

Государственное образовательное учреждение
высшего профессионального образования
**«Томский государственный университет
систем управления и радиоэлектроники»**



**ТЕМАТИЧЕСКИЙ
РЕФЕРАТИВНЫЙ СБОРНИК № 44-1/1**

**“Light Emitting Diode”
(«Светодиоды»)
Журнальные публикации**

Источник: *Digital Library IEEEExplore*
Язык: *английский*
Глубина поиска: *2009 – 2011 гг.*
Дата формирования: *март 2011 г.*
Составитель: *В.И. Карнышев*

Томск – 2011

ТЕМАТИЧЕСКИЙ РЕФЕРАТИВНЫЙ СБОРНИК № 44-1/1

"Light Emitting Diode"

(«Светодиоды»)

Журнальные публикации

"Organic vapor jet printing at micrometer resolution using microfluidic nozzle arrays"

Organic vapor jet printing with a print head comprised of a microfluidic Si nozzle array is used to deposit parallel lines of an organic semiconductor thin film with a line width of 16 μm and edge resolution of 4 μm . Line width and feature size are functions of process conditions, depending strongly on nozzle-to-substrate separation distance. Experimental results are accurately characterized by a direct simulation Monte Carlo model. The model suggests that feature sizes of <1.5 μm are attainable by this printing process. The ability of the print head to codeposit doped films is demonstrated by growing the emissive layer of a green phosphorescent organic light emitting diode sandwiched between hole and electron transport layers deposited by vacuum thermal evaporation. This device had an external quantum efficiency of $8.8 \pm 1.3\%$, comparable to a similar device entirely grown by vacuum thermal evaporation. [J1]

"Polarized spontaneous emission from blue-green m-plane GaN-based light emitting diodes"

The polarization of spontaneous emission was investigated for various indium compositions and quantum wells on m-plane oriented gallium nitride (GaN) light emitting diodes (LEDs) grown on bulk-GaN substrates. Internal light scattering and depolarization was mitigated with application of absorber materials to the LED die. The polarization ratio (ρ) was measured under electrical injection for devices with InGaN active regions emitting up to 520 nm and observed as high as 96%. Values of ρ were independent of drive current. The valence band energy separation (ΔE) was characterized using spectral measurement and temperature dependent optical analysis of valence band hole distributions. [J2]

"Surface-plasmon-induced light absorption on a rough silver surface"

We investigate light absorption in metal films, silver and aluminum, with different surface roughness. Measurements using an integrating sphere show that the reflectance in silver decreases significantly with increasing surface roughness whereas the reflectance in aluminum is almost constant. The experimental results agree well with numerical simulations in which the surface roughness of metal is described properly. In particular, the simulations demonstrate that the absorption by surface-plasmon-polaritons excited on a rough silver surface causes the surface-dependent reflectance in silver. This study suggests a convenient and feasible rule to rationally design a backside metal reflector toward high-efficiency light-emitting diodes and photovoltaics. [J3]

"Improved Extraction Efficiency of Light-Emitting Diodes by Wet-Etching Modifying AZO Surface Roughness"

In this letter, the AlGaInP light-emitting diodes (LEDs) between the air and GaP layer are added to the textured ZnO:Al (AZO) films in order to improve light extraction of the device. At 20 mA, the relative luminous intensity of textured AZO LEDs is increased by 129.9% when compared with the conventional sample. Furthermore, the far-field radiation pattern was improved with intensity not only at 0° , but also from 60° to 300° . Due to loss of internal Fresnel efficiency and critical angle efficiency, textured AZO LEDs are significantly improved by the wet-etching technique. The surface treatment of AZO films generates surface texturing that is characterized as random crater. It presents a better far-field radiation pattern when compared with nontextured AZO films. This letter has demonstrated the far-field radiation pattern and the theory for enhancing light emission efficiency of LEDs. [J4]

"Integer charge transfer states in organic light-emitting diodes: Optical detection of hole carriers at the anode | organic interface"

Hole carriers that reside at the anode | hole-transport-layer (HTL) interface, creating a dipole layer, have been observed in organic light-emitting diode (OLED) and model devices using charge modulation spectroscopic

techniques. These interfacial carriers have been observed with various HTL materials and several anode compositions at voltages such that the HTL is reverse-biased. The cation density at an ITO|CFx|NPB interface is estimated to be approximately $1.4 \times 10^{13}/\text{cm}^2$, or approximately 10% of a molecular layer. [NPB is 4,4'-bis[N-(1-naphthyl)-N-phenylamino]biphenyl. CFx is a fluorocarbon polymer.] The cations represent the integer charge-transfer states whose presence has been inferred from ultraviolet photoelectron spectroscopy studies of various conductor|organic interfaces. Anions of an organic hole-injecting material, 1,4,5,8,9,11-hexaazatriphenylene hexacarbonitrile (HAT-CN) were also observed. Conditions near the injecting contacts often determine the electric field profile and drive voltage of an OLED. Elucidation of these conditions is important to a complete understanding and detailed modeling of OLED operation. [J5]

"Efficiency measurement of GaN-based quantum well and light-emitting diode structures grown on silicon substrates"

The optical efficiency of GaN-based multiple quantum well (MQW) and light emitting diode (LED) structures grown on Si(111) substrates by metal-organic vapor phase epitaxy was measured and compared with equivalent structures on sapphire. The crystalline quality of the LED structures was comprehensively characterized using x-ray diffraction, atomic force microscopy, and plan-view transmission electron microscopy. A room temperature photoluminescence (PL) internal quantum efficiency (IQE) as high as 58% has been achieved in an InGaN/GaN MQW on Si, emitting at 460 nm. This is the highest reported PL-IQE of a c-plane GaN-based MQW on Si, and the radiative efficiency of this sample compares well with similar structures grown on sapphire. Processed LED devices on Si also show good electroluminescence (EL) performance, including a forward bias voltage of

3.5 V at 20 mA and a light output power of 1 mW at 45 mA from a $500 \times 500 \mu\text{m}^2$ planar device without the use of any additional techniques to enhance the output coupling. The extraction efficiency of the LED devices was calculated, and the EL-IQE was then estimated to have a maximum value of 33% at a current density of 4 A cm^{-2} , dropping to 30% at a current density of 40 A cm^{-2} for a planar LED device on Si emitting at 455 nm. The EL-IQE was clearly observed to increase as the structural quality of the material increased for devices on both sapphire and Si substrates. [J6]

"Enhanced Output Power of Near-Ultraviolet InGaN/AlGaIn LEDs With Patterned Distributed Bragg Reflectors"

A 400-nm near-ultraviolet InGaN/AlGaIn light-emitting diode (LED) with a patterned distributed Bragg reflector (PDBR) mask is the subject of this paper. The design of the PDBR mask on the GaN/sapphire substrate attempts to reduce the threading dislocation density in the epitaxial template and enhance light extraction efficiency via the reflective behavior of the DBR. Under an injection current of 20 mA, the forward voltages of the PDBR and conventional LEDs were 3.51 and 3.52 V, respectively. This result indicates that the operating voltage of the PDBR LED does not arise by this PDBR mask design. In addition, the leakage current of the PDBR LED sample (1.36 nA at -5 V) is found to be lower than that of the conventional LED (11 nA). We also discovered that the light output power for the PDBR LED was approximately 39% higher (at 20 mA) than the conventional LED, and this significant improvement in performance is attributed not only to the GaN template crystalline quality reform but also due to the light extraction enhancement via the PDBR mask. [J7]

"Exciton formation as a rate limiting step for charge recombination in disordered organic molecules or polymers"

The exciton formation (direct charge recombination) is studied and quantified as a function of material physical-properties such as the exciton binding energy, the exciton lifetime, and the mechanism causing the electronic disorder. By using a model that is an extension of a charge transport model [Y. Preezant and N. Tessler, Phys. Rev. B 74, 235202 (2006)] we are able to compare the direct exciton formation rate with the one predicted by the Langevin model. Using reasonable material parameters we find that in many cases the overall balance between free charge carrier and excitons is significantly affected by the exciton formation rate with its values being significantly low compared to the Langevin rate. We also find that in order to describe the complete recombination process it is important to introduce an intermediate state which we term exciton-precursor. This is in contrast to the common practice of using the Langevin model which embeds the assumption that the exciton formation rate is negligibly fast. The relations found between the physical-properties and the recombination rate can explain why certain materials exhibit Langevin rate while others exhibit significantly suppressed rates. This would eventually lead to the design of new materials better suited for either photocells or light-emitting diodes. [J8]

"Improvement of ESD Level of GaN-Based LEDs Using Antiparallel Ga- and N-Polar Domains in p-GaN Layer"

Electrostatic discharge (ESD) endurance ability of InGaN blue light-emitting diodes is significantly improved when antiparallel Ga- and N-polar domains coexist within the p-type GaN-layer region. The inversion of Ga to N polarity in this region, which is verified using convergent-beam electron diffraction, was induced by the stress accumulated in the underlying layers. A typical p-type GaN layer, which is composed of a periodical arrangement of Ga-polar domains (width, 450 nm) and antiparallel Ga- and N-polar domains (width, 150 nm), improves the negative human-body mode ESD 4000 V pass yields to greater than 90%. [J9]

"Ultraviolet Electroluminescence From ZnO-Based n-i-p Light-Emitting Diodes"

The p-type ZnO films were obtained using codeposition of ZnO and sources by the vapor cooling condensation system. With an adequate postannealing temperature, the p-type conductive behaviors of the resulting ZnO films could be achieved due to the activation of Li-N dual acceptor. According to the emission energy of free electron to acceptor hole level, the acceptor binding energy of 137 meV was obtained. Furthermore, the ZnO-based n-i-p ultraviolet light-emitting diodes were deposited on sapphire substrates using the vapor cooling condensation system. A rectifying diode-like behavior and ultraviolet emission were observed from the ZnO-based n-i-p light-emitting diodes. [J10]

"Indoor Channel Characteristics for Visible Light Communications"

In this letter, we present indoor multipath dispersion characteristics for visible light communications (VLC). Since the VLC uses a wide spectrum between 380 nm and 780 nm, the conventional narrowband model for infrared may not apply. We generalize the Barry's model by including wavelength-dependent white LED characteristics and spectral reflectance of indoor reflectors. We perform a computer simulation to compare the power delay profile of the VLC with that of infrared communications. From our studies, we show that the VLC provides a larger transmission bandwidth than infrared communications. [J11]

"Enhancement in Light Emission From Hg-Cd-Te Due to Surface Patterning"

Enhancement of light emission from HgCdTe due to surface patterning has been studied by means of photoluminescence (PL) spectroscopy. A triangular pattern of circular holes was etched into the CdTe layer grown on top of HgCdTe thin-film and multiple quantum well samples. Two different pattern lattice constants were used, giving lattice constant aGto emission wavelength ratios of 0.9, 1.2, and 2.1. The surface pattern was found to give 26%-35% enhancement in measured PL intensity. [J12]

"Planar Lighting System Using Array of Blue LEDs to Excite Yellow Remote Phosphor Film"

This investigation demonstrates a novel light-emitting system with an array of blue light-emitting diodes (LEDs). Unlike a conventional lighting system that is constructed from white LEDs, the proposed planar lighting system uses blue LEDs to excite a YAG: Ce³⁺+yellow phosphor film remotely, yielding a high lumen efficiency with uniform and planar light-emission. The phosphor film herein acts as a wavelength converter and a light diffuser simultaneously. The optical properties of the proposed lighting system, angular color deviation and light-emitting uniformity, are studied. Eventually, a high lumen efficiency (73.0 lm/W) and thin lighting module (7.5 mm-thick) was demonstrated without the use of any conventional diffuser plate or light guiding plate (LGP). A low color deviation ($\Delta u'v' = 0.025$) and a high light-emitting uniformity (Uniformity= 82%) were achieved. Hence, the proposed lighting system exhibited superior optical performance using a compact module. [J13]

"A Novel Adaptive Dimming LED Backlight System With Current Compensated X-Y Channel Drivers for LCD TVs"

In this paper, a novel two-dimensional adaptive dimming and current compensation technique with X-Y channels for light-emitting diode (LED) backlight system in LCD TVs is proposed. The proposed LED backlight has matrix structured LED modules with row and column switches to control the brightness of individual division block. It shows local dimming effects such as reduced power consumption and high dynamic contrast ratio even with much less number of LED drivers than that of the conventional two-dimensional local dimming method. Therefore, low cost and compact design of LED drivers can be achieved. This paper also contains a new adaptive dimming algorithm and image compensation technique for the proposed LED backlight system. Moreover, luminance difference among blocks caused by different I-V characteristics of LED and the luminance variation caused by temperature change are compensated by current sensing system. The proposed dimming technique is verified by simulation and experimental results based on a RGB-LED backlight of a 32-inch LCD TV. [J14]

"Characteristics of dotlike green satellite emission in GaInN light emitting diodes"

An unwanted green satellite emission in blue GaInN light emitting diodes (LEDs) has been investigated under various electrical bias conditions and temperatures. The dot-shaped green satellite emission appears only under electrically biased conditions of the LED (but not under photoluminescence excitation) and contributes directly to a high subthreshold leakage current of the LED. A weak temperature dependency of the green satellite emission intensity is observed indicating that tunneling-assisted radiative recombination involving Mg acceptors is the origin of the green emission. [J15]

"Efficient organic light-emitting devices with platinum-complex emissive layer"

We report efficient organic light-emitting devices having a platinum-complex emissive layer with the peak external quantum efficiency of 17.5% and power efficiency of 45lm W⁻¹. Variation in the device performance with platinum-complex layer thickness can be attributed to the interplay between carrier recombination and intermolecular interactions in the layer. Efficient white devices using double platinum-complex layers show the external quantum efficiency of 10%, the Commission Internationale d'Éclairage coordinates of (0.42, 0.41), and color rendering index of 84 at 1000cd m⁻². [J16]

"Localization of surface plasmon polaritons in hexagonal arrays of Moire cavities"

In view of the progress on the confinement of light, we report on the dispersion characteristics of surface plasmon polaritons (SPPs) on two-dimensional Moire surfaces in the visible part of the electromagnetic spectrum. Polarization dependent spectroscopic reflection measurements show omnidirectional confinement of SPPs. The resonance wavelength of SPP cavity modes can be adjusted by tuning the propagation direction of SPPs. The results may have an impact on the control of spontaneous emission and absorption with applications in light emitting diodes and solar cells, as well as in quantum electrodynamics experiments. [J17]

"Uniform Illumination Design by Configuration of LED Array and Diffuse Reflection Surface for Color Vision Application"

Illumination uniformity and color mixing results are essential for color vision applications. In this paper, an indirect method is proposed for the uniform illumination, and a mathematically simulated algorithm is developed. We integrate the method of light-emitting diode (LED) array and diffuse reflection surface for uniform illumination system. By considering each single LED as an imperfect Lambertian emitter, we discuss the irradiance distribution over a sphere's inner surface to the three-ring LED array. The sphere's inner surface is a diffuse reflection surface with high hemisphere reflectance. Using the bi-directional reflectance distribution functions (BRDF) of the sphere's inner surface, we simulate the uniformity of the LED illumination at varying distances. Finally, we design a practical LED illumination. The uniformity of practical LED illumination agrees with the simulated result. The results demonstrate the usefulness of this method for uniform illumination design. [J18]

"Improved Electrostatic Discharge Protection in GaN-Based Vertical Light-Emitting Diodes by an Internal Diode"

We first fabricated GaN-based vertical light-emitting diodes (LEDs) with electrostatic discharge (ESD) protection internal diode. Despite the reduced emitting area due to the internal diode, the LEDs with the internal diode give a forward voltage of 3.42 V at 350 mA similar to that (3.40) of LEDs without the internal diode. It is shown that the output power of the LEDs with the internal diode is reduced by about 6% at 350 mA compared to reference LEDs without the internal diode. It is, however, further shown that the LEDs without the internal diode give a yield of 0% at the reverse voltages above 400 V, while the LEDs with the internal diode show a yield of $\sim 90\%$ at reverse voltages of 2-4 kV. [J19]

"Midinfrared electroluminescence from PbTe/CdTe quantum dot light-emitting diodes"

Midinfrared electroluminescence of epitaxial PbTe quantum dots in CdTe with emission in the 2-3 μ m wavelength range is demonstrated up to room temperature. The light-emitting diode structures were grown by molecular beam epitaxy with the active PbTe quantum dots embedded in the intrinsic zone of a CdTe/CdZnTe p-i-n junction on GaAs (100) substrates. The current and temperature dependences of the electroluminescence emission are presented. The comparison with photoluminescence measurements shows that midinfrared light-emission from the diodes originates from the quantum dots. [J20]

"Interconnected alternating-current light-emitting diode arrays isolated by laser micromachining"

The fabrication and operation of a monolithic InGaN alternating-current light-emitting diode (LED) based on the bridge rectifier design are demonstrated. The device consists of on-chip interconnected LED elements that have been isolated by direct-write laser micromachining, a powerful tool well-suited for rapid device prototyping. The

effects of capacitors coupled to the dc path of the rectifier have been investigated. Although an increase of radiant flux can be achieved through capacitive voltage smoothening, the wall-plug efficiency drops as a result. The device can be applied to 12Vrms lighting applications. [J21]

"Design of selective emitting media within a cylindrical tube for conversion of wasted heat energy to electrical energy"

Thermophotovoltaic (TPV) energy conversion is the conversion of heat energy to electrical energy via light. This manuscript focuses on the geometric design of emitting material within an exhaust tube to convert wasted heat energy to light, and achieve an optimal amount of irradiance at the PV diode cells. Due to the large value of the absorption coefficient for the selectively emitting erbia-doped nanofibers under discussion, the diffusion approximation to the equation of radiation transfer is used. This approximate equation is solved for emission from hot-spot sources within the emitting material. Several geometric distributions of the emitting material are considered. Within an axisymmetric geometry all erbia-doped nanofibers, all quartz wool, and mixtures of disk-shaped or cylindrical shell shaped distributions of nanofibers and wool are investigated. Within a polar geometry all erbia-doped nanofibers, all quartz wool, and mixtures of spoke-shaped or cylindrical shell shaped distributions are investigated. In both geometries the mixture distributions consist of alternating thin layers of emitting and non-emitting material. Homogenization techniques are applied to these distributions to define expressions for the effective absorption and scattering coefficients for these spatially distributed emitting structures. The effective expressions are input into the diffusion approximation that is solved for the spectral irradiance. The net radiation obtained from these emitting structures is examined to optimize the geometry of the TPV material to maximize emission with use of minimal TPV material. Results show that disk-shaped bands or spokes allow for maximum irradiation in the radial direction toward the diode collectors. A large volume fraction of erbia-doped nanofibers is optimal when hot spots are close to the diodes. Smaller volume fractions work better when hot spots are away from the diodes due to reabsorption of emitted light by the emitting material. [J22]

"Influence of GaSb and AlGaInAsSb as Barrier Material on 2.8- μ m GaSb-Based Diode Laser Properties"

GaSb-based diode lasers emitting at a wavelength of 2.8 μ m have been grown. The devices feature GaSb or Al_{0.21}Ga_{0.58}In_{0.21}As_{0.20}Sb_{0.80} barrier layers for the quantum wells, respectively. The transparency current density, modal gain, internal absorption, and characteristic temperature have been investigated on both devices. Since the barrier layers serve at the same time as waveguide for the laser light, the optical properties and the impact on device performance have been determined. The refractive index for Al_{0.21}Ga_{0.58}In_{0.21}As_{0.20}Sb_{0.80} has been estimated to be 3.26. [J23]

"Improvement of Surface Emission for GaN-Based Light-Emitting Diodes With a Metal-Via-Hole Structure Embedded in a Reflector"

This work demonstrates the feasibility of gallium nitride (GaN)-based light-emitting diodes (LEDs) with a metal-via-hole structure embedded in a reflector on the backside of sapphire substrate. Luminescence intensity for the surface-emitting LEDs is enhanced by mirroring efficaciously the downward light emitted from the InGaN/GaN multiquantum wells (MQWs) owing to the deep ladder-shaped inclined reflector on the backside of substrate. A metal-via-hole structure with a deep ladder shape was also processed with a wet-etching method at a high temperature to pattern the sapphire substrate deeply. The electroplating method was used to fill the area of patterned sapphire substrate with copper subsequently to produce a heat spreader path through the metal-via-hole and to strengthen the sapphire substrate with the void structure. Experimental results indicate that the GaN-based surface-emitting LEDs with a reflector for the planar, deep ladder-shaped sapphire, and metal-via-hole structures exhibit a luminescence intensity of 37%, 178%, and 226%, respectively, which are higher than the conventional ones under an injection current of 20 mA. A more stable peak wavelength shift is also observed for the metal-via-hole LED structure. [J24]

"Indoor Optical Wireless MIMO System With an Imaging Receiver"

This letter reports an experimental demonstration of an indoor optical wireless multiple-input-multiple-output (MIMO) system with an imaging receiver. The system setup consists of a 2×2 array of white light-emitting diodes (LEDs) and a 3×3 photodetector array, separated by a range of 2 m. The system operates at a bit rate of 2 Mb/s/channel, with error-free operation at certain positions within the system coverage area. An overview of the design specifications, optical design, and experimental setup are reported in this letter, together with results and discussion of how the system might be improved. [J25]

"Investigation of the Carrier Dynamic in GaN-Based Cascade Green Light-Emitting Diodes Using

the Very Fast Electrical-Optical Pump-Probe Technique"

For the first time, the internal carrier dynamic inside GaN-based green light-emitting diodes (LEDs) during operation has been directly observed using the demonstrated electrical-optical pump-probe technique. Short electrical pulses (~100 ps) were pumped into high-speed cascade green LEDs, and the output optical pulses were probed using high-speed photoreceiver circuits. Using such a method, the recombination time constant of the carriers can be directly measured without any assumption about the recombination process. A high-speed cascade LED structure was adopted in the experiments to eliminate the influence of the RCdelay time on the measured responses. Our measurement results indicate that both single- and three-LED cascade structures have the same internal response time due to current continuity. Furthermore, based on responses measured under different temperatures (from 25°C to 200°C), the origin of the efficiency droop in GaN-based green LEDs under a high bias current density may be attributed to the strong nonradiative Auger effect rather than device heating or carrier overflow. The demonstrated measurement scheme and high-speed cascade device structure offer a novel and simple way to straightforwardly investigate the internal carrier dynamic inside the active layers of the LED during forward-bias operation. [J26]

"Cascaded Superlattice InAs/GaSb Light-Emitting Diodes for Operation in the Long-Wave Infrared"

Superlattice InAs/GaSb light-emitting diodes with peak emission wavelength of 8.6 μm and output power approaching 190 μW at 77 K from a 120 \times 120 μm^2 mesa are demonstrated. Output power in excess of 600 μW was demonstrated from a 520 \times 520 μm^2 mesa at 1 A drive current and 50% duty cycle. Devices were grown by molecular beam epitaxy on lightly n-doped GaSb substrates and employed a 16-stage cascaded active region configuration to improve current efficiency and increase optical output. Emitting regions were coupled by semi-metallic tunnel junctions consisting of a p-GaSb layer and a thickness-graded InAs/GaSb superlattice stack. [J27]

"Nearly Diffraction-Limited Tapered Lasers at 675 nm With 1-W Output Power and Conversion Efficiencies Above 30%"

High brightness, highly efficient tapered lasers emitting around 675 nm have been developed. The devices have a 500- μm -long straight section and a 1500- μm -long tapered section with a flare angle of 3°. At a temperature of 25°C and a current of 1.5 A, the lasers emit an output power of nearly 1.2 W. The maximum conversion efficiency of 31% is reached at an output power of 1 W. The emitted beam is nearly diffraction-limited with a beam propagation ratio (second moments) of 2.2. [J28]

"Optical Properties of the Partially Strain Relaxed InGaN/GaN Light-Emitting Diodes Induced by p-Type GaN Surface Texturing"

Partial strain relaxation from the light-emitting diode (LED) with surface-textured p-GaN was observed. The textured device possesses less efficiency droop and a higher current level at the efficiency maximum, as compared with the planar one. The results suggest that surface roughening affects not only the external light extraction but also the internal quantum efficiency. Furthermore, the photoluminescent (PL) measurement at low temperature reveals that the percentage increment of the optical power of the textured LED over that of the planar LED becomes lower. In addition to the effect of frozen nonradiative defect states, the PL difference is related to the strain-correlated quantum-confined Stark effect. [J29]

"Design of Infrared Electronic-Toll-Collection Systems With Extended Communication Areas and Performance of Data Transmission"

Based on our previous works in the design of an infrared emitter for electronic-toll-collection (ETC) applications, we use the unidirectional cosines functions to approximate the irregular radiation pattern for typical infrared low-cost commercial light-emitting diodes (LEDs) with a half-intensity angle $\Phi_{1/2} = 10^\circ$. With the aid of this approximation, the main characteristics of the performance of an infrared ETC system utilizing this type of LED as the emitter can be investigated based on the received signal strength of the system. For on-off keying, a simple model connecting the received signal strength and the bit error rate (BER) of the system is further established. From the calculated or the measured received signal strength of the system, it is not difficult to estimate the system performance in terms of the BER by this simple model. Roughly speaking, for a typical setting of the circuit parameters and a typical uplink and downlink data-transmission protocol, the data transmission can be very successful in terms of a very low BER if the received signal strength is 1.3 times stronger than the signal strength received at the communication boundary. The emitter presented in this paper is able to produce a relatively extended communication area in the vehicle-traveling direction, resulting in longer communication time interval for the data transmission between the onboard unit (OBU) and the roadside unit (RSU) than conventional emitters. Furthermore, the design presented in this paper is validated by experimental

measurement to demonstrate its effectiveness. [J30]

"On the Adjustment of the Color Temperature of White Light-Emitting Diodes by Femtosecond Laser Patterning"

We show that femtosecond (fs) laser microstructuring of light-emitting diode (LED) encapsulates has a high potential for the fine-tuning of the color temperatures of white LED packages. The number of scattering centers that are fabricated within the volume of the encapsulate allows the precise adjustment of the color temperature of the device to the desired value. This opens possibilities to achieve color reproducibility among individual LED packages with highest accuracy. [J31]

"A Universal-Input Single-Stage High-Power-Factor Power Supply for HB-LEDs Based on Integrated Buck-Flyback Converter"

Due to the high rise in luminous efficiency that high-brightness light-emitting diodes (HB-LEDs) have experienced in recent years, many new applications have been researched. This paper covers a streetlight LED application using the offline integrated buck-flyback converter (IBFC) developed in previous works. In this application, the converter is used to provide power-factor correction from a universal ac source. A control loop using the LM3524 IC has been implemented for testing the feasibility of Enabling pulsewidth modulation dimming mode. First, the LED load has been linearized and modeled in order to calculate the IBFC topology properly. Second, the converter has been designed and tested at the laboratory. The converter has also been modeled in order to design a fixed-frequency constant-current control. The dynamics of all the stages involved in the closed loop have been taken into account in order to develop an adequate controller. Finally, the experimental results obtained from the laboratory tests are discussed. [J32]

"A Method for Fabricating Practically Channel-Corner-Free Polycrystalline Silicon Thin-Film Transistors"

The influences of metal-induced laterally crystallized silicon channel corners on the performance and reliability of thin-film transistors (TFTs) were investigated. It was found that the TFT with the channel width, mostly applied to active matrix organic light-emitting diodes, had weak immunity to electrical stresses because of the heaviest weight of silicide-rich channel corner on the channel width by the geometric effect. The proposed TFT fabrication, which is composed of two consecutive adjacent step switches, makes TFTs practically channel-corner-free, resulting in high reliability. Moreover, it enables TFTs to have more current flow paths that maintain a high performance. [J33]

"Efficiency Enhancement in Organic Light-Emitting Devices With a Magnetic Doped Hole-Transport Layer"

Magnetic field effects on tris-(8-hydroxyquinoline) aluminum-based organic light-emitting devices (OLEDs) by employing Fe₃O₄ as a magnetic dopant in the hole-transport layer (HTL) have been studied. The magnetic doped OLEDs exhibit efficient injection and transport of holes, and its performances are further enhanced after a magnetic field is applied. The enhancement of luminance and current efficiency of 20% and 24% has been obtained from the magnetic doped devices, while they are only 8% and 9%, respectively, for the nondoped devices under an applied magnetic field of 500 mT. Organic magnetoresistance induced by the magnetic doped HTL is the main origin of increased electroluminescence for the magnetic doped OLEDs. [J34]

"Vertically Mounted InGaN-on-Sapphire Light-Emitting Diodes"

An InGaN/GaN light-emitting diode (LED) chip mounted in a vertical configuration (vmLED) is demonstrated, exhibiting significant enhancement to light extraction, compared with a LED mounted in a conventional planar geometry. By flipping the chip orthogonally, two large illumination surfaces of the device are exposed for direct light extraction. Comparisons, through ray-trace modeling and experiment data with conventional surface-mounted LEDs, indicate that the vmLEDs achieve superior light extraction efficiency. A sapphire-prism-mounted vmLED is further proposed to improve heat sinking, which is well suited for higher current operations. [J35]

"Angular CCT Uniformity of Phosphor Converted White LEDs: Effects of Phosphor Materials and Packaging Structures"

In this work, we studied the effect of different packaging parameters on the angular homogeneity of correlated color temperature (CCT) in phosphor-in-cup light-emitting diode (LED) packages, including phosphor particle concentration, phosphor-layer surface curvature, and lens surface curvature, using a Monte Carlo ray tracing

simulation tool. An optimized packaging geometry with convex phosphor layer was achieved with good CCT uniformity and highest lumen efficiency. Moreover, an approach was developed for the prediction of color uniformity and lumen efficiency when varying the surface curvature of either phosphor layer or clear lens, since the inconsistency of phosphor layer or lens cap happened commonly to the fabricated phosphor conversion white LEDs (pc-WLEDs). [J36]

"Portable Fluorescence Lifetime Detection for Chlorophyll Analysis in Marine Environments"

This paper describes the proof-of-concept performance of a low-cost phase fluorometer designed to capture the fluorescence lifetime of chlorophyll in various stages of healthy marine life. The proof-of-concept experimental demonstration is completed using fluorescein as a close simulant of chlorophyll. Results are extrapolated analytically using simulation to project performance limits (detection and lifetime) in chlorophyll rich environments. The designed system is able to compete with the fundamental performance limits of existing fluorometers designed for chlorophyll analysis while reducing power consumption by a factor of 20, power supply by an order of magnitude or more (to 12 V), and cost by a factor of ten (to a target low-volume system cost of \$1000). [J37]

"Top 11 technologies of the decade"

The most powerful technologies take a while to mature. But when they do, they can rapidly retire mainstays that are decades old. Given in this paper are the top 11 technologies of the decade which are smartphones, social networking, voice over IP, LED lighting, multicore CPU, cloud computing, drone aircraft, planetary rovers, flexible AC transmission, digital photography and class-D audio. [J38]

"The lightbulb that really is a better idea [JTools & Toys]"

LED bulbs change the lighting equation. The paper presents the LED light bulb that produce as much as incandescent bulbs for less than a fifth the electricity and heat, they last up to 20 years, and they fit in standard sockets, and discussed its advantage, economical analysis and benefits over the other light bulb. So even as you try to figure out which of your current fixtures might be suitable for LED bulbs, expect them to be far more commonly seen at new stores, restaurants, and offices. [J39]

"Color Range Images Captured by a Four-Phase CMOS Image Sensor"

As 3-D displays become more common, the demand for 3-D-related products is rapidly increased. Three-dimensional image sensors based on the time-of-flight (TOF) technique are one of these products and are applied to many applications. In this paper, a new pixel based on the continuous-wave modulation method was proposed to measure the TOF and was embedded in a test complementary metal-oxide-semiconductor (CMOS) image sensor. Compared with other range imagers, no complex control signals, high operating voltage, or multilevel control voltages are needed in this pixel. The chip, with 92 Ч 30 pixels, was fabricated using the Taiwan Semiconductor Manufacturing Company's 0.18- μm CMOS standard process, and a time-switched color measurement was applied to this rangefinder system. A pulse train of red, green, and blue lights is emitted sequentially from a light-emitting diode array. The distance is easily calculated from the phase differences, and the color information is estimated using the difference in reflection coefficients under a different light. The measured distance and color are compared with the actual distance and color-corrected images. A color range image with a distance error of 3.56 cm and an L^*a^*b color difference of 40.23 can be observed. This rangefinder system provides a new perspective to capturing a colored range image. [J40]

"Light Extraction Investigation for Thin-Film GaN Light-Emitting Diodes With Imbedded Electrodes"

Light extraction in thin-film GaN light-emitting diodes (LEDs) prepared with Si substrates pretreated by surface roughening and imbedded electrodes were studied. The LEDs were fabricated with a roughened p-GaN layer, followed by epilayer transferring. There are four types of LEDs: conventional LEDs (C-LED), n-side-up thin GaN LEDs with imbedded electrodes and a KOH-roughened n-GaN (first-type LED), p-side-up thin GaN LEDs with a KOH-roughened n-GaN (second-type LED), and n-side-up thin GaN LEDs with imbedded electrodes and without KOH-roughened n-GaN (third-type LED). The electrical properties of the LEDs are almost the same. However, they differ in luminance intensity. The luminance intensities (at 350 mA) of C-LED, first-type, second-type, and third-type LEDs are 3468, 9105, 7610, and 7047 mcd, respectively. The brightest LED is first-type LED. This may be due to emission surface with pyramidal-textured surface and without light shading electrodes. They enhance the light extraction for first-type LEDs. [J41]

"Numerical Study of Blue InGaN Light-Emitting Diodes With Varied Barrier Thicknesses"

This letter demonstrates the outcomes of numerical investigation of the InGaN light-emitting diodes with varied

barrier thicknesses. Compared with the original structure with equal barrier thickness, the analyses focus on hole injection efficiency, carrier distribution, electron leakage, and radiative recombination. Simulation approach yields to a result that, when varied barrier thicknesses are used, more than one quantum well contributes to radiative recombination at high injection current which leads to the improvement of efficiency droop. Further analysis indicates that the thinner barrier located close to the p-side layers is beneficial for increasing hole injection, which leads to the reduction of electron leakage; moreover, holes can be confined in more quantum wells in such condition as well. [J42]

"Powering LED Using High-Efficiency SR Flyback Converter"

A multifunction circuit is presented herein and applied to a synchronously rectified flyback converter, with the circuit not only playing the role of an LCsnubber but also detecting the zero crossing of the current to reduce switching loss and feeding the peripheral circuit. Hence, such a converter has high efficiency all over the operating range and, together with one front-end power-factor-correction ac-dc converter, is applied to feeding a LED streetlight. In this paper, the basic operating principles of the proposed topology are first illustrated in detail, and second, some simulated and experimental results are provided to demonstrate the effectiveness of the proposed topology. [J43]

"An Interleaved Flyback Converter Featured With Zero-Voltage Transition"

This paper proposes an interleaved flyback converter, which is remarked with zero-voltage-switched active switches and reduced reverse-recovery loss on the rectifying diodes. The converter is composed of two parallel-operated identical flyback converters and an auxiliary inductor shunted between the diodes. This converter can provide up to 500 W power with highest efficiency as high as 91%. In addition, burst-mode control is equipped to drive the converter at low load. Even at 50-W output, the efficiency is higher than 83%. [J44]

"Improved Optical and ESD Characteristics for GaN-Based LEDs With an Layer"

Nitride-based light-emitting diodes (LEDs) with an $\text{Al}_x\text{Ga}_{1-x}\text{N}$ layer are proposed and fabricated. By providing a larger series resistance in the vertical direction, it was found that the $\text{Al}_x\text{Ga}_{1-x}\text{N}$ layer could enhance LED output intensity due to the enhanced current spreading. It was also found that LEDs with $\text{Al}_x\text{Ga}_{1-x}\text{N}$ layer thicknesses of 0.15, 0.2, and 0.25 μm could endure electrostatic discharge surges up to ~ 1200 , ~ 1800 , and ~ 3000 V, respectively. [J45]

"A Problem of Infrared Electronic-Toll-Collection Systems: The Irregularity of LED Radiation Pattern and Emitter Design"

According to our measurements, the radiation pattern of many low-cost commercial light-emitting diodes (LEDs) is not smooth. Some LEDs even have serious irregularities that affect the performance of infrared communication systems. For systems where a definite communication area is required, such as electronic-toll-collection (ETC) applications, this problem is particularly serious. In this paper, we first present our measured results for the radiation pattern of several typical low-cost commercial LEDs, showing that almost all of them are irregular to some extent. We then use the most acceptable model with a suitable half-intensity angle to construct the emitter of an ETC system. The design was calculated with the aid of an optimization algorithm to determine the mounting angle for each LED such that the system has an extended communication area in the longitudinal direction, i.e., in the vehicle traveling direction, and can withstand high signal attenuation. For a typical LED with half-intensity angle $\Phi_{1/2} = 13^\circ$, a very simple two-group structure for the emitter is obtained, and the analysis results are verified by experimental measurements. [J46]

"Enhanced Performance of Nitride-Based Blue LED With Step-Stage MQW Structure"

A step-stage InGaN/GaN multiquantum-well (MQW) structure can enhance the efficiency of GaN-based light-emitting diodes (LEDs). Compared to dual-stage MQW LEDs, the step-stage MQW LEDs have lower forward voltage and higher light output. The measured light output power of step-stage LEDs operating at 350 mA shows an increase of approximately 23% with an external quantum efficiency (EQE) increase of 6.6%, when compared to dual-stage LEDs. [J47]

"Combining Illumination Dimming Based on Pulse-Width Modulation With Visible-Light Communications Based on Discrete Multitone"

In the field of indoor wireless networks, visible-light communications is garnering increasing attention. One of the type of emitters used in this technology is white light-emitting diodes, which can synergistically provide both illumination and data transmission. Discrete multitone modulation is attractive for visible-light communications.

One of the issues to be addressed in these synergetic use cases is how to incorporate light dimming while not corrupting the communication link. In this paper, the performance of a visible-light communication system combining pulse-width modulation for dimming and discrete multitone for data transmission was investigated. Performance indicators were addressed, i.e., the signal-to-interference ratio due to dimming and the achievable bit-error ratio in the absence of additional noise. By aid of simulations it was shown that practical communication is only feasible when the line rate of the dimming modulation is at least twice the frequency assigned to the largest multitone subcarrier frequency. The results demonstrate that under this constraint and when using a suitably modified demodulation scheme, dimming does not influence the data transmission. [J48]

"Performance characteristics of GaN-based light-emitting diodes fabricated with AgNi, AgCu, and AgAl-alloy reflectors"

We report on the performance characteristics of GaN-based light-emitting diodes (LEDs) fabricated with Ag-alloy p-type reflectors including AgNi, AgCu, and AgAl. Compared to the reference LEDs fabricated with Ag, LEDs fabricated with AgNi and AgCu produced smaller forward voltages and higher light output power. Under optimized thermal annealing conditions, the forward voltages obtained were 3.56, 3.29, 3.28, and 3.44 V, the light output powers were 14.38, 15.73, 14.40, and 12.77 mW, and the power efficiencies were 20.2%, 23.91%, 21.95%, and 18.45% for LEDs fabricated with Ag, AgNi, AgCu, and AgAl, respectively. The surface morphology of Ag-alloy was also found to be smoother than that of Ag, suggesting that Ag-alloy reflectors, particularly AgNi, are very promising for practical applications. [J49]

"Droop improvement in high current range on PSS-LEDs"

The droop property of blue GaN light emitting diodes (LEDs) has been improved by creating a 9 quantum well (QW) LED on a patterned sapphire substrate (PSS). The droop ratio was improved from 45.9 to 7.6%. At a wavelength of 447nm, and with standard on-header packaging, the 9QW PSS-LED had an output power of 27.6mW and an EQE of 49.7% at a current of 20mA. The output power of the 9QW PSS-LED remains linear with increasing drive current, even up to relatively high current density, and the EQE is almost constant. [J50]

"Electroluminescence From Polar Nonlinear Optical Chromophore With Low Turn-On Voltage"

Structure property relationships have been studied for polar and non-polar electro-luminescent molecules. The polar chromophore with a large red-shift shows a lower turn-on voltage than its non-polar counterparts. The I-V curves show characteristic diode behavior. The external quantum efficiency measurements for the polar molecule shows a four times higher quantum efficiency than the other molecules. [J51]

"Multicolor Virtual Matrix LED Display Controlled by D-Type Flip-Flop Drivers"

Light-emitting diode (LED) displays are currently experiencing a growing interest in many applications such as publicity, mass shows, etc., because of their high performance in terms of component reliability, brightness, power efficacy, modularity and scalability. However, the complexity of the control architecture of the present designs, based on current drivers, is the biggest obstacle to a significant cost reduction and massive spreading of this technology. In this paper, a new control architecture based on D-type flip-flops registers (HC logic) is presented. This design reduces in a significant way the cost and complexity of the large LEDs displays. It works as a write only memory on the basis "it is seen what is saved". This design is adequate for variable brightness screens on multicolor displays. [J52]

"Flexible multilayer inverted polymer light-emitting diodes with a gravure contact printed Cs₂CO₃ electron injection layer"

Here we demonstrate high efficiency, flexible inverted polymer light-emitting diodes in which the bottom-contact cesium carbonate electron injection layer is gravure contact printed. The poly(9,9-dioctylfluorene-alt-benzothiadiazole) emissive/electron transport layer, the poly(9,9-dioctylfluorene-alt-N-(4-butylphenyl)-diphenylamine) hole transport/electron blocking layer and the poly(3,4-ethylene dioxythiophene):poly(styrene sulfonate) hole injection layer were sequentially spin-coated from solution using orthogonal solvent formulations with appropriate wetting properties. By switching from indium-tin-oxide (ITO) on glass to ITO on poly(ethylene terephthalate) and using gravure contact printing instead of spin-coating, Cs₂CO₃ smoothness and morphology was optimized, resulting in an approximately fivefold increase in current efficiency and power efficiency at 100cd/m². [J53]

"Theoretical study of polarization-doped GaN-based light-emitting diodes"

Insufficient hole injection is a major impediment to the luminescence efficiency of III-nitride light-emitting diodes

(LEDs). In our previous work by Zhang et al [Appl. Phys. Lett. 97, 062103 (2010)], high-density mobile three-dimensional hole gas is obtained in Mg-doped Al composition graded AlGaIn layer with Al composition linearly decreasing from a certain value to 0. In this paper, it is revealed by a theoretical study that the hole injection efficiency in blue-light GaN-based LEDs can be greatly enhanced by using this polarization-doped method. An increase in the electroluminescence intensity and the internal quantum efficiency in polarization-doped GaN-based LEDs is observed, in comparison with a conventional LED. [J54]

"Vertical ZnO nanorod/Si contact light-emitting diode"

Blue-white light emission was obtained from glass/indium tin oxide (ITO)/n-ZnO nanorod array (NRA)/p+-Si vertical contact light emitting diodes (VCLEDs). The nanoscale p-n heterojunction VCLEDs were formed by direct engagement n--tipsof n-ZnO NRA grown vertically on an ITO/glass substrate with p+-Si wafer. Proposed configuration of the VCLED allows creating a high density ($\sim 10^9 \text{cm}^{-2}$) of self-assembled ZnO/Si nanodiodes with point junctions of high quality due to structural perfection of the Si wafer and the tips of ZnO nanorods as well as providing a high injection current and light emission from the NRA VCLED required for solid state lighting. [J55]

"A host sensitized reddish-orange $\text{Gd}_2\text{MoO}_6:\text{Sm}^{3+}$ phosphor for light emitting diodes"

An intense reddish-orange phosphor, $\text{Gd}_2\text{MoO}_6:\text{Sm}^{3+}$, was developed by solid state chemistry. The photoluminescence excitation and emission spectra, concentration effect are investigated. The results show an efficient energy transfer from MoO_6 -group to Sm^{3+} occurs and Sm^{3+} ion emits an intense reddish-orange light with high color purity and an excellent reproduction quality of optical properties. These results demonstrate that Sm^{3+} ion with low 4f-4f absorption efficiency in near ultraviolet region can play a role of activator in narrow reddish-orange emitting phosphor potentially useful in 370nm GaN-based light emitting diode through efficient energy feeding by charge transfer absorption of MoO_6 -group. [J56]

"Efficient up-conversion of triplet excitons into a singlet state and its application for organic light emitting diodes"

A material possessing a very small energy gap between its singlet and triplet excited states, ΔE_{1-3} , which allows efficient up-conversion of triplet excitons into a singlet state and leads to efficient thermally activated delayed fluorescence (TADF), is reported. The compound, 2-biphenyl-4,6-bis(12-phenylindolo[2,3-a] carbazole-11-yl)-1,3,5-triazine, breaks the restriction of a large energy gap, with a ΔE_{1-3} of just 0.11 eV, while maintaining a high fluorescent radiative decay rate ($k_r \sim 10^7$). The intense TADF provides a pathway for highly efficient electroluminescence. [J57]

"AlGaIn based deep ultraviolet light emitting diodes with high internal quantum efficiency grown by molecular beam epitaxy"

We report the development of AlGaIn based deep ultraviolet light emitting diodes (UV-LEDs) by molecular beam epitaxy. By growing the AlGaIn well layer under Ga-rich conditions to produce strong potential fluctuations, internal quantum efficiency of a quantum well structure emitting at 300 nm was found to be 32%. By combining such Ga-rich growth condition in the active region with polarization field enhanced carrier injection layers, deep UV-LEDs emitting at 273 nm were obtained with output power of 0.35 mW and 1.3 mW at 20 mA continuous wave and 100 mA pulsed drive current, respectively. The maximum external quantum efficiency was 0.4%. [J58]

"Polymer Infrared Proximity Sensor Array"

A near-infrared proximity sensor array is achieved by integrating a polymer light-emitting diode and a polymer photodetector (PD). A green emission is converted into deep red peaked at 670 nm by the inorganic phosphor Intematix R670 with quantum efficiency of over 20%. A bandpass filter is used to select a spectral tail of phosphor luminescence with a wavelength above 700 nm. The emissive polymer is green polyfluorene. The infrared PD contains a thick film of a blend of poly(3-hexylthiophene) and (6,6)-phenyl-C61-butyric acid methyl ester up to a thickness of 8 μm . Position of a moving object at a distance of 10 cm is detected in real time by the array with dynamic images displayed on the computer screen. [J59]

"Determination of the trap-assisted recombination strength in polymer light emitting diodes"

The recombination processes in poly(p-phenylene vinylene) based polymer light-emitting diodes (PLEDs) are investigated. Photogenerated current measurements on PLED device structures reveal that next to the known Langevin recombination also trap-assisted recombination is an important recombination channel in PLEDs, which has not been considered until now. The dependence of the open-circuit voltage on light intensity enables us to

determine the strength of this process. Numerical modeling of the current-voltage characteristics incorporating both Langevin and trap-assisted recombination yields a correct and consistent description of the PLED, without the traditional correction of the Langevin prefactor. At low bias voltage the trap-assisted recombination rate is found to be dominant over the free carrier recombination rate. [J60]

"Improvement of voltage and charge balance in inverted top-emitting organic electroluminescent diodes comprising doped transport layers by thermal annealing"

We present investigations of top emitting organic light emitting devices (OLED) comprising n- and p-doped organic charge transport layers. It has been found previously that in comparison to noninverted p-i-n OLEDs, inverted n-i-p OLEDs show reduced device performances after fabrication. These differences can be eliminated by subsequent thermal annealing of the whole n-i-p OLED. After this process, the n-i-p OLED exhibits a superior low driving voltage of 2.9 V at 1000cd/m² and shows an increase in external quantum efficiency from 11% to almost 15% which we ascribe to a modified charge balance within the intrinsic organic emission layer. [J61]

"Reduced molybdenum oxide as an efficient electron injection layer in polymer light-emitting diodes"

We report a significant improvement in the performance of single layer polymer light-emitting diodes (PLEDs), based on the green emitting copolymer poly[(9,9-dioctylfluorenyl-2,7-diyl)-co-(1,4-benzo-{2, 1',3}-thiadiazole)], upon inserting a very thin layer of partially reduced molybdenum oxide (MoO_x, where x=2.7) at the polymer/Al cathode interface. Both fully oxidized (x=3) and partially reduced (x=2.7) thin molybdenum oxide layers were investigated as electron injection layers and their influence on PLED device performance was examined. Improved current density, luminance, and efficiency was achieved only in the case of devices with a thin partially reduced MoO_{2.7} film as electron injection layer, as a result of improved electron injection and more facile transfer at the modified polymer/Al interface. [J62]

"InP/InAlGaAs light-emitting transistors and transistor lasers with a carbon-doped base layer"

Characteristics of InP/InAlGaAs light-emitting transistors (LETs) and transistor lasers (TLs) using carbon (C) for p-type doping of the base region were investigated. The N-InP/p-In_{0.52}(Al_{0.4}Ga_{0.6})_{0.48}As/N-In_{0.52}Al_{0.48}As LETs show a current gain of 0.22 and light emission at wavelength of $\lambda = 1610$ nm. The low current gain is attributed to the short minority carrier lifetime in the C-doped base with a quantum well. The TL demonstrates continuous-wave operation at -190 °C with a threshold current of $I_B = 35$ mA. By comparing the optical output characteristics of the TL and a laser diode with similar structure, it is suggested that the low differential quantum efficiency and the high threshold current density in the TL is related to the strong inter-valence band absorption in the heavily doped base layer. [J63]

"Deep-ultraviolet light-emitting diodes with gradually increased barrier thicknesses from n-layers to p-layers"

In this work, the structure with gradually increased barrier thicknesses from the n-layers to p-layers is proposed to replace the traditional structure with equal barrier thickness in deep-ultraviolet AlGaIn light-emitting diodes. Simulation approach yields to a result that, when increased barrier thicknesses are used, the distribution of electron and hole carriers inside the active region becomes quite uniform, which leads to efficient recombination of electrons and holes and thereby a significant enhancement in output power. [J64]

"The effect of trimethylgallium flows in the AlInGaIn barrier on optoelectronic characteristics of near ultraviolet light-emitting diodes grown by atmospheric pressure metalorganic vapor phase epitaxy"

The letter reports a theoretical and experimental study on the device performance of near ultraviolet light-emitting diodes (LEDs) with quaternary AlInGaIn quantum barrier (QB). The indium mole fraction of AlInGaIn QB could be enhanced as we increased the trimethylgallium flow rate. It was found the AlInGaIn/InGaIn LEDs can reduce forward voltage and improve light output power, compared with conventional GaIn QB. By using advanced device simulation, it should be attributed to a reduction in lattice mismatch induced polarization mismatch in the active layer, which results in the suppression of electron overflow. [J65]

"Numerical Study of ZnO-Based LEDs"

2-D numerical simulation is employed to assess a number of possible design approaches aimed at optimizing the internal quantum efficiency (IQE) of ZnO-based light-emitting diodes (LEDs) grown along the c -axis. First,

the relative performance of similar ZnO-based and GaN-based LED structures is compared and discussed. Second, the effects on IQE of thickness, doping, and alloy composition of the MgZnO electron blocking layer (EBL) is studied in order to maximize the carrier confinement in the active region. The optimum number of quantum wells is also addressed, and different strategies for barrier doping are considered, showing that, if the EBL is doped p -type, a similar doping in the barriers is not required to compensate for the spontaneous and piezoelectric interface charges and to enhance hole transport. Different choices of the geometrical and doping parameters of the n -type access region are considered, and the impact of different values of the electron mobility is determined. Finally, the analysis of a ZnO/BeZnO LED structure suggests that the incorporation of BeZnO layers does not provide significant advantages. [J66]

"Effect of Surface Texture and Backside Patterned Reflector on the AlGaInP Light-Emitting Diode: High Extraction of Waveguided Light"

This paper describes a novel structure of an AlGaInP light-emitting diode (LED) to extract the waveguided light for high-brightness applications. Four devices are considered and compared. They are AlGaInP-sapphire LEDs with: 1) a planar Ag reflector (LED-A); 2) a patterned Ag reflector (LED-B); 3) a planar Ag reflector and surface-roughened features (LED-C); and 4) a patterned Ag reflector and surface-roughened features (LED-D). The patterned Ag reflector can be used to direct some of the waveguided light that bounces within the AlGaInP LED and sapphire substrate to the top escape cone of the LED surface. Additionally, the roughened features, which are randomly distributed on the LED surface, enable the waveguided light that is trapped inside the LED chip to be coupled efficiently into the air. As a result, the external quantum efficiencies of LED-A, LED-B, LED-C, and LED-D measured at $I=350\text{ mA}$ are $\eta=9.20\%$, 10.46% , 15.22% , and 16.75% , respectively. [J67]

"GaAs-based near-infrared up-conversion device fabricated by wafer fusion"

Reported for the first time is a full GaAs-based room-temperature near infrared (NIR) up-conversion device fabricated by wafer-fusing a GaAsSb/GaAs pin photodetector (PD) with a GaAs/AlGaAs light emitting diode (LED). NIR photons with wavelengths in the range $1.3\text{--}1.6\text{ }\mu\text{m}$ were up-converted to $0.87\text{ }\mu\text{m}$. [J68]

"Water-related abnormal instability of transparent oxide/organic hybrid thin film transistors"

We have fabricated fully patterned transparent oxide/organic hybrid transistors on glass substrates that contain In-Ga-Zn-O as the active layer and a poly(4-vinyl phenol-co-methyl methacrylate) copolymer as the dielectric layer. These devices exhibit a saturation mobility of $6.04\text{ cm}^2/\text{V s}$, a threshold voltage value of 3.53 V , a subthreshold slope of 360 mV/decade , and an on-off ratio of 1.04×10^9 at a maximum processing temperature of $200\text{ }^\circ\text{C}$. We found that the bias stability characteristics of the hybrid transistors are dependent on the ambient conditions, but can also be dramatically improved by applying a hydrophobic organic passivation layer to the gate insulator. [J69]

"Optical design of organic light emitting diodes"

Out-coupling of light from organic light emitting diodes (OLEDs) is a significant challenge for the application of OLEDs in solid state lighting. Most of the light is trapped in the stratified thin film structure and the glass substrate. In this study, an optical model is developed to simulate the optical electrical field for OLEDs with a stratified structure based on the dipole source term and transfer matrix approach. The exciton distribution is also considered in the proposed model. OLEDs with weak microcavity are selected to evaluate the model. Calculation of the electroluminescence spectrum, device efficiency as well as the angular dependence is shown to have a good agreement with the experimental data. Moreover, by using the weak microcavity design, an OLED of more than 70% improved efficiency is achieved. [J70]

"Optimization of Thermal Management by Integration of an SCGM, a Finite-Element Method, and an Experiment on a High-Power LED Array"

This paper proposes an original idea to minimize heat concentrations of high-power light-emitting diode (LED) arrays. The purpose of this paper is to investigate temperature distribution with and without an optimal process of high-power LED arrays by experiment and a numerical method in order to achieve an optimal design of LED arrays for thermal management. This paper develops an effective method to design each LED position for decreasing thermal concentrations in high-power LED arrays. In this paper, temperature profiles are measured by a thermal infrared camera and a thermocouple and compared with simulated results under different power. The optimal method is adopted by a simplified conjugate gradient method combined with a finite-element method. This method proves reliability of simulated results in advance. Through this optimal method, efficiency of heat removal will be enforced as an extra cooling device is added. The important part is that this optimal design

will not affect brightness through an illumination analysis. [J71]

"A spintronic source of circularly polarized single photons"

We present a spintronic single photon source which emits circularly polarized light, where the helicity is determined by an applied magnetic field. Photons are emitted from an InGaAs quantum dot inside an electrically operated spin light-emitting diode, which comprises the diluted magnetic semiconductor ZnMnSe. The circular polarization degree of the emitted light is high, reaching 83% at an applied magnetic field of 2 T and 96% at 6 T. Autocorrelation traces recorded in pulsed operation mode prove the emitted light to be antibunched. The two circular polarization states could be used for representing quantum states $|0\rangle$ and $|1\rangle$ in quantum cryptography implementations. [J72]

"Predictive modeling of the current density and radiative recombination in blue polymer-based light-emitting diodes"

The results of a combined experimental and modeling study of charge transport, recombination and light emission in blue organic light-emitting diodes (OLEDs) based on a polyfluorene derivative are presented. It is shown that the measured temperature-dependent current-voltage curves and the voltage-dependent current efficiency are accurately described using an OLED device model that is based on the separately determined unipolar electron and hole mobility functions. The recombination rate is calculated using the Langevin formula, including recombination of holes with free as well as trapped electrons. The light emission is obtained from the exciton formation profile using independently determined values of the exciton radiative decay probability, the average dipole orientation, and assuming a fraction of singlet excitons $\eta_S = (22 \pm 3)\%$, close to the quantum-statistical value. No additional free parameter is used. This shows that predictive one-dimensional device modeling of OLEDs is feasible. [J73]

"Directionality control through selective excitation of low-order guided modes in thin-film InGaN photonic crystal light-emitting diodes"

This letter explores the impact of quantum well placement and photonic crystal (PhC) etch depth on the emission directionality of thin-film InGaN PhC light-emitting diodes (LEDs). The far-field pattern of 800-nm-thick PhC LEDs is tuned by varying only the etch depth of a surface-patterned hexagonal PhC from 90 to 440 nm. This dependence on etch depth is shown to arise from the preferential excitation of a subset of the allowed guided modes. Selective excitation of the TE₀ and TE₁ modes is utilized to achieve a vertically directional emission pattern comprised of only these two modes. [J74]

"Enhanced optical output power of green light-emitting diodes by surface plasmon of gold nanoparticles"

We demonstrate the surface plasmon (SP) enhanced green light-emitting diodes (LEDs). The Au nanoparticles were embedded in the p-GaN of LEDs. The photoluminescence and electroluminescence measurements showed improved optical properties of LEDs with Au nanoparticles due to an increase in the spontaneous emission rate by resonance coupling between the excitons in multiple quantum wells and localized surface plasmons in Au nanoparticles. The optical output power of SP-enhanced green LEDs with Au nanoparticles was increased by 86% without showing degradation of the electrical characteristics of LEDs compared to LEDs without Au nanoparticles. [J75]

"Misfit dislocation formation at heterointerfaces in (Al,In)GaN heteroepitaxial layers grown on semipolar free-standing GaN substrates"

Semipolar GaN-based light emitting devices show great promise because of reduced polarization-related electric fields in the quantum wells and the potential for high indium uptake in In_xGa_{1-x}N quantum wells. In semipolar GaN, the (0001) slip plane is inclined with respect to the film normal, thus shear stresses are present on this plane for nominally misfitting layer growth. We present scattering contrast transmission electron microscopy studies of (1122) and (2021) semipolar GaN-based laser diode structures. Misfit dislocations were observed at the nominally misfitting heterointerfaces in the (1122) structures with line direction $[1100]$ and Burgers vector in the (0001) plane. Similar observations are reported for the (2021) structures. Overall, the results are consistent with stress relaxation by threading dislocation glide. [J76]

"6-DOF tracker using LED directivity"

Proposed is a new concept for a 6-DOF optical tracker exploiting the directivity of an LED. To verify the concept,

a low-noise, linear optical sensor was designed, a working prototype was built that solves a source-localisation problem in real time, and its performance, compared with a reference tracker, was evaluated. [J77]

"Self-Assembled Periodic Silica Nanosphere Arrays on Wet-Etched Patterned Sapphire Substrate for a High-Light-Extraction-Efficiency Light-Emitting Diode"

We have developed a periodical self-assembled method of patterning the sapphire substrate with silica nanospheres for light-emitting diode (LED) applications. Using this method, silica nanospheres were directed to self-assemble in a periodic fashion on a wet-etched patterned sapphire substrate (WPSS). Moreover, we fabricated an InGaN/GaN-based LED on the silica-nanosphere-assembled WPSS. The light output power of the resultant LED was about 2.23 and 1.7 times higher than that of the LEDs grown on planar sapphire and WPSS, respectively. Moreover, the light extraction efficiency of the silica-nanosphere-assembled WPSS LED was 37% higher than that of conventional LED. [J78]

"On the symmetry of efficiency-versus-carrier-concentration curves in GaInN/GaN light-emitting diodes and relation to droop-causing mechanisms"

The internal quantum efficiency (IQE)-versus-carrier-concentration (n) curves of GaN-based light-emitting diodes have been frequently described by the ABC model: $\text{IQE} = Bn^2 / (A + Bn^2 + Cn^3)$. We show that this model predicts IQE-versus- n curves that have even symmetry. Phase-space filling makes the Band C coefficients concentration-dependent. We also show that IQE-versus- n curves that take into account phase-space filling possess even symmetry. In contrast, experimental IQE-versus- n curves exhibit asymmetry. The asymmetry requires a fourth-power or higher-power contribution to the recombination rate and provides insight into the mathematical form of the droop-causing mechanisms. [J79]

"Electromechanical phenomena in semiconductor nanostructures"

Electromechanical phenomena in semiconductors are still poorly studied from a fundamental and an applied science perspective, even though significant strides have been made in the last decade or so. Indeed, most current electromechanical devices are based on ferroelectric oxides. Yet, the importance of the effect in certain semiconductors is being increasingly recognized. For instance, the magnitude of the electric field in an AlN/GaN nanostructure can reach 1-10 MV/cm. In fact, the basic functioning of an (0001) AlGaN/GaN high electron mobility transistor is due to the two-dimensional electron gas formed at the material interface by the polarization fields. The goal of this review is to inform the reader of some of the recent developments in the field for nanostructures and to point out still open questions. Examples of recent work that involves the piezoelectric and pyroelectric effects in semiconductors include: the study of the optoelectronic properties of III-nitrides quantum wells and dots, the current controversy regarding the importance of the nonlinear piezoelectric effect, energy harvesting using ZnO nanowires as a piezoelectric nanogenerator, the use of piezoelectric materials in surface acoustic wave devices, and the appropriateness of various models for analyzing electromechanical effects. Piezoelectric materials such as GaN and ZnO are gaining more and more importance for energy-related applications; examples include high-brightness light-emitting diodes for white lighting, high-electron mobility transistors, and nanogenerators. Indeed, it remains to be demonstrated whether these materials could be the ideal multifunctional materials. The solutions to these and other related problems will not only lead to a better understanding of the basic physics of these materials, but will validate new characterization tools, and advance the development of new and better devices. We will restrict ourselves to nanostructures in the current article even though the measurements and calculations of the bulk electromechanical coefficients remain challenging. Much of the literature has focused on InGaN/GaN, AlGaN/GaN, ZnMgO/ZnO, and ZnCdO/ZnO quantum wells, and InAs/GaAs and AlGaN/AlN quantum dots for their optoelectronic properties; and work on the bending of nanowires have been mostly for GaN and ZnO nanowires. We hope the present review article will stimulate further research into the field of electromechanical phenomena and help in the development of applications. [J80]

"DFE Versus MLSE Electronic Equalization for Gigabit/s SI-POF Transmission Systems"

In this letter, we compare three different types of electronic equalization techniques to compensate the limited bandwidth of gigabit/s step-index polymer optical fiber (SI-POF) transmission systems. In particular, we experimentally analyze the performance of a feed-forward equalizer (FFE), a feed-forward plus decision feedback equalizer (FFE+DFE), and a maximum likelihood sequence estimator (MLSE) equalizer in an optical link composed of a resonant cavity light-emitting diode (RC-LED), 50 m of SI-POF, and a photodiode. The investigation is carried out on a real hardware experiment based on available POF optoelectronics, while the equalization is implemented in software using an off-line processing approach. We show that the FFE+DFE solution pays only a limited penalty versus the much more complex MLSE algorithm. Our result shows that the FFE+DFE solution is a very good compromise between performance and complexity for a gigabit/s SI-POF

system. [J81]

"Top-Emitting Organic Light-Emitting Diodes With Step-Doped Emission Layers"

High-efficiency top-emitting organic light-emitting diodes (OLEDs) with step-doped emission layers are numerically investigated. The simulation results demonstrate that the OLEDs with step-doped emission layers have better electrical performance and higher emitting intensity than those without step-doped design. Compared to conventional OLED devices, step-doped OLEDs with Fabry-Pérot microcavity not only have fixed wavelength but also have narrow emission spectral width. The simulation results suggest that the OLED structure with step-doped design in a Fabry-Pérot microcavity has superior performance and hence is beneficial for the display applications. [J82]

"Leakage Current Characteristics of Nitride-Based InGaN Light-Emitting Diode"

Leakage current characteristics have been investigated for nitride-based InGaN light-emitting diodes (LEDs) with different levels of Si-doping conditions applied to the n-type InGaN/GaN layer. The tested LED samples had an emission wavelength of 445 nm. Based on the analysis of temperature-dependent I_{V} characteristics measurements, the reverse leakage current, I_{R} , was predominantly influenced by the lowering of Poole-Frenkel (PF) barrier for low electric field ($< 2.5 \times 10^6$ V/cm) and, for high electric field region ($> 8 \times 10^7$ V/cm), phonon-assisted tunneling (PAT) dominates the I_{R} mechanism. The I_{R} is influenced by the Si-doping density of InGaN/GaN layer that may be present near the end of depletion regions of tested samples. [J83]

"Towards Color Stable Blue Primary for Displays: Suppress Field-Dependent Color Change in a Multilayered Electroluminescent Device"

A blue fluorescent organic compound, 1-phenyl-3,4-dimethyl-1H-pyrazolo[3,4-b]quinoline (PAQ5), is a suitable emitter to enable a color stable blue emission from multilayered light emitting devices. The dopant PAQ5 functioned as an energy trap and an emitter having its HOMO/LUMO levels lying inside the band gap of the host to secure an efficient energy transfer; it also reduced barrier height for electron injection and improved electron transporting of the emitting layer. It lowered the turn-on electric field and enhanced luminance gradually as the dopant concentrations increased. A bright and color stable blue emission having CIE (x,y) = (0.168, 0.100) was obtained. Field-dependent color change of such multilayered devices within a wide range of driving electric fields was suppressed by PAQ5 dopant. A color purity of 0.815 was achieved. [J84]

"Erratum: "Multilayered graphene used as anode of organic light emitting devices" [JAppl. Phys. Lett. 96, 133301 (2010)]"

{no data available} [J85]

"Digital Holographic Three-Dimensional Video Displays"

Holography aims to record and regenerate volume filling light fields to reproduce ghost-like 3-D images that are optically indistinguishable from their physical 3-D originals. Digital holographic video displays are pixelated devices on which digital holograms can be written at video rates. Spatial light modulators (SLMs) are used for such purposes in practice; even though it is desirable to have SLMs that can modulate both the phase and amplitude of the incident light at each pixel, usually amplitude-only or phase-only SLMs are available. Many laboratories have reported working prototypes using different designs. Size and resolution of the SLMs are quite demanding for satisfactory 3-D reconstructions. Space-bandwidth product (SBP) seems like a good metric for quality analysis. Even though moderate SBP is satisfactory for a stationary observer with no lateral or rotational motion, the required SBP quickly increases when such motion is allowed. Multi-SLM designs, especially over curved surfaces, relieve high bandwidth requirements, and therefore, are strong candidates for futuristic holographic video displays. Holograms are quite robust to noise and quantization. It is demonstrated that either laser or light-emitting diode (LED) illumination is feasible. Current research momentum is increasing with many exciting and encouraging results. [J86]

"Emission enhancement from nonpolar a-plane III-nitride nanopillar"

A nonpolar a-plane GaN-based light emitting structure was patterned by self-assembled SiO₂ nanosphere lithography and subsequent inductively coupled plasma (ICP) etch to define an array of nanopillar light emitters. The photoluminescence (PL) intensity was enhanced by ~110% after the anisotropic ICP etch, compared with an unprocessed sample, which is attributed to a reduction in wave-guiding effects in the thin film. Additionally, the anisotropic ICP etch caused minimal wavelength shift in the dominant 3.34 eV near-bandedge radiative

transition. A subsequent photoelectrochemical (PEC) etch process of the a-plane GaN nanopillars preferentially etched the underlying n-type layers, leaving a wider p-type cap. The n-type layers wet-etched by recession of the N-polar (000-1) plane (perpendicular to the a-plane growth axis) via formation of the distinctive pyramid-shaped facets. The PL intensity was enhanced by 168% after ICP and PEC etching although the peak emission occurred at a lower energy. The combination of nanosphere lithography and ICP was highly effective in improving the light extraction efficiency in a-plane nonpolar GaN-based light emitting diodes. [J87]

"Nitride-Based LEDs With High-Reflectance and Wide-Angle Ag Mirror SiO₂/TiO₂ DBR Backside Reflector"

Nitride-based light-emitting diodes (LEDs) with a backside reflector combining a SiO₂/TiO₂ distributed Bragg reflector (DBR) and an Ag mirror were simulated and fabricated. With combining the three-pair SiO₂/TiO₂ DBR and an Ag mirror, it was found that we can significantly enhance the 96% reflectance of Ag mirror to 99.1% with an incident angle of 0°. Furthermore, reflectance of the proposed reflector depends slightly on incident light wavelength and the incident angle. With 350-mA current injection, it was found that the output powers were 122, 138, 153, 156, and 162 mW for the LEDs without reflector, with an Al mirror, with Al₃DBR mirror, with an Ag mirror, and with Ag₃DBR mirror, respectively. [J88]

"The Emission Properties of Integrated Organic Light Emitting Diodes With Organic Photo Sensor for Emotional Lighting Applications"

This letter reports on a study of the emission properties of organic light-emitting diodes (OLEDs) controlled by an organic photo sensor (OPS) based on poly-3-hexylthiophene (P3HT) and [6, 6]-phenyl-C61butyric acid methyl ester for emotional lighting applications. The emission characteristics exhibit the changes in the current and luminance of an OLED as a function of time when different illumination levels are exposed to the OPS. The luminance of the OLED increases from 283.4 to 1134 cd/m² when the OPS is exposed to different illumination levels from full dark to 500 mW/cm² using a xenon lamp. [J89]

"Luminescence degradation in phosphorescent organic light-emitting devices by hole space charges"

We studied electroluminescence degradation in phosphorescent organic light-emitting devices (PHOLEDs) and found that two distinctive mechanisms are responsible for device degradation depending on the device structure. For a device without a hole blocking layer (HBL), excess holes penetrate into the electron transport layer (ETL) and lead to the deterioration of the ETL adjacent to the interface of the emitting layer. The lower electron transport capacity of the degraded ETL alters the balance in hole/electron injection into the emitting layer and results in a decrease in the luminescence efficiency of the PHOLEDs. For a device with a HBL, on the other hand, holes accumulate and become trapped in the emitting layer, and result in a decrease in the luminescence efficiency of the PHOLEDs, likely due to their role in acting as exciton quenchers or as nonradiative charge recombination centers. [J90]

"Highly simplified phosphorescent organic light emitting diode with >20% external quantum efficiency at >10,000 cd /m²"

A simplified trilayer green phosphorescent organic light emitting diode with high efficiency and an ultralow efficiency roll-off has been demonstrated. In particular, the external quantum efficiency drops <1% from 100 to 5,000 cd/m² and remains as high as 21.9% at 10,000 cd/m². The power efficiency is also significantly improved, reaching 78.0 lm/W at 100 cd/m², 50.5 lm/W at 5,000 cd/m², and 42.8 lm/W at 10,000 cd/m². The working mechanism of this simple device structure with an unprecedented high efficiency is also discussed. [J91]

"Influence of As on the Morphologies and Optical Characteristics of GaSb/GaAs Quantum Dots"

The influence of As atoms on the morphologies of GaSb quantum dots (QDs) is investigated. Without any special treatment, GaSb quantum rings (QRs) are observed in the embedded GaSb layer even when the uncapped layer reveals QD like morphologies. With intentional As supply after the uncapped GaSb QD deposition, a QD to QR transition is observed. The phenomenon suggests that insufficient Sb atoms on the GaSb QDs would lead to the QD to QR transition as in the case of embedded GaSb layers. With extended Sb soaking time following GaSb deposition, QD structures could be well maintained for the embedded GaSb layers. A light-emitting diode operated at room temperature is fabricated based on the GaSb/GaAs QD structure. Identical peak positions in photoluminescence and electroluminescence (EL) spectra of the device show that type-II GaSb QDs are responsible for the observed EL. [J92]

"Raman and emission characteristics of a-plane InGaN/GaN blue-green light emitting diodes on r-sapphire substrates"

Raman and emission properties of a nonpolar a-plane InGaN/GaN blue-green light emitting diode (LED) on an r-sapphire substrate are investigated and compared with a conventional c-plane blue-green LED. The output power of the a-plane LED was 1.4 mW at 20 mA. The c-plane LED has higher EQE, but it reaches the maximum at a lower forward current and the droop is faster than the a-plane counterpart. As the reverse bias increased, a blueshift in the PL spectra was not observed in the a-plane structure, which is indicative of an absence of quantum confined Stark effects. However, a strong blueshift in the electroluminescence spectra was still present, which means the In localization effects are relevant in nonpolar InGaN/GaN quantum wells. In the Raman spectra, a strong anisotropy of E2(high) phonon modes was observed. By comparing the frequency of the E2(high) modes, we demonstrate that the residual compressive strain in an a-plane LED is significantly smaller than in the polar counterpart. [J93]

"A novel target-type low pressure drop bidirectional optoelectronic air flow sensor for infant artificial ventilation: Measurement principle and static calibration"

An optoelectronic target-type volumetric air flow-rate transducer for bidirectional measurements is presented. The sensor is composed of a T-shaped target and two nominally identical LED-photodiode couples which are operated in differential mode. The sensitive surfaces of the photodiodes are differentially shadowed by the deflection of the target, which in turn depends on the gas flow-rate. The principle of operation is described in mathematical terms and the design parameters have been optimized in order to obtain the highest sensitivity along with minimal pressure drop and reduced dimensions. The sensor is placed in a 20 mm diameter hose and was tested with air flow-rate in the typical temperature range of mechanical ventilation between 20 and 40 °C. The theoretical model was validated through experiments carried out in the volumetric flow range from -7.0 to +7.0 l min⁻¹. The nonlinear behavior allows sensitivities equal to 0.6 V l⁻¹min for flow rates ranging from -2.0 to +2.0 l min⁻¹, equal to 2.0 V l⁻¹min for flow rates ranging from -3.0 to -2.0 l min⁻¹ and from +2.0 to +3.0 l min⁻¹, up to 5.7 V l⁻¹min at higher flow rates ranging from -7.0 to -3.0 l min⁻¹ and from +3.0 to +7.0 l min⁻¹. The linear range extends from 3.0 to 7.0 l min⁻¹ with constant sensitivity equal to 5.7 V l⁻¹min. The sensor is able to detect a flow-rate equal to 1.0 l min⁻¹ with a sensitivity of about 400 mV l⁻¹min. The differential nature of the output minimizes the influence of the LEDs' power supply variations and allows to obtain a repeatability in the order of 3% of full scale output. The small pressure drop produced by the sensor placed in-line the fluid stream, of about 2.4 Pa at 7 l min⁻¹, corresponds to a negligible fluid dynamic resistance lower than 0.34 Pa l⁻¹min. [J94]

"Strong light extraction enhancement in GaInN light-emitting diodes by using self-organized nanoscale patterning of p -type GaN"

We report on a self-organized nanoscale patterning method by using oblique angle deposition to enhance the light extraction in a GaInN light-emitting diode (LED). The method offers one-step processing with good controllability of the feature size and density of the nanopatterns by varying the deposition angle during oblique angle deposition, eliminating the need for photolithography and annealing. A 5-nm-thick silver (Ag) film, when deposited by using oblique angle deposition, spontaneously forms a nanoscale island-like morphology on the substrate. This method is used to texture p-type GaN with nanoscale features, which results in increased light extraction from a GaInN LED. At 100 mA, the nanotextured LED shows a 46% higher light output than a standard LED with unpatterned (planar) p-type GaN. [J95]

"Mechanism for the direct electron injection from Al cathode to the phosphine oxide type electron transport layer"

A high efficiency blue fluorescent organic light-emitting diode without LiF electron injection layer was developed. Aluminum electrode was directly deposited on a phosphine oxide type electron transport layer and the observed quantum efficiency was as high as 6.13%. The ultraviolet photoemission spectroscopy data clearly indicated that the electron injection barrier (the offset between Al Fermi level and the lowest unoccupied molecular orbital of the organic layer) is less than 0.1 eV, which led us to believe that more efficient electron injection through the lower barrier is mainly responsible for the high efficiency. [J96]

"Charge transport, carrier balance, and blue electrophosphorescence in diphenyl[4-(triphenylsilyl)phenyl]phosphine oxide devices"

Diphenyl[4-(triphenylsilyl)phenyl]phosphine oxide (EMPA1) displays a wide highest occupied molecular orbital-lowest unoccupied molecular orbital gap (4.1 eV), singlet (4.3 eV) and triplet (3.4 eV), and an electron-dominated charge transport that follows a trap-free space charge limited model with an average electron mobility of 5.74×10⁻⁴

6cm² V-1 s-1 and a hole mobility of 1.1410-6cm² V-1 s-1. At high driving voltages (>6V), ambipolar charge transport is observed, resulting in a balanced charge density in the active layer. Highly efficient blue phosphorescent organic light-emitting diodes were realized, showing a high external quantum efficiency (21%) and a luminance efficiency of 45 cd/A using a bis[2-(4',6'-difluorophenyl)-pyridinato-N,C2']iridium(III) picolinate dopant. [J97]

"Violet electroluminescence from p-GaN thin film/n-GaN nanowire homojunction"

The difficulty associated with the precise positioning of nanowires has been one of the most significant issues hindering nanoelectronic integration. In this paper, we employed dielectrophoretic force to manipulate n-type GaN nano- and microwires onto a p-type GaN thin film to form a pristine p-n homojunction. The GaN wires were attracted to the n-type Ohmic metal in a direction parallel to the electric field, which was consistent with our simulation results. Violet electroluminescence emanated from the point of the n-GaN wire in contact with the p-GaN thin film. This p-n homojunction device displayed forward conduction above 6-9 V and current rectifying behavior down to a -20 V reverse bias. The current-voltage characteristics are distinctive of a p-n homojunction formed without deleterious damage or contamination. [J98]

"White LED Based on YAG : Ce,Gd Phosphor and CdSe-ZnS Core/Shell Quantum Dots"

Core/shell CdSe-ZnS quantum dots (QDs) with a peak emission wavelength of 618 nm and size of ~ 5.5 nm were synthesized by thermal deposition approach. High photoluminescence efficiency with a quantum yield of more than 48% has been achieved. Red-shift of a peak emission wavelength from 532 to 568 nm was realized by doping Gd³⁺ ions into the YAG: Ce³⁺ to substitute some Y³⁺ ions. To compensate the poor color rendering index (CRI) of the YAG: Ce-based white light-emitting diode (LED) due to the lack of red spectral component, CdSe-ZnS QDs were blended into YAG: Ce³⁺, Gd³⁺ phosphors. Prominent spectral evolution has been achieved by increasing the content of QDs. White LED combining a blue LED with the blends of phosphor and QDs with a weight ratio of 1:1, has been demonstrated with an improved CRI value of 90. [J99]

"Defect-related tunneling mechanism of efficiency droop in III-nitride light-emitting diodes"

The quantum efficiency of GaN-based light-emitting diodes (LEDs) is investigated at temperatures 77-300 K. It is found that the efficiency droop is due to a decrease in the internal quantum efficiency (IQE) in the low-energy part of the emission spectrum. The efficiency starts to decrease at a temperature independent forward voltage of U_{max} ≈ 2.9V. At this voltage tunneling current through the LED-structure begins to dominate. It is suggested that the external quantum efficiency droop is related to reduction of the IQE due to tunneling leakage of carriers from the quantum well (QW) to defect states in barriers, and to reduction of the injection efficiency by excess tunneling current under QW through deep defect states in barriers. [J100]

"Photolithographic patterning of subwavelength top emitting colloidal quantum dot based inorganic light emitting diodes on silicon"

The combination of lithographic patterning and nanostamping methods makes it possible to accurately define diffraction-limited multicolor (wavelengths 560-620 nm) light sources on a silicon substrate. We demonstrate a postprocessing technique that utilizes standard photolithography process to pattern the cathode of top emitting diode. Correlation of electroluminescence, photoluminescence, and atomic force microscopy topography showed that the emission region is well defined through the robust multiscale patterning techniques, with the fineness of the emitting area mainly limited by the point spread function of the observing microscope. [J101]

"Development of a light-emitting diode tachistoscope"

This paper describes a new method for rapid visual stimulus delivery, the light-emitting diode (LED) tachistoscope. An array of white LEDs provided a luminous intensity greater than 1 000 000 mcd. This array was placed behind a liquid crystal display (LCD) to function as a backlight; switching it on and off determined the visibility of the display. Commands to illuminate for periods from 1 ms to continuously on were relayed from a computer to the LED array. Changes in luminous intensity at the surface of a LED and the LCD were recorded via oscilloscope. The required duration of light pulses consistently matched the durations displayed, with only microsecond discrepancies due to turn-on and turn-off delays. Images were illuminated on the LCD screen for as little as 1 ms, with the amplitude of the luminance consistent across trials. The LED tachistoscope can be used with any computer to display images extremely briefly, potentially at the submillisecond level, providing superior performance to traditional and computer monitor tachistoscopes. [J102]

"Photometer for monitoring the thickness of inkjet printed films for organic electronic and sensor"

applications"

Inkjet printed organic thin films are being used for a variety of electronic and sensor applications with advantages that include ease of fabrication and reproducibility. Construction and use of a low-cost photometer based on a light-emitting diode (LED) light source and a photodiode detector are described. The photometer attaches to the exit of the printer with the transparent substrate onto which the film is printed passing between the LED and photodiode. By measuring the output voltage of the detector, the transmittance and absorbance of the inkjet printed film can be calculated in real-time. Since absorbance is linearly proportional to thickness in the Beer-Lambert regime, the thickness of the film may be monitored and controlled by varying the number of passes through the printer. Use of the photometer is demonstrated for inkjet printed films of monolayer-protected colloidal gold nanoparticles that function as chemical vapor sensors. The photometer may find applications in both research and quality control related to the manufacture of organic electronic devices and sensors and enables "feedback-controlled" inkjet printing. [J103]

"Study of electric characteristics and diffusion effects of 2-methyl-9,10-di(2-naphthyl)anthracene doped with cesium fluoride by admittance spectroscopy"

In this work, the admittance spectroscopy studies show that doping cesium fluoride (CsF) into 2-methyl-9,10-di(2-naphthyl)anthracene (MADN) can greatly decrease the resistance of MADN and raises the Fermi level from deep level to only 0.1 eV below the lowest unoccupied molecular orbital, resulting in enhancing the electron injection. In addition, the diffusion width of CsF from doped MADN layer into tris(8-quinolinolato)aluminium is clearly observed by capacitance-frequency measurement and is about 9.4 nm. Moreover, the diffusion width is significant to be affected by external thermal. [J104]

"InGaN gallium nitride light-emitting diodes with reflective electrode pads and textured gallium-doped ZnO contact layer"

We demonstrate a GaN-based light-emitting diode (LED) with nonalloyed metal contacts and textured Ga-doped ZnO (GZO) contact layer to serve as the n- and p-type electrode pads, respectively. Compared with the conventional LEDs with flat surface and Cr/Au metal contacts, the nonalloyed Ag/Cr/Au contacts used in the present experimental LEDs play the role of reflector to prevent the emitted light from absorption by the opaque electrode pads. Enhancement of light output power observed from the experimental LEDs is also due to the textured GZO layer that can disperse the angular distribution of photons at the GZO/air interface. With an injection current of 20 mA, the output power of experimental LEDs can be improved markedly by a magnitude of 30% compared with conventional GaN-based LEDs. [J105]

"Study of InGaN-GaN Light-Emitting Diodes With Different Last Barrier Thicknesses"

This work reports a theoretical and experimental study on the device performance of blue InGaN-GaN light-emitting diodes (LEDs) with different last barrier thicknesses. The experimental results show that the employment of a 25-nm-thick p-type GaN last barrier in GaN LEDs can improve the light output power from 35.6 to 40.2 mW at 50 mA. By using advanced device simulation, it is shown that the effective energy barrier created by the p-type AlGaIn electron blocking layer (EBL) is significantly decreased due to the band bending at the interface between GaN last barrier and AlGaIn EBL. The use of a p-type GaN last barrier before the growth of AlGaIn EBL can provide a higher energy barrier to suppress the electron overflow and then enhance the light output power. [J106]

"Fast Voltage-Programmed Pixel Architecture for AMOLED Displays"

We present a fast voltage programming scheme for active-matrix organic light-emitting diode (AMOLED) displays using amorphous silicon (a-Si) thin-film transistor (TFT) backplane technology. The proposed scheme uses on-pixel measurement of the threshold voltage (V_{th}) of the drive TFT. In contrast to the conventional voltage driving, V_{th} is not measured by discharging a capacitor through a diode-connected TFT. Thus, the accuracy-speed tradeoff does not limit the performance of the new driving scheme. A 4-TFT 2-capacitor pixel circuit is implemented based on the new driving scheme, and its performance is verified by circuit-level simulations using AIM-SPICE. Simulation results show that for a programming time of 33 ns, less than 2.5% change in the OLED current can be achieved for a 5-V shift in the threshold voltage of the drive TFT. [J107]

"Electroluminescence observation of nanoscale phase separation in quaternary AlInGaIn light-emitting diodes"

Anomalous temperature-dependent electroluminescence (EL) of $\text{Al}_{0.06}\text{In}_{0.02}\text{Ga}_{0.92}\text{N}/\text{Al}_{0.1}\text{Ga}_{0.9}\text{N}$ multiple-quantum-well light-emitting diodes was investigated. At low temperatures and low currents, the EL was

dominated by narrow peaks arising from GaN band edge (3.47 eV) and AlGaIn localized state emission (3.59 eV). At 150 K, as thermalized carriers surmounted a static nanobarrier surrounding In-rich nanoclusters, the EL shifted to low-energy emission at 3.39 eV. These EL anomalies are evidence that, contradictory to theoretical predictions, there remains a strong effect of compositional fluctuation toward nanoscale phase separation in low In/Al AlInGaIn alloys. During the interphase transfer at 150 K, the majority of excitons underwent nonradiative decay, leading to a sharp decrease in quantum efficiency by over one order of magnitude. [J108]

"Soft and Hard Failures of InGaIn-Based LEDs Submitted to Electrostatic Discharge Testing"

This letter reports an extensive analysis of the degradation mechanisms of InGaIn-based light-emitting diodes (LEDs) submitted to reverse-bias electrostatic discharge (ESD). The results of this analysis indicate that two different failure modes, namely, "soft" and "hard" degradations, can be induced by ESD pulses. The "soft" failure mode takes place as a consequence of ESD events with moderate voltage/current levels and consists in a decrease in the reverse-bias leakage current of LEDs. This effect is due to the annihilation of some of the defective paths responsible for leakage-current conduction, possibly triggered by the injection of relatively high reverse-bias current densities. "Hard" failure takes place when high-voltage/current ESD pulses are applied to an LED. After hard failure, LEDs behave as short circuits. This process is due to the high voltage levels reached by the junction during an ESD event (with subsequent dielectric rupture) or to the injection of extremely high current densities through one of the localized paths responsible for reverse-current conduction. [J109]

"Large-Area Flexible Ultrasonic Imaging System With an Organic Transistor Active Matrix"

We have successfully fabricated a large-area flexible ultrasonic imaging system by integrating a polymeric ultrasonic-transducer array sheet with an active matrix of organic field-effect transistors. The ultrasonic sheet comprises 8 x 8 ultrasonic sensing cells with an effective size of 25 ГfB— 25 cm². The organic transistors exhibit mobility of 0.1 and 0.5 cm²/V ГfB·s at the low operation voltage of 1 mV and in the saturation regime, respectively. When an ac signal is applied between source and drain electrodes for the transistors with a grounded gate, the on/off ratio is larger than 10⁴ at the carrier frequency of 40 kHz. In the linear sensing array comprising eight ultrasonic cells, crosstalk is suppressed sufficiently low, and the on/off ratio exceeds 10⁴. Images in free space are obtained for multiple-target objects over this sheet. [J110]

"Microplasma Current Switch and Its Characteristics"

A microplasma current switch (MPCS) for a device operated in a current-mode-like organic light-emitting diodes, which features matrix addressability and current switching, is presented, as well as its architecture and operational principle. The MPCS utilizes the intrinsic memory and conductivity of plasmas to achieve matrix addressability and current switching. We have fabricated a 100 mm ?? 100 mm MPCS panel with a cell pitch of 1080 ??m ?? 1080 ??m. Matrix addressability and current switching are verified. Moreover, the current-voltage curve of the unit cell is measured and analyzed. It exhibits the characteristic of a floating-double-probe diagnosing plasma parameters, so that we estimate the plasma density and electron temperature from it. [J111]

"Efficiency Improvement of GaN-Based LEDs With a Nanorod Array and a Patterned Sapphire Substrate"

The enhancement of light extraction from GaN-based light-emitting diodes (LEDs) with a patterned sapphire substrate (PSS) and a SiO₂/12-fold photonic quasi-crystal (PQC) structure using nanoimprint lithography is presented. At a driving current of 20 mA on transistor-outline-can package, the light output powers of LED with a PSS and LED with a PSS and a SiO₂/PQC structure are enhanced by 35% and 48%, compared with the conventional LED. In addition, the higher output power of the LED with a PSS and a SiO₂/PQC structure is due to better reflectance on PSS and higher epitaxial quality on an n-GaN using a SiO₂/12-fold PQC structure pattern. These results provide promising potential to increase output powers of commercial light-emitting devices. [J112]

"Light-Output-Power Enhancement of GaN-Based Light-Emitting Diodes on an n-GaN Layer Using a Photonic Quasi-Crystal Overgrowth"

GaN-based LEDs with a SiO₂oxide PQC pattern on an n-GaN layer by nanoimprint lithography are fabricated and investigated. At a driving current of 20 mA on a Transistor-Outline-can package, the light output power of LED III (d = 1.2 μm) was enhanced by a factor of 1.20. The internal-quantum-efficiency result offers promising potential to enhance the light output power of commercial light-emitting devices with a SiO₂oxide PQC structure on an n-GaN layer. [J113]

"Measurement of Electron Temperature and Density Using Stark Broadening of the Coaxial Focused Plasma for Extreme Ultraviolet Lithography"

We have generated an Ar plasma in a dense plasma focus device with coaxial electrodes for extreme ultraviolet (EUV) lithography and investigated an emitted visible light for electrooptical plasma diagnostics. We have applied an input voltage of 4.5 kV to the capacitor bank of 1.53 μF , and the diode chamber has been filled with Ar gas of 8-mtorr pressure. The inner surface of the cylindrical cathode has been attached by an acetal insulator. Also, the anode is made of tin metal. If we assumed that the focused plasma regions satisfy the local thermodynamic equilibrium conditions, the electron temperature and density of the coaxial plasma focus could be obtained by the Stark broadening of optical emission spectroscopy. The Lorentzian profile for the emission lines of Ar I of 426.629 nm and Ar II of 487.99 nm were measured with a visible monochromator. In addition, the electron density has been estimated by the full-width at half-maximum (FWHM) of its profile. To find the exact value of FWHM, we observed the instrumental line broadening of the monochromator with a Hg-Ar reference lamp. The electron temperature has been calculated using the two relative electron-density ratios of the Stark profiles. In case of electron density, it has been observed by the Stark broadening method. This experimental result shows the temporal behavior of the electron temperature and density characteristics for the focused plasma. The EUV emission signal whose wavelength is about 6-16 nm has been detected by using a photodetector (AXUV-100 Zr/C, IRD). The result compared the electron temperature and density with the temporal EUV signal. The electron density and temperature were observed to be 10^{16}cm^{-3} and 20-30 eV, respectively. [J114]

"Laser-induced Zn doping in GaN based light-emitting diode"

By laser-induced Zn doping, hole concentration in the p-type GaN contact layer of conventional GaN-based light-emitting diodes (LEDs) is increased and improvement of the LED property is confirmed. Compared with LED with no use of laser-induced doping, the forward voltage under 20 mA current is decreased from 3.33 to 3.13 V and the thermal resistance of the chip is decreased from 18.6 to 9.7 K/W. In addition, the lifetime of the device is increased about 41%. These results are attributed to the improvement of the p-type Ohmic contact due to laser-induced doping of Zn to the p-GaN contact layer. [J115]

"Light Extraction Enhancement of a GaN-Based Light-Emitting Diode Through Grating-Patterned Photoelectrochemical Surface Etching With Phase Mask Interferometry"

The enhancement of light extraction by fabricating a surface grating structure around the mesa of a light-emitting diode (LED) with an approach combining photoelectrochemical (PEC) wet etching and phase mask interferometry is demonstrated. The PEC etching rate is controlled by the intensity of illuminating UV light, which is spatially modulated by the fringe pattern of phase mask interferometry, for forming the grating structure. Without affecting the resistance characteristics of the device, the diffraction of such a grating structure leads to LED output enhancement by > 43% on either the top or bottom side. [J116]

"An LED Model for Intensity-Modulated Optical Communication Systems"

Modulating the intensity of light-emitting diodes (LEDs) with analog signals, especially in the case of the bipolar optical orthogonal frequency-division-multiplexing (O-OFDM) signal, leads to significant signal degradation due to LED nonlinearity. The LED transfer function distorts the signal amplitude and forces the lower peaks to be clipped at the LED turn-on voltage. Additionally, the upper peaks are purposely clipped before modulating the LED to avoid chip overheating. The induced distortion can be controlled by optimizing the bias point or backing-off the average O-OFDM signal power. In this letter, a model that incorporates amplitude distortion and that provides a parameterized upper clipping is proposed. Through Monte Carlo simulations, the model can be used to determine the optimum bias point and to optimize the O-OFDM signal power. In this context, a novel concept of soft-clipping of the upper peaks is presented. It is shown that soft-clipping is an effective approach to reduce nonlinearity distortion and to enhance symbol error performance. [J117]

"Highly efficient orange-red phosphorescent organic light-emitting diode using 2,7-bis(carbazol-9-yl)-9,9-ditolyfluorene as the host"

We demonstrate an efficient orange-red organic light-emitting diode using a host, 2,7-bis(carbazol-9-yl)-9,9-ditolyfluorene, doped with tris(2-phenylquinoline) iridium(III). The device exhibits a high current efficiency of 44.8 cd/A at 1000cd/m^2 . This may be attributed to the adoption of the host, which favors the injection of holes, as well as the emissive-layer architecture enabling excitons to form on host and hence favoring efficient energy-transfer from host to guest. Moreover, an electron-confining layer is used to modulate excessive holes to be injected into emissive layer and confine the electrons, which would in turn balance the injection of both carriers and improve efficiency. [J118]

"Light- and ion-gauge-induced space charges in tris-(8-hydroxyquinolate) aluminum-based organic light-emitting diodes"

We report space charge formation in tris-(8-hydroxyquinolate) aluminum (Alq3)-based organic light-emitting diodes induced by light irradiation and ion-gauge (IG) operation during device fabrication. An analysis of the capacitance-voltage curves of the light-treated devices reveals the presence of uniformly distributed negative space charges in the Alq3 layer. Spatial inhomogeneity of the orientation polarization as well as electrons trapped in the Alq3 film can be the origin of the negative space charge. We also found that positively charged species can be included in the device due to IG operation. [J119]

"Physical mechanisms for hot-electron degradation in GaN light-emitting diodes"

We report investigations on the degradation of GaN-based light-emitting diodes due to high dc current stress by examining two types of devices with the same fabrication procedures except for the growth conditions for the InGaN quantum wells (QWs). Higher trimethylindium and triethylgallium fluxes are used for type A devices resulting in a threefold increase in the InGaN QWs growth rate compared to type B devices. Detailed structural and optoelectronic properties of the devices are investigated by transmission electron microscopy, atomic force microscopy, thermal imaging, I-V measurements, and the low-frequency noise properties of the devices as a function of the stress time, t_s . The experimental data show that the QWs in type B devices are dominated by spiral growth and they have substantially higher strain nonuniformity than type A devices. The highly strained GaN/InGaN interfaces in device B are also responsible for the faster increase in the defect density due to hot-electron injection. The defects enhance the trap-assisted tunneling in the multiple quantum wells (MQWs) resulting in the development of hot spots among type B devices after high current stressing of the MQWs. This in turn leads to an increase in the defect generation rate resulting in a thermal run-away condition that ultimately resulted in the failure of the device. The data show that an increase in the growth rate in the InGaN layer led to the domination by the step flow growth mode over the spiral growth mode in the MQWs. This is the main reason for the reduction in the dislocation density in type A devices and hence their increase in device reliability. [J120]

"Mg doping of GaN grown by plasma-assisted molecular beam epitaxy under nitrogen-rich conditions"

Acceptor doping of GaN with Mg during plasma-assisted molecular beam epitaxy, under N-rich conditions and a relatively high growth temperature of 740 °C, was investigated. The p-doping level steadily increases with increasing Mg flux. The highest doping level achieved, determined from Hall measurements, is $2.14 \times 10^{18} \text{ cm}^{-3}$. The corresponding doping efficiency and hole mobility are 4.9% and $3.7 \text{ cm}^2/\text{V s}$ at room temperature. Cross-sectional transmission electron microscopy and photoluminescence measurements confirm good crystalline and optical quality of the Mg-doped layers. An InGaN/GaN quantum dot light emitting diode ($\lambda_{\text{peak}} = 529 \text{ nm}$) with p-GaN contact layers grown under N-rich condition exhibits a low series resistance of 9.8Ω . [J121]

"Enhanced Electroluminescence Efficiency of Phosphorescent Organic Light-Emitting Diodes by Controlling the Triplet Energy of the Hole-Blocking Layer"

This letter reports on the effect of the triplet energy (ET) of the hole-blocking layer (HBL) on triplet exciton quenching between the emissive layer (EML) host and the HBL of phosphorescent organic light-emitting diodes (PHOLEDs). Using different EML hosts and HBLs having different ET's and electron mobilities, the effects of the ET's of the HBL have been analyzed. When the ET of the HBL is lower than that of the EML host, the PHOLEDs show significant dependence of reduced device performances. PHOLEDs having a 3-(4-biphenyl)-4-phenyl-5-tert-butylphenyl-1,2,4-triazole HBL show 65% improved external quantum efficiency (EQE) at 500 cd/m^2 with a 4,4',4''-tris(N-carbazolyl)-triphenyl-amine host than that with an N,N'-dicarbazolyl-4,4''biphenyl host, while PHOLEDs having a 2,9-dimethyl-4,7-diphenyl-1,10-phenanthroline HBL show 41% reduced EQE. To solve the remaining key issue of developing highly efficient PHOLEDs, the ET of matching the EML and the HBL is extremely desirable and is also explored. [J122]

"A Novel Phototherapy Device"

Phototherapy is the standard treatment for severe cases of hyperbilirubinemia in newborns. Phototherapy exposes the infants to light in the range of 400-500 nm to isomerize unconjugated bilirubin in the skin. Any light source that produces this wavelength can be used, including the sun (though there is a risk of sunburn), fluorescent or halogen lamps, or, more recently, light-emitting diodes. Despite the well-established efficacy of phototherapy devices and their relative simplicity-being not much more than a floor lamp-phototherapy devices

are too expensive for developing world hospitals to purchase, with typical hospital models ranging from US\$3,000 to US\$5,000. In addition, the resource-poor setting presents a more challenging engineering problem than most. Phototherapy devices are frequently donated to developing world hospitals. However, donated phototherapy devices typically run for no more than a few months once donated and, even then, offer little value to some hospitals. Given this background, we set out to design a phototherapy device specifically for use in the developing world. As a minimum, we knew that it had to have a light source with an extraordinarily long life span and have battery backup so that it could run during frequent power outages. Our design uses LEDs and is powered by a car or motorcycle battery. In this article, we present the full engineering design cycle, starting with needs identification and continuing through several cycles of engineering field trials and results with comments on the differences between the engineering design cycle executed in, and for, the developing world. [J123]

"New Technologies in Electric-Powered Vehicles [JAutomotive Electronics]"

Presents the latest news in automotive electronics. [J124]

"ZnO-GaN Hybrid Heterostructures as Potential Cost-Efficient LED Technology"

Reliable and reproducible p-type doping is the main challenge for fabricating highly efficient ZnO-based light-emitting diodes. During the last few years, the lack of reliable p-type conductivity in ZnO has initiated research concerning the combination of ZnO and other semiconductors, which can then be doped p-type. One of these concepts is the combination of ZnO with GaN heterostructures aiming at the fabrication of hybrid LEDs. We discuss the problems as well as potential benefits from a combination of ZnO and GaN hybrid heterostructures in a single device. We also present our recent results on ZnO-GaN hybrid LEDs using an inverted LED concept. The hybrid LEDs have an external quantum efficiency of more than 35%. [J125]

"High-Power (110" > mW) Superluminescent Diodes by Using Active Multimode Interferometer"

We have designed and fabricated, for the first time to our knowledge, novel superluminescent diodes by using active multimode interferometers that emit at a wavelength of 1.55 μ m. An output power as high as 115 mW was obtained with a wide 3-dB bandwidth of 50 nm and low spectral ripple of 0.03 dB. In addition, they showed stable single-transverse-mode outputs up to the maximum output power. [J126]

"On the Aging Effects of 4H-SiC Schottky Photodiodes Under High Intensity Mercury Lamp Irradiation"

Ultraviolet (UV) germicidal irradiation uses high-power 254-nm radiation from low-pressure mercury discharge lamps to kill or inactivate viral, bacterial, and fungal species. Since UV germicidal irradiation effectiveness depends primarily on the UV dose delivered to the microorganisms, it is essential to monitor the power emitted from the source by using appropriate UV-light detectors. We report on preliminary aging tests performed on high signal-to-noise ratio 4H-SiC Schottky photodiodes under high intensity mercury lamp irradiation (10 mW/cm²). [J127]

"Measurement of extraction and absorption parameters in GaN-based photonic-crystal light-emitting diodes"

The light extraction efficiency of photonic-crystal (PhC) light-emitting diodes (LEDs) relies on the competition between the PhC extraction and dissipation mechanisms of the guided light within the LED. This work presents the experimental determination of the PhC extraction length of each guided mode and the absorption coefficient of the active region (AR) and quantum wells (QWs) from the observation of the LED far-field emission using a high-resolution angle-spectrum-resolved measurement. The angular and spectral linewidths of the extracted guided modes reveal, depending on the spectral range, the modal extraction length of the PhCs, the AR absorption length, or a combination of both. Modes with a high confinement with the QWs presented a shorter absorption length compared with their extraction length by a shallow surface PhC (95-nm-deep), meaning that the AR absorption was a more efficient mechanism than the PhC extraction. The measured modal extraction length of the shallow surface PhC varied in the range of 55-120 μ m, which determines the minimum dimensions of the device and the maximum acceptable dissipation length for an efficient extraction of the guided light by the PhCs. This paper presents also a discussion on the PhC designs that yield PhC extraction lengths shorter than other dissipation lengths, a fundamental requirement for high-efficiency PhC LEDs. The same technique was also applied to estimate the absorption coefficient of the InGaN-based QWs, and can be extended to experimentally determine losses by metallic layers from electrical contacts or other dissipation mechanisms, which are parameters of interest to a broader class of optoelectronic devices, not only PhC LEDs. [J128]

"Near-ultraviolet light emitting diodes using strained ultrathin InN/GaN quantum well grown by metal organic vapor phase epitaxy"

The near-ultraviolet (UV) light emitting diodes (LED) using ultrathin InN/GaN quantum well (QW) are fabricated by metal organic vapor phase epitaxy. The x-ray diffraction measurement shows well-defined satellite peaks, which implies abrupt interfaces and good layer periodicity of the QWs. The electroluminescence only exhibits a near-UV emission centered at approximately 3.14-3.18 eV without other emission peaks even the common yellow luminescence, which further confirms the advantages of the near-UV LED especially the minimization of phase separation, interdiffusion, and defects in the QWs. The near-UV emission is found to be stable even under high pulsed injection-current in contrast to the conventional InGaN based LED. This behavior indicates effective avoidance of the redshift related to the many body effect as well as the blueshift induced by band filling effect, localized states in the barrier, and the quantum confined stark effect. The realization of the near-UV LED using the ultrathin InN/GaN QW would facilitate the application of near-UV solid-state lighting source. [J129]

"Photonic Transitions (1.4 eV-2.8 eV) in Silicon p np Injection-Avalanche CMOS LEDs as Function of Depletion Layer Profiling and Defect Engineering"

p+np+CMOS Si LED structures were modeled in order to investigate the effect of various depletion layer profiles and defect engineering on the photonic transitions in the 1.4-2.8 eV, 450-750 nm regime. Modeling shows that by utilizing a short linear increasing E-field in the p+n reverse-biased junction with a gradient of approximately 5 ГfB— 105V cm-1ГfB· ГfBm-1, and injecting carriers from an adjacent p+n junction, increased localized optical yield by a factor 50-100. A number of device designs were realized using CMOS 0.35 ГfBm technology. The device design involves normal CMOS design and processing procedures with no excessive microdimensioning. The current devices operated in the 6-8 V, 1 ГfBmA-2 mA regime, and yield emission intensities of up to 100 nW ГfBm-2. The current emission levels are about three orders higher than the low-frequency detectability limit of Si CMOS p-n detectors of corresponding area, which make diverse electro-optical applications such as MOEMS devices, and diverse optical signal processing and wave-guiding and the development of ГfBsmart chipsГfB feasible in standard CMOS integrated circuitry. [J130]

"Improvement of quantum efficiency by employing active-layer-friendly lattice-matched InAlN electron blocking layer in green light-emitting diodes"

Improvement of the internal quantum efficiency in green-light emitting diodes has been achieved using lattice-matched InAlN electron-blocking layers. Higher electroluminescence intensities have been obtained due to better electron confinement in the device active region. The device efficiency has also been found to significantly depend on the InAlN growth temperature. Optimized InAlN growth at 840 °C results in a lower growth rate and longer growth times than at 780 °C. The observed reduction in emission efficiency for InAlN layers grown at higher temperatures is possibly attributed to thermal damage in the green active region. [J131]

"Impedance spectroscopy as a probe for the degradation of organic light-emitting diodes"

Impedance spectroscopy is a powerful method for characterizing the electrical properties of materials and their interfaces. In this study we use capacitance measurements to investigate the degradation of electrically aged bottom-emitting organic light-emitting diodes with different polymeric hole injection layers. The devices comprise a heterojunction between a hole transporting triphenyl-diamine and an electron transporting and green emitting aluminum chelate complex [Alq3, tris-(8-hydroxyquinoline) aluminum]. A detailed analysis of the capacitance as function of frequency and dc bias yields information about trapped and interfacial charges as well as the dynamics of injected charges. We find that the loss of luminance and the increase in drive voltage of stressed devices is accompanied by a deterioration of hole injection and the formation of positively charged quenching centers at or close to the organic heterojunction. Using a new polymeric hole injection layer leads to improved device stability. [J132]

"Influence of the hole blocking layer on blue phosphorescent organic light-emitting devices using 3,6-di(9-carbazolyl)-9-(2-ethylhexyl)carbazole as host material"

Organic blue light-emitting devices are essential for the development of future light sources and display technology. Here, we present a highly efficient host-guest system suitable for blue light emission, consisting of the wide gap host material 3,6-di(9-carbazolyl)-9-(2-ethylhexyl)carbazole (TCz1) and the phosphorescent blue emitter iridium(III)bis[(4,6-difluorophenyl)-pyridinato-N,C2']picolate (FIrpic). We investigate charge carrier balance as a function of hole blocking layer thickness. For optimized structures, devices with a quantum efficiency as high as 14.3% and a luminous efficacy of 21 lm/W at a luminance of 1000cd/m2 are realized. [J133]

"Properties of TiO₂-based transparent conducting oxide thin films on GaN(0001) surfaces"

Anatase Nb-doped TiO₂ transparent conducting oxide has been formed on GaN(0001) surfaces using a sputtering method. Amorphous films deposited at room temperature were annealed at a substrate temperature of 500 °C in vacuum to form single-phase anatase films. Films with a thickness of 170 nm exhibited a resistivity of $8.4 \times 10^{-4} \Omega \text{ cm}$ with absorbance less than 5% at a wavelength of 460 nm. Furthermore, the refractive index of the Nb-doped TiO₂ was well matched to that of GaN. These findings indicate that Nb-doped TiO₂ is a promising material for use as transparent electrodes in GaN-based light emitting diodes (LEDs), particularly since reflection at the electrode/GaN boundary can be suppressed, enhancing the external quantum efficiency of blue LEDs.

[J134]

"Detailed studies on energy loss mechanism in phosphor-sensitized fluorescent polymer light-emitting devices"

We studied the main energy loss mechanism in electroluminescent (EL) processes in phosphor-sensitized fluorescent polymer light-emitting devices. The used organometallic phosphor is fac-tris(2-phenyl-pyridine) iridium [Ir(ppy)₃] and the used red fluorescent dye is 4-(dicyanomethylene)-2-t-butyl-6-(1,1,7,7-tetramethyljulolidyl-9-enyl)-4H-pyran (DCJTB). The investigation found that due to the stronger electron trapping ability of DCJTB than that of Ir(ppy)₃, the excitons prefer to form on DCJTB molecules. The charge trapping on the DCJTB molecules obviously restrains the function of the phosphor-sensitizer Ir(ppy)₃. Moreover, the energy transfer from phosphorescent triplet state (T_p) to the fluorescent triplet state (T_f) also has great negative impact on the phosphor-sensitized fluorescent process. We clearly demonstrated these energy loss processes by steady-state and transient photoluminescence and comparison of device efficiency. [J135]

"A chip-level electrothermal-coupled design model for high-power light-emitting diodes"

An advanced three-dimensional electrothermal-coupled simulation model basing on finite-element method numerical simulation is developed to study the electrical and thermal properties of chip-level high-power GaN-based light-emitting diodes (LEDs). The current spreading, heat generation, and transfer in the device are comprehensively considered in this model. The current-spreading effect of the transparent current-spreading layer and the thermal performance of LEDs with interdigitated-electrodes are investigated. The simulation results prove that the temperature distribution in the active layer is strongly affected by the electrode pattern. The obvious heat accumulation in LEDs with conventional interdigitated-electrode patterns can be seen both in the simulated results and the infrared measured results. The heat transfer efficiency can be improved by using a symmetry electrode pattern design. The thermal management of the bump configurations in flip-chip LEDs is also studied. A more reasonable and thermal effective bump configuration is presented, and the simulated results show that a lower average temperature and more uniform heat distribution in the chips can be obtained. [J136]

"Droop in InGaN light-emitting diodes: A differential carrier lifetime analysis"

To investigate the variation in internal quantum efficiency in InGaN structures, we measure the differential carrier lifetime of an InGaN/GaN double-heterostructure light-emitting diode under varying electroluminescence injection conditions. By coupling this measurement to an internal quantum efficiency measurement, we determine the carrier density and the radiative and nonradiative contributions to the lifetime without making any assumptions on recombination processes. We find that droop is caused by a shortening of the nonradiative lifetime with current. The observed shortening of both radiative and nonradiative lifetimes with current is found to be in excellent agreement with an ABC model including phase-space filling. [J137]

"Growth and characteristics of GaInN/GaN multiple quantum well light-emitting diodes"

We demonstrate GaInN multiple quantum well (MQW) light-emitting diodes (LEDs) having ternary GaInN quantum barriers (QBs) instead of conventional binary GaN QBs for a reduced polarization mismatch between QWs and QBs and an additional separate confinement of carriers to the MQW active region. In comparison with GaInN LEDs with conventional GaN QBs, the GaInN/GaN LEDs show a reduced blueshift of the peak wavelength with increasing injection current and a reduced forward voltage. In addition, we investigate the density of pits emerging on top of the MQW layer that are correlated with V-defects and act as a path for the reverse leakage current. The GaInN/GaN MQW structure has a lower pit density than the GaInN/GaN MQW structure as well as a lower reverse leakage current. Finally, the GaInN/GaN MQW LEDs show higher light output power and external quantum efficiency at high injection currents compared to the conventional GaInN/GaN MQW LEDs. We attribute these results to the reduced polarization mismatch and the reduced lattice mismatch in the GaInN/GaN MQW active region. [J138]

"Negative Terminal Capacitance of Light Emitting Diodes at Alternating Current (AC) Biases"

Measurement of obvious negative capacitance (NC) at large forward bias of light-emitting diodes (LEDs), using an alternating current (AC) small signal, together with direct current (DC) I-V plot, has shown that the NC grows exponentially with the forward applied voltage. The experimental results are unexpected and are in conflict with Shockley's p-n junction theory which only includes increasing diffusion capacitance and certainly no negative capacitance. The experiment also shows that the ideal factor of LEDs is about 4, which far exceeds the traditional theory value. However, these results support the comprehensive p-n junction theory presented by Hess. Using the framework of his theory, the NC could be interpreted distinctly. [J139]

"GaN-Based Light-Emitting Diodes With Pillar Structures Around the Mesa Region"

This study presents the numerical and experimental demonstrations for the enhancement of light extraction efficiency in nitride-based light-emitting diodes (LEDs) with textured sidewall and micro-sized pillar waveguides (TSMPW) and nano-textured sidewall and nano-pillars (NTSNP) around the mesa. Using hydrothermal ZnO nanorods as the etching hard mask, the authors successfully formed vertical GaN nano-pillars on the mesa-etched regions. It was found that electrical characteristics observed from the proposed LEDs were near the same as the control samples without the pillars. Output power enhancement of LED with TSMPW was about 11% compared with conventional LEDs, and the output power enhancement of LED was greater than 45% upon replacement of TSMPW with the NTSNP structure. The light extraction efficiency enhancement factors of the LEDs with TSMPW and NTSNP structures simulated by finite-difference time-domain analysis were 16.6% and 23%, respectively. [J140]

"Enhanced electron capture and symmetrized carrier distribution in GaInN light-emitting diodes having tailored barrier doping"

The confinement of electrons to the active region of GaInN light-emitting diodes (LEDs) is limited by the (i) inefficient electron capture into polar quantum wells, (ii) electron-attracting properties of electron-blocking layers (EBL), (iii) asymmetry in electron and hole transport, and (iv) unfavorable p-doping in the EBL for high Al content. To counteract these mechanisms, we employ tailored Si-doping in the quantum barriers (QBs). Experiments show a 37.5% enhancement in light-output power at high currents of one-QB-doped LEDs over all-QB-doped LEDs. These results are consistent with simulations showing that QB doping can be used to symmetrize the electron and hole distribution. [J141]

"InGaN Light-Emitting Diodes With the Inverted Cone-Shaped Pillar Structures"

An InGaN-based light-emitting diode (LED) with an inverted cone-shaped pillar structure was fabricated through a plasma dry etching process and a photoelectrochemical (PEC) process. The undercut structure was fabricated through a bandgap-selective PEC etching process that occurred at the InGaN active layer. Then, the inverted cone-shaped pillar structure was formed through a bottom-up crystallographic etching process in a hot potassium hydroxide solution. The light-output power of the LED with an inverted cone-shaped pillar structure had a 42% enhancement compared with the standard LED without the pillar structure at a 20-mA operating current. A higher light intensity of the PEC-treated LED was observed around the mesa-edge region and the pillar structures as a result of a higher light-scattering process occurring at the inverted cone-shaped structure. [J142]

"Fiber optic sensor for the measurement of concentration of silica in water with dual wavelength probing"

The design, development, and characterization of a fiber optic evanescent wave based sensor with selectivity suitable for concentration measurement are presented. The sensor that is made up of a step index plastic multimode fiber can be used for the measurement of silica in water. Generally evanescent wave fiber optic sensors employ a single source and detector that show change in output optical power irrespective of the interacting species, i.e., they lack selectivity. This design employing two sources provides excellent selectivity, and the differential arrangement further enhances sensitivity and repeatability. Advantages of this design include the use of inexpensive and easily available light-emitting diode sources that match the analytical wavelength of the samples. The use of dual wavelength probing topology enhances the selectivity, sensitivity, and repeatability, which cannot be achieved by single source evanescent wave fiber optic sensors. [J143]

"Multilayered graphene used as anode of organic light emitting devices"

In this report, we find multilayered graphene, which has good transparency, conductivity and suitable work function, can be used as the anode for the organic light emitting device. Our device structure is

Al/glass/multilayered graphene/V2O5/NPB/CBP:(ppy)2Ir(acac)/Bphen/Bphen:Cs2CO3/Sm/Au. The maximum luminance efficiency and maximum power efficiency reach 0.75 cd/A and 0.38 lm/W, respectively. We believe that by optimizing the hole density and uniforming the thickness of the multilayered graphene anode, the device efficiency can be remarkably increased in the future. [J144]

"Large Gamut Backlight for an LCD With Four Primaries"

A small backlight unit having four LEDs of different colors is designed and fabricated. Traditionally, the backlight units are lit by white cold cathode fluorescent lamps or by white LEDs. Our backlight unit utilizes four monochromatic LEDs. LEDs are located at corners of the light guide. Outcoupling is accomplished using large period blazed-gratings. The master plate for the light guide is fabricated by laser lithography. The final lightguide is UV-casted on a PMMA plate using an electroplated nickel tool. Proposed backlight unit enlarges significantly the gamut of LCD, if the color filters of the LCD panel have been chosen appropriately. The brightness uniformity and the white balance of the backlight are analyzed by a fiber spectrometer. The brightness uniformity of the backlight is good, over 85%. White balance of the backlight should be further improved. [J145]

"Detector-Based Calibration for Illuminance and Luminance Meters-Experimental Results"

The connection between illuminance and luminance measurements is considered to create a traceability link among a highly accurate illuminance meter, which is considered as an internal standard of the Photometric Laboratory, University of Padova, Padova, Italy, and other illuminance meters or photometric heads and luminance meters. After an introduction on the main involved definitions and equations linking the illuminance and the luminance measurements, this paper presents the instruments to which the procedures are applied and, at the end, results regarding the absolute calibration of the instruments under test, the check of their linearity, and the analysis of their spectral responsivity within the visible range. Following this way, this paper shows the main results in the connection among instruments devoted specifically to illuminance and luminance measurements. Then, it also introduces a comparison to other photometric heads, e.g., sensors that are part of more complex systems, like an integrating sphere for luminous flux measurement. In this last case, it has no significance to evaluate the difference between the absolute outputs, but it is interesting to compare the response of the two devices considering their linearity and their relative spectral response. A special section devoted to the evaluation of the spectral response presents a new simple but effective method. The application of a detector-based method allows a significant reduction of the uncertainty in the internal calibration of the photometric instruments, granting the continuity of the Photometric Laboratory operation contemporarily. [J146]

"Enhanced Output Power of InGaN-Based Light-Emitting Diodes With AlGaIn/GaN Two-Dimensional Electron Gas Structure"

We demonstrate high-performance InGaIn-based light-emitting diodes (LEDs) with tunneling-junction-induced 2-D electron gas (2DEG) at an AlGaIn/GaN heterostructure, which is inserted in the middle of the P+-GaIn contact layer of a conventional LED structure. The output power of a LED with a 2DEG insertion layer shows 17% enhancement compared to that of a conventional LED at 20 mA. This enhancement in output power for the LED with a 2DEG insertion layer could be attributed to both enhanced hole-injection efficiency and lateral current spreading by the presence of 2DEG at the AlGaIn/GaN heterostructure. [J147]

"Development of a Low-Cost FPGA-Based SSVEP BCI Multimedia Control System"

This paper proposes a low-cost field-programmable gate-array (FPGA)-based brain-computer interface (BCI) multimedia control system, different from the BCI system, which uses bulky and expensive electroencephalography (EEG) measurement equipment, personal computer, and commercial real-time signal-processing software. The proposed system combines a customized stimulation panel, a brainwave-acquisition circuit, and an FPGA-based real-time signal processor and allows users to use their brainwave to communicate with or control multimedia devices by themselves. This study also designs a light-emitting diode stimulation panel instead of cathode ray tube or liquid-crystal display used in existing studies, to induce a stronger steady-state visual evoked potential (SSVEP), a kind of EEG, used as the input signal of the proposed BCI system. Implementing a prototype of the SSVEP-based BCI multimedia control system verifies the effectiveness of the proposed system. Experimental results show that the subjects' SSVEP can successfully control the multimedia device through the proposed BCI system with high identification accuracy. [J148]

"Relationship between thermal and luminance distributions in high-power lateral GaN/InGaN light-emitting diodes"

The relationship between the thermal and luminance distributions in high-power lateral GaN/InGaN light-emitting

diodes (LEDs) is demonstrated. By using a three-dimensional electrical circuit model and experimentally measured thermal and luminance images of the LED chips, it is shown that thermal and luminance distributions have close correlation and that uniform current density is essential to improve the thermal and luminance properties of LED chips. [J149]

"Board certified"

Breadboarding a new circuit is a key skill and an important step in many projects-especially early on, when you need to move wires around and substitute components. But that very flexibility also makes it easy to knock wires out. Eventually, if your project is a keeper, you're going to want something with a bit more permanence. [J150]

"Room-temperature operation type-II GaSb/GaAs quantum-dot infrared light-emitting diode"

A GaSb/GaAs quantum-dot light-emitting diode (QD LED) with a single GaSb QD layer is investigated in this paper. The room-temperature photoluminescence peak blueshift with increasing excitation power densities suggests a type-II alignment of the GaSb/GaAs heterostructures. Significant electroluminescence (EL) is observed for the device under forward biases, which suggests that pronounced dipole transitions occur at the GaSb/GaAs interfaces. With increasing forward biases, the observed EL peak blueshift confirms that the origin of luminescence is from the type-II GaSb/GaAs QD structures. A model is established to explain the operation mechanisms of the type-II QD LED. [J151]

"Design and implementation of power-aware LED light enabler with location-aware adaptive middleware and context-aware user pattern"

Recent advances in ubiquitous technologies facilitate location-aware and power-aware systems that can provide predefined services. Recent research efforts are based on control mechanisms for standby power reduction. Conventional systems are only designed for power reduction of the consumer electronics. However, due to their architectural limitations, the recent systems are not flexible with respect to LED light control for power reduction. We need to consider efficient autonomous power control based on intelligent devices and the power-aware service prediction in networked environments. In this paper, we propose a power-aware LED light enabler with light sensors, motion sensors and network interfaces. The LED light enabler also communicates with context-aware middleware using an intelligent power gateway that adaptively determines the optimal power control by analyzing user living patterns using sensing data obtained by devices. Our power-aware LED light enabler with adaptive middleware dynamically reconfigures the power-aware services. The proposed adaptive middleware facilitates the learning mechanism which analyzes the illumination and the user activity, and controls the LED lights only when users exist around the devices. Our enabler reduces power consumption up to 58% in comparison to a basic lighting system at the real office testbed. [J152]

"Space-charge-limited current in organic light emitting diodes"

A physically based mathematical model for the dc current of single-carrier organic light emitting diodes is presented. The model accounts for the most important physical quantities that influence the carrier mobility and thus the device current itself: temperature, charge carrier concentration, and electric field. It is rigorously developed basing on the variable range hopping transport theory and extends the pioneering work of Mark and Helfrich [J. Appl. Phys. 33, 205 (1962)] to large electric fields typical of light emitting diodes. It was validated on experimental data collected from devices of different materials in a wide range of operating conditions. Thanks to the effective electric field approach, the mathematical expression is simple, accurate and suitable for CAD applications. [J153]

"Current-Based Testing of Optical Feedback Pixel Driver"

A testing scheme of an optical feedback pixel driver is proposed, discussed and simulated by HSPICE. A basic characteristic of the specific circuit is that the gray scales of the pixel are created by pulse width modulation. So, the integral of the output $I_{\text{pixelcurrent}}$ (which is proportional to I_{oled}) has to be measured or calculated and used for testing. The testing procedure that is proposed enables the detection and identification of common processing defects up to 96%, as verified from simulation results. Although $I_{\text{pixelcurrent}}$ is tend to be very low, the measuring system used, using special instrumentation ICs, is successfully simulated and verified by HSPICE. [J154]

"Light-Rail Transit Systems"

The authors describe a state-of-the-art and innovative light-rail vehicle for the Greater Phoenix area in Arizona. The Phoenix 70% low-floor light-rail vehicle was designed and built by KinkiSharyo International LLC to reflect

the needs of the unique operating environment found in Phoenix. [J155]

"Woven Thin-Film Metal Interconnects"

The next step in the evolution of electronic textiles (e-textiles) involves the integration of electronics at the yarn level. We aim to integrate "electronic yarns" into textiles by fabricating thin-film devices and interconnects on plastic strips and weaving them into a fabric using a commercial weaving machine. Since interconnect lines are exposed to very small applied bending radii during weaving, we studied changes in interconnect resistance for applied bending radii ranging from 5 mm to 100 μm . We then wove textiles using different weaving patterns and measured the strip bending radius in the textile. Interconnect lines ruptured at bending radii of 120 μm , corresponding to a tensile bending strain of 16.73 %. The smallest bending radius within the textiles was ~ 165 μm , making all weaving patterns suitable for e-textile fabrication. Finally, we wove strips with interconnect lines and light-emitting diodes using a commercial weaving machine. [J156]

"Electroluminescence From Ferromagnetic Fe-Doped ZnO Nanorod Arrays on p-Si"

Vertically aligned Fe-doped ZnO nanorod arrays (ZnO:Fe NRAs) with weak ferromagnetism at room temperature (RT) have been fabricated by in situ doping of Fe into ZnO nanorods (NRs) using a simple thermal chemical vapor deposition method. Structure analyses indicated that the NRs have a single-crystalline wurtzite structure without any detectable segregated cluster or impurity phase. Both photoluminescence and electroluminescence (EL) showed near-band-edge and broad defect-band emissions at RT. The EL from ZnO:Fe NRAs/p-Si light-emitting diodes red shifted with increasing current injections, which was ascribed to the doping effect of the Fe. [J157]

"Improvement of peak quantum efficiency and efficiency droop in III-nitride visible light-emitting diodes with an InAlN electron-blocking layer"

InAlN electron-blocking layers (EBLs) are shown to improve the emission intensity and to mitigate the efficiency droop problem in III-nitride-based visible light-emitting diodes (LEDs). Using an $\text{In}_{0.18}\text{Al}_{0.82}\text{NEBL}$ in blue LEDs, we have achieved a significant improvement in the electroluminescence emission intensity and a mitigated efficiency droop compared to similar LEDs without an EBL or with an $\text{Al}_{0.2}\text{Ga}_{0.8}\text{NEBL}$. This indicates that an $\text{In}_{0.18}\text{Al}_{0.82}\text{NEBL}$ is more effective in electron confinement and reduces the efficiency droop possibly caused by carrier spill-over than conventional AlGaIn EBLs. [J158]

"Particular Failure Mechanism of GaN-Based Alternating Current Light-Emitting Diode Induced by GaO Oxidation"

This investigation describes the unique failure mechanism of the Wheatstone bridge circuit-type alternating current light-emitting diode (WB AC-LED). The micro-LEDs in WB AC-LED rectifying branches were reverse biased, and therefore, positive charges (holes) accumulated in the n-type GaN layer under the active region and combined with the GaN material and OH-ions to generate GaO oxidation grains. The GaO generation speed was fast with high reverse voltage applied to micro-LEDs, and the expansion of GaO dimensions degraded the opto-electrical characteristics and eventually caused failure of the WB AC-LED. The root-mean-square reverse voltage dropped across each micro-LED from -13.1 to -6.7 V with different micro-LEDs array arrangements extended the WB AC-LED lifetime from being less than 650 h to more than 1600 h, respectively. [J159]

"A Microcontroller-Based IR Range Finder System With Dynamic Range Enhancement"

The present paper describes the development of a microcontroller-based infrared (IR) range finder system, employing two IR light-emitting diodes (LEDs) and an IR sensor. The system employs a software array-based approach where both the burst frequency of IR energy transmitted by the IR LEDs and the duration of this energy transmission in one sweep are progressively reduced, in a bid to increase the possibility of sensing the IR energy reflected back from the object. The proposed system can perform dynamic range enhancement, by utilizing an intelligent scheme, where, the output from the IR sensor system is used as a feedback to adaptively switch one of the IR LEDs. Experimental studies confirm that our developed system can indeed implement dynamic range enhancement, when compared to a conventional IR range finder system. [J160]

"Spin injection and circular polarized electroluminescence from InAs-based spin-light emitting diode structures"

We have investigated circularly polarized electroluminescence (EL) from hybrid II-Mn-VI/III-V light emitting diodes (LED's) at low temperatures in magnetic fields upto 10 T. Both magnetic (the Brillouin paramagnet $\text{Cd}_{1-x}\text{Mn}_x\text{Se}$) and nonmagnetic (CdSe) injectors were studied. Electrons, spin unpolarized (n-CdSe) or spin-polarized

(n-CdMnSe), were injected into wide InAs quantum wells, where they recombined with unpolarized holes injected from p-type InAs/AlAsSb layers. Detailed measurements and modeling of the circular polarization of the resulting midinfrared EL were carried out to explore and quantify the additional complexities of this materials system compared with the extensively studied GaAs-based spin-LED structures. We show that optical and spin polarization in narrow gap semiconductors such as InAs are not simply related to each other. To analyze the complex relationship, we have developed and used a detailed rate equation model, which incorporates the band-structure of electrons and holes in a magnetic field, a finite ratio of recombination and spin-flip times, and the spin polarization of the CdMnSe spin-aligner as a function of injection current. The latter was determined in situ by circular polarized photoluminescence measurements on the injector material. Experimentally, the circular polarization degrees of magnetic and nonmagnetic structures are observed to be very similar, when the magnetic samples have low effective Mn incorporation. This results from a combination of the consequently low spin polarization of the aligner and comparable spin and recombination life times in InAs. [J161]

"Polarization modification in InGaN/GaN multiple quantum wells by symmetrical thin low temperature-GaN layers"

Light emitting diodes (LEDs) using InGaN/GaN quantum wells (QWs) with thin low temperature GaN (LT-GaN) layers bounding each InGaN layer are grown by metal-organic vapor phase epitaxy. The light output power of such LEDs increases by a factor of 2 at a drive current density of 35A/cm² compared to that from reference LEDs without the LT-GaN. The blueshift in the emission wavelength is 5.2 nm when the current density increases from 3 to 50A/cm², which is much smaller than the shift 8.1 nm from reference LEDs. Moreover, the efficiency droop at high current injection is also reduced by 28%, and current density at which peak efficiency is observed increases from 1 to 2A/cm². High resolution transmission electron microscopy of the QWs bounded with LT-GaN shows higher quality and less strain compared to the reference samples. The better performance of LEDs incorporating the LT-GaN layers is attributed to suppressed polarization from piezoelectric fields. [J162]

"Observation of hole hopping via dopant in MoO_x-doped organic semiconductors: Mechanism analysis and application for high performance organic light-emitting devices"

Conduction mechanism in molybdenum trioxide (MoO_x)-doped hole- and electron-type organic semiconductors is investigated. The used hole-transporting materials are N,N'-diphenyl-N,N'-bis(1-naphthylphenyl)-1, 1'-biphenyl-4, 4'-diamine, 4,4''-tri(N-carbazolyl)triphenylamine, 4, 4'-N,N-dicarbazole-biphenyl, and pentacene and the used electron-transporting material is (8-quinolinolato) aluminum (Alq₃). It can be seen that the hole conductivity is significantly enhanced upon MoO_x doping, and more importantly, dominant hole current could be realized in a typical electron-transport material Alq₃ by doping MoO_x. Hence, high efficiency organic light-emitting devices can also be achieved even using MoO_x-doped Alq₃ film as hole transporting layer. The mechanism investigation indicates that the MoO_x plays an important role in the hole transport. It is showed that the MoO_x serves as the hole hopping sites, whereas the used organic materials serve as the transport medium and determine the magnitude of transport current. Furthermore, it is found that doping MoO_x into the organic materials also reduces the energy and position disorders of the doped organic films, which are well demonstrated by the study on transport characteristics of the doped films at various temperatures. [J163]

"Enhancement of ultraviolet electroluminescence based on n-ZnO /n-GaN isotype heterojunction with low threshold voltage"

Ultraviolet light-emitting diodes based on simple n-ZnO/n-GaN isotype heterojunction have been fabricated using a radio frequency magnetron sputtering system. Ultraviolet emission peaking around 368nm with a full-width at half maximum of 7nm was observed at room temperature when the devices were under sufficient forward bias. With the presence of an i-MgO layer inserted between the ZnO and GaN layers, the ultraviolet emission intensity and output power have been much enhanced, while the threshold voltage drops down to 2.5 V. The electroluminescence mechanisms in these devices were discussed in terms of the band diagrams of the heterojunctions. [J164]

"Enhanced Light Extraction Mechanism of GaN-Based Light-Emitting Diodes Using Top Surface and Side-Wall Nanorod Arrays"

Using a self-catalyst vapor-liquid-solid mechanism, random indium-tin-oxide (ITO) nanorod arrays were deposited on the top surface and side-wall of GaN-based light-emitting diodes (LEDs) by electron-beam deposition. When the side-wall nanorod arrays and the top surface ITO nanorod arrays were deposited at an oblique-angle of 45°, roughened surface morphology and matched refractive index of 1.6 between air and the p-GaN layer could be obtained. Comparing the conventional LEDs without ITO nanorod arrays, a 34% light output power increase was attributed to the roughened top and side-wall surface morphology and the matched

refractive index caused by the ITO nanorod arrays. Not only were the side-wall nanorod arrays used to increase light output power, but the light output divergence angle could be widened by using side-wall nanorod arrays.

[J165]

"White luminescence from single-layer devices of nonresonant polymer blends"

Poly(9,9'-dioctyl fluorene) (F8) and poly(4,4'-diphenylene diphenylvinylene) (PDPV) are conjugated polymers with optical transitions that are nonresonant thanks to the particular structural features of PDPV that yield a very large Stokes' shift (1.14 eV) between absorption and emission spectra. We present steady-state and time-resolved photoluminescence (PL) experiments showing that F8:PDPV blends are "optically disconnected" systems for which the emission spectra and PL quantum yields are the linear combination of the contributions of the individual constituents with weights given by the respective absorption coefficients and concentration in the films. Single-layer light-emitting diodes incorporating F8:PDPV blends show white electroluminescence resulting from the simultaneous exploitation of the spectral features of both blend constituents (Commission Internationale de l'Eclairage, CIE, coordinates: $x=0.27$ and $y=0.36$, in the case of 8:2 F8:PDPV molar ratio). [J166]

"A PDM-Based Digital Driving Technique Using Delta-Sigma ($\Delta\Sigma$) Modulation for QVGA Full-Color AMOLED Display Applications"

We propose a digital driving technique using pulse-density modulation (PDM) for an active-matrix organic light-emitting diode (AMOLED) to effectively suppress the false image contour in conventional pulsewidth modulation (PWM) while achieving considerably low operating frequency. A compact first-order digital $\Delta\Sigma$ modulator provides the PDM signal to the panel. A 2.2-inch QVGA AMOLED system using the proposed technique shows no false image contour problem while allowing relaxed minimum gate scan time. [J167]

"InGaN-Based High-Power Flip-Chip LEDs With Deep-Hole-Patterned Sapphire Substrate by Laser Direct Beam Drilling"

A high-performance flip-chip light-emitting diode (LED) with deep-hole-patterned sapphire substrate was fabricated by laser direct beam drilling. The output power of the LED was measured to be as high as 145 mW at a forward current of 350 mA, which is improved by 19% compared to that of the reference LED. This significant enhancement of the LED with deep-hole-patterned sapphire is attributed to the increase of extraction efficiency, resulting from the increase in photon escape probability due to enhanced light scattering at the deep-hole pattern. [J168]

"Parallel Phase-Shifting Digital Holography Capable of Simultaneously Capturing Visible and Invisible Three-Dimensional Information"

We propose a parallel phase-shifting digital holography capable of simultaneously capturing both outside three-dimensional (3D) information of the object such as a surface of an object which human being can perceive (visible information) and internal 3D information of the object (invisible information) using a visible laser light and an invisible laser light. This technique can carry out phase-shifting interferometry for each light with a single-shot exposure, because an interference fringe image in which the information of each light and each phase-shift is spatially multiplexed is recorded by a phase-shifting array device and a wavelength-filter array. We numerically simulated the proposed technique, and the effectiveness of the proposed technique was shown by evaluating the simulation results using a correlation coefficient. Also we conducted a preliminary experiment using a red filter and a near-infrared filter placed 8 cm apart from each other as objects containing both visible and invisible 3D information. A He-Ne laser operated at 633 nm and a diode laser operated at 830 nm were used as a visible light source and an invisible light source, respectively. The 3D imaging capability of the proposed technique was successfully demonstrated by the preliminary experiment, and the validity of the technique was also confirmed by evaluating root mean square errors of the reconstructed images. Also the capability for simultaneously 3D capturing of outside (visible) information and internal (invisible) information was demonstrated by a preliminary experiment. [J169]

"Telescope Aiming Point Tracking Method for Bioptic Driving Surveillance"

A bioptic telescope is a visual aid used by people with impaired vision when driving in many U.S. states, though bioptic driving remains controversial. Objective data on how and when bioptic drivers use the telescope and what they look at with it are crucial to understanding the bioptic telescope's effects on driving. A video-based technique to track the telescope's aiming point is presented in this paper. With three infrared retro-reflective markers pasted on the bioptic spectacles frame, its movement is recorded using an infrared camera unit with infrared LED illuminators. The angles formed by the three markers are used to calculate the telescope's aiming

points, which are registered with road scene images recorded by another camera. The calculation is based on a novel one-time calibration method, in which the light spot from a head-mounted laser pointer projected on a wall while the scanning is recorded by the scene camera, in synchronization with the infrared camera. Interpolation is performed within small local regions where no samples were taken. Thus, nonlinear interpolation error can be minimized, even for wide-range tracking. Experiments demonstrated that the average error over a $70^\circ \times 48^\circ$ field was only 0.86° , with lateral head movement allowed. [J170]

"Challenges and Opportunities in GaN and ZnO Devices and Materials"

This special issue addresses to a large extent the challenges and opportunities in GaN and ZnO devices and materials deemed critical to both the GaN- and ZnO-based technologies. There are twenty articles in this special issue. [J171]

"Stacking fault formation in the long wavelength InGaN/GaN multiple quantum wells grown on m-plane GaN"

Nonpolar GaN-based light emitting diodes (LEDs) and laser diodes (LDs) show great promise. However, long wavelength emitters ($\lambda > 500\text{nm}$) have reduced performance in comparison with violet and blue nonpolar emitters. We present results of transmission electron microscopy studies of long wavelength (1100) m-plane GaN LED series and m-plane GaN LDs grown on high quality bulk GaN substrates. In basal plane stacking faults form in the high In content $\text{In}_x\text{Ga}_{1-x}\text{N}$ quantum wells ($x \approx 0.26$) for thicker wells. The faults are bounded by sessile Frank-Shockley partial dislocations that likely limit the radiative efficiency of long wavelength m-plane emitters. [J172]

"Sequential low-voltage detecting method for multistring LED BLU circuit"

A new low-voltage detecting method for a multichannel LED back lighting unit is proposed. The proposed method detects the lowest voltage drops among the multichannel LED strings with a reduced number of devices, and it provides feedback voltage to control the stages of the boost converter for minimising the power consumption in the LED driving circuit. [J173]

"High-Performance Quantum Cascade Lasers With Single Phonon-Continuum Depopulation Structures"

We report high performance $\lambda \sim 8.6 \mu\text{m}$ quantum cascade lasers based on 5 quantum well single phonon-continuum (SPC) depopulation scheme, grown by metal organic vapor-phase epitaxy. Devices with SPC depopulation structures exhibit high device performances in pulsed and continuous wave (CW) operation due to a large dipole matrix element (3.0 nm) and short depopulation time (0.22 ps). A 4 mm-long, 8 μm -wide, high reflective (HR)-coated buried-hetero-structure laser with 33 cascade stages, for active region, demonstrates a high output power of 313 mW, a threshold current density of 1.35 kA/cm^2 , and slope efficiency of 547 mW/A at 30°C in CW operation. The maximum CW lasing temperature of the device is observed to be 120°C . Furthermore, by using a higher number of cascade stages ($N=70$) in a 4 mm-long, 22 μm -wide, HR-coated ridge laser, a high peak power of 6.3 W is obtained together with a high wall-plug efficiency (WPE) of 10.8%, a slope efficiency of 2.7 W/A , and a threshold current density of 0.76 kA/cm^2 in pulsed operation at 300 K. The measured WPE of over 10% at room temperature is close to the theoretical values. [J174]

"Enhancing outcoupling efficiency of indium-tin-oxide-free organic light-emitting diodes via nanostructured high index layers"

We fabricated organic light-emitting diodes with one-dimensional Bragg gratings as light extraction elements for substrate and waveguide modes. A Ta_2O_5 layer was introduced to obtain a high refractive index contrast to the subsequent anode layer. As anode we employed a highly conductive polymer. Laser interference lithography and physical plasma etching were used to pattern gratings into the Ta_2O_5 layer with a lattice constant of 370 nm and various grating depths. Mainly attributed to the outcoupling of the substrate modes, the structured devices exhibit a luminous flux which is up to four times higher compared to the unstructured reference devices. [J175]

"II-VI semiconductor color converters for efficient green, yellow, and red light emitting diodes"

II-VI compound semiconductor quantum-well heterostructures were fabricated for use as efficient, narrow-spectrum, photoluminescent color converters to generate green, yellow, or red light when photopumped with blue GaInN light emitting diodes (LEDs). This approach promises high efficiencies in a wide range of wavelengths that includes the green-yellow portion of the spectrum where conventional LEDs offer relatively low efficiency. External quantum conversion efficiencies of 60%-70% and output spectra with full width at half maximum of 15

nm were achieved using CdZnSe-CdMgZnSe quantum wells grown by molecular beam epitaxy on InP substrates. [J176]

"Easy Process and Performance Improvement for Top-Emission Organic Light-Emitting Diodes by Using UV Glue as the Insulation Layer on Copper Substrate"

A high heat dissipation material (copper, Cu) was employed as the substrate for top emission organic light-emitting diodes (TEOLEDs). The UV glue was spin-coated onto the Cu substrate as the insulation layer to effectively improve Cu surface roughness and reduce process complexity. From the optoelectronic results, the optimized device with the Cu substrate shows the maximum luminance of 14110 cd/m² and luminance efficiency of 7.14 cd/A. The surface and junction temperatures are measured to discuss the heat-dissipating effect on device performance. From the results, TEOLED fabricated on a Cu substrate has lower junction (55.34°C) and surface (25.7°C) temperatures, with the lifetime extended seven times. We employed Cu foil as the substrate for flexible TEOLED with maximum luminance of 10310 cd/m² and luminance efficiency of 7.3 cd/A obtained. [J177]

"Hole transport in the organic small molecule material alpha -NPD : evidence for the presence of correlated disorder"

In this paper the hole mobility in the amorphous small molecule material N,N'-bis(1-naphthyl)-N,N'-diphenyl-1,1'-biphenyl-4,4'-diamine (alpha -NPD), which is frequently used in organic light-emitting diodes, is studied. From an analysis of the temperature and layer thickness dependence of the steady-state current density in sandwich-type alpha -NPD-based hole-only devices, it is found that a conventional mobility model assuming a Poole-Frenkel type field dependence and neglecting the carrier density dependence is not appropriate. Consistent descriptions with equal quality are obtained within the framework of two forms of the Gaussian disorder model (GDM and CDM), within which the presence of energetic disorder is described by a Gaussian density of states and within which spatial correlations between the site energies are absent or are included, respectively. Both models contain a carrier density dependence of the mobility. Based on a comparison of the site densities as obtained from both models with the molecular density, we argue that the analysis provides evidence for the presence of correlated disorder. [J178]

"CMOS Imaging of Pin-Printed Xerogel-Based Luminescent Sensor Microarrays"

We present the design and implementation of a luminescence-based miniaturized multisensor system using pin-printed xerogel materials which act as host media for chemical recognition elements. We developed a CMOS imager integrated circuit (IC) to image the luminescence response of the xerogel-based sensor array. The imager IC uses a 26 Ч 20 (520 elements) array of active pixel sensors and each active pixel includes a high-gain phototransistor to convert the detected optical signals into electrical currents. The imager includes a correlated double sampling circuit and pixel address/digital control circuit; the image data is read-out as coded serial signal. The sensor system uses a light-emitting diode (LED) to excite the target analyte responsive luminophores doped within discrete xerogel-based sensor elements. As a prototype, we developed a 4 Ч 4 (16 elements) array of oxygen (O₂) sensors. Each group of 4 sensor elements in the array (arranged in a row) is designed to provide a different and specific sensitivity to the target gaseous O₂ concentration. This property of multiple sensitivities is achieved by using a strategic mix of two oxygen sensitive luminophores ([Ru(dpp)₃]²⁺ and [Ru(bpy)₃]²⁺) in each pin-printed xerogel sensor element. The CMOS imager consumes an average power of 8 mW operating at 1 kHz sampling frequency driven at 5 V. The developed prototype system demonstrates a low cost and miniaturized luminescence multisensor system. [J179]

"Surface 210 nm light emission from an AlN p-n junction light-emitting diode enhanced by A-plane growth orientation"

(1120)A-plane AlN p-n junction light-emitting diode (LED) with a wavelength of 210 nm is demonstrated. The electroluminescence from the A-plane LED is inherently polarized for the electric field parallel to the [0001] c-axis due to a negative crystal-field splitting energy. The polarization ratio (electric-field component ratio of parallel and perpendicular to c-axis) is as high as 0.9. The radiation pattern of the A-plane LED shows higher emission intensity along the surface normal, while that of a conventional (0001) C-plane LED shows lower emission intensity along the surface normal. The different radiation patterns can be explained by the polarization property. [J180]

"Electron Beam Evaporation of Tungsten Oxide Films for Gas Sensors"

Pure and iron incorporated nanostructured Tungsten Oxide (WO₃) thin films were investigated for gas sensing applications using noise spectroscopy. The WO₃ sensor was able to detect lower concentrations (1-10 ppm) of

NH₃, CO, CH₄, and Acetaldehyde gases at operating temperatures between 100°C to 250°C. The iron-doped Tungsten Oxide sensor (WO₃:Fe) showed some response to Acetaldehyde gas at relatively higher operating temperature (250°C) and gas concentration of 10 ppm. The sensitivity of the WO₃ sensor towards NH₃, CH₄ and Acetaldehyde at lower operating temperatures (50°C-100°C) was significant when the sensor was photo-activated using blue light-emitting diode (Blue-LED). From the results, photo-activated WO₃ thin film that operates at room temperature appeared to be a promising gas sensor. The overall results indicated that the WO₃ sensor exhibited reproducibility for the detection of various gases and the WO₃:Fe indicated some response towards Acetaldehyde gas. [J181]

"Corrosion Estimation of Stainless Steel in Nitric Acid by an Optoelectronic Instrument Based on Diffuse Light Scattering Pattern Measurement"

This paper presents the design and implementation of an optoelectronic instrument for measuring corrosion of metal surfaces, based on measurement of lightwave scattering pattern. The instrument consists of a thin beam light emitting diode (LED) that illuminates a tiny spot on the metal surface, and an array of photodiodes spread over a hemispherical structure covering the surface to record the light scattering pattern. A mathematical model of light scattering by a corroded metal surface is constructed in which a newly defined corrosion factor is correlated to light scattering pattern. The corrosion factor derived from the scattering pattern gives a measure of the degree of corrosion in a scale from 0 to 100. The temporal behavior of corrosion of stainless steel samples immersed in nitric acid of various concentrations is presented graphically. A semi empirical mathematical model describing the corrosion and dissolution processes in terms of the well-known bilogarithmic laws fits very well with the experimental results. The measured corrosion factor and the corresponding roughness factor as measured by an atomic force microscope are compared to show the relation between the two. [J182]

"Highly polarized polymer-based light-emitting diodes fabricated by using very thin photoaligned polyimide layers"

Polarized polymer-based light-emitting diodes (PLEDs) have been fabricated by inserting a very thin photoaligned polyimide film into the device structure. The photoaligned polyimide film was used to form a highly oriented layer of light-emitting polymer, poly (9,9-dioctylfluorenyl-2,7-diyl) (PFO). The polyimide contains azobenzene in the backbone structure, allowing us to control the alignment of its backbone structure by optical treatment. Since the photoalignment treatment is scratch-free, the thickness of the photoaligned film can be reduced below 4 nm without decreasing its alignment ability for PFO. Even though polyimide is a good insulator, such a very thin photoaligned film can be inserted into PLED structures. We examined the influence of the thickness of the photoaligned polyimide film and the light-emitting layer on the polarization ratio and the current efficiency of the polarized PLEDs. Using a 2.9 nm-thick polyimide photoalignment layer and a 101 nm-thick PFO light-emitting layer, we have succeeded in fabricating a polarized PLED with a current efficiency of 0.3 cd/A at 150 cd/m² and polarization ratios of 46 at 434 nm, 27 at 460 nm, and 20 for integrated intensity from 400 to 600 nm. [J183]

"Emission color control from blue to red with nanocolumn diameter of InGaN/GaN nanocolumn arrays grown on same substrate"

A novel technology for controlling the In composition of InGaN quantum wells on the same wafer was developed, which paved the way for the monolithic integration of three-primary-color nano-light-emitting diodes. In the experiment, InGaN/GaN multiple quantum well nanocolumn arrays with nanocolumn diameters from 137 to 270 nm were prepared on the same substrate with the Ti-mask selective area growth by rf-plasma-assisted molecular beam epitaxy. The emission color changed from blue to red (from 479 to 632 nm in wavelength) with increasing nanocolumn diameter. The emission color change mechanism was clearly explained by the beam shadow effect of the neighboring nanocolumns. [J184]

"Low efficiency droop in blue-green m-plane InGaN/GaN light emitting diodes"

We investigated the electroluminescence and relatively external quantum efficiency (EQE) of m-plane InGaN/GaN light emitting diodes (LEDs) emitting at 480 nm to elucidate the droop behaviors in nitride-based LEDs. With increasing the injection current density to 100 A/cm², the m-plane LEDs exhibit only 13% efficiency droop, whereas conventional c-plane LEDs suffer from efficiency droop at very low injection current density and the EQE of c-plane LEDs decrease to as little as 50% of its maximum value. Our simulation models show that in m-plane LEDs the absence of polarization fields manifest not only the hole distribution more uniform among the wells but also the reduction in electron overflow out of electron blocking layer. These results suggest that the nonuniform distribution of holes and electron leakage current due to strong polarization fields are responsible for the relatively significant efficiency droop of conventional c-plane LEDs. [J185]

"Growth of Bulk GaN and AlN: Progress and Challenges"

GaN-based optoelectronic and electronic devices such as light-emitting diodes (LEDs), laser, and heterojunction field-effect transistors (HFETs) typically use material grown on foreign substrates such as sapphire, Si, and SiC. However, thermal and lattice mismatch present prevent attainment of quality films deemed necessary by ever increasing demand on device performance. In fact in LEDs intended for solid state lighting, internal quantum efficiencies near 100% might be needed, and further these high efficiencies would have to be retained at very high injection current levels. On the electronic device side, high radio-frequency (RF) power, particularly high-power switching devices, push the material to its limits. Consequently, as has been the case for other successful semiconductor materials systems, native substrates must be developed for the GaN family. In this paper, various approaches such as high-pressure nitrogen solution (HPNS), ammonothermal, and Na flux methods, and an intermediary technique called the hydride vapor phase epitaxy (HVPE; to a lesser extent as there is a review devoted to this technique in this issue) along with their strengths and challenges are discussed. [J186]

"Intersubband Transition-Based Processes and Devices in AlN/GaN-Based Heterostructures"

We report on the physics, epitaxial growth, fabrication, and characterization of optoelectronic devices based on intersubband transitions in the AlN/GaN material system. While in 1999, only results of optical absorption experiments could be shown, photodetectors and modulators with operation frequencies beyond 10 GHz as well as optically pumped light emitters have been demonstrated recently. This is the reason for a comprehensive report on the most important properties of such devices. Beside some basic theoretical considerations, we will concentrate on the fabrication and characterization of modulators, switches, photodetectors, and light emitters. At the end of this paper, an outlook to future trends and developments in this emerging field will be given. [J187]

"Space-charge-limited hole current in poly(9,9-dioctylfluorene) diodes"

Characterization of the hole transport in blue-emitting polymers as poly(9,9-dioctylfluorene) (PFO) is strongly hindered by their large ionization potential of 6 eV. Using common anodes as poly(3,4-ethylenedioxythiophene)/poly(styrenesulphonic acid) leads to a strongly injection limited current. We demonstrate that molybdenum trioxide forms an Ohmic hole contact on PFO, enabling the observation of a space-charge-limited current (SCLC). This allows a direct determination of the hole mobility PFO of $1.34 \cdot 10^{-9} \text{ m}^2/\text{V s}$ at room temperature, in good agreement with previously reported mobility values determined by time-of-flight measurements. [J188]

"Evidence of intermolecular species formation with electrical aging in anthracene-based blue organic light-emitting devices"

Electrical aging mechanism in blue emitting organic light-emitting devices (OLEDs) based on 9,10-bis (2-naphthyl)-2-t-butylanthracene (TBADN) fluorescent emitter is investigated using a number of techniques, including delayed electroluminescence measurements. The studies reveal that electrical aging is associated with an increasing concentration of an intermolecular species with a weak characteristic luminescence at around 535 nm. This species is capable of charge trapping, and thus plays a role as an electron-hole recombination center with prolonged electrical driving. Weak green luminescence from this species leads to an increased green/blue emission ratio, and causes the color purity loss in aged devices. The results also suggest that this species is also efficient in dissipating excitation energy nonradiatively, hence is capable of quenching TBADN singlet excitons, contributing to the observed efficiency loss with electrical aging. [J189]

"High Brightness GaN Vertical Light-Emitting Diodes on Metal Alloy for General Lighting Application"

In this paper, we show the many advantages of the GaN-based vertical light-emitting diodes (VLEDs) on metal alloy over conventional LEDs in terms of: better current spreading, vertical current path for low operation voltage, better light extraction, flexible chip size scaling, higher driving current density, faster heat dissipation, and good reliability. The GaN VLED on metal alloy exhibits very good current-voltage behavior with low operated voltage and low serial dynamic resistance. The low operation junction temperature of GaN VLED on metal alloy demonstrates excellent heat dissipation capabilities. Chip size scaling without efficiency loss shows a unique property of GaN VLED on metal alloy. The GaN VLED on metal alloy also enables top surface engineering for efficient light extraction to further light output. A high-power white LED having efficiency of 120 lumen/W was achieved through a combination of reflector, surface engineering, and optimization of the n-GaN layer thickness. Coupled with good reliability and mass production ability, the GaN VLED on metal alloy is very suitable for general lighting application. [J190]

"Very-High Temperature (200 C) and High-Speed Operation of Cascade GaN-Based Green Light-Emitting Diodes With an InGaN Insertion Layer"

We demonstrate a novel type of linear cascade green light-emitting diode (LED) arrays as a light source for in-car or harsh environment plastic optical fiber (POF) communications. To further enhance its dynamic and static performance, an InGaN layer is inserted between an n-type GaN cladding layer and InGaN-GaN multiple quantum wells as an efficient current spreading layer. Compared with the control device without that layer, our three-LED cascade array demonstrates a smaller turn-on voltage (9.3 versus 11 V at 20 mA) and a larger output power (25.5 versus 22.5 mW at 180 mA), corresponding to an enhancement of around 31% in wall-plug efficiency. Furthermore, under the constant voltage bias of an in-car battery (12 V), our three-LED array exhibits an electrical-to-optical 3-dB bandwidth (100 versus 40 MHz) performance superior to that of the control device. Even under high-temperature dynamic operation, we observe that the InGaN insertion layer gives strong enhancement of modulation speed with negligible degradation of the output power, unlike the red resonant-cavity LEDs conventionally used for POF. We achieve 200-Mb/s error-free transmission at 200°C which is the highest operation temperature among all the reported high-speed LEDs. [J191]

"Vibration energy harvesting using highly (001)-oriented Pb (Zr ,Ti)O 3 thin film"

Energy conversion from mechanical vibration into electric power was investigated using the piezoelectric Pb(Zr,Ti)O₃ lead zirconate titanate (PZT) thin film with highly (001)-orientation. The piezoelectric d₃₁ constant was found to be as large as -150 pC/N. The generated electric voltage under vibration acceleration of 45m/s² at 2450 Hz for the PZT/Si cantilever exceeded 2 V and the operation of light emitting diode lighting was demonstrated. The average output power of 100μW was obtained at the impedance-matched load resistance of 2.2kΩ. The generated power density of 50μW/mm³ was much larger than that of conventional piezoelectric harvesters. [J192]

"Localized Surface Plasmon-Enhanced Nitride-Based Light-Emitting Diode With Ag Nanotriangle Array by Nanosphere Lithography"

We describe a method to enhance the light output power of nitride-based light-emitting diodes (LEDs) through the coupling of multiple quantum wells (MQWs) with localized surface plasmon (LSP). The LSP was generated on an Ag nanotriangle array (NTA) on a 40-nm-thick p-type GaN layer beneath the p-pad of the LED, which was partially etched by inductively coupled plasma system. The Ag NTA was fabricated by nanosphere lithography. The resonant frequency of a generated LSP can be precisely controlled by changing the size of the polystyrene nanosphere and the Ag deposition thickness. Under the optimum conditions, the light output power of LED with an Ag NTA was 15.4% higher than LED without an Ag NTA at an inject current of 20 mA. The improvement in light output power can be attributed to the coupling effect between MQW and LSP. [J193]

"Solid-State Lighting: An Integrated Human Factors, Technology, and Economic Perspective"

Solid-state lighting is a rapidly evolving technology, now virtually certain to someday displace traditional lighting in applications ranging from the lowest-power spot illuminator to the highest-power area illuminator. Moreover, it has considerable headroom for continued evolution even after this initial displacement. In this paper, we present a high-level overview of solid-state lighting, with an emphasis on white lighting suitable for general illumination. We characterize in detail solid-state lighting's past and potential-future evolution using various performance and cost metrics, with special attention paid to inter-relationships between these metrics imposed by human factors, technology, and economic considerations. [J194]

"Effect of P-Type Last Barrier on Efficiency Droop of Blue InGaN Light-Emitting Diodes"

P-type doping in the last barrier is proposed to improve the efficiency droop of the blue InGaN light-emitting diodes (LEDs). The light-current curves, energy band diagrams, carrier concentrations, radiative recombination efficiency, and internal quantum efficiency of the blue LEDs under study are investigated. The simulation results show that the efficiency droop is significantly improved when the last undoped GaN barrier in a typical blue LED is replaced by a p-type GaN barrier. The simulation results suggest that the improvement in efficiency droop is mainly due to the decrease of electron current leakage and increase of hole injection efficiency. [J195]

"A Novel Passive Offline LED Driver With Long Lifetime"

This paper describes a patent-pending passive offline light-emitting diode (LED) driver that has no controlled semiconductor switches, electrolytic capacitors, auxiliary power supply, and control board. It can provide a fairly smooth current from the ac mains to drive LED strings. The new circuit has the advantages of high input power

factor, high energy efficiency and luminous efficacy, long lifetime, stable luminous output, and high robustness against extreme weather conditions. In addition, over 90% of the driver material is recyclable, leading to reduction of electronic waste. It is particularly suitable public LED lighting systems, such as road lighting systems. Experimental results based on a 50-W system are included in the paper to confirm the validity of the proposal. Due to the circuit simplicity, an energy efficiency exceeding 93.6% has been achieved. [J196]

"Microcavity enhanced silicon light emitting pn-diode"

An electrically driven silicon light emitting diode with two distributed Bragg reflectors is reported. The active material is a Si pn-junction fabricated by boron ion implantation into an n-type silicon-on-insulator wafer. The cavity with a thickness of a few wavelengths is formed by amorphous Si/SiO₂ multilayer stacks. A strong narrowing and enhancement of the electroluminescence at a resonant wavelength of $\lambda = 1146 \text{ nm}$ is observed with a quality factor of $Q = 143$ and a finesse of $F = 11$. [J197]

"Improvement of electron injection in inverted bottom-emission blue phosphorescent organic light emitting diodes using zinc oxide nanoparticles"

We fabricated highly efficient iridium(III) bis[(4,6-di-fluorophenyl)-pyridinato-N,C2'] picolinate doped inverted bottom-emission blue phosphorescent organic light-emitting diodes, with an electron injection layer of zinc oxide (ZnO) nanoparticles (NPs). The ZnO NPs layer lowers the turn-on voltage by about 4 V and significantly enhances the efficiency. The device with ZnO NPs shows peak efficiencies of 16.5 cd/A and 8.2%, about three times higher than those of the device without ZnO NPs. Since the ZnO NPs layer has a wide band gap, good electron transporting properties and low work function, it can be utilized as an effective electron injection layer with good transparency. [J198]

"AlGaN based highly sensitive radio-frequency UV sensor"

The response of the AlGaN based radio-frequency (rf) sensor to deep ultraviolet (UV) illumination was investigated. Illumination by UV light emitting diodes with wavelengths from 280 to 375 nm significantly decreased rf oscillator frequency due to change in the impedance of AlGaN-based metal-semiconductor-metal structure. The UV-induced frequency shift attains 400 kHz from the oscillator dark frequency of 144.5 MHz with the highest sensitivity of 40 kHz/($\mu\text{W}/\text{cm}^2$) at 280 nm wavelength and UV power density less than 7.4 $\mu\text{W}/\text{cm}^2$. The AlGaN-based rf oscillator allows for a wireless visible-blind and solar-blind UV sensing. [J199]

"The latest video projectors can fit inside tiny cameras or cellphones yet still produce big pictures [JLittle Gizmo, Big Picture]"

The latest video projectors can fit inside tiny cameras or cellphones yet still produce big pictures. What a pico projector does is simple: It takes a digital image and sends it out as a beam of light, creating an image that's much bigger than the originating device. Every pico projector needs chips to process and decode the image data for the hardware, a light source, typically LEDs or laser diodes, and mirrors and optics, to direct and focus the image. [J200]

"Electroluminescence behavior of ZnO/Si heterojunctions: Energy band alignment and interfacial microstructure"

n-ZnO/p-Si heterojunction light-emitting diodes (LEDs) show weak defect-related electroluminescence (EL). In order to analyze the origin of the weak EL, the energy band alignment and interfacial microstructure of ZnO/Si heterojunction are investigated by x-ray photoelectron spectroscopy. The valence band offset (VBO) is determined to be $3.15 \pm 0.15 \text{ eV}$ and conduction band offset is $-0.90 \pm 0.15 \text{ eV}$, showing a type-II band alignment. The higher VBO means a high potential barrier for holes injected from Si into ZnO, and hence, charge carrier recombination takes place mainly on the Si side rather than the ZnO layer. It is also found that a 2.1 nm thick SiO_x interfacial layer is formed at the ZnO/Si interface. The unavoidable SiO_x interfacial layer provides to a large number of nonradiative centers at the ZnO/Si interface and gives rise to poor crystallinity in the ZnO films. The weak EL from the n-ZnO/p-Si LEDs can be ascribed to the high ZnO/Si VBO and existence of the SiO_x interfacial layer. [J201]

"Thermophotonic heat pump-a theoretical model and numerical simulations"

We have recently proposed a solid state heat pump based on photon mediated heat transfer between two large-area light emitting diodes coupled by the electromagnetic field and enclosed in a semiconductor structure with a nearly homogeneous refractive index. Ideally the thermophotonic heat pump (THP) allows heat transfer at Carnot efficiency but in reality there are several factors that limit the efficiency. The efficient operation of the THP is

based on the following construction factors and operational characteristics: (1) broad area semiconductor diodes to enable operation at optimal carrier density and high efficiency, (2) recycling of the energy of the emitted photons, (3) elimination of photon extraction losses by integrating the emitting and the absorbing diodes within a single semiconductor structure, and (4) eliminating the reverse thermal conduction by a nanometer scale vacuum layer between the diodes. In this paper we develop a theoretical model for the THP and study the fundamental physical limitations and potential of the concept. The results show that even when the most important losses of the THPs are accounted for, the THP has potential to outperform the thermoelectric coolers especially for heat transfer across large temperature differences and possibly even to compete with conventional small scale compressor based heat pumps. [J202]

"Energy-Recycling (ER) Technique for a Direct-Lit Intelligent Power Management Backlight Unit (BLU)"

A field-sequential-color (FSC) liquid crystal display (LCD) technique with a direct-lit red, green, and blue LED backlight driver is proposed to achieve low weight, thin, perfect image quality, and low-power consumption of LCD television. The FSC technique performs a pseudorandom color sequence in the spatial and temporal domains to reduce color-breakup and motion-blur effects. The direct-lit RGB-LED backlight driver increases brightness, contrast, and uniformity due to the removal of a color filter. In this paper, the proposed FCS-LCD controller uses a single LED driver to switch the driving voltage alternatively between 36 V for driving 12-series G- or B-LEDs and 24 V for 12-series R-LEDs. The proposed energy-recycling technique can harvest the extra energy when the driving voltage switches from 36 to 24 V. Experimental results show that energy saving is higher than 17% of the conventional driving method. [J203]

"Improved electroluminescence from n-ZnO/AlN/p-GaN heterojunction light-emitting diodes"

n-ZnO/p-GaN heterojunction light-emitting diodes with and without a sandwiched AlN layer were fabricated. The electroluminescence (EL) spectrum acquired from the n-ZnO/p-GaN displays broad emission at 650 nm originating from ZnO and weak emission at 440 nm from GaN, whereas the n-ZnO/AlN/p-GaN exhibits strong violet emission at 405 nm from ZnO without GaN emission. The EL intensity is greatly enhanced by inserting a thin AlN intermediate layer and it can be attributed to the suppressed formation of the GaOxinterfacial layer and confinement effect rendered by the AlN potential barrier layer. [J204]

"Power Recycling of Large-Area OLEDs Using Solar Cells"

We demonstrate that power recycling is feasible by merging a large-area (30 4120 mm²) OLED panel and a solar cell into each other. The power recycling efficiency of 0.152% is achieved under the illumination of one side-emitting white OLED at 2450 cd/m² when the conversion efficiency of a reference solar cell is 4% and the distance between the OLED and solar cell is 1.5 mm. We have found that the power recycling efficiency is decreased under high brightness due to a decrease in the power efficiency of OLED and a loss of current induced by the resistance of a transparent electrode. We have also shown that local heat generation of the large-area OLED panel would be an issue for power recycling. [J205]

"Erratum: "High-refractive-index TiO₂-nanoparticle-loaded encapsulants for light-emitting diodes" [JJ. Appl. Phys. 103, 083120 (2008)]"

First Page of the Article [J206]

"Modeling of injection characteristics of polar and nonpolar III-nitride multiple quantum well structures"

Carrier confinement and injection characteristics of polar and nonpolar III-nitride quantum well (QW) light-emitting diode or laser diode structures are compared. We demonstrate that strongly inhomogeneous QW injection in multiple-QW (MQW) active region is one of the possible reasons holding back the advance of nonpolar laser structures. In polar structures, strong interface polarization charges induce the nonuniform carrier distribution among the active QWs so that the extreme p-side QW always dominates the optical emission. On the contrary, in nonpolar MQW structures, the inhomogeneity of QW populations is supported mainly by QW residual charges and the prevailing QW is the one closest to the n-side of the diode. For both polar and nonpolar structures, the QW injection inhomogeneity is strongly affected by the QW carrier confinement and becomes more pronounced in longer wavelength emitters with deeper active QWs. We show that in nonpolar structures indium incorporation into optical waveguide layers improves the uniformity of QW injection. On the contrary, QW injection in polar structures remains inhomogeneous even at high-indium waveguide layer compositions. We show, however, that polarization-matched design of the electron-blocking layer can noticeably improve the injection uniformity in polar

MQW structure and enhance the structure internal quantum efficiency. [J207]

"Control of magnetoconductance through modifying the amount of dissociated excited states in tris-(8-hydroxyquinoline) aluminum-based organic light-emitting diodes"

Magnetoconductance (MC) is generally believed to be controlled by the ratio of singlet to triplet excited states. In this study, it is found that the MC magnitude of tris-(8-hydroxyquinoline) aluminum-based organic light-emitting diodes decreases substantially upon the introduction of narrow band gap fluorescent dopants. Since singlet to triplet ratio of excited states keeps unchanged in doped devices, this large reduction in MC means that other underlying mechanism affects the MC. The charge carrier trapping effect is proposed here to vary the magnitude of MC. By using this trapping effect, the controlling of the total amount of dissociated electron-hole pairs and consequently the magnitude of MC are realized by changing the dopant's concentration or band gaps. [J208]

"InGaN-based light-emitting diodes grown and fabricated on nanopatterned Si substrates"

InGaN-based light-emitting diodes (LEDs) were grown and fabricated on nanoscale patterned Si (111) substrates (NPSi). Using anodized aluminum oxide as the etch mask, the NPSi was prepared with an average nanopore diameter of 150 nm and interpore distance of 120 nm. LEDs grown on NPSi exhibit relaxed tensile stress relative to the ones grown on microscale patterned Si (111) substrates (MPSi). Nanoheteroepitaxial lateral overgrowth was significantly promoted on NPSi, which led to extensive dislocation bending and annihilation. The devices made on NPSi exhibit lower leakage current and higher light output power as compared with those on MPSi. [J209]

"Solution-Processed Flexible ITO-Free Organic Light-Emitting Diodes Using Patterned Polymeric Anodes"

We discuss a thin-film spin-coating and patterning process of a conductive polymer electrode for flexible organic light-emitting diodes (OLEDs). For the polymeric anode, dimethylsulfoxide (DMSO)-doped poly(3,4-ethylenedioxythiophene):poly(styrene sulfonate) (PEDOT:PSS) has been spin coated on a non-ionic surfactant layer that was pre-coated on the polyethersulfone (PES) substrate. A peel-off method has then been employed to pattern the conductive polymer anode without UV irradiation or heat treatment involved. A peel-off pattern is induced by different adhesion energy among a hydrophobic flexible substrate, a hydrophilic polymeric anode layer, and an adhesive film peeler that is in contact with the polymer anode. With this process technology, we have successfully fabricated solution-processed flexible green OLEDs, showing a peak luminescence of 6000 and a maximum current efficiency of 16.2 cd/A. [J210]

"ZnO Devices and Applications: A Review of Current Status and Future Prospects"

ZnO is an attractive material for applications in electronics, photonics, acoustics, and sensing. In optical emitters, its high exciton binding energy (60 meV) gives ZnO an edge over other semiconductors such as GaN if reproducible and reliable p-type doping in ZnO were to be achieved, which currently remains to be the main obstacle for realization of bipolar devices. On the electronic side, ZnO holds some potential in transparent thin film transistors (TFTs) owing to its high optical transmittivity and high conductivity. Among the other promising areas of application for ZnO are acoustic wave devices, due to large electromechanical coupling in ZnO, and devices utilizing nanowires/nanorods such as biosensors and gas sensors and solar cells, since it is relatively easy to produce such forms of ZnO nanostructures, which have good charge carrier transport properties and high crystalline quality. Despite the significant progress made, there is still a number of important issues that need to be resolved before ZnO can be transitioned to commercial use, not to mention the stiff competition it is facing with GaN, which is much more mature in terms of devices. In this paper, recent progress in device applications of ZnO is discussed and a review of critical issues for realization of ZnO-based devices is given. [J211]

"GaN-Based Light-Emitting Diodes: Efficiency at High Injection Levels"

Light-emitting diodes (LEDs) have become quite a high-performance device of late and are revolutionizing the display and illumination sectors of our economy. Due to demands for better performance and reduced energy consumption there is a constant race towards converting every single electron hole pair in the device to photons and extracting them as well while using only the minimum required voltage. This raises the bar on GaN-based LEDs in terms of elimination of nonradiative recombination processes not just at low but just as importantly if not more at very high injection levels needed for high brightness sources, and design of heterostructures for efficient electron and hole recombination without carrier loss and voltage/photon energy conversion loss. The haunting efficiency droop observed in GaN-based LEDs at high injection levels has been attributed to nonradiative Auger recombination, but can be simply explained by electron spillover. Investigations of quantum well (QW) InGaN

LED structures with different barrier heights, widths, and doping suggest that limited hole transport in the active region and the resulting electron spillover is responsible for efficiency droop at high injection levels. In this paper, highly critical, demanding, and challenging nature of high-efficiency high-brightness LEDs, in particular the basics surrounding the internal quantum efficiency of LED structures and the ongoing research/development, will be discussed. [J212]

"Doping Asymmetry Problem in ZnO: Current Status and Outlook"

ZnO has gained considerable interest recently as a promising material for a variety of applications. To a large extent, the renewed interest in ZnO is fuelled by its wide direct band gap (3.3 eV at room temperature) and large exciton binding energy (60 meV) making this material, when alloyed with, e.g., Cd and Mg, especially attractive for light emitters in the blue/ultraviolet (UV) spectral region. Unfortunately, as with other wide-gap semiconductors, ZnO suffers from the doping asymmetry problem, in that the n-type conductivity can be obtained rather easily, but p-type doping proved to be a formidable challenge. This doping asymmetry problem (also dubbed as the p-type problem in ZnO) is preventing applications of ZnO in light-emitting diodes and potential laser diodes. In this paper, we provide a critical review of the current experimental efforts focused on achieving p-type ZnO and discuss the proposed approaches which could possibly be used to overcome the p-type problem. [J213]

"Enhanced light extraction in light-emitting diodes with photonic crystal structure selectively grown on p-GaN"

We report on the properties of green light-emitting diodes (LEDs) with a photonic crystal (PC) structure on p-GaN. A PC structure was fabricated by the selective area epitaxy of p-GaN using SiO₂nanopillars. The electrical characteristics of LEDs with PC were not degraded and the optical output power of green LEDs with PC was increased by 70% at 20 mA of injection current compared with that of conventional LEDs without PC. This enhancement of optical output power was attributed to the improvement in light extraction efficiency by the SiO₂/p-GaN PC layer on p-GaN. [J214]

"Sensor Applications Based on the Cutoff Properties of Liquid-Filled Ge-Doped Microstructured Fibers"

The cutoff properties of the fundamental mode of liquid filled Ge-doped microstructured fiber can be exploited in a novel set of wavelength encoded sensor applications. A number of temperature, strain and vibration sensors have been implemented using a Ge-doped core Y-shaped microstructured fiber. The temperature sensitivity of the cutoff wavelength is 25 nm/°C, more than two orders of magnitude higher than the values reported for fiber Bragg gratings. Similarly, the strain sensitivity is 16.8 pm/μ, about one order of magnitude higher than a fiber Bragg grating. Amplitude interrogation of the sensor heads can be implemented in rather easy configurations using a light emitting diode or a laser diode, without requiring an accurate selection of the laser wavelength. This permits, for example, the development of vibration sensors with fast time response, at least better than 0.1 ms. [J215]

"Heinrich Welker"

Heinrich Welker's work as a theoretical physicist in the 1950s, 1960s, and 1970s focused on the then novel fields of superconductivity and CMOS technology. Specifically, his theoretical and experimental research on gallium arsenide laid the foundations for a range of diversified industries. His pioneering ideas are at the origin of the major technology developments that led to the 1970 inauguration of the Arpanet, precursor of the Internet. Compound semiconductors are the building blocks of light-emitting devices, such as lasers, and of light-detecting devices such as photocells. They opened the way to CD players and DVD recorders, sophisticated night-vision equipment, fiber optical communications systems, solar photovoltaic panels, flat-panel displays, mobile phones, and all devices that make up the technological revolution that shapes so many aspects of our lives. [J216]

"Dual wavelength GaSb based type I quantum well mid-infrared light emitting diodes"

We have designed and developed dual wavelength type I quantum well light emitting diodes (LEDs) operating at 2μm and 3-3.4μm wavelengths with independently controlled intensities. The room temperature quasicontinuous wave output power was 2.8 mW at 2μm and 0.14 mW at 3μm. The design of the dual wavelength structure allows for monolithically integrating LED pixels with different wavelengths opening the way for the fabrication of multiwavelength LED arrays for multispectral and hyperspectral imaging applications. [J217]

"Influences of evaporation temperature on electronic structures and electrical properties of

molybdenum oxide in organic light emitting devices"

The influence of evaporation temperatures on the electronic structures of molybdenum oxide (MoOx) films and the electrical properties of organic light emitting diodes were investigated. MoOx films evaporated at a high temperature and a high deposition rate are close to a stoichiometric phase, but become less effective when they are used as a hole injection layer. However, when MoOx is evaporated at a lower temperature and a slower rate, there are large amounts of defect-related states present in the forbidden gap, which make the films behave like a high work function conductor and an effective hole injection layer. [J218]

"Transfer of GaN-Based Light-Emitting Diodes From Silicon Growth Substrate to Copper"

III-nitride light-emitting diodes (LEDs) grown on Si (111) substrates have the potential of low-cost manufacturing for solid-state lighting and display, by taking advantage of the well-developed IC technologies of silicon. In this letter, LEDs grown on silicon substrates were transferred onto copper substrates, to maximize light extraction and heat dissipation. On Si substrates, 300 \times 300 μ m² multiple quantum well InGaN LEDs were first grown and processed. The top surface of the fabricated devices was then temporarily bonded to a sapphire wafer and the Si substrate was chemically etched. Ti/Al/Ti/Au layers were deposited on the backside of LEDs. An 80- μ m-thick copper layer was electroplated and the temporary bonding was removed, resulting in LEDs on copper substrate. The optical output power of LEDs on copper increased by \sim 70% as compared to that of the LEDs on silicon. The improved performance was attributed to the removal of the light-absorbing Si substrate and the good thermal conductivity of copper. [J219]

"SAR-Controlled Adaptive Off-Time Technique Without Sensing Resistor for Achieving High Efficiency and Accuracy LED Lighting System"

A successive approximation register (SAR) is utilized to control adaptive off-time in order to regulate accurate light-emitting diode (LED) current and improve efficiency of LED driver. The proposed SAR-controlled adaptive off-time technique without the external sensing resistor can sense the current flowing through LEDs during the turning on of the N-type power MOSFET, as well as provide adaptive off-time depending on the input voltage and the numbers of LED, to obtain an accurate LED current. Experimental results show the inductor current ripple is kept within $\pm 15\%$ of the DC current. As a result, line regulation is guaranteed in this proposed design. [J220]

"Pulsed Excitation of OLEDs With a Remote Metallic Cathode"

In this paper, we report on the behavior of organic LEDs (OLEDs) with a remote metallic cathode under pulsed excitation. Devices comprising poly(triarylamine) as the hole-transporting layer, Alq₃:DCM2 as the light-emitting layer, and PTCDI-C13H₂₇ as the electron-transporting layer are analyzed and their performance is compared to conventional OLED device structures comprising the same organic materials. We demonstrate that the dependence of the light intensity on the applied pulsewidth is mainly determined by charge injection into the active light-emitting layer and show that pulses down to 1 ns can be applied to the device without affecting the light intensity. This latter observation suggests that pulsed excitation may be able to reduce the accumulation of triplets in the device. In this way, triplet-state losses, which are major loss mechanisms with respect to the high photon density required for an electrically pumped organic laser, will be suppressed. [J221]

"Stark Effects Model Used to Highlight Selective Activation of Failure Mechanisms in MQW InGaN/GaN Light-Emitting Diodes"

This paper demonstrates the feasibility of creating specific defects in double-heterostructure InGaN/GaN commercial light-emitting diodes by neutron irradiation. Using controlled neutron energy, only one failure mechanism can be activated. Defects are located on the side of the chip and increase the leakage current driven by the well-known Poole-Frenkel effect with $E_c - E_T = 130$ meV electron trap energy level. The maximal amplitude of the optical spectrum also reveals a drop of about 20% associated with the rise of the leakage current. The Stark effect model highlights the origin of the degradation. [J222]

"A Ring-Shaped Photodiode Designed for Use in a Reflectance Pulse Oximetry Sensor in Wireless Health Monitoring Applications"

We report a photodiode for use in a reflectance pulse oximeter for use in autonomous and low-power homecare applications. The novelty of the reflectance pulse oximeter is a large ring shaped backside silicon pn photodiode. The ring-shaped photodiode gives optimal gathering of light and thereby enable very low light-emitting diode (LED) driving currents for the pulse oximeter. The photodiode also have a two layer SiO₂/SiN interference filter yielding 98% transmission at the measuring wavelengths, 660 nm and 940 nm, and suppressing other

wavelengths down to 50% transmission. The photodiode has a radius of 3.68 mm and a width of 0.78 mm giving an area of 18 mm². The capacitance of the photodiode is measured to 34.5 nF. The quantum efficiency of the photodiode is measured to 55% and 62% at 660 nm and 940 nm, respectively. It is acceptable for this prototype but can be improved. The sensor also has an on-chip integrated Au thermistor for measuring the skin temperature of the body. The thermistor has a Temperature Coefficient of Resistance of $2.7\Gamma, B \cdot 10^{-3} K^{-1}$ and a repeatability on temperature measurements of $\Gamma, B \pm 0.26\Gamma, B^{\circ}C$. The photodiode is fabricated in a clean room environment by two diffusion processes and an Advanced Silicon Etch to make the hole in the middle for the LEDs. The sensor is designed to be integrated in a sticking patch of hydrocolloid polymer together with integrated electronics, radio communication unit, and a coin cell battery. The reflectance pulse oximetry sensor is demonstrated to work in a laboratory setup with a Ledtronics dual LED with wavelengths of 660 and 940 nm. Using this setup photoplethysmograms which clearly show the cardiovascular cycle have been recorded. The sensor is shown to work very well with low currents of less than 10 mA. [J223]

"Design of a GaN White Light-Emitting Diode Through Envelope Function Analysis"

In this paper, we present an envelope function analysis technique for the design of the emission spectra of a white quantum-well light-emitting diode (QWLED). The nanometric heterostructure that we are dealing with is a multiple QW, consisting of periods of three single QWs with various well thicknesses. With the aid of 6 Γ B—6 Luttinger Hamiltonian, we employ the combination of two methods, $k\Gamma, B$ -p perturbation and the transfer matrix method, to acquire the electron and hole wave functions numerically. The envelope function approximation was considered to obtain these wave functions for a special basis set. While adjacent valence sub-bands have been determined approximately, the conduction bands are approximated as parabolic. The effect of Stokes shift has also been taken into account. The dipole moment matrix elements for interband atomic transitions are evaluated via the correlation between the electron and hole envelope functions, for both orthogonal polarizations, thus simplifying the calculation of the photoluminescence intensity. Spatial variations in the hole/electron wave functions have been examined with the introduction of piezoelectric and spontaneous polarization internal fields. We theoretically establish the possibility of a highly efficient InGaN red emitter, resulting in a uniform luminescence in red, green, and blue emissions from a white light emitting diode by adjusting the material composition, internal field, and well thickness. [J224]

"Effects of Moist Environments on LED Module Reliability"

Unless their reliability is no longer a concern, light-emitting diodes (LEDs) will be unable to be used for broader applications. One important factor in the operating environment of LEDs is moisture, which is always present if the packaging is not hermetically sealed. In order to investigate the effects of moisture on the reliability of LEDs, several high-power white LEDs were subjected to extremely moist conditions at different temperature points in this study. Different light-output regression rates were measured. Digital microscopy was used to observe moisture diffusion on the LED module. The results demonstrate that the light output of LEDs decreases as the environmental moisture changes. Moisture diffuses into the interfaces of the packaging material, which not only decreases light output but may also disable the LED module due to electronic failure. [J225]

"Si Nano-Dots and Nano-Pyramids Dependent Light Emission and Charge Accumulation in ITO/SiO₂/p-Si MOS Diode"

The current blocking and charge accumulation effects of an ITO/Si-rich SiO₂/p-Si MOS diode with buried Si nano-dots and SiO₂/Si interfacial Si nano-pyramids are characterized. The ITO/Si-rich SiO₂/p-Si MOS diodes exhibits the 3.5 $\Gamma, B \pm 0.2$ nm large Si nano-dots with volume density of 4-5 Γ B—1018cm⁻³. At the SiO₂/p-Si interface, the area density of Si nano-pyramids is increasing from 1.3 Γ B—109 to 1.6 Γ B—1011cm⁻², which greatly decreases turn-on voltage of the MOS diode from 182 to 52 V, thus enhancing the electro-luminescent power from 17.5 to 50.4 nW. The current blocking phenomenon of such a MOS diode become serious with lengthening step-voltage delay, indicating that a significant charge accumulation associated with a strong screening field is generated within Si-rich SiO₂ layer. It was observed that the turn-on voltage with Si nano-pyramids evidently decreases to 31.6 V under reverse biased conditions for tunneling holes. Counter-clockwise C-V hysteresis analysis reveals a flat-band voltage shift of 8.5 V for electron and -12.9 V for hole, showing nonlinear function with either Si nano-dot volume or density. The C-t retention shows higher charge loss rate for electrons (7.6%) than for holes (1.5%) within 0.5 hr due to low SiO₂/Si nano-dot barrier. [J226]

"An Ultra-Low-Power Pulse Oximeter Implemented With an Energy-Efficient Transimpedance Amplifier"

Pulse oximeters are ubiquitous in modern medicine to noninvasively measure the percentage of oxygenated hemoglobin in a patient's blood by comparing the transmission characteristics of red and infrared light-emitting

diode light through the patient's finger with a photoreceptor. We present an analog single-chip pulse oximeter with 4.8-mW total power dissipation, which is an order of magnitude below our measurements on commercial implementations. The majority of this power reduction is due to the use of a novel logarithmic transimpedance amplifier with inherent contrast sensitivity, distributed amplification, unilateralization, and automatic loop gain control. The transimpedance amplifier, together with a photodiode current source, form a high-performance photoreceptor with characteristics similar to those found in nature, which allows LED power to be reduced. Therefore, our oximeter is well suited for portable medical applications, such as continuous home-care monitoring for elderly or chronic patients, emergency patient transport, remote soldier monitoring, and wireless medical sensing. Furthermore, our design obviates the need for an A-to-D and digital signal processor and leads to a small single-chip solution. We outline how extensions of our work could lead to submilliwatt oximeters. [J227]

"Design Criteria for Near-Ultraviolet GaN-Based Light-Emitting Diodes"

We discuss, through numerical device simulation, a number of possible design approaches intended for optimizing the internal quantum efficiency (IQE) of light-emitting diodes based on InGaN quantum wells (QWs) grown along the c-axis emitting in the near-ultraviolet region. We study the effects on IQE of thickness, doping, and alloy composition of the electron and hole blocking layers in order to maximize the confinement of both carrier species in the active region. We discuss the selection of the number of QWs to be employed in the active region and their optimum width, and we show the comparatively minor effects of the thickness of the barrier layers. We also compare different strategies for barrier doping, confirming that a p-type doping in all barriers helps to compensate the spontaneous and piezoelectric surface charges and to enhance hole transport. Finally, we evaluate the impact of Auger recombination on IQE and its role in the experimentally observed efficiency droop. Whenever possible, we suggest practical design criteria and provide technologically feasible sets of design parameters. [J228]

"Heterostructured White Light-Emitting Diode: Nanoscale Interface Analysis and Electroluminescence Studies"

n-ZnO/n-GaAs heterostructured light-emitting diodes have been fabricated by a low-cost ultrasonic spray pyrolysis technique. Nanoscale interface analysis was carried out with scanning transmission electron microscopy. An ~ 8.6-nm-thick amorphous GaAsZnInO was found in the n-ZnO/n-GaAs interface. A strong and broad white electroluminescence band centered at ~ 525 nm and a weak near-infrared emission peaked at ~ 815 nm were observed when n-GaAs was positively biased. The 815-nm emission is believed to be related to the interface layer, and the 525-nm emission is assigned to the recombination of electrons from conduction band to deep-level holes in the ZnO layer. [J229]

"Guest Editorial Special Issue on Light-Emitting Diodes"

There are eight invited papers and 12 contributed papers in this special issue on light-emitting diodes. [J230]

"High Efficiency GaN Light-Emitting Diodes With Two Dimensional Photonic Crystal Structures of Deep-Hole Square Lattices"

We report the enhanced light extraction of a square lattice photonic crystal GaN LED with a lattice constant of 460 nm and holes with a depth of 500 nm drilled through InGaN/GaN multiple quantum wells (MQWs) using laser holography and inductively coupled plasma reactive ion etching. In spite of the etching through the MQWs leading to undesirable surface recombination, the photonic crystal LEDs exhibited 1.37 times higher light extraction than that of the LEDs without photonic crystals at 20 mA. Theoretical studies using the 3-dimensional finite-difference time domain method show that the increase of the extraction efficiency with increasing etch depth is due to the increase of the density of the leaky modes into the air. [J231]

"Nitride Nanocolumns for the Development of Light-Emitting Diode"

The progress of light-emitting-diode (LED) development based on nitride nanocolumn (NC) growth, including InGaN/GaN quantum-well (QW) growth on NCs and regularly arranged GaN NC growth, is first reviewed. Then, the coalescence-overgrowth results based on patterned GaN NC growth are introduced. The overgrowth quality dependence on NC cross-sectional size and NC spacing size is discussed. Generally, a smaller NC dimension and spacing size lead to higher overgrowth quality, including lower threading dislocation (TD) density and larger lateral domain size. Next, the emission enhancement results of blue- and green-emitting InGaN/GaN QW and LED structures based on NC growth and coalescence overgrowth are presented. Significant enhancements (up to ~100% output intensity increase in a blue LED) are demonstrated. For LED applications, the TD density reduction in an overgrown GaN template can more effectively enhance the emission efficiency of a blue LED,

when compared with a green LED. [J232]

"Five-Primary-Color LCDs"

We demonstrate a wide color gamut and high brightness LCD TV using a conventional cold cathode fluorescent lamp (CCFL) backlight with five-primary (red, green, blue, yellow, and cyan) colors. Without changing the CCFL backlight and pixel size, the color gamut is widened from ~72% to ~90% and meanwhile the white brightness is increased by more than 20%, as compared to the three-primary. We also validate our simulation results using a 32" five-primary multi-domain vertical alignment LCD TV prototype. The agreement is reasonably good. [J233]

"Mechanisms of lighting enhancement of Al nanoclusters-embedded Al-doped ZnO film in GaN-based light-emitting diodes"

Aluminum (Al)-doped ZnO (AZO) films with embedded Al nanoclusters were proposed and utilized to enhance the light output power and maximum operation current of GaN-based light-emitting diodes (LEDs). The AZO films were sputtered using ZnO and Al targets in a magnetron cosputtering system. With Al dc power of 7 W and ZnO 100 W ac power, the electron concentration of $4.14 \times 10^{20} \text{ cm}^{-3}$, electron mobility of $16.2 \text{ cm}^2/\text{V s}$, and resistivity of $7.24 \times 10^{-4} \Omega \text{ cm}$ were obtained for the deposited AZO film annealed at 600°C for 1 min in a N_2 ambient. As verified by a high resolution transmission electron microscopy, the deposited AZO films with embedded Al nanoclusters were clearly observed. A 35% increase in light output power of the GaN-based LEDs with Al nanoclusters-embedded AZO films was realized compared with the conventional LEDs operated at 500 mA. It was verified experimentally that the various characteristics of GaN-based LEDs including the antireflection, light scattering, current spreading, and the light extraction efficiency in light emission could be significantly enhanced with the use of Al nanoclusters-embedded AZO films. [J234]

"Multilayer structured polymer light emitting diodes with cross-linked polymer matrices"

Currently, there is great interest in manufacturing multilayer polymer light emitting diode (PLED) structures via low-cost solution-based spin-casting or printing methods. The difficulty with this approach is that solvent from freshly deposited films often dissolves the underlying layers. This letter demonstrates that fully operational multilayer PLED structures can be fabricated via a solution process by embedding the hole transport material in cross-linked inert polymer matrices that protect the functional material while subsequent layers are deposited using the same solvent. The resulting devices exhibited greatly improved quantum efficiency compared with devices that did not employ cross-linked polymer matrices. [J235]

"Low-temperature electroluminescence quenching of AlGaIn deep ultraviolet light-emitting diodes"

The temperature-dependent electroluminescence (EL) properties of AlGaIn deep ultraviolet light-emitting diodes (LEDs) have been studied. The low-temperature EL quenching is observed in 265 nm LEDs with p-type AlGaIn heterostructure, which has not previously been reported in such short wavelength devices. However, this phenomenon disappears in those with a thin i-AlIn electron blocking layer (EBL). It is found that the electron overflow becomes more severe at low temperature in the LEDs without EBL, whereas it is suppressed effectively in those with AlIn EBL. On the basis of a model of temperature-dependent efficiency, the EL quenching is explained by the competition of electron overflow and radiative recombination. [J236]

"Size-dependent light output, spectral shift, and self-heating of 400 nm InGaIn light-emitting diodes"

We have systematically investigated the impact of device size scaling on the light output, spectral shift, and self-heating of 400 nm InGaIn light-emitting diodes (LEDs). Devices with diameters in the range 20-300 μm have been studied. It is shown that smaller LED pixels can deliver higher power densities (despite the lower absolute output powers) and sustain higher current densities. Investigations of the electroluminescence characteristics of differently sized pixels against current density reveal that the spectral shift is dominated by blueshift at the low current density level and then by redshift at the high current density level, owing to the competition between the bandgap shrinkage caused by self-heating and band-filling effects. The redshift of the emission wavelength with increasing current density is much faster and larger for the bigger pixels, suggesting that the self-heating effect is also size dependent. This is further confirmed by the junction-temperature rise measured by the established spectral shift method. It is shown that the junction-temperature rise in smaller pixels is slower, which in turn explains why the smaller redshift of the emission wavelength with current density is present in smaller pixels. The measured size-dependent junction temperature is in reasonable agreement with finite element method simulation results. [J237]

"Analysis of metal-oxide-based charge generation layers used in stacked organic light-emitting"

diodes"

We study electron and hole injection in MoO₃ charge generation layers (CGLs) commonly used for establishing balanced injection in multilayer stacked organic light-emitting diodes (SOLEDs). A compound CGL consisting of 100-Å-thick MoO₃ and Li-doped 4,7-diphenyl-1,10-phenanthroline in a 1:1 molar ratio is demonstrated to have a high electron generation efficiency. Charge injection from the compound CGL is modeled based on a two-step process consisting of tunneling-assisted thermionic emission over an injection barrier of (1.2 ± 0.2) eV and a trap level due to oxygen vacancies at (0.06 ± 0.01) eV above the MoO₃ valence band edge. Peak external quantum efficiencies (EQEs) of $(10.5 \pm 0.2)\%$, $(10.1 \pm 0.2)\%$, $(8.6 \pm 0.2)\%$, and $(8.9 \pm 0.2)\%$ are obtained for tris-(phenylpyridine)iridium-based electrophosphorescent OLEDs with indium tin oxide (ITO) anode/CGL cathode, CGL anode/CGL cathode, CGL anode/Al cathode, and ITO anode/Al cathode contacts, respectively. Based on our analysis, a three-element green emitting electrophosphorescent SOLED is demonstrated with a peak forward-viewing EQE = $(24.3 \pm 1.0)\%$ and a power efficiency of (19 ± 1) lm/W. [J238]

"Geometric centre tracking of tagged objects using a low power demodulation smart vision sensor"

In this study, a modulated light detecting smart CMOS image sensor is presented. The design has the ability to sense asynchronous signals transmitted from electronic markers such as flashing light emitting diodes (LEDs) tagged on moving objects. The geometric centre of the detected region is returned as the output result. With the presented sensor, object localisation and position detection functions are simplified, performed at higher speeds in real time and power requirement is reduced. The sensor in-pixel processing filters out the background image data, detects the modulated marker regions and projects the extracted region on the two axes, while the geometric centre extraction units placed at each axis identify the coordinates assigned to the marker. The design presents less sensitivity to object texture compared with techniques based on edge extraction or binarisation. The sensor has been designed as a 64 ГrB— 64 pixel VLSI CMOS chip in the 0.35 ГrBim standard CMOS technology and analysed in the presence of mismatches and noise. Issues such as sensor array scalability, speed and power dissipation are also examined in this study and features of the sensor are reported and compared with some previous designs. [J239]

"Effect of neutron irradiation on electrical and optical properties of InGaN/GaN light-emitting diodes"

InGaN/GaN multiquantum well light-emitting diodes (LED) with emission wavelength of 450 nm were irradiated with average energy of 9.8 MeV and dose of 5.54×10^{11} cm⁻² neutrons. Right after irradiation, the forward current of the irradiated LEDs was decreased as a result of the creation of deep levels by the neutron-induced lattice displacement. However, unstable lattice damages resulting from the collisions with the incoming neutrons were removed at room temperature 6 days after the irradiation. The diode turn-on voltage, ideality factor, and optical emission intensity were recovered to preirradiated state by self-annealing process at room temperature. [J240]

"Correlation of energy band alignment and turn-on voltage in organic light emitting diodes"

The correlation of energy alignment and turn-on voltage of organic light emitting diodes (OLEDs) was investigated. With identical hole transport layers (HTLs) and electron transport layers (ETLs), the turn-on voltages of OLEDs are always the same, regardless of the cathode structures, such as Ca, Al, LiF/Al, and Cs₂CO₃/Al. For devices with various combinations of HTLs and ETLs, the turn-on voltages are equal to the energy difference between the lowest unoccupied molecular orbital of ETLs and the highest occupied molecular orbital of HTLs, taking into consideration of vacuum level shift at organic interfaces measured from ultraviolet photoemission spectroscopy. [J241]

"Enhancing the Brightness of Parallax Barrier Based 3D Flat Panel Mobile Displays Without Compromising Power Consumption"

This paper presents an alternative approach for achieving higher optical efficiency in conventional parallax barrier 3D mobile displays. The method entails modifying and enhancing the protrusion structure of conventional multi-domain vertical alignment (MVA) pixel arrays plus the storage capacitors (C_{st}) of the pixel circuitry which increase effective pixel transmission area by a factor of 1.07. Hiding the modified storage capacitor under the parallax barrier strip increases the barrier gap or slit size by a factor of 1.52. The result is a structure that enhances mobile displays' optical efficiency by a compounded factor slightly over 60% without compromising power consumption. [J242]

"Characteristics of an AlGaInP-Based Light Emitting Diode With an Indium-Tin-Oxide (ITO) Direct Ohmic Contact Structure"

An AlGaInP multi-quantum-well (MQW) light-emitting diode (LED) with a direct Ohmic contact structure, formed

by an indium-tin-oxide (ITO) transparent film and AuBe diffused thin layer, is fabricated and studied. By the deposition of an AuBe metallic thin layer on the surface of Mg-doped GaP window layer, followed by a thermal activation process, a direct Ohmic contact between ITO and p-GaP layers can be obtained. Experimentally, under an injection current of 20 mA, a dynamic resistance of 5.7 Ω , and a forward voltage of 1.91 V, are obtained. In addition, a higher external quantum efficiency of 9.7% and a larger maximum light output power of 26.6 mW are found for the studied LED. As compared with the conventional LED without this structure, the external quantum efficiency of the studied device is increased by 26% under the injection current of 100 mA. This is mainly attributed to the reduced series resistance resulted from the relatively uniform distribution of AuBe atoms near the GaP layer surface and the effective current spreading ability by the use of ITO film. Moreover, the life behavior is not degraded by using this AuBe diffused layer for the studied LED under a 20 mA operation condition. [J243]

"UV Electroluminescence and Structure of n-ZnO/p-GaN Heterojunction LEDs Grown by Atomic Layer Deposition"

Atomic layer deposition technique and subsequent rapid thermal annealing (RTA) were implemented to grow high-quality ZnO epilayers for the fabrication of n-ZnO/p-GaN heterojunction LEDs. The X-ray diffraction measurement reveals that the ZnO epilayer has high crystallinity with c-axis orientation. Transmission electron microscopy images present that the ZnO layer is a single crystal, including only a few survivals of threading dislocations, which were generated in the GaN layer deposited by metal-organic chemical vapor deposition on the c-Al₂O₃ substrate and most of which were eliminated at the n-ZnO/p-GaN interface. An interfacial layer 4-5 nm thick caused by the RTA treatment was observed between the n-ZnO and p-GaN layers. Room temperature UV electroluminescence (EL) at 391 nm from ZnO was achieved at a low injection current about 10 mA. It is concluded that the competition between the ELs from the n-ZnO and p-GaN (around 425 nm) may be ascribed to the ZnO/GaN interface states coupled with the differences between the n-ZnO and p-GaN in carrier concentration and light emission efficiency. [J244]

"Target Practice"

Discusses how the projects in the Winners & Losers issue are chosen and evaluated. [J245]

"Efficient spin injection into semiconductor from an Fe /GaO x tunnel injector"

We examined the electrical injection of spin-polarized electrons into a GaAs-based light-emitting diode structure from a Fe/GaO tunnel injector whose electron-charge injection efficiency was comparable to that of a conventional Fe/n⁺-AlGaAs ohmic injector. A high circular polarization of electroluminescence up to 20% was observed at 2 K. The combination of effective spin- and charge-injection efficiencies makes GaOx a promising tunnel barrier for GaAs-based spintronic devices. [J246]

"You've got that glow"

A light-therapy machine called ReGen, produced by Energist, in Swansea, Wales, uses high intensity LEDs, which the company claims will soften skin, smooth wrinkles, and erase blemishes. Each of the four light boxes has a 255- by 70-millimeter panel containing 1024 LEDs. At wavelengths of 415 nanometers, they glow blue; when they're set at 630 nm, they're red. A third mode--which produces purple light by mixing blue and red--is claimed to combine the benefits of both treatments. Twenty minutes twice a week is supposed to reduce the signs of aging. [J247]

"4G in the U.S.A."

Fourth-generation wireless got its official start in the United States one year ago when Clearwire Wireless made Portland, Ore., the first city to be covered by its WiMax wireless "last mile" broadband connection. Twelve months later, the shape of wireless's future is now clearly outlined: WiMax has the early lead but will eventually be overtaken by another technology. [J248]

"III-Nitride-Based Light-Emitting Diodes With GaN Micropillars Around Mesa and Patterned Substrate"

In this paper, the textured-sidewall mesa and GaN microsize pillars (Γ , Bi -pillars) around the mesa region were fabricated on III-nitride light-emitting diodes (LEDs) with a patterned sapphire substrate (PSS). We demonstrated that the light-waveguide mode outside the mesa region of III-nitride LEDs could be disrupted by a GaN Γ , Bi -pillar around the mesa region and PSS. We found that the power enhancement of LEDs with textured sidewall, Γ , Bi -pillars around the mesa, and PSS from ray-tracing simulation was about 65% larger than that of

conventional LEDs. It was found that we could achieve a high power enhancement of about 60% of LEDs with textured sidewall, Γ ,Bi $\bar{\Gamma}$ -pillars around the mesa, and a patterned substrate, and it was close to the result of simulation. It was also found that the light intensity outside the mesa region with Γ ,Bi $\bar{\Gamma}$ -pillars of LEDs with or without a patterned substrate would decay in proportion to the distance away from the mesa edge, by studying the light emission intensity image of the whole LEDs. The decay lengths for the textured sidewall and Γ ,Bi $\bar{\Gamma}$ -pillars around the mesa LEDs with or without a patterned substrate are 12 and 17 Γ ,Bi $\bar{\Gamma}$ m, respectively. We understand that the light outside the mesa region could be extracted earlier by introducing the GaN Γ ,Bi $\bar{\Gamma}$ -pillars and patterned substrate together. [J249]

"Influence of Die Attach Layer on Thermal Performance of High Power Light Emitting Diodes"

In this paper, the influence of the die attach adhesive (DAA) layer on the thermal performance of high power light emitting diodes was first investigated by using finite element analysis, and some key results were verified by the experimental data. Effective thermal management of the studied light emitting diode package can be achieved by selecting a DAA material with a proper thermal conductivity and by manipulating the geometry parameters of the DAA layer, such as the DAA area, and the bond-line thickness. The significance of DAA thermal conductivity to heat dissipation was further demonstrated by an analysis of the bottleneck to heat transfer. [J250]

"Self-Assembled Two-Dimensional Surface Structures for Beam Shaping of GaN-Based Vertical-Injection Light-Emitting Diodes"

Enhanced light extraction and beam shaping of GaN-based vertical-injection light-emitting diodes (VI-LEDs) employing biomimetic surface structures were demonstrated. The biomimetic surface structures were fabricated using self-assembled polystyrene nanospheres serving as a monolayer mask, and followed by anisotropic inductively coupled plasma reactive ion etching. The light output power of the VI-LEDs with the patterned structures exhibited an efficiency enhancement factor of 68% at a driving current of 350 mA, compared to those without any surface structures. The structures also resulted in a modified heart-shaped radiation pattern, which is preferable for backlight applications in flat panel displays. [J251]

"Toward a Germanium Laser for Integrated Silicon Photonics"

It has been demonstrated theoretically and experimentally that germanium, with proper strain engineering and n-type doping, can be an efficient light emitter and a gain medium at its direct bandgap within the third optical communication window (~1520-1620 nm). In this paper, we systematically discuss the effect of strain, doping, and temperature on the direct-gap optical gain in germanium. For electrically pumped devices, properties and design guidelines of Ge/Si heterojunction are also analyzed and compared with the results from fabricated Ge/Si heterojunction LEDs. [J252]

"Mechanism Investigation of p-i-n ZnO-Based Light-Emitting Diodes"

Using a cosputtering technique to deposit P-ZnO: AlN film and using a vapor cooling condensation system to deposit n-ZnO: In and i-ZnO films on sapphire substrates, thin-film-type ZnO-based light-emitting diodes (LEDs) were fabricated. A Nd: YAG laser with a wavelength of 413 nm is utilized to identify the defect-related emissions of p-ZnO, i-ZnO, and n-ZnO films. The characteristics of i-ZnO layer of ultraviolet (UV) emissions were analyzed using temperature-dependent photoluminescence. The mechanism of the UV electroluminescence emission peak at 3.20 eV observed from the p-i-n ZnO-based LEDs were attributed to the low deep-level defects and the radiative recombination occurred in the i-ZnO layer. [J253]

"LED-Based Optical Device for Chronic In Vivo Cerebral Blood Volume Measurement"

We demonstrate a reflectivity-based cerebral blood volume sensor comprised of surface-mount light-emitting diodes on a flexible substrate with integrated photodetectors in a form factor suitable for direct brain contact and chronic implantation. This reflectivity monitor is able to measure blood flow through the change of the surface reflectivity and, through this mechanism, detect the cerebral-blood-volume changes associated with epileptic seizures with a signal-to-noise (SNR) response of 42 dB. The device is tested in an in vivomodel confirming its compatibility and sensitivity. The data taken demonstrate that placing the sensor into direct brain contact improves the SNR by more than four orders of magnitude over current noncontact technologies. [J254]

"Recent Advances in ZnO-Based Light-Emitting Diodes"

ZnO has attracted considerable attention for optical device applications because of several potential advantages over GaN, such as commercial availability of bulk single crystals and a larger exciton binding energy (~60 meV

compared with ~25 meV for GaN). Recent improvements in the control of background conductivity of ZnO and demonstrations of p-type doping have intensified interest in this material for applications in light-emitting diodes (LEDs). In this paper, we summarize recent progress in ZnO-based LEDs. Physical and electrical properties, bandgap engineering, and growth of n- and p-type ZnO thin films are also reviewed. [J255]

"GaN-Based LEDs With AZO:Y Upper Contact"

We report the fabrication of GaN-based light-emitting diodes (LEDs) with ytterbium-doped alumina-zinc-oxide (AZO:Y) upper contact. It was found that AZO and AZO:Y are both highly transparent in the visible region with good thermal stability optically. However, it was found that AZO:Y is much more thermally stable electrically, as compared with AZO. Furthermore, it was found that the output power of GaN LEDs with AZO upper contact decreased significantly from 2.80 to 2.30 mW after 700°C annealing. With the same annealing condition, it was found that output power decreased only slightly from 2.77 to 2.69 mW for the LEDs with AZO:Y upper contact. [J256]

"Temperature Measurement Technique for Stabilizing the Light Output of RGB LED Lamps"

The efficiency of light-emitting-diode (LED) lights approaches that of fluorescent lamps. LED light sources find more applications than conventional light bulbs due to their compactness, lower heat dissipation, and real-time color-changing capability. Stabilizing the colors of red-green-blue (RGB) LED lights is a challenging task, which includes color light intensity control using switching-mode power converters, color point maintenance against LED junction temperature change, and limiting LED device temperature to prolong the LED lifetime. In this paper, we present a LED junction temperature measurement technique for a pulsedwidth modulation diode forward current controlled RGB LED lighting system. The technique has been automated and can effectively stabilize the color without the need for using expensive feedback systems that involve light sensors. Performance in terms of chromaticity and luminance stability for a temperature-compensated RGB LED system will be presented. [J257]

"Bridging Physics to Electronics-An Outreach Effort"

Physics has been an important part of the science curriculum in high schools. Without the appropriate high school physics background, it is difficult for a student subsequently to pursue an electronics engineering program at the university level since a good understanding of many concepts in physics is required to comprehend the material covered in electronics-related courses. Unfortunately, a phenomenon observed in today's high schools is a clear diminution of student interest in physics, leading to dwindling physics class sizes compared to a decade ago. The lack of interest in and passion for physics at the high school level ultimately leads to smaller intakes at the university level for electronics engineering courses and/or lower qualification cutoffs for students entering the programs. This results in a significant reduction in good students graduating from engineering programs. This paper will first share survey results that reveal possible reasons behind the decreasing number of students entering engineering programs. Two concerted efforts launched from the National University of Singapore (NUS) to arrest the declining interest in high schools will then be presented. [J258]

"A High-Efficiency Dimmable LED Driver for Low-Power Lighting Applications"

This paper presents a dimmable light-emitting diode (LED) driver with adaptive feedback control for low-power lighting applications. An improved pulsedwidth modulation dimming technique is studied for regulating the LED current and brightness. Under universal input voltage operation, high efficiency and high power factor can be achieved by a coupled inductor single-ended primary inductance converter power factor correction (PFC) converter with a simple commercial transition-mode PFC controller. The operation principles and design considerations of the studied LED driver are analyzed and discussed. A laboratory prototype is also designed and tested to verify the feasibility. [J259]

"Transient Charge Feedforward Driver for High-Speed Current-Mode Data Driving in Active-Matrix OLED Displays"

A transient charge feedforward driver (TCFD) is presented for high-speed current-mode data driving in active-matrix organic LED (AMOLED) displays. In order to provide charging current for the parasitic capacitance of a column line (CL), TCFD adaptively generates the required charging current by taking advantage of the parasitic capacitance of another adjacent CL. The TCFD can dramatically enhance the data driving speed by driving a CL with the summing current of data and the required charging current. The adaptive generation of the required charging current and the summing operation are realized by the simultaneous operation of negative- and positive-feedback loops. The loop transfer function is revealed and the stability conditions are discussed. By applying the TCFD, a 70 ns driving speed is achieved for 20 nA of data current. The driving speeds are almost

constant for CL conditions up to 6 k Ω and 40 pF. The TCFD is fabricated in a standard 0.35- μ m CMOS process and the performance of the TCFD is evaluated by on-chip panel emulation. [J260]

"Comparative Study on the Structural Designs of LED Devices and Systems Based on the General Photo-Electro-Thermal Theory"

An investigation into the effects of the structures of both LED devices and systems on the luminous performance is presented. Single-chip and multichip LED structures and concentrated and distributed LED systems are studied and compared. Practical tests on both of the device and system levels have confirmed the theoretical predictions that parallel LED structures can lead to much lower thermal resistance and thus higher luminous output. The results of this paper contribute to new information for both LED device manufacturers and system designers toward the optimization of the LED technology. [J261]

"An Optically Coupled System for Quantitative Monitoring of MRI-Induced RF Currents Into Long Conductors"

The currents induced in long conductors such as guidewires by the radio-frequency (RF) field in magnetic resonance imaging (MRI) are responsible for potentially dangerous heating of surrounding media, such as tissue. This paper presents an optically coupled system with the potential to quantitatively measure the RF currents induced on these conductors. The system uses a self shielded toroid transducer and active circuitry to modulate a high speed light-emitting-diode transmitter. Plastic fiber guides the light to a photodiode receiver and transimpedance amplifier. System validation included a series of experiments with bare wires that compared wire tip heating by fluoroptic thermometers with the RF current sensor response. Validations were performed on a custom whole body 64 MHz birdcage test platform and on a 1.5 T MRI scanner. With this system, a variety of phenomena were demonstrated including cable trap current attenuation, lossy dielectric Q-spoiling and even transverse electromagnetic wave node patterns. This system should find applications in studies of MRI RF safety for interventional devices such as pacemaker leads, and guidewires. In particular, variations of this device could potentially act as a realtime safety monitor during MRI guided interventions. [J262]

"A Method of Reducing the Peak-to-Average Ratio of LED Current for Electrolytic Capacitor-Less AC-DC Drivers"

This paper proposes a concept of electrolytic capacitor-less light-emitting diode (LED) driver, which converts the commercial ac voltage to a pulsating current with twice the line frequency driving high-brightness LEDs. As no electrolytic capacitor is used, this driver possesses the unique advantage of long lifetime to match with that of LEDs. A method of injecting the third and fifth harmonics into the input current to reduce the peak-to-average ratio of the output current is also proposed. While ensuring that the input power factor is higher than 0.9 to meet regulation standards such as ENERGY STAR, the proposed method allows the peak-to-average ratio of the output current to be reduced to 1.34 theoretically, which is beneficial for the safe operation of the LEDs. As an example, a flyback-based electrolytic capacitor-less LED driver is proposed, and its operation is analyzed. In order to inject the third and fifth harmonics into the input current, the function of the duty cycle in a half-line cycle is derived. It is then simplified to a fitting function, which can be easily implemented with the input voltage sensing. A 25 V, 0.35 A output prototype is built and tested in the laboratory, and the experimental results are presented to verify the effectiveness of the electrolytic capacitor-less LED driver and its control method. [J263]

"LED Driver Circuit with Series-Input-Connected Converter Cells Operating in Continuous Conduction Mode"

This paper introduces an LED driver circuit implemented by series-input-connected converter cells with a common duty cycle control approach operating from a dc voltage bus. With this structure, low-voltage high-frequency ICs and low-profile components can be applied in high-voltage applications. Flexibility is provided for the cells to work under different voltage supply conditions by simply changing the number of series converters. With the converters operating in continuous conduction mode, the common duty cycle control approach enables automatic line voltage sharing and output current copying. The approach results in a control-to-output transfer function of the system close to that of a single converter for ease of feedback loop design. The modular approach also allows continued operation in the presence of open-circuit LED failures. Design considerations and experimental results are presented for a 25-W three-cell system with 9 Luxeon K2 high-brightness LEDs, demonstrating line voltage sharing, output current copying, and LED failure response. [J264]

"GaN Substrates for III-Nitride Devices"

Despite the rapid commercialization of III-nitride semiconductor devices for applications in visible and ultraviolet

optoelectronics and in high-power and high-frequency electronics, their full potential is limited by two primary obstacles: i) a high defect density and biaxial strain due to the heteroepitaxial growth on foreign substrates, which result in lower performance and shortened device lifetime, and ii) a strong built-in electric field due to spontaneous and piezoelectric polarization in the wurtzite structures along the well-established [0001] growth direction for nitrides. Recent advances in the research, development, and commercial production of native GaN substrates with low defect density and high structural and optical quality have opened opportunities to overcome both of these obstacles and have led to significant progress in the development of several optoelectronic and high-power devices. In this paper, the recent achievements in bulk GaN growth development using different approaches are reviewed; comparison of the bulk materials grown in different directions is made; and the current achievements in device performance utilizing native GaN substrate material are summarized. [J265]

"Impact of Trapped Charge and Interface Defects on the Degradation of the Optical and Electrical Characteristics in OLEDs"

Electroluminescence degradation mechanisms in small-molecule-based organic light-emitting diodes (OLEDs) have been investigated. We focused on intrinsic degradation phenomena that determine the decrease in the optical power of OLEDs during standard operation. The study was carried out on simplified OLED structures, by means of combined optical and electrical characterization techniques. The results of this analysis provide information on the physical processes responsible for OLED degradation, suggesting a strong correlation between the reduction in the luminance intensity of the devices and the creation of both positive trapped charge and neutral electron traps at the Alq3/NPD interface. The evidence reported in this paper supports the hypothesis that degradation is due to the instability of the cationic Alq3 species. [J266]

"High-Efficiency Blue Emitting Phosphorescent OLEDs"

In this paper, we will show our latest results on high-efficiency blue phosphorescent organic light-emitting diodes (PHOLEDs). Effects of triplet exciton confinement, exciton energy transfer and charge trapping, and charge balance on iridium(III)bis [(4,6-di-fluorophenyl)-pyridinato-N,C2'] picolate (FIrpic)-based blue PHOLEDs will be presented. By optimizing the aforementioned device parameters, a high-efficiency blue PHOLED with 59 cd/A (48 lm/W at 100 cd/m²) was demonstrated. [J267]

"Ultraviolet ZnO Nanorod/P-GaN-Heterostructured Light-Emitting Diodes"

Both i-ZnO and n-ZnO: In nanorod arrays were grown on a p-GaN layer with an anodic alumina membrane template using a vapor cooling condensation method. Electroluminescence emissions were observed from the resulting p-n (p-GaN/n-ZnO: In nanorod array) and p-i-n (p-GaN/i-ZnO nanorod array/n-ZnO: In nanorod array) heterostructured light-emitting diodes (LEDs). The ultraviolet emission peak at 386 nm observed in the p-i-n heterostructured LEDs was attributed to radiative recombination of the near-band edge in the i-ZnO nanorods. Using power-law fitted current-voltage relationships, it was shown that a space-charge-limited current and associated effects occurred in the p-n and p-i-n nanorod heterostructured LEDs. [J268]

"High-Power and High-Efficiency InGaN-Based Light Emitters"

In this paper, we report on the latest advancements in improving AlGaInN-based visible-light-emitting-diode (LED) efficiency in epitaxy, chip, and package designs. We investigate the fundamental origin of the typical high current Γ -droop of efficiency observed in such LEDs. We show that this effect is most likely not caused by incomplete carrier injection or carrier escape but that it is rather a fundamental material property of InGaN/GaN-heterostructure-based light emitters. The droop can be reduced in improved epitaxial LED active-layer designs. We show how this can be achieved by lowering InGaN volume carrier density in multiple quantum wells (MQWs) and thick InGaN layers. Improved epitaxial MQW structures are then combined with a new advanced chip concept. It is optimized for high efficiency at high current operation and arbitrary scalability and can be manufactured at low cost. This is accomplished by improving light-extraction efficiency, homogenizing the emission pattern, reducing forward voltage, and lowering thermal resistance. The improved high current efficiency can be fully exploited by mounting the chip in the highly versatile new OSLO SSL package. It features very stable package materials, a small footprint, and an electrically isolated design decoupling electrical and thermal contacts. [J269]

"Polymer-MEMS-Based Optoelectronic Display"

In this paper, a novel all-polymer integrated microsystem, which realizes a 2-D display by integrating a 1-D array of polymer light-emitting diodes (PLEDs) with a polymer scanner of microelectromechanical system (MEMS), is presented. Electronic modulation of PLEDs forms the first dimension of the display (fast scan), and the scanner actuation orthogonal to the direction of PLED lineup forms the second one (slow scan). MEMS

scanner (actuator) is fabricated on a polymer composite (FR4 material) with a double-sided process using lithography to pattern copper lines and laser micromachining to cut the scanner outline. PLEDs are fabricated on polyethylene terephthalate sheets. They have a thin-film structure of indium tin oxide, poly (3,4-ethylenedioxythiophene) poly (styrenesulfonate), poly [2-methoxy-5-(2'-ethyl-hexyloxy)-1,4-phenylene vinylene], and aluminum. The scanner is actuated electromagnetically in its slow-scan resonance mode at 49 Hz, generating a maximum displacement of 3.5 mm at a drive power of 84 mW with the help of a mini permanent magnet attached to the tip of the scanner and an off-chip energizing coil. Turn-on voltage of a PLED is 7.5 V, and each one generate a luminance of 0.3 cd/m² at 13 V, consuming 1.1-mA current. Successful operation of the integrated-display system is shown by forming a checker box image with a resolution of 20 ГрБ— 7 and a size of 9 mm by 3.4 mm. [J270]

"Ohmic-Contact Technology for GaN-Based Light-Emitting Diodes: Role of P-Type Contact"

GaN-based semiconductors are of great technological importance for the fabrication of optoelectronic devices, such as light-emitting diodes (LEDs) and laser diodes. The further improvement of LED performance can be achieved through the enhancement of external quantum efficiency. In this regard, high-quality p-type ohmic electrodes having low contact resistance and high transmittance (or reflectivity), along with thermal stability, must be developed because p-type ohmic contacts play a key role in the performance of LEDs. In this paper, we review recent advances in p-type ohmic-contact technology for GaN-based LEDs. A variety of methods for forming transparent and reflective ohmic contacts are introduced. [J271]

"Electrostatic Reliability Characteristics of GaN Flip-Chip Power Light-Emitting Diodes With Metal-Oxide-Silicon Submount"

The electrostatic reliability characteristics of gallium nitride flip-chip (FC) power light-emitting diodes (PLEDs) with metal-oxide-silicon (MOS) submount are investigated for the first time. The electrostatic damage reliability of the reported diode submount and that of our proposed simple structure MOS submount are fabricated and compared. Their corresponding electrostatic protection capabilities are increased from 200 V (conventional PLED) to 500 V (FC-LED on diode submount), to 500 V (FC-LED on MOS submount with a SiO₂ thickness of 297 Å, B_i), and even to a value as high as 1000 V (FC-LED at a SiO₂ thickness of 167 Å, B_i), which are much higher than the PLED industrial test value of 150 V at -5 V/-10 Г, B_i A criterion and are also much more robust than the previous academic reports. [J272]

"Comparison of InGaN-Based LEDs Grown on Conventional Sapphire and Cone-Shape-Patterned Sapphire Substrate"

To improve the external quantum efficiency, a high-quality InGaN/GaN film was grown on a cone-shape-patterned sapphire substrate (CSPSS) by using metal-organic chemical vapor deposition. The surface pattern of the CSPSS seems to be more helpful for the accommodative relaxation of compressive strain related to the lattice mismatch between GaN and a sapphire substrate because the growth mode of GaN on the CSPSS was similar to that of the epitaxial lateral overgrowth. The output power of a light-emitting diode (LED) grown on the CSPSS was estimated to be 16.5 mW at a forward current of 20 mA, which is improved by 35% compared to that of a LED grown on a conventional sapphire substrate. The significant enhancement in output power is attributed to both the increase of the extraction efficiency, resulted from the increase in photon escaping probability due to enhanced light scattering at the CSPSS, and the improvement of the crystal quality due to the reduction of dislocation. [J273]

"Nonpolar and Semipolar III-Nitride Light-Emitting Diodes: Achievements and Challenges"

It has been several years since InGaN/GaN light-emitting diodes (LEDs) on nonpolar and semipolar orientations were first demonstrated. Prominent performance and inherent potential of these crystallographic orientations have been revealed as bulk-GaN substrates of arbitrary orientations became available for epitaxial device growth. At this point in time, we intend to survey the progress made to date and prospect the future requirements for further device improvements. The discussion begins with a historical background: how nonpolar/semipolar orientations were introduced to III-nitride LEDs and why they are beneficial. The discussion then provides information on elementary crystallography and piezoelectricity in addition to the electronic band structure of wurtzite crystals. Later in this paper, LED reports are collected to develop comprehensive knowledge of the past research efforts and trends. Nonpolar and semipolar orientations provide not only high LED performances, e.g., optical output power and wavelength ranges, but also unique functions, e.g., polarized light emission, which will explore new fields of applications. [J274]

"A Review on the Physical Mechanisms That Limit the Reliability of GaN-Based LEDs"

We review the failure modes and mechanisms of gallium nitride (GaN)-based light-emitting diodes (LEDs). A number of reliability tests are presented, and specific degradation mechanisms of state-of-the-art LED structures are analyzed. In particular, we report recent results concerning the following issues: 1) the degradation of the active layer induced by direct current stress due to the increase in nonradiative recombination; 2) the degradation of LEDs submitted to reverse-bias stress tests; 3) the catastrophic failure of advanced LED structures related to electrostatic discharge events; 4) the degradation of the ohmic contacts of GaN-based LEDs; and 5) the degradation of the optical properties of the package/phosphors system of white LEDs. The presented results provide important information on the weaknesses of LED technology and on the design of procedures for reliability evaluation. Results are compared with literature data throughout the text. [J275]

"Efficiency Improvement of GaN-Based LEDs With Microrod Array and Textured Sidewalls"

High-performance nitride-based light-emitting diodes (LEDs) grown with SiO₂microrod array have been demonstrated. The light output power of LEDs with SiO₂microrod array was 9.03% higher than conventional LEDs at the injection current of 20 mA. The improvement contributed to the enhancement of the light extraction efficiency, and epitaxial GaN film quality improved by direct heteroepitaxial lateral overgrowth with SiO₂microrod array. The light output power could be further enhanced by about 18.36% as compared with the conventional LEDs when adopting the textured sidewall surface which use buffered oxide etch to remove SiO₂microrod arrays and use NaOH to etch the sidewall again into an inverted pyramid shape. After the texturing process, the LEDs show higher electroluminescence intensity and broader far-field pattern. Furthermore, the LEDs with SiO₂microrod array and additional wet-etching process will not affect the electrical property. [J276]

"Laboratory Thin-Film Encapsulation of Air-Sensitive Organic Semiconductor Devices"

We present an approach, which is compatible with both glass and polymer substrates, to in-laboratory handling and intra-laboratory shipping of air-sensitive organic semiconductors. Encapsulation approaches are presented using polymer/ceramic and polymer/metal thin-film barriers using commercially available materials and generally available laboratory equipment. A technique for depositing an opaque vapor barrier, a transparent vapor barrier, and an approach to storing and shipping air-sensitive thin-film organic semiconductor devices on both polymer and glass substrates are presented. Barrier performance in air was tested using organic light-emitting diodes (OLEDs) as test devices. The half-life performance of OLEDs on plastic substrates in air exceeded 700 h, and that on glass exceeded 500 h. Commercially available heat-seal barrier bag systems for device shipping and storage in air were tested using a thin film of metallic calcium to test water permeation. More than four months of storage of a metallic calcium film in a heat-sealed foil bag was demonstrated in the best storage system. These approaches allow for the encapsulation of samples for longer duration testing and transportation than otherwise possible. [J277]

"Deep-Ultraviolet Light-Emitting Diodes"

Compact solid-state deep-ultraviolet (DUV) light-emitting diodes (LEDs) go far beyond replacing conventional DUV sources such as mercury lamps. DUV LEDs enable new applications for air, water, and surface sterilization and decontamination, bioagent detection and identification, UV curing, and biomedical and analytical instrumentation. We review materials growth, device physics, design, fabrication, and performance of DUV LEDs with wavelength ranging from 210 to 365 nm, describe prototype systems for water purification and sterilization, and discuss other emerging applications and systems using DUV LEDs. [J278]

"Blue Organic LEDs With Improved Power Efficiency"

High-power-efficiency blue fluorescent organic light-emitting devices have been demonstrated by simultaneously doping two hole-conduction layers of 4, 4', 4''-Tris(N-3-methylphenyl-N-phenyl-amino) triphenylamine (m-MTDATA), and N, N'-diphenyl-N, N'-bis(1-naphthyl)-(1, 1'-biphenyl)-4, 4'-diamine (NPB) with 2, 3, 5, 6-tetrafluoro-7,7,8,8-tetracyano-quinodimethane (F4-TCNQ) as well as doping two ambipolar emission layers with p-bis(p-N, N-diphenyl-aminostyryl) benzene (DSA-Ph). By doping the two host layers with DSA-Ph to form the double emission layer, the current efficiency is enhanced due to the extended emission zone. We further increase the performance by introducing the doping F4-TCNQ into the hole-injection and transporting layers to reduce the transport barrier at the m-MTDATA:F4TCNQ/NPB and to enhance the hole injection and conduction. The luminance and power efficiencies reach 8.9 cd/A and 4.5 lm/W, respectively. [J279]

"Highly efficient fluorescent-phosphorescent triplet-harvesting hybrid organic light-emitting diodes"

We demonstrate highly efficient white and nonwhite hybrid organic light-emitting diodes (OLEDs) in which singlet and triplet excited states, generated in the recombination zone, are utilized by fluorescence and

phosphorescence, respectively. The excited states are formed at a blue fluorescent light-emitting layer (LEL), and the triplets diffuse through a spacer layer to one or more phosphorescent LEL(s). A key feature enabling the triplet diffusion in such OLEDs is the use of a blue fluorescent emitter with triplet energy above, or not much below, that of the fluorescent host. Additional material properties required for triplet harvesting are outlined. At 1000cd/m² a blue and yellow harvesting OLED shows 13.6% external quantum efficiency, 3.8 V, 30.1 lm/W, and color characteristics suitable for display application. High-efficiency harvesting R+G+Bwhite, and B+G and B+Rnonwhite OLEDs are also demonstrated. The triplet-harvesting mechanism was verified in all devices by physical methods including spectral analysis, time-resolved electroluminescence, magnetic field effect, and electron paramagnetic resonance. [J280]

"Multivariable Robust Control for a Red-Green-Blue LED Lighting System"

This paper proposes a novel control structure for a red-green-blue (RGB) LED lighting system, and applies multivariable robust control techniques to regulate the color and luminous intensity outputs. RGB LED is the next-generational illuminant for general lighting or liquid crystal display backlighting. The most important feature for a polychromatic illuminant is color adjustability; however, for lighting applications using RGB LEDs, color is sensitive to temperature variations. Therefore, suitable control techniques are required to stabilize both luminous intensity and chromaticity coordinates. In this paper, a robust control system was proposed for achieving luminous intensity and color consistency for RGB LED lighting in a three-step process. First, a multivariable electrical-thermal model was used to obtain RGB LED luminous intensity, in which a lookup table served as a feedforward compensator for temperature and power variations. Second, robust control algorithms were applied for feedback control design. Finally, the designed robust controllers were implemented to control the luminous and chromatic outputs of the system. From the experimental results, the proposed multivariable robust control was deemed effective in providing steady luminous intensity and color for RGB LED lighting. [J281]

"Degradation Mechanisms of InGaN Laser Diodes"

We discuss various mechanisms of laser diode degradation based on our own experiments and on the available literature data. In most of the cases, degradation of InGaN laser diodes occurs through the increase of the threshold current with almost constant slope efficiency. The threshold current change follows frequently the square root on time dependence. Though this type of behavior has usually been attributed to magnesium acceptor diffusion, no firm proof of such a hypothesis has so far been presented. In contrast, there is an increasing number of reported experiments showing that the most important factor contributing to fast (hours), and medium time (hundreds of hours) degradation is the process of carbon deposition. This process involves photochemical reactions leading to the decomposition of hydrocarbons existing in the laser diode environment. This process resembles very closely the mechanism responsible for 980-nm laser diode degradation and known as Package Induced Failure. [J282]

"Effects of additional Ce 3+ doping on the luminescence of Li₂SrSiO₄:Eu²⁺ yellow phosphor"

Additional Ce³⁺-doping improves the luminescence of Li₂SrSiO₄:Eu²⁺, a yellow phosphor for ultraviolet or blue light-emitting diodes. By examining the photoluminescence of Li₂SrSiO₄:Eu²⁺, Li₂SrSiO₄:Ce³⁺, and Li₂SrSiO₄:Ce³⁺,Eu²⁺, it was confirmed that the energy transfer from Ce³⁺ to Eu²⁺ ions contributes little to the enhanced luminescence of Li₂SrSiO₄:Ce³⁺,Eu²⁺. Alternatively, we suggested that Ce³⁺ ions could stabilize the Li vacancies, inhibit the oxidation of Eu²⁺ to Eu³⁺, and consequently increase emission intensity, based on the characterizations with decay time and synchrotron light source x-ray absorption measurements. The proposed argument was validated with first principle calculations of the defect formation energies. [J283]

"Determination of molecular dipole orientation in doped fluorescent organic thin films by photoluminescence measurements"

The orientation of the transition dipole moments of fluorescent organic molecules doped into a matrix material is determined by photoluminescence measurements of the angular dependent emission spectra and by comparison with simulations. The analysis of two small molecular materials doped into a 4,4'-bis(N-carbazole)-biphenyl matrix is demonstrated, yielding a horizontal orientation of 91% for 4,4'-bis[4-(diphenylamino)styryl]biphenyl and a completely random orientation in case of tris-(8-hydroxyquinoline)aluminum (Alq₃). This expeditious technique does not require detailed information about the optical properties of the dopant, making this method particularly suitable for characterizing newly developed materials for organic light-emitting diodes with enhanced light-outcoupling efficiency. [J284]

"Nonsaturating Drain Current Characteristic in Short-Channel Amorphous-Silicon Thin-Film Transistors"

Nonsaturating drain current characteristics are analyzed in terms of the channel length modulation (CLM) and the self-heating effect. According to this analysis, the nonsaturating drain current arises if the effective channel length is sufficiently reduced such that the CLM effect leads to a superlinear increase of the drain current beyond saturation. The extracted CLM parameter was around $\Gamma_{Bi} = 1/15 \Gamma_{Bi}/V$ for the samples investigated, and a nonsaturating characteristic was observed in hydrogenated-amorphous-silicon (a-Si:H) thin-film transistors (TFTs) with a channel length of $10 \Gamma_{Bi}$ or less. Furthermore, in a bias-temperature-stressed short-channel a-Si:H TFT, which has a laterally nonuniform threshold voltage, the experimental data showed a pronounced nonsaturating current in the reverse output characteristics and a much lower and flatter characteristic in the forward I_d - V_{ds} data. The nearly flat forward saturation characteristic is discussed in terms of the cancellation of the CLM effect by the effect from the rising threshold voltage at the pinchoff point as the drain bias increases. The pronounced nonsaturating reverse characteristic is explained in terms of the compounding effects of the rising CLM current and the rising current due to the falling threshold voltage of the pinchoff point. We also discuss a split-channel design to suppress the nonsaturating drain currents in a-Si:H TFTs. [J285]

"Intermix and match"

Ultra-broadband light sources for biomedical imaging are a step closer to reality with the demonstration of a new type of controlled intermixed superluminescent diode. The first broadband high-power quantum dot superluminescent diodes (QD-SLDs) to have been intermixed to have a significant blue-shift in their operating wavelength have been demonstrated by researchers at the University of Sheffield in the UK. This result could open the door to high bandwidth active devices comprising regions of different wavelengths that could meet the demands of, for example, optical imaging of the eye and other skin tissue. [J286]

"Balanced charge transport and enhanced white electroluminescence from a single white emissive polymer via thermal annealing"

The effect of thermal annealing on electroluminescence of polyfluorene-based single white emissive polymer is demonstrated. Both color purity and light-emitting efficiency of the devices are enhanced via thermal annealing. It is found that thermal annealing can induce the formation of crystalline polyfluorene phase that acts as an efficient blue fluorescent dopant for enhancing blue emission and hence color purity of the white light. Most importantly, the hole and electron transport is balanced after thermal annealing that favors improving the light-emitting efficiency. A light-emitting efficiency of 10 cd/A is achieved after thermal annealing, about 30% increase compared to the as-produced device. [J287]

"Efficiency droop in 245-247 nm AlGaIn light-emitting diodes with continuous wave 2 mW output power"

We report on 245-247 nm AlGaIn-based deep ultraviolet (DUV) light-emitting diodes with continuous wave output power up to 2 mW. DUV diodes with peak emission wavelength of 245 and 247 nm exhibit turn-on voltage less than 10 V. At room temperature and cw operation the maximum external quantum efficiency was close to 0.18%, which is the highest value published to date for devices with peak emission wavelength shorter than 250 nm. A large external efficiency droop observed at current densities above 100 A/cm^2 is attributed to self-heating, carrier spillover from the QWs into the barrier layers or the p-type cladding layer, and/or Auger recombination. A semiempirical equation was proposed to describe the efficiency droop in DUV diodes at a high current injection. [J288]

"Direct Prediction Methods on Lifetime Distribution of Organic Light-Emitting Diodes From Accelerated Degradation Tests"

Accelerated degradation testing (ADT) expedites product degradation by stressing the product beyond its normal use. To extrapolate the product's reliability at use condition, the ADT requires a known functional link relating the harsh testing environment to the usual use environment. Practitioners are often faced with a great challenge to designate an explicit form of the stress-degradation relationship a priori in accelerated degradation models. In this paper, we propose three methods to make direct inference on the lifetime distribution itself without invoking arbitrary assumptions on the degradation model: delta approximation, multiple imputation of failure-times, and the lifetime distribution-based (LDB) method. The methods are easy to implement without computational difficulty, hence they have potential in a wide range of applications for estimating lifetime distributions from ADT data. We applied the methods to two ADT data sets including a real application of commercial organic light-emitting diodes (OLED). The analysis of the examples and simulation results suggests parametric LDB and multiple imputation method as more potential alternatives to traditional failure-time approaches, especially for the case where there is neither enough physical background, nor historical evidence supporting presumed relationships between stress and the parameters of the degradation model. [J289]

"Enhanced optical power and low forward voltage of GaN-based light-emitting diodes with Ga-doped ZnO transparent conducting layer"

Ga-doped ZnO (ZnO:Ga) films were grown by metalorganic chemical vapor deposition as transparent conducting layers for GaN light-emitting diodes (LEDs). The forward voltage of LEDs with ZnO:Ga was 3.3 V at 20 mA. The low forward voltage was attributed to the removal of a resistive ZnGa₂O₄ phase, decreased resistivity of ZnO:Ga films, and increased hole concentration in p-GaN by thermal annealing process. The light output power of LEDs with ZnO:Ga was increased by 25% at 20 mA compared to that of LEDs with Sn-doped indium oxide due to the enhanced transmittance and the increased hole concentration in p-GaN. [J290]

"Inkjet Printed RGB Quantum Dot-Hybrid LED"

We report DC driven full color inkjet printed quantum-dots light-emitting devices. The inkjet was used to print monochromatic red, green, and blue, as well as integrate red-green-blue light-emitting quantum dots onto a substrate having QVGA display. The performance of the inkjet printed monochrome devices was on the same order as that of spin coated ones. For the full color RGB devices, a video brightness of 100 cd/m² is achieved at 9.3 V. [J291]

"Characteristics of a GaN-Based Light-Emitting Diode With an Inserted p-GaN/i-InGaN Superlattice Structure"

An interesting GaN-based light-emitting diode (LED) with a ten-period i (undoped)-InGaN/p (Mg doped)-GaN (2.5 nm/5 nm) superlattice (SL) structure, inserted between a multiple-quantum well (MQW) structure and a p-GaN layer, is fabricated and studied. This inserted SL can be regarded as a confinement layer of holes to enhance the hole injection efficiency. As compared with a conventional LED device without the SL structure, the studied LED exhibits better current spreading performance and an improved quality. The turn-on voltage, at 20 mA, is decreased from 3.32 to 3.14 V due to the reduced contact resistance as well as the more uniformity of carriers injection. A substantially reduced leakage current (10⁻⁷ to 10⁻⁹ A) and higher endurance of the reverse current pulse are found. The measured output power and external quantum efficiency (EQE) of the studied LED are 13.6 mW and 24.8%. In addition, as compared with the conventional LED without the SL structure, the significant enhancement of 25.4% in output power as well as the increment of 5% in EQE are observed due to the superior current spreading ability and reduction of dislocations offered by the SL structure. [J292]

"The challenge of unity wall plug efficiency: The effects of internal heating on the efficiency of light emitting diodes"

We develop a self-consistent model to describe the internal heating of high power light emitting diodes (LEDs) and use this model to simulate the operation of GaAs-AlGaAs double heterostructure LEDs. We account for the heating by nonradiative recombination processes in the simulations and solve self-consistently the steady state junction temperature. Based on the simulation results, we discuss the plausibility of unity conversion efficiency in LEDs and also the mechanisms underlying the efficiency droop. We show that the rise in the junction temperature limits the light output available from LEDs and further degrades the efficiency of operation at high operating currents. In addition to high power applications we study the optimal operating point and discuss the methods to increase the efficiency of LEDs toward the thermodynamical limits. [J293]

"Comprehensive Modeling of Superluminescent Light-Emitting Diodes"

We present a self-consistent electric and optic model for superluminescent light-emitting diodes (SLED) using 3D finite-element method. The carrier transport is calculated by the drift-diffusion method, which is coupled with the radiative recombination obtained from the solution of Shrodinger-Poisson equations self-consistently. The spontaneous emission noise is described by the fundamental theory using the Green's function method. Our model allows 2D treatment of the carrier dynamics and optical confinement on the transverse plane, along with the electronic and optical variation on the longitudinal axis. The theoretical model has been benchmarked with an InP-based edge-emitting SLED. The device has nonidentical quantum wells with broad bandwidth from 1300 to 1600 nm. The results show the importance of 3D effects and demonstrate the validity of the model. [J294]

"Improved Performance of GaN-Based Blue LEDs With the InGaN Insertion Layer Between the MQW Active Layer and the n-GaN Cladding Layer"

In this study, we demonstrate the effect of GaN-based blue light-emitting diodes (LEDs), using an InGaN layer inserted between the n-type GaN cladding layer and the active layer (InGaN/GaN multiple quantum well), on improving device performances. With a 20-mA current injection, the results indicate that the typical output power

(or forward voltage) of light-emitting diodes grown with, and without, the InGaN insertion layer are approximately 18.1 (3.1) and 15.3(3.5) mW (V), respectively. This corresponds to an enhancement in output power (wall-plug efficiency) of around 18% (33%), with the use of the InGaN insertion layer. In addition, the electrostatic discharge (ESD) endurance voltages increased from 1000 V to 6000 V when the InGaN insertion layer was applied to the GaN/sapphire-based LEDs. The improvement of output power and ESD endurance voltage could be mainly due to the fact that the Si-doped InGaN insertion layer played the role of a current-spreading layer, which led to a lower possibility of junctions suffering a large current density in specific local sites. [J295]

"The smart power strip"

First Page of the Article [J296]

"Remarkable increase in the efficiency of N,N'-dimethylquinacridone dye heavily doped organic light emitting diodes under high current density"

We demonstrated a remarkable rise of external quantum efficiency (EQE) of N,N'-dimethylquinacridone (DMQA) heavily doped organic light-emitting diodes with tris-(8-hydroxyquinolinato) aluminum as host at large current density. The EQE of 5.0 wt % DMQA doped device increased 42% as the current density rises from 20 to 300mA/cm². At 300mA/cm², the EQE of 1.8 wt % DMQA doped device equals to that of the optimal concentration (0.8 wt %) doped device, which behaves a flat trend curve with the increase of current density. Whereas, another green fluorescent dye (Coumarin6) doped device with the same structure indicates straight falling dependence of EQE on increasing current density. The EQE increase is attributed to the dissociation of excimer species formed by interaction of higher concentration DMQA molecules into DMQA monomer excitons under high current density. [J297]

"Structural Parameter Dependence of Light Extraction Efficiency in Photonic Crystal InGaN Vertical Light-Emitting Diode Structures"

Light extraction efficiency (LEE) in thin-film InGaN vertical light-emitting diode (LED) structures with photonic crystal patterns is studied using the three-dimensional finite-difference time-domain simulation. We systematically investigate the dependence of LEE on various structural parameters of photonic crystal vertical LEDs such as the thickness of the p-GaN and n-GaN layers, and air-hole depth and size. It is found that high LEE of > 80% is obtainable from unencapsulated photonic crystal LEDs for a wide range of structural parameters. In particular, higher LEE is observed for the structures with relatively long-period photonic crystal patterns and possible mechanisms for the large enhancement of LEE are discussed. [J298]

"Enhancement of light extraction in ultraviolet light-emitting diodes using nanopixel contact design with Al reflector"

We report on a nanopixel contact design for nitride-based ultraviolet light-emitting diodes to enhance light extraction. The structure consists of arrays of Pd ohmic contact pixels and an overlying Al reflector layer. Based on this design a twofold increase in the light output, compared to large area Pd square contacts is demonstrated. Theoretical calculations and experiments reveal that a nanopixel spacing of 1μm or less is required to enable current overlap in the region between the nanopixels due to current spreading in the p-GaN layer and to ensure current injection into the entire active region. Light emitted in the region between the nanopixels will be reflected by the Al layer enhancing the light output. The dependence of the light extraction on the nanopixel size and spacing is investigated. [J299]

"Stable temperature characteristics of InGaN blue light emitting diodes using AlGaIn/GaN/InGaIn superlattices as electron blocking layer"

P-type AlGaIn/GaN/InGaIn superlattices were incorporated in a InGaN based blue light emitting diode as electron blocking layer to minimize the temperature dependence on optical output power. For the characteristic temperatures in range of 10 to 100 °C and at operation current of 350 mA, the external quantum efficiency varied by less than 0.5%. For the presented device, the negative characteristic temperature was shown to occur below temperature of 50 °C. The improved temperature stability in optical output power is thought to be attributed to (1) the efficiency of hole carrier transport in AlGaIn/GaN/InGaIn superlattices and (2) the enhanced blocking of electron overflow between multiple quantum wells and AlGaIn/GaN/InGaIn superlattices. [J300]

"Study of Light Emission Enhancement in Nanostructured InGaN/GaN Quantum Wells"

Recently, InGaN/GaN quantum wells with different nanostructures such as nanoholes and nanorods have been

proposed to enhance the light emitting efficiency. This paper calculates the influence of nanostructures to the strain and band profile of the quantum well. The effects of strain relaxation and surface states are analyzed, which could possibly influence the diode emission properties. Our calculation results show that the strain relaxation and the surface state pinning play important roles in enhancing the light emission, reducing the quantum confined Stark effect, and causing the blue shift of the spectrum. Our calculation results provide useful information in analyzing emission properties of nanohole arrays and similar structures. [J301]

"Forward tunneling current in GaN-based blue light-emitting diodes"

Forward tunneling current in InGaN/GaN multiquantum-well blue light-emitting diodes grown on sapphire substrate was studied by temperature-variable current-voltage (I-V) measurement. All semilog I-V curves obtained in the temperature range from 100 to 300 K exhibit two successive linearly dependent regions at low forward bias. The corresponding slopes appear to be insensitive to temperature, which indicates a dominant defect-assisted tunneling process. It is found that the tunneling current varies approximately as a function of $\exp(-\beta E_g + \lambda eV)$, where β and λ are constants independent of temperature and voltage. The temperature- and voltage-dependence of forward tunneling current are explained by thermally induced band gap shrinkage and bias-induced route change of diagonal tunneling, respectively. The likely tunneling entities involved in the forward tunneling process are also discussed. [J302]

"Resonant Tunneling in III-Nitrides"

Wide-bandgap semiconductors can sustain high temperatures and high power operation in various important applications such as transistors, light-emitting diodes, and lasers. Although in embryonic stage, one can expect such a resilience in GaN resonant tunneling diodes (RTDs) and superlattices as well with distinct applications. Because of the negative differential conduction, the double barrier resonant tunneling structures could be the basis for new high-power coherent microwave sources operating in W-band and terahertz. In this paper, recent progress in wide-bandgap semiconductor RTDs is discussed. [J303]

"Effects of Basal Stacking Faults on Electrical Anisotropy of Nonpolar a-Plane () GaN Light-Emitting Diodes on Sapphire Substrate"

We report on the effects of basal stacking faults (BSFs) on the electrical anisotropy and the device characteristics of nonpolar a-plane GaN (1120) light-emitting diodes (LEDs) on r-plane (1102) sapphire substrates. The sheet resistance in the direction parallel to the c-axis [0001] is 18%-70% higher than the one in the direction parallel to the m-axis [1100]. The anisotropic conductivity of faulted a-plane GaN films can be explained by carrier scatterings from BSFs. It is also shown that the output power of nonpolar a-plane GaN LEDs are significantly influenced by the presence of BSFs, which laterally hampers the carrier transport in the n-GaN layer, especially in the direction parallel to the c-axis in faulted nonpolar nitride films. [J304]

"Ring Remote Phosphor Structure for Phosphor-Converted White LEDs"

An efficient packaging configuration for high-power white light-emitting diodes (LEDs), consisting of an inverted cone lens encapsulant and a surrounding ring remote phosphor layer, is present. Ray-tracing simulations demonstrate that the package extraction efficiency of the ring remote phosphor structure exceeds 93%. With the implementation of the ring remote phosphor structure, the ring remote phosphor device has a maximum luminous efficacy of 145 lm/W at 20 mA and a maximum luminous flux of 132 lm at 400 mA. The enhancements are attributed to reduced absorption of the re-emitting yellow light by the LED chip, and the reduction of the trapping light inside the flat remote phosphor layer in normal remote phosphor structure. [J305]

"Performance of Flip-Chip Thin-Film GaN Light-Emitting Diodes With and Without Patterned Sapphires"

We report on improved device performance of flip-chip (FC) GaN-based light-emitting diodes (LEDs) by combining patterned sapphire substrate (PSS) and thin-film techniques. It was found that an FC LED grown on a conventional planar sapphire exhibits a power enhancement factor of only 36.3% after the thin-film processes of substrate removal and surface roughening. In contrast, the as-fabricated FC LED grown on a PSS showed a power enhancement factor of up to 62.3% without any postprocess as compared with the light output power of an original conventional FC LED. Further intensity improvement to 74.4% could be achieved for the FC LED/PSS sample with the thin-film processes. [J306]

"Direct Submount Cooling of High-Power LEDs"

Rapidly increasing light emitting diode (LED) heat fluxes necessitate the development of aggressive thermal

management techniques that can intercept the dissipated heat directly in the submount. Microgap coolers, which eliminate solid-solid thermal interface resistance and provide direct contact between chemically inert, dielectric fluids and the back surface of an active electronic component, offer a most promising approach for cooling high-power LEDs. This paper focuses on the two-phase thermofluid characteristics of a dielectric liquid, FC-72, flowing in an asymmetrically heated chip-scale microgap channel, 10 mm wide \times 37 mm long, with channel heights varying from 110 μm to 500 μm and channel wall heat fluxes of 200 kW/m². The experimental two-phase, area-averaged heat transfer coefficients of FC-72 reached 10 kW/m²·K, significantly higher than the single-phase FC-72 values, thus providing cooling capability in the range associated with water under forced convection. Data obtained for single-phase water yielded very good agreement with predictions for the convective heat transfer coefficients and served to validate the accuracy of the experimental apparatus and measurement technique. It is shown that this two-phase cooling approach could be used to dissipate in excess of 600 kW/m² in the submount of high-power LEDs. [J307]

"Highly efficient blue organic light emitting device using indium-free transparent anode Ga:ZnO with scalability for large area coating"

Organic light emitting devices have been achieved with an indium-free transparent anode, Ga doped ZnO (GZO). A large area coating technique was used (RF magnetron sputtering) to deposit the GZO films onto glass. The respective organic light emitting devices exhibited an operational voltage of 3.7 V, an external quantum efficiency of 17%, and a power efficiency of 39 lm/W at a current density of 1 mA/cm². These parameters are well within acceptable standards for blue OLEDs to generate a white light with high enough brightness for general lighting applications. It is expected that high-efficiency, long-lifetime, large area, and cost-effective white OLEDs can be made with these indium-free anode materials. [J308]

"Technique to evaluate the diode ideality factor of light-emitting diodes"

A photoluminescence technique has been demonstrated on InGaN/GaN light-emitting diodes (LEDs) to evaluate their diode ideality factors. Selectively excited active regions produce potential differences between two contact terminals in addition to luminescence, from which the rate of recombination and terminal voltage have been related. Obtained ideality factors on commercial LEDs were between 1.1 and 2.4, which were significantly smaller than values determined via current-voltage characteristics. The ideality factor has been discussed from the viewpoint of direct-band-gap light-emitting pn-junctions, and the notion that quantum-well structure takes over the role of the recombination plane introduced by the Sah-Noyce-Shockely analysis is proposed. [J309]

"Color Filter-Less LCDs in Achieving High Contrast and Low Power Consumption by Stencil Field-Sequential-Color Method"

The field-sequential-color liquid crystal display (FSC-LCD) without a color filter enables high light efficiency, wide color gamut, and low material cost. However, the visual defect of color breakup (CBU) is perceived when relative velocities exist between the screen image and the human eye. We proposed the Stencil-FSC method with a 240-Hz field rate to make CBU imperceptible. Given the Stencil-FSC method, the hardware parameters were optimized to reduce hardware complexity while maintaining sufficient suppression of CBU. After implementing Stencil-FSC on a 32-in FSC-LCD, the image contrast ratio was shown to be ten times more than that of a conventional CCFL LCD, and the average power consumption was reduced to less than 35 W—a 67% savings in power consumption. [J310]

"Temperature and excitation power dependent photoluminescence intensity of GaInN quantum wells with varying charge carrier wave function overlap"

For the realization and the improvement of GaN-based optoelectronic devices (light emitting diodes and laser diodes) emitting from the ultraviolet to the red wavelength range GaInN quantum well structures with high internal quantum efficiency are of great importance. To determine parameters which affect the internal quantum efficiency, we have analyzed the emission intensity of GaInN quantum well structures with varied electron and hole wave function overlap by temperature and excitation power dependent and by time-resolved photoluminescence. The quantum confined Stark effect reduces the temperature dependent photoluminescence emission intensity for thick polar quantum wells at low temperature. But near room temperature, these thick polar GaInN quantum wells feature less relative intensity loss than thinner polar quantum wells. This behavior can partially be assigned to increased screening effects and higher quantum well barriers for thicker quantum wells. Additionally, excitation power dependent photoluminescence points to a transition from a radiative recombination based on excitons at 10 K to a bimolecular recombination at room temperature for thick c-plane quantum wells. This transition may also affect the intensity decrease by a changed carrier diffusivity. [J311]

"Organic light emitting complementary inverters"

We show that p- and n-type light emitting field-effect transistors (LEFETs) can be made using "superyellow" as a light-emitting polymer, poly(2,5-bis(3-tetradecylthiophen-2-yl)thieno[3,2-b]thiophene) as a p-type material and a naphthalene di-imide as an n-type material. By connecting two of these LEFETs, we have demonstrated a light emitting complementary inverter (LECI). The LECI exhibited electrical and optical characteristics in the first and third quadrant of the transfer characteristics with voltage gain of 6 and 8, respectively. [J312]

"Controlling carrier accumulation and exciton formation in organic light emitting diodes"

It is found that the device performance of organic light emitting diodes (OLEDs) can be significantly improved by separating the carrier accumulation zone from the exciton formation interface. The improvement is explained by suppression of exciton quenching caused by accumulated carriers at the exciton formation interface. It is also found that the position of the exciton formation interface in OLEDs correlates well with the interfacial dipole measured using ultraviolet photoelectron spectroscopy at the interface between a hole transport layer and an electron transport layer. The findings of this work provide useful material selection guidelines in designing high performance OLEDs. [J313]

"Chemical reactivity of aromatic hydrocarbons and operational degradation of organic light-emitting diodes"

We report the study of the chemical reactivity of representative hydrocarbon organic light-emitting diode (OLED) materials-fully aromatic derivatives of anthracene and tetracene in the OLED environment. In addition to the participation in free-radical chemistry initiated by homolytic bond dissociation reactions of arylamines, the hydrocarbons appear to initiate and undergo dehydrogenation reactions following the electronic excitation caused by the recombination of charge carriers or by the absorption of a photon. A chemical product of the intramolecular dehydrogenation reaction, cyclization, was identified in photoexcited films of representative anthracene derivative and detected in electrically degraded OLEDs utilizing this material in the emissive layer. Other analogous intra- and intermolecular dehydrogenation reactions initiated by the excited states of hydrocarbons are also expected to occur in operating OLEDs. The stepwise transfers of hydrogen atoms or ions to neighboring molecules are likely to yield, at least in part, neutral or ionic forms of performance-damaging species-nonradiative recombination centers and luminescence quenchers. A comparison of the luminescence losses and quantities of the identified degradation product in OLEDs and photoexcited films suggests that the dehydrogenation mechanism plays a minor but not negligible part in the operational degradation of modern OLEDs utilizing hydrocarbons as emissive layer hosts. [J314]

"Device physics of highly sensitive thin film polyfluorene copolymer organic phototransistors"

We report on solution processed, highly light sensitive thin film transistors (TFTs) based on poly(9,9-dioctylfluorene-co-bithiophene) (F8T2). Transistors without heat treatment showed the highest saturation mobility, while devices annealed at 280 °C showed the highest drain current. The latter annealed transistors were found to give highly stable and reproducible performance over many light cycles. Measurements were carried out using an inorganic light emitting diode (LED) light source with a peak wavelength of 465 nm and 19 nm bandwidth from 0 to 400 mW/cm² light intensity on TFTs with an F8T2 film thickness of 30 nm. The TFT OFF current was found to increase both with light intensity and gate bias. The bulk photogenerated carrier density was calculated to change from 5.4 × 10¹¹ to 1.4 × 10¹³ cm⁻³ over the measured light intensity range. The TFT saturation mobility did not change with light intensity, remaining constant at 1.2 × 10⁻⁴ cm²/V s. The TFT ON current instead increased due to a shift in the turn-on voltage V_T. This changed from -27 to -20 V over the measured light intensity range, initially changing rapidly but then saturating at higher intensity values. Contact resistance R_C measurements showed large values in the dark. R_C rapidly decreases with increasing light intensity, again saturating at higher values. - From these results, we propose a phototransistor model in which illumination varies the device performance by effecting injection. By considering this shift in R_C as photoassisted barrier lowering which additionally varies the width of the region depleted of carriers between the injecting interface and the channel, it is possible to explain the observed shift in V_T as a change in the fraction of the gate bias dropped across the contact capacitance C_C. By operating the phototransistor at a value of V_g = -5 V (below V_T), it was possible to achieve a highly linear response of the photocurrent with light intensity. Alternatively, by operating at a value of V_g = -40 V (above V_T), it was possible to maximize the photoresponsivity within the measured range. A photoresponsivity of 18.5 A/W at 5 mW/cm² light intensity was achieved. [J315]

"White Light Emission Characteristics of Polymer-Encapsulated CdSe Nanocrystal Films"

A white, cadmium selenide (CdSe) nanocrystal-based phosphor light-emitting diode (LED) was fabricated in this

work using a commercial ultraviolet (UV) LED topped with a thin film of nanocrystals encapsulated in a polymer. A range of film thicknesses were fabricated and different wavelength LEDs were employed to analyze their influences on the emission properties of the phosphor LEDs. The absorbance and emission intensity of light passing through the films were optimized without compromising the excellent inherent color quality of the white-light nanocrystals. These results indicate a potential to improve the color quality and lower the scattering losses found in current white LEDs based on much larger, micron-sized phosphors. [J316]

"ac excitation of organic light emitting devices utilizing conductive charge generation layers"

The ac-field-induced charge carrier generation and recombination is studied in an asymmetric conjugated polymer light emitting device based on one injecting electrode and one electrode separated by an insulating layer. Under operation with 130 kHz light intensity emitted by the device exhibits a pronounced asymmetry with respect to the polarity of the electric field. Numerical simulations show that this behavior can be explained by the significantly different mobilities of electrons and holes in the conjugated polymer. This approach enables insight into the device physics of organic light emitting devices with internal charge generation and allows direct investigation of hole and electron mobilities in one single device. [J317]

"Enhanced fluorescence by surface plasmon coupling of Au nanoparticles in an organic electroluminescence diode"

A significant increase in electroluminescence was achieved through coupling with localized surface plasmons in a single layer of Au nanoparticles. We fabricated a thin-film organic electroluminescence diode, which consists of an indium tin oxide (ITO) anode, a Au nanoparticle array, a Cu phthalocyanine hole transport layer, a tris(8-hydroxyquinolinato) aluminum (III) electron transport layer, a LiF electron injection layer, and an Al cathode. The device structure, with size-controlled Au particles embedded on ITO, can be used to realize the optimum distance for exciton-plasmon interactions by simply adjusting the thickness of the hole transport layer. We observed a 20-fold increase in the molecular fluorescence compared with that of a conventional diode structure. [J318]

"Near-infrared electroluminescence and stimulated emission from semiconducting nonconjugated polymer thin films"

We present the results of a study on near-infrared electroluminescence and optical amplification in semiconductor thin films based on a nonconjugated polymer doped with luminescent and electron-transport molecules. A single-layer light-emitting diode is fabricated on an indium tin oxide-coated glass substrate with poly(9-vinylcarbazole) containing an electron-transport material, 2-(4-Biphenyl)-5-(4-tert-butylphenyl)-1,3,4-oxadiazole and a near-infrared-emitting compound, 2-(6-(p-dimethylaminophenyl)-2,4-neopentylene-1,3,5-hexatrienyl)-3-ethylbenzothiazolium perchlorate. The single-layer structure shows near-infrared electroluminescence with a turn-on voltage of 13 V. The same structure is characterized under transversal pulsed photopumping with a frequency-doubled Nd: yttrium aluminum garnet laser. With increasing pump fluence, the edge emission at 0.82 μm shows both significant gain narrowing and superlinear intensity increase, which indicate the existence of optical gain by stimulated emission. Our results provide impetus for the development of near-infrared polymer lasers and optical amplifiers. [J319]

"Interchain and intrachain emission branching in polymer light-emitting diode doped by organic molecules"

A blend of the polymer poly[2-(2-ethylhexyloxy)-5-methoxy-1,4-phenylenevinylene] (MEH-PPV) and the electron-transport molecule tris-(8-hydroxyquinoline) aluminum (Alq3) has been investigated by means of electroluminescence and fluorescence spectroscopy, upon variation of the Alq3 content in the blend. A decreased interchain emission is observed upon increasing Alq3 content, due to lower packing of the MEH-PPV chains which leads to a reduction in the interchain interaction, excimer formation, and emission probability. A branching of MEH-PPV interchain and intrachain emissive contributions is clearly time resolved and analyzed as a function of the Alq3 content. At high doping concentration, direct emission from Alq3 molecules is observed. [J320]

"Engineer on a mission"

A Jesuit priest and electrical engineer finds a new calling in Africa [J321]

"Polarization-charge tunnel junctions for ultraviolet light-emitters without p -type contact"

Polarization-charge tunnel junctions for ultraviolet light-emitters ($\lambda = 360\text{nm}$) are modeled using the k-p multiband quantum transmitting boundary method. It is shown that polarization-charge tunnel junctions can

carry sufficient current to be viable for ultraviolet emitters. Sources of inefficiency in existing ultraviolet emitters are discussed, including poor hole-injection efficiency and optical absorption in the p-type GaN contact layers. It is demonstrated that polarization-charge tunnel junctions can deliver improvements in both areas, by eliminating the need for p-type contacts, and by enabling the use of a p-side-down structure, which is shown to have favorable characteristics for carrier transport compared to conventional p-side-up structures. [J322]

"Analysis of reverse tunnelling current in GaInN light-emitting diodes"

The characteristics of the reverse leakage current of GaInN/GaN multiple quantum well light-emitting diodes (LEDs) are examined with various n-type GaN doping concentrations and interpreted by using a tunnelling current model. Changing the doping concentration of the n-type GaN influences the tunnelling probability of electrons into the conduction band and thus the reverse leakage current. Reducing the doping concentration of the top 150 nm portion of the n-type GaN layer by half decreases the tunnelling probability, resulting in decrease of the reverse leakage current by 80% at 10%V without deterioration of any forward electrical properties of LEDs. [J323]

"Recoverable electroluminescence from a contaminated organic/organic interface in an organic light-emitting diode"

An organic/organic interface, like an electrode/organic interface in an organic light-emitting diode (OLED), can be severely affected by ambient contamination. However, we surprisingly found that the contaminated surface or interface can be "cured" by depositing a thin interfacial layer containing a strong reducing agent onto the contaminated surface before finishing the fabrication of the device. For example, in comparison with a regular OLED, an OLED having a 5-min ambient exposure to the light-emitting layer/electron-transporting layer interface drops its initial electroluminescence (EL) intensity by 50%. The decreased EL intensity due to the 5-min ambient exposure can be fully recovered and the improved operational stability can be realized after curing the contaminated interface using a thin Li interfacial layer. The experimental results provide a useful method to cope with the interfacial contamination in OLEDs during a manufacturing process. In addition, our results support the failure mechanism of an Alq-based OLED suggested by [Papadimitrakopoulos et al, Chem. Mater. 8, 1363 (1996)]. [J324]

"High extraction efficiency light-emitting diodes based on embedded air-gap photonic-crystals"

This letter reports on high extraction efficiency light-emitting diodes (LEDs) based on embedded two-dimensional air-gap photonic crystals (PhCs). High refractive index contrast provided by the air gaps along with high interaction of the embedded PhCs with the guided light resulted in an efficient extraction of all guided modes in the LED, in contrast to the common surface PhC configuration. Embedded PhC LEDs presented an enhanced directional light emission compared to non-PhC LEDs. High extraction efficiency, close to unity, provided by the encapsulated embedded PhC LEDs demonstrates the capability of this approach to achieve high efficiency devices with directional light emission. [J325]

"Note: Investigation of a null measurement of optical absorbance using a pulse width modulated light-emitting diode"

We examined the possibility of making a null measurement of optical absorbance by using pulse-width modulation to control the intensity of a light-emitting diode (LED). This type of measurement is intriguing because the instrumental sources of noise are different from those in the traditional absorbance measurement. Our experiment employed phototransistor detectors and a RC integrator to measure the amount of light being transmitted. However, instead of measuring the ratio of the detector voltages for a blank and sample, we measured the ratio of the LED duty cycles required to give the same detector voltage for a blank and a sample. Using this method, it is presumed that the same amount of light reaches the detector during measurement of the blank and sample. [J326]

"Effect of Mg doping in the barrier of InGaN/GaN multiple quantum well on optical power of light-emitting diodes"

We report on Mg doping in the barrier layers of InGaN/GaN multiple quantum wells (MQWs) and its effect on the properties of light-emitting diodes (LEDs). Mg doping in the barriers of MQWs enhances photoluminescence intensity, thermal stability, and internal quantum efficiency of LEDs. The light output power of LEDs with Mg-doped MQW barriers is higher by 19% and 27% at 20 and 200 mA, respectively, than that of LEDs with undoped MQW barriers. The improvement in output power is attributed to the enhanced hole injection to well layers in MQWs with Mg-doped barriers. [J327]

"Design considerations of high performance optical code division multiple access: a new spectral amplitude code based on laser and light emitting diode light source"

A new code of optical code division multiple access (OCDMA) based on spectral amplitude coding (SAC) is described and analysed. The coding technique is called random diagonal (RD) code. One of the important properties of this code is that the cross-correlation at data segment is always zero, which means that phase intensity induced noise (PIIN) is reduced. From the construction of RD code sequence, the authors can see that the RD code is constructed using code segment and data segment. Using this code property, RD code is implemented using coherent source (multi-laser) and incoherent source (light emitting diode) for the code segment and data segment, respectively. RD code using two multi-sources (incoherent and coherent) can be considered as an effective way for maximising the capacity while minimising the cost of SAC-OCDMA. It is shown that the system using this new code matrices not only suppresses PIIN, but also allows a larger number of active users compared with other codes. [J328]

"Organic light-emitting diodes containing multilayers of organic single crystals"

Double-heterostructure (DH) organic light-emitting diodes (OLEDs) with thick carrier transport layers based on organic single crystals have been fabricated. Although the total thickness of the organic layers ($\sim 1.4\text{ }\mu\text{m}$) is one order of magnitude greater than that of conventional thin-film OLEDs, a current density of 100 mA/cm^2 was achieved at 19 V. The major advantage of the single crystal-based DH-OLED was that a very low applied electric field ($\sim 104\text{ V/cm}$) was required for the onset of carrier injection and transport, because of the high carrier mobilities of the single crystal layers. [J329]

"Multifunctional integrating sphere setup for luminous flux measurements of light emitting diodes"

A multifunctional setup based on the absolute integrating sphere method for measuring luminous flux of light emitting diodes (LEDs) is presented. The total luminous flux in 2π and 4π geometries and partial luminous flux with variable cone angle can be measured with the same custom-made integrating sphere. The number and area of ports and baffles of the sphere was minimized. The sphere has three ports: a main port, a detector port, and an auxiliary port, located in the same hemisphere. The other hemisphere is free of ports. The main port is used for the calibration of the sphere as well as for the LED under test. Only one absolute calibration of the integrating sphere photometer is needed for measuring LEDs in all three geometries. The spatial nonuniformity correction is needed only for LEDs with low directivity or having significant minor beams. The expanded uncertainty ($k=2$) for the measurement setup varies between 1.2% and 4.6% depending on the measurement geometry, color, and the angular spread of the LED light beam. A complete calibration procedure of the constructed integrating sphere photometer is presented as well as comparison measurements with a goniophotometer. [J330]

"Emission zone control in blue organic electrophosphorescent devices through chemical modification of host materials"

We report blue organic light-emitting devices with iridium (III) bis[(4,6-difluorophenyl)-pyridinato- $N,C2'$] picolinate as an emitter doped into a series of phosphine oxide-based host materials that have significantly different charge transport properties: 4-(diphenylphosphoryl)- N,N -diphenylaniline (HM-A1), N -(4-diphenylphosphoryl phenyl) carbazole (PO12), 9-[6-(diphenylphosphoryl)pyridin-3-yl]-9H-carbazole (HM-A5), and 6-(diphenylphosphoryl)- N,N -diphenylpyridin-3-amine (HM-A6). Depending on the nature of the host material, the location of the emission zone can be moved within the emissive layer from the hole transport layer interface to the electron-transport layer interface. The charge transport properties of the materials were evaluated using single carrier devices. [J331]

"Doping and optimal electron spin polarization in n-ZnMnSe for quantum-dot spin-injection light-emitting diodes"

Utilizing the diluted magnetic semiconductor ZnMnSe for electron spin alignment near-perfect spin state preparation in semiconductor quantum dots has been demonstrated. We show that the electron spin polarization depends strongly on the electron concentration in ZnMnSe:Cl. Using a model which takes accurately the Zeeman sublevel occupation into account, we can explain well the experimentally observed results. We find that the electron concentration must be below the effective density of states to obtain full electron spin polarization and best device operation. This is especially important in II-VI spin-aligner materials with a low density of states. [J332]

"Improved crystal quality and performance of GaN-based light-emitting diodes by decreasing the slanted angle of patterned sapphire"

Periodic triangle pyramidal array patterned sapphire substrates (PSSs) with various slanted angles were fabricated by wet etching. It was found beside normal wurtzite GaN, zinc blende GaN was found on the sidewall surfaces of PSS. The crystal quality and performance of PSS-LEDs improved with decrease in slanted angle from 57.4° to 31.6°. This is because most of the growth of GaN was initiated from c-planes. As the growth time increased, GaN epilayers on the bottom c-plane covered these pyramids by lateral growth causing the threading dislocation to bend toward the pyramids. [J333]

"Wavelength-stable cyan and green light emitting diodes on nonpolar m-plane GaN bulk substrates"

We report the development of 480 nm cyan and 520 nm green light emitting diodes (LEDs) with a highly stable emission wavelength. The shift is less than 3 nm when the drive current density is changed from 0.1 to 38 A/cm². LEDs have been obtained in GaInN-based homoepitaxy on nonpolar m-plane GaN bulk substrates. For increasing emission wavelength we find a large number of additional dislocations generated within the quantum wells (24108 to 1010 cm⁻²) and a decrease in the electroluminescence efficiency. This suggests that the strain induced generation of defects plays a significant role in the performance limitations. [J334]

"Study on Hydrogen Ion-Implanted Characteristic of Thin-Film Green Resonant-Cavity Light-Emitting Diodes"

This letter investigates the effects of hydrogen ion implantation on the characteristics of InGaN-based green resonant-cavity light-emitting diodes (RCLEDs). RCLEDs with ion implantation were fabricated by implanting hydrogen ion (H⁺) in a selective area. The implanted region was used to form current-confinement layers due to an existing deep-level (~ 512 nm, 2.4 eV). Superior directionality was also obtained because the selective area of p-GaN layer of RCLEDs with ion implantation provided a low refractive index. The light emission enhancement was due to the high current density increasing and the total reflection of the emission ray. The electroluminescence spectrum exhibited narrow full-width at half-maximum of 45 nm for the RCLEDs with ion implantation. The fiber-coupled power of RCLEDs with H⁺ implantation was 2.2 times greater than that of a similar structure without H⁺ implantation at an injection current of 20 mA. [J335]

"Finite-Difference Time-Domain Modeling of Periodic and Disordered Surface Gratings in AlInSb Light Emitting Diodes With Metallic Back-Reflectors"

Two-dimensional finite-difference time-domain modeling is undertaken to study the optical behaviour of midinfrared AlInSb light-emitting diode devices with close metallic back reflectors. The location of the source and mirror is investigated in detail and optimised for peak emission at $\lambda_0 = 4 \mu\text{m}$. A periodic surface grating is added and it is found that greater than 98% of the light at a specific wavelength may be extracted for specific grating parameters, an enhancement of ~ 20-fold. A novel type of grating termed disordered-periodic is then studied and is shown to have a much broader spectral response with more than 50% of the power extracted across a broad wavelength range. [J336]

"Angularly Uniform White Light-Emitting Diodes Using an Integrated Reflector Cup"

We report on white light-emitting diodes (LEDs) with a truncated-conical (TC) geometry produced by laser micromachining. A blue LED was shaped into a circular disc with 50°-inclined sidewall using a modified laser micromachining setup. A layer of Al was coated onto the inclined sidewall and the bottom surface to form an integrated reflector. Due to the highly reflective mirror, laterally propagating photons are redirected into the upward direction, contributing to an increase of 21.7% of light intensity in the normal direction. With quantum dots applied to the surface, white light emission from this TC-LED structure demonstrated a 37% enhancement in color uniformity, compared with a conventional device. [J337]

"GaN-Based Power Flip-Chip LEDs With an Internal ESD Protection Diode on Cu Sub-Mount"

The authors demonstrate the fabrication of 1 mm × 1 mm GaN-based power flip-chip light-emitting diodes (LEDs) with an internal electrostatic discharge (ESD) protection diode on Cu sub-mount. With the internal diode, it was found that forward voltage of the LED increased from 3.22 to 3.38 V while output power decreased from 366.5 to 273.9 mW when under 350 mA current injection due to the reduced light emitting area. It was also found that we can achieve a significantly better ESD robustness by building the internal diode inside the LED chip. Furthermore, it was found that 90% of the LEDs with internal diode survived with an applied reverse ESD surge of 12000 V and 25% of the LEDs can even endure 20000 V reverse ESD stressing. [J338]

"Efficiency Dependence on Degree of Localization States in GaN-Based Asymmetric Two-Step Light-Emitting Diode With a Low Indium Content InGaN Shallow Step"

GaN-based asymmetric two-step light-emitting diodes (LEDs) with a low indium content (LI_n) InGaN shallow step was proposed and fabricated. It was found the LI_n-InGaN shallow step can significantly enhance phase separation and/or inhomogeneous indium distribution in the active In_{0.27}Ga_{0.73}N layer. By inserting an In_{0.08}Ga_{0.92}N shallow step, it was found that we can enhance LED output power by a factor of 2.27 with an injection current of 20 mA. [J339]

"An Integrated Port Camera and Display System for Laparoscopy"

In this paper, we built and tested the port camera, a novel, inexpensive, portable, and battery-powered laparoscopic tool that integrates the components of a vision system with a cannula port. This new device 1) minimizes the invasiveness of laparoscopic surgery by combining a camera port and tool port; 2) reduces the cost of laparoscopic vision systems by integrating an inexpensive CMOS sensor and LED light source; and 3) enhances laparoscopic surgical procedures by mechanically coupling the camera, tool port, and liquid crystal display (LCD) screen to provide an on-patient visual display. The port camera video system was compared to two laparoscopic video systems: a standard resolution unit from Karl Storz (model 22220130) and a high definition unit from Stryker (model 1188HD). Brightness, contrast, hue, colorfulness, and sharpness were compared. The port camera video is superior to the Storz scope and approximately equivalent to the Stryker scope. An ex vivostudy was conducted to measure the operative performance of the port camera. The results suggest that simulated tissue identification and biopsy acquisition with the port camera is as efficient as with a traditional laparoscopic system. The port camera was successfully used by a laparoscopic surgeon for exploratory surgery and liver biopsy during a porcine surgery, demonstrating initial surgical feasibility. [J340]

"A route to improved extraction efficiency of light-emitting diodes"

The electroluminescence from an n-MgZnO/i-ZnO/MgO/p-GaN asymmetric double heterojunction has been demonstrated. With the injection of electrons from n-MgZnO and holes from p-GaN, an intense ultraviolet emission coming from the ZnO active layer was observed. It is revealed that the emission intensity of the diode recorded from the MgZnO side is significantly larger than that from the MgO side because of the asymmetric waveguide structure formed by the lower refractive index of MgO than that of MgZnO. The asymmetric waveguide structure reported in this letter may promise a simple and effective route to light-emitting diodes with improved light-extraction efficiency. [J341]

"Internal potential distribution in organic light emitting diodes measured by dc bridge"

Internal potential distribution of organic light-emitting diodes (OLEDs) is an essential problem. By using dc bridge to eliminate errors due to high resistance of the devices at low bias, the potential distribution has been accurately measured for both double-layer and single-layer OLEDs. It is found that the electric field inside the device is not uniform, and the potential distribution changes with external bias. This phenomenon could be the effect of space charge originating from the unequal injections of holes and electrons, which is confirmed by the results of the device with modified work function of the anode. [J342]

"Variable sensitivity of organic light-emitting diodes to operation-induced chemical degradation: Nature of the antagonistic relationship between lifetime and efficiency"

The efficiency of any organic light-emitting diode (OLED) decreases with prolonged operation. In fluorescent OLEDs containing the standard hole-transporting material NPB [N,N'-diphenyl-N,N'-bis(1-naphthyl)-1,1'-biphenyl-4,4'-diamine], prolonged operation also results in chemical degradation of the NPB. Qualitatively and quantitatively, the extent and location of chemical changes are consistent with the hypothesis that chemical degradation of NPB is largely responsible for the loss of device efficiency and that the degradation is initiated by bond-breaking in excited-state NPB. Blue fluorescent OLEDs with low operating voltages and high luminance efficiencies tend to lose efficiency much faster than OLEDs with higher operating voltages and lower efficiencies. Even so, the two types exhibit approximately the same kind and degree of chemical degradation after operation for equal times at equal current densities. In the low-voltage OLEDs, the electric field in the light-emitting layer is weaker, and the concentration of NPB radical-cations near the emission zone is smaller than in the higher-voltage devices. Apparently for this reason, degradation products impair the luminescent efficiency more severely in the low-voltage OLEDs. Such differing sensitivity of low-voltage and high-voltage OLEDs to the same amount of chemical degradation is further demonstrated by experiments with OLEDs that have been doped intentionally with a contaminant modeling a degradation product at realistic concentrations. It is also supported by a substantial recovery of efficiency after a conversion of a degraded low-voltage device into a high-voltage device

by replacement of the cathode and electron-injecting interface. [J343]

"Blue-green and white color tuning of monolithic light emitting diodes"

A blue light emitting diode (LED) is grown on top of a (Ga, In)N/GaN multiple quantum well (QW) acting as a light converter from blue to green-yellow wavelength. The blue light is produced by electrical injection, while the green-yellow emitting QWs are optically pumped by the blue photons. It is shown that the final color of the LED is strongly dependent on the blue pumping wavelength, the absorption and the internal quantum efficiency of the light converter. Depending on these parameters, blue to green LEDs or even white LEDs can be obtained. In addition, the injection current dependence of the LED electroluminescence is measured and analyzed. A very low blueshift is observed as a function of the injection current. It is explained by the fact that the carrier density per QW in the light converter stays relatively low compared to the case of classical current-injected green LEDs. [J344]

"Sustainable energy-efficient wireless applications using light"

As we step further into the 21st century, the demand for sustainable energy-efficient technology grows higher. The important area of electric lighting, currently dominated by decades-old incandescent and fluorescent sources, is being taken over by white light emitting diodes, which are solid state devices with much greater energy savings. Replacement of current inefficient lighting by these LEDs will result in reduction of global carbon dioxide emissions, a major cause of global warming, among other things. WLEDs hold the potential, in the field of photonics, to be as transformational as the transistor was in electronics. This core device has the potential to revolutionize how we use light, including not only for illumination, but also for communications, sensing, navigation, imaging, and many more applications. In this tutorial we highlight some of the potentials. [J345]

"Solution processed polymer light-emitting diodes utilizing a ZnO/organic ionic interlayer with Al cathode"

This letter reports polymer light-emitting diodes that employ a soluble zinc oxide (ZnO) nanoparticle (NP) and organic ionic interlayer as an electron-injection layer exhibits remarkable enhancement of device performance despite aluminum cathode. The ionic solution infiltrated into ZnO NP layer, which contains poly(ethylene oxide) and tetra-n-butylammonium tetrafluoroborate, significantly lowers the large electron-injection barrier by forming a permanent interfacial dipole. The polymer, phenyl substituted poly(para-phenylene vinylene) known as "Super Yellow," yellow light-emitting diodes employing the ZnO NP and ionic interlayer show a maximum efficiency of 6.3 cd/A at a 1209cd/m² and 5.4 V. The maximum brightness of the device reached 24000cd/m² at 9 V. [J346]

"GaN nanostructure design for optimal dislocation filtering"

The effect of image forces in GaN pyramidal nanorod structures is investigated to develop dislocation-free light emitting diodes (LEDs). A model based on the eigenstrain method and nonlocal stress is developed to demonstrate that the pyramidal nanorod efficiently ejects dislocations out of the structure. Two possible regimes of filtering behavior are found: (1) cap-dominated and (2) base-dominated. The cap-dominated regime is shown to be the more effective filtering mechanism. Optimal ranges of fabrication parameters that favor a dislocation-free LED are predicted and corroborated by resorting to available experimental evidence. The filtering probability is summarized as a function of practical processing parameters: the nanorod radius and height. The results suggest an optimal nanorod geometry with a radius of 50b(26 nm) and a height of 125b(65 nm), in which b is the magnitude of the Burgers vector for the GaN system studied. A filtering probability of greater than 95% is predicted for the optimal geometry. [J347]

"Mechanisms of high quality i-ZnO thin films deposition at low temperature by vapor cooling condensation technique"

A comparative mechanism investigation on the structural and optoelectronic properties of i-ZnO thin films, deposited on the silicon substrates at various temperatures were conducted. The experimental results verified that the i-ZnO films deposited at a low temperature have better quality over the conventional high temperature deposited ones. This low temperature deposition by using vapor cooling condensation technique has been successfully used to fabricate optoelectronic devices, such as UV light-emitting diodes and UV photodetectors. The mechanisms responsible for the fact that the low temperature deposited samples had better quality were analyzed in terms of the adsorption/desorption and diffusion of ZnO particles in the growth process. [J348]

"1.54 μ m emitters based on erbium doped InGaN p-i-n junctions"

We present here on the growth, fabrication and electroluminescence (EL) characteristics of light emitting diodes

(LEDs) based on Er-doped InGaN active layers. The p-i-n structures were grown using metal organic chemical vapor deposition and processed into 3004300mcm2mesa devices. The LEDs exhibit strong emissions at 1.0 and 1.54mcm, due to Er intra-4ftransitions, under forward bias conditions. The emitted EL intensity increases with applied input current without exhibiting saturation up to 70 mA. The integrated power over the near infrared emission, measured at room temperature from the top of a bare chip, is about 2mu W. The results represent a significant advance in the development of current injected, chip-scale emitters and waveguide amplifiers based on Er doped semiconductors. [J349]

"The fabrication of GaN-based nanopillar light-emitting diodes"

InGaN/GaN multiple quantum well-based light-emitting diode (LED) nanopillar arrays were fabricated using Ni self-assembled nanodots as etching mask. The Ni nanodots were fabricated with a density of 64108-1.54109cm-2and a dimension of 100-250 nm with varying Ni thickness and annealing duration time. Then LED nanopillar arrays with diameter of approximately 250 nm and height of 700 nm were fabricated by inductively coupled plasma etching. In comparison to the as-grown LED sample an enhancement by a factor of four of photoluminescence (PL) intensity is achieved for the nanopillars and a blueshift as well as a decrease in full width at half maximum of the PL peak are also observed. The method of additional chemical etching was used to remove the etching-induced damage. Then nano-LED devices were further completed using a planarization approach to deposit p-type electrode on the tips of nanopillars. The current-voltage curves of both nanopillars and planar LED devices are measured for comparison. [J350]

"Analysis of the physical processes responsible for the degradation of deep-ultraviolet light emitting diodes"

This paper reports an extensive analysis of the degradation of deep-ultraviolet light-emitting diodes submitted to dc stress test. The study was carried out by means of combined electrical and optical characterization techniques. Results described in the paper indicate that the following: (i) stress can induce a significant decrease in the optical power emitted by the devices; (ii) optical power decrease is more prominent at low measuring current levels, thus suggesting that degradation is related to an increase in the concentration of defects; (iii) stress induces a significant increase in the green-yellow parasitic emission of the devices; and (iv) stress causes a localized increase in the apparent charge distribution profiles in the active region of the devices. Experimental evidence collected within this work suggest that degradation is due to an increase in the defectiveness in the active layer of the devices, with subsequent worsening of their radiative efficiency. [J351]

"The effects of energetic disorder and polydispersity in conjugation length on the efficiency of polymer-based light-emitting diodes"

Energetic disorder plays a critical role in governing the performance of organic light-emitting diodes (OLEDs). This is particularly true for polymer-based OLEDs in which disorder can be controlled but not eliminated. Contrary to the common assumption that energetic disorder has only a negative effect on performance, we provide experimental evidence of improved efficiency when the energetic disorder is increased upon deliberate addition of traps via an increase in polymer chain length distribution. We use numerical calculations to extract the mechanisms responsible for the observed improvements and discuss the general conditions under which traps can be introduced to increase device efficiency. [J352]

"Effect of the Phosphor Geometry on the Luminous Flux of Phosphor-Converted Light-Emitting Diodes"

The effect of the phosphor geometry on the luminous flux of phosphor-converted light-emitting diodes (pcLEDs) is analyzed. Five phosphor geometries are investigated based on ray-tracing simulations. Results show that the curvature of the convex surface is an important factor to influence the luminous flux, and the remote-phosphor pcLED with the phosphor layer of a hemispherically top surface can achieve an improvement of more than 12% compared with the conventional dispersed-coating pcLED. [J353]

"Publisher's Note: "III-nitride nanopyramid light emitting diodes grown by organometallic vapor phase epitaxy" [JJ. Appl. Phys. 108, 044303 (2010)]"

First Page of the Article [J354]

"Effects of strain on defect structure in II-VI green color converters"

State-of-the-art green emission efficiency has been achieved with light-emitting diodes incorporating CdMgZnSe

color-converting quantum well heterostructures, although dark line defects (DLDs) limit the device reliability. We have determined that misfit strain plays an important role in the formation of extended stacking faults (SFs) and DLDs in II-VI green converters. Even small strain causes SFs to extend to accommodate misfit strain and extended SFs further give rise to DLDs when they intersect active regions. Detailed strain relaxation mechanisms for both tensile and compressive strain have been investigated, which may apply for other semiconductor heterostructures with an fcc lattice. Careful control of the layer strain via close lattice matching prevents the extension of SFs and leads to DLD-free converters. [J355]

"Investigation of Optical Performance of InGaN MQW LED With Thin Last Barrier"

In this work, the optical performance of the blue InGaN light-emitting diodes (LEDs) with varied last barrier thickness is investigated. The experimental measurement shows that the optical power of the InGaN LED with thinner last barrier is apparently improved. According to simulation analysis, thinner last barrier is beneficial for increasing the hole injection efficiency and holes can inject into more quantum wells within the active region. With better hole injection efficiency, the leakage electrons from active region to p-side layers are depressed correspondingly. Therefore, the radiative recombination and optical power are enhanced accordingly when the thinner last barrier is utilized. [J356]

"Equilibrium strain and dislocation density in exponentially graded Si 1-x Ge x /Si (001)"

We have calculated the equilibrium strain and misfit dislocation density profiles for heteroepitaxial Si_{1-x}Ge_x/Si(001) with convex exponential grading of composition. A graded layer of this type exhibits two regions free from misfit dislocations, one near the interface of thickness y_1 and another near the free surface of thickness $h - y_d$, where h is the layer thickness. The intermediate region contains an exponentially tapered density of misfit dislocations. We report approximate analytical models for the strain and dislocation density profile in exponentially graded Si_{1-x}Ge_x/Si(001) which may be used to calculate the effective stress and rate of lattice relaxation. The results of this work are readily extended to other semiconductor material systems and may be applied to the design of exponentially graded buffer layers for metamorphic device structures including transistors and light emitting diodes. [J357]

"Tunnel injection In 0.25 Ga 0.75 N /GaN quantum dot light-emitting diodes"

Hole tunnel injection is incorporated in the design of In_{0.25}Ga_{0.75}N/GaN quantum dot light-emitting diodes with peak emission at $\lambda = 500$ nm. Calculations show that cold holes are uniformly injected into all five quantum dot layers in the active region. Measurements were made on devices having different thicknesses, t_{eff} , of the In_{0.43}Al_{0.57}N hole tunnel barrier. The best performance is exhibited by a device with $t_{eff} = 1.5$ nm. The maximum external quantum efficiency is 0.66% at 220 A/cm², and an efficiency droop of 20% at 360 A/cm² is tentatively attributed to reduced Auger recombination and leakage of hot carriers. [J358]

"Analysis of thermal properties of GaInN light-emitting diodes and laser diodes"

The thermal properties, including thermal time constants, of GaInN light-emitting diodes (LEDs) and laser diodes (LDs) are analyzed. The thermal properties of unpackaged LED chips are described by a single time constant, that is, the thermal time constant associated with the substrate. For unpackaged LD chips, we introduce a heat-spreading volume. The thermal properties of unpackaged LD chips are described by a single time constant, that is, the thermal time constant associated with the heat spreading volume. Furthermore, we develop a multistage R_{th}C_{th} thermal model for packaged LEDs. The model shows that the transient response of the junction temperature of LEDs can be described by a multiexponential function. Each time constant of this function is approximately the product of a thermal resistance, R_{th}, and a thermal capacitance, C_{th}. The transient response of the junction temperature is measured for a high-power flip-chip LED, emitting at 395 nm, by the forward-voltage method. A two stage R_{th}C_{th} model is used to analyze the thermal properties of the packaged LED. Two time constants, 2.72 ms and 18.8 ms are extracted from the junction temperature decay measurement and attributed to the thermal time constant of the LED GaInN/sapphire chip and LED Si submount, respectively. [J359]

"Influence of Architecture-Controlled GaN Rod Arrays on the Output Power of GaN LEDs"

We report the influence of controlled lengths and densities of GaN rod arrays on the output power of GaN light-emitting diodes (LEDs). The morphology-controlled GaN rod arrays are fabricated via using ZnO rod arrays as a dry etching mask. Our investigation indicates that the output power of GaN LEDs has a strong dependence on the lengths and densities of GaN rod arrays. The variation of output power of GaN LEDs with GaN rod arrays is caused by the Fabry-Perot resonance of the film composed by GaN rod arrays. The theoretical analysis also shows a good agreement with the measurement results. [J360]

"Enhanced efficiency of CdMgZnSe down-converted light emitting diodes using light extraction features fabricated by laser-speckle lithography"

We report a method of making a wavelength converted, light-emitting diode (LED) having light extraction features based on coherent speckle patterns. These patterns have random feature size, random feature distribution, and random feature shape. The features were produced using a maskless lithography process based on exposing photoresist with a laser-induced coherent optical speckle pattern. A wet chemical etching process was then used to transfer the resist pattern into the underlying surface of the semiconductor wavelength converter layer. The external quantum efficiency of a wavelength converter with emitting surfaces having such extraction features showed a twofold increase compared to a wavelength converter without extraction features. While demonstrated here using semiconductor wavelength converters, this approach could also be applied to light extraction in conventional LED structures. [J361]

"Current crowding effect on the ideality factor and efficiency droop in blue lateral InGaN/GaN light emitting diodes"

By examining two types of lateral InGaN/GaN light emitting diodes with different contact patterns, we demonstrate that in the intermediate range of current where the space-charge region dominates in the device performance, the ideality factor (β) increases from 1.9 (current spreading design) up to 2.4 (current crowding design). This modification of β -factor could be erroneously treated as the change of free carrier recombination nature. The current crowding design is also responsible for the local overheating and heavier efficiency droop that occurs at the characteristic current 2.3 times smaller in comparison with the current spreading design. [J362]

"Highly efficient white organic light-emitting diodes based on fluorescent blue emitters"

Beside inorganic LEDs and fluorescent lamps, organic light-emitting diodes (OLEDs) are evolving into a serious alternative to incandescent lamps. Up to now, it was assumed that all-phosphorescent OLEDs are required for reaching sufficiently high efficiencies. However, the stability of phosphorescent blue emitters is a major challenge. We present a novel approach to achieve highly efficient (up to 90 lm/W at 1000cd/m² using a macroextractor) white light emission from OLEDs. The here presented combination of a fluorescent blue and a phosphorescent red emitter simultaneously allows for a strong blue emission and efficient triplet transfer to the phosphor. The spectrum is extended in the green and yellow region by a full phosphorescent unit stacked on top of the triplet harvesting device. This superposition of four different emitters results in color coordinates close to illuminant A and a color rendering index of 80. Furthermore, color stability is given with respect to varying driving conditions and estimations of the electrical and optical efficiencies are provided. [J363]

"Experimental evaluation of video transmission through LED illumination devices"

In this paper we describe the implementation of a prototype of an optical wireless system based on visible white LED lamps, which allows a video broadcasting to reach a bit rate of 2 Mbps. This technology is usually called VLC or Visible Light Communications and presents several advantages as the robustness against EM interference, safety for human eye and security against undesired network access. These conditions make this system suitable for co-existing with commercial RF networks -WiFi, Bluetooth, etc.-, especially for in-house applications. For the uplink channel we have also included in the prototype an infrared 115 kbps transceiver. This VLC system could be used for supporting data transmission applied to low-speed sensor network connections as well. The electronic structure of a low-cost VLC transceiver, based on commercial off-the-shelf components and LED lamps is presented too. The modulation process and the Ethernet interface implemented in each access point are also described. Finally, some conclusions and application scenarios are drawn. [J364]

"Mechanism of optical degradation in microstructured InGaN light-emitting diodes"

While the enhancement of light extraction efficiency from microstructured InGaN light-emitting diodes (μ LED) has been firmly established, there is concern over the effect of microstructuring on the device lifetimes. A study on the electrical characteristics and reliability of μ LED arrays has been carried out. Despite improved optical performance, expanded device sidewalls served to accelerate the rate of optical degradation, adversely affect the lifetimes of devices. Through current-voltage plots and noise spectrum measurements, vertical current conduction along the plasma-damaged sidewalls was identified as the key degradation mechanism. [J365]

"A numerical study of Auger recombination in bulk InGaN"

Direct interband and intraband Auger recombination due to electron-electron-hole and hole-hole-electron

transitions in bulk InGaN is investigated by first-order perturbation theory including Fermi statistics, realistic electronic structures obtained by nonlocal empirical pseudopotential calculations, and their corresponding wavevector-dependent dielectric functions. Our results confirm that the intraband Auger coefficient is negligible in alloy compositions relevant for solid-state lighting and indicate that the resonant enhancement associated with interband transitions for wavelengths ranging from blue to green cannot account for the efficiency droop experimentally observed in GaN-based light emitting diodes. [J366]

"Bright Lights, Big City"

The paper presents the celebrations of the a little shop in New York city, the glory of the light bulb in the waning days of incandescence lamp. [J367]

"Solution-processed ZnO nanocrystals in thin-film light-emitting diodes for printed electronics"

Thin-film light-emitting diodes (LEDs) containing solution-processed ZnO nanocrystals (NCs) were prepared as printed electronics. The electroluminescent (EL) properties of thin-film LEDs were investigated along with the structural and photoluminescence (PL) properties of the ZnO NCs. Scanning electron microscope and x-ray diffraction studies revealed that the crystal sizes D were ranged from 5-11 nm, and can be controlled by varying growth time t in the Zn^{2+}/OH -solution at 40 °C. The time evolution of D was analyzed using Lifshitz-Slyozov-Wagner theory, showing that growth is limited by diffusion. The results of PL studies indicated that increases in the peak energies in the ultraviolet (UV) region could be attributed to the quantum-size effects on the exciton emission in the NCs with a small D , the ZnO surfaces became sufficiently passivated as D increases. Printed layers containing well-passivated ZnO NCs with different D of 8-11 nm were used as emission layers in thin-film LEDs together with pentacene hole transport layers. The current-voltage characteristics were analyzed using the trapped-charge-limited current mechanism. EL spectral measurements revealed the presence of weak UV emission that increased slightly as D decreased. [J368]

"Development of LED smart switch with light-weight middleware for location-aware services in smart home"

In recent years, the home network has focused on service diversity and the intelligent enhancement of devices for providing user-centric services. Recent studies dealing with home network systems aggregate the sensor data and manage various devices for reasoning the adaptive services. However, home network systems, especially intelligent devices, are difficult to implement due to the high setup cost and the problems with interconnection among other devices in a home domain. Therefore, we consider the intelligent implementation of light switch present in whole spaces. We propose a LED Smart switch with light-weight middleware which provides location-aware service and pattern-based service prediction. The proposed switch with an embedded sensor manages active and passive events according to the sensor data analysis and the service reasoning. Furthermore, the LED smart switch locates the user and interconnects among other switches over a network connection. The smart switch using a LED display provides simple information service, such as weather forecast, stock information, and the light status, using icons and digitalized voices. To evaluate the efficiency of our switch, we implemented testbed, in a home and an office. Our switch reduces the service response time by up to 12% for our experiment. [J369]

"A luminance adjusting algorithm for high resolution and high image quality AMOLED displays of mobile phone applications"

A luminance adjusting algorithm using light sensing scanner is proposed for small-sized high resolution and high image quality active matrix organic light emitting diode (AMOLED) displays such as smartphone applications. By using simple pixel structure with the proposed algorithm, high aperture ratio in high resolution display can be achieved. Experimental results show that the standard deviation of luminance improves from 7.07 to 1.81 LSB when the proposed adjusting method is used to 3.5-inch AMOLED display with 8-bit gray scale. [J370]

"Improved calibration technique of the infrared imaging bolometer using ultraviolet light-emitting diodes"

The technique used until recently utilizing the Ne-He laser for imaging bolometer foils calibration [B. J. Peterson et al, J. Plasma Fusion Res. 2, S1018 (2007)] has showed several issues. The method was based on irradiation of 1 cm spaced set of points on a foil by the laser beam moved by set of mirrors. Issues were the nonuniformity of laser power due to the vacuum window transmission nonuniformity and high reflection coefficient for the laser. Also, due to the limited infrared (IR) window size, it was very time consuming. The new methodology uses a compact ultraviolet (uv) light-emitting diodes installed inside the vacuum chamber in a fixed position and the foil

itself will be moved in the XY directions by two vacuum feedthroughs. These will help to avoid the above mentioned issues due to lack of a vacuum window, fixed emitters, higher uv power absorption, and a fixed IR camera position. [J371]

"Operation stability enhancement in organic photovoltaic device by a metal doped organic exciton blocking layer"

While metal diffusion in organic layers have been considered as causes for performance degradation in organic light-emitting devices, we show that suitable metal doping can instead improve physical stability of organic films. By using a metal doped organic exciton blocking layer (EBL), enhanced stability is demonstrated in unpackaged CuPc/C60organic photovoltaic devices (OPV). While devices with a pure organic EBL of bathocuproine and tris(8-hydroxyquinolato)aluminum (Alq3) show over 20% decreases in efficiency for first 150 min of operation, the device with magnesium-doped Alq3EBL shows less than 5% variation in efficiency during the same period. [J372]

"Epitaxial growth and interfacial magnetism of spin aligner for remanent spin injection: [JFe /Tb]n /Fe /MgO /GaAs -light emitting diode as a prototype system"

We have successfully grown and characterized [Fe/Tb]10/Fe(001)/57Fe(001)/MgO(001) multilayer contacts on a GaAs-based light emitting diode. Using 57Fe conversion-electron Mossbauer spectroscopy at room temperature (RT) and at 4.2 K, we provide atomistic proof of large perpendicular Fe spin components in zero external field at and below RT at the 57Fe(001)/MgO(001) interface. Further, indirect evidence of large interfacial Fe atomic moments is provided. Our contacts serve as a prototype spin aligner for remanent electrical spin injection at RT. [J373]

"An Advanced External Compensation System for Active Matrix Organic Light-Emitting Diode Displays With Poly-Si Thin-Film Transistor Backplane"

An advanced method for externally compensating the nonuniform electrical characteristics of polycrystalline silicon thin-film transistors (TFTs) and the degradation of organic light-emitting diode (OLED) devices is proposed, and the method is verified using a 14.1-in active matrix OLED (AMOLED) panel. The proposed method provides an effective solution for high-image-quality AMOLED displays by removing IR-drop and temperature effects during the sensing and displaying operations of the external compensation method. Experimental results show that the electrical characteristics of TFTs and OLEDs are successfully sensed, and that the stained image pattern due to the nonuniform luminance error and the differential aging of the OLED is removed. The luminance error range without compensation is from -6.1% to 9.0%, but it is from -1.1% to 1.2% using the external compensation at the luminance level of 120 cd/m² in a 14.1-inch AMOLED panel. [J374]

"Enhancing the Brightness of GaN Light-Emitting Diodes by Manipulating the Illumination Direction in the Photoelectrochemical Process"

In this report, a cost-effective photoenhanced electrochemical (PEC) process was proposed to assist in forming a deep undercut sidewall and rough surface on a GaN light-emitting diode (LED). As a result, a 51% improvement in light extraction efficiency was obtained compared to a standard LED without the PEC process. Manipulating the direction of light illumination during the PEC process produced an undercut angle and rough surface on the sidewall of GaN LED, which enhanced light extraction by about 14% compared to a sample prepared using the conventional PEC process. A simulation based on a two-dimensional finite-difference time-domain method was established to investigate the light output intensity for LED samples by manipulating different illumination directions in the PEC processes. Simulation results indicated that photons have a higher probability of being emitted from the undercut sidewall and cone-like surface of the LED structure formed by the PEC process; this improved the light extraction efficiency of GaN LED. [J375]

"Polymer grating imbedded organic light emitting diodes with improved out-coupling efficiency"

Organic light emitting diodes with enhanced external light coupling efficiency are demonstrated by incorporating a polymeric diffraction grating fabricated directly on top of the indium tin-oxide (ITO) electrode. Compared to the previous inorganic diffraction gratings fabricated under the ITO electrode, the polymer grating prepared by convenient lithography facilitates the fabrication process and provides good compatibility with conventional production facilities. In spite of the reduction in the emitting area, the luminance efficiency is improved by 72% by imbedding the polymer grating. The strong scattering of the guided mode enables the device to have negligible wavelength dispersion. [J376]

"Octave-spanning frequency comb generated by 250 fs pulse train emitted from 25 GHz externally phase-modulated laser diode for carrier-envelope-offset-locking"

Proposed is an approach to achieving a carrier-envelope-offset (CEO)-locked frequency comb with 25 GHz mode spacing in the telecommunications wavelength region. To achieve the approach, a 250 fs laser pulse train at a 25 GHz repetition rate was developed by intensity- and phase-modulating a seed light emitted from a continuous-wave laser diode and propagating it through a dispersive fibre. Using the authors developed tellurite photonics crystal fibre with a high-nonlinear coefficient, octave-spanning supercontinuum generation in the 1.5 μm band from a 250 MHz gated pulse train for CEO frequency detection was demonstrated. [J377]

"Integration of LED chip within patch antenna geometry for hybrid FSO/RF communication"

A free space optical (FSO)/radio frequency (RF) dual mode communication transmitter using a LED integrated within the geometry of a planar patch antenna on a shared substrate is demonstrated. An experimental FSO link is constructed with a bare die visible LED and a commercial silicon photodetector. The antenna radiating at a centre frequency of 10 GHz, provides a simultaneously operated backup RF channel for the FSO data communication link to enhance reliability. A data rate of 20 Mbits is achieved for the FSO data communication. [J378]

"Red-emitting fluorescent organic light emitting diodes with low sensitivity to self-quenching"

Concentration quenching is a major impediment to efficient organic light-emitting devices (OLEDs). We herein report on OLEDs based on a fluorescent amorphous red-emitting starburst triarylamine molecule [4-di(4'-tert-butylbiphenyl-4-yl)amino-4'-dicyanovinylbenzene, named FVIN], exhibiting a very small sensitivity to concentration quenching. OLEDs are fabricated with various doping levels of FVIN into Alq3, and show a remarkably stable external quantum efficiency of 1.5% for doping rates ranging from 5% up to 40%, which strongly relaxes the technological constraints on the doping accuracy. An efficiency of 1% is obtained for a pure undoped active region, along with deep red emission ($x=0.6$; $y=0.35$ in the Commission Internationale de l'Energie (CIE) coordinates). A comparison of FVIN with the archetypal 4-dicyanomethylene-2-methyl-6-(p-dimethylaminostyryl)-4H-pyran dye is presented in an identical multilayer OLED structure. [J379]

"Determination of the interface delta -hole density in a blue-emitting organic semiconductor diode by electromodulated absorption spectroscopy"

The hole density at the interface of a poly(fluorene-alt-triarylamine) (TFB) with p-doped poly(3,4-ethylenedioxythiophene) (PEDT) anodes has been determined from electromodulation of the TFB subgap polaron band. At 295 K, this delta -hole density σ_{OSC} is approximately $1.4 \times 10^{12} \text{ cm}^{-2}$, for which the current-voltage characteristics indicate an Ohmic contact. However at 30 K, σ_{OSC} falls to $2.4 \times 10^{11} \text{ cm}^{-2}$, and the contact characteristics approach the injecting-blocking boundary. The PEDT/TFB vacuum offset inside the device is inferred to be 0.1 eV, and so the Fermi level is not as deeply pinned in the TFB gap as suggested by ultraviolet photoemission measurements. [J380]

"Transient electroluminescence dynamics in small molecular organic light-emitting diodes"

Intriguing electroluminescence (EL) spikes, following a voltage pulse applied to small molecular OLEDs, are discussed, elucidating carrier and exciton quenching dynamics and their relation to device structure. At low temperatures, all devices exhibit spikes at 70-300 ns and μs -long tails. At 295 K only those with a hole injection barrier, carrier-trapping guest-host emitting layer, and no strong hole-blocking layer exhibit the spikes. They narrow and appear earlier under post-pulse reverse bias. The spikes and tails are in agreement with a revised model of recombination of correlated charge pairs (CCPs) and initially unpaired charges. Decreased post-pulse field-induced dissociative quenching of singlet excitons and CCPs, and possibly increased post-pulse current of holes that "turn back" toward the recombination zone after having drifted beyond it are suspected to cause the spikes' amplitude, which exceeds the dc EL. [J381]

"C and Si codoping method for p -type AlN"

Aluminum Nitride (AlN), the largest direct band gap material (6.2 eV) in the III-nitride semiconductors, is emerging as an important semiconductor due to its promising applications in the development of solid-state ultraviolet light sources in the form of light-emitting diodes and laser diodes. However, the applications have been limited by absence of p-type AlN. In view of the extremely low 10^{10} cm^{-3} hole concentration in p-type AlN reported up to date, we propose a method of C:Si codoping in AlN. We have performed ab initio density functional pseudopotential calculations to investigate the energies of separated C acceptor binding to Cn-Si ($n=0$,

1, 2, and 3, respectively) complexes in wurtzite AlN. The results show that the C_{n+1} -Si complexes are favorable and stable. In N-rich growth condition, the formation level of C2-Si complex is -0.24 eV, suggesting high doping concentration can be formed. The calculated activation energy for C2-Si is only 0.19 eV, which is 0.28 eV lower than that for a single C acceptor. The results suggest the codoping of C:Si is an effective p-type doping method in AlN. [J382]

"Visible light emission from self-catalyzed GaInP/GaP core-shell double heterostructure nanowires on silicon"

The authors report on the formation, structural analyses, and optical properties of GaInP/GaP self-catalyzed core-shell double heterostructure nanowires (NWs) grown on Si(111) substrates. The NW growth is initiated with the formation of Ga droplets as catalysts, followed by the growth of GaP core and GaInP double heterostructure shells. Structural analyses elucidate the existence of interfaces among GaP core and GaInP double heterostructure shells. Light emissions at 640 and 800 nm are observed at 77 K from GaInP core-shell double heterostructure NWs and surface states of GaInP layers, respectively. The signal from the surface state can be mitigated via surface passivation with ammonium sulfide solution. These results will enable the realization of novel NW-based light-emitting diodes or nanolasers grown on Si substrates utilizing mature Si technologies. [J383]

"Mn-doped nanocrystals in light-emitting diodes: Energy-transfer to obtain electroluminescence from quantum dots"

We fabricate light-emitting diodes (LEDs) based on Mn-doped ZnS nanocrystals along with hole-transporting N,N'-bis(3-methylphenyl)-N,N'-diphenyl-benzidine (TPD). With Mn-doping, ZnS nanostructures exhibit a strong photoluminescence. The LEDs exhibit electroluminescence (EL) from Mn-doped ZnS quantum dots and TPD. In order to open up channels for energy-transfer from TPD to quantum dots and to achieve EL from only the nanoparticles, we grow core-shell nanoparticles with Mn-doped ZnS in the core and CdS as the shell layer. Excitons formed in TPD can now transfer their energy directly to the shell-layer to yield EL from only the nanoparticles. [J384]

"Lattice site location of optical centers in GaN:Eu light emitting diode material grown by organometallic vapor phase epitaxy"

Eu-doped GaN was grown by organometallic vapor phase epitaxy at temperatures from 900 to 1100 °C. Eu incorporation is influenced by temperature with the highest concentration found for growth at 1000 °C. In all samples, Eu is incorporated entirely on substitutional Ga sites with a slight displacement which is highest (0.2Å) in the sample grown at 900 °C and mainly directed along the c-axis. The major optical Eu³⁺ centers are identical for in situ doped and ion-implanted samples after high temperature and pressure annealing. The dominant Eu³⁺ luminescence lines are attributed to isolated, substitutional Eu. [J385]

"Emission mechanisms of passivated single n-ZnO:In/i-ZnO/p-GaN-heterostructured nanorod light-emitting diodes"

The single n-ZnO:In/i-ZnO/p-GaN-heterostructured n-i-p nanorod was deposited using a vapor cooling condensation system. The photoelectrochemical system was used to directly passivate the nanorod sidewall surface with a Zn(OH)₂ layer. The electrical performance of the passivated and unpassivated single nanorod was measured using a conductive atomic force microscopy. The resulting nanorod light-emitting diodes were investigated for understanding the relevant light emission mechanisms. Since the nonradiative recombination centers, native defects, and dangling bonds existed on the nanorod sidewall surface were effectively passivated, the resultant surface leakage current was reduced and the near-band emission intensity of the nanorod light-emitting diode was increased accordingly. [J386]

"Note: Scanned multi-light-emitting-diode illumination for volumetric particle image velocimetry"

We describe the development of both multilevel two-dimensional and grid-based three-dimensional illumination systems for volumetric particle image velocimetry (PIV) that uses a single camera and an arbitrary number of low powered lasers. This flexible system is robust and capable of capturing results over a range of spatiotemporal scales determined by the choice of camera, the depth of field of the lens, and the laser power. The system is demonstrated on a rotating spin-up experiment where we extract high fidelity velocity fields at up to 62 frames/s at a spatial resolution of 2352x1728 pixels. The flexibility and economy offered by this system—approximately one-tenth that of a comparable commercial package—may make it attractive to many laboratory users. [J387]

"Multispectral imaging of the ocular fundus using light emitting diode illumination"

We present an imaging system based on light emitting diode (LED) illumination that produces multispectral optical images of the human ocular fundus. It uses a conventional fundus camera equipped with a high power LED light source and a highly sensitive electron-multiplying charge coupled device camera. It is able to take pictures at a series of wavelengths in rapid succession at short exposure times, thereby eliminating the image shift introduced by natural eye movements (saccades). In contrast with snapshot systems the images retain full spatial resolution. The system is not suitable for applications where the full spectral resolution is required as it uses discrete wavebands for illumination. This is not a problem in retinal imaging where the use of selected wavelengths is common. The modular nature of the light source allows new wavelengths to be introduced easily and at low cost. The use of wavelength-specific LEDs as a source is preferable to white light illumination and subsequent filtering of the remitted light as it minimizes the total light exposure of the subject. The system is controlled via a graphical user interface that enables flexible control of intensity, duration, and sequencing of sources in synchrony with the camera. Our initial experiments indicate that the system can acquire multispectral image sequences of the human retina at exposure times of 0.05 s in the range of 500–620 nm with mean signal to noise ratio of 17 dB (min 11, std 4.5), making it suitable for quantitative analysis with application to the diagnosis and screening of eye diseases such as diabetic retinopathy and age-related macular degeneration.

[J388]

"Multiwavelength Blue Light Source Based on MgO : PPLN SHG Using Vertically Stacked Grating-Coupled Surface-Emitting Lasers"

In this letter, we present the first experimental results of frequency doubling the output of vertically stacked grating coupled surface-emitting laser/dual-grating reflector devices with different emitting wavelengths. We used a multigrating 5% magnesium-oxide-doped periodically poled lithium niobate (MgO: PPLN) crystal as the nonlinear conversion medium. In pulse operation, 0.6 W of multiwavelength total second-harmonic peak power was obtained. The individual emitter output is focused into each channel of the crystal by diffractive beam shaping optical element array to minimize the footprint area of the whole setup. [J389]

"The properties of tris (8-hydroxyquinoline) aluminum organic light emitting diode with undoped zinc oxide anode layer"

Transparent and conductive undoped zinc oxide films were prepared by atomic layer deposition method for use in tris (8-hydroxyquinoline) aluminum (Alq3)-based organic light emitting diodes. The properties of the ZnO layers were investigated. The ZnO/CuI/Alq3/poly(ethylene glycol) dimethyl ether/Al device turned on at 7.9 V and demonstrated external quantum efficiency of 1.5% which is better comparing to the same structure but with indium tin oxide as anode layer. [J390]

"Influence of electromechanical effects and wetting layers on band structures of AlN/GaN quantum dots and spin control"

In a series of recent papers we demonstrated that coupled electromechanical effects can lead to pronounced contributions in band structure calculations of low dimensional semiconductor nanostructures (LDSNs) such as quantum dots (QDs), wires, and even wells. Some such effects are essentially nonlinear. Both strain and piezoelectric effects have been used as tuning parameters for the optical response of LDSNs in photonics, band gap engineering, and other applications. However, the influence of spin orbit effects in presence of external magnetic field on single and vertically coupled QD has been largely neglected in the literature. The electron spin splitting terms which are coupled to the magnetic field through the Pauli spin matrix in these QDs become important in the design of optoelectronic devices as well as in tailoring properties of QDs in other applications areas. At the same time, single and vertically stacked QDs are coupled with electromagnetic and mechanical fields which become increasingly important in many applications of LDSN-based systems, in particular, where spin splitting energy is important. These externally applied electric and magnetic fields as well as the separation between the vertically coupled QDs can be used as tuning parameters. Indeed, as electromagnetic and elastic effects are often significant in LDSNs, it is reasonable to expect that the externally applied magnetic fields oriented along a direction perpendicular to the plane of two-dimensional electron gas in the QDs may also be used as a tuning parameter in the application of light emitting diodes, logic devices, for example, OR gates, AND gates and others. In this paper, by using the fully coupled model of electroelasticity, we analyze the influence of these effects on optoelectronic properties of QDs. Results are reported for III-V type semiconductors with a major focus given to AlN/GaN based QD systems. [J391]

"An intentionally positioned (In,Ga)As quantum dot in a micron sized light emitting diode"

We have integrated individual (In,Ga)As quantum dots (QDs) using site-controlled molecular beam epitaxial growth into the intrinsic region of a p-i-n junction diode. This is achieved using an in situ combination of focused ion beam pre patterning, annealing, and overgrowth, resulting in arrays of individually electrically addressable (In,Ga)As QDs with full control on the lateral position. Using microelectroluminescence spectroscopy we demonstrate that these QDs have the same optical quality as optically pumped Stranski-Krastanov QDs with random nucleation located in proximity to a doped interface. The results suggest that this technique is scalable and highly interesting for different applications in quantum devices. [J392]

"Analysis of InGaN-delta-InN quantum wells for light-emitting diodes"

The design of InGaN-delta-InN quantum wells (QWs) leads to significant redshift for nitride active region with large electron-hole wave function overlap ($\Gamma_{e,h}$) and spontaneous emission rate. The analysis was carried out by using self-consistent six-band k -pband formalism. The design of active region consisting of 30 E In_{0.25}Ga_{0.75}NQW with InN delta-layer leads to large $\Gamma_{e,h}$ of >50% with emission wavelength in the yellow and red spectral regimes, which is applicable for nitride-based light-emitting diodes. [J393]

"Carrier recombination mechanisms and efficiency droop in GaInN/GaN light-emitting diodes"

We model the carrier recombination mechanisms in GaInN/GaN light-emitting diodes as $R = A_n + B_n n^2 + C_n n^3 + f(n)$, where $f(n)$ represents carrier leakage out of the active region. The term $f(n)$ is expanded into a power series and shown to have higher-than-third-order contributions to the recombination. The total third-order nonradiative coefficient (which may include an $f(n)$ leakage contribution and an Auger contribution) is found to be $8.4 \times 10^{-29} \text{ cm}^3 \text{ s}^{-1}$. Comparison of the theoretical $ABC + f(n)$ model with experimental data shows that a good fit requires the inclusion of the $f(n)$ term. [J394]

"Drooping as a simple characterization tool for extraction efficiency and optical losses in light emitting diodes"

We extend the previous droop models developed for InGaN light emitting diodes (LEDs) by accounting for the light extraction and show that drooping can be used to quantify both the extraction efficiency and the optical losses in LEDs. Our model allows very simple characterization of LEDs by an integrating sphere and therefore provides an attractive characterization tool to measure the most important loss parameters of various LED structures. In particular, the approach allows evaluation of the effects of various optical losses and photon recycling on the efficiency and consequently allows more efficient optimization of the LED structures. As an additional benefit, our measurement method does not necessarily require any fitting of the data. [J395]

"Internal efficiency of InGaN light-emitting diodes: Beyond a quasiequilibrium model"

We propose a model to better investigate InGaN light-emitting diode (LED) internal efficiency by extending beyond the usual total carrier density rate equation approach. To illustrate its capability, the model is applied to study intrinsic performance differences between violet and green LEDs. The simulations show performance differences, at different current densities and temperatures, arising from variations in spontaneous emission and heat loss rates. By tracking the momentum-resolved carrier populations, these rate changes are, in turn, traced to differences in bandstructure and plasma heating. The latter leads to carrier distributions that deviate from the quasiequilibrium ones at lattice temperature. [J396]

"Near-Infrared Organic Light-Emitting Diodes Based on Donor-pi-Acceptor Oligomers"

This letter reports efficient near-infrared (NIR) electroluminescence (EL) of organic light-emitting diodes (OLEDs) based on two donor-pi-acceptor oligomers. The energy gap can be tuned by changing the conjugated length, strengths of the acceptor component, and nonplanarity. EL with peak emission wavelengths of 775 and 905 nm were observed from the two NIR oligomers. External quantum efficiencies up to 3.54%, electrical-to-optical power efficiencies up to 15.8 mW/W, and turn-on voltage of 4.5 V were achieved in OLEDs based on these NIR emitters. [J397]

"The Impact of Inhomogeneities in the Phosphor Distribution on the Device Performance of Phosphor-Converted High-Power White LED Light Sources"

We present a study by optical ray-tracing in order to determine the impact of an inhomogeneous phosphor distribution in the color conversion elements (CCE) of phosphor-conversion-based white LED light sources. It turns out that in particular the color temperature and its angular variation, but also the flux-output are highly sensitive towards phosphor distribution variations. [J398]

"Enhancement of light power for strain-compensated hybrid InGaN/InGaN/MgZnO light-emitting diodes"

Electronic and optical properties of strain-compensated InGaN/InGaN/MgZnO quantum well (QW) structures using a MgZnO substrate are investigated using the multiband effective mass theory. A strain-compensated InGaN/InGaN/MgZnO QW structure with a larger strain shows larger matrix element than that with a smaller strain. The spontaneous emission peak rapidly increases with increasing compressive strain because the matrix element is enhanced for the strain-compensated QW structure with a larger strain. In addition, we find that the strain-compensated QW structure with the larger Mg composition in the substrate has greater spontaneous emission peak than the strain-compensated QW structure with the smaller Mg composition in the substrate.

[J399]

"Suppression of roll-off characteristics of electroluminescence at high current densities in organic light emitting diodes by introducing reduced carrier injection barriers"

We experimentally investigated suppression of the roll-off characteristics of the electroluminescence efficiency at high current densities in organic light emitting diodes (OLEDs). To increase exciton density, we propose a nonheterostructure OLED that consists of a single emitting layer of 4,4'-bis[(N-carbazole)styryl]biphenyl (BSB-Cz) and layers locally with doped donors/acceptors on the cathode and anode sides. The OLED exhibited suppression of the roll-off characteristics at high current densities over 100 A/cm² with balanced bipolar injection and transport, resulting in the high exciton density of 10²⁴ cm⁻³ s⁻¹. Furthermore, amplified spontaneous emission with a relatively low threshold of $E_{th} = 24 \mu\text{J}/\text{cm}^2$ was obtained by optically pumping the single-layer device. However, to realize electrical excitation it was necessary to reduce the lasing threshold by two orders of magnitude or to inject a 100 times higher current density. [J400]

"Improvement in output power of a 460 nm InGaN light-emitting diode using staggered quantum well"

Staggered quantum well structures are studied to eliminate the influence of polarization-induced electrostatic field upon the optical performance of blue InGaN light-emitting diodes (LEDs). Blue InGaN LEDs with various staggered quantum wells which vary in their indium compositions and quantum well width are theoretically studied and compared by using the APSYS simulation program. According to the simulation results, the best optical characteristic is obtained when the staggered quantum well is designed as In_{0.20}Ga_{0.80}N (1.4 nm)-In_{0.26}Ga_{0.74}N (1.6 nm) for blue LEDs. Superiority of this novelty design is on the strength of its enhanced overlap of electron and hole wave functions, uniform distribution of holes, and suppressed electron leakage in the LED device. [J401]

"Light output enhancement of GaN-based flip-chip light-emitting diodes fabricated with SiO₂/TiO₂ distributed Bragg reflector coated on mesa sidewall"

We report on the enhanced light output of GaN-based flip-chip light-emitting diodes (LEDs) fabricated with SiO₂/TiO₂ distributed Bragg reflector (DBR) on mesa sidewall. At the wavelength of 400 nm, five pairs of SiO₂/TiO₂ DBR coats on the GaN layer showed a normal-incidence reflectivity as high as 99.1%, along with an excellent angle-dependent reflectivity. As compared to the reference LED, the LED fabricated with the DBR-coated mesa sidewall showed an increased output power by a factor of 1.32 and 1.12 before and after lamp packaging, respectively. This could be attributed to an efficient reflection of the laterally guided mode at the highly reflective mesa sidewall, enhancing the subsequent extraction of light through the sapphire substrate.

[J402]

"Cost effective design and implementation of scanning-based LED backlight for LCD module"

Blurring effects in liquid crystal display can be observed in motion pictures if the response time of the liquid crystal molecules is not fast enough. In this study, a cost-effective architecture for backlight control system is proposed with scanning based method. A backlight control process employed with sequential lighting of the backlit pixels to reduce the blurring effects on LCD. Based on the sequential control, a 42-inch white light backlight module system with 1440 LED devices can be driven by only two driver chips. The prototyping backlight system had been implemented within one PCB in success. The measurement results from the laboratory demonstrate that the backlight system can save power dissipation and provide enough brightness for LCD. The proposed backlight system can be not only to reduce the implementation cost but also to shrink the driving board size. The implementation cost can be reduced by about 70% compared with the conventional architecture. [J403]

"Blue Light-Emitting Diodes With an Embedded Native Gallium Oxide Pattern Structure"

InGaN-based light emitting diodes (LEDs) were embedded by an insulated disk-array gallium oxide (Ga_2O_3) pattern structure that was formed through a photoelectrochemical oxidation process on a GaN layer. A 4- μm -diameter native Ga_2O_3 pattern with a top air-void structure was observed in the lower undoped GaN layer acting as a lateral overgrowth mask and as a light scattering center. In the patterned- Ga_2O_3 LED structure (PGO-LED), the light output power had an approximate 28% enhancement when compared to a conventional LED at 20 mA. In the PGO-LED structure, the lower piezoelectric field and the slightly higher internal quantum efficiency in the InGaN active layers were both measured through a bias-dependent and temperature-dependent microphotoluminescence measurement. The LED structure consists of Ga_2O_3 disk-array patterns with top air-void structures that increase external quantum efficiency for nitride-based LED applications. [J404]

"Optical polarization characteristics of ultraviolet (In)(Al)GaN multiple quantum well light emitting diodes"

The polarization of the in-plane electroluminescence of (0001) orientated (In)(Al)GaN multiple quantum well light emitting diodes in the ultraviolet-A and ultraviolet-B spectral range has been investigated. The intensity for transverse-electric polarized light relative to the transverse-magnetic polarized light decreases with decreasing emission wavelength. This effect is attributed to rearrangement of the valence bands at the Gamma -point of the Brillouin zone with changing aluminum and indium mole fractions in the (In)(Al)GaN quantum wells. For shorter wavelength the crystal-field split-off hole band moves closer to the conduction band relative to the heavy and light hole bands and as a consequence the transverse-magnetic polarized emission becomes more dominant for deep ultraviolet light emitting diodes. [J405]

"Green light emission from the edges of organic single-crystal transistors"

We have fabricated ambipolar light-emitting field-effect transistors made of 1,4-bis(5-phenylthiophen-2-yl)benzene (AC5) single crystals, which have 35% fluorescent quantum efficiency. The obtained hole and electron mobilities were $2.9 \times 10^{-1} \text{ cm}^2/\text{V s}$ and $6.7 \times 10^{-3} \text{ cm}^2/\text{V s}$, respectively. These are the highest values among AC5 transistors. Importantly, although the light emission from the crystal surface was less than the detection level of the camera, we observed bright and polarized light emission from the edge of the single crystals. This polarized edge emission is attributed to the strong self-assembled light-confining nature and perfectly aligned transition dipole moments, which are advantageous for future laser devices. [J406]

"A Fully Integrated RF-Powered Contact Lens With a Single Element Display"

We present progress toward a wirelessly-powered active contact lens comprised of a transparent polymer substrate, loop antenna, power harvesting IC, and micro-LED. The fully integrated radio power harvesting and power management system was fabricated in a 0.13 μm CMOS process with a total die area of 0.2 mm^2 . It utilizes a small on-chip capacitor for energy storage to light up a micro-LED pixel. We have demonstrated wireless power transfer at 10 cm distance using the custom IC and on-lens antenna. [J407]

"Generation of amber III-nitride based light emitting diodes by indium rich InGaN quantum dots with InGaN wetting layer and AlN encapsulation layer"

Indium rich InGaN nanostructures grown by metalorganic chemical vapor deposition were incorporated in InGaN/GaN quantum wells for long wavelength generation. These results were achieved by optimizing the growth temperature of the nanostructures, InGaN quantum well, the AlN capping layer and the GaN barrier layers. Before the growth of nanostructures, a thin InGaN wetting layer was included to reduce the lattice mismatch as well as to enhance the deposition of indium-rich InGaN nanostructures. These individual quantum wells were each subsequently capped with an AlN layer which better preserved the In-rich phase in the nanostructures and prevented the indium interdiffusion between the InGaN/GaN heterojunctions. The AlN capping layer also reduces the effect of piezoelectric field in the active layers of the light emitting diodes as seen from the reduction in the blueshift in the electroluminescence peaks with higher injection currents. The energy band profile of such a structure is discussed. [J408]

"Efficiency droop alleviation in InGaN/GaN light-emitting diodes by graded-thickness multiple quantum wells"

InGaN/GaN light-emitting diodes (LEDs) with graded-thickness multiple quantum wells (GQW) was designed and grown by metal-organic chemical vapor deposition. The GQW structure, in which the well-thickness increases along [0001] direction, was found to have superior hole distribution as well as radiative recombination distribution

by performing simulation modeling. Accordingly, the experimental investigation of electroluminescence spectrum reveals additional emission from the narrower wells within GQWs. Consequently, the efficiency droop can be alleviated to be about 16% from maximum at current density of 30 to 200 A/cm², which is much smaller than that for conventional LED (32%). Moreover, the light output power was enhanced from 18.0 to 24.3 mW at 20 A/cm².

[J409]

"The ultralow driven current ultraviolet-blue light-emitting diode based on n-ZnO nanowires/i - polymer/p-GaN heterojunction"

Under the ultralow driven current of 25 μ A an ultraviolet (UV)-blue electroluminescence (EL) with a weak defect-related emission could be obtained for the n-type (n-)ZnO nanowires (NWs)/insulating (i-)polymer/p-type (p-)GaN light-emitting diode (LED). The i-MgO layer was also explored as a carrier blocking layer for the comparison. For the i-polymer inserted LED the EL emission peak was located at 400 nm, by analyzing the spectra it is believed that the emission includes several compound originations from both ZnO and GaN. The flexible carrier blocking layer, such as i-polymer, could effectively confine the radiative recombination zone.

[J410]

"Electrical annealing for flexible organic light-emitting diodes having poly(3,4-ethylenedioxythiophene):poly(styrene sulfonate) anodes"

We present a postproduction method of electrical annealing (E-annealing) to improve the performance of flexible organic light-emitting diodes (FOLEDs) having conductive polymer anodes on a polyethersulfone substrate. The polymer that was used for the anodes was dimethylsulfoxide-doped poly(3,4-ethylenedioxythiophene):poly(styrene sulfonate). It was found that E-annealing of the fabricated FOLEDs can reduce the turn-on voltage and enhance the brightness with reduced flowing current, thereby enhancing the device efficiency. With the E-annealing method, we have successfully demonstrated efficient solution-processed green FOLEDs, which show a peak luminescence of 6 100 cd/m² and a maximum current efficiency of 16.4 cd/A. An ion migration model to explain the phenomena related to the improvement of FOLEDs is also proposed.

[J411]

"Competitive emission process in mixed single layer top-emission organic light emitting device with reduced efficiency roll-off"

The authors investigate efficiency roll-off in 5,6,11,12-tetraphenylanthracene (rubrene)-based mixed single layer top-emission organic light emitting devices by codoping with special additive dopants. The efficiency roll-off is suppressed after codoping rubrene with phenoxazone (Nile red). Due to dual nature of rubrene acting as electron hopping site and hole trap, it not only captures carrier producing light but also transfers energy to Nile red and then produces light. Meanwhile, Nile red molecules can also get energy from host directly. There exists a competitive process between three emission mechanisms, which depress self-quenching of dye molecules during emission, resulting in improved efficiency and lowered driving voltage. [J412]

"Stress-induced current and luminescence modulations in an organic light-emitting device"

The responses of the electrical and optical characteristics of an organic light-emitting device (OLED) with fac-tris(2-phenylpyridinato-N, C2') iridium (III) [Ir(ppy)₃] doped in a polymer matrix to compressive stresses were studied. The OLED converted stresses as low as 6.8 kPa into measurable and reversible changes in both current density and electroluminescence (EL) intensity. The current showed a nearly linear characteristic response with sensitivity up to 105 μ A/kPa, whereas EL decreased by three orders of magnitude at 100 kPa. The latter was attributed to increased nonradiative back energy transfer between Ir(ppy)₃ and neighboring host molecules. It is expected that similar OLEDs built on large curved surfaces may directly image stress distributions at a high-resolution and sense touch on a par with a human finger. [J413]

"Organic light emitting diodes using NaCl:N,N'-bis(naphthalene-1-yl)-N,N'-bis(phenyl)benzidine composite as a hole injection buffer layer"

Composite buffer layers of N,N'-bis(naphthalene-1-yl)-N,N'-bis(phenyl)benzidine (NPB) and NaCl at the anode/organic interface were found to be very effective on the hole injection enhancement from an indium tin oxide anode to the hole-transport layer (HTL) of NPB. Two maxima of significant current injection with respect to compositional variation were observed, implying multiple injection mechanisms of the tunneling effect and other interfacial effects. From a longer operation lifetime, the enhanced device stability was also confirmed as compared with a standard device with copper phthalocyanine as the hole injection layer. Those results are partly attributed to the better mechanical contact between anode and HTL via the composite buffer, observed from

atomic force microscopy measurement. [J414]

"AlGaInP LEDs Prepared by Contact-Transferred and Mask-Embedded Lithography"

The authors applied a simple, low-cost, mass-producible contact-transferred and mask-embedded lithography (CMEL) to texture p-GaP window layer for the fabrication of AlGaInP light-emitting diodes (LEDs) emitting at 612 nm. Under 20 mA current injection, it was found that forward voltages were 2.25, 2.39, 2.29, 2.39, 2.24, 2.21, and 2.25-V while the 20 mA output powers were 1.43, 1.42, 1.38, 1.35, 1.28, 1.22, and 1.16 mW for CMEL-400-nm LED, CMEL-600-nm LED, CMEL-800-nm LED, CMEL-1- μ m LED, CMEL-2- μ m LED, CMEL-3- μ m, and the conventional LED without CMEL, respectively. [J415]

"Optically-addressed two-terminal multicolor photodetector"

A two-terminal multicolor photodetector that is most advantageous for greater than two bands is proposed. This two-terminal design is particularly significant for focal plane arrays as it maximizes the fill factor and simplifies the readout integrated circuits. Individual color detection is realized with appropriate optical biasing. This concept is demonstrated experimentally using a three-color photodetector and biasing light emitting diodes. The measured linear dynamic range is greater than four orders of magnitude, making it a practical device for a broad range of applications. [J416]

"Optical polarization anisotropy of tensile strained InGaN/AlInN quantum wells for TM mode lasers"

In this paper, we discuss the optical characteristics and polarization anisotropy of a tensile strained polar c-plane InGaN/AlInN quantum well. We found that if the quantum well is under the tensile strain, the $|Z\rangle$ -like state will be lifted up so that the emitted light will be TM mode. In addition, with a particular aluminum composition of the AlInN alloy as the barrier for the tensile strained InGaN quantum well, it is possible to reduce quantum-confined Stark effect. The self-consistent Poisson and 646k-pSchrodinger solver has been used for studying light emitting characteristics. Our results show that the tensile strained InGaN quantum well on AlInN barrier has much larger optical gain and lower threshold carrier density compared to the conventional InGaN/GaN system, and it has a potential to be TM light source for edge emitting laser diodes with the photonic crystal cavity made by nanorod arrays. [J417]

"Concentration quenching of electroluminescence in neat Ir (ppy)₃ organic light-emitting diodes"

We studied concentration quenching of electroluminescence (EL) in organic light-emitting diodes with a neat fac-tris(2-phenylpyridinato-N, C2') iridium (III) [Ir(ppy)₃] emitting layer of different thicknesses sandwiched between electron and hole blocking layers. The intensity of the green emission decreased rapidly with increasing Ir(ppy)₃ thickness and was reversely correlated with the tail band emission. The overall light output power reached the minimum at 4 nm, and attained a saturated value for Ir(ppy)₃ thicker than 6 nm. These results are interpreted as evidence that concentration quenching in Ir(ppy)₃ originates from both short and long-range energy transfer between excited and ground states of molecules. The EL quenching magnitude was found to be independent of the injection current, indicating that biexcitonic annihilation plays a minor role. [J418]

"Optical studies of degradation of AlGaIn quantum well based deep ultraviolet light emitting diodes"

Aging under high current stress of AlGaIn quantum well based light emitting diodes with high and low Al content in the wells emitting at 270 nm and 335 nm, respectively, has been studied by scanning near field optical spectroscopy and far field electroluminescence, photoluminescence and time-resolved photoluminescence. In the high Al content devices emission band related to optical transitions in the cladding involving nitrogen vacancies has been found. Evolution of this band during aging suggests that the role of N vacancies is crucial in the aging process by aiding defect generation and formation of high conductivity channels. [J419]

"Optimization of the Yellow Phosphor Concentration and Layer Thickness for Down-Conversion of Blue to White Light"

A cerium-doped gadolinium-yttrium garnet yellow emitting phosphor was used to optimize the phosphor layer for down-conversion of blue light from InGaIn inorganic light-emitting diode (iLED) to white. Optical, morphological and elemental characterizations of phosphor were carried out. Various amounts of the phosphor were dispersed in polymethyl methacrylate polymer (PMMA)-chlorobenzene solution. The phosphor layer thickness was optimized by varying the volume of the phosphor-PMMA mixture. Using a blue emitting (458 nm) iLED, a two times larger luminance efficacy (lm/W) was obtained from down-converted white light using a 37.5 μ m thick 25 mm \times 25 mm film prepared from 30 mg of phosphor in 500 μ l of the PMMA-chlorobenzene solution. [J420]

"Top-emitting organic light-emitting diodes: Influence of cavity design"

We report on red top-emitting organic light-emitting diode structures with higher order cavities. The emission zone is placed in the first, second, and third antinodes of the electric field in the cavity by increasing the hole transport layer thickness. Furthermore, the thicknesses of the cathode and the capping layer are varied to achieve high efficiencies. Using doped charge transport layers and a phosphorescent emitter, we reach up to 29%, 17%, and 12% external quantum efficiencies for first, second, and third order devices, respectively. An optical model is further used to analyze the angular dependent emission. [J421]

"Minimal Viewing Distance Calculation in LED Display Panels"

Light-emitting diode (LED) display panels have received more attention recently. These panels usually are placed in public places such as streets, squares, highways, and stadiums for live broadcasting of sporting events, TV programs, advertisements, and movie clips. An important characteristic of these panels is the minimum distance to see contiguous images on the panel with desirable quality which is referred to as the minimal viewing distance and is represented by dV. The minimal viewing distance depends on the pixel shape and pitch of the panel. In this paper, we study the relationship between the minimal viewing distance and the pixel shape and position and then provide a method to reduce this distance. This method can be used to manufacture panels with particular diagonal and distance of pixels for a required dV for a specific location. [J422]

"Droop in III-nitrides: Comparison of bulk and injection contributions"

We study mechanisms which are thought to contribute to efficiency droop in III-nitrides. We first observe droop in a photoluminescence (PL) experiment on bulk GaN, which confirms the existence of a bulk contribution to droop, unrelated to piezoelectric fields or alloy fluctuations. We then perform biased-PL on a series of InGaN light-emitting diodes to estimate the potential impact of carrier leakage on PL experiments. We conclude that carrier leakage is only significant at very low pump densities and does not contribute to droop, thus validating the use of PL to characterize droop. [J423]

"New Pixel Design on Emitting Area for High Resolution Active-Matrix Organic Light-Emitting Diode Displays"

We propose new pixel design on emitting area and corresponding shadow mask design for high resolution active-matrix organic light-emitting diodes (AMOLEDs) to overcome the limitation of conventional shadow mask process. The proposed scheme has the extended emitting area into adjacent sub-pixel and gives flexibility for manufacturing shadow mask with quarter resolution compared with conventional requirement. The proposed scheme can use normal pixel driving circuit; however, anode electrode in each sub-pixel covers adjacent pixels to extend its own emitting aperture area for high resolution AMOLEDs. We have successfully implemented this scheme in a 4.3-in-sized WVGA (854 Ч RGB Ч 480) AMOLED using p-type advanced-solid phase crystallization (A-SPC) backplane technology and top emissive organic light-emitting diode (OLED) device structure and evaluated key performance characteristics. [J424]

"Polycrystalline Silicon TFTs Threshold Voltage Compensated Bias Current Generator for Analog Circuit Design"

A new bias current generator (BCG) with threshold voltage compensation for analog circuit design implemented with low-temperature polycrystalline silicon thin-film transistors (LT poly-Si TFTs) is proposed. The proposed topology can be used in AMOLED display applications or in other poly-Si TFTs current mode analog circuits. The functionality of the proposed circuit has been verified through simulations with HSpice. In order to obtain realistic simulations, parameters extraction in fabricated LT poly-Si TFTs was made. The simulation results indicate that the output current is independent from the transistors threshold voltage, without requiring additional capacitors or control signals for the threshold voltage compensation. Furthermore, low supply voltage is needed (10 V) and the impact of the threshold voltage variations was reduced from 54% to 3% for an output current of 2.5 μ A. [J425]

"Study on the Electron Overflow in 264 nm AlGaIn Light-Emitting Diodes"

The dependence of electron overflow on injection current, operating temperature, and structure of p-type layers was investigated in 264 nm AlGaIn light-emitting diodes (LEDs). Both increasing current and decreasing temperature resulted in the increase of electron overflow due to the insufficient barrier height and the increase of electrical field in p-type layers, respectively. The use of heterostructure as p-type layer was more favorable to suppress the overflow than single layer owing to the higher barrier for electron overflow and the lower barrier for

hole injection induced by the polarization field. Both simulation and experiment showed that the insert of thin i-AlN interlayer between active region and p-type layers can suppress the electron overflow effectively due to the further increase of barrier height. The optical properties of such LEDs were improved significantly and the maximum output power was increased by two orders of magnitude. [J426]

"Solution processable single layer organic light-emitting devices with a single small molecular ionic iridium compound"

We herein report on the occurrence of bright and efficient electrophosphorescence from a simple organic light-emitting diode (OLED) with a single organic layer comprised of a small molecular ionic iridium compound, formed using a solution process. The studied small molecular ionic iridium compound is $[\text{Ir}(\text{dfppy})_2(\text{bpy})]^+\text{PF}_6^-$, which exhibits excellent film-forming properties, bright green photoluminescence, and efficient bipolar carrier transport with balanced electron and hole mobilities of about $10^{-5}\text{cm}^2/(\text{V s})$. A high performance of the device was achieved by using a phosphorescent OLED (PHOLED) that was fabricated using the $[\text{Ir}(\text{dfppy})_2(\text{bpy})]^+\text{PF}_6^-$ compound, with a peak brightness of about $18\,000\text{cd/m}^2$ and a peak current efficiency of 12 cd/A . A peak power efficiency of 2.5 lm/W was measured at 2800cd/m^2 . These results suggest that the small molecular ionic iridium compound is a promising material for bright and efficient PHOLEDs manufactured using a simple solution process. [J427]

"Optoelectronic properties of p-n and p-i-n heterojunction devices prepared by electrodeposition of n-ZnO on p-Si"

The importance of silicon based optoelectronic devices is due to the well developed silicon technology and its potential for device integration. ZnO/Si light emitting diodes reported in the literature are based mainly on ZnO films grown by the vapor-phase techniques. Electrodeposition, a cost-effective and simple method, has not been explored adequately for the fabrication of such devices. In this study, ZnO films were electrodeposited on the (100) plane of highly B-doped p-Si substrates. Heterojunction devices (p-n and p-i-n) were constructed and characterized by means of current-voltage, capacitance-voltage, photocurrent spectroscopy, photoluminescence, and electroluminescence measurements. Electrodeposition yields compact films with a native donor density 10^{17}cm^{-3} . Diffusion of boron from Si into ZnO, during an annealing process, yields graded p-n junctions with enhanced electroluminescence. Devices exhibit a reasonably good photoresponse in the ultraviolet-blue range. The absorption of subband gap photons in ZnO shows an Urbach tail with a characteristic energy of 115 meV . The absorption and emission of light involves two prominent defect levels in ZnO, namely, L1 and E1. [J428]

"Effect of an asymmetry AlGaIn barrier on efficiency droop in wide-well InGaIn double-heterostructure light-emitting diodes"

External-quantum-efficiency (EQE) and efficiency droop in wide-well InGaIn double-heterostructure light-emitting diodes have been investigated. It was found that the insertion of an AlGaIn barrier between the n-type GaIn layer and the InGaIn well resulted in higher peak EQE and reduced efficiency droop at a higher injection level. EQE was improved by 5.7% and 25.8% over that of a sample without an AlGaIn barrier at a current density of 104.3A/cm^2 and 521A/cm^2 , respectively. It is suggested that the mechanism is attributed to an electron decelerating effect that enlarges the effective active region. [J429]

"A New Individually Addressable Micro-LED Array for Photogenetic Neural Stimulation"

Here, we demonstrate the use of a micro light emitting diode (LED) array as a powerful tool for complex spatiotemporal control of photosensitized neurons. The array can generate arbitrary, 2-D, excitation patterns with millisecond and micrometer resolution. In particular, we describe an active matrix control address system to allow simultaneous control of 256 individual micro LEDs. We present the system optically integrated into a microscope environment and patch clamp electrophysiology. The results show that the emitters have sufficient radiance at the required wavelength to stimulate neurons expressing channelrhodopsin-2 (ChR2). [J430]

"Optical second harmonic generation at heterojunction interfaces of a molybdenum trioxide layer and an organic layer"

We have observed optical second harmonic generation (SHG) from a space charge layer (SCL) in a stacked indium tin oxide (ITO)/molybdenum trioxide (MoO_3)/N'-N'-diphenyl-N'-bis(1-naphthyl)-1,1'-biphenyl-4,4'-diamine (α -NPD) system. When the MoO_3 thicknesses were increased, the SHG signals from this system decreased sharply at smaller MoO_3 thicknesses, and were saturated at MoO_3 thicknesses larger than 1 nm . These results prove the vital role of SCL in improvement of drive voltages of organic light-emitting diodes. [J431]

"Color-tunable multilayer organic light emitting diode composed of DNA complex and tris(8-hydroxyquinolino)aluminum"

In this study, the voltage-controlled color tunability of an organic light emitting diode composed of a DNA/Polyaniline/Ru(bpy)₃²⁺ complex (as the hole transport layer) and tris(8-hydroxyquinolino)aluminum (as the electron transport layer) was demonstrated. At applied voltage of 5 V, green emission was observed from Alq₃. As the voltage was increased, the emission color changed from green to yellow (14 V) to orange (16 V) and finally to red (18 V), with strong contribution of red emission from Ru(bpy)₃²⁺. This color tunability of the emission was principally a result of the shift in the carrier recombination region with an increase in applied voltage. [J432]

"Electroluminescence from AlN nanowires grown on p-SiC substrate"

Aluminum nitride (AlN) nanowires were prepared by the carbothermal reduction method. A heterojunction light-emitting diode (LED) was fabricated by depositing randomly aligned AlN nanowires onto p-type 4H-SiC substrate. When a forward bias voltage greater than 8 V was applied to the LED, a broad band emission peaked at 417 nm could be observed. The peak deconvolution revealed four emission peaks at 400, 420, 468, and 525 nm. These emission peaks may be attributed to the radiative recombination between electrons from trap-level states and holes from the valence band of the AlN nanowires. [J433]

"Development of a High-Lumen Solid State Down Light Application"

Light-emitting diode (LED)-based solid-state lighting (SSL) products have been exceeding the predicted performances especially at the chip and package levels. This has led to new SSL-based products for energy savings and long lifetimes. Large amounts of government funding and private investments have been made during the last decade to accelerate and guide the technology. This paper focuses on the development of an LED-based high-lumen luminaire technology. The critical subcomponents of the luminaire are the LED light engine (LED chips and optical system), thermal management, and driver electronics. Each of these subcomponents will be discussed in detail for a 100 W incandescent replacement technology. The paper addresses system integration of each of the subcomponents. While the design of new products evolve, the lack of reliability data poses a risk of premature failure of LED-based products. Premature failures would trigger customer rejection and may delay market penetration. Therefore, luminaire reliability is an important aspect of luminaire design. In cohort with this notion, finally, the luminaire reliability has been discussed. [J434]

"Quantification of energy loss mechanisms in organic light-emitting diodes"

The external quantum efficiency of organic light-emitting diodes (OLEDs) is limited by several loss mechanisms. By applying a numerical model for the efficiency analysis of OLED devices, we analyze the distribution of the different energy loss mechanisms in bottom and top emission organic light-emitting diodes. We validate the findings by the comparison with experimental data measured on red state-of-the-art p-i-n devices containing the red phosphorescent emitting dye iridium(III)bis[2-methyldibenzo-(f, h)quinoxaline](acetylacetonate) [Ir(MDQ)₂(acac)]. The model is used to design extremely efficient bottom and top emission diodes with 21% and 27% external quantum efficiencies, respectively. [J435]

"Effects of the intermediate SiO₂ layer on polarized output of a light-emitting diode with surface plasmon coupling"

The variation behaviors of the output intensity and polarization ratio of InGaN/GaN quantum well (QW) light-emitting diodes (LEDs) with surface plasmon (SP) coupling by inserting SiO₂ intermediate layers between the p-GaN layers and surface Ag grating structures are demonstrated. The insertion of the SiO₂ layer is expected to reduce the metal dissipation of SP energy and extend the near-field distribution range of the induced SP for generating more favored SP-QW coupling effects. The Ag grating period for optimizing SP-QW coupling is increased when a SiO₂ layer is added to the device, which is consistent with the simulation results of the momentum matching of SP polariton and the resonance behavior of localized SP. The almost unpolarized outputs from other LED samples fabricated with an epitaxial structure of thicker p-GaN layer, which leads to weak SP-QW coupling, indicate that the observed polarization ratios are due to near-field SP-QW coupling, instead of far-field diffraction. [J436]

"Polarized edge emission from GaN-based light-emitting diodes sandwiched by dielectric/metal hybrid reflectors"

Edge-emitting c-plane GaN/sapphire-based light-emitting diodes (LEDs) sandwiched by two dielectric/metal

hybrid reflectors on both sapphire and GaN surfaces were studied to determine their light emission polarization. The hybrid reflectors comprised dielectric multiple thin films and a metal layer. The metal layers of Au or Ag used in this study were designed to enhance the polarization ratio from S-polarization (transverse electric wave, TE) to P-polarization (transverse magnetic wave, TM). The two sets of optimized dielectric multi thin films served as matching layers for wide-angle incident light on both sapphire and GaN surfaces. To determine which reflector scheme would achieve a higher polarization ratio, simulations of the reflectance at the hybrid reflectors on sapphire (or GaN) interface were performed before the fabrication of experimental LEDs. Compared with conventional c-plane InGaN/GaN/sapphire LEDs without dielectric/metal hybrid reflectors, the experimental LEDs exhibited higher polarization ratio (ITE-max/ITM-max) with $r=2.174$ (3.37dB) at a wavelength of 460 nm. In contrast, the original polarized light (without dielectric/metal hybrid reflectors) was partially contributed ($r=1.398$) by C-HH or C-LH (C band to the heavy-hole sub-band or C band to the crystal-field split-off sub-band) transitions along the a-plane or m-plane direction. [J437]

"Light out-coupling enhancement of organic light-emitting devices with microlens array"

Light out-coupling efficiency of organic light-emitting devices from high-index glass substrate into air is enhanced by attaching ordered microlens arrays, which are fabricated by a roll-to-roll mold transfer process. The dependence of microlens geometries on light extraction is analyzed experimentally and theoretically. An increase of 60% in the light out-coupling with an optimized elliptical microlens array is achieved over a conventional device without affecting the electroluminescent spectrum. [J438]

"Thermal stability of Si-doped InGaN multiple-quantum wells for high efficiency light emitting diodes"

Excitation power dependent photoluminescence (PL) spectroscopy was employed to determine the thermal degradation of InGaN quantum wells (QWs) structure with different Si doping in well region. At a low excitation power density, PL intensity of undoped InGaN well was significantly decreased, while those of interfacial and full Si-doped InGaN well were slightly reduced by rapid thermal annealing (RTA) process. However, PL measurement with high excitation power density showed that PL intensities of InGaN QWs regardless of Si doping were almost similar with/without RTA process. In addition, x-ray diffraction results indicated that Si-doping in well could improve the interfacial quality of InGaN QWs. Therefore, we suggest that Si doping suppress the generation of nonradiative recombination centers by thermal degradation at weaker localization states which could be easily filled by low excitation carriers. [J439]

"Characteristics of efficiency droop in GaN-based light emitting diodes with an insertion layer between the multiple quantum wells and n -GaN layer"

We have studied the characteristics of efficiency droop in GaN-based light emitting diodes (LEDs) with different kinds of insertion layers (ILs) between the multiple quantum wells (MQWs) layer and n-GaN layer. By using low-temperature (LT) (780 °C)n-GaN as IL, the efficiency droop behavior can be alleviated from 54% in reference LED to 36% from the maximum value at low injection current to 200 mA, which is much smaller than that of 49% in LED with InGaN/GaN short-period superlattices layer. The polarization field in MQWs is found to be smallest in LED with InGaN/GaN SPS layer. However, the V-shape defect density, about $5.34 \times 10^8 \text{ cm}^{-2}$, in its MQWs region is much higher than that value of $2.94 \times 10^8 \text{ cm}^{-2}$ in LED with LT n-GaN layer, which will lead to higher defect-related tunneling leakage of carriers. Therefore, we can mainly assign this alleviation of efficiency droop to the reduction of dislocation density in MQWs region rather than the decrease of polarization field. [J440]

"Efficiency dependence on alkali metal compound/Al bilayer cathode in organic light-emitting diodes"

The use of alkali metal compound/Al bilayer cathodes of LiF/Al and Liq/Al caused a dramatic luminous efficiency change of one order of magnitude in organic light-emitting diodes (OLEDs) comprising 2-methyl-9,10-bis(naphthalene-2-yl)anthracene (MADN) as an electron-transporting layer (ETL). In contrast, the use of the same two electrodes yielded similar efficiency in OLEDs comprising of tris(8-hydroxyquinoline) aluminum(III) (Alq3) as an ETL. The dramatic change is attributed to different behaviors of LiF/Al and Liq/Al cathodes toward the ETL. It is revealed that organic alkali metal complex/Al, such as Liq/Al, is superior to inorganic alkali metal compound/Al, such as LiF/Al, as a standard bilayer cathode to investigate the effectiveness of electron-transporting materials for high-efficiency OLEDs. [J441]

"Temperature rise in InGaN/GaN vertical light emitting diode on copper transferred from silicon probed by Raman scattering"

The authors report on a Raman scattering study of self-heating in InGaN/GaN-based thin film vertical light emitting diode (VLED) on copper successfully transferred from silicon (111). The LED structures grown on bulk Si are transferred to a copper substrate host using electroplating and sacrificial removal of silicon by grinding, lapping and dry etching. The light emission characteristics of such VLEDs are studied by electroluminescence measurements. Due to self-heating at very high injection current, the temperature of the p-side down VLED without encapsulation and packaging increases rapidly and correlates well with the I-V characteristics. The Raman measurements allow probing of temperature profiles when these VLEDs are driven at current up to 1 A. [J442]

"Magnetic field effects on the electroluminescence of organic light emitting devices: A tool to indicate the carrier mobility"

The magnetoelectroluminescence (MEL) of organic light emitting devices with a N,N'-bis(1-naphthyl)-N,N'-diphenyl-1,1'-biphenyl-4,4'-diamine:tris-(8-hydroxyquinoline) aluminum (NPB:Alq3) mixed emission layer (EML) has been investigated. We find that MEL is maximized when the volume ratio of NPB of the mixed EML reaches 30% and the EML thickness is 40 nm. The features of MEL under various magnetic field strengths are insensitive to the change in EML thickness and mixing ratio. Meanwhile, MEL has a close relationship with the carrier mobility. We have conducted a theoretical study to further verify the relationship. Our experimental and theoretical results confirm that MEL can function as a tool to indicate the mobility. [J443]

"513 Mbit/s Visible Light Communications Link Based on DMT-Modulation of a White LED"

We report a visible-light wireless point-to-point communication link operating at 513 Mbit/s gross transmission rate (net Mbit/s). The bit-error ratio of the uncoded data was smaller than for an illumination level of 1x. The link was based on a commercial thin-film high-power phosphorescent white LED, an avalanche photo diode, and off-line signal processing of discrete multitone signals. Quadrature-amplitude modulation, bit- and power-loading, as well as symmetrical clipping were successfully employed in pushing the gross transmission rate beyond 500 Mbit/s. Adaptation of the clipping level increased the data rate only by 2%, while simulations predicted an enhancement of 20%. Obstacles towards higher data rates as well as potential remedies are discussed. We predicted that data rates of over 1 Gbit/s can be achieved with the same setup and under the same experimental conditions if these obstacles are overcome. [J444]

"A study of the role of dislocation density, indium composition on the radiative efficiency in InGaN/GaN polar and nonpolar light-emitting diodes using drift-diffusion coupled with a Monte Carlo method"

In this paper, we apply the Poisson, drift-diffusion, and Schrodinger solver coupled with the Monte Carlo method to study the in-plane carrier dynamics in the InGaN c-plane and nonpolar plane quantum well light-emitting diode device. Carrier diffusion, scattering, radiative recombination, and trapping by dislocation defects in the quantum well are studied. The impact of carrier dynamics on the internal quantum efficiency (IQE) in the quantum well with different indium compositions, dislocation densities, polarization effect, and interface roughness is studied. Our results show that (for dislocations densities in typical devices) due to the large radiative lifetime from the quantum confined Stark effect, nonradiative recombination caused by the dislocation defects plays a dominated role in limiting the IQE. In the nonpolar quantum well, the IQE is much better than in the c-plane case but is still strongly influenced by dislocation density. Our results show that to achieve 100% IQE, the dislocation density levels need to be lower than 10^6 cm^{-2} and 10^7 cm^{-2} for c-plane and nonpolar plane InGaN quantum well, respectively. Our results are also compared with published experimental work and have shown a good agreement. [J445]

"A local dimming algorithm for low power LCD TVs using edge-type LED backlight"

A local dimming algorithm is proposed to reduce the power consumption of LCD TVs using edge-type LED backlight. The proposed local dimming algorithm is implemented by matrix driving of orthogonally located LEDs at the edge of the backlight. The dimming rate of LED string is determined according to target luminance of local blocks and modified to reduce image distortion. The backlight power saving ratios of four typical images are 23.2-53.2 % and 30.2- 54.3% by using proposed division and rate algorithms, respectively. PSNR is greater than 48 dB using proposed local dimming algorithms. [J446]

"Degradation of InGaN-based laser diodes analyzed by means of electrical and optical measurements"

In this paper we present a detailed analysis of the degradation of InGaN-based laser diodes carried out by

means of electrical and optical techniques. The study is based on the comparison between the degradation kinetics of laser diodes and light-emitting diode (LED)-like samples, i.e., devices with the same epitaxial structure as the lasers, but with no ridge and facets. Results described in the following indicate that degradation of lasers and LED-like samples is due to the same mechanism, possibly involving the generation of point defects within the active region of the devices. Furthermore, since degradation occurs both in lasers and in LED-like samples (i.e., structures with no current confinement), results suggest that degradation of lasers is not correlated with the geometry of the devices, nor to worsening of current confinement under the ridge. [J447]

"Correlations for predicting the surface wettability for organic light-emitting-diode patterns by x-ray photoelectron spectroscopy analysis"

X-ray photoelectron spectroscopy (XPS) and contact angle measurements have been made to characterize patterned organic light-emitting-diode (OLED) substrates comprising indium-tin-oxide and a photoresist, both of which are modified by treatment with oxygen and tetrafluoromethane in a radiofrequency (13.56 MHz) low-power (~ 1 W) capacitively coupled plasma as a function of time. Correlations between the surface chemical compositions from XPS and the contact angle, θ , are evaluated in order that the wettability of very small areas may be predicted. Very clear correlations for both the indium-tin-oxide and the photoresist surfaces are obtained enabling the prediction of the contact angles for these plasma-treated OLED materials from XPS data to a standard uncertainty of 9% in $\cos \theta$. These correlations need to be extended to a wider range of compositions in order to establish the physicochemical properties of particular surface functional groups that control water contact angles by this method. [J448]

"Experimental observation of polarized electroluminescence from edge-emission organic light emitting devices"

We have observed a strongly polarized edge-emission from an organic light emitting device (OLED) with a silicon anode and a stacked Sm/Au (or Ag) cathode. For the OLED with a Sm/Au cathode, the transverse magnetic (TM) mode is stronger than the transverse electric (TE) mode by a factor of 2, while the polarization ratio of TM:TE is close to 300 for that with a Sm/Ag cathode. The polarization results from the scattering of surface plasmon polaritons at the device boundary. Such a silicon-based OLED is potentially an electrically excited SPP source in plasmonics. [J449]

"Thermal Resistance and Reliability of High-Power LED Packages Under WHTOL and Thermal Shock Tests"

The light emitting diode (LED) packaging problems associated with high cost, high junction temperature, low luminous efficiency, and low reliability have to be resolved before the LED gaining more market acceptance. In this paper, chip-on-plate (CoP) LED packages with and without phosphors are evaluated in terms of thermal resistance and reliability under wet and high-temperature operation life (WHTOL) and thermal shock tests. The WHTOL test is with the condition of 85°C/85%RH and 350 mA of forward current for 1008 h, while thermal shock test is with 200 cycles at temperature ranging from -40°C to 125°C. The thermal behavior of the CoP packages was analyzed by 1-D thermal resistance circuit (1-D TRC) with and without spreading angle, 3-D TRC method, and 2-D axisymmetric finite element method. The feasibility of these analyses was evaluated and discussed in detail by comparing those results with experimental measurements. The reliability results indicated that all CoP packages with phosphors in the silicone encapsulant failed after 309 h in the WHTOL test, but all those without phosphors still survived after 1008 h. The failure modes were found to be the debonding of the aluminum wire from the chip or copper pad of the substrate. However, after the aluminum wire was replaced by gold wire, all the packages with and without phosphors passed after 1008 h. For these survival packages in the WHTOL test, their thermal resistances of junction-to-air and junction-to-aluminum substrate increased by about 12 and 9°C/W, respectively. Moreover, it was also found that there is a difference of 38°C/W in the junction-to-air thermal resistances for the packages between under natural and forced convections in the chamber during the WHTOL test. This might yield the different reliability data, unless the flow conditions in the test chamber are specified in this standard test. Furthermore, all the packages with and without phosphors could pass 200--cycles in thermal shock test, with minor changes in the thermal resistances. However, the degradation of luminous flux in the packages with phosphors was found to be greater than those without phosphors by 14% vs. 9%. [J450]

"A novel sequential-color RGB-LED backlight driving system with local dimming control and dynamic bus voltage regulation"

Higher luminance efficacy, wider color gamut, lower power consumption, faster response, longer operation life, lesser environmental impacts, and local dimming capability make RGB LED backlight driving system suitable for high end LCD applications. In this paper, a digitally controlled four-phase interleaved RGB LED backlight driving

system for LCD panels is proposed. Field color sequential (FCS) techniques, local dimming control (LDC) and dynamic bus voltage regulation (DBVR) technologies are implemented in the proposed system. FCS can improve the power efficiency and image quality, LDC can reduce the power consumption and enhance the image contrast ratio and DBVR can maximize the driving system's efficiency. Only one power converter is required in the proposed system; therefore the system configuration is very simple. Finally, experimental results are provided to validate the effectiveness and correctness of the proposed system. According to the experimental results, the presented system can successfully drive the RGB LED backlight module, and the color-mixing, local dimming and bus voltage regulation functions can be successfully realized. [J451]

"A Vertically Integrated CMOS Microsystem for Time-Resolved Fluorescence Analysis"

We describe a two-chip micro-scale time-resolved fluorescence analyzer integrating excitation, detection, and filtering. A new 848 array of drivers realized in standard low-voltage 0.35- μm complementary metal-oxide semiconductor is bump-bonded to AlInGaN blue micro-pixelated light-emitting diodes (micro-LEDs). The array is capable of producing sample excitation pulses with a width of 777 ps (FWHM), enabling short lifetime fluorophores to be investigated. The fluorescence emission is detected by a second, vertically-opposed 16 \times 4 array of single-photon avalanche diodes (SPADs) fabricated in 0.35- μm high-voltage CMOS technology with in-pixel time-gated photon counting circuitry. Captured chip data are transferred to a PC for further processing, including histogramming, lifetime extraction, calibration and background/noise compensation. This constitutes the smallest reported solid-state microsystem for fluorescence decay analysis, replacing lasers, photomultiplier tubes, bulk optics, and discrete electronics. The system is demonstrated with measurements of fluorescent colloidal quantum dot and Rhodamine samples. [J452]

"Die Bonding for a Nitride Light-Emitting Diode by Low-Temperature Sintering of Micrometer Size Silver Particles"

Die-bonding for a nitride light-emitting diode (LED) by sintering of micrometer size Ag particles in air at 200°C was investigated. Micrometer size Ag particles absorb oxygen remarkably well at 200°C and above, and on sintering, they form a porous layer. The activating temperature of the sintering is in good agreement with the oxygen adsorption temperature. Sintering does not progress in the absence of oxygen. A reduction of thermal resistance and an improvement of reliability are achieved by the sintered layer as a die attach to a surface-mount-type LED. This mounting method is useful in the die bonding of electronic components, and is an alternative technique to high-temperature lead soldering. [J453]

"Hole injection and efficiency droop improvement in InGaN/GaN light-emitting diodes by band-engineered electron blocking layer"

A graded-composition electron blocking layer (GEBL) with aluminum composition increasing along the [0001] direction was designed for c-plane InGaN/GaN light-emitting diodes (LEDs) by employing the band-engineering. The simulation results demonstrated that such GEBL can effectively enhance the capability of hole transportation across the EBL as well as the electron confinement. Consequently, the LED with GEBL grown by metal-organic chemical vapor deposition exhibited lower forward voltage and series resistance and much higher output power at high current density as compared to conventional LED. Meanwhile, the efficiency droop was reduced from 34% in conventional LED to only 4% from the maximum value at low injection current to 200A/cm². [J454]

"Analysis of Thermal and Luminous Performance of MR-16 LED Lighting Module"

Light emitting diode (LED) with a long lifetime, low power consumption, and low pollution has been successfully applied in many products. However, due to its low electro-optical conversion efficiency, high percentage of input power transformed to redundant heat, thus increasing the LED temperature. This phenomenon decreases the luminous flux, changing light color, and useful life span of LED. Therefore, thermal management becomes an important issue in high power LED. In this paper, the variation of luminous flux and light color for different LED lighting modules under long time operation has been measured and discussed. In addition, a detailed finite element model of LED lighting module, MR-16, with a corresponding input power and suitable boundary conditions is established by using the ANSYS finite element analysis program. Furthermore, to validate the simulation results, the current-voltage-temperature method for characterization of a diode is utilized to measure the junction temperature of LED chip indirectly and compare with simulation results. After the simulation is validated, various thermal performance assessments under the different design parameters of the LED package and lighting module are also investigated in this paper. The methodology and analysis results of this paper can provide a guideline for the LED lighting module such as MR-16 design in the future. [J455]

"Coupled Thermal and Thermo-Mechanical Design Assessment of High Power Light Emitting"

Diode"

Coupled thermal and mechanical design issues in a high power light emitting diode (LED) package platform are investigated using numerical models. A thermal resistance network model and a 3-D finite element model are built for thermal and stress analyses. They are validated with the experimental data and subsequently utilized to study the effect of key parameters on the junction temperature and the thermal strains. An extensive parametric analysis is conducted to assess the effect of design and material parameters on the junction temperature and thermal strains of the high power LED under study. Based on the results, the desired parameters of adhesives for high power LED applications are identified and an example of an LED thermo-mechanical design protocol is presented. [J456]

"Understanding efficiency droop effect in InGaN/GaN multiple-quantum-well blue light-emitting diodes with different degree of carrier localization"

Two light-emitting diode samples are grown with InGaN and GaN underlying layers beneath the multiple quantum wells (MQWs), respectively. By measuring the carrier lifetime as a function of photon energy, it is found that the MQW with InGaN underlying layer has a higher degree of carrier localization. Comparison between the external quantum efficiency and injection current of these two samples reveals that efficiency droop at small injection current is attributed to the delocalization of carriers, while further droop at a higher injection current is due mostly to the carrier leakage demonstrated through temperature-dependent electroluminescence measurements. [J457]

"Enhancement of current injection in inverted organic light emitting diodes with thermal annealing"

The enhancement of current density in inverted organic light emitting diodes is achieved by thermal annealing after device process. The current-voltage characteristics of annealed devices are improved as compared to that of nonannealed devices. The current improvement is attributed to the increase in electron injection efficiency from the inverted cathodes. X-ray and ultraviolet photoemission spectroscopy were also carried out to investigate the origins of the enhancement. The result shows that the activation of doping effect of the inverted Alq3trilayers occurs after thermal annealing. However, the current density is still not compatible to that of normal devices with Alq3trilayers as the cathode on the top. The reason is found to be related to the oxidation of aluminum cathodes, which are deposited first in the inverted devices. [J458]

"Influence of carrier dynamics on the modulation bandwidth of quantum-dot based nanocavity devices"

We theoretically investigate the modulation response of quantum-dot based nanocavity light emitting devices. For high Purcell enhancement factors, our theory predicts the possibility of decreasing the modulation bandwidth with increasing scattering rate into the lasing quantum-dot state. This counterintuitive effect is investigated using a microscopic semiconductor model. The resulting guidelines for possible optimizations of quantum-dot based nanocavity laser devices are given. [J459]

"Future direction of direct writing"

Direct write technology using special inks consisting of finely dispersed metal nanoparticles in liquid is receiving an undivided attention in recent years for its wide range of applicability in modern electronic industry. The application of this technology covers radio frequency identification-tag (RFID-tag), flexible-electronics, organic light emitting diodes (OLED) display, e-paper, antenna, bumpers used in flip-chip, underfilling, frit, miniresistance applications and biological uses, artificial dental applications and many more. In this paper, the authors have reviewed various direct write technologies on the market and discussed their advantages and shortfalls. Emphasis has given on microdispensing deposition write (MDDW), maskless mesoscale materials deposition (M3D), and ink-jet technologies. All of these technologies allow printing various patterns without employing a mask or a resist with an enhanced speed with the aid of computer. MDDW and M3D are capable of drawing patterns in three-dimension and MDDW, in particular, is capable of writing nanoinks with high viscosity. However, it is still far away for direct write to be fully implemented in the commercial arena. One of the hurdles to overcome is in manufacturing conductive inks which are chemically and physically stable, capable of drawing patterns with acceptable conductivity, and also capable of drawing patterns with acceptable adhesiveness with the substrates. The authors have briefly discussed problems involved in manufacturing nanometal inks to be used in various writing devices. There are numerous factors to be considered in manufacturing such inks. They are reducing agents, concentrations, oxidation, compact ability allowing good conductivity, and stability in suspension. [J460]

"Silicon emitter for shortwave infrared (1.6-3 mcm) band by light down-conversion"

No silicon-based light emitting diodes exist for shortwave infrared (1.6-3.0μm) band due to bandgap limitations imposed on luminescence wavelengths. To alleviate this problem, we propose a photonic device in which below-bandgap radiation comes as the result of the thermal emission enhanced by free charge carriers generated by the above-bandgap excitation (light downconversion). With this approach, we demonstrate high-temperature ($T > 300\text{K}$) large-area ($20 \times 20\text{mm}^2$) Si emitter with stable high-power output ($\sim 100\text{mW/cm}^2$) and prescribed spectrum inside the 1.6-3.0μm band for applications such as dynamic scene simulation devices operating at frequencies above 1 kHz. [J461]

"3-D without four eyes"

New glasses-free 3-D devices are about to hit the market, and their backers are hoping they'll make 3-D spectacles as obsolete as Smell-O-Vision. These gadgets, described as "autostereo" to distinguish them from the kind requiring eyewear, will include not only game consoles like the one I've been playing with but also cameras, cellphones, and tablet computers. Among the first will be autostereo 3-D TVs, just now hitting stores in Japan, and Nintendo's 3DS handheld games console, due for release worldwide early next year. To perceive three dimensions, a person's eyes must see different, slightly unaligned images. In the real world, the spacing between the eyes makes that happen naturally. On a video screen, it's not so simple; one display somehow has to present a different and separate view to each eye. Some systems handle this challenge by interspersing the left and right views; they're called multiplexed. Others, called sequential, alternate left and right views. Whatever the approach, the displays then use optical or technological tricks to direct the correct view to the correct eye. For example, the bulkiest glasses used with currently available 3-D TVs are active-shutter glasses. They contain a set of miniature LCD panels that synchronize with the large LCD screen in the TV. When the main screen is showing an image destined for your right eye, a liquid-crystal shutter in the left lens of the glasses makes that lens opaque, and vice versa. This sequential system switches between images meant for each eye dozens of times a second, creating a smooth 3-D effect. It works well. In theory, at least. According to a survey of 1400 Americans by the market research firm Interpret, a quarter of gamers got headaches from 3-D, a fifth complained of eyestrain, and one in six said that they felt disoriented or dizzy after playing. In a similar survey of 2000 Americans by the market research firm NPD Group, over half said that having to wear glasses would discourage them-- from upgrading to 3-D altogether. And the glasses aren't cheap. Hightech 3-D specs cost US \$100 or more, and a pair bought from, say, Sony typically won't work with a Panasonic or LG Electronics TV. [J462]

"Reduced efficiency roll-off in electrophosphorescent devices by a short-living rhenium emitter with well-matched energy levels"

We demonstrated reduced efficiency roll-off in electrophosphorescent devices based on a rhenium [Re(I)] complex, {9, 9-Di-[9'-(4"-phenoxybutyl)-9'H-carbazyl]-9-H-4,5-Diazafluorene Re(CO)₃Br} (Re-PCDF). The devices based on Re-PCDF exhibited the peak luminance of 7888 cd/m² and the maximum efficiency of 7.41 cd/A, respectively. Remarkably, the devices exhibited very small efficiency roll-off with only ca. 28%, which is much better than the reported Re(I) complexes based devices. Such excellent performances could be ascribed to the short luminescent lifetime of Re-PCDF and well-matched energy levels between the singlet host and the triplet emitter. The detailed mechanisms of such small efficiency roll-off were also investigated. [J463]

"Electroluminescence of green CdSe/ZnS quantum dots enhanced by harvesting excitons from phosphorescent molecules"

We demonstrated the enhancement of electroluminescence from green CdSe/ZnS quantum dots (QDs) in hybrid QD/organic light-emitting diodes (LEDs) by employing blue phosphorescent dyes bis(4,6-difluorophenyl)pyridinato-N,C2)picolinatoiridium (FIrpic) as efficient exciton harvesters and energy transfer donors. Precise control over the position and concentration of the donors doped in a fluorescent host led to complete exciton energy transfer from FIrpic molecules located within the Forster distance of 8 nm from the QD layer, and a 2.5-fold increase in the quantum efficiency of the QD-LEDs. [J464]

"Controlling charge balance and exciton recombination by bipolar host in single-layer organic light-emitting diodes"

Highly efficient single-layer organic light-emitting diodes with reduced efficiency roll-off are demonstrated by using a bipolar host material of 2,5-bis(2-(9H-carbazol-9-yl)phenyl)-1,3,4-oxadiazole (o-CzOXD) doped with iridium complexes as the emissive layer. For example, the green single-layer device, employing fac-tris(2-phenylpyridine)iridium Ir(ppy)₃ as dopant, shows a peak current efficiency of 45.57 cd A⁻¹, corresponding to external quantum efficiency (EQE) of 12.42%, and still exhibits efficiencies of 45.26 cd A⁻¹ and 40.42 cd A⁻¹ at luminance of 1000 and 10 000 cd m⁻², respectively. In addition, the yellow and red single-layer devices, with

bis(2-(9,9-diethyl-9H-fluoren-2-yl)-1-phenyl-1H-benzimidazol-N,C3)iridium(acetylacetonate) (fbi)2Ir(acac) and bis(1-phenylisoquinolinolato-C2,N)iridium(acetylacetonate) (piq)2Ir(acac) as emitter, also show high EQE of 7.04% and 7.28%, respectively. The transport properties of o-CzOXD film are well investigated by current-voltage measurement, from which both hole and electron mobility are determined. It is found that the o-CzOXD shows appealing bipolar transport character, which is favor for the balanced charge distribution in the whole doped zone. More importantly, the multifunctional role of hole trapping and electron transporting of the iridium complex in o-CzOXD further balances the charge carriers and broadens the recombination zone. As a result, the recombination of electrons and holes is significantly improved and the triplet-triplet annihilation and triplet-polaron quenching processes are effectively suppressed, eventually leading to the high efficiency as well as the reduced efficiency roll-off. [J465]

"Effects of Nanometer-Scale Photonic Crystal Structures on the Light Extraction From GaN Light-Emitting Diodes"

This paper reports on the effect of nanometer-scale photonic crystal structures on the enhancement of the light extraction in GaN light-emitting diodes. Photonic crystals with hole or pillar-patterned structures with lattice constants of 460, 600, 750, and 920 nm are fabricated on indium-doped tin oxide (ITO) electrodes and/or p-GaN layers using laser holography and reactive ion etching. It is found that the light extraction efficiency depends strongly on the distance between the photonic crystal and the active layer, as well as the lattice constant for both structures. Photonic crystal light-emitting diodes (LEDs) with a lattice constant of 750 nm and hole depths of 260 nm in the ITO layer show an increase in light extraction of up to 32%, compared to conventional LEDs, without degradation in the electrical properties while a maximum enhancement of 26% is obtained from the device with a lattice constant of 460 nm and pillar heights of 60 nm on the p-GaN layer. The dependence of the extraction efficiency on the lattice constant is also calculated using a 3-D finite-difference time-domain method and compared with experimental results. [J466]

"The Impact of Spectral and Spatial Exciton Distributions on Optical Emission From Thin-Film Weak-Microcavity Organic Light-Emitting Diodes"

We present an analytical model for the optical emission produced by sources located in a thin-film weak-microcavity formation and study the effects of the ensemble spectral and spatial distribution on the device emission properties. However derived for a general stratified media configuration, the formulation results are highly applicable for the study of nanometric organic light-emitting devices. Rigorously developed into closed-form analytical expressions using the device's thin-film weak-microcavity characteristics, they enable clear observation of the underlying physical processes that determine the emission properties of the device, as well as the impact of the exciton ensemble spectral and spatial distributions on these properties. For the sake of simplicity and clarity, we focus on a 2-D canonical configuration excited by impulsive (line) sources. Our results show that the spectral distribution of the ensemble diminishes interference effects originated in the weak microcavity formed between the substrate/air and cathode/active layer interfaces, while the spatial distribution can only impact the slow-varying component of the emission pattern, which is the consequence of the source-image interference near the highly reflecting cathode. For a typical device, the quasi-Lambertian emission pattern reported experimentally is reproduced. It should be pointed out that the incorporation of both rigorous electromagnetic analysis and the source spectral and spatial broadening effects is addressed in our report, to the best of our knowledge, for the first time. This results in a precise model capable of repeating and interpreting experimental and simulated data. [J467]

"Light Output Enhancement of GaN-Based Light-Emitting Diodes Using ZnO Nanorod Arrays Produced by Aqueous Solution Growth Technique"

ZnO nanorod arrays were successfully deposited on GaN-based light-emitting diodes (LEDs) using the aqueous solution growth technique. A 20.3% light output enhancement of the LEDs with ZnO nanorod array was obtained at an injection current of 100 mA. With the presence of the ZnO nanorod array, divergence of the light output was reduced and the light output was confined in a smaller escape cone of about 30° rather than 42° of the conventional LEDs. Current-voltage characteristics and electroluminescence measurements confirmed that there was no significant change in electrical and optical properties of these LEDs with ZnO nanorod arrays. [J468]

"InGaN/GaN White Light-Emitting Diodes Embedded With Europium Silicate Thin Film Phosphor"

This article describes the successful fabrication of europium-silicate thin film phosphor and its application to InGaN/GaN white light-emitting diodes (LEDs) in order to improve the photometric properties of the LEDs, including their correlated color temperatures (CCT) and color rendering index (CRI). The europium-silicate

compounds are deposited on GaN templates grown on sapphire substrates by RF-sputtering and then annealed at 1000°C in an N₂ ambient to form a thin film phosphor that produces yellow or red emissions. The thin film phosphor is then patterned with stripes to grow a GaN buffer layer by epitaxially laterally overgrown GaN (ELOG) techniques, on which LED structures are grown by metal organic chemical vapor deposition. The ELOG sample shows no pits on the surface, and the full widths at half maximum (FWHMs) of its X-ray rocking curve for the (002) and (102) planes are as low as 249 and 416 arcsec, respectively. The optical spectrum from the embedded thin film phosphor is adjusted to have a maximum intensity at 560-600 nm and a FWHM as wide as 90 nm to make up for the low efficiency at these wavelengths of conventional YAG-based yellow phosphor. Finally, we observed a tristimulus coordinate (x, y) = (0.33, 0.39), CCT = 5607 K, and CRI = 77.6 from the white LEDs with thin film phosphor as compared with (x, y) = (0.30, 0.28), CCT = 8467 K, and CRI = 66.52 for the white LEDs without thin film phosphor. [J469]

"Highly-directional emission patterns based on near single guided mode extraction from GaN-based ultrathin microcavity light-emitting diodes with photonic crystals"

This study investigates the distribution of highly-directional far-field emission on GaN-based ultrathin microcavity light-emitting diodes (uMCLEDs) with photonic crystals (PhCs). The ultrathin 550 nm cavity, PhC lattice constant of 370 nm, and hole depth of 250 nm in the GaN PhC uMCLED provide near single guided mode extraction and a pattern of high directionality radiation. Angular-spectral-resolved electroluminescence measurements reveal photon-band structure agreement with the fundamental mode effective refractive index dispersion curve. In addition, GaN PhC uMCLED increase the output power extraction efficiency by 145.9% ($\times 2.464$) compared with GaN non-PhC uMCLED, and a directional far-field emission pattern at half intensity of nearly $\pm 15^\circ$. [J470]

"Comparison of ultraviolet- and charge-induced degradation phenomena in blue fluorescent organic light emitting diodes"

We compare the degradation of organic light emitting diodes (OLEDs) by UV light and by electrical driving. We prove that the exponential dependence of the half-lifetime on the current density known from electrical aging is also valid for UV-degradation. The influence of excitons on the degradation of OLEDs is determined and we experimentally distinguish between the influence of singlet and triplet excitons. We conclude that singlet excitons are the main cause of degradation for Spiro-DPVB(2,2',7,7'-tetrakis(2,2-diphenylvinyl)spiro-9,9'-bifluorene)-based OLEDs by a comparison of the degradation of electrically driven and UV-excited OLEDs. [J471]

"InGaN staircase electron injector for reduction of electron overflow in InGaN light emitting diodes"

Ballistic and quasiballistic electron transport across the active InGaN layer are shown to be responsible for electron overflow and electroluminescence efficiency droop at high current levels in InGaN light emitting diodes both experimentally and by first-order calculations. An InGaN staircase electron injector with step-like increased In composition, an "electron cooler," is proposed for an enhanced thermalization of the injected hot electrons to reduce the overflow and mitigate the efficiency droop. The experimental data show that the staircase electron injector results in essentially the same electroluminescence performance for the diodes with and without an electron blocking layer, confirming substantial electron thermalization. On the other hand, if no InGaN staircase electron injector is employed, the diodes without the electron blocking layer have shown significantly lower (three to five times) electroluminescence intensity than the diodes with the blocking layer. These results demonstrate a feasible method for the elimination of electron overflow across the active region, and therefore, the efficiency droop in InGaN light emitting diodes. [J472]

"High efficiency and low roll-off blue phosphorescent organic light-emitting devices using mixed host architecture"

We report high efficiency and low roll-off for blue electrophosphorescent organic light emitting devices based on a mixed host layer architecture. The devices were fabricated using a mixed layer of di-[4-(N,N-ditolyl-amino)-phenyl]cyclohexane, a hole transport material, and 2,8-bis(diphenylphosphoryl)dibenzothiophene, an electron transport material, as the host layer doped with the blue phosphor iridium (III) bis[(4,6-difluorophenyl)-pyridinato-N,C2']picolinate. Using a mixed layer as the host allowed us to achieve high power efficiency (59 lm/W at 100cd/m²), low turn-on voltage (2.7 V for >10cd/m²), and low roll-off in these devices. [J473]

"High-power and high-speed organic three-dimensional transistors with submicrometer channels"

Three-dimensional organic field-effect transistors with high current density and high switching speed are developed with multiple submicrometer channels arranged perpendicularly to substrates. The short channel length is defined by the height of a multicolumnar structure without an electron-beam-lithography process. For

devices using dinaphtho[2,3-b:2',3'-f]thieno[3,2-b]thiophene, extremely high current density exceeding 10A/cm² and fast switching within 0.2 μs are realized with an on-off ratio of 105. The unprecedented performance is beyond general requirements to control organic light-emitting diodes, so that even more extensive applications to higher-speed active-matrices and display-driving circuits can be realized with organic semiconductors. [J474]

"Nitrogen doped Mg_xZn_{1-x}O /ZnO single heterostructure ultraviolet light-emitting diodes on ZnO substrates"

We have grown nitrogen-doped Mg_xZn_{1-x}O:N films on Zn-polar ZnO single crystal substrates by molecular beam epitaxy. As N-sources, we employed NO-plasma or NH₃ gas itself. As x increased, optimum growth temperature window for smooth film morphology shifted to higher temperatures, while maintaining high N-concentration (1.4×10^{19} cm⁻³). The heterostructures of Mg_xZn_{1-x}O:N ($0.1 \leq x \leq 0.4$)/ZnO were fabricated into light emitting diodes of 500-μm-diameter. We observed ultraviolet near-band-edge emission ($\lambda = 382$ nm) with an output power of 0.1 μW for a NO-plasma-doped LED and 70 μW for a NH₃-doped one at a bias current of 30 mA. [J475]

"Comparison on the electroluminescence of Si-rich SiN_x and SiO_x based light-emitting diodes"

Electroluminescence (EL) of the metal-insulator-semiconductor light-emitting diodes (MISLEDs) made by Si-rich SiN_x and SiO_x films with buried Si nanocrystals are compared. The SiN_x facilitates carrier transport and EL from MISLED with turn-on current and voltage of 4 μA and 12 V by reducing barrier heights at indium tin oxide /SiN_x and SiN_x/Si-nc interfaces. The SiN_x MISLED exhibits larger charge loss rate of 12% within 200 s and shorter delay time of 3.86×10^{-4} s than SiO_x one, which limit its external EL quantum efficiency by strong carrier escaping effect due to the insufficient carrier confinement in Si nanocrystals with low interfacial barriers. [J476]

"Color tunable light-emitting diodes based on p⁺-Si /p-CuAlO₂ /n-ZnO nanorod array heterojunctions"

Wide-range color tuning from red to blue was achieved in phosphor-free p⁺-Si/p-CuAlO₂/n-ZnO nanorod light-emitting diodes at room temperature. CuAlO₂ films were deposited on p⁺-Si substrates by sputtering followed by annealing. ZnO nanorods were further grown on the annealed p⁺-Si/p-CuAlO₂ substrates by vapor phase transport. The color of the p-CuAlO₂/n-ZnO nanorod array heterojunction electroluminescence depended on the annealing temperature of the CuAlO₂ film. With the increase of the annealing temperature from 900 to 1050 °C, the emission showed a blueshift under the same forward bias. The origin of the blueshift is related to the amount of Cu concentration diffused into ZnO. [J477]

"Manipulating the Microcavity Structure for Highly Efficient Inverted Top-Emitting Organic Light-Emitting Diodes: Simulation and Experiment"

A comprehensive theoretical and experimental study on inverted top-emitting organic light-emitting diodes (ITOLEDs) with a microcavity structure is demonstrated. In the ITOLEDs, tris-(8-hydroxyquinoline) aluminum (Alq₃) is used as the emitting material and the outcoupling capping layer, and the 2, 9-dimethyl-4, 7-diphenyl-1, 10-phenanthroline is used as the hole/exciton-blocking layer to confine most emitting dipoles exactly at the desired resonant position. A classical optical model is adopted to simulate the electroluminescence intensity and the spectral characteristics as a function of a viewing angle. The factors that influence optical interference effects and light outcoupling are discussed systematically. The optimized ITOLED shows an enhanced outcoupling efficiency and highly saturated colors compared with that of the corresponding conventional bottom-emitting light-emitting diode while the angular dependence of the emission wavelength is minimized. [J478]

"Degradation Evaluation of -IGZO TFTs for Application to AM-OLEDs"

We have evaluated the characteristic degradation of amorphous-InGaZnO₄ thin-film transistors (α-IGZO TFTs) to apply to active-matrix organic light-emitting diode displays (AM-OLEDs) using current-voltage (I-V) and capacitance-voltage (C-V) curves and an extraction technique of trap densities. First, the degradation was a parallel shift of the I-V and C-V curves after a short time, mainly caused by fixed charge injection into the gate insulator when gate voltage stress was applied by supposing switching TFTs in AM-OLEDs. Second, the degradation was a parallel shift of the I-V curve and slope dullness of the C-V curve after a long time, mainly caused by trap generation in the channel layer when drain current stress was applied by supposing driving TFTs in AM-OLEDs. We should note that two different degradation modes occur when α-IGZO TFTs are applied to AM-OLEDs. [J479]

"A 0.5-Hz High-Pass Cutoff Dual-Loop Transimpedance Amplifier for Wearable NIR Sensing"

Device"

This brief describes a fully integrated dual-loop transimpedance amplifier with bandpass response for wearable near-infrared (NIR) sensing operating at low frequency: one loop to lower the lower band cutoff frequency and another loop for self-regulating DC photocurrent to prevent saturation at later stages. The circuit was implemented in a 0.35- μm CMOS process and achieved a DC photocurrent rejection ranging from 2.7 to 15 μA and a -3-dB high-pass cutoff frequency from 0.5 to 110 Hz by using on-chip capacitors. Both total harmonic distortion and spurious-free dynamic range are better than -42 dB . It achieves an improvement of 390 times in capacitor reduction compared with the traditional DC rejection technique. [J480]

"Optimized Thermal Management From a Chip to a Heat Sink for High-Power GaN-Based Light-Emitting Diodes"

To improve heat dissipation of sapphire-based LEDs, we develop a new LED package with a dual heat spreader design. The first heat spreader is a cup-shaped copper sheet, which was directly contacted with sapphire to enhance heat dissipation of the chip itself. The second heat spreader is the die-bonding material of diamond-added AgSnCu solder and a high thermal conductive metal-core printed circuit board (MCPCB), where the conventional dielectric layer was replaced with a thin diamond-like layer. Characterization results demonstrate that the diamond-added composite solder is useful in reducing LED thermal resistance, thus avoiding the thermal accumulation phenomenon. In addition, a LED packaged on the new MCPCB exhibits smaller total thermal resistance and larger light output power. [J481]

"Pseudo Zero-Dimension Dimming for Power Reduction in Field Sequential Color Liquid Crystal Display Systems"

Expensive hardware is required by the conventional two-dimensional (2-D) light-emitting diode (LED) dimming technique to obtain high-contrast and low-power in the field sequential color (FSC) technique. Thus, based on real-time image data, the pseudo zero-dimension (0-D) LED dimming technique is proposed to further reduce power dissipation in the D-FSC technique, which allows the intelligent selection of an adequate color sequence. The multi-liquid crystal and backlight (LC/BL) algorithm utilizes the D-FSC technique in temporal and spatial domains. It not only utilizes the pseudo 0-D technique to effectively reduce the color breakup (CBU) effect without greatly increasing frame rate, but also to reduce power consumption. On the backlight module, CBU suppression can be substantially improved and power dissipation can be reduced by at least 12.5%. Power consumption can also be further reduced through the re-dimming improvement in the proposed pseudo 0-D dimming technique. [J482]

"Lateral current injection photonic crystal membrane light emitting diodes"

A novel method for fabricating photonic crystal membrane light emitting diodes is presented. The device employs a transverse diode structure and injects carriers laterally through a photonic crystal patterned at the p-n junction within a membrane. Details of the fabrication process as well as electrical and optical characteristics of the devices are presented. [J483]

"Investigation of the Electrostatic Discharge Performance of GaN-Based Light-Emitting Diodes With Naturally Textured p-GaN Contact Layers Grown on Miscut Sapphire Substrates"

The electrostatic discharge (ESD) characteristics of GaN-based light-emitting diodes (LEDs) with naturally textured p-GaN contact layers grown on c-axis miscut sapphire substrates are studied and demonstrated. Based on the machine model, the device grown on a 0.35° miscut sapphire shows the highest ESD tolerance, whereas the device grown on a 0.2° miscut sapphire exhibits the poorest tolerance. It is found that this phenomenon is primarily related to the presence of maximum capacitance C_m values rather than the difference in defect densities between LEDs. The variation in C_m values is caused by the parasitic capacitance effect induced by different p-GaN surface morphologies between the studied devices. This observation gives us a more reliable application in improving the ESD performance based on the device grown on a 0.35° miscut sapphire. [J484]

"Enhanced Illumination Sensing Using Multiple Harmonics for LED Lighting Systems"

This paper considers frequency division multiplexing (FDM) based illumination sensing in light emitting diode (LED) lighting systems. The purpose of illumination sensing is to identify the illumination contributions of spatially distributed LEDs at a sensor location, within a limited response time. In the FDM scheme, LEDs render periodical illumination pulse trains at different frequencies with prescribed duty cycles. The problem of interest is to estimate the amplitudes of the individual illumination pulse trains. In our previous work, an estimation approach was proposed using the fundamental frequency component of the sensor signal. The number of LEDs

that can be supported by this estimation approach is limited to around 100 LEDs at a response time of 0.1 s. For future LED lighting systems, however, it is desirable to support many more LEDs. To this end, in this paper, we seek to exploit multiple harmonics in the sensor signal. We first derive upper limits on the number of LEDs that can be supported in the presence of frequency offsets and noise. Thereafter, we propose a low complexity successive estimation approach that effectively exploits the multiple harmonics. It is shown that the number of the LEDs can be increased by a factor of at least five, compared to the estimation approach using only the fundamental frequency component, at the same estimation error. [J485]

"Direct and indirect band gap room temperature electroluminescence of Ge diodes"

Germanium is a promising material for electrically pumped light emitters integrated on silicon. In this work, we have investigated the room temperature electroluminescence of pure germanium diodes grown by metal organic chemical vapor deposition. The dependence of the optical response of the p-n diodes is studied as a function of the injected current. Both direct and indirect band gap recombinations are observed at room temperature around 1.6 and 1.8 μm . The amplitude of the direct band gap recombination is equivalent to the one of the indirect band gap. [J486]

"Thermally induced surface instabilities in polymer light emitting diodes"

The role of thermal gradients and their attendant mechanical stresses in the overall stability of organic electronic devices has been elucidated through the occurrence of spiral shaped blisters that develop on the surface of suitably biased polymer light emitting diodes. A model based on the spontaneous disordering (or ordering) of polymeric thin film systems has been used to explain the formation and growth of these blisters. The model is shown to provide insights into how thermal stresses affect the overall stability of organic electronic devices. The implications of the results are then discussed for the design of flexible organic electronic devices. [J487]

"Precision laser micromachining of trenches in GaN on sapphire"

Trench formation for device isolation on GaN light-emitting diode (LED) wafers via nanosecond ultraviolet laser micromachining is demonstrated. Trenches with smooth sidewalls and flat bottom surfaces are produced. Unlike wafer scribing with laser beams, the formation of trenches requires that the incident fluence is sufficient for laser ablation of GaN, yet low enough to prevent ablation of the sapphire substrate. Owing to the dissimilar ablation thresholds between GaN and sapphire, the etch process terminates automatically at the GaN/sapphire interface. The effect of the following parameters on the trench properties and quality has been investigated: focus offset, pulse energy, pulse repetition rate, scan speed, and the number of scan passes. It was found that optimal focus offset and pulse energy, a high pulse repetition rate, and single cycle of slow scanning are the key factors for obtaining a trench with tapered sidewall and smooth bottom surface, which is suitable for the laying of interconnects conformally across the trench for device interconnection. This technique has been successfully applied to the rapid prototyping of interconnected LED arrays on a single chip, where metal interconnects run continuously across the micromachined trenches to connect the individual LED devices. [J488]

"Efficient electron spin injection in MnAs-based spin-light-emitting-diodes up to room temperature"

Studies of ferromagnetic MnAs in recent years have revealed a wide range of properties desirable for spintronic applications. Previously studied MnAs spin-light-emitting-diodes exhibited a low value of spin injection into the device active region. In this work, we have investigated injection of spin polarized electrons from MnAs into AlGaAs(n)/GaAs(i)/AlGaAs(p) n-i-p structures. The band-edge electroluminescence emitted from these devices has a saturation circular polarization of 26% at 7 K and B=2T. Using optical pumping measurements the corresponding electron spin polarization was determined to be 52%. Emission persists up to room temperature, with a saturation circular polarization of 6% at B=2T. [J489]

"The aspect ratio effects on the performances of GaN-based light-emitting diodes with nanopatterned sapphire substrates"

The nanopatterned sapphire substrates (NPSSs) with aspect ratio that varied from 2.00 to 2.50 were fabricated by nanoimprint lithography. We could improve the epitaxial film quality and enhance the light extraction efficiency by NPSS technique. In this work, the aspect ratio effects on the performances of GaN-based light-emitting diodes (LEDs) with NPSS were investigated. The light output enhancement of GaN-based LEDs with NPSS was increased from 11% to 27% as the aspect ratio of the NPSS increases from 2.00 to 2.50. Owing to the same improvement of crystalline quality by using various aspect ratios of NPSS, these results indicated that the aspect ratio of the NPSS is strongly related to the light extraction efficiency. [J490]

"Polyethyleneoxide/sodium dodecyl sulfate as hole-blocking/electron-transporting layer for high-performance blue polymer light-emitting diode with oxygen- and moisture-stable aluminum cathode"

We present the case of the blend of polyethyleneoxide (PEO) with sodium dodecyl sulfate (SDS) as a hole-blocking (HB)/electron-transporting (ET) layer to allow the use of oxygen- and moisture-stable aluminum (Al) as the cathode for achieving high-performance polymer light-emitting diode. With inserting the PEO-SDS layer (at the weight ratio 1:1.25), the blue-emitting device with poly(9,9-di-n-octylfluorene) exhibits the maximum brightness 12 300cd/m² and current efficiency 2.8 cd/A, much higher than the device without this layer (0.3cd/m² and 0.005 cd/A) and that using CsF/Al as the cathode (5835cd/m² and 1.06 cd/A). This HB-ET layer can also improve the performances of poly[2-methoxy-5-(2-ethylhexyloxy)-1,4-phenylene vinylene]-based device with Al as the cathode. [J491]

"Temperature dependence of superluminescence in InGaN-based superluminescent light emitting diode structures"

We have studied the temperature dependence of electroluminescence in superluminescent light emitting diode InGaN structures emitting light at 405 nm. Devices were fabricated in the "tilted ridge" geometry. We measured the superluminescence emission as a function of temperature from 263 to 295 K and observed a very pronounced power sensitivity with temperature. Simple modeling of the optical intensity reveals that the main temperature dependence is related to the spontaneous emission factor in the amplified spontaneous emission and the temperature dependence of gain is of secondary importance. This result strongly suggests the need for reducing nonradiative recombination in superluminescent devices. [J492]

"Influence of polarization fields on carrier lifetime and recombination rates in InGaN-based light-emitting diodes"

We study differential carrier lifetimes in InGaN light-emitting diodes (LEDs) of varying wavelengths. Increase in wavelength is correlated with an increase in lifetime, due to the impact of the polarization fields on carrier overlap. This effect explains the early onset of droop in longer-wavelength LEDs. [J493]

"Numerical analysis of efficiency droop induced by piezoelectric polarization in InGaN/GaN light-emitting diodes"

The effects of piezoelectric polarization on efficiency droop in InGaN/GaN light-emitting diodes (LEDs) have been investigated using numerical analysis. The simulation results showed that the severe band bending in InGaN quantum-well was improved as the piezoelectric polarization is reduced, resulting in the improved overlap of electron and hole wave functions. As a results, the internal quantum efficiency increases and efficiency droop significantly reduces. The reduction in piezoelectric polarization could be derived by applying a tensile stress to relax compressive stress in GaN epilayer, improving the efficiency droop of vertical-structure LEDs, agree well with simulation ones. [J494]

"Structure and Ultraviolet Electroluminescence of Nanocomposite/ -GaN Heterostructure Light-Emitting Diodes"

We fabricated and characterized ultraviolet (UV) light-emitting diodes (LEDs) composed of n-ZnO/SiO₂-ZnO nanocomposite/p-GaN heterostructures. Significant UV electroluminescence at 387 nm from the n-ZnO layer in this heterostructure LED was observed at a forward-bias current of as low as 1.8 mA. This is ascribed to the high quality of the n-ZnO layer and the effective function of the SiO₂-ZnO nanocomposite layer. The SiO₂-ZnO nanocomposite layer accomplishes the role of current blocking by forming the larger energy barrier for electron injection from n-ZnO into p-GaN and also contributes to, due to its low refractive index, higher light extraction efficiency from the n-ZnO layer. [J495]

"Air stable, ambipolar organic transistors and inverters based upon a heterojunction structure of pentacene on N,N'-ditridecylperylene-3,4,9,10-tetracarboxylic di-imide"

In this paper, we report on the fabrication and electrical characterization of top-contact, ambipolar organic field-effect transistors (OFETs) and inverters based upon a heterostructure of p-type pentacene on n-type N,N'-ditridecylperylene-3,4,9,10-tetracarboxylic di-imide (P13), using the neutral cluster beam deposition (NCBD) method. The device characteristics measured as a function of both P13 and pentacene layer thicknesses revealed that OFETs with thicknesses of P13 (300 Å) and pentacene (200 Å) showed high air-stability and well-balanced ambipolarity with hole and electron mobilities of 0.12 and 0.08cm²/V s. The complementary inverters,

comprising two identical ambipolar OFETs, were found to operate both in the first and third quadrants of the transfer curves and exhibited a high voltage inversion gain of 13, good noise margins, and little hysteresis under ambient conditions. The results presented demonstrate that the NCBD-based ambipolar transistors and inverters qualify them as promising potential candidates for the construction of high-performance, organic thin film-based integrated circuits. [J496]

"Investigation of dominant effect on efficiency droop in InGaN light emitting device"

To understand a major effect on efficiency droop, radiative characteristics of InGaN laser diodes (LDs) of emission wavelength of 445nm are studied at subthreshold levels for different active structures; (1) InGaN single quantum well (SQW), (2) double quantum wells (DQWs) with Si-doped barrier, and (3) DQWs with undoped barrier. For InGaN LDs with DQWs, the absolute radiative efficiency is most dominant for the case of undoped barrier, and least for the case of Si-doped barrier. The efficiency droop in InGaN LDs with DQWs, regardless of the doping condition of barriers, is typical of reported InGaN light emitting devices, whereas for the InGaN LD with SQW, the efficiency droop is significantly improved for all current density levels due to the least polarization field of InGaN QW. [J497]

"High-Performance Poly-Si TFTs Using Ultrathin Gate Dielectric for Monolithic Three-Dimensional Integrated Circuits and System on Glass Applications"

High-performance poly-Si thin-film transistors (TFTs) using an ultrathin high- κ metal gate stack with a subthreshold swing (SS) of 193 mV/dec when operating at room temperature and maximum thermal budget of 700°C are readily compatible with monolithic 3-D integrated circuits (3D-ICs) and silicon-on-glass (SOG) applications. The SS is reduced to 31 mV/dec, and the on/off current ratio is increased to 108 at 77 K; the result is a significant reduction of leakage current and lower power consumption. Long-channel TFTs have a higher drain current noise spectral density S_{ID} and a smaller exponential frequency factor (γ) due to the influence of numerous grain boundaries on carrier transport, as confirmed by gap state density extraction. These devices may pave the way for high-performance circuit designs and applications, such as monolithic 3D-ICs, SOG, and active-matrix organic LED. [J498]

"Enhanced Light Output of GaN-Based Vertical-Structured Light-Emitting Diodes With Two-Step Surface Roughening Using KrF Laser and Chemical Wet Etching"

A two-step roughening process that uses a KrF excimer laser and KOH chemical etching for the n-GaN layer surface of vertically structured GaN-based light-emitting diodes (VLEDs) to yield circular protrusions with hexagonal cones atop for light extraction enhancement is demonstrated. A possible mechanism of the formation of the circular protrusions commenced by laser irradiation with nonuniform etching rates at sites with various dislocation densities was investigated. An improvement in light output power of about 95% at 350-750 mA compared to that of flat VLEDs was obtained for the two-step roughened VLEDs, which is attributed to the increase in surface emission area and dimensions of roughness, and, in particular, the decrease in the n-GaN layer thickness. [J499]

"Enhancement of light extraction from GaN-based green light-emitting diodes using selective area photonic crystal"

We report the development of a GaN-based green light-emitting diode (LED) with a selective area photonic crystal (SPC) structure, which was formed outside the p-bonding electrode on p-GaN. As a result, the optical output power of LEDs with SPC was enhanced by 78% compared to that without PC. In addition, the forward voltage, series resistance, and leakage current of LEDs with SPC were remarkably improved. These results show that the light extraction efficiency of green LEDs can be greatly increased using the SPC structure, with no degradation of electrical properties. [J500]

"Modeling of Tunable Luminescence in Multiple Rare Earth Co-Doped Glasses"

As luminescence from co-doping systems is highly sensitive to the glass host and concentration of active ions due to complicated electronic transitions within respective active ions and complex energy transfer between them, it is desirable to develop a theoretical model to design and optimize the co-doping system before the fabrication and measurement of the sample. In this paper, we present a numerical approach to model the generation of tunable visible luminescence in multiple rare earth co-doped glasses. According to our research, a glass system with a special combination of Tb³⁺, Sm³⁺ and Dy³⁺ ions can emit tunable luminescence. When glasses co-doped with proper doping concentration of Tb³⁺/Sm³⁺/Dy³⁺ ions are excited by different wavelength in the range of 370-410 nm, the luminescent color can be tuned from yellowish white to orange-red. Our work

suggests that the tunable luminescence from multiple rare earth co-doped glasses could have further application in colorful light emitting and other display devices. [J501]

"Evidence of electron conductivity in polysilanes and its implications in design of ultraviolet emitting devices"

Polysilanes are thought to be primarily hole conducting. Consequently, poor efficiency of a polysilane based light emitting diode is explained on the basis of propensity of the charge carriers to nonradiatively recombine near the cathode. We fabricated a single layer device based on poly(n-octylphenylsilane) with a calcium cathode. This device, however, cannot be analyzed on the basis of a single carrier (hole) transport and the device, unexpectedly, exhibits an injection limited current, though no barrier to hole injection exists. Simulation based analysis reveals bipolar transport, with electron mobility much greater than the hole mobility. This now also makes polysilane electron transport layers possible. In addition, we establish that the time-of-flight measured mobilities in polysilanes may not be relevant to electronic devices, which employ much thinner layers. Based on these observations, the basis for device design is revised. Accordingly, a N, N-diphenyl-N, N-bis(1-naphthyl)(1,1-biphenyl)-4,4 diamine layer is inserted between the polysilane and cathode, in which a lowered electron injection barrier allows current to increase by ten times and electroluminescent quantum efficiency by eight times. Simulation of the current in the device shows that increase in current is originating from at least ten-fold increase in electron concentration. An alternative method employing bathocuproine for blocking holes, however, is not found useful in the case of polysilanes. [J502]

"Effects of Patterned Sapphire Substrates on Piezoelectric Field in Blue-Emitting InGaN Multiple Quantum Wells"

The strain and piezoelectric fields in InGaN blue light-emitting diodes on a GaN layer, which is grown on a planar sapphire substrate or patterned sapphire substrates (PSSs), such as a micro-sized PSS and a nano-sized PSS (NPSS), are investigated by micro-Raman spectroscopy and electroreflectance (ER) spectroscopy. The obtained piezoelectric field in InGaN multiple quantum wells (QWs) grown on the planar substrate is 0.83 MV/cm, and it is 0.70 MV/cm for the case of the NPSS. These results are attributed to the fact that the GaN layers on the PSSs have a smaller residual strain compared to that on the planar sapphire, and thus, strain reduction in the GaN layer can reduce the piezoelectric field in the InGaN QWs grown on top of it. [J503]

"Performance Analysis of the CCD Pixel Binning Option in Particle-Image Velocimetry Measurements"

This paper proposes convenient methods to increase the dynamic speed range in particle-image velocimetry (PIV) measurements, which employ a charge-coupled device (CCD) camera binning option. Although the binning procedure decreases spatial resolution along specified dimensions, its ability to increase the camera frame rate and preserve the field-of-view are important advantages, which need to be thoroughly investigated. In order to demonstrate the advantages of the CCD binning option, we have carried out experiments both on static images of in-plane particle displacements and on dynamic images of real-fluid flows. In the first experiment, we have analyzed static images of 0.5, 1, and 1.9 μm size fluorescent polystyrene microparticles placed on thick quartz glass plate and illuminated by high-power LED. The in-plane images were captured at various CCD binning options, the distance between particles was then calculated using cross-correlation analysis and a subpixel interpolation scheme based on a Gaussian filter. In the second experiment, the fluid flow in a $30 \times 300 \times 50\,000 \mu\text{m}$ microchannel was recorded at various CCD binning modes, and then, evaluated using ensemble-averaged normalized cross-correlation analysis with Gaussian subpixel interpolation. Velocity profiles obtained at various CCD binning modes were compared with those obtained at the normal mode. Error analysis has shown that despite the loss of the spatial resolution, the advantages of pixel binning, specifically increased sensitivity and a total full-frame rate, can be useful in PIV measurements, especially in laminar-fluid flows. [J504]

"Time resolved studies of catastrophic optical mirror damage in red-emitting laser diodes"

We have observed the changing light intensity during catastrophic optical mirror damage (COMD) on the timescale of tens of nanoseconds using red-emitting AlGaInP quantum well based laser diodes. Using as-cleaved facets and this material system, which is susceptible to COMD, we recorded the drop in light intensity and the area of damage to the facet, as a function of current, for single, high current pulses. We found that in the current range up to 40 A, the total COMD process up to the drop of light intensity to nonlasing levels takes place on a timescale of hundreds of nanoseconds, approaching a limiting value of 200 ns, and that the measured area of facet damage showed a clear increase with drive current. Using a straightforward thermal model, we propose an explanation for the limiting time at high currents and the relationship between the time to COMD and the area of damaged facet material. [J505]

"Highly Flexible AM-OLED Display With Integrated Gate Driver Using Amorphous Silicon TFT on Ultrathin Metal Foil"

This paper introduces the technology behind developing of flexible AM-OLED displays with improved color and reduced bending radius. Developing a-Si TFT fabrication technology using 80- μm ultrathin stainless steel foil as the substrate and integrating driver electronic in the display panel, we were able to demonstrate a full-color AM-OLED displayed in a curvature of less than 5 cm bending radius. Total panel thickness of 0.30 mm, brightness of 100 cd/m^2 and color reproducibility of 63% were achieved. [J506]

"GaN-Based Resonant-Cavity Light-Emitting Diodes With Top and Bottom Dielectric Distributed Bragg Reflectors"

Dielectric distributed Bragg reflectors (DBRs) were employed as the top and bottom mirrors to form a Fabry-Perot resonator of GaN-based resonant-cavity light-emitting diodes. The DBR consisting of TiO_2 and SiO_2 dielectric pairs was deposited using an electron-beam deposition system with optical monitoring system to obtain high reflection precisely at blue light wavelength. The pairs of top and bottom reflectors were 9 and 10 that represent high reflection of 93.2% and 95% at a blue wavelength of 448 nm, respectively. An increase of 245% of light output intensity and a decrease of 10 nm of the full-width at half-maximum of the light output intensity were attributed to the resonance effect caused by the top and bottom DBRs. [J507]

"Efficient hybrid organic-inorganic light emitting diodes with self-assembled dipole molecule deposited metal oxides"

We investigate the effect of self-assembled dipole molecules (SADMs) on ZnO surface in hybrid organic-inorganic polymeric light-emitting diodes (HyPLEDs). Despite the SADMs being extremely thin, the magnitude and orientation of SADMs dipole moment effectively influenced the work function of the ZnO. As a consequence, the charge injection barrier between the conduction band of the ZnO and the lowest unoccupied molecular orbital of poly(9,9'-dioctylfluorene)-co-benzothiadiazole could be efficiently controlled resulting that electron injection efficiency is remarkably enhanced. The HyPLEDs modified with a negative dipolar SADMs exhibited enhanced device performances, which correspond to approximately a fourfold compared to those of unmodified HyPLEDs. [J508]

"Stable Temperature Characteristics and Suppression of Efficiency Droop in InGaN Green Light-Emitting Diodes Using Pre-TMIn Flow Treatment"

We present experimental results on the improved performance and high stable temperature characteristics of the InGaN green light-emitting diode (LED) with pre-trimethylindium (pre-TMIn) flow treatment. By using pre-TMIn flow treatment, a relatively large radiative coefficient ($B = 3.34 \times 10^{-11} \text{ cm}^3 \cdot \text{s}^{-1}$) corresponding to a 9.2% enhancement in the internal quantum efficiency, as well as a significant reduction of leakage paths for injected carriers, was obtained. Most important, the pre-TMIn flow treatment evidently reduces the dependence of the external quantum efficiency on temperature and efficiency droop of green LEDs. The improvement is thought to be attributable to the preferential formation of In-rich dots upon pre-TMIn flow treatment, which effectively suppresses the trapping of excitons by threading dislocations and the overflowing of injected carriers outside the active regions at elevated temperatures. [J509]

"Energy barrier, charge carrier balance, and performance improvement in organic light-emitting diodes"

The charge injection properties of poly(3,4-ethylenedioxythiophene):polystyrene sulfonate anodes are crucial for performance of organic photovoltaics and organic light-emitting diodes (OLEDs). A simple method for tuning hole injection efficiency using UV-ozone is shown to change anode work-function and optimized carriers balance in the devices and improved efficiency in OLEDs. The optimum time of treatment and work-function differs with device architecture. [J510]

"Enhanced luminescence properties of highly threaded conjugated polyelectrolytes with potassium counter-ions upon blending with poly(ethylene oxide)"

The photophysics and electroluminescence (EL) of thin films of unthreaded and cyclodextrin-encapsulated poly(4,4'-diphenylenevinylene) (PDV) with potassium counteranions, blended with poly(ethylene oxide) (PEO) are investigated as a function of the PEO concentration. We show that three main factors contribute to increasing the photoluminescence (PL) quantum efficiency as a result of suppressed intermolecular interactions, namely: the high degree of encapsulation of the polyrotaxanes, the relatively large counteranion (e.g., compared

to lithium), and the complexation of the rotaxanes with PEO. By facilitating cationic transport to the negative electrodes, PEO also leads to devices with enhanced electron injection and improved charge balance, whose operation therefore resembles that of "virtually unipolar" light-emitting electrochemical cells. This effect, together with the enhanced PL efficiency, leads to higher EL efficiency for both polyrotaxanes and unthreaded polymers, upon addition of the PEO. We show that the concurrent exploitation of the various strategies above lead to an overall EL efficiency that is approximately twice the value previously reported for Li-based PDV. A blueshift of the EL spectrum during the devices turn-on is also reported and analyzed in terms of interference and doping effects. [J511]

"Optical Chip-to-Chip Link System by Using Optical Wiring Method for Reducing EMI"

This paper describes a new optical link system which consists of a metal optical bench, a module printed circuit board, a driver/receiver integrated circuit, a vertical-cavity surface-emitting laser/photo diode (VCSEL/PD) array, and an optical link block with plastic optical fibers for reducing electromagnetic interference (EMI) noise. For the optical interconnection between the light-sources and detectors, an optical wiring method whose distinctive features include the absence of EMI noise and easy assembly is proposed. The results clearly demonstrate that the use of an optical wiring method can provide robust, cost-effective assembly and easy-repair. We successfully achieved a 4.5 Gb/s data transmission rate without EMI problems. [J512]

"Identification of the nature of trapping centers in polyspirobifluorene based diodes by using electrical characterization"

The trap parameters in hole-only diodes using a blue emitting polyspirobifluorene copolymer were explored by using two complementary techniques such as: charge based deep level transient spectroscopy and thermally stimulated current. The trap analyses have been further completed by the measurements of the current-voltage characteristics as a function of the temperature. The use of unipolar structures allowed us to determine hole traps in the devices and further to identify electron traps in bipolar structures. Two hole traps which are located at 0.19 and 0.37 eV from the highest occupied molecular orbital, have been identified in blue polyspirobifluorene based devices. In bipolar diodes, four electron traps are determined and are located at 0.32, 0.58, 0.74, and 0.83 eV from the lowest unoccupied molecular orbital. We also showed that the use of a palladium electrode introduced new trap states of mean activation energy of 0.4 eV. As the nature of the cathode changes from Ba/Al to Pd, these traps are inferred to be related to the interface of polymer/Pd contact. [J513]

"Measurement of initial motion of a flying golf ball with multi-exposure images for screen-golf"

Recently, realistic sports games have been one of the growth industries of the indoor entertainment field. In particular, screen-golf, which is played indoors with real golf clubs and balls, has shown an outstanding growth rate in South Korea. It consists of a sensor, a computer graphics engine, an interior, and other elements. The sensor is the most essential component among them. It measures the initial conditions of a flying golf ball, the velocity, the horizontal angle, and the vertical angle. Until 2008, most commercialized products were infrared LED type sensors, but these are associated with relatively low accuracy and a narrow measurement range compared to those that utilize a camera. In spite of the better performance, camera-based screen-golf sensors are not broadly employed in the screengolf market because they remain expensive compared with other screen-golf sensors. In this study, a new type of camerabased sensor system that captures multi-exposure images and ball tracking algorithms are suggested. These measure the initial condition of a flying golf ball from captured images. The suggested system was verified in an environment equal to that of a real screen-golf store. [J514]

"Efficient resource allocation for rapid link recovery and visibility in visible-light local area networks"

Visible-light communication provides many advantages over other forms of communications, such as visibility, high SNR (Signal to Noise Ratio), easy installation, freedom of interference from radio or electromagnetic waves, usage of license free frequency band, and high security. Furthermore, the exponentially increasing requirements and quality of LEDs (Light Emitting Diodes) have encouraged the development of visible-light communication that makes use of LEDs. In a visible-light communication system, an LOS (Line of Sight) link between two transceivers should be guaranteed due to the straightness of the visible-light signal. However, link failure caused by temporary blocking or poor orientation of a transmitter frequently occurs, causing burst frame errors. In this paper, we focus on how to let a user know about link failure as quickly as possible, in order that the link failure problem may be solved by realigning the transmission signal towards the receiver. This is furthermore a relatively straightforward matter, by the very nature of this system being a visible means of communication. It is also required that the visibility should be supported when a user attempts initial access procedure. Nevertheless, by supporting visibility, system performance can be degraded because some additional resources are required for the visibility to be enabled. In this paper, we propose three schemes for supporting visibility without reducing

system performance in a visible-light local area network [J515]

"High-Speed Visible Light Communications Using Individual Pixels in a Micro Light-Emitting Diode Array"

The high-frequency modulation of individual pixels in III-nitride-based micro-pixel light-emitting diode arrays, where each array consists of 16×16 individually addressable $72\text{-}\mu\text{m}$ -diameter pixels, are reported. The devices investigated have peak emission wavelengths at 370, 405, and 450 nm, respectively. The optical -3-dB modulation bandwidth of a typical pixel from the 450-nm-emitting device was found to be approximately 245 MHz. Data transmission at rates of up to 1 Gb/s is demonstrated from a single pixel emitting at 450 nm, using on-off keying nonreturn-to-zero modulation, with a bit-error ratio of less than 1×10^{-10} . Such devices have potential for free-space or fiber-coupled visible light communications. [J516]

"Design method for area-efficient and uniform channel DACs"

A current-mode driving scheme has significant advantages over other competing driving method, and the scheme does not require the time-consuming threshold voltage sampling process used in recent voltage-mode driving methods. Design considerations for compact and uniform channel DACs in current-mode AMOLED display data drivers are addressed in detail. Furthermore, an 8 bit area-efficient cascaded-dividing DAC and a 9 bit segmented DAC are designed in accordance with the suggested DAC design method. The presented DACs perform outstandingly when compared in terms of a composite DAC performance that comprises chip area, power consumption, sampling frequency, and DAC bit resolution. [J517]

"Enhancement of electroluminescence in GaN-based light-emitting diodes by metallic nanoparticles"

The enhanced electroluminescence of GaN-based light-emitting diodes (LEDs) with noble metallic nanoparticles (MNPs) is demonstrated. The sample with well-designed Ag MNPs has shown the best performance enhancement of 126% in electroluminescent intensity compared with a conventional LED sample, even though the MNPs are placed at least 200 nm away from the quantum-well active layer. The MNPs provide enhanced photon scattering and coupling between localized surface plasmon resonance (LSPR) modes and photon modes internally trapped in a device. To investigate this effect, the peculiarities of the LSPR and the corresponding structural properties of the MNPs are discussed through the effective medium approach. [J518]

"High extraction efficiency GaN-based light-emitting diodes on embedded SiO₂ nanorod array and nanoscale patterned sapphire substrate"

In this paper, GaN-based LEDs with a nanoscale patterned sapphire substrate (NPSS) and a SiO₂ photonic quasicrystal (PQC) structure on an n-GaN layer using nanoimprint lithography are fabricated and investigated. The light output power of LED with a NPSS and a SiO₂PQC structure on an n-GaN layer was 48% greater than that of conventional LED. Strong enhancement in output power is attributed to better epitaxial quality and higher reflectance resulted from NPSS and PQC structures. Transmission electron microscopy images reveal that threading dislocations are blocked or bended in the vicinities of NPSS layer. These results provide promising potential to increase output power for commercial light emitting devices. [J519]

"Data driving methods and circuits for compact and high-image-quality AMOLED mobile displays"

To implement a compact and high-image-quality AMOLED mobile display, a previously proposed panel DAC concept was elaborated and improved. Three types of pixel structures for the panel DAC have been presented and discussed in terms of the yield, aperture ratio and timing margin. Also, the functional feasibility of the panel DAC has been verified by fabrication and measurement of low-temperature poly-Si TFT test circuits. The circuit area of the 8-bit DAC consisting of the 6-bit resistor-string-based DAC and the 2-bit cyclic panel DAC is increased by 26.7% compared with that of the 6-bit resistor-string-based DAC, whereas the conventional 8-bit resistor-string-based DAC quadruples the circuit area. [J520]

"Synergistic effect on the efficiency of polymer light-emitting diodes upon blending of two green-emitting polymers"

Light-emitting diodes based on blends of the two green-emitting polymers, poly(9,9-dioctylfluorene-alt-benzothiadiazole), F8BT, and poly(9,9-dioctylfluorene-alt-bithiophene), F8T2, show efficiencies that lie in between those of the devices based on the neat polymers (with a maximum efficiency of approximately 4 cd/A for the devices with magnesium cathodes based on F8BT), except for the blend with 5% by weight of F8T2,

which is more efficient than the device based on neat F8BT (a maximum efficiency of approximately 5 cd/A is obtained). In view of the lower photoluminescence efficiency of F8T2, we attribute this improvement to the improved hole transport brought about by F8T2, though it is surprising that 5% by weight, is enough to significantly improve the charge balance within the emissive layer. A detailed photophysics study was carried out for the neat polymers and their blends and no clear evidence for energy transfer between the components was found. This unanticipated devices performance improvement points to the need of a deeper screening of available conjugated luminescent polymers. [J521]

"Fabrication of ZnO photonic crystals by nanosphere lithography using inductively coupled-plasma reactive ion etching with CH₄/H₂/Ar plasma on the ZnO/GaN heterojunction light emitting diodes"

This article reports fabrication of n-ZnO photonic crystal/p-GaN light emitting diode (LED) by nanosphere lithography to further booster the light efficiency. In this article, the fabrication of ZnO photonic crystals is carried out by nanosphere lithography using inductively coupled plasma reactive ion etching with CH₄/H₂/Ar plasma on the n-ZnO/p-GaN heterojunction LEDs. The CH₄/H₂/Ar mixed gas gives high etching rate of n-ZnO film, which yields a better surface morphology and results less plasma-induced damages of the n-ZnO film. Optimal ZnO lattice parameters of 200 nm and air fill factor from 0.35 to 0.65 were obtained from fitting the spectrum of n-ZnO/p-GaN LED using a MATLAB code. In this article, we will show our recent result that a ZnO photonic crystal cylinder has been fabricated using polystyrene nanosphere mask with lattice parameter of 200 nm and radius of hole around 70 nm. Surface morphology of ZnO photonic crystal was examined by scanning electron microscope. [J522]

"Study on MoO_{3-x} films deposited by reactive sputtering for organic light-emitting diodes"

The authors investigate the role of reduced molybdenum trioxide [MoO_{3-x} (x ≤ 1)] films in organic light-emitting diodes, particularly from the viewpoint of the oxidation state of Mo. MoO_{3-x} films were deposited by reactive sputtering under a mixture of argon (Ar) and oxygen (O₂). The O₂ gas-flow ratio (GFR) [O₂/(Ar+O₂)] was adjusted between 10% and 100%. Mo with six, five, and four valence electrons was detected in MoO_{3-x} film deposited with an O₂GFR of 10% and 12.5%, whereas, under higher O₂GFRs, only six valence electrons for Mo in the MoO_{3-x} film were detected. N,N'-di(1-naphthyl)-N,N'-diphenylbenzidine (α-NPD) layer, hole-transport material, were deposited over the MoO_{3-x} layer by subsequent vacuum evaporation. At the α-NPD/MoO_{3-x} interface, it was found that α-NPD cations were generated and that MoO_{3-x} was reduced, which provided evidence of charge transfer across the interface by Raman spectroscopy and x-ray photoelectron spectroscopy. [J523]

"Development of High-Performance Optical Silicone for the Packaging of High-Power LEDs"

Silicone materials with a relatively high-refractive index have been introduced for the encapsulation of high-power light-emitting diodes (LEDs), and LEDs with relatively short wavelengths. However, most of those existing silicone encapsulants still suffer from thermal and radiation induced degradations and thus lead to reliability issues and a shorten lifetime. A new high-performance silicone has been developed and its performance is compared with other commercial silicone and optical grade epoxy in high-power white LEDs. The new materials had been found to suffer less loss in the lumen output during the aging test and high-temperature/high-humidity test, as well as the Joint Electron Devices Engineering Council (JEDEC) reliability test. It is concluded that this material is excellent for the packaging of high-power white LEDs and high-power colored LEDs, because of its ability in maintaining high-transparency and great radiation/thermal resistance. [J524]

"Optical Wireless Communication Systems in the Mb/s to Gb/s Range, Suitable for Industrial Applications"

For future short- and mid-range industrial applications, optical wireless (OW) communication systems are expected to play a major role. When moderate transmission rates (100 Mb/s range) are required, OW communications present a viable and promising technology, supplemental to conventional radio wireless systems. Advanced approaches based on diversity techniques and adaptive signal processing show potential to achieve both high spatial coverage and high bit rates of more than 100 Mb/s. Visible-light communication systems using white phosphorescent LEDs equally present an interesting application potential, combining illumination with data transfer. When high data volumes (100 Gb/s range) need to be transmitted, tailored optical data links provide a solution of choice. Exemplarily, a scalable (24-140 Gb/s) optical data link is presented, developed for future implementation in maskless lithography systems. The link comprises a high-speed data buffer with synchronizable architecture and scalable throughput (N < 24 Gb/s), an optical free-space transmission solution, and finally, a 45-channel low-noise optical receiver chip based on BiCMOS 0.6 μm technology. [J525]

"CMOS Optoelectronic Lock-In Amplifier With Integrated Phototransistor Array"

We describe the design and development of an optoelectronic lock-in amplifier (LIA) for optical sensing and spectroscopy applications. The prototype amplifier is fabricated using Taiwan Semiconductor Manufacturing Co. complementary metal-oxide semiconductor 0.35- μm technology and uses a phototransistor array (total active area is $400\text{ }\mu\text{m} \times 640\mu\text{m}$) to convert the incident optical signals into electrical currents. The photocurrents are then converted into voltage signals using a transimpedance amplifier for subsequent convenient signal processing by the LIA circuitry. The LIA is optimized to be operational at 20-kHz modulation frequency but is operational in the frequency range from 13 kHz to 25 kHz. The system is tested with a light-emitting diode (LED) as the light source. The noise and signal distortions are suppressed with filters and a phase-locked loop (PLL) implemented in the LIA. The output dc voltage of the LIA is proportional to the incident optical power. The minimum measured dynamic reserve and sensitivity are 1.31 dB and 34 mV/ μW , respectively. The output versus input relationship has shown good linearity. The LIA consumes an average power of 12.79 mW with a 3.3-V dc power supply. [J526]

"Light Output Enhancement of Near UV-LED by Using Ti-Doped ITO Transparent Conducting Layer"

With Ti doping, the transmittance of indium-tin-oxide (ITO) thin film is greatly enhanced in near the ultraviolet (UV) range. After annealing at 500 °C in vacuum, the transmittance of Ti-doped ITO (Ti: ITO) thin film at 380 nm is larger than that of pure ITO thin film by 22%. And, the resistivity of annealed Ti: ITO thin film is equivalent with that of ITO thin film ($4.248 \times 10^{-4} \Omega \cdot \text{cm}$). Using Ti: ITO as TCL, the light output power of UV light-emitting diode (LED) is enhanced by 52.1%, compared to UV-LED (380 nm) with an ITO transparent conducting layer. [J527]

"Light-emitting dendrimer film morphology: A neutron reflectivity study"

We have used neutron reflectivity (NR) measurements to probe the physical structure of phosphorescent dendrimer films. The dendrimers consisted of fac-tris(2-phenylpyridyl)iridium(III) cores, biphenyl-based dendrons (first or second generation), and perdeuterated 2-ethylhexyloxy surface groups. We found that the shape and hydrodynamic radius of the dendrimer were both important factors in determining the packing density of the dendrimers. "Cone" shaped dendrimers were found to pack more effectively than "spherical" dendrimers even when the latter had a smaller radius. The morphology of the films determined by NR was consistent with the measured photoluminescence and charge transporting properties of the materials. [J528]

"Reduction in the efficiency droop effect of a light-emitting diode through surface plasmon coupling"

The reduction in the external quantum efficiency (EQE) droop effect of an InGaN/GaN quantum-well (QW) light-emitting diode (LED) through the mechanism of surface plasmon (SP) coupling with QW is demonstrated. With a current spreading grid pattern on the mesa surface, a smaller grid period leads to more effective carrier transport into the QW regions of Ag deposition for stronger SP-QW coupling such that the droop effect is more significantly reduced, as indicated by the increase in injection current density of maximum EQE and the decrease in drooping slope. The claim of the SP-QW coupling effect in the samples of thin p-GaN is supported by the different droop behaviors of the LED samples fabricated with another epitaxial structure of thick p-GaN, in which the SP-QW coupling effect is expected to be weak. [J529]

"Numerical simulation of charge transport in disordered organic semiconductor devices"

For the design of organic semiconductor devices such as organic light-emitting devices and solar cells, it is of crucial importance to solve the underlying charge transport equations efficiently and accurately. Only a fast and robust solver allows the use of fitting algorithms for parameter extraction and variation. Introducing appropriate models for organic semiconductors that account for the disordered nature of hopping transport leads to increasingly nonlinear and more strongly coupled equations. The solution procedures we present in this study offer a versatile, robust, and efficient means of simulating organic semiconductor devices. They allow for the direct solution of the steady-state drift-diffusion problem. We demonstrate that the numerical methods perform well in combination with advanced physical transport models such as energetic Gaussian disorder, density-dependent and field-dependent mobilities, the generalized Einstein diffusion, traps, and its consistent charge injection model. [J530]

"Revised hole injection mechanism of a thin LiF layer introduced between pentacene and an indium tin oxide anode"

Hole injection enhancement has been reported for organic thin-film transistors and light-emitting diodes at the

indium tin oxide (ITO) anode side by introducing a LiF layer, which is usually used as an electron injection layer at the cathode side to reduce the electron injection barrier. We report a revised mechanism for the hole injection enhancement by studying a prototype interface of pentacene/LiF/ITO anode. Upon deposition of LiF on ITO, the work function of ITO decreases, and energy level realignment occurs between the pentacene and ITO. The hole injection barrier from the ITO to the pentacene highest occupied molecular orbital increases significantly with LiF insertion. Thus, the reduction in the hole injection barrier is not a critical factor for the hole injection enhancement. We suggest that a LiF insulating buffer layer enhances both injection barriers and tunneling through the barrier when a bias is applied. [J531]

"The measured dependence of the lateral ambipolar diffusion length on carrier injection-level in Stranski-Krastanov quantum dot devices"

Using the segmented contact method we separate and numerically evaluate the components making up the threshold current density dependence of quantum dot ridge waveguide lasers. An increasing internal optical mode loss and an increasing lateral out-diffusion current are the significant processes in ridges of widths between 4 and 10 μm , with no significant contribution from a deteriorating gain-mode overlap. By fitting a diffusion length model to the lateral out-diffusion process, we extract the ambipolar diffusion length, L_d , as a function of intrinsic carrier injection-level which covers carrier densities appropriate for functioning light-emitting diode and laser devices. The measured dependence fits a diffusion mechanism involving the thermal redistribution of carriers via the wetting-layer and most significantly leads to two regimes where L_d can be reduced in self-assembled quantum-dot systems. Only one of these is shown to be beneficial to the overall efficiency of the device, while the other is at the expense of undesired high-order nonradiative recombination processes at high injection-levels. Covering a peak modal gain range of approximately 5 to 11 cm^{-1} over injection-levels of 65 to 122 meV at 350 K, this dependence caused L_d to change from 0.75 to 1.50 μm , with the maximum occurring at 84 meV where the peak modal gain is 6 cm^{-1} . Decreasing the temperature to 300 K reduced L_d to <0.75 μm over approximately the same injection-level range. [J532]

"Si-based packaging platform for LED module using electroplating method"

A method for fabricating a Si-based packaging platform with a reflector and electrode-guided interconnections is proposed for the packaging component of a high-power light-emitting diode (LED) module. The reflector is fabricated by Ni/Au/Ag-electroplating which is patterned by SU-8 2075 and 4620 negative photo-resistors and the electrical interconnections are formed by Cu/Au-electroplating in the same body. The heat generated by the LED chip is dissipated directly to the Si body through the large metal-plated platform. This method is suitable for high-efficiency and low-cost LED packaging. [J533]

"Determination of Junction Temperature in InGaN and AlGaInP Light-Emitting Diodes"

The junction temperature of a light-emitting diode (LED) directly and greatly affects its performances. Therefore, the reliable measurement and accurate estimation of the junction temperature of an LED is extremely important. This paper proposes an approach for directly determining the dependence of junction temperature on injected currents in InGaN and AlGaInP LEDs. Various important physical parameters that affect the junction temperature of an LED are also considered. [J534]

"Modal Behavior, Spatial Coherence, and Beam Quality of a High-Power Gain-Guided Laser Array"

In this paper, we investigate the modal behavior and the spatial coherence properties of a gain-guided laser array emitting an optical output power of more than 50 W in quasi-continuous-wave operation at a wavelength of 1070 nm and above. The lateral near- and far-field intensity profiles and the Wigner distribution function were measured from low to high output power. The array modes were calculated by solving the waveguide equation taking into account the power-dependent temperature distribution and were also experimentally determined by a modal decomposition of the cross spectral density. The analysis revealed that, at a low power, a single array mode lases, whereas at high power, multiple single stripe modes dominate the lasing due to the thermally induced index rise under the stripes. [J535]

"A High-Speed Current-Mode Data Driver With Push-Pull Transient Current Feedforward for Full-HD AMOLED Displays"

A push-pull transient current feedforward driver is designed to have a complete push-pull function and loop gain control that enhances the data current drivability. The sink and source current capability of the proposed driver makes it insensitive to the initial voltage levels on the data lines and provides a reduced settling time. The gain control in the positive feedback loop offers a fast settling time without ringing over the complete range of pixel

drive currents. The data driver exhibits a settling time of better than 6 μ s for drive currents from 20 nA to 5 μ A into an equivalent full-HD AMOLED display panel parasitic load of 4 k Ω series resistance and 90 pF shunt capacitance. The driver consumes a static current of 4.5 μ A/channel. [J536]

"Instabilities in Amorphous Oxide Semiconductor Thin-Film Transistors"

Thin-film transistors (TFTs) fabricated using amorphous oxide semiconductors (AOS) exhibit good electron mobility (5 to $>$; 50 cm²/V \cdot s), they are transparent, and they can be processed at low temperatures. These new materials show a great promise for high-performance large-area electronics applications such as flexible electronics, transparent electronics, and analog current drivers for organic light-emitting diode displays. Before any of these applications can be commercialized, however, a strong understanding of the stability and reliability of AOS TFTs is needed. The purpose of this paper is to provide a comprehensive review and summary of the recently emerging work on the stability and reliability of AOS TFTs with respect to illumination, bias stress, ambient effects, surface passivation, mechanical stress, and defects, as well as to point out areas for future work. An overview of the TFT operation and expected reliability concerns as well as a brief summary of the instabilities in the well-known Si₃N₄/a-Si:H system is also included. [J537]

"Hierarchical Life Prediction Model for Actively Cooled LED-Based Luminaire"

The lifetime of an actively-cooled light emitting diode (LED)-based luminaire is dependent not only on the junction temperature of LEDs, but also on the reliability of active cooling devices. We propose a novel hierarchical model to assess the lifetime of an actively cooled LED-based luminaire that can provide light output equivalent to a 100 W incandescent lamp. After design considerations for LED-based luminaires with active cooling are discussed, the proposed model is described using component-level sub-physics-of-failure models. The model is implemented to predict the lifetime of a LED-based recessed downlight with synthetic jet cooling. The effects of the time-dependent performance degradation mechanisms of the active cooling device on the lifetime of the luminaire are also discussed. [J538]

"Boosting Green GaInN/GaN Light-Emitting Diode Performance by a GaInN Underlying Layer"

The light output of 530 nm green GaInN/GaN light-emitting diodes on sapphire has been nearly doubled by the insertion of a 130-nm GaInN underlayer (UL) between the n-GaN electron injection layer and the quantum-well (QW) active region. Under variation of the alloy composition, best results were obtained for an x = 6.3% Ga_{1-x}In_xN UL. By low-temperature depth-resolved cathodoluminescence spectroscopy, an interplay of the impurity-related donor-acceptor pair recombination, the UL, and the QW emission has been observed. We propose that the resonance and level alignments between the defect and UL levels reroute excitation toward radiative recombination in the QWs. [J539]

"ZnO-organic hybrid white light emitting diodes grown on flexible plastic using low temperature aqueous chemical method"

We demonstrate white light luminescence from ZnO-organic hybrid light emitting diodes grown at 90 °C on flexible plastic substrate by aqueous chemical growth. The configuration used for the ZnO-organic hybrid white light emitting diodes (WLEDs) consists of a layer of poly (9, 9-dioctylfluorene) (PFO) on poly (3, 4-ethylenedioxythiophene) poly (styrenesulfonate) coated plastic with top ZnO nanorods. Structural, electrical, and optical properties of these WLEDs were measured and analyzed. Room temperature electroluminescence spectrum reveals a broad emission band covering the range from 420 to 750 nm. In order to distinguish the white light components and contribution of the PFO layer we used a Gaussian function to simulate the experimental data. Color coordinates measurement of the WLED reveals that the emitted light has a white impression. The color rendering index and correlated color temperature of the WLED were calculated to be 68 and 5800 K, respectively. [J540]

"Studies on Optical Consistency of White LEDs Affected by Phosphor Thickness and Concentration Using Optical Simulation"

Effects of variations of yttrium aluminum garnet:Ce phosphor thickness and concentration on optical consistency of produced white light-emitting diodes (LEDs) including the consistency of brightness and light colors were studied by optical simulation. Five packaging methods with different phosphor locations were compared. Optical models of LED chip and the phosphor were presented and a Monte Carlo ray-tracing simulation procedure was developed. Both color binning and brightness level were used to sort the simulated LEDs to evaluate their optical consistency. Results revealed that the optical consistency of white LEDs strongly depends on how the phosphor thickness and the concentration vary. To obtain desired color binning, conformal phosphor coating is not a

favorable packaging method due to its low brightness level and poor brightness consistency by large shifts of the brightness level as the phosphor thickness and concentration varying. Planar remoter phosphor improves the brightness level and its consistency, but realization of high color consistency becomes more difficult due to its smaller variation ranges of the phosphor thickness and concentration. Hemispherical remoter phosphor can fulfill the requirements of both high color consistency and high brightness consistency due to its capability of larger variation ranges of the phosphor thickness and concentration. By applying this method with thick phosphor thickness or high phosphor concentration, this method can be a promising packaging method for the low cost production. [J541]

"Modeling high power light-emitting diode spectra and their variation with junction temperature"

Spectral radiant flux is the primary optical characteristic of a light source, determining the luminous flux and color. Much research is dedicated to the modeling of light-emitting diode (LED) spectra and their temperature dependence, allowing for the simulation of optical properties in various applications. Most of the spectral radiant flux models that have been published so far are purely mathematical. For this paper, spectral radiant fluxes of commercial single color LED packages have been measured in a custom made integrating sphere at several junction temperatures by active cooling and heating with a Peltier element. A spectrum model at 300 K is constructed where the Boltzmann free carrier distribution and carrier temperature are included. Subsequently, the model is extended with the carrier temperature variation, the band gap energy shift, and the nonradiative recombination rate decrease with junction temperature. As a result, the skewness variation, peak frequency shift, and peak value change in the spectrum with temperature can be predicted. The model has been validated by comparing flux and color coordinates of measured and simulated spectra at 340 K junction temperature. In practice, only two spectral flux measurements at different junction temperatures are needed to accurately simulate a single color spectrum at any temperature. [J542]

"Speedup of Dynamic Response of Organic Light-Emitting Diodes"

We demonstrate that large-area organic light-emitting diodes (OLEDs) exhibit slow dynamic response due to their capacitor-like behaviors. In particular, the discharge dynamics of large-area OLEDs is observed to be relatively slower, compared with the charge dynamics. To find ways to increase the response speed of large-area OLEDs, we make an in-depth study of transient electroluminescence (EL) of OLEDs in response to voltage pulses (i.e., pulse separation), device configurations (i.e., device length), and various material parameters (e.g., carrier mobility, exciton lifetime, and energy level offset). The EL response speed can be increased by applying high bias voltage and reducing the device length. Meanwhile, the pulse separation affects the response speed of the second pulse. As the pulse separation is decreased, the ratio of the delay time of the second pulse to the delay time of the first pulse is found to be reduced, whereas the ratio of the peak luminance of the second pulse to the peak one of the first pulse is getting increased. We have also shown that the dependence of the delay time on the carrier mobility, exciton lifetime, and energy level offset is less pronounced. This study may provide design guidelines of OLEDs for practical applications including ac-driven displays and next-generation visible-light communications (VLCs). [J543]

"Crosstalk Study of the Single-Photon Response of a Flat-Panel PMT for the RICH Upgrade at LHCb"

The ring imaging Cherenkov (RICH) detector at LHCb is now read out by hybrid photon detectors. In view of its upgrade, a possible option is the adoption of the flat-panel photon multiplier tube (PMT). An important issue for good reconstruction of the Cherenkov rings is a negligible level of crosstalk. We have experimentally studied the crosstalk from the 16 Ч 16-pixels Hamamatsu H9500 PMT. Results have shown that, for the single-photon response, the statistics tied to the small number of electrons generated at the first dynode of the PMT chain (a few units) leads to a number of crosstalk signals that are a small fraction of the fired pixel. With the H9500, in a Cherenkov ring, only one or two pixels are expected to generate crosstalk. As a consequence, crosstalk cannot be considered a limit in the use of the H9500 for the upgrade of the RICH at LHCb. [J544]

"Optical and thermal depth profile reconstructions of inhomogeneous photopolymerization in dental resins using photothermal waves"

Photopolymerization is a process that depends, among other factors, on the optical properties of polymerized materials. In turn, this process affects longitudinal light transport in these materials, thereby altering their optical absorption coefficient which is thus expected to exhibit depth dependence. Furthermore, polymerization affects the thermal properties of these materials. A robust theoretical approach to the study of the depth-dependent optical absorption coefficient, $\beta(x)$, and thermal diffusivity, $\alpha(x)$, in materials exhibiting depth profiles of these parameters has been developed through the photothermal inverse problem based on the concept of the

thermal-harmonic oscillator. Using this concept in the frequency-domain nonhomogeneous photothermal-wave boundary-value problem, the simultaneous reconstruction of arbitrary simultaneous optical and thermal depth profiles was achieved using a multiparameter fitting method to the experimental amplitude and phase. As a first application of the theory to partially polymerized Alert Composite (shade A3) dental resin, with curing induced by a blue light-emitting diode, the beta (x) and alpha (x) depth profiles were reconstructed from photothermal radiometric frequency-scanned data. A strong anticorrelation of these two depth profiles was observed and was interpreted in terms of photochemical processes occurring during the optical (photocuring) creation of long polymeric chains in the resin. The photothermally reconstructed depth profiles may have implications for the optimization of blue light curing methods using such resins in dental clinical practice. [J545]

"Interplay of cavity thickness and metal absorption in thin-film InGaN photonic crystal light-emitting diodes"

Thin-film InGaN photonic crystal (PhC) light-emitting diodes (LEDs) with a total semiconductor thickness of either 800 nm or 3.45 μm were fabricated and characterized. Increased directional radiance relative to Lambertian emission was observed for both cases. The 800-nm-thick PhC LEDs yielded only a slight improvement in total light output over the 3.45- μm -thick PhC LEDs. Simulations indicate that, except for ultrathin devices well below 800 nm, the balance between PhC extraction and metal absorption at the backside mirror results in modal extraction efficiencies that are almost independent of device thickness, but highly dependent on mirror reflectivity. [J546]

"Insertion of an organic interlayer for hole current enhancement in inverted organic light emitting devices"

We report the enhancement of hole current density in the hole transport part of an inverted top-emission organic light emitting diode by applying an organic insertion layer of 1,4,5,8,9,11-hexaazatriphenylene-hexacarbonitrile (HAT-CN). Poor hole transporting performance of Al/4,4'-bis(N-phenyl-1-naphthylamino)biphenyl (NPB)/indium tin oxide is greatly improved by the HAT-CN insertion between Al and NPB layer. The highest occupied molecular orbital level onset of the NPB bends toward Fermi level at the HAT-CN/NPB interface. This extra charge generation layer made of pure organic molecules substantially enhances hole injection from Al anode as revealed by the results of ultraviolet photoelectron spectroscopy and J-V measurement data. [J547]

"Photodegradation of the organic/metal cathode interface in organic light-emitting devices"

We study the photostability of organic light-emitting devices (OLEDs). Irradiating OLEDs by external illumination is found to result in a gradual increase in driving voltage and decrease in electroluminescence (EL) efficiency. This photoinduced degradation in device performance is found to be caused by changes at the organic/metal cathode interface that lead to a deterioration in electron injection. Evidence of photodegradation of the same interface, inherently, by device own EL, is also reported. The results uncover an important degradation mechanism in OLEDs and shed the light on a phenomenon that might limit the stability of other organic optoelectronic and photovoltaic devices. [J548]

"GaN-based light emitting diodes with embedded SiO₂ pillars and air gap array structures"

We demonstrated GaN-based light emitting diodes (LEDs) with different embedded heights of SiO₂ pillars and air gap array structures. The air gap on top of the SiO₂ pillars were also realized using the enhanced epitaxial lateral overgrowth mode. With the embedded SiO₂ pillars and air gap array structures, we achieved a smaller reverse leakage current due to the lateral growth-induced crystal quality improvement. Moreover, under 20 mA current injections, the output powers were 3.04, 4.23, 4.66, and 4.44 mW for conventional LED, LEDs with embedded 200 and 500 nm height of SiO₂ pillars and air gaps, 500 nm height of SiO₂ pillars and air gaps, and 700 and 400 nm height of SiO₂ pillars and air gaps, respectively. We found that the embedded 500 nm height SiO₂ pillars and 500 nm height air gap array structures could enhance LED output power by more than 50% due to the enhanced guided-light scattering efficiency in our study. [J549]

"Surface electronic structure of ZrB₂ buffer layers for GaN growth on Si wafers"

The electronic structure of epitaxial, predominantly single-crystalline thin films of zirconium diboride (ZrB₂), a lattice-matching, conductive ceramic to GaN, grown on Si(111) was studied using angle-resolved ultraviolet photoelectron spectroscopy. The existence of Zr-derived surface states dispersing along the Γ -M direction indicates a metallic character provided by a two-dimensional Zr-layer at the surface. Together with the measured work function, the results demonstrate that the surface electronic properties of such thin ZrB₂(0001) buffer layers are comparable to those of the single crystals promising excellent conduction between

nitride layers and the substrate in vertical light-emitting diodes on economic substrates. [J550]

"Direct measurement of the magnetic field effects on carrier mobilities and recombination in tri-(8-hydroxyquinoline)-aluminum based light-emitting diodes"

The magnetic field effects on the carrier mobilities and recombination in tri-(8-hydroxyquinoline)-aluminum (Alq3) based light-emitting diodes have been measured by the method of transient electroluminescence. It is confirmed that the magnetic field has no effect on the electron and hole mobilities in Alq3 layers and can decrease the electron-hole recombination coefficient. The results imply that the dominant mechanism for the magnetic field effects in Alq3 based light-emitting diodes is the interconversion between singlet e-h pairs and triplet e-h pairs modulated by the magnetic field when the driving voltage is larger than the onset voltage of the electroluminescence. [J551]

"Enhanced efficiency and reduced roll-off in nondoped phosphorescent organic light-emitting devices with triplet multiple quantum well structures"

Highly efficient nondoped phosphorescent organic light-emitting devices (NPOLEDs) with triplet multiple quantum well structures are fabricated by using 4,4'-N,N'-dicarbazole-biphenyl and an iridium(III) complex as the potential barrier layer and the potential well layer/light-emitting layer, respectively. Remarkably, such NPOLED with an optimized device configuration achieves reduced current efficiency roll-off, which slightly decreases from its peak value of 31.5 cd/A at 19.8 mA/cm² to 29.2 cd/A at 100 mA/cm². We attribute this improvement to the efficient triplet exciton confinement effect and the suppression of triplet-triplet annihilation which occurs via single-step long range (Forster-type) energy transfer between excited molecules. [J552]

"Improved luminescence properties of Eu-doped GaN light-emitting diodes grown by atmospheric-pressure organometallic vapor phase epitaxy"

We investigated the luminescence properties of Eu-doped GaN (GaN:Eu) grown by atmospheric-pressure organometallic vapor phase epitaxy. The GaN:Eu exhibited radiant red emission due to the intra-4f shell transition of Eu³⁺ ions at room temperature. The intensity of the dominant peak was about 4 times higher than that in the sample grown at 10 kPa, even though the Eu concentration was only half that of the 10 kPa sample. This was mainly caused by the enhancement of the energy transfer from the GaN host to Eu ions. The enhanced energy transfer resulted in improved luminescence properties of a GaN:Eu light-emitting diode. [J553]

"Study of Top and Bottom Photonic Gratings on GaN LED With Error Grating Models"

The gallium nitride (GaN) light-emitting-diode (LED) top-bottom (or transmission-reflection) grating simulation results with error grating model are presented. The microstructure GaN bottom hole and top pillar gratings are calculated and compared with the non-grating (flat) case. Grating shapes simulated are either conical or cylindrical. A direct comparison of 181 different combined transmission-reflection grating cases using the finite difference time domain method is presented. The simulation results show that simple or direct combinations of the optimized top grating with the optimized bottom grating only produce a 42% light extraction improvement compared to the non-grating case, which is much lower than that of an optimized single grating case. This is due to the mismatch of grating parameters with the direct addition of the second grating structure, which changes the optical field distribution in the LEDs. Therefore, it is very important to optimize both top and bottom gratings simultaneously for the double-grating design. We also show the optimization of a double grating structure can achieve better performance than a single grating. Finally, transmission-reflection error gratings are also presented. It is also the first time to present randomization in GaN LED grating design and its effects in fabrication. Our data shows that the favorable light extraction improvement is at approximately 10-15% randomization. The randomization can achieve 230% improvement over the original grating at a randomization intensity factor of 12.8%. [J554]

"Invited Review Article: IceCube: An instrument for neutrino astronomy"

Neutrino astronomy beyond the Sun was first imagined in the late 1950s; by the 1970s, it was realized that kilometer-scale neutrino detectors were required. The first such instrument, IceCube, is near completion and taking data. The IceCube project transforms 1 km³ of deep and ultratransparent Antarctic ice into a particle detector. A total of 5160 optical sensors is embedded into a gigaton of Antarctic ice to detect the Cherenkov light emitted by secondary particles produced when neutrinos interact with nuclei in the ice. Each optical sensor is a complete data acquisition system including a phototube, digitization electronics, control and trigger systems, and light-emitting diodes for calibration. The light patterns reveal the type (flavor) of neutrino interaction and the energy and direction of the neutrino, making neutrino astronomy possible. The scientific missions of IceCube

include such varied tasks as the search for sources of cosmic rays, the observation of galactic supernova explosions, the search for dark matter, and the study of the neutrinos themselves. These reach energies well beyond those produced with accelerator beams. The outline of this review is as follows: neutrino astronomy and kilometer-scale detectors, high-energy neutrino telescopes: methodologies of neutrino detection, IceCube hardware, high-energy neutrino telescopes: beyond astronomy, and future projects. [J555]

"A nondamaging electron microscopy approach to map In distribution in InGaN light-emitting diodes"

Dark-field inline electron holography and, for comparison, high-resolution transmission electron microscopy are used to investigate the distribution of indium in GaN-based commercial high-efficiency green light-emitting diodes consisting of InGaN multiquantum wells (QWs). Owing to the low electron doses used in inline holography measurements; this technique allows to map the indium distribution without introducing any noticeable electron beam-induced damage which is hardly avoidable in other quantitative transmission electron microscopy methods. Combining the large field of view with a spatial resolution better than 1 nm, we show that the InGaN QWs exhibit random alloy nature without any evidence of nanometer scale gross indium clustering in the whole active region. [J556]

"Electronic structures of MoO₃-based charge generation layer for tandem organic light-emitting diodes"

The role of MoO₃ in charge generation layers for tandem organic light-emitting diodes is investigated. The electronic structure of a typical MoO₃-based charge generation layer, consisting of N,N'-bis(1-naphthyl)-N,N'-diphenyl-1,1'-biphenyl-4,4'-diamine, MoO₃, and Mg doped 4,7-diphenyl-1,10-phenanthroline (NPB/MoO₃/Mg:Bphen) is identified to be a p/n/n junction. It is shown that MoO₃ can pronouncedly modify the energy level alignment, beneficial to charge separation at the NPB/MoO₃ interface and electron injection at the MoO₃/Mg:Bphen interface from MoO₃ into suitable molecular energy levels of adjacent emission units. Moreover, Mg:Bphen is favorable to block holes flowing from the anode side directly into the adjacent emission unit. [J557]

"Optimization of a Photonically Controlled Microwave Switch and Attenuator"

A silicon-based photoconductive switch and attenuator for microwave signals has been demonstrated and optimized for low insertion loss and high attenuation response upon illumination from a standard infrared LED. This device is fabricated within a coplanar waveguide for easy integration into a planar antenna for photonic control of an array. A general tradeoff exists between the goals of low insertion loss and high attenuation range. However, design and process enhancements are found to improve the device performance. A device that offers up to 20-dB attenuation with insertion loss of only 0.6 dB at 2.0 GHz is demonstrated. These devices show a frequency range where the insertion phase shift upon attenuation is significantly less than 1°/dB. [J558]

"The Robockey Cup"

Each fall, a group of intrepid students converge in a classroom on the third floor of the University of Pennsylvania's Towne Engineering Building for what they know will be one of the most challenging courses in their academic career. That first class begins with a discussion of where it will end. In particular, we talk about what they will accomplish in the final project, where they will design, fabricate, assemble, program, and debug small teams of autonomous hockey-playing robots, complete with wireless communications, infrared puck sensing, and enough onboard computational power to handle just about any task that can dream up. Most of the students look incredulous; after all, many of them have never built a circuit or written C code before. [J559]

"InGaN/GaN nanorod array white light-emitting diode"

Conventional InGaN/GaN light-emitting diodes based on planar quantum well structures do not allow for efficient long-wavelength operation beyond the blue region due to a strong quantum confined Stark effect in lattice-mismatched polar InGaN quantum wells. Here we overcome the limitation by using self-assembled GaN nanorod arrays as strain-free growth templates for thick InGaN nanodisks. In combination with enhanced carrier localization and high crystalline quality, this approach allows us to realize full-color InGaN nanodisk emitters. By tailoring the numbers, positions, and thicknesses of polychromatic nanodisk ensembles embedded vertically in the GaN nanorod p-n junction, we are able to demonstrate natural white (color temperature 6000K) electroluminescence from InGaN/GaN nanorod arrays. [J560]

"External efficiency and carrier loss mechanisms in InAs/GaInNAs quantum dot light-emitting diodes"

The electroluminescence (EL) characteristics of a set of InAs/GaInNAs quantum dot (QD) light-emitting diodes with varying In and N contents are analyzed. Room-temperature EL around 1.5 μm is obtained with 15% In and 2% N in the QD capping layer. It is shown that the addition of N results in a degradation of the external efficiency, η_{ext} , probably due to an increase in the nonradiative recombination in the QD heterostructure and an increase in the carrier escape from the QD to the capping layer, which yield a degradation of the current injection efficiency into the QD. Nevertheless, η_{ext} can be partially recovered if a postgrowth rapid thermal annealing is performed, although this also results in a blueshift in the EL peak wavelength. The different contributions to the EL spectra are also analyzed and identified by looking at their dependence on injected current and temperature. It is found that N-containing devices show two radiative transitions. The lowest energy transition has been ascribed to the QD ground state recombination, whereas the higher energy transition has been attributed to recombination of carriers confined in the capping layer. Moreover, the carrier loss mechanisms responsible for the quenching of the EL in the dilute nitride-based devices are studied. It is found that the EL thermal quenching has an activation energy which can be ascribed to carrier escape from the QD to the capping layer. [J561]

"Electroluminescence from ZnO nanoflowers/GaN thin film p-n heterojunction"

Dielectrophoretic force was employed to position ZnO nanoflowers on a p-type GaN thin film prepatterned with Ti/Al/Ni/Au n-type and Ni/Au p-type contact metallizations. Analytical and finite element calculations were employed to determine the optimal alternating current frequency to attract the randomly dispersed ZnO nanoflowers to the n-type contact located on but isolated from the p-GaN thin film. The n-type ZnO nanoflower/p-type GaN thin film heterojunction displayed rectifying current-voltage behavior characteristic of a pristine p-n junction diode and emitted violet light under forward bias above 4.7-5.5 V. [J562]

"Direct hole injection in to 4,4'-N,N'-dicarbazole-biphenyl: A simple pathway to achieve efficient organic light emitting diodes"

The conventional carrier-blocking design of the exciton formation zone used in nearly all organic light emitting diodes is shown to be problematic, due to exciton quenching from accumulated radical cations. To reduce exciton quenching, a single layer of 4,4'-N,N'-dicarbazole-biphenyl (CBP) is used as hole transport layer, resulting in a dramatically improved device efficiency even at high luminance (e.g., 20.5 cd/A at 100 000 cd/m² for fluorescent green). Various high work function transition metal oxides (WO₃, V₂O₅, and MoO₃) coated on indium tin oxide anodes have been shown to enable direct hole injection into the deep highest occupied molecular orbital of CBP (6.1 eV). [J563]

"The contribution of sidewall light extraction to efficiencies of polygonal light-emitting diodes shaped with laser micromachining"

The light extraction efficiencies of InGaN/GaN blue light-emitting diodes (LEDs) of different geometries ranging from a triangle to a decagon have been simulated by ray-tracing. The conventional rectangular LED was found to be the most inefficient among the investigated polygons, and light extraction through the device sidewalls was the key factor. The results were experimentally verified by fabricating LEDs shaped into polygons by nanosecond-pulsed laser micromachining, which proved the simulated results. The mechanism of light extraction in polygonal LEDs is discussed in detail. [J564]

"On the origin of efficient electron injection at phosphonate-functionalized polyfluorene/aluminum interface in efficient polymer light-emitting diodes"

Ultraviolet and x-ray photoelectron spectroscopy are used to explore the underlying mechanism of efficient electron injection at phosphonate-functionalized polyfluorene (PF-EP)/Al interface in polymer light-emitting diodes (PLEDs). It is proposed that both the favorable interfacial dipoles of phosphonate groups and intense coordination interaction between the phosphonate groups and Al at PF-EP/Al interface are responsible for the efficient electron injection. As a result, the PLEDs with PF-EP/Al cathode demonstrate superior performance compared to the PLEDs with Ba or Ca cathode due to efficient electron injection and suppressed exciton-quenching at cathode interface. [J565]

"High-Luminance White-Light Point Source Using Ce,Sm : YAG Double-Clad Crystal Fiber"

Ce and Sm ions codoped yttrium aluminum garnet (Ce,Sm: YAG) double-clad crystal fibers (DCFs) were successfully fabricated using the codrawing laser-heated pedestal growth method. At a pump wavelength of 446 nm, white-light point source was produced from a 10--core DCF. The amplified spontaneous emissions and the residual pump resulted in a directional high brightness point source. A luminance of $4.5 \times 10^9 \text{ cd/m}^2$ was

generated. The luminous flux of the point white light was 6.2 lm. When coupled to a 200-core multimode fiber, the output power and coupling efficiency were 4.8 mW and 36.8%, respectively. Point white-light sources are useful for biomedical endoscopic application and long-range directive illumination. The generated broadband yellow emission can also be served as the light source for optical coherence tomography system. Using the 91-nm yellow emission, an axial resolution of 1.5-optical coherence tomography can be achieved for ultrahigh-resolution ocular and industrial applications. [J566]

"Viewing-Zone Control of Light-Emitting Diode Panel for Stereoscopic Display and Multiple Viewing Distances"

We propose methods to control viewing zones of a large screen consisting a full-color LED panel. Large parallax barriers have been developed for public 3D displays. By changing pixel arrangements, viewing positions and the number of perspectives are reconfigurable. The response of a viewer's position caused by a shift of viewing zone was detected to evaluate the design of stereoscopic viewing zone. Furthermore, an array of slits has been utilized to provide different information at multiple viewing distances for digital signage. [J567]

"Inverse Source Coding for Dimming in Visible Light Communications Using NRZ-OOK on Reliable Links"

This letter proposes an inverse source coding scheme to mitigate the severe performance degradation caused by light dimming in visible light communications using on-off keying on reliable links. The proposed scheme meets the ratio of 0's to 1's for the dimming target, and transmission efficiency approaches the theoretical maximum, entropy. It outperforms the existing time-multiplexing scheme, and the difference in performance becomes larger the more the dimming target deviates from 50%. There might be several ways to implement inverse source coding and this letter presents an example utilizing Huffman coding. [J568]

"VIS-NIR Imaging Spectroscopy of Mercury's Surface: SIMBIO-SYS/VIHI Experiment Onboard the BepiColombo Mission"

The Visible and Infrared Hyperspectral Imager (VIHI) is one of the three optical heads of the Spectrometers and Imagers for MPO BepiColombo Integrated Observatory SYStem (SIMBIO-SYS) experiment onboard European Space Agency's BepiColombo cornerstone mission to Mercury. The other two optical heads of SIMBIO-SYS are a stereo camera and a high-resolution image camera. The experiment is designed to scan the Hermean surface from a polar orbit with the three channels to map the physical, morphological, tectonic, and compositional properties of the planet. The main scientific objectives of SIMBIO-SYS are the study of Mercury's surface geology and stratigraphy, the surface composition, the regolith properties, the crustal differentiation, impact, and volcanic processes. The VIHI experiment uses a high-performance optical layout (Schmidt telescope and spectrometer in Littrow configuration) which allows investigating the 400-2000-nm spectral range with 256 spectral channels (6.25 nm/band sampling). The instrument has an instrument field of view (FOV) of 250 μ rad corresponding to a spatial scale of about 100 m/pixel at perihelion and 375 m at aphelion. The instrument operates in pushbroom configuration, sampling the surface of Mercury with an FOV of 64 \times 0.25 mrad. The main technical challenges of this experiment are focal-plane design (cadmium-mercury-telluride thinned to improve the efficiency at visible wavelengths), short dwell time (from about 40 ms at equator to about 100 ms at poles), thermal control, mechanical miniaturization, radiation hardening, high data rate, and compression. A description of the internal calibration unit concept and functionalities is given. [J569]

"Pulsewidth Modulation With Current Uniformization for AM-OLEDs"

We propose a novel conception of driving methods, pulsewidth modulation with current uniformization, for active-matrix organic light-emitting diode displays (AM-OLEDs). This driving conception can simultaneously achieve precise grayscale and exceedingly improve luminance uniformity. We evaluate a concrete example, in which a pixel circuit includes seven transistors and a driving period consists of addressing-programming and light-emitting periods. The working and the tolerance against characteristic deviations of thin-film transistors and OLEDs are confirmed using circuit simulation and actual equivalent circuits. [J570]

"Structural Effects on Highly Directional Far-Field Emission Patterns of GaN-Based Micro-Cavity Light-Emitting Diodes With Photonic Crystals"

This study theoretically and experimentally investigates the highly directional far-field emission patterns of GaN photonic crystal (PhC) micro-cavity light-emitting diodes (MCLEDs) depending on varying structural parameters. Angular-spectra-resolved electroluminescence measurements reveals the behavior of guided-mode extraction which is significantly affected by the structural parameters of GaN PhC MCLEDs, where the GaN cavity

thickness decides the extracted guided mode numbers, PhC lattice constant influences the distribution of far-field emission, and PhC hole depth affects the interaction with guided modes. The proposed GaN ultrathin MCLED (uMCLED) with PhC lattice constant of 420 nm and deep hole depth of 250 nm exhibited a maximum output light extraction efficiency of 248% under one-watt input power compared to GaN non-PhC uMCLED and produced a directional far-field emission pattern at half intensity near 17° . The present results indicate that highly directional light extraction enhancement could contribute to developments of many applications, especially for etendue-limited applications such as pico- projectors. [J571]

"Hot electron effects on efficiency degradation in InGaN light emitting diodes and designs to mitigate them"

Hot electrons and the associated ballistic and quasiballistic transport, heretofore neglected endemically, across the active regions of InGaN light emitting diodes (LEDs) have been incorporated into a first order simple model which explains the experimental observations of electron spillover and the efficiency degradation at high injection levels. The model is in good agreement with experiments wherein an adjustable barrier hot electron stopper, commonly called the electron blocking layer (EBL), is incorporated. The model is also in agreement with experiments wherein the electrons are cooled, eliminating hot electrons, inside a staircase electron injector (SEI) prior to their injection into the active region. Thermionic emission from the active region, even if one uses an uncharacteristically high junction temperature of 1000 K, fails to account for the carrier spillover and the experimental observations in our laboratory in samples with varying EBL barrier heights. The model has been successfully applied to both m-plane (lacking polarization induced electric field) and c-plane (with polarization induced field) InGaN double heterostructure (DH) LEDs with a 6 nm active region featuring a variable barrier hot electron stopper, and a SEI, and the various combinations thereof. The choice of DH LEDs stems from our desire to keep the sample structure simple as well as the model calculations. In this paper, the theoretical and experimental data along with their comparison followed by an insightful discussion are given. The model and the approaches to eliminate carrier spillover proposed here for InGaN LEDs are also applicable to GaN-based laser diodes. [J572]

"Highly efficient, single-layer organic light-emitting devices based on a graded-composition emissive layer"

We demonstrate highly efficient electrophosphorescence from devices comprising a single organic layer. High efficiency is realized by combining both hole- and electron-transporting host materials (HTMs and ETMs, respectively) into a single, graded-composition emissive layer with the green phosphorescent emitter fac-tris(2-phenylpyridine) iridium (III). The composition is continuously graded to realize nearly 100% HTM at the anode and nearly 100% ETM at the cathode. Peak external quantum and power efficiencies of $\eta_{EQE} = (19.3 \pm 0.4)\%$ and $\eta_P = (66.5 \pm 1.3) \text{ lm/W}$ are realized at a luminance level of 600 cd/m². [J573]

"III-nitride nanopyramid light emitting diodes grown by organometallic vapor phase epitaxy"

Nanopyramid light emitting diodes (LEDs) have been synthesized by selective area organometallic vapor phase epitaxy. Self-organized porous anodic alumina is used to pattern the dielectric growth templates via reactive ion etching, eliminating the need for lithographic processes. (In,Ga)N quantum well growth occurs primarily on the six {1101} semipolar facets of each of the nanopyramids, while coherent (In,Ga)N quantum dots with heights of up to 20 nm are incorporated at the apex by controlling growth conditions. Transmission electron microscopy (TEM) indicates that the (In,Ga)N active regions of the nanopyramid heterostructures are completely dislocation-free. Temperature-dependent continuous-wave photoluminescence of nanopyramid heterostructures yields a peak emission wavelength of 617 nm and 605 nm at 300 K and 4 K, respectively. The peak emission energy varies with increasing temperature with a double S-shaped profile, which is attributed to either the presence of two types of InN-rich features within the nanopyramids or a contribution from the commonly observed yellow defect luminescence close to 300 K. TEM cross-sections reveal continuous planar defects in the (In,Ga)N quantum wells and GaN cladding layers grown at 650–780 °C, present in 38% of the nanopyramid heterostructures. Plan-view TEM of the planar defects confirms that these defects do not terminate within the nanopyramids. During the growth of p-GaN, the structure of the nanopyramid LEDs changed from pyramidal to a partially coalesced film as the thickness requirements for an undepleted p-GaN layer result in nanopyramid impingement. Continuous-wave electroluminescence of nanopyramid LEDs reveals a 45 nm redshift in comparison to a thin-film LED, suggesting higher InN incorporation in the nanopyramid LEDs. These results strongly encourage future investigation--s of III-nitride nanoheteroepitaxy as an approach for creating efficient long wavelength LEDs. [J574]

"Electroluminescence from Er-doped Si-rich silicon nitride light emitting diodes"

Electrical devices based on Erbium (Er) doping of silicon nitride have been fabricated by reactive cosputtering

and intense, room temperature Er electroluminescence was observed in the visible (527, 550, and 660 nm) and near-infrared (980 and 1535 nm) spectral ranges at low injection voltages (<5 V EL turn on). The electrical transport mechanism in these devices was investigated and the excitation cross section for the 1535 nm Er emission was measured under electrical pumping, resulting in a value ($1.24 \times 10^{-15} \text{ cm}^2$) comparable to optical pumping. These results indicate that Er-doped silicon nitride has a large potential for the engineering of light sources compatible with Si technology. [J575]

"Highly-selective wettability on organic light-emitting-diodes patterns by sequential low-power plasmas"

Patterned organic light-emitting-diode substrates were treated by oxygen (O_2) and tetrafluoromethane (CF_4) radio-frequency (rf, 13.56 MHz) plasmas of low-power (close to 1 W) that were capacitively-coupled. An unexpected wettability contrast (water contact angle difference up to 90°) between the indium-tin-oxide anode and the bank resist regions was achieved, providing excellent conditioning prior to the ink-jet printing. This selectivity was found to be adjustable by varying the relative exposure time to the O_2 and CF_4 sequential plasmas. Static contact angle measurements and extensive x-ray photoelectron spectroscopy analyses showed that the wetting properties depend on the carbon and fluorine chemical functional groups formed at the outermost surface layers, whereas atomic force microscopy images did not show a morphological change. Plasma optical emission spectroscopy and ion mass spectroscopy suggested that surface functionalization was initiated by energy transfer from ionic species (O^+ , O_2^+ , CF^+ , CF_2^+ , and CF_3^+) and excited neutrals (O^* and F^*). The absolute ion fluxes measured on the substrates were up to $10^{14} \text{ cm}^{-2} \text{ s}^{-1}$ and the ion energies up to 20 eV, despite the low powers applied during the process. [J576]

"Solvothermal synthesis of designed nonstoichiometric strontium titanate for efficient visible-light photocatalysis"

SrTiO_3 powders with various Sr/Ti atomic ratios were synthesized by microwave-assisted solvothermal reactions of SrCl_2 and $\text{Ti}(\text{OC}_3\text{H}_7)_4$ in KOH aqueous solutions. The nanoparticles of perovskite type SrTiO_3 structure with the particle size of 30–40 nm were synthesized. The photocatalytic activity was determined by deNO_x ability using light emitting diode lamps of various wavelengths such as 627 nm (red), 530 nm (green), 445 nm (blue), and 390 nm (UV). The photocatalytic activity significantly changed depending on the Sr/Ti atomic ratio, i.e., the strontium rich sample (Sr/Ti atomic ratio > 1) showed excellent visible light responsive photocatalytic activity for the oxidative destruction of NO. [J577]

"Light Extraction Study on Thin-Film GaN Light-Emitting Diodes With Electrodes Covering by Wafer Bonding and Textured Surfaces"

Textured n-side-up GaN LEDs with interdigitated imbedded electrodes (IIEs), high-reflection mirror, and double-side roughening on both p-GaN and undoped-GaN layers are investigated. The IIE structure can eliminate electrode shading. The epitaxial layers of the devices are grown on (0001) sapphire substrates by metal-organic chemical vapor deposition. The devices are subsequently fabricated with wafer bonding, laser lift off, and chemical dry/wet etching techniques. The n-side-up structure is useful for enhancing light extraction and increasing light output power. Luminance intensity performance (at 350-mA injection current) is 160% and 20% higher than those of the conventional structure and the p-side-up structure with high-reflection mirror on silicon substrate and with electrode shading, respectively. The performance of p-side-up glue bonding LED (at 350-mA injection current) is only 120% higher than the conventional structure. The light extraction efficiency of n-side-up thin-film LEDs is better than that of p-side-up thin-film LEDs. [J578]

"Optimized Microcavity and Photonic Crystal Parameters of GaN-Based Ultrathin-Film Light-Emitting Diodes for Highly Directional Beam Profiles"

This study experimentally investigates the highly directional far-field emission distributions of GaN ultrathin-film light-emitting diodes (uTFLEDs) with optimized microcavity thickness and photonic crystal (PhC) parameters. Results show that directionality depends on guided mode extraction behaviors and strong microcavity effects. The proposed GaN PhC uTFLED exhibited an output power extraction efficiency enhancement of 278% (3.78) compared to GaN non-PhC uTFLED, and produced a directional far-field emission pattern at half intensity near $\pm 17^\circ$. [J579]

"Reduction in the Efficiency-Droop Effect of InGaN Green Light-Emitting Diodes Using Gradual Quantum Wells"

The effect of gradual indium gallium nitride (InGaN) quantum wells (QWs) on the suppression of efficiency-droop

in green light-emitting diodes (LEDs) is numerically investigated. The presented scheme increases the internal quantum efficiency by 45.5% at $I=20$ mA and 55.7% at $I=100$ mA, indicating a considerable reduction of efficiency-droop. This improvement is attributable mainly to the use of the gradual InGaN QW's structure that significantly alleviates band bending in the valence band, improving the transport efficiency of injected holes above that of conventional LEDs. The radiative recombination is thus enhanced as the overlap between electron and hole wave functions is increased. Most importantly, the leakage of injected electrons to p-type region is correspondingly reduced, in turn suppressing the efficiency-droop in the LED. [J580]

"Photosensitive biosensor array system using optical addressing without an addressing circuit on array biochips"

This paper introduces a photosensitive biosensor array system with a simple photodiode array that detects photocurrent changes caused by reactions between probe and target molecules. Using optical addressing, the addressing circuit on the array chip is removed for low-cost application, and real cell addressing is achieved using an externally located computer-controllable light-emitting diode array module. The fabricated biosensor array chip shows a good dynamic range of 1-100 ng/mL under prostate-specific antigen detection, with an on-chip resolution of roughly 1 ng/mL. [J581]

"Spin-injection device prospects for half-metallic Fe₃O₄:Al_{0.1}Ga_{0.9}As interfaces"

Electrical spin-injection across the Fe₃O₄:Al_{0.1}Ga_{0.9}As interface has been measured. We quantify this effect in an In_{0.2}Ga_{0.8}As:GaAs spin-light emitting diode optical device. The optical polarization signal is maintained from 4.2 up to 200 K without influence of the metal-insulator Verwey transition in the bulk of the Fe₃O₄ film. An incomplete oxidation at the interface may be detrimental for this device, as it has a similar spin-injection efficiency to that of Fe:Al_{0.1}Ga_{0.9}As. Ambient temperature operation of this device may be possible although the present polarization levels remain too low for practical spintronic applications. We demonstrate the first step in the integration of molecular beam epitaxy-grown magnetic oxides into III-V semiconductor devices. [J582]

"Disordered antireflective nanostructures on GaN-based light-emitting diodes using Ag nanoparticles for improved light extraction efficiency"

In this study, we demonstrate GaN light-emitting diodes (LEDs) with antireflective subwavelength structures (SWS) for enhanced light extraction efficiency. To eliminate the internal Fresnel reflection, SWS were fabricated on an indium-tin-oxide (ITO) surface using an overall dry etch process of Ag nanoparticles. The average size of the Ag nanoparticles was carefully chosen by theoretical calculation of the reflective diffraction efficiency using a rigorous coupled-wave analysis (RCWA) method. Improvement in light output power of 30.2% was achieved for the fabricated ITO SWS LEDs compared to conventional LEDs, with no significant increase in the forward voltage. [J583]

"Full spin-coated multilayer structure hybrid light-emitting devices"

We report on a multilayer structure hybrid light-emitting device (HLED) using a water/alcohol-soluble polymer poly(9,9-bis{30-[(N,N-dimethyl)-N-ethylammonium]-propyl}-2,7-fluorene dibromide) as an electron-transporting layer and a close-packed quantum dot-layer (QD-layer) as an emitting layer. The device was realized by full spin-coating technology without thermal evaporation process for the deposition of organic layers. The QD-layer was a mixture of QDs with two different sizes, in which large size QD-emitters were dispersed in small size QDs to weaken the concentration quenching. The device achieved a maximum power efficiency of 0.58 lm/W, which nearly quadrupled that of the HLED with a plain large size QD-EML. [J584]

"Fast current programming method using current amplifier for active matrix organic light emitting diode displays"

A fast and accurate current programming method with a current unity-gain amplifier which provides high gain and driving capability has been designed. Experimental results show that the maximum error of the programming current in pixels is less than 0.22 least significant bit using the proposed current driving method and the lowest grey-level current, 6.7 nA, can be successfully programmed within 19 s. The power consumption of the proposed current driving method with a channel is 10.5 W. This performance is good enough to apply to a 12-inch-wide extended graphics array resolution format active matrix organic light emitting diode display with 8-bit greyscale. [J585]

"Removing GaAs substrate by nitric acid solution"

A two-step removing GaAs substrate technique by using HNO₃ solution is reported. In the authors' experiments,

as compared with other ratios, the etch rate of $\text{HNO}_3:\text{H}_2\text{O}_2:\text{H}_2\text{O}=1:6:1$ is faster. In addition, the etched surface by nitric acid solution has about 0.15 μm of surface smoothness. The high selectivity of $\text{HNO}_3:\text{H}_2\text{O}_2:\text{H}_2\text{O}=1:4:1$ for GaAs/GaN is demonstrated with smooth morphology whose roughness is about 4.57 nm. The advantages of this technique are easy, repeatable, and no contamination. It is a very useful process in the light-emitting diode fabrication. [J586]

"Formation of low-resistance Ohmic contacts to N-face n-GaN for high-power GaN-based vertical light-emitting diodes"

We report on the formation of low-resistance Ohmic contacts to N-face n-GaN for high-power vertical light-emitting diodes using an Al-Ga solid solution (50 nm)/Ti(30 nm)/Al(200 nm) scheme and compare them with Ti(30 nm)/Al(200 nm) contacts. The Al-Ga solid solution layer is introduced to minimize the formation of Ga vacancies near the N-face n-GaN surface. It is shown that, unlike the Ti/Al contacts, the Al-Ga solid solution/Ti/Al contacts exhibit Ohmic behavior with a resistivity of $4.1 \times 10^{-4} \Omega \text{ cm}^2$, even after annealing at 250 °C. X-ray photoemission spectroscopy and secondary ion mass spectrometry examinations are performed to understand the temperature dependence of the electrical properties. [J587]

"Origin of magnetic field effect enhancement by electrical stress in organic light emitting diodes"

Recently, it has been discovered that the magnetic field effect (MFE) in organic light emitting diodes (OLEDs) based on poly(para-phenylene vinylene) can be enhanced by exposing the diode to moderate electrical stress. Here, we disclose the mechanism behind this way of improving the MFE. We first show that electronic traps in general play an important role for the MFE. Optical depletion of available trap states by infrared illumination leads to a decrease in the MFE. Furthermore, we demonstrate that annealing of the OLED at high temperatures eliminates the MFE improvement of the previously performed electrical conditioning. However, the improvement can be restored by subsequent conditioning at higher current or voltage. Thus it is likely that electrical stress is accompanied by a transformation of the polymer morphology or conformation resulting in a formation of energetic traps for charge carriers. [J588]

"Charge separation and transport behavior of a two-dimensional charge sheet at organic donor-acceptor heterointerfaces"

Charge separation and transport behavior were investigated at an organic heterolayered interface consisting of a 4,4',4"-tris[3-methylphenyl(phenyl)amino] triphenylamine (m-MTDATA) organic donor and a hexadecafluoro-copper-phthalocyanine (F16CuPc) organic acceptor. A two-dimensional charge sheet of electron-hole pairs was induced due to the formation of charge-transfer complexes at the heterointerface. The induced charges could be separated by application of an electric field perpendicular to the heterointerface. The charge-separation behavior was independent of the work function of the contact electrodes but was strongly dependent on the energy-level alignment between the highest occupied molecular orbital of the donor molecules and the lowest unoccupied molecular orbital of the acceptor molecules. This enabled the preparation of an organic light-emitting diode without injecting holes from the anode. The charge-transport behavior along the heterointerface was also investigated by fabricating laterally arranged contact electrodes. The F16CuPc/m-MTDATA heterointerface exhibited high conductivity of 0.001 S/cm, which is seven orders of magnitude higher than that of a single-layer F16CuPc or m-MTDATA film. In situ electrical measurements during formation of the heterointerface enabled the effective thickness of the charge sheet to be determined as being accumulated within 2-3 nm, which corresponds to the bilayer of both F16CuPc and m-MTDATA. [J589]

"Electronic and optical properties of InGaN quantum dot based light emitters for solid state lighting"

In this paper, we have made a systematic study of the electronic and optical properties of InGaN based quantum dot light emitters. The valence force field model and 646k-p method have been applied to study the band structures in InGaN or InN quantum dot devices. Piezoelectric and spontaneous polarization effects are included. A comparison with InGaN quantum wells shows that InGaN quantum dots can provide better electron-hole overlap and reduce radiative lifetime. We also find that variation in dot sizes can lead to emission spectrum that can cover the whole visible light range. For high carrier density injection conditions, a self-consistent method for solving quantum dot devices is applied for better estimation of device performance. Consequences of variations in dot sizes, shapes, and composition have been studied in this paper. The results suggest that InGaN quantum dots would have superior performance in white light emitters. [J590]

"Insights into thermal degradation of organic light emitting diodes induced by glass transition through impedance spectroscopy"

Highly sensitive alternate current (ac) impedance measurements with variable temperature have been performed to investigate the optical and electrical failure mechanisms during the glass transition phenomena in the archetypal ITO/TPD/Alq3/Alorganic light emitting diode (OLED) structure. Since the device degradation is mainly related to the lower glass transition temperature (T_g) of the N,N'-Bis(3-methylphenyl)-N,N'-diphenylbenzidine (TPD), this study is focused on the frequency response of thin TPD films approaching the glassy region. The related experimental data are discussed in the framework of the universal dielectric response model. By ac measurements, TPD glass transition temperature is located and temperature regions with different OLED behaviors are evidenced. The relation between the behaviors of TPD frequency response and of the OLED electro-optical response, while the temperature approaches the glass transition region, is discussed. [J591]

"p-Si /beta -FeSi 2 /n-Si double-heterostructure light-emitting diodes achieving 1.6 mcm electroluminescence of 0.4 mW at room temperature"

Electroluminescence at an emission power of over 0.4 mW is achieved at an emission wavelength of 1.6mcm using a p-Si/beta -FeSi2/n-Si double-heterostructure light-emitting diode. This emission power is obtained at room temperature under current injection of 460 mA, corresponding to an external quantum efficiency of approximately 0.1%. Photoluminescence and time-resolved photoluminescence measurements for devices with different thicknesses of beta -FeSi2 indicate that radiative recombination rate increased as the thickness of the beta -FeSi2 active layer is increased. [J592]

"Luminescence enhancement and emission color adjustment of white organic light-emitting diodes with quantum-well-like structures"

In recent years, white-light organic light-emitting diodes (OLEDs) have attracted considerable attention because of their potential applications in displays, backlight units, and general lighting. In this paper, we describe the fabrication of a high-luminance white-light OLED with dual-emission layers (EMLs). The 2,9-dimethyl-4,7-diphenyl-1,10-phenanthroline hole blocking layers (HBLs) were prepared to enhance the luminance and adjust the emission color of the device. For the device with a single-HBL structure, the excess holes were accumulated at the red EML (REML)/HBL1 interface. Consequently, most of the carriers were recombined in the REML, which led to a redshifted light emission. On the contrary, the device with a dual-HBL structure showed a blueshifted light emission. The device with a quantum-well-like structure increased the carrier trapping and recombination probabilities; as a result, a lower current density and a higher luminance intensity of the device were achieved. The maximum luminance intensity was 33 600 cd/m² at 13 V, with CIE coordinates at (0.32, 0.32); the maximum current efficiency was 7.06 cd/A at 10 V; and the maximum power efficiency was 2.62 lm/W at 7 V and 294 cd/m². [J593]

"Hadamard transform microchip electrophoresis combined with laser-induced fluorescence detection using a compact neodymium-doped yttrium aluminum garnet laser emitting at 532 nm"

Hadamard transform electrophoresis combined with laser-induced fluorescence (LIF) detection on a microchip was demonstrated. A compact, diode-pumped neodymium-doped yttrium aluminum garnet laser was employed as the light source for LIF detection. The analytical conditions were optimized using rhodamine B as the analyte. Under optimal conditions, the signal-to-noise ratio (S/N) of the analyte was improved by a factor of 7.5 by means of Hadamard transformation based on a 255-order cyclic Smatrix. Additionally, the relationship between fluorescence intensity and analyte concentration was linear with a correlation coefficient of 0.993 in the inverse Hadamard transformed data at the concentration range from 25 to 100 pM. The results indicate that the present method is applicable to quantitative analysis at the concentration lower than the concentration limit of detection in a conventional method. The concentration limit of detection was 25 pM (the relative standard deviation of the peak height was 5.2%). The present technique was successfully applied to the separation of a mixture containing 1.9 nM phenylalanine and 1.9 nM glutamic acid labeled with rhodamine B isothiocyanate. The S/Ns of the analyte peaks were improved up to 10 in the inverse Hadamard transformed data derived from a 127-order cyclic Smatrix, while neither peak was lower than the limit of detection (S/N > 3) in conventional microchip electrophoresis by a single injection. [J594]

"Leakage current improvement of nitride-based light emitting diodes using CrN buffer layer and its vertical type application by chemical lift-off process"

We report the electrical characteristics of vertical and lateral type light emitting diodes (LEDs) grown with CrN buffer layer. The LED with CrN buffer showed lower reverse leakage current than the reference sample grown with conventional low-temperature GaN buffer. It was also observed that the density of open core screw dislocation was smaller by one order of magnitude, which was thought to relate to the leakage current of devices. The vertical type LED fabricated by chemical etching of CrN buffer showed lower series resistance,

lower turn-on voltage, and larger light output power than those of the conventional LEDs. [J595]

"Quantum efficiency enhancement in nanocrystals using nonradiative energy transfer with optimized donor-acceptor ratio for hybrid LEDs"

The quantum efficiency enhancement in nanocrystal solids is critically important for their efficient use as luminophors on color-conversion light emitting diodes (LEDs). For this purpose, we investigate energy gradient mixture of nanocrystal solids for recycling their trapped excitons by varying their donor-acceptor nanocrystal ratios and study the resulting quantum efficiency enhancement as a function of the donor-acceptor ratio in the solid film for hybrid LEDs. We achieve a maximum quantum efficiency enhancement of 17% in these nanocrystal solids when the donor-acceptor ratio is 1:1, demonstrating their highly modified time-resolved photoluminescence decays to reveal the kinetics of strong energy transfer between them. [J596]

"Exciton-related electroluminescence from ZnO nanowire light-emitting diodes"

The authors study the microscopic origin of the electroluminescence from zinc oxide (ZnO) nanowire light-emitting diodes (LEDs) fabricated on a heavily doped p-type silicon (p-Si) substrate. By comparing the low-temperature photoluminescence and electroluminescence of a single nanowire LED, bound- and free-exciton related recombination processes, together with their longitudinal-optical phonon replicas, can be identified as the origin of both electroluminescence and photoluminescence. [J597]

"An investigation on the light-emission mechanism of metal-insulator-semiconductor light-emitting diodes with different SiGe quantum well structures"

The SiGe quantum well (QW) tunneling diodes with different Si cap thickness are designed in this work to investigate the detailed mechanism of light emission for the metal-insulator-semiconductor (MIS) light-emitting diode (LED). At the accumulation (negative) gate bias, the electrons tunnel from the metal gate to the SiGe QW semiconductor substrate (p-type). Meanwhile, the negative gate bias also attracts holes in the interface of insulator and SiGe QW semiconductor and then the tunneling electrons can recombine with holes to emit the infrared. LEDs with different Si/SiGe/Si structure are used to investigate the light-emission mechanism and prove that the region of infrared emission is mainly from the interface of the insulator and semiconductor, not from the neutral region in the semiconductor substrate. The accurate energy band and carrier concentration in the SiGe QW structure with operated bias are also simulated and compared it with the experimental data. It shows that the concentrations of the tunneling electrons, which will be drifted by the gate bias, plays the main role on the light emission and limits the light-emission region near the interface of insulator and semiconductor. This work helps us understand clearly the light-emission mechanism of the MIS LED, developed continuously by our group in the decade. [J598]

"Light emission and photoluminescence from high-k dielectrics containing Ge nanocrystals"

A metal/HfAlO/Si light emitting diode with Ge nanocrystals embedded in HfAlO has the visible light emission (610nm) and the infrared emission (760nm). The image and Ge content are measured by the transmission electron microscopy and Raman spectroscopy. The photoluminescence of Ge nanocrystals embedded in HfAlO has a peak wavelength at 700nm, while the peak wavelength at 725nm is observed for Ge nanocrystals embedded in HfO₂. The difference of it may be due to the larger band gap of HfAlO as compared to HfO₂. [J599]

"Enhanced ultraviolet electroluminescence from p-Si/n-ZnO nanorod array heterojunction"

The authors report enhanced ultraviolet electroluminescence at room temperature from a diode structure consisting of vertically oriented ZnO nanorod arrays grown on a p-typed silicon substrate. Excitonic emitting peak at wavelength of 385nm with a full width at half maximum (FWHM) of 23nm and a defect-related visible emitting peak at the wavelength of 546nm with a FWHM of 124nm are observed from this structure under forward-bias voltage. The intensity ratio of the ultraviolet peak and the visible peak reaches 4.7. The scanning electron microscope, x-ray diffraction, energy dispersive x ray, I-V, and electroluminescence measurements demonstrate that good crystal structure and rectifying diodelike behavior are obtained and defect-related visible light emission is greatly restrained. [J600]

"High-speed electroluminescence modulation of a conjugated-polymer light emitting diode"

To maximize the electroluminescence (EL) switching rate that can be generated in an organic-based light emitting diode, we fabricated a device having an active area of 0.018mm² which is based on a 1:1 blend of the high charge-carrier mobility conjugated polymers poly[diocetylfluorene-co-N-(4-butylphenyl) diphenylamine] and

poly[9,9'-dioctylfluorene-co-benzothiadiazole]. Our devices have a 50% cutoff frequency of 26 MHz and a maximum EL modulation rate of 63 MHz at a drive voltage of 3.8 V. Such switching rates are suitable for short-range video transmission via plastic optical fibers, suggesting possible applications as optical communication light sources. [J601]

"Efficient single-component light-emitting electrochemical cells with an ion-conducting water-soluble polyfluorene"

Polymer light-emitting diodes (PLEDs) and light-emitting electrochemical cells (LECs) were fabricated using a water-soluble conjugated polymer with ion-conducting side chains. The water-soluble polymer was spin-coated on the emitting layer of a PLED and was used as an electron-injecting layer. The PLED showed enhanced performance with LEC behavior due to both the mobile ions and ion-conducting side groups of the polymer. A single-component and single-layer device was also fabricated, which showed typical LEC behavior with 1.13% maximum external quantum efficiency after complete ion migration. [J602]

"An ambipolar phosphine oxide-based host for high power efficiency blue phosphorescent organic light emitting devices"

We report blue electrophosphorescent organic light emitting devices with an ambipolar host material, 4-(diphenylphosphoryl)-N,N-diphenylaniline (HM-A1), doped with Irpic (iridium(III)bis[(4,6-difluorophenyl)pyridinato-N,C2']picolinate). The ambipolar nature of the host was verified using single carrier devices. The power efficiency of devices with PO15 (2,8-bis(diphenylphosphoryl)dibenzothiophene) electron transport layer (ETL) showed optimized performance when the ETL thickness was 500 Å, giving a peak power efficiency of 46 lm/W (corresponding external quantum efficiency (EQE) of 17.1%). The EQE and power efficiency at the brightness of 800 cd/m² were measured with no light outcoupling enhancement and found to be 15.4% and 26 lm/W, respectively. [J603]

"Tilted-charge high speed (7 GHz) light emitting diode"

We demonstrate a higher speed form of light emitting diode (LED), an asymmetrical two-junction tilted-charge LED, utilizing an n-type buried "drain" layer beneath the p-type "base" quantum-well (carrier and photon) active region. The drain layer tilts and pins the charge in the manner of a heterojunction bipolar light emitting transistor (HBLT), selecting and allowing only "fast" recombination (recombination lifetime τ_{Bof} of the order of base transit time τ_t). The tilted-charge LED, simple in design and construction, is capable of operation at low current in spontaneous recombination at a 7 GHz bandwidth or even higher with more refinement. [J604]

"Enhanced hole injection in organic light-emitting devices by using Fe₃O₄ as an anodic buffer layer"

Hole injection improvement in organic light-emitting devices with Fe₃O₄ as a buffer layer on indium tin oxide (ITO) has been demonstrated. The luminance and the current density are significantly enhanced by using the Fe₃O₄/ITO anode, as well as the turn-on voltage is reduced by 1.5 V compared to the devices without the buffer. Results of atom force microscopy, x ray, and UV photoelectron spectroscopy studies reveal that the enhanced hole injection is attributed to the modification of the ITO surface and the reduced hole-injection barrier by the insertion of the Fe₃O₄ thin film between the ITO and hole-transporting layer. [J605]

"Effect of electron blocking layer on efficiency droop in InGaN/GaN multiple quantum well light-emitting diodes"

The effect of an electron blocking layer (EBL) on the efficiency droop in InGaN/GaN multiple quantum well light-emitting diodes (LEDs) is investigated. At low current density, the LEDs with a p-AlGaIn EBL show a higher external quantum efficiency (EQE) than LEDs without an EBL. However, the EQE of LEDs without an EBL is higher than LEDs with an EBL as injection current density is increased. The improved EQE of LEDs without an EBL at high current density is attributed to the increased hole injection efficiency. [J606]

"Realization of high efficiency microcavity top-emitting organic light-emitting diodes with highly saturated colors and negligible angular dependence"

An alternative way to optimize the emission characteristics of a microcavity top-emitting organic light-emitting diode (TOLED) based on a simple device structure is demonstrated via combining a comprehensive theoretical analysis in the microcavity effects with the experimental modification in the carrier injection of both electrodes. It can be seen that the resulting TOLED exhibits much higher efficiencies and a more saturated color than those of

the corresponding conventional bottom-emitting device, as well as hardly detectable color shift with viewing angles. Such a strategy may be more feasible in practical application for active-matrix organic light-emitting diode displays. [J607]

"4.3 GHz optical bandwidth light emitting transistor"

We demonstrate a quantum-well base heterojunction bipolar light emitting transistor (HBLT) operating in the common collector configuration with a 3 dB optical response bandwidth f_{3dB} of 4.3 GHz. The HBLT has a current gain, $\beta = |\Delta I_C / \Delta I_B|$ as high as 30, and can be operated as a three-port device to provide simultaneously an optical and electrical output with gain. The f_{3dB} of 4.3 GHz corresponds to an effective carrier recombination lifetime of 37 ps, and shows that "fast" spontaneous recombination can be harnessed for high-speed modulation. [J608]

"Metal organic chemical vapor deposition of crack-free GaN-based light emitting diodes on Si (111) using a thin Al₂O₃ interlayer"

Crack-free GaN light emitting diodes (LEDs) have been grown by metal organic chemical vapor deposition on Si(111) substrates using an atomic layer deposition-grown Al₂O₃ interlayer. Devices on Si show a longer emission wavelength compared to those on sapphire. This is attributed to tensile strain in the layers on Si, which may increase indium incorporation. Internal quantum efficiency is similar on both substrates. Luminescence intensity versus current density measurements show higher efficiency for the LEDs on Si relative to sapphire at high drive currents. These results show comparable performance characteristics for GaN-based devices on Si and sapphire substrates. [J609]

"Improving emission enhancement in surface plasmon coupling with an InGaN/GaN quantum well by inserting a dielectric layer of low refractive index between metal and semiconductor"

The improved emission enhancement in surface plasmon polariton (SPP) coupling with an InGaN/GaN quantum well (QW) by inserting a SiO₂ layer of lower refractive index between the deposited Ag and GaN layers is experimentally and numerically demonstrated. The inserted SiO₂ layer leads to reduced SPP dissipation rate, increased evanescent field intensity beyond a certain depth in GaN, and decreased SPP density of state. The combination of these factors can result in further emission enhancement of QW through SPP coupling. For light-emitting diode application, the elongated evanescent field coverage can release the constraint of thin p-type GaN for effective SPP coupling. More importantly, the reduced SPP dissipation can result in more effective emission in such an SPP-QW coupling mechanism. [J610]

"Laser micromachining of optical microstructures with inclined sidewall profile"

Laser micromachining has been proved to be a useful tool for the formation of microstructures in semiconductor and optical materials. It is also widely adopted for dicing of light-emitting diode chips. The authors propose a modified laser micromachining setup which enables three-dimensional structures to be formed. A mirror is inserted in the optical path between the focusing optics and the machining plane so that the beam strikes the sample at an oblique angle. By translating and/or rotating the sample as micromachining is carried out, various three-dimensional structures such as a pyramid or a conic section can be obtained. Trenches as small as 10 μm on sapphire have been realized with nanosecond ultraviolet laser pulses. Laser-induced damage, due to resolidification of the ablation melt, accumulates with increasing scans of the beam; it can be removed by chemical and mechanical treatment. [J611]

"Dual luminescence from organic/inorganic hybrid p-n junction light-emitting diodes"

We fabricated a hybrid p-n junction structure using n-type InGaN/GaN multiple quantum wells (MQWs) and p-type N,N'-diphenyl-N,N'-bis(1-naphthyl)-1,1'-biphenyl-4,4'-diamine (α-NPD). The hybrid structure shows a good current rectifying characteristic similar with conventional p-n junction diodes. Electroluminescence (EL) of the hybrid device exhibits two emission bands originated from InGaN/GaN MQWs, as well as α-NPD layer. The EL properties can be explained by either (or both) electron-hole charge transport between the components or (and) efficient energy transfer via Foster mechanism. The device characteristics could be applicable to various multicolor light-emitting diodes by constructing other organic/inorganic hybrid junctions. [J612]

"Carrier localization degree of In_{0.2}Ga_{0.8}N /GaN multiple quantum wells grown on vicinal sapphire substrates"

In this work, we have grown In_{0.2}Ga_{0.8}N/GaN multiple quantum well (MQWs) epitaxial structure on vicinal sapphire substrates by low pressure metal-organic chemical vapor deposition and investigated the relationship

between carrier localization degree and vicinal angles of sapphire substrates. The optical analysis confirmed that the In_{0.2}Ga_{0.8}N/GaNMQWs grown on 0.2°-off sapphire substrate exhibited the smallest carrier localization degree and more ordered In_{0.2}Ga_{0.8}N/GaNMQW structure. In addition, mechanisms for carrier localization in In_{0.2}Ga_{0.8}N/GaNMQWs grown on vicinal substrate were discussed based on the results obtained from the power and temperature dependent photoluminescence measurements. The Raman spectrum showing the in-plane compressive stress of the GaN epitaxial structures grown on vicinal sapphire substrates revealed the relation between the dislocation density and the carrier localization degree in MQWs. From transmission electron microscopy images, the threading dislocation density (TDD) of In_{0.2}Ga_{0.8}N/GaNMQWs grown on 0.2° vicinal sapphire substrate at the bottom of n-GaN layer was about $9.4 \times 10^8 \text{ cm}^{-2}$ and reduced to $3.0 \times 10^8 \text{ cm}^{-2}$ at the top of n-GaN layer. We also obtained the TDD of $5.6 \times 10^7 \text{ cm}^{-2}$ in the MQW region and only $1.0 \times 10^7 \text{ cm}^{-2}$ in the p-GaN region. Based on the results mentioned above, 0.2°-off substrate can offer In_{0.2}Ga_{0.8}N/GaNMQW blue light-emitting diode structures with benefits, such as high crystal quality, low defects, and small carrier localization degree. [J613]

"Effects of gate insulator using high pressure annealing on the characteristics of solid phase crystallized polycrystalline silicon thin-film transistors"

The oxidizing ambient was built using high pressure H₂O vapor at 550 °C. For the solid phase crystallization (SPC) polycrystalline silicon (poly-Si) that is annealed for 1 h at 2 MPa, the oxide thickness is about 150 Å. The oxide layer is approximately 90 Å above the original surface of the poly-Si and 60 Å below the original surface. The oxide layer is used as the first gate insulator layer of thin-film transistors (TFTs). The heating at 550 °C with 2 MPa H₂O vapor increased the carrier mobility from 17.6 cm²/V s of the conventional SPC process to 30.4 cm²/V s, and it reduced the absolute value of the threshold voltage (V_{th}) from 4.13 to 3.62 V. The subthreshold swing also decreased from 0.72 to 0.60 V/decade. This improvement is attributed mainly to the reduction in defect density at the oxide/poly-Si interface and in the poly-Si film by the high pressure annealing (HPA) process. Since the realization of excellent performance at the oxide/poly-Si interface and in poly-Si depends on the defect density, the poly-Si having the thermal oxide formed by a combined process of SPC and HPA may be well suited for fabrication of poly-Si TFTs for flat panel displays such as active matrix organic light emitting diodes. [J614]

"A high-performance tandem white organic light-emitting diode combining highly effective white-units and their interconnection layer"

By utilizing 2,9-dimethyl-4,7-diphenyl-1,10-phenanthroline:Li/MoO₃ as an effective charge generation layer (CGL), we extend our recently demonstrated single-emitting-layer white organic light-emitting diode (WOLED) to realize an extremely high-efficiency tandem WOLED. This stacked device achieves maximum forward viewing current efficiency of 110.9 cd/A and external quantum efficiency of 43.3% at 100 A/cm² and emits stable white light with Commission Internationale de L'Eclairage coordinates of (0.34, 0.41) at 16 V. It is noted that the combination of effective single units and CGL is key prerequisite for realizing high-performance tandem WOLEDs. [J615]

"Erratum: "High output power density from GaN-based two-dimensional nanorod light-emitting diode arrays" [JAppl. Phys. Lett. 94, 141111 (2009)]"

First Page of the Article [J616]

"Reduction in Shockley-Read-Hall generation-recombination in AlInSb light-emitting-diodes using spatial patterning of the depletion region"

A technique for the reduction in Shockley-Read-Hall recombination in semiconductor diodes, in which areas of the depletion region are removed, is described and preliminary results obtained using AlInSb light-emitting-diodes (LEDs) are presented. Both the electrical and optical characteristics of the devices were significantly improved by removing parts of the depletion region using dry etching, with an average increase in the zero bias differential resistance and LED emission at low currents by a factor of 2. [J617]

"Investigation of Forster-type energy transfer in organic light-emitting devices with 4-(dicyanomethylene)-2-*t*-butyl-6-(1,1,7,7-tetramethyljulolidin-4-yl-vinyl)-4H-pyran doped cohost emitting layer"

Organic light-emitting devices (OLEDs) with cohosted emitter, which is composed of 9,10-di(2-naphthyl)anthracene (ADN) and tris(8-hydroxy-quinolino) aluminum (Alq₃) and doped with 4-(dicyanomethylene)-2-*t*-butyl-6-(1,1,7,7-tetramethyljulolidin-4-yl-vinyl)-4H-pyran (DCJTB), were fabricated and

studied. The efficiency of OLEDs with a cohost emitter was higher than that with a single host emitter. For the cohost emitter with ADN/Alq3 weight ratio of 75:25, the 3.4 cd/A efficiency of the resulted OLEDs was obtained. It is found that the absorption spectra of DCJTb and the emission spectra of Alq3 changed with the composition of the emitter. This phenomenon is attributed to the polarization effect. On the basis of the Forster's theory, the resulted overlap integral exhibits the highest value for this cohost emitter. The experimental results reveal that the cascade energy transfer plays an important role in the luminance efficiency enhancement of the cohost emitter in OLEDs. [J618]

"Microstructure and luminescent properties of novel InGaP alloys on relaxed GaAsP substrates"

We present a metal organic chemical vapor deposition (MOCVD) growth study of unconventional alloys of InGaP (with In fraction of 0.2-0.4) grown on fully relaxed GaAsP virtual substrates for the application of high performance visible light emitting diodes (LEDs) and lasers in the green to red range of the visible spectrum. Several defects which are harmful to optical performance were identified, characterized, and removed. These include CuPt-B order (which lowers band gap), phase separation or short range order (which contributes to leakage currents and reduces luminescence) and undulation of the virtual substrate surface (which prevents high quality epitaxial growth). Each of these defects is understood through a two-step growth model which describes the formation and subsequent randomization of defects during growth. Through control of MOCVD parameters including growth temperature, V/III ratio, growth rate, and surfactant we demonstrate growth of extremely high quality InGaP heterostructures which hold promise for fabrication of light emitting devices. [J619]

"High power light emitting diode based setup for photobleaching fluorescent impurities"

Single molecule fluorescence experiments, with their associated low signals, require very low background fluorescence in the sample. Even high purity liquids will often possess large numbers of fluorescent impurities that are difficult to completely remove through standard purification techniques such as distillation and recrystallization. We have constructed a simple setup in which such impurities can be photobleached before final sample preparation. The instrument consists of high power light emitting diodes, and it delivers almost 10 W of light to the sample without the heating associated with more conventional light sources or the cost and safety concerns associated with a high power laser. [J620]

"Measurement of urinary calcium using AT89C51RD2 microcontroller"

A simple and inexpensive absorption technique for determination of calcium ion in urine samples is developed, comprising a light emitting diode (650 nm) as the light source and photodiode as the detector with AT89C51RD2 microcontroller. The design of the system and details of interface, calibration, and procedure of operation are explained in this paper. Software is developed to monitor sample processing and to display the results in liquid crystal display screen. With 15 μ l sample volume, a linear output is obtained in the range of 2.5-7.5 mM calcium with a detection limit of 0.06 mM. Interferences from other cations such as monovalent ion and divalent ion are investigated in the expected range, which are normally present in clinical samples, and absorption changes over the pH range of 3-12 are also determined. This system has been demonstrated successfully for the successive assay of calcium in urine samples, with the results comparing well to those achieved and in good agreement with values obtained with the current clinical spectrophotometric method at 95% of confidence level. [J621]

"Fabrication and characterization of the substrate-free InGaN-based resonant-cavity light-emitting diodes for plastic optical fiber communications"

In this article, the authors report on the realization of substrate-free InGaN-based thin-film resonant-cavity light-emitting diodes (TF-RCLEDs). Experimentally, the sapphire substrate was stripped by using the laser lift-off technique. The $\lambda/4$ -thick Ta₂O₅/SiO₂ distributed Bragg reflector and the metallic Ag film with mirror reflectivities of 68% and 97% were, respectively, coated onto the top and bottom of the substrate-free LEDs to form a Fabry-Perot cavity. The performances of LEDs are characterized by light output power, external quantum efficiency, emission spectrum, angular-resolved intensity distribution, and dynamic response. As a result, the fabricated TF-RCLEDs exhibit a low operating voltage of 3.34 V at 20 mA, a maximum light output power of 6.3 mW at 140 mA, and an external quantum efficiency of 5.5% at 4 mA. In addition, the TF-RCLEDs show temperature insensitivity as compared to the normal LEDs directly grown on the sapphire substrates. Furthermore, the 50% viewing angle of TF-RCLED is smaller than that of normal LED, i.e., 146° versus 168° at 60 mA. Finally, the eye pattern of the TF-RCLEDs is improved compared to that of the normal LEDs as operated at the data transmission rate of 100 Mbit/s. These results exhibit that the InGaN-based TF-RCLEDs are excellent candidates for the use in short-distance plastic optical fiber communications. [J622]

"Fabrication and characterization of novel hybrid green light emitting diodes based on substituting n-type ZnO for n-type GaN in an inverted p-n junction"

Details of the fabrication and characterization of hybrid green light emitting diodes, composed of n-ZnO/(InGa)N/p-GaN on AlN/sapphire, are reported. Scanning electron microscope, atomic force microscopy, high resolution x-ray diffraction, and photoluminescence were used to study the hybrid device. The effects of solvents, annealing, and etching on n-ZnO are discussed. Successful hybridization of ZnO and (In)GaN into a green light emitting diode was realized. [J623]

"Light emitting diode fault detection using p-n junction photovoltaic effect"

This paper proposes an online noncontact fault detection method during light emitting diode (LED) chip packaging, which is based on the photovoltaic effect in p-n junctions. Once a LED chip bonded on a lead frame is illuminated, the photocurrent will flow through the loop circuits formed by the lead frame. Through characterization of the weak photovoltaic response in the lead frame with the 20 LED chips, five LED faults, including chip defects (chip quality and chip contamination) and bonding deficiencies (disconnection, debonding, and rebonding), can be detected before packaging. A high-sensitivity photocurrent detection instrument has been developed to detect different color (red, yellow, green, and blue) and different size LED chips (9-15 mil) on LED assembly line. A key feature of the new instrument is the capability to tune and implement the maximum output power (photocurrent) in the loop lead frame by designing the high-efficiency magnetic core, the magnetic coil and the detecting system. Experiments demonstrate that the photovoltaic behaviors for LED p-n junctions are directly related to the LED electroluminescent characteristics, and the internal optoelectronic characteristics and the external Ohmic contact performances can be derived by detecting the photocurrent of LED chips. The LED online noncontact fault detection instrument based on the photovoltaic effect can be used to substitute for the ordinary electroluminescence online contact fault detection instrument. [J624]

"Efficiency of light emission in high aluminum content AlGaIn quantum wells"

High quality multiple quantum well Al_{0.35}Ga_{0.65}N active layers with narrow wells designed for ultraviolet (UV) light-emitting diodes using the phonon engineering approach are characterized using quasi-steady-state and time-resolved photoluminescence spectroscopy. The photoluminescence intensity decrease with temperature increasing from 10 to 300 K was very small, and the upper limit of the internal quantum efficiency (IQE) of up to 70% was estimated based on this temperature dependence. Carrier lifetime measurements yielded the lower bound of the IQE to be 35% under optical pumping, whereas IQE of 25% was estimated from the measured external quantum efficiency and the light extraction efficiency calculated by ray tracing. The observed photoluminescence features and the high IQE are interpreted as a consequence of strong carrier (exciton) localization. [J625]

"Design and implementation of a system with a multielement thermopile for monitoring temperature of a plane"

In this paper, we report the design of a system equipped with a multielement thermopile for measuring the temperature of a given plane. We evaluate the performance of our measurement system, which comprises a microcontroller, an analog-to-digital converter, a liquid crystal display (LCD), light-emitting diodes (LEDs), a buzzer, laser pointers, and a rotary encoder. We use different types of display modes such as an LCD for displaying the measured temperature, LEDs which colors indicate the temperature range, and an RS-232 or a wireless interface that transmits the temperature values to be displayed as different colors on a PC screen. The buzzer/alarm in the system is activated when the threshold temperature is reached. The system is inexpensive, portable, and can be used for two-dimensional temperature measurements; further, its emissivity can be easily adjusted. The effective detection range of this system is from -20 to 115 °C, and the field of view is 41°×32°; the measurement error is confined to ±1 °C. The experimental results demonstrate the effectiveness of the system in monitoring the temperature of a remote plane. Hence, it is possible to identify a hot spot that occurred in the electrical heating equipment or a smoldering source hidden in upholstery. [J626]

"High sensitivity photoconductivity based measurement setup for the determination of effective recombination lifetime in silicon wafers"

We describe a high sensitivity measurement setup for the determination of recombination parameters in semiconductors at low levels of carrier injection. The setup is based on a lock-in amplifier and on a commercially available contactless conductivity detector. The information on recombination is extracted through the analysis, assuming quasi-steady-state conditions, of the low frequency, sinusoidally modulated photoconductivity signal induced by the illumination of a 950 nm light emitting diode array. Experimental results show a substantial

increase in sensitivity with respect to traditional transient or quasi-steady-state techniques based on the same detection principle. The sensitivity bonus can be exploited for the extension of the carrier injection range for which effective recombination lifetime is measurable, both in the case of p-type and n-type wafers. [J627]

"GaSb-Based Type I Quantum-Well Light-Emitting Diode Addressable Array Operated at Wavelengths Up to 3.66 μm "

Type I GaSb-based light-emitting diodes (LEDs) have been demonstrated while operating at room temperature at wavelengths up to 3.66 μm with approximately 200 μW of quasi-continuous-wave optical power. A mid-infrared 6 times 6 addressable array of Type I LEDs was also demonstrated. [J628]

"Optical enhancement of room temperature ferromagnetism in Er-doped GaN epilayers"

We report on the enhancement of magnetic properties of Er-doped GaN epilayer structures, grown by metal-organic chemical vapor deposition, with illumination from a light emitting diode. Single and multiple Er-doped epilayers were grown with Er concentrations up to 10^{21}cm^{-3} . All samples exhibited hysteresis behavior at room temperature as measured by an alternating gradient magnetometer. When the samples were illuminated at a wavelength of 371 nm, an increase in saturation magnetization was observed for each sample. The percentage increase for multiple layer samples ranged from 10%-25% indicating possible device applications. [J629]

"Determination of Sit-to-Stand Transfer Duration Using Bed and Floor Pressure Sequences"

The duration of a sit-to-stand (SiSt) transfer is a representative measure of a person's status of physical mobility. This paper measured the duration unobtrusively and automatically using a pressure sensor array under a bed mattress and a floor plate beside the bed. Pressure sequences were extracted from frames of sensor data measuring bed and floor pressure over time. The start time was determined by an algorithm based on the motion of the center of pressure (COP) on the mattress toward the front edge of the bed. The end time was determined by modeling the foot pressure exerted on the floor in the wavelet domain as the step response of a third-order transfer function. As expected, young and old healthy adults generated shorter SiSt durations of around 2.31 and 2.88 s, respectively, whereas post-hip fracture and post-stroke adults produced longer SiSt durations of around 3.32 and 5.00 s. The unobtrusive nature of pressure sensing techniques used in this paper provides valuable information that can be used for the ongoing monitoring of patients within extended-care facilities or within the smart home environment. [J630]

"Technological Aspects of Solid-State and Incandescent Sources for Miner Cap Lamps"

Light-emitting diodes (LEDs) are emerging as viable replacements for incandescent (INC)-based cap lamps used in mining. The photometric and energy characteristics of these light sources differ in important ways. This paper describes the performance of LED and INC sources in cap lamps in terms of correlated color temperature, color rendering, light output, electric power, ambient temperature and air flow, and light source aging. Importantly, these characteristics can influence a miner's ability to spot mining hazards thus impacting safety. Second, some of these characteristics interact with the operating life of the cap lamp's battery power, such that differences between LED and INC sources can be magnified toward the end of a 10-h battery discharge cycle. Empirically, we have determined that after 8 h at an ambient temperature of 25degC, the average light output of an INC cap lamp can decrease to about 69% of its initial value when powered by a lead-acid battery, and it can decrease to about 65% of its initial value when powered by a nickel-hydride battery. An LED-based cap lamp using a constant current drive circuit can maintain about 96% of its initial value when powered by a nickel-hydride battery. Real-world tests addressing the effects of ambient temperature and air flow on the light output of an LED and INC cap lamp were conducted in the National Institute for Occupational Safety and Health Safety Research Coal Mine. The LED cap lamp yielded a vertical average illuminance improvement of approximately 9.5%, and the INC cap lamp yielded a vertical average illuminance degradation of approximately 4%. The differences between LED and INC cap lamps were further quantified by the calculation of Idquomesopic luminancerdquo data that indicated for the same photopic luminance (i.e., as measured using a conventional light meter) the LED cap lamp could be up to 38% more efficient than the INC cap lamp with a lead-acid battery at the end of the 10-h driving cycle. Lastl--y, accelerated life tests were used to empirically determine light output depreciation as the INC light source age approached its useful life. There was about a 35% decrease in light output. This is quite considerable, particularly given that the light output will decrease an additional 30% to 45% over the period of a 10-h shift. The implications of the differences between LED and INC sources are discussed. This information is crucial in determining how visual performance could be affected for real-world conditions where batteries discharge during the work shift and as the light source ages. To date, only idealized conditions have been used for LED and INC cap lamp visual performance research. [J631]

"460-nm InGaN-Based LEDs Grown on Fully Inclined Hemisphere-Shape-Patterned Sapphire Substrate With Submicrometer Spacing"

This letter investigates 460-nm InGaN-based light-emitting diodes (LEDs) grown on a hemisphere-shape-patterned sapphire substrate (HPSS) with submicrometer spacing. The full-width at half-maximum of the (102) plane rocking curves for GaN layer grown on a conventional sapphire substrate (CSS) and HPSS are 480 and 262 arcsec, respectively. Such improvement is due to the reduction of the pure edge threading dislocations. At the forward current of 20 mA, the light output power of the LEDs grown on CSS and HPSS were 4.05 and 5.86 mW, respectively. This improvement of 44% light-output power can be attributed to the improved quality of the material and the increase of the light extraction by the fully inclined facets of the HPSS. [J632]

"Partial Polarization Matching in GaInN-Based Multiple Quantum Well Blue LEDs Using Ternary GaInN Barriers for a Reduced Efficiency Droop"

GaInN-based multiple-quantum-well (MQW) blue LEDs with ternary GaInN barriers polarization-matched to GaInN wells are fabricated. Single-layered Ga_{0.9}In_{0.1}N and Ga_{0.9}In_{0.1}N/GaN multiple-layered quantum barriers (MLQBs) are used for 50% polarization matching. Compared to conventional GaInN/GaN MQW LEDs, the polarization-matched LED with GaInN/GaN MLQBs shows a higher light output power in a high injection current regime, resulting in reduced efficiency droop, along with a minimal blue-shift of emission with injection current, reduced ideality factor, and reduced forward voltage. These results are attributed to a reduced magnitude of polarization sheet charges at heterointerfaces between the GaInN well and the GaInN barrier, and the resultant reduced internal polarization field in the MQWs, thereby minimizing electron leakage current and efficiency droop. [J633]

"Effect of Phosphor Particle Size on Luminous Efficacy of Phosphor-Converted White LED"

In this paper, the influence of YAG:Ce phosphor particle sizes on the lumen output and the conversion efficiency of both in-cup phosphor and top remote phosphor LED packages are investigated with 3-D ray-tracing simulations. The lumen output and the conversion efficiency of both types of phosphor-converted (pc) white LED packages are dependent on the size of YAG:Ce particles. The lumen output and conversion efficiency of both types of pc-white LED packages are minimal at the phosphor particle size with the size parameter of around one and are highest at the particle size in micron size. The simulation results show that both in-cup and top remote phosphor packages have the highest lumen output and the highest conversion efficiency at the particle size of around 20 μm . [J634]

"Midinfrared electroluminescence from pentanary-quaternary heterojunction light-emitting diodes"

InAs-GaInAsSbP-InAsSbP double heterojunction light-emitting diodes were fabricated which exhibit electroluminescence near 3.7 μm at room temperature. Radiative recombination from band-tail states associated with alloy disorder and localized potential fluctuations was observed, as well as emission from states localized at the InAs-pentanary heterointerface. [J635]

"Highly conductive modulation doped composition graded p-AlGaIn/(AlN)/GaN multiheterostructures grown by metalorganic vapor phase epitaxy"

In this study, we present theoretical and experimental results regarding highly conductive modulation doped composition graded p-AlGaIn/(AlN)/GaN multiheterostructures. Based on simulation results, several multiheterostructures were grown by metalorganic vapor phase epitaxy. Using high resolution x-ray diffraction and x-ray reflectometry, the abruptness of the AlGaIn/AlN/GaN interfaces could be determined. Using electron holography, the energetic profile of the valence band could be measured, yielding important information about the vertical carrier transport in such multiheterostructures. The electrical properties of the samples were investigated by measuring the lateral (σ_L) and vertical (σ_V) conductivity, respectively. The free hole concentration of a sample optimized in terms of lateral conductivity was measured to be $1.24 \times 10^{19} \text{ cm}^{-3}$ (295 K) with a mobility of $7 \text{ cm}^2/\text{Vs}$, yielding a record σ_L of $13.7 (\Omega \text{ cm})^{-1}$. Low temperature Hall measurements (77 K) proved the existence of a two-dimensional hole gas at the AlN/GaN interface, as the lateral conductivity could be increased to $30 (\Omega \text{ cm})^{-1}$ and no carrier freeze out was observable. By substituting the p-GaN layer in a light emitting diode (LED) with an AlGaIn/GaN multiheterostructure, the overall voltage drop could be reduced by more than 100 mV ($j=65 \text{ A/cm}^2$). Furthermore improved current spreading on the p-side of LEDs with integrated AlGaIn/AlN/GaN multiheterostructures could be proved by μ -electroluminescence, respectively. [J636]

"Citizen Sensing, Social Signals, and Enriching Human Experience"

In this article, I introduce the exciting paradigm of citizen sensing enabled by mobile sensors and human computing—that is, humans as citizens on the ubiquitous Web, acting as sensors and sharing their observations and views using mobile devices and Web 2.0 services. [J637]

"Sunlight-style color-temperature tunable organic light-emitting diode"

We demonstrate a man-made lighting device of organic light-emitting diode (OLED) capable of yielding a sunlight-style illumination with various daylight chromaticities, whose color temperature ranges between 2300 and 8200 K, fully covering those of the entire daylight at different times and regions. The OLED employs a device architecture capable of simultaneously generating all the emissions required to form a series of daylight chromaticities. The wide color-temperature span may be attributed to that the recombination core therein can easily be shifted along the different emissive zones simply by varying the applied voltage via the use of a thin carrier-modulating layer. [J638]

"Ultraviolet electroluminescence from ZnO/NiO-based heterojunction light-emitting diodes"

Ultraviolet light-emitting diodes based on ZnO/NiO heterojunctions were fabricated on commercially available n+-GaN/sapphire substrates using a radio frequency magnetron sputtering system. Near band edge emission of ZnO peaking at 370nm with a full-width at half maximum of 7nm was achieved at room temperature when the devices were under sufficient forward bias. With the help of an electron blocking i-Mg_{1-x}Zn_xO(0 < x < 1) layer inserted between the ZnO and NiO layers, the emission intensity has been much enhanced and the threshold current drops down to 23 from 70mA. The results were discussed in terms of the band diagrams of the heterojunctions. [J639]

"Advantages of blue InGaN multiple-quantum well light-emitting diodes with InGaN barriers"

The advantages of blue InGaN light-emitting diodes (LEDs) with InGaN barriers are studied. The L-I curves, carrier concentrations in the quantum wells, energy band diagrams, and internal quantum efficiency are investigated. The simulation results show that the InGaN/InGaN LED has better performance over its conventional InGaN/GaN counterpart due to the enhancement of electron confinement, the reduced polarization effect between the barrier and well, and the lower potential barrier height for the holes to transport in the active region. The simulation results also suggest that the efficiency droop is markedly improved when the traditional GaN barriers are replaced by InGaN barriers. [J640]

"Improved output power of GaN-based light-emitting diodes grown on a nanopatterned sapphire substrate"

This letter describes the improved output power of GaN-based light-emitting diodes (LEDs) formed on a nanopatterned sapphire substrate (NPSS) prepared through etching with a self-assembled monolayer of 750-nm-diameter SiO₂ nanospheres used as the mask. The output power of NPSS LEDs was 76% greater than that of LEDs on a flat sapphire substrate. Three-dimensional finite-difference time-domain calculation predicted a 40% enhancement in light extraction efficiency of NPSS LEDs. In addition, the reduction of full widths at half maximum in the omega -scan rocking curves for the (0 0 2) and (1 0 2) planes of GaN on NPSS suggested improved crystal quality. [J641]

"White light generation from Dy³⁺-doped ZnO-B₂O₃-P₂O₅ glasses"

Dysprosium doped ZnO-B₂O₃-P₂O₅ (ZBP) glasses were prepared by a conventional melt quenching technique in order to study the luminescent properties and their utility for white light emitting diodes (LEDs). X-ray diffraction spectra revealed the amorphous nature of the glass sample. The present glasses were characterized by infrared and Raman spectra to evaluate the vibrational features of the samples. The emission and excitation spectra were reported for the ZBP glasses. Strong blue (484 nm) and yellow (574 nm) emission bands were observed upon various excitations. These two emissions correspond to the 4F_{9/2}→6H_{15/2} and 4F_{9/2}→6H_{13/2} transitions of Dy³⁺ ions, respectively. Combination of these blue and yellow bands gives white light to the naked eye. First time, it was found that ZnO-B₂O₃-P₂O₅ glasses efficiently emit white light under 400 and 454 nm excitations, which are nearly match with the emissions of commercial GaN blue LEDs and InGaN LED, respectively. CIE chromaticity coordinates also calculated for Dy³⁺: ZBP glasses to evaluate the white light emission. [J642]

"From Fireflies to Fault-Tolerant Swarms of Robots"

One of the essential benefits of swarm robotic systems is redundancy. In case one robot breaks down, another robot can take steps to repair the failed robot or take over the failed robot's task. Although fault tolerance and robustness to individual failures have often been central arguments in favor of swarm robotic systems, few studies have been dedicated to the subject. In this paper, we take inspiration from the synchronized flashing behavior observed in some species of fireflies. We derive a completely decentralized algorithm to detect non-operational robots in a swarm robotic system. Each robot flashes by lighting up its on-board light-emitting diodes (LEDs), and neighboring robots are driven to flash in synchrony. Since robots that are suffering catastrophic failures do not flash periodically, they can be detected by operational robots. We explore the performance of the proposed algorithm both on a real-world swarm robotic system and in simulation. We show that failed robots are detected correctly and in a timely manner, and we show that a system composed of robots with simulated self-repair capabilities can survive relatively high failure rates. [J643]

"Design and Implementation of RGB LED Drivers for LCD Backlight Modules"

In this paper, a backlight module driver driving high-power red, green, and blue light-emitting diodes (RGB LEDs) for a 19-in liquid crystal display is proposed. The DC-DC series resonant converters (SRCs) with zero-voltage switching and constant-output-current control are implemented to drive the RGB LED arrays. Phase-shifted pulsewidth modulation dimming control is adopted to effectively narrow the load variations and improve the output voltage regulations of the SRCs. A DSP-based hysteresis control algorithm is performed to track the white-color point and the specified backlight luminance. Analysis and design considerations of the proposed drivers are presented in detail. Experimental results agree well with the theoretical predictions and confirm the validity of the proposed approach. [J644]

"Optical Simulation and Fabrication of Nitride-Based LEDs With the Inverted Pyramid Sidewalls"

In this study, the numerical and experimental demonstrations for the enhancement of light-extraction efficiency in nitride-based LEDs with randomly inverted pyramid sidewalls (IPSSs) by chemical etching of the chip edge are presented. With 20 mA injection current, it was found that forward voltages were 3.69 and 3.75 V while output powers were 7.07 and 8.95 mW for the conventional LED and inverted pyramid sidewall LED, respectively. The larger LED output power is attributed to the increased light-extraction efficiency by IPSSs. [J645]

"Effects of disorder in a photonic crystal on the extraction efficiency of a light-emitting diode"

We analyze the effects of disorder in a photonic crystal (PC) on the extraction efficiency of a light-emitting diode (LED) by using a full-vectorial finite-difference time-domain method. The extraction efficiency of the ordered PC LED (EEOPL) and the extraction efficiency of the disordered PC LED (EEDPL) are compared. The physical explanation for the difference between the EEOPL and EEDPL is given through the mechanism of the guided modes and leaky modes. When the frequencies are in the leaky mode region, the EEOPL and EEDPL are comparable even if some disorder exists in the fabrication process. [J646]

"Opening the light extraction cone of high index substrates with plasmonic gratings: Light emitting diode applications"

The opening of the light extraction cone of a high index substrate (GaP) is demonstrated using plasmonic gratings. We show that the excitation of surface plasmons on the metal grating leads to the extraction of light otherwise undergoing total internal reflection in the substrate with high efficiency. This effect has an immediate application in the context of light emitting diodes, where resonant metal gratings are promising for the design of dual purpose electric contact/extraction structures. [J647]

"Monolithic LED Microdisplay on Active Matrix Substrate Using Flip-Chip Technology"

A monolithic high-resolution (individual pixel size 300times300 μm^2) active matrix (AM) programmed 8times8 micro-LED array was fabricated using flip-chip technology. The display was composed of an AM panel and a LED microarray. The AM panel included driving circuits composed of p-type MOS transistors for each pixel. The n-electrodes of the LED pixels in the microarray were connected together, and the p-electrodes were connected to individual outputs of the driving circuits on the AM panel. Using flip-chip technology, the LED microarray was then flipped onto the AM panel to create a microdisplay. [J648]

"Near-IR Optical Upconverter With Integrated Heterojunction Phototransistor and Organic Light-Emitting Diode"

In this letter, we report a near-infrared (NIR) optical upconverter consisting of an integrated InGaAs-InP heterojunction phototransistor (HPT) with an organic light-emitting diode (OLED), which converts 1.5- μm IR

light to visible light with a built-in electrical gain. The device was fabricated through direct tandem integration of an OLED with an inorganic InGaAs-InP HPT. Incoming 1.5- μm optical radiation is absorbed by the HPT, generating an amplified photocurrent. The resultant photocurrent drives the OLED that emits at 545 nm. Upconversion is demonstrated at room temperature with a gain of 15 from the HPT and an overall external upconversion efficiency of 0.15 W/W. [J649]

"Characteristics of a-Plane Green Light-Emitting Diode Grown on r-Plane Sapphire"

In this work, we have successfully grown a-plane green light-emitting diodes (LEDs) on r-plane sapphire and investigated the device characteristics of a-plane green LEDs. The apparent emission polarization anisotropy was observed and the polarization degree was as high as 67.4%. In addition, the electroluminescence (EL) spectra first revealed a wavelength blue-shift with increasing drive current to 20 mA, which could be attributed to the band-filling effect, and then the EL peak become constant. The current-voltage curve showed the forward voltage of a-plane LED grown on r-plane sapphire substrate was 3.43 V and the differential series resistance was measured to be about 24 Ω as 20-mA injected current. Furthermore, the output power was 240 μW at 100-mA drive current. [J650]

"Improved Performance of AlGaInP LEDs by a Periodic GaP-Dish Mirror Array"

A periodic GaP-dish mirror structure was introduced into AlGaInP light-emitting diodes (LEDs) through wet etching and Si wafer bonding process. It was found that the performance of these GaP-dish LEDs was better than that of conventional LED transferred to Si substrate (LED-C). In addition, the output power of GaP-dish LEDs was increased with the decrease of GaP-dish diameter. When the GaP-dish diameter decreased to 3 μm , the output power reached 2.2 mW, which was two times higher than that of LED-C. [J651]

"Improving the lifetime of white polymeric organic light-emitting diodes"

We report on efficient polymeric white organic light-emitting diodes with unprecedented stability. The investigated devices are based on an electroluminescent copolymer of electron and hole-transporting units and red-, green-, and blue-emitting chromophores. We find that the glass transition of the polymer ($T_g=182.5^\circ\text{C}$) is the process determining the relation between thermal annealing during fabrication and device lifetime. For devices annealed below T_g , the device lifetime significantly increases with increasing annealing temperature. For annealing temperatures above T_g , however, the current density in the devices rapidly increases while their lifetime slightly decreases. Insight into the underlying processes is provided by atomic force microscopy phase imaging and by UV/visible and fluorescence spectroscopy. We also investigated the influence of the operating temperature of the device: besides the commonly known fact that elevated operating temperatures reduce the lifetime, we discovered that the acceleration coefficient, which determines the scaling of the device lifetime with applied current density, was reduced. At the glass transition, the device lifetime no longer depended on the current density. The device lifetime was improved even further by introducing an additional cross-linkable hole-transport layer. Optimized devices achieve a half-luminance lifetime of 1860 h when operated at room temperature and at an initial luminance of 500 cd m^{-2} . As a result of the relatively balanced stability of the three chromophores, the emission spectrum remains virtually unchanged over the entire device lifetime. Finally, to reduce the time required for the lifetime measurements, we propose to analyze the voltage increase over the first 10-50 h of the lifetime test and find that this allows precisely estimating the lifetime of our devices. [J652]

"High-Efficiency InGaN/GaN Light Emitters Based on Nanophotonics and Plasmonics"

We report novel methods to enhance light emission efficiencies from InGaN/GaN quantum wells (QWs) based on nanophotonics and plasmonics. First, the nanoscopic optical properties were observed and characterized based on the carrier localization and the quantum confinement Stark effect depending on the In composition of InGaN. Based on the results, we proposed that the emission efficiencies should be improved by making nanostructures, and showed actual enhancement of photoluminescence (PL) intensities by using fabricated random nanodisk and arrayed nanopillar structures. Moreover, surface plasmon (SP) coupling technique was used to enhance blue and green light emissions from InGaN/GaN QWs. We obtained a 14-fold increase in the PL intensity along with a 7-fold increase in the internal quantum efficiency (IQE) of light emission from InGaN/GaN when nanostructured Ag layers were deposited 10 nm above the QWs. The possible enhancement mechanism was discussed and reproduced by using the 3-D finite-difference time-domain simulations. Electron-hole pairs in InGaN QWs couple to electron oscillations at the metal surface and produce SPs instead of photons or phonons. This new path increases the spontaneous emission rate and the IQEs. The SP-emitter coupling technique would lead to superbright and high-speed solid-state light-emitting devices that offer realistic alternatives to conventional fluorescent light sources. [J653]

"Growth of embedded photonic crystals for GaN-based optoelectronic devices"

We present three different techniques to fabricate embedded photonic crystals in GaN-based structures by metal organic chemical vapor deposition, geared toward high efficiency and high directionality light emitting diodes. Compared to the usual lateral epitaxial overgrowth, the novelty lies in the very short grating periods (varying from 180 to 350 nm) and the two-dimensional triangular nature of the grating. Coalescence was obtained over air-gap photonic crystals with thicknesses down to 70 nm, an essential requirement to obtain an efficient interaction between the optical guided modes and the photonic crystals. The quality and surface morphology of the overgrown layers were assessed by transmission electron microscopy and atomic force microscopy measurements. The thin coalesced GaN layer presented a fairly smooth surface (rms roughness of 1.27 nm for a 20420mcm2scan) with no extra defects created by the embedded photonic crystals. [J654]

"Waveform Design Methods for Piezo Inkjet Dispensers Based on Measured Meniscus Motion"

Waveform design methods for piezo inkjet dispensers based on measured meniscus motion are presented. The meniscus motion is measured from charge-coupled-device camera images wherein strobe lights from light-emitting diodes are synchronized with the jetting signal. Waveforms for the piezo dispenser are designed such that the number of experiments can be significantly reduced compared to conventional methods. Furthermore, the designed waveform can also be evaluated by the measured meniscus motion since the motion is directly related to jetting behavior. [J655]

"Optical Design of LCOS Optical Engine and Optimization With Genetic Algorithm"

This paper demonstrates an optical design of miniature of LCOS optical engine and optics with white light-emitting diode (LED) and the most importantly, proposes a new optimization method for non-image optics via Genetic Algorithm (GA) written in Optical Software ASAP, in order to achieve best performance for light efficiency and uniformity. Thanks to the development of modern digital equipment, optimization work for non-image optics plays a role in modern optical engineering. So far Least Damping Square, Taguchi Fuzzy, and simulation annealing methods have been introduced and some of them has been applied to many items of commercial simulation software. However, GA is first introduced in this paper for non-image optical design and optimization, although it has been for many years been used as effective optimization method in image optics; In this paper, GAs are written in the form of macro language from ASAP. During the design process, we used one OPTEK Technology OVS3WBCR44 LED as the light source of the general projection display. Because of the extensiveness of the LEDs, the collection efficiency within the desired acceptance angle was not expected to be high. Due to the particular acceptance angle (cone), we needed a condenser lens system, which satisfied the light small angle incident to 0.59-in liquid-crystal-on-silicon (LCOS) pixels. The optical engine in this paper is designed for a compact LCOS projector with a white LED light source and the employment of an LCOS panel has been reduced to one piece in order to get the best volumetric size. Optical design specification is mainly for an 11"projected screen, whose objective distance is close to 420 mm with fixed focal lens. GA methods are applied in this research in order to achieve maximum brightness and uniformity. Compared to traditional optimization methods, such as Least Damping Square, the GA used in this research gives reasonably good results. [J656]

"Luminance Uniformity of Large-Area OLEDs With an Auxiliary Metal Electrode"

One of the key issues of a large-area organic light-emitting diode (OLED) for flat panel lighting applications is to enhance the uniformity of light emission. In this work, we have investigated the effect of an auxiliary metal (chrome) electrode in association with a device configuration on the luminance uniformity of a large-area (15 times 15 cm²) white OLED. We demonstrate that the ratio between the effective horizontal resistance of anode (indium-tin-oxide (ITO) with the grid patterned metal electrode) and the vertical resistance of the OLED device is the critical factor to determine the luminance uniformity. Moreover, the luminance uniformity is shown to be a function of the current density and degraded with increasing current density. Namely, the OLED panel with the 200- μ m-wide metal lines exhibits the luminance uniformity as high as 90% at 200 mA and 85% at 500 mA. [J657]

"A Simple Method for Comparative Study on the Thermal Performance of LEDs and Fluorescent Lamps"

A simple method is proposed to measure the heat dissipation of LEDs and fluorescent lamps in an open system that allows light energy to escape. Based on this method, a comparative study on the thermal and luminous performance of high-brightness LEDs and fluorescent lamps is presented. At rated power, T5 and T8 fluorescent lamps generate about 73%-77% of their total power as heat, while three types of high-brightness LEDs dissipate about 87%-90% of input power as heat. Heat dissipation is an important factor particularly for air-conditioned

buildings when overall energy efficiency is considered. T5 fluorescent lamps perform better than some existing LEDs in terms of luminous efficacy and heat generation in this study. [J658]

"Blue Light Source Based on a ppKTP SHG Using a Grating-Coupled Laser Diode"

In this letter, we present the first experimental results of a single-pass second-harmonic (SH) generation from a grating-coupled surface-emitting laser (GCSEL) with integrated dual-grating reflector. In pulse operation, the maximum SH peak power was obtained at 0.66 W, yielding a normalized conversion efficiency of $0.6 \times 10^{-3} \text{ W}^{-1}$. A high-level monolithical integration of the GCSEL device led to a compact blue light source, which was based on a frequency-doubled near-IR laser diode. [J659]

"Investigation of Efficiency Droop Behaviors of InGaN/GaN Multiple-Quantum-Well LEDs With Various Well Thicknesses"

Efficiency droop behavior of InGaN/GaN multiple-quantum-well LEDs with various well thicknesses is discussed. It is demonstrated that LED samples with thinner well structures possess higher external quantum efficiencies with stronger droop behaviors. The efficiency droop behavior is contributed by dislocation recombination, Auger recombination in an active region, and carrier overflow out of an active region. Simulation results suggest that at the current density region of 10-100 A/cm², Auger recombination is a dominant mechanism for efficiency droop behavior, while at high current density region of 100-200 A/cm², carrier overflow starts to be the major mechanism for the change of efficiency droop behaviors. [J660]

"Study of electrical characterization of 2-methyl-9, 10-di (2-naphthyl)anthracene doped with tungsten oxide as hole-transport layer"

An efficient p-doped transport layer composed of an ambipolar material, 2-methyl-9,10-di(2-naphthyl)anthracene (MADN) and tungsten oxide (WO₃) has been developed. The admittance spectroscopy studies show that the incorporation of WO₃ into MADN can greatly improve the hole injection and the conductivity of the device. Moreover, when this p-doped layer was incorporated in the tris(8-quinolinolato)aluminum-based device, it achieved a current efficiency of 4.0 cd/A and a power efficiency of 2.4 lm/W at 20 mA/cm². This work paves the way to simplify the fabrication of future p-i-n organic light-emitting devices with a single common ambipolar MADN material. [J661]

"Green/Yellow Solid-State Lighting via Radiative and Nonradiative Energy Transfer Involving Colloidal Semiconductor Nanocrystals"

LEDs made of In_xGa_{1-x}N and (Al_xGa_{1-x})_{1-y}In_yP suffer from significantly reduced quantum efficiency and luminous efficiency in the green/yellow spectral ranges. To address these problems, we present the design, growth, fabrication, hybridization, and characterization of proof-of-concept green/yellow hybrid LEDs that utilize radiative and nonradiative [Förster resonance energy transfer (FRET)] energy transfers in their colloidal semiconductor nanocrystals (NCs) integrated on near-UV LEDs. In our first NC-LED, we realize a color-converted LED that incorporate green-emitting CdSe/ZnS core/shell NCs ($\lambda_{\text{PL}} = 548 \text{ nm}$) on near-UV InGaN/GaN LEDs ($\lambda_{\text{EL}} = 379 \text{ nm}$). In our second NC-LED, we implement a color-converted FRET-enhanced LED. For that, we hybridize a custom-design assembly of cyan- and green-emitting CdSe/ZnS core/shell NCs ($\lambda_{\text{PL}} = 490 \text{ and } 548 \text{ nm}$) on near-UV LEDs. Using a proper mixture of differently sized NCs, we obtain a quantum efficiency enhancement of 9% by recycling trapped excitons via FRET. With FRET-NC-LEDs, we show that it is possible to obtain a luminous efficacy of 425 lm/W opt and a luminous efficiency of 94 lm/W, using near-UV LEDs with a 40% external quantum efficiency. Finally, we investigate FRET-converted light-emitting structures that use nonradiative energy transfer directly from epitaxial quantum wells to colloidal NCs. These proof-of-concept demonstrations show that FRET-based NC-LEDs hold promise for efficient solid-state lighting in green/yellow. [J662]

"Wide-Angle Beam Propagation Method Using Local Reference Indices"

Inspired by the local dimming technology in liquid crystal displays, we propose a modified wide-angle beam propagation formulation with local reference indices for the first time to improve the performance in wide-angle simulation. The reference indices in the proposed formulation are spatially varying in both propagation and transverse directions, instead of a single reference index over the whole computation domain as in commonly used formulation. The proposed formulation is simple and only a minor modification from conventional one, and extra computation effort is relatively small. It can greatly improve the accuracy in modeling for wide-angle cases. [J663]

"Highly balanced ambipolar mobilities with intense electroluminescence in field-effect transistors based on organic single crystal oligo(p-phenylenevinylene) derivatives"

Single crystal organic field-effect transistors (FETs) based on highly luminescent oligo(p-phenylenevinylene) (OPV) derivatives are fabricated. Although OPV single crystal FETs show both p- and n- type FET operation, we found that an increase in the conjugation length of the OPV derivatives from three phenylene rings (P3V2) to four phenylene rings (P4V3) results in an improvement in the electron mobility by an order of magnitude, while retaining the high hole mobility. This molecular design, using P4V3, achieved an ambipolar light-emitting OFET with well-balanced high hole ($0.12 \text{ cm}^2/\text{V s}$) and electron ($0.11 \text{ cm}^2/\text{V s}$) mobilities, leading to intense electroluminescence. [J664]

"Study of polarization properties of light emitted from a -plane InGaN/GaN quantum well-based light emitting diodes"

This paper discusses the optical characteristics of a nonpolar a-plane InGaN/GaN quantum well with different indium compositions, quantum well widths, and injection carrier densities. The self-consistent Poisson and 646k-pSchrodinger solver has been applied to study the band structures in nonpolar a-plane InGaN-based quantum well light emitting diodes (LEDs). We find that the larger indium composition and smaller well width make the energy separation of $|Y\rangle$ -like state to $|Z\rangle$ -like state larger, and as a result enhance the polarization ratio of light. However, the polarization ratio decreases as the carrier injection increases, which might be a drawback for high power applications. We have studied the optimization condition for designing the a-plane InGaN quantum well LED for applications, such as liquid crystal display backlight modules and lasers, which would be useful information for device designs. [J665]

"Top-emission Si-based phosphor organic light emitting diode with Au doped ultrathin n-Si film anode and bottom Al mirror"

We report a highly efficient top-emission Si-based phosphor organic light emitting diode (PhOLED) with an ultrathin polycrystalline n-Si:Au film anode and a bottom Al mirror. This anode is formed by magnetron sputtering followed by Ni induced crystallization and then Au diffusion. By optimizing the thickness of the n-Si:Au film anode, the Au diffusion temperature, and the other parameters of the PhOLED, the highest current and power efficiencies of the n-Si:Au film anode PhOLED reached $85 \pm 9 \text{ cd/A}$ and $80 \pm 8 \text{ lm/W}$, respectively, corresponding to an external quantum efficiency of $21 \pm 2\%$ and a power conversion efficiency of $15 \pm 2\%$, respectively, which are about 60% and 110% higher than those of the indium tin oxide anode counterpart and 70% and 50% higher than those of the bulk n+-Si:Au anode counterpart, respectively. [J666]

"Novel -Activated Glass Ceramics Precipitated With Green and Red Phosphors for High-Power White LED"

We have obtained Eu^{2+} -doped glass-ceramic phosphors, where the two-phosphor crystals of green and red were precipitated by novel GC preparation "frozen sorbet" method and postceraming process. The as-made GC consisted of glass and spherical $\beta\text{-Ca}_2\text{SiO}_4\text{:Eu}^{2+}$ crystal phases with size of about 20-40 μm . After ceramization, $\text{Ca}_3\text{Si}_2\text{O}_7\text{:Eu}^{2+}$ crystals were also precipitated in addition to the $\beta\text{-Ca}_2\text{SiO}_4$ crystal. The photoluminescence had two broad emission bands: at 515 nm from $\text{Eu}^{2+}:\beta\text{-Ca}_2\text{SiO}_4$ and at 600 nm from $\text{Eu}^{2+}:\text{Ca}_3\text{Si}_2\text{O}_7$. Judging from the cathodoluminescence mapping images of microstructure, two emission bands peaked at 515 and 600 nm were observed from different parts in the GC. With increasing heat-treatment temperature, the color coordinates shifted from green range to center region, which corresponds to pure white in the International Commission on Illumination chromaticity diagram. Eu^{2+} -doped calcium silicate GC containing $\beta\text{-Ca}_2\text{SiO}_4$ and $\text{Ca}_3\text{Si}_2\text{O}_7$ are suitable phosphor as the use of phosphor converting white LED with high color rendering. [J667]

"A hybrid control scheme for driving current sources of pm-oled panel"

This paper proposes a new amplitude width modulation (AWM) scheme for PM-OLED (passive matrix organic light emission device) data driver IC. The data driver controls brightness of OLED by adjusting the amplitude and width of the current through OLED. There are two conventional modulation schemes; pulse amplitude modulation (PAM) and pulse width modulation (PWM). The PWM suffers from lower light emitting efficiency at lower luminance levels. The PAM gives us large chip area, due to DACs for each column. The proposed AWM accurately controls the current level using MSB data and increases luminance using LSB data that improves inefficiencies of the PAM and PWM. We fabricated a one channel data driver chip with AWM using a 0.18 μm standard CMOS process. The proposed scheme reduces power consumption 50% compared with PWM. [J668]

"Interfacial electronic structure of a hybrid organic-inorganic optical upconverter device: The role of interface states"

Organic-inorganic hybrid heterojunctions are critical for the integration of organic electronics with traditional Si and III-V semiconductor microelectronics. The amorphous nature of organic semiconductors eliminates the stringent lattice-matching requirements in semiconductor monolithic growth. However, as of yet it is unclear what driving forces dictate the energy-level alignment at hybrid organic-inorganic heterojunctions. Using photoelectron spectroscopy we investigate the energy-level alignment at the hybrid organic-inorganic heterojunction formed between S-passivated InP(100) and several commonly used hole injection/transport molecules, namely, copper phthalocyanine (CuPc), N,N'-diphenyl-N,N'-bis-(1-naphthyl)-1-1'-biphenyl-4,4'-diamine (α -NPD), and fullerene (C60). The energy-level alignment at the hybrid organic-inorganic heterojunction is found to be consistent with traditional interface dipole theory, originally developed to describe Schottky contacts. Contrary to conventional wisdom, hole injection from S-passivated InP(100) into an organic semiconductor is found to originate from interface states at or near the Fermi level, rather than from the valence band maximum of the semiconductor. As a result the barrier height for hole injection is defined by the offset between the surface Fermi level of the S-passivated InP(100) and the highest occupied molecular orbital of the organic. This finding sheds new light on the unusual trend in device performance reported in literature for such hybrid organic-inorganic heterojunction devices. [J669]

"Tailoring the work function of indium tin oxide electrodes in electrophosphorescent organic light-emitting diodes"

We investigate the use of organic surface modifiers based on phosphonic acid anchoring groups that react with the surface of indium tin oxide (ITO) in order to modify its work function, surface energy, and the charge injection in organic multilayer electrophosphorescent devices. The phosphonic acid surface modifiers, possessing different substituting groups, are found to tune the work function of ITO in the range of 4.40-5.40 eV. These surface modifiers have been tested as an interfacial layer between the ITO anode and hole transport layers (HTL) that are either processed from the vapor phase or from solution. The use of this interfacial layer with a solution-processible HTL results in high quantum and luminous efficiencies of 20.6% and 68 cd/A at 100cd/m² (17.5% and 60 cd/A at 1000cd/m²). The enhanced performance of the devices incorporating phosphonic acid modifiers could be associated with an improved charge injection and a better compatibility with the hydrophobic nature of the organic layer. The performance of these devices is also compared to that of devices in which ITO is modified with other well-known techniques such as air plasma treatment or the use of a layer of poly(3,4-ethylenedioxythiophene)/poly(styrenesulfonate). [J670]

"Electronic structures of Ba-on-Alq3 interfaces and device characteristics of organic light-emitting diodes based on these interfaces"

The device performance of organic light-emitting diodes was significantly improved by inserting a Ba coverage (Θ_{Ba}) of 1 nm between tris(8-quinolinolato)aluminum (III) (Alq3) and the cathode. This improvement was attributed to the lowering of the electron-injecting barrier height that was induced by the formation of a new gap state from an interfacial chemical reaction, as well as band bending due to Fermi level pinning. However, the device with Θ_{Ba} above 1 nm showed poor device performance. The spectroscopic results indicated that the Alq3 molecules started to decompose by the reaction between Ba and the phenoxide moiety of the molecule. [J671]

"Optical absorption and emission of fully conjugated heterocyclic aromatic rigid-rod polyelectrolytes containing sulfonated pendants"

Fully conjugated and rodlike poly[(1,7-dihydrobenzo[1,2-d:4,5-d']diimidazole-2,6-diyl)-2-(2-sulfo)-p-phenylene] (sPBI) was synthesized and fabricated for monolayer light emitting diodes showing a threshold voltage of 4.5 V and an emission λ_{max} of 530 nm. Intractable sPBI was derivatized for a fully conjugated water soluble rigid-rod polyelectrolyte sPBI-PS(Li⁺) which was doped with LiCF₃SO₃ or LiN(CF₃SO₂)₂ for optical absorption, electrical conductivity, and luminescent emission. sPBI-PS(Li⁺) light emitting electrochemical cells doped with 0.41 and 1.01 wt % of LiN(CF₃SO₂)₂ showed a threshold voltage of 2.8 V and a tenfold increase in electroluminescence intensity (at λ_{max} = 514 nm) which did not increase with its conductivity. [J672]

"Excitation resolved color conversion of CdSe/ZnS core/shell quantum dot solids for hybrid white light emitting diodes"

In this paper, for their use as nanoluminophors on color-conversion white light emitting diodes (LEDs), we present spectrally resolved relative quantum efficiency and relative color (photon) conversion efficiency of

CdSe/ZnS core/shell nanocrystal (NC) emitters in the solid-state film. We observe that both the averaged relative quantum efficiency and the averaged relative photon conversion efficiency of these NC solids increase with the increasing photon pump energy. Therefore, the excitation LED platform emitting at shorter wavelengths facilitates such NC luminophor solids to be more efficiently pumped optically. Furthermore, we investigate the spectral time-resolved spectroscopy of NCs in solution and in film with 0.4-2.4 nmol integrated number of NCs in the spectral range of 610-660 nm. We observe that the average lifetime of NCs increases toward longer wavelengths as the number of in-film NCs increases. With the increased amount of NCs, the average lifetime increases even further and the emission of NCs is shifted further toward red. This is attributed to the enhanced nonradiative energy transfer between these NCs due to the inhomogeneous size distribution. Thus, in principle, for fine tuning of the collective color of NCs for color-conversion LEDs, it is important to control the energy transfer by changing the integrated number of NCs. [J673]

"Tungsten oxide doped N,N'-di(naphthalen-1-yl)-N,N'-diphenyl-benzidine as hole injection layer for high performance organic light-emitting diodes"

By introducing tungsten oxide (WO₃)doped N,N'-di(naphthalen-1-yl)-N,N'-diphenyl-benzidine (NPB) hole injection layer, the great improvement in device efficiency and the organic film morphology stability at high temperature were realized for organic light-emitting diodes (OLEDs). The detailed investigations on the improvement mechanism by optical, electric, and film morphology properties were presented. The experimental results clearly demonstrated that using WO₃doped NPB as the hole injection layer in NPB/tris (8-quinolinolato) aluminum (Alq₃)-based device, the maximum efficiency reached 6.1cd A⁻¹ and 4.8lm W⁻¹, which were much higher than 4.5cd A⁻¹ and 1.1lm W⁻¹ of NPB/Alq₃ device without hole injection layer. The device with WO₃doped NPB hole injection layer yet gave high efficiency of 6.1cd A⁻¹ (2.9lm W⁻¹) even though the device was fabricated at substrate temperature of 80 °C. These results adequately indicated that WO₃doped NPB was a promising hole injection layer for high efficiency and high stability OLEDs. [J674]

"Ultimate limit and temperature dependency of light-emitting diode efficiency"

We discuss the ultimate limit of performance of semiconductor light-emitting diodes (LEDs) and its dependence on temperature. It is known that in high quality semiconductor materials it is, in principle, possible to reach wall plug efficiencies exceeding unity, which allows electroluminescent cooling in addition of very high efficiency light emission. Our simulation results suggest a few fairly simple measures that may further improve the external quantum efficiency (EQE) of LEDs toward the electroluminescent cooling limit. These include reducing the current density, modifying the LED structure by making thicker active regions and barrier layers, and doping of the active material. Our calculations also indicate that, contrary to the present understanding, operating LEDs at relatively high temperatures of 400-600 K may, in fact, improve the performance. [J675]

"The Li₃PO₄/Al bilayer: An efficient cathode for organic light emitting devices"

In this contribution an efficient cathode material for organic light emitting diodes (OLEDs) is introduced consisting of a thin layer of the metal salt lithium phosphate (Li₃PO₄) deposited between the organic semiconductor and an Al cathode. The bilayer cathode Li₃PO₄/Al enables a device performance of small molecule based OLEDs competitive to the benchmark cathode LiF/Al. While current densities and luminances of both systems are alike, the use of Li₃PO₄ substantially increases the device lifetime. It will be shown that the improved device characteristics can be ascribed to a stably enhanced electron injection. We demonstrate that neither a field enhancement across the Li₃PO₄ layer due to accumulated holes nor a possible charge transfer doping by the Li₃PO₄ is the reason for the improved electron injection. Investigation of the Li₃PO₄/Al interface by Kelvin probe techniques disclosed a work function lowering of the cathode that facilitates electron injection and finally explains the improvement in performance of respective organic light emitting diodes. [J676]

"Coupling light from an organic light emitting diode (OLED) into a single-mode waveguide: Toward monolithically integrated optical sensors"

Evanescent coupling is used to couple light from a polymer light emitting diode (PLED) into a planar single-mode waveguide. The PLED is monolithically integrated on top of the waveguide in a stacked configuration. Due to the waveguide's proximity, the emission zone of the PLED and the waveguide modes overlap substantially, so that the PLED can directly excite the modes. An additional spacer layer between PLED and waveguide is shown to improve the coupling efficiency by about a factor of 5. For iridium-based diodes PLED-to-waveguide coupling efficiencies of as high as 3.2% have been obtained. [J677]

"Ultraviolet-light-emitting AlN:Gd thin-film electroluminescence device using an energy transfer from Gd 3+ ions to N₂ molecules"

An ultraviolet (UV)-light-emitting AlN:Gd thin-film electroluminescence device (TFELD) was demonstrated for application to flat-panel lighting. AlN:Gd thin films were deposited by rf magnetron sputtering at 200 °C and applied to an ac-voltage-driven TFELD with a double-insulating structure as an emission layer. UV-light emission was observed over a threshold voltage of 270 V for a 5 kHz sinusoidal ac voltage. Electroluminescence (EL) spectra were compared with photoluminescence and cathodoluminescence spectra of AlN:Gd originating from Gd³⁺ 6P_j→8S_{7/2} transitions and with an emission spectrum of the second positive system (C₃Pi u→B₃Pi g) of N₂ molecules. As a result, an energy transfer from Gd³⁺ 6P_j→8S_{7/2} to N₂C₃Pi u→B₃Pi g is discussed as a likely mechanism for the UV EL. Finally, a preliminary result, associated with the conversion from UV light into blue-green light via a phosphor, is demonstrated for the color tunability of the TFELD. [J678]

"Studies of the degradation mechanism of organic light-emitting diodes based on tris(8-quinolinolate)aluminum Alq and 2-tert-butyl-9,10-di(2-naphthyl)anthracene TBADN"

Previously, radical cation of tris(8-quinolinolate)aluminum (Alq^{•+}) has been associated with the instability of Alq films subjected to holes-only electrical current. Yet, the questions remain (i) whether Alq^{•+} is the primary source of the intrinsic degradation of bipolar organic light-emitting diodes (OLEDs) based on Alq, (ii) whether Alq^{•+} reactions result in deep charge traps in holes-only devices as found in bipolar counterparts, and (iii) whether radical cations can be a common source of degradation of OLEDs irrespective of materials. With regards to generality of hole-current-related degradation, it is interesting to examine the behavior of 9,10-diarylanthracenes (DAAs)-the practically important class of blue-fluorescing light-emitting-layer hosts. These questions prompted our comparative study of the effects of unipolar currents in Alq and 2-tert-butyl-9,10-di(2-naphthyl)anthracene (TBADN), which was chosen as a representative material of the DAA class. First, we identified device structures allowing for rigorous and stable unipolar conduction. Interestingly, even in pristine holes-only devices, our voltammetric measurements indicated that Alq contains a substantial density of deep hole traps (far deeper than what can be explained by energetic disorder), which can be charged by passing holes-only current and seemingly discharged by exposure to white light. As for aged holes-only Alq devices, they exhibited symptoms qualitatively matching those of aged bipolar Alq devices, viz., photoluminescence (PL) loss, transition voltage (V₀) rise, and drive voltage (V_d) rise. Notably, PL and V₀ are linearly correlated in both holes-only and bipolar devices, which reinforces the supposed link between Alq^{•+} and the degradation in both types of devices. Yet, there are indications the Alq^{•+} instability may not be the only degradation pathway in bipolar devices. Even though our observations for holes-only Alq devices agree qualitatively with previously reported ones, we observe far slower degradation rates [Alq PL fades up to 500 times slower in holes-only devices, while Alq electroluminescence (EL) fades 50 times slower in bipolar control devices]. It is possible that impurities play a significant, perhaps crucial role in the degradation mechanism of both bipolar and holes-only devices, especially the relatively shorter-lived ones. In sharp contrast to Alq, all three observables (PL, V₀, and V_d) indicate that holes-only current in TBADN (neat or doped with a perylene-based blue dopant) does not result in degradation in the time that is sufficient for the corresponding bipolar control devices to lose 60%-80% of EL and 20%-30% of PL. We find that the electrons-only current in Alq or TBADN does not result in degradation either. Thus, the degradation of Alq and DAA bipolar devices may be caused by fundamentally dissimilar mechanisms: while hole current may damage the former, it does not appear to affect the latter, suggesting that the initiation step is different. [J679]

"Shell-dependent electroluminescence from colloidal CdSe quantum dots in multilayer light-emitting diodes"

We report electroluminescence (EL) of colloidal CdSe/CdS, CdSe/ZnS, and CdSe/CdS/CdZnS/ZnS core/shell quantum dots (QDs) in multilayer light-emitting diodes (LEDs) fabricated by spin coating a near monolayer of the core/shell QDs on cross-linkable hole transporting layers. It is found that CdSe/CdS QD-LEDs exhibit a faster decrease in EL quantum efficiency (~2% at a brightness of 100 cd/m²) with increasing current density and lower maximum brightness than those of CdSe/ZnS QD-LEDs. A more significant redshift and spectral broadening of the EL observed in CdSe core/shell QDs with a CdS or CdS/CdZnS/ZnS shell than with a ZnS shell indicate that the electron wave function can penetrate into the shell under electric field. The difference in device performance and EL spectra results from conduction band offsets between the CdSe cores and CdS or ZnS shells, suggesting the existence of the exciton ionization in the QD-LEDs. [J680]

"Colloidal nanocrystal-based light-emitting diodes fabricated on plastic toward flexible quantum dot optoelectronics"

We report the demonstration of mechanically flexible quantum dot light emitting diodes (QD-LEDs) of all three primary colors (red, green, and blue). The QD-LEDs have been fabricated over poly(ethylene-terephthalate) substrates and exhibited high brightness, saturated colors, and pronounced flexibility with a critical bending radius of 5mm. The efficiencies of the flexible QD-LEDs are comparable with the devices fabricated on rigid substrates, suggesting the intrinsic flexibility of quantum dot-based optoelectronic devices. [J681]

"Coalescence overgrowth of GaN nanocolumns on sapphire with patterned metal organic vapor phase epitaxy"

High-quality coalescence overgrowth of patterned-grown GaN nanocolumns on c-plane sapphire substrate with metal organic chemical vapor deposition is demonstrated. Although domain structures of a tens of micron scale in the overgrown layer can be identified with cathodoluminescence measurement, from atomic force microscopy (AFM) measurement, the surface roughness of the overgrown layer in an area of 545mcm² is as small as 0.411 nm, which is only one-half that of the high-quality GaN thin-film template directly grown on sapphire substrate (the control sample). Based on the AFM and depth-dependent x-ray diffraction measurements near the surface of the overgrown layer, the dislocation density is reduced to the order of 10⁷cm⁻², which is one order of magnitude lower than that of the control sample and two to three orders of magnitude lower than those of ordinary GaN templates for fabricating light-emitting diodes. Also, the lateral domain size, reaching a level of 2.7mcm, becomes three times larger than the control sample. Meanwhile, the ratio of photoluminescence intensity at room temperature over that at low temperature of the overgrown sample is at least six times higher than that of the control sample. Although the strain in nanocolumns is almost completely released, a stress of 0.66GPa is rebuilt when the coalescence overgrowth is implemented. [J682]

"Electronic and chemical properties of molybdenum oxide doped hole injection layers in organic light emitting diodes"

The origins of barrier lowering leading to high efficient organic light emitting devices with incorporation of molybdenum oxide (MoO_x) in anode structures are investigated. Ultraviolet and x-ray photoemission spectra reveal that p-type doping effects in the organic films and carrier concentration increase at the anode interfaces cause the hole injection barrier lowering. The gap states, which help carrier injection from the anodes, resulted from the oxygen deficiency in MoO_x due to the interaction of organic materials and MoO_x. [J683]

"Correlation analysis of electrical and optical low frequency fluctuation in organic device degradation"

Low frequency electrical and optical noise fluctuations of organic light emitting diodes were obtained simultaneously. It had been observed that the voltage and optical noises increased gradually with time as the device was subjected to constant current stress. Correlation between the device electrical and optical noise was established. Computation of the correlation coefficients between the voltage and luminescence noises had been devised and implemented. Results suggested that the correlation increased with the noise frequency and this phenomenon was concluded to be the result of some photons going undetected at low frequencies. It was further observed that the correlation was more consistent under low device current when the current efficiency was higher. [J684]

"Enhanced performance of GaN-based light emitting diode with isoelectronic Al doping layer"

The effects of isoelectronic Al doping into epitaxial GaN films grown by metal organic chemical vapor deposition on sapphire substrates were investigated. It was found, based on the measured electron mobility and x-ray analysis, that there is a limiting point of the incorporation of Al into GaN in improving the crystal quality. The electron mobility of the undoped GaN film was 178cm²/V s and the value greatly increased to 524cm²/V s by doping a small amount of Al (up to 0.45% in concentration) into the GaN layer. A further increase in the Al concentration resulted in a degradation of the electron mobility, which decreased to 138cm²/V s when the Al concentration was 0.82%. The output power of a side view light emitting diode (LED) with the Al-doped GaN layer was estimated to be 15.76 mW at a forward current of 20 mA, which improved by 19% compared to that of a conventional LED. These results show that a small amount of Al incorporation into a GaN layer improves the electrical and optical properties of the layer, which are attributed to the reduction of Ga vacancy and associated defects, such as dislocations. [J685]

"High-brightness, high-color-purity, white organic light-emitting diodes featuring multiple emission layers"

We have developed high-brightness, high-color-purity, white organic light-emitting diodes featuring three

emission layers: (i) the green light-emitting material 1,3,5-tris(1-pyrenyl)benzene (TPB3), (ii) the host material 1,4-bis(2,2-diphenylvinyl)biphenyl (DPVBi) doped with the blue dye di(4-fluorophenyl)amino-di(styryl)biphenyl (DSB), and (iii) tris(8-hydroxyquinoline)aluminum (Alq3) doped with the red dye 4-(dicyanomethylene)-2-tert-butyl-6-(1,1,7,7-tetramethyljulolidyl-9-enyl)-4H-pyran (DCJTB). A device having the configuration indium tin oxide (1300E)/N,N'-bis(1-naphthyl)-N,N'-diphenyl-1,1'-biphenyl-4,4'-diamine (500 E)/TPB3 (200 E)/DPVBi: 2wt %DSB (150E)/Alq3: 2wt %DCJTB (150E)/Alq3(350 E)/LiF (8 E)/Al (2000 E) exhibited a white emission with a maximum luminance at 15 V of 55 800cd/m², a maximum current efficiency of 4.06 cd/A at 13 V, a maximum power efficiency of 2.24 lm/W at 5 V, and a maximum external quantum efficiency of 2.45% at 5 V. The Commission Internationale de l'Eclairage coordinates of (0.33, 0.32) changed only slightly upon varying the potential from 9 to 13 V. We attribute the high brightness and color purity of the emitted white light to the high electroluminescence of the hosts and dopants, the relatively high efficiency of the energy transfer from the hosts to the dopants, and the high control over the thicknesses and dopant concentrations of the red-, green-, and blue-emitting layers, resulting in suitable numbers of partial excitons being generated in each of those three layers. [J686]

"Full-solution-processed blue organic light emitting device based on a fluorescent 1,3,5-tristyrylbenzene stilbenoid small molecule"

A full-solution-processed blue organic light emitting diode display based on a small molecule built on a fluorescent stilbenoid core has been fabricated and characterized. The structure of the blue device is ITO/PEDOT:PSS/active layer/Al. The optical characterization of the 1,3,5-tristyrylbenzene endowed with alkoxy (OC₆H₁₃) chain active layer reveals a change in the excited molecular level configuration due to the molecular packing in the thin film that gives as a result a large Stokes shift in the solid state. The electroluminescence in the deep-blue region of the single layer device corresponds well with the photoluminescence emission of the thin films (438nm) and is independent of the applied voltage. Raman analysis confirms the stability of the compound through the fabrication process. From the I-V study, an effective hole mobility of 9.34·10⁻⁶ cm²/Vs for the active layer has been obtained. [J687]

"Defect-related light emission in the 1.4-1.7 μm range from Si layers at room temperature"

High density of crystal defects is formed in Si layers during their growth on the nanostructured surface composed of dense arrays of Ge islands grown on oxidized Si substrates. Although these defect-rich Si layers exhibit intense photoluminescence only at low temperatures, the forward-biased diodes with the Si layers located in the region of the p-i-n junction can emit light at room temperature. The difference suggests that the influence of thermal emission of carriers from defect states on the light emission intensity is essentially reduced when the spatial distribution of carrier density is governed by the bias voltage and band bending. The results show that Si layers emitting light in the 1.4-1.7 μm range at room temperature can be prepared by means of growth. [J688]

"Enhancement of current-voltage characteristics of multilayer organic light emitting diodes by using nanostructured composite films"

With the aim of improving the photonic efficiency of an organic light emitting diode (OLED) and its display duration, both the hole transport layer (HTL) and the emitting layer (EL) were prepared as nanostructured thin films. For the HTL, nanocomposite films were prepared by spin-coating a homogeneous solution of low molecular weight poly(4-styrenesulfonate) (PEDOT-PSS) and surfactant-capped TiO₂ nanocrystals onto low resistivity indium tin oxide (ITO) substrates; for the EL, nanocrystalline titanium oxide (nc-TiO₂)-embedded Poly[2-methoxy-5-(2'-ethyl-hexyloxy)-1,4-phenylene vinylene] (MEH-PPV+nc-TiO₂) conjugate polymers were spin-coated onto the HTL. Also, for a shallow contact of Al/LiF/MEH-PPV instead of Al/MEH-PPV a super LiF thin film was deposited onto the EL by vacuum evaporation. The resulting multilayer OLED had the following structure of Al/LiF/MEH-PPV+nc-TiO₂/PEDOT-PSS+nc-TiO₂/ITO. Characterization of the nanocomposite films showed that both the current-voltage (I-V) characteristics and the photoluminescent properties of the nanocomposite materials were significantly enhanced in comparison with the standard polymers. OLEDs made from these layers would exhibit a large photonic efficiency. [J689]

"Microanalyses of the reverse-bias leakage current increase in the laser lift off GaN-based light emitting diodes"

Microanalyses of the reverse-bias leakage current increase in the laser lift off (LLO) GaN-based light emitting diodes were performed. It was found that the amount of dislocations did not obviously change after LLO process in our experiments. The conductive-atomic force microscopy images and transmission electron microscope (TEM) images results revealed that almost all screw dislocations became to be related with leakage current and the current intensity increased over 100 times after the LLO process; however, only nanopipes corresponded to leakage current in the sample without the laser irradiation. Scanning TEM images indicated microstructure

changes induced by LLO process. Amount of point defects around dislocations might be responsible for the increase in leakage current by providing more levels for tunneling. [J690]

"Light enhancement of Al nanoclusters embedded in Al-doped ZnO films of GaN-based light-emitting diodes"

The aluminum (Al)-doped ZnO (AZO) films embedded with Al nanoclusters were employed to enhance the light output power of III-nitride-based light-emitting diodes (LEDs). The ZnO and Al targets were sputtered using a magnetron cosputtering system. Al nanoclusters embedded in AZO films were found in the AZO films deposited with Al dc power of 10W and ZnO rf power of 100W using high resolution transmission electron microscopy. An increase of 20% in the light output power of the GaN-based LEDs with AZO films embedded with Al nanoclusters can be obtained compared to the conventional LEDs operated at 500mA. [J691]

"Characterization of blue-green m-plane InGaN light emitting diodes"

High indium content blue-green (460-520 nm) m-plane InGaN light emitting diodes (LEDs) were grown on low defect-density m-plane GaN substrates. Systematic studies were performed on packaged blue-green LED lamps by using a range of well and barrier thicknesses. Photoluminance and electroluminescence peak wavelengths increased while the well width was increased from 2 to 4 nm. The highest output power was achieved for well width of 2.5 nm. The output power improved significantly with the increase in barrier thickness. Nearly blueshift-free emission was observed in all LEDs from 1-400A/cm² current density under pulsed operation. [J692]

"Measuring the profile of the emission zone in polymeric organic light-emitting diodes"

The profile of the emission zone (PEZ) in the emissive layer (EML) of polymeric organic light-emitting diodes (OLEDs) is determined by fitting the measured electroluminescence spectrum of the device with a series of simulated spectra that correspond to different emitter locations. The studied OLEDs are based on two different blue-emitting conjugated polymers. In one case, the PEZ is confined to a 10 nm thin sheet at the anode indicating electron dominated current in the EML. In OLEDs based on the other emitter, the PEZ spreads over the entire EML. [J693]

"The Ultra Weak Variational Formulation Applied to Radiation Problems With Macroscopic Sources in Inhomogeneous Domains"

This paper shows the applicability of the ultraweak variational formulation for radiation problems that typically occur during the simulation of active optoelectronic devices. In frequency domain, we investigate the field generated by a macroscopic source (i.e., no point source) embedded in a layered medium with varying refractive index. The analysis focuses on large 2-D simulation domains up to 1000 λ times 1000 λ . A comparison with various reference solutions shows the applicability of the approach. Special focus is put on computational efficiency aspects such as information reduction and parallelization. [J694]

"High efficiency GaN-based light-emitting diodes fabricated on dielectric mask-embedded structures"

We report on the enhanced quantum efficiency of GaN-based light-emitting diodes (LEDs) fabricated on inverted hexagonal pyramid dielectric mask (IHPDM)-embedded structure. The ray-tracing calculation showed that the extraction efficiency of LEDs fabricated on IHPDM-embedded structure could be enhanced up to 56%. Compared to the reference, the n-GaN template grown on IHPDM-embedded structure also showed a reduction in the dislocation density by 57%, leading to an increase in photoluminescence intensity by 82%. The LED fabricated on IHPDM-embedded structure exhibited a reduction in the forward leakage current by one order of magnitude (1.5V) and an enhancement in the output power by 41%. [J695]

"Complete suppression of surface leakage currents in microperforated blue light-emitting diodes"

We investigated the effects of thermal annealing and sulfide passivation on the electrical characteristics of GaN-based light-emitting diodes (LEDs) whose active regions were integrated with a plasma-etched microhole array resembling a photonic crystal structure. Thermal annealing removed most plasma damage in the near-surface bulk region, whereas (NH₄)₂S treatment only passivated the defect states at the immediate surface, each producing a partial recovery of the electrical characteristics. It was found that annealing at 700 °C used in conjunction with prolonged sulfide passivation eliminated all the effects of plasma damage and resulted in a complete suppression of surface leakage in the microperforated LEDs. [J696]

"Flexible full color organic light-emitting diode display on polyimide plastic substrate driven by amorphous indium gallium zinc oxide thin-film transistors"

We have fabricated 6.5 in. flexible full-color top-emission active matrix organic light-emitting diode display on a polyimide (PI) substrate driven amorphous indium gallium zinc oxide thin-film transistors (a-IGZOTFTs). The a-IGZOTFTs exhibited field-effect mobility (μ_{FE}) of $15.1 \text{ cm}^2/\text{V s}$, subthreshold slope of 0.25 V/dec , threshold voltage (V_{TH}) of 0.9 V . The electrical characteristics of TFTs on PI substrate, including a bias-stress instability after 1 h long gate bias at 15 V , were indistinguishable from those on glass substrate and showed high degree of spatial uniformity. TFT samples on 10 nm thick PI substrate withstood bending down to $R=3 \text{ mm}$ under tension and compression without any performance degradation. [J697]

"Near-infrared optical upconverter based on i-In_{0.53}Ga_{0.47}As/C₆₀ photovoltaic heterojunction"

A near-infrared to visible light optical upconverter by the integration of an i-In_{0.53}Ga_{0.47}As/C₆₀ junction and an organic light emitting diode is reported. This device shows the photovoltaic effect of an i-In_{0.53}Ga_{0.47}As/C₆₀ heterojunction and potential application in a pixelless upconversion imaging device. [J698]

"Effect of chip geometry on breakdown voltage of GaInN light-emitting diodes"

Reverse leakage current characteristics of GaInN/GaN multiple quantum well light-emitting diodes (LEDs) with various chip geometries are examined. The effect of chip geometry on the reverse leakage current is negligible at a low voltage, but becomes apparent at a high voltage. The reverse breakdown voltage of LEDs decreases as the angle of vertex in the chip geometry decreases presumably because of a highly localised electric field strength near the vertex. This suggests that a chip geometry with a rounded vertex is suitable for reliable high-power LEDs. [J699]

"Sight and insight-[Jengineering vision]"

Health applications are not the only ideas being investigated for smart contact lenses. Over the past year, technology enthusiasts on the internet have been excitedly blogging about the research of Babak Parviz and colleagues at the University of Washington. These researchers have demonstrated a contact lens that includes an electronic circuit and red light-emitting diodes (LEDs) that are just one-third of a millimetre across. The components are constructed away from the delicate organic materials used for contact lenses and then reconstructed on the lens using self-assembly. [J700]

"Direct evidence for degradation of polaron excited states in organic light emitting diodes"

We investigate the intrinsic degradation mechanisms of the prototypical phosphorescent emissive material fac-tris(2-phenylpyridine) iridium [Ir(ppy)₃] doped into the host 4, 4'-bis(3-methylcarbazol-9-yl)-2,2'-biphenyl (mCBP) by separately evaluating the effects of unipolar current, optical excitation, and their combination. We find that the mCBP anion is unstable and becomes more so in its excited state. Degradation due to the formation of defect states is evident from changes in the capacitance-voltage characteristics and from increasing drive voltage over time of a unipolar test device. These changes are understood within the framework of trapped-charge-limited transport, allowing for the determination of rate constants for each degradation mechanism. We also observe degradation of the hole transport material 4, 4'-bis[N-(1-naphthyl)-N-phenyl-amino]-biphenyl under sub-energy-gap illumination and suggest that this instability may proceed through excitation of its cationic state. These results provide direct evidence for polaron-induced degradation that limits the operational lifetime of organic light emitting diodes. [J701]

"A Driving Scheme for Active-Matrix Organic Light-Emitting Diode Displays Based on Current Feedback"

This paper presents a method of driving active-matrix organic light-emitting diode (AMOLED) displays with amorphous silicon (a-Si) thin-film transistors (TFTs). By using current feedback, the method effectively compensates for the effect of shift in the threshold voltage (V_T) of a-Si TFTs on the OLED current. A CMOS transresistance amplifier is used as the column driver to cancel the effect of large parasitic capacitance of data lines. An accelerating pulse is used at the start of the programming cycle to improve the settling at low currents. A detailed analysis has been done to investigate the effect of circuit components on the sensitivity of the OLED current to V_T shift and the settling behavior of the circuit. Prototypes of pixel circuits and the transresistance amplifier were fabricated in an a-Si TFT process and a $0.8\text{-}\mu\text{m}$ 20-V CMOS technology, respectively. Measurements show less than 5% change in the OLED current for 2.5-V shift in V_T of TFTs. Settling times smaller than 50 μs were achieved for parasitic capacitances of 50-200 pF and programming currents as small as 200 nA. [J702]

"Magnetic field dependent triplet-triplet annihilation in Alq₃-based organic light emitting diodes at different temperatures"

The magnetic field dependent current and electroluminescence (EL) of aluminum tris-(8-hydroxyquinoline) (Alq₃)-based organic light emitting diodes (OLEDs) have been measured at different temperatures. At low temperatures, the magnetic field effects consist of a rapid rising in EL in low field regime followed by a slow falling at high fields and a continuous increase in current for all applied magnetic fields. The high field decrease in the EL is weakened and even vanishes at higher temperatures, which is attributed to the field affected triplet-triplet annihilation process. Other possible mechanisms about the magnetic field effects on electronic processes in OLEDs are also discussed. [J703]

"Effect of N-Type AlGaIn Layer on Carrier Transportation and Efficiency Droop of Blue InGaIn Light-Emitting Diodes"

The effect of an n-type AlGaIn layer on the physical properties of blue InGaIn light-emitting diodes (LEDs) is investigated numerically. The p-type AlGaIn electron-blocking layer is usually used in blue LEDs to reduce the electron leakage current. However, the p-type AlGaIn layer also retards the injection of holes, which leads to the degradation of efficiency at high current. To improve the efficiency droop of blue InGaIn LEDs at high current, an n-type AlGaIn layer below the active region is proposed to replace the traditional p-type AlGaIn layer. The simulation results show that the improvement in efficiency droop is due mainly to the sufficiently reduced electron leakage current and more uniform distribution of holes in the quantum wells. [J704]

"Temperature dependences of photoluminescence and electroluminescence spectra in light-emitting diodes"

The temperature influence on the luminescence characteristics of light-emitting diodes (LEDs) is investigated to reveal the connection of photoluminescence (PL) with photon absorption and electroluminescence (EL) through current injection. By inspecting the PL and EL spectra at identical injection intensities, it has been found that the normalized spectra in PL and EL exhibit obvious similarities in shape and apparent differences in spectral characteristic values. Furthermore, the differences are found to originate from the junction temperatures in diverse injection modes. The observations are conducted on AlGaInP red LED chips. [J705]

"Violet light-emitting diodes grown on crack-free AlGaIn templates"

This study investigates the violet light-emitting diodes (LEDs) grown on crack-free AlGaIn templates, which were prepared on GaN and AlN nucleation layers (NLs) over sapphire substrates by metal-organic chemical-vapor deposition using a two-step growth method. Symmetric and asymmetric x-ray diffraction patterns show that the LED structure grown on the AlGaIn template with a GaN NL exhibits a better crystalline quality as compared to that with an AlN NL. When observed from the analyses of secondary-ion-mass spectroscopy and transmission-electron microscopy, it is found that the thickness and the indium composition in the InGaIn wells of InGaIn/GaNmultiquantum wells are slightly different at the growth temperatures of 720 and 750°C. In addition, the LEDs with GaN NL exhibit a narrower full width at half maximum of the excitonic peaks than those with AlN NL. [J706]

"A Single-Chip CMOS Smoke and Temperature Sensor for an Intelligent Fire Detector"

A single-chip CMOS smoke and temperature sensor for use as an intelligent fire detector is proposed. The proposed smoke sensor measures smoke density based on the light-scattering method. The temperature sensor is integrated with the smoke sensor not only to sense heat from a fire but also to compensate for the temperature dependency of the smoke sensor. The prototype chip includes an on-chip photodiode (PD), pixel circuit, correlated double sampling (CDS) circuit, and analog-to-digital converter (ADC). The prototype chip was fabricated using a 0.35- μ m CMOS process and was placed inside the smoke detection chamber, while the thermistor for the temperature sensor is placed outside the chamber. The measurement results show plusmn 1% smoke detection accuracy over the range 4% ~ 25% and plusmn1degC temperature-sensing accuracy over the range 25degC ~ 95degC. The power consumption of the prototype chip is 220 nW, excluding the infrared light-emitting diode (IR LED). [J707]

"Interface properties of a Li₃PO₄/Al cathode in organic light emitting diodes"

Recently Li₃PO₄/Al has been introduced as an alternative cathode for the commonly used LiF/Al system for organic light emitting diodes (OLEDs) due to its competitive electron injection properties. In the present article the interfaces of the organic semiconductor with the Li₃PO₄/Al bilayer cathode are investigated using photoelectron

spectroscopy to elucidate the origin behind the efficient electron injection. Therefore, a thick Li₃PO₄ layer was vacuum deposited onto an indium tin oxide substrate and characterized in order to learn about the stoichiometry of evaporated Li₃PO₄. During evaporation Li₃PO₄ decomposes, forming a layer consisting of P₂O₅ and LiPO₃. In a second step the interface between Li₃PO₄ and Alq₃[tris(8-hydroxyquinoline) aluminum] was investigated, whereupon Li₃PO₄ coverage Alq₃ molecules decompose, forming aluminum oxide or aluminum phosphate leaving 8-quinolinol molecules behind. A similar reaction occurs at the Li₃PO₄/Al interface where again an oxidation of the metallic aluminum points toward the formation of aluminum oxide or phosphate. A work function lowering of up to 180 meV observed once Al was covered by Li₃PO₄ is likely to be caused by the polar nature of all generated or deposited species. A simple estimate of the surface potential drop caused by those dipoles can account for the work function lowering and explain the highly efficient electron injection property of the Li₃PO₄/Al cathode in an OLED. [J708]

"GaN-Based LEDs With Mesh ITO p-Contact and Nanopillars"

In this letter, the authors report the fabrication of GaN-based light-emitting diodes (LEDs) with mesh indium-tin-oxide p-contact and nanopillars on patterned sapphire substrate. Using hydrothermal ZnO nanorods as the etching hard mask, the authors successfully formed vertical GaN nanopillars inside the mesh regions and on the mesa-etched regions. It was found that 20-mA forward voltage and reverse leakage currents observed from the proposed LED were only slightly larger than those observed from the conventional LEDs. It was also found that output power of the proposed LED was more than 80% larger than that observed from conventional LED prepared on flat sapphire substrate. [J709]

"Para-sexiphenyl-CdSe/ZnS nanocrystal hybrid light emitting diodes"

CdSe/ZnS core/shell nanocrystals (NCs) are integrated into para-sexiphenyl (p-6P) based hybrid light emitting diodes, to obtain green and red emission in addition to blue emission originated from p-6P. For the active region of the devices, ultrathin layers of p-6P and NCs are deposited by hot wall epitaxy and spin casting, respectively, resulting in current-voltage characteristics with small leakage currents and low onset voltages. The achieved electroluminescence exhibits narrow emission line widths and thus high color purity, as required for color display applications. [J710]

"Organic light-emitting diodes using 3,6-difluoro-2,5,7,7,8,8-hexacyanoquinodimethane as p-type dopant"

We demonstrate that 3,6-difluoro-2,5,7,7,8,8-hexacyanoquinodimethane (F₂-HCNQ) can serve as an excellent electrical doping material for hole transport materials with the highest occupied molecular orbital level as high as 5.4 eV, such as N,N'-di(naphthalene-1-yl)-N,N'-diphenyl-benzidine (NPB). With its relatively strong electron-accepting ability and high thermal stability, F₂-HCNQ doped NPB organic light-emitting diode (OLED) showed improved power efficiency with low driving voltage. The tris(8-hydroxyquinoline)aluminum based OLED with F₂-HCNQ doped NPB layer and Cs₂O doped bathophenanthroline electron transport layer exhibits power efficiency of 3.6 lm/W with driving voltage of 3.2 V at 100 cd/m². [J711]

"Improved performance of polymer light-emitting diodes with nanocomposites"

The characteristics of a hybrid polymer light-emitting diode (HPLED) with an active layer of poly [2-methoxy,5-(2-ethylhexoxy)-1,4-phenylenevinylene] blended with Au-capped TiO₂ nanocomposites are reported. Both the increased current in the active layer and low turn-on voltage were attributed to incorporation of Au-capped TiO₂ in the electroluminescent polymer. The maximal brightness of 11 630 cd/m² was observed in HPLED with a 1:1 ratio of Au-capped TiO₂. The enhanced performance was attributed to the roughness assisted charge transport induced by the Au-capped TiO₂ nanocomposites in the active polymer. [J712]

"Color-variable highly efficient organic electrophosphorescent diodes manipulating molecular exciton and excimer emissions"

A simple way of tuning the emission color and electroluminescence efficiency from vacuum-deposited emitters of phosphorescent organic light emitting diodes (LEDs) is demonstrated. For each color a single-emissive layer consisting of a blend of two materials, one of Pt(N C N) complex series [where (N C N)=di(2-pyridinyl)benzene-based tridentate ligands] as either the low-concentration bluish green (molecular) phosphorescence emitter or high-concentration red (excimer) phosphorescence emitter, and (4,4',4''-tris(N-carbazolyl)-triphenylamine) as the host was employed. By adjusting the relative amount of blue and red emissive species, the color of the light emission was tuned from bluish green through green and white up to red. Very high external quantum efficiency (up to 18.3±0.5%) and current efficiency (up to 44.8±0.5 cd/A) at

500cd/m² four-layer devices were achieved with white and greenish light emitting layers, respectively. It is found that the introduction of electron-withdrawing fluorine atoms at the central ring and electron-donating groups at the lateral rings of the Pt complex leads to a blueshift in the molecular and excimer emissions, respectively. This allows to refine colors and optimize the efficiency of the LEDs by selecting suitable substituents. [J713]

"Optimized efficiency and angular emission characteristics of white top-emitting organic electroluminescent diodes"

The concept of an additional capping layer, which is deposited onto the semitransparent top contact, is applied to minimize microcavity effects for white light emission from top-emitting organic light emitting devices (OLEDs). The influence on the optical properties of such devices with silver as top electrode material is discussed using an analytical method and numerical simulations. The results of the theoretical findings are experimentally verified for inverted top emitting devices on opaque substrates, showing broad spectral bandwidth and angle-independent color coordinates. [J714]

"High efficiency electroluminescence devices using a series of Ir(III)-tetrazolate phosphors: Mechanisms for the drive current evolution of quantum yield"

We demonstrate high-brightness and high-efficiency blue-green to yellow-green electrophosphorescent organic light-emitting diodes employing a series of organic Ir complexes [Ir-(C_N)₂(N_N)]. Three different complexes have been synthesized showing high photoluminescence solid blend efficiencies up to 44%. A low current density increase of the electroluminescence (EL) external quantum efficiency ($\phi_{EL(EXT)}$) is observed and a maximum of $\phi_{EL(EXT)} = 10.6\% \pm 0.8\%$ photon/e and power efficiency $\eta = 27 \pm 2$ lm/W are achieved at a current density of $j = 0.01$ mA/cm². We examine various electronic processes that underlie a nonmonotonous current density dependence of the EL quantum efficiency of electrophosphorescent light-emitting diodes. The shape of $\phi_{EL(EXT)}$ versus j is shown to reflect a trade off between electron-hole encounter and charge carrier transit times, electric field effect on electron-hole pair dissociation time, and current driven triplet molecular exciton lifetime. [J715]

"The origin of the high diode-ideality factors in GaInN/GaN multiple quantum well light-emitting diodes"

We report on a significant decrease in the diode-ideality factor of GaInN/GaN multiple quantum well light-emitting diodes (LEDs), from 5.5 to 2.4, as Si-doping is applied to an increasing number of quantum barriers (QBs). The minimum ideality factor of 2.4 is obtained when all QBs are doped. It is shown that polarization-induced triangular band profiles of the undoped QBs are the major cause of the high ideality factors in GaInN/GaN LEDs. Numerical simulations show excellent agreement with the measured ideality factor value and its dependence on QB doping. [J716]

"On resonant optical excitation and carrier escape in GaInN/GaN quantum wells"

Recently, photoluminescence studies using resonant optical excitation in GaInN layers have been used to investigate the physical origin of efficiency droop in GaInN/GaN light-emitting diodes. In these studies, it has been assumed that in the case of resonant excitation, where electron-hole pairs are generated in the GaInN layers only, carrier transport effects play no role. We report that in contrast to this assumption, carrier escape from quantum wells does take place and shows strong dependence upon the duration of excitation and bias conditions. We also discuss the time scales required to reach steady-state conditions under pulsed optical excitation. [J717]

"Inkjet printing of light emitting quantum dots"

We demonstrate the fabrication of diodes having inkjet printed light emitting quantum dots layer. Close packing of printed layer is shown to be influenced by surface morphology of the underlying polymer layer and size variance of quantum dots used. We extend our approach to printing quantum dots onto a quarter video graphics array substrate (76 800 monochrome pixels). The purity of emitted electroluminescent spectra of resulting devices is related to coverage integrity of printed layer, which in turn is shown to be affected by the number of printed drops per pixel. [J718]

"Evaluation of GaN substrates grown in supercritical basic ammonia"

GaN crystals grown by the basic ammonothermal method were investigated for their use as substrates for device regrowth. X-ray diffraction analysis indicated that the substrates contained multiple grains while secondary ion

mass spectroscopy (SIMS) revealed a high concentration of hydrogen, oxygen, and sodium. Despite these drawbacks, the emission from the light emitting diode structures grown by metal organic chemical vapor deposition on both the c-plane and m-plane epitaxial wafers was demonstrated. The SIMS depth profiles showed that the diffusion of the alkali metal from the substrate into the epitaxial film was small, especially in the m-direction. [J719]

"Measurement of electron overflow in 450 nm InGaN light-emitting diode structures"

Test structures were developed to experimentally measure the presence of electron overflow in light-emitting diodes (LEDs) under typical bias conditions. These test structures are comprised of a standard LED structure with an extra Mg-doped quantum well inserted on the p-type side of the electron blocking layer. Electrons escaping the active region recombine in the extra quantum well and the corresponding photon emission is observed. No electron overflow was observed at low current densities. At intermediate current densities where efficiency droop occurs, overflow was observed and increased with increasing current density. The onset of electron overflow occurred at slightly lower current densities than the onset of efficiency droop. Auger-assisted overflow, a by-product of the Auger process, is considered in addition to traditional overflow mechanisms. [J720]

"Laser desorption/ionization time-of-flight mass spectrometry: A predictive tool for the lifetime of organic light emitting devices"

For improving the lifetime of organic light emitting devices (OLEDs), the analysis of the chemical degradation requires a deep understanding of the involved reaction pathways. We show that the dissociation reactions of phosphorescent emitters and the additional complexations with the used surrounding blocking layers are the dominant intrinsic degradation mechanisms in long living p-i-n-type OLEDs. We use the laser desorption/ionization (LDI) time-of-flight mass spectrometry to correlate the laser-induced ion formation with the observed lifetime of the organic devices. The superlinear correlation between the LDI forced reactions and the lifetimes allows the prediction of the lifetime of an OLED with new materials. [J721]

"Broadband and omnidirectional antireflection from conductive indium-tin-oxide nanocolumns prepared by glancing-angle deposition with nitrogen"

Characteristic formation of highly oriented indium-tin-oxide (ITO) nanocolumns is demonstrated using electron-beam evaporation with an obliquely incident nitrogen flux. The nanocolumn material exhibits broadband and omnidirectional antireflective characteristics up to an incidence angle of 70° for the 350-900 nm wavelength range for both s- and p-polarizations. Calculations based on a rigorous coupled-wave analysis indicate that the superior antireflection arises from the tapered column profiles which collectively function as a gradient-index layer. Since the nanocolumns have a preferential growth direction which follows the incident vapor flux, the azimuthal and polarization dependence of reflectivities are also investigated. The single ITO nanocolumn layer can function as antireflection contacts for light emitting diodes and solar cells. [J722]

"Room temperature GaAs exciton-polariton light emitting diode"

Room temperature GaAs polariton emission is demonstrated under electrical injection. Temperature and angle-resolved electroluminescence measurements on a polariton light emitting diode clearly show the persistence of Rabi splitting and anticrossing behavior at temperatures as high as 315 K. We show that by increasing the number of quantum wells in the structure, the cutoff temperature for the strong coupling regime can be pushed beyond room temperature, in good agreement with theory. Our results suggest that optimally designed GaAs microcavities are perfectly suited for room temperature polaritronics. [J723]

"Enhanced light extraction efficiency of GaN-based light-emitting diodes with ZnO nanorod arrays grown using aqueous solution"

We report a dramatic increase in the light extraction efficiency of GaN-based blue light-emitting diodes (LEDs) by ZnO nanorod arrays on a planar indium tin oxide (ITO) transparent electrode. ZnO nanorods were grown into aqueous solution at the low temperature of 90 °C. With 20 mA current injection, the light output efficiency of the LED with ZnO nanorod arrays on ITO was increased by about 57% with no increase in a forward voltage over the conventional LEDs with planar ITO. The increased light extraction by the ZnO nanorod arrays is due to the formation of sidewalls and a rough surface, resulting in a multiple photon scattering at the LED surface. [J724]

"AlN/AlGaIn short-period superlattice sacrificial layers in laser lift-off for vertical-type AlGaIn-based deep ultraviolet light emitting diodes"

Large-area (1 cm^2) laser lift-off (LLO) wafer separation of $\text{Al}_{0.45}\text{Ga}_{0.55}\text{N}$ layers from AlN /sapphire templates has been demonstrated by using 200-period $\text{AlN}/\text{Al}_{0.22}\text{Ga}_{0.78}\text{N}$ short-period superlattice (SPSL) sacrificial layers instead of conventional GaN photoabsorbing layers. The SPSL functions as the photoabsorbing and mechanically weakened layer in the LLO process. This SPSL-assisted LLO technique promises future progress of vertical-type deep ultraviolet light emitting diodes and freestanding AlN - AlGaIn bulk substrates. [J725]

"Very low voltage and stable p-i-n organic light-emitting diodes using a linear S,S-dioxide oligothiophene as emitting layer"

Very low voltage organic light-emitting diodes using a fluorescent linear S,S-dioxide oligothiophene as emitting layer has been realized using a p-i-n structure. The device reaches a remarkable luminance of $10\,000\text{ cd/m}^2$ at only 9 V, which is two orders of magnitude higher than the simple bilayer structure already reported for this active material. Due to the doping of the transport layers, a maximum power efficiency of 2.1 lm/W was reached against 0.2 lm/W of the corresponding undoped device. As a consequence of this higher power efficiency, the reduced self-heating of the p-i-n device structure, compared to the undoped devices, determines the best operating condition to check the intrinsic stability of the emitting layer. Aging measurements reveal indeed a very high stability, with extrapolated device lifetimes at about 108 and 2200 h at starting luminances of 100 and 3200 cd/m^2 , respectively. [J726]

"Wafer-Level Packaged Light-Emitting Diodes Using Photodielectric Resin"

A large area ($1600\text{ }\mu\text{m}$ times $800\text{ }\mu\text{m}$) high-brightness light-emitting diode (HB LED) employing rearranged metal pads and multipassivation layers is presented. To enlarge the active layer with a smaller mesa area and improve package productivity using large bonding pads, two electrodes were used to fabricate the LED; a primary electrode was in contact with the n, p-GaN as a conventional LED, and the second electrode was connected to the primary electrode with a passivation layer having photodielectric resin interposed between them. The LED was directly bonded to the metal-core printed circuit board without wire bonding or epoxy molding. The resultant HB LED has a low forward voltage ($\sim 3.2\text{ V}$ at 350 mA) due to the optimized n, p-contact scheme, and an optical power of 75 mW with no encapsulation. [J727]

"Some bright spots in the gloom"

The technology industry is suffering mightily from the global economic crisis. Worldwide semiconductor revenue is expected to drop 24.1 percent in 2009, to US \$194.5 billion, according to Gartner, a technology research firm in Stamford, Conn. Meanwhile, revenue from enterprise software—that is, corporate-scale systems—will be flat at about \$222 billion. Still, there are some sectors that will gain, some bright spots in the gloom. [J728]

"Modulated Infrared Electroluminescence From Organic Light-Emitting Diodes"

Modulated infrared electroluminescence from organic light-emitting diodes (OLEDs) based on rare earth complexes (tris-dibenzoylmethanato-mono-bathophenanthroline) erbium or neodymium were fabricated. The modulations were realized by varying the device configuration and by varying an applied forward bias at room temperature. We found that the intensity of EL peak at $1.54\text{ }\mu\text{m}$ was reduced by a factor of almost 20 times as the Nd complex layer thickness in the OLEDs was increased from 1 nm to 5 nm. The intensity ratio of the $1.54\text{ }\mu\text{m}$ (Nd) to $1.06\text{ }\mu\text{m}$ (Er) decreases from 0.82 to 0.53 as the forward bias increases from 6.5 V to 18 V. The effects of the modulation of these IR emissions were also discussed. [J729]

"Transabdominal Fetal Heart Rate Detection Using NIR Photoplethysmography: Instrumentation and Clinical Results"

In obstetrics, fetal heart rate (FHR) detection remains the standard for intrapartum assessment of fetal well-being. In this paper, a low-power ($<55\text{ mW}$) optical technique is proposed for transabdominal FHR detection using near-infrared photoplethysmography (PPG). A beam of IR-LED (890 nm) propagates through to the maternal abdomen and fetal tissues, resulting in a mixed signal detected by a low-noise detector situated at a distance of 4 cm. Low-noise amplification and 24-bit analog-to-digital converter resolution ensure minimum effect of quantization noise. After synchronous detection, the mixed signal is processed by an adaptive filter to extract the fetal signal, whereas the PPG from the mother's index finger is the reference input. A total of 24 datasets were acquired from six subjects at 37 plusmn 2 gestational weeks. Results show a correlation coefficient of 0.96 ($p\text{-value} < 0.001$) between the proposed optical and ultrasound FHR, with a maximum error of 4%. Assessment of the effect of probe position on detection accuracy indicates that the probe should be close to fetal tissues, but not necessarily restricted to head or buttocks. [J730]

"Blue Flexible Transparent Organic Light-Emitting Devices"

Blue transparent organic light-emitting devices (TOLEDs) and blue flexible OLEDs (FOLEDs) have been fabricated on glass and plastic films, respectively. We have also fabricated blue flexible transparent OLEDs (FTOLEDs) having both flexibility and transparency by using indium-tin-oxide:cesium (ITO:Cs) as a cathode. A Cs-incorporated ITO electrode is useful for the fabrication of not only a TOLED on a glass substrate but also a flexible TOLED on a plastic film. [J731]

"High-Performance InGaN-Based Green Resonant-Cavity Light-Emitting Diodes for Plastic Optical Fiber Applications"

High-performance InGaN-based green resonant-cavity light-emitting diodes (RCLEDs) with a plating Cu substrate for plastic optical fiber communication applications are reported. Good stability of emission wavelength was obtained at 0.016 nm/mA. The RCLEDs presents low temperature dependence, showing only a 3% drop in light output power as the temperature increasing from 25 to 85degC. The superior performance can be attributed to the decreased dynamic series resistance and the enhanced thermal dissipation of the heat sink substrate. [J732]

"Robotic baby seal could diminish dementia"

It's soft, it's cute, it's cuddly, and it's powered by two 32-bit reduced-instruction-set-computer microprocessors. Paro may look like a toy, but it's quickly attracting the serious attention of rehabilitation researchers. [J733]

"Guest Editorial"

The 13 papers in this special issue highlight some of the recent developments in flexible electronics technology, covering flexible displays, thin-film transistors (TFTs), organic light-emitting diodes (OLEDs), sensors. etc. Most of the papers in this issue were presented at the 2007 International Symposium for Flexible Electronics and Displays (ISFED-2007). [J734]

"Electrical Properties of Trilayer Organic Light-Emitting Diodes With a Mixed Emitting Layer"

We investigate the electrical properties of three different trilayer organic light-emitting diodes (OLEDs), one of which is based on a conventional layered structure and the others on a blended structure where an emitting layer (EML) is uniformly or stepwise mixed with an electron transport layer (ETL), Tris-(8-hydroxyquinoline) aluminum (Alq3). By way of simulations, we visualize the electrical behaviors that provide a clear understanding on why the uniformly mixed structure enhances further the longevity of OLEDs, compared to the other configurations. Namely, the uniformly mixed structure has the lowest concentration of positive charges in the ETL (thereby reducing oxidative degradation of Alq3) and weakest electric field (decreasing the probability of Joule heating), followed by the stepwise mixed one and then the layered one. However, such blended structures show lower recombination efficiency due to the delocalization of carriers (recombination), which has been demonstrated by simulations of the current balance. [J735]

"Color control of multilayer stacked white polymer light-emitting diodes using a quantum dot as an interlayer"

Color tunable multilayer stacked white polymer light-emitting diodes (WPLEDs) have been developed using a quantum dot as an interlayer. Multilayer WPLEDs were fabricated by a stamp transfer printing method and the charge transport of WPLEDs could be controlled by the quantum dot interlayer. The use of the quantum dot as the interlayer shifted the color coordinate of blue/yellow stacked WPLEDs from (0.34, 0.41) to (0.41, 0.48). The electron trapping effect of the quantum dot was responsible for the color shift in the multilayer stacked WPLEDs. [J736]

"Correlation of lifetime and recombination zone in green phosphorescent organic light-emitting diodes"

The lifetime of green phosphorescent organic light-emitting diodes was correlated with the charge leakage and recombination zone of the devices. The lifetime of green devices was decreased in the device with an electron leakage out of an emitting layer into a hole transport layer. In particular, the decrease in lifetime at high luminance was significant in the device with an electron leakage into the hole transport layer. In addition, the recombination zone of green devices was shifted from the hole transport layer side to the electron transport layer side during driving. [J737]

"Low temperature magnetic field effects in Alq 3 -based organic light emitting diodes"

The magnetic field effects on injection current and electroluminescence have been investigated for aluminum tris(8-hydroxyquinoline) (Alq3)-based organic light emitting diodes at the temperature of 12 K. The experimental traces of electroluminescence exhibit a rapid rising at low magnetic field, followed by a decrease at high field strength, whereas the injection current increases continuously. The drive dependence of the high field effect of the quantum efficiency matches that which is expected for the triplet-triplet annihilation process, indicating that the delayed fluorescence from the triplets' annihilation significantly contributes to the field dependent light emission in our devices. [J738]

"Sr 3 Al 2 O 5 Cl 2 :Ce 3+ ,Eu 2+ : A potential tunable yellow-to-white-emitting phosphor for ultraviolet light emitting diodes"

The Sr₃Al₂O₅Cl₂:Ce³⁺,Eu²⁺ phosphors were prepared by solid state reaction. The obtained phosphors exhibit a strong absorption in the UV-visible region and have two intense emission bands at 444 and 609 nm. The energy transfer from the Ce³⁺ to Eu²⁺ ions was observed, and the critical distance has been estimated to be about 24.5 Å by spectral overlap method. Furthermore, the developed phosphors can generate lights from yellow-to-white region under the excitation of UV radiation by appropriately tuning the activator content, indicating that they have potential applications as an UV-convertible phosphor for white light emitting diodes. [J739]

"Enhancement of Light Extraction From Resonant Cavity Light-Emitting Diodes Using a 2-D Grating Embossed in TiO Sol-Gel"

To enhance the light extraction efficiency of a resonant cavity light-emitting diode (RCLED), a soft embossing technique was developed to fabricate a 2-D grating on the RCLED output surface. The optimal 2-D grating parameter was designed by a rigorous coupled wave analysis code. By embossing the 2-D grating on the output of a commercial RCLED, a 49% light extraction enhancement was achieved using a novel high refractive index (n= 2) TiO₂sol-gel and a 24% enhancement using a UV curable polymer with lower refractive index (n= 1.56). The overall emission pattern was also modified making the patterned RCLED potentially easier to couple into a fiber. [J740]

"Design of an RGB LED Backlight Circuit for Liquid Crystal Display Panels"

This paper presents a red, green, and blue (RGB) light-emitting diode (LED) backlight circuit for liquid crystal display (LCD) panels. Some studies have been conducted to devise dimming methods that regulate the RGB LED currents. In this paper, design considerations for the RGB LED backlight are presented. A laboratory prototype for 20-in panels is implemented and tested. The color gamut of an LCD panel with the designed RGB LED backlight is measured and discussed. The experimental results of the laboratory prototype are also shown to verify feasibility of the findings. [J741]

"Near-infrared photon upconversion devices based on GaNAsSb active layer lattice matched to GaAs"

Room-temperature full GaAs-based near-infrared (NIR) upconversion has been demonstrated by connecting lattice-matched GaNAsSb/GaAs p-i-n photodetectors in series with commercial GaAs/AlGaAs light-emitting diodes (LEDs). Due to the avalanche gain in GaNAsSb/GaAs photodetectors and high internal efficiency in GaAs/AlGaAs LEDs, the upconversion efficiency of the integrated system reaches 0.048 W/W under -7 V bias, much higher than any existing NIR upconverters without amplifying structures. We have further investigated the dependence of the upconversion efficiency on applied bias and incident light intensity. The present work establishes an experimental base for direct epitaxial growth of full GaAs-based NIR upconverters with high upconversion efficiencies. [J742]

"Blue to deep UV light emission from a p-Si /AlN /Au heterostructure"

Undoped AlN thin film has been grown on p-Si(111) by metal-organic chemical-vapor deposition. The p-Si/AlN/Au heterostructured light-emitting diode was further fabricated and investigated. The current-voltage characteristic showed a typical back-to-back diode behavior, which is responsible for the electroluminescence at both forward and reverse bias. A deep UV emission at 283 nm as well as a UV emission at 380 nm was observed from the forward biased p-Si/AlN/Au diode, while a blue emission at 490 nm was detected from the diode under reverse bias. The recombination mechanism for each emission band was discussed based on the energy band diagram. [J743]

"Control performance of a single-chip white light emitting diode by adjusting strain in InGaN underlying layer"

Light emission from green to white in a single-chip light emitting diode is modulated by adjusting the strain in InGaN underlying layer (UL) embedded below an active layer of InGaN/GaN multiple quantum wells. Transmission electron microscopy combined with x-ray reciprocal space mapping reveals that indium phase separation in InGaN quantum well active layer is enhanced by using a partly relaxed InGaN UL and In-rich quantum dots with different size and indium composition are formed. They emit multicolor lights whose mixing produces white light. Quality of the white light could be controlled by modulation on relaxation degree of the InGaN UL. [J744]

"Efficient bilayer phosphorescent organic light-emitting diodes: Direct hole injection into triplet dopants"

In phosphorescent organic light-emitting diodes (OLEDs), a hole transporting layer is traditionally thought to be required to facilitate hole injection into the host molecule. It is found that fac-tris(2-phenylpyridine)iridium [Ir(ppy)₃] doped into 4,4'-N,N'-dicarbazole-biphenyl can be used to directly inject and transport holes from an indium tin oxide anode, and thus simplify the device structure and selection of materials. The efficiencies of the simplified bilayer OLEDs exceed 41 lm/W and 57 cd/A at a brightness of 100cd/m². We attribute the excellent performance to direct hole injection from the anode to Ir(ppy)₃ dopant. [J745]

"Highly efficient single-emitting-layer white organic light-emitting diodes with reduced efficiency roll-off"

By codoping blue and orange phosphorescent dyes into a single host material, a highly efficient white organic light-emitting diode (WOLED) with Commission Internationale de L'Eclairage coordinates of (0.38, 0.43) at 12 V is demonstrated. Remarkably, this WOLED achieves reduced current efficiency roll-off, which slightly decreases from its maximum value of 37.3-31.0 cd/A at 1000cd/m². The device operational mechanism is subsequently investigated in order to unveil the origin of the high performance. [J746]

"Output power enhancement of GaN light emitting diodes with p -type ZnO hole injection layer"

We report an enhancement of the optical output power of GaN light emitting diodes (LEDs) by addition of a p-type ZnO layer located in close proximity to the active layer (ZnO/GaN LEDs). Arsenic (As)-doped p-ZnO was used as a hole-injecting layer to overcome the drop in external quantum efficiency of GaN LEDs at high drive currents-the so-called "efficiency droop." The output power in ZnO/GaN LEDs was improved up to 40%. This result is useful for development of highly efficient GaN LEDs operating at high current densities that will play a critical role in replacement of incandescent lamps by high efficiency solid-state light bulbs. [J747]

"Nanoparticle-induced resonant tunneling behaviors in small molecule organic light-emitting devices"

We report a hybrid nanoparticle/organic device with strong resonant tunneling behavior by introducing ligand-capped Ag nanoparticles between indium tin oxide and hole transport layer in small molecule organic light-emitting devices. The dependences of resonant tunneling current on the thickness of the organic layers are investigated. For the optimized device, a peak-to-valley current ratio as high as 4.5 and narrow peak width about 1.8 V are obtained. Combining with the analysis of current-voltage behavior, the mechanism based on the charge trapping effect of Ag nanoparticles is proposed to interpret the operation of the hybrid device. Finally, the emission characteristics of hybrid devices are also studied. [J748]

"The effect of the internal capacitance of InGaN-light emitting diode on the electrostatic discharge properties"

The electrostatic discharge (ESD) properties of the InGaN-light emitting diode (LED) were investigated in terms of the internal capacitance of the InGaN-LED. The LEDs with higher internal capacitance were found to be more resistant to external ESD impulses. The internal capacitance of the InGaN-LED was controlled by the silicon doping level of the n-GaN layer bordering the active layer. The human body model ESD yield at -500 V was increased from 27% to 94% by increasing the internal capacitance. Moreover, the high ESD pass yield was maintained up to -7000 V. [J749]

"Acoustoelectric luminescence from a field-effect n-i-p lateral junction"

A surface-acoustic-wave (SAW) driven light-emitting-diode structure that can implement a single-photon source

for quantum-cryptography applications is demonstrated. Our lateral n-i-p junction is realized starting from an undoped GaAs/AlGaAs quantum well by gating. It incorporates interdigitated transducers for SAW generation and lateral gates for current control. We demonstrate acoustoelectric transport and SAW-driven electroluminescence. The acoustoelectric current can be controlled down to complete pinch-off by means of the lateral gates. [J750]

"Directional light extraction enhancement from GaN-based film-transferred photonic crystal light-emitting diodes"

Experimental investigation of the directionality in the far-field pattern and light extraction enhancement in collected cone were performed in GaN-based film-transferred photonic crystal (PhC) light-emitting diodes (FTLEDs). Angular-resolved measurement revealed directional profile and azimuthal anisotropy in the far-field distribution with guided modes extraction. Good agreement according to Bragg's diffraction theory and free photon band structure were achieved. The light enhancement in PhC FTLEDs compared to non-PhC FTLEDs within the collection cone angle was obtained according to measured three-dimensional far-field patterns. In a $\pm 20^\circ$ collection cone, collected light was enhanced by a factor of 2.4 for the collimated PhC FTLED. [J751]

"Three-dimensional organic field-effect transistors with high output current and high on-off ratio"

High-performance three-dimensional organic field-effect transistors are developed with multiple vertical channels of organic semiconductors. Advanced processes of vacuum depositing high-mobility and air-stable dinaphtho[2,3-b:2',3'-f]thieno[3,2-b]thiophene thin films on a series of horizontally elongated vertical walls have maximized the output current to 0.60 A/cm² area with the application of -10 V for both drain-source and gate voltages. The on-off ratio is as high as 106. Carrier mobility of the organic semiconductor is typically 0.30 cm²/V s and deviation among ten devices is within 10%. The performance meets requirement for such application as driving organic light-emitting diodes in active-matrix displays. [J752]

"High efficiency blue phosphorescent organic light emitting diodes using a simple device structure"

High efficiency blue phosphorescent organic light emitting diodes have been developed by using a simple device structure. A derivative of spirobifluorene based phosphine oxide was used both as a host and an electron transport layer with an exciton blocking function. A maximum quantum efficiency of 19.2% and a current efficiency of 37.2 cd/A were obtained by using a simple device structure without a hole blocking layer. [J753]

"Optical and electrical characteristics of Ag-doped perylene diimide derivative"

In this paper, a highly conductive and strongly absorptive organic thin film by doping Ag into N,N'-bis(2,6-diisopropylphenyl)-1,7-bis(4-methoxy-phenyl) perylene-3,4,9,10-tetracarboxydiimide (MPPDI) was demonstrated. Strong absorption resulted from the broadband absorption of MPPDI at visible range and plasmon-enhanced absorption around 420 nm of Ag nanoparticles. Ag dopants in MPPDI acted as quenchers, which resulted in a dramatic decrease in photoluminescence intensity of MPPDI. Besides, J-V characteristics of Ag:MPPDI thin film changed from trapped-charge-limited current to Ohmic conduction with increasing Ag concentrations. Conductivity of 1.15 $\times 10^{-6}$ Ω^{-1} cm was achieved when MPPDI/Ag=5:1. This organic thin film has potential applications for low-reflectance organic light-emitting diode and organic photovoltaic device. [J754]

"Reduction in efficiency droop, forward voltage, ideality factor, and wavelength shift in polarization-matched GaInN/GaN multi-quantum-well light-emitting diodes"

Blue light-emitting diodes (LEDs) with polarization-matched GaInN/GaN multi-quantum-well (MQW) active regions are grown by metal-organic vapor-phase epitaxy. The GaInN/GaN MQW structure reduces the magnitude of polarization sheet charges at heterointerfaces in the active region. The GaInN/GaN MQW LEDs are shown to have enhanced light-output power, reduced efficiency droop, a lower forward voltage, a smaller diode ideality factor, and decreased wavelength shift, compared with conventional GaInN/GaN MQW LEDs. [J755]

"Organic light-emitting diodes with carbon nanotube cathode-organic interface layer"

Improved performance of organic light-emitting diodes (OLEDs) was achieved by implementing a carbon nanotube (CNT) layer at the cathode-organic interface, spin coated between the organic layer and the cathode. The small geometry of CNTs could enable the enhancement of the electric field around them, thus increasing electron injection efficiency from the cathode to the organic layer. In addition, as measured from the x-ray absorption and emission spectroscopy, incorporation of CNT could reduce the lowest unoccupied molecular orbital of the organic material at the cathode-organic interface, thus effectively decreasing the barrier for electron

injection. Increased electron injection and luminance characteristics were demonstrated for both polymer and small molecule based OLED devices. [J756]

"Correlation between the microstructure and electroluminescence properties of Er-doped metal-oxide semiconductor structures"

Optical response of a rare earth (RE)-doped SiO₂ layer is known to deteriorate markedly at room temperature due to RE clustering. The key challenge is therefore to probe the ongoing processes at the microscopic level and the subsequent impact on the luminescence properties with increasing RE concentration. Here, we report how the Er electroluminescence in a metal-oxide-semiconductor structure has been affected by increasing Er content. Our results indicate that the Er oxide clustering is anticipated by the formation of Si-based oxygen-deficiency centers during postimplantation annealing and leads to a strong quenching of the short-wavelength (350-500 nm) Er electroluminescence. [J757]

"Microcavity top-emitting organic light-emitting devices integrated with diffusers for simultaneous enhancement of efficiencies and viewing characteristics"

We show that integrating diffuser films with microcavity top-emitting organic light-emitting devices (OLEDs) provide a convenient approach for simultaneously achieving large quantum- efficiency enhancement (1.38 times compared to top-emitting devices without diffusers and 2.1 times compared to conventional bottom-emitting devices) and improving viewing characteristics (more saturated/stable colors over angles, emission patterns more Lambertian, pixel sharpness remained) of top-emitting microcavity OLEDs for display applications. Most importantly, the fabrication of the diffuser films is simple and effective. These features may make it attractive for use in enhancing OLED performances in various applications. [J758]

"Metal mirror assisting light extraction from patterned AlGaInP light-emitting diodes"

We demonstrate light extraction from metal reflector-based AlGaInP photonic crystal (PhC) light-emitting diodes (LEDs). The photons reflected by a high-reflectivity, small-absorption, bottom Ag mirror steadily interact with the PhC, and thus enhanced light extraction is achieved. The square lattice PhC patterns are fabricated on an upper n-doped AlGaInP surface with a depth of 500 nm. An optical power measurement using an integration sphere shows that the extraction efficiency of the PhC LED is 1.8 times larger than that of the nonpatterned LED. A three-dimensional finite difference time domain simulation is performed to understand the output enhancement extracted by the PhC and the effect of internal absorption. [J759]

"GaN light-emitting diode with monolithically integrated photonic crystals and angled sidewall deflectors for efficient surface emission"

In order to obtain efficient surface emission, we propose and demonstrate a GaN light-emitting diode (LED) structure. A two-dimensional photonic crystal (PC) pattern is integrated to the sapphire substrate before the epigrowth by employing laser holography. In addition, angled sidewall deflectors (ASDs) are formed on the mesa sidewalls. Both the PC and ASDs redirect guided photons into the surface-normal direction. When compared to a conventional LED structure, we could obtain a twofold increase in the total surface emission and the surface-normal emission intensity enhanced by a factor of 2.5. [J760]

"Reduced nonthermal rollover of wide-well GaInN light-emitting diodes"

Nonthermal rollover (or efficiency droop) of the electroluminescence (EL) efficiency has been investigated for near-UV-emitting (AlGaIn)N single-well light-emitting diodes (LED) with varying GaInN well widths grown on substrates with different dislocation densities (DDs). For each DD the well width of the mesa-LEDs has been optimized for maximum EL efficiency at high operating currents. LEDs on freestanding GaN (DD4.4107cm⁻²) with an 18 nm thick GaInN wide-well active region show the highest efficiency, and the output power-versus-current characteristic remains linear up to the highest pulsed current density of 750A/cm². In contrast, LEDs on sapphire grown with conventional low-temperature nucleation (DD109cm⁻²) exhibit the optimum well width at 3 nm and show significant nonthermal rollover. [J761]

"High-efficiency staggered 530 nm InGaIn/InGaIn/GaN quantum-well light-emitting diodes"

Optical properties of staggered 530 nm InGaIn/InGaIn/GaN quantum-well (QW) light-emitting-diodes are investigated using the multiband effective mass theory. These results are compared with those of conventional 530 nm InGaIn/GaN QW structures. A staggered InGaIn/InGaIn/GaN QW structure is shown to have much larger spontaneous emission than a conventional InGaIn/GaN QW structure. This can be explained by the fact that a staggered QW structure has much larger matrix element than a conventional QW structure because a spatial

separation between electron and hole wave functions is substantially reduced with the inclusion of a staggered InGaN layer. A staggered QW structure shows that the peak position at a high carrier density (530 nm) is similar to that at a noninjection level. [J762]

"Direct measurement of electric field screening in light emitting diodes with conjugated polyelectrolyte electron injecting/transport layers"

Electroabsorption spectroscopy was used to directly probe the electric fields in a polymer light emitting diode that utilizes a conjugated polyelectrolyte electron transporting/injection layer. The electric field in the emitting layer was found to be negligible at applied biases greater than the built-in field of the device. Holes injected at these biases accumulate at the emitting layer/conjugated polyelectrolyte interface and screen the field from the emitting layer to the conjugated polyelectrolyte layer. In conjunction with mobile ions that redistribute the field in the conjugated polyelectrolyte layer, this leads to greatly improved electron injection from high work function cathodes. [J763]

"Highly efficient and stable organic light-emitting diode using 4,4'-bis(N-carbazolyl)-9,9'-spirobifluorene as a thermally stable host material"

We demonstrated efficient and stable organic light-emitting diodes (OLEDs) using 4,4'-bis(N-carbazolyl)-9,9'-spirobifluorene (CFL), which has spirobifluorene and two carbazole moieties, as a thermally stable host and tris(1-phenylisoquinolinolato-C2,N) iridium(III) [Ir(piq)3] or tris(2-phenylpyridine)iridium(III) [Ir(ppy)3] as a guest. Glass transition temperature of CFL was 151 °C. The efficiency of OLEDs that use CFL as a host and Ir(piq)3 as a guest were higher than that of an OLED, which uses conventional 4,4'-bis(N-carbazolyl)-1,1'-biphenyl (CBP) as a host. The external quantum efficiency of the OLED using CFL and Ir(piq)3 was 13%. The lifetime of the OLED using CFL as the host was longer than that of the OLED using CBP. [J764]

"Determination of localized-state distributions in organic light-emitting diodes by impedance spectroscopy"

A method for determining localized-state distributions in organic light-emitting diodes by impedance spectroscopy is proposed on the basis of a theory for single-injection space-charge-limited current. The method is sensitive and has high energy resolution. The applicability of the method is demonstrated in polyfluorene-based Green K (Sumation™) light-emitting polymer; the localized-state distributions in this polymer are mapped out in the energy range of 0.3-0.8 eV, both below the conduction-band mobility edge and above the valence-band mobility edge. [J765]

"Single-layer triplet white polymer light-emitting diodes incorporating polymer oxides: Effect of charge trapping at phosphorescent dopants"

This paper describes the effects of charge trapping on the device performances of triplet polymer light-emitting diodes (PLEDs) after the cathode contact had been improved through the blending of poly(ethylene glycol) (PEG) into the active layer. The external quantum efficiency (EQE) was enhanced when the dopant tended to trap electrons. In contrast, we observed no EQE enhancement for the device featuring a hole-trapping dopant. Because PEG promoted electron injection, more electrons were trapped in the triplet molecules, thereby enhancing the probability of recombination. Finally, after incorporating PEG, we further achieved white PLEDs exhibiting both high EQE and high power efficiency. [J766]

"Rapid efficiency roll-off in high-quality green light-emitting diodes on freestanding GaN substrates"

InGaN/GaN multiple-quantum-well green light-emitting diodes (LEDs) were grown on freestanding GaN and sapphire substrates. The density of microstructural defects in the LED on GaN was substantially reduced, leading to a significant reduction in defect-assisted tunneling currents and an improved injection efficiency under low bias. The LED on GaN outperformed the LED on sapphire at low injection currents and exhibited a 65% peak internal quantum efficiency. However, it suffered from even more dramatic efficiency roll-off, which occurs at a current density as low as 0.3 A/cm². This behavior is explained as the combined result of efficient current injection and significant carrier overflow in a high-quality LED. [J767]

"TiN/Al Ohmic contacts to N-face n-type GaN for high-performance vertical light-emitting diodes"

We report on the electrical properties of TiN(30 nm)/Al(200 nm) Ohmic contacts to N-face n-type GaN for high-performance vertical light-emitting diodes and compare them with those of Ti(30 nm)/Al(200 nm) contacts. Both the as-deposited samples show Ohmic behaviors with contact resistivity of (6.0-7.2) × 10⁻⁴ Ω cm². However,

annealing the samples at 300 °C causes the degradation of their electrical properties. Furthermore, unlike the TiN/Al contacts, the Ti/Al contacts suffer from aging degradation when exposed to air. Based on the x-ray photoemission spectroscopy and secondary ion mass spectrometry results, Ohmic formation and degradation mechanisms are briefly described and discussed. [J768]

"Spin injection in silicon at zero magnetic field"

In this letter, we show efficient electrical spin injection into a SiGe based p-i-n light emitting diode from the remanent state of a perpendicularly magnetized ferromagnetic contact. Electron spin injection is carried out through an alumina tunnel barrier from a Co/Pt thin film exhibiting a strong out-of-plane anisotropy. The electron spin polarization is then analyzed through the circular polarization of emitted light. All the light polarization measurements are performed without an external applied magnetic field, i.e., in remanent magnetic states. The light polarization as a function of the magnetic field closely traces the out-of-plane magnetization of the Co/Pt injector. We could achieve a circular polarization degree of the emitted light of 3% at 5 K. Moreover this light polarization remains almost constant at least up to 200 K. [J769]

"High output power density from GaN-based two-dimensional nanorod light-emitting diode arrays"

Here we propose and realize a scheme for making a direct contact to a two-dimensional nanorod light-emitting diode (LED) array using the oblique-angle deposition approach. And, more importantly, we demonstrate highly efficient electrical carrier injection into the nanorods. As a result, we show that at a 20 mA dc current injection, the light output power density of our nanorod LED array is 3700 mW cm⁻². More general, this contact scheme will pave the ways for making direct contacts to other kinds of nanoscale optoelectronic devices. [J770]

"Light-extraction enhancement in GaN-based light-emitting diodes using grade-refractive-index amorphous titanium oxide films with porous structures"

Amorphous titanium oxide (a-TiOx:OH) films prepared by plasma-enhanced chemical-vapor deposition at 200 and 25 °C are in turn deposited onto the GaN-based light-emitting diode (LED) to enhance the associated light extraction efficiency. The refractive index, porosity, and photocatalytic effect of the deposited films are correlated strongly with the deposition temperatures. The efficiency is enhanced by a factor of 1.31 over that of the uncoated LEDs and exhibited an excellent photocatalytic property after an external UV light irradiation. The increase in the light extraction is related to the reduction in the Fresnel transmission loss and the enhancement of the light scattering into the escape cone by using the graded-refractive-index a-TiOx:OH film with porous structures. [J771]

"Low voltage efficient simple p-i-n type electrophosphorescent green organic light-emitting devices"

We present simple p-i-n structures with double-emitting and mixed-emitting layers for highly efficient phosphorescent green devices. Using a wide band-gap hole transporting material of 4,4'-bis(tris(N-carbazolyl)-triphenylamine) and a wide band-gap electron transporting material of bis[2-(2-hydroxyphenyl)-pyridine]beryllium, the bilayered p-i-n structure with no heterointerface barriers has been realized. A very low onset voltage value of 2.4 V corresponding to the energy of 2.4 eV of green electroluminescence, which is close to the photon energy of dopant emitting molecules (2.3-2.4 eV), is achieved in this simple p-i-n device configuration. Maximum current- and power-efficiency values of 53.3 cd/A and 61.4 lm/W and low rolloff of current efficiency (6%) are demonstrated in the simple p-i-n green phosphorescent devices, promising for the practical and economical high brightness applications. [J772]

"High speed pulsed electrical spin injection in spin-light emitting diode"

We demonstrate high speed pulsed electrical spin injection from a CoFeB/MgO spin injector into a AlGaAs/GaAs semiconductor light emitting diode. Under pulsed electrical excitation, time-resolved electroluminescence on nanosecond time scale exhibits a plateau of circular polarization degree as high as 15% under a 0.8 T magnetic field. It follows an initial decay that could be due to electron spin-relaxation process in the quantum well embedded in the intrinsic region of the diode. The temporal buildup of the electronic spin polarization degree in the quantum well is much faster than the rise time of electroluminescence intensity. [J773]

"Study of efficient and stable organic light-emitting diodes with 2-methyl-9,10-di(2-naphthyl)anthracene as hole-transport material by admittance spectroscopy"

An organic light-emitting device with enhanced efficiency by employing 2-methyl-9,10-di(2-naphthyl)anthracene (MADN) as hole-transport material (HTM) has been developed. The admittance spectroscopy studies indicate that using MADN as HTM can reduce the amount of hole carriers injected into the device leading to a well-

balanced carrier recombination. The green fluorescent 10-(2-benzothiazolyl)-1,1,7,7-tetramethyl-2,3,6,7-tetrahydro-1H,5H,11H-benzo[*l*]pyrano-[6,7,8-*ij*]quinolizin-11-one doped tris(8-quinolinolato)aluminum device achieved a current efficiency of 21.8 cd/A and a power efficiency of 10.4 lm/W at 20mA/cm² that are 65% higher than those of the control device. The green-doped device also achieved a long half-decay lifetime of 22 000h at an initial brightness of 500cd/m². [J774]

"Spin injection studies into GaAs quantum wells in the presence of confined electrons"

We compare the electroluminescence spectra (spectral composition and polarization characteristics) of two types of Fe-based AlGaAs/GaAs n-i-ppspin light emitting diodes (spin LEDs). In type A spin LEDs the GaAs quantum well (QW) does not contain any confined carriers, while in type B LEDs the GaAs QW is occupied by confined electrons generated by excess n-type doping in the AlGaAs(n) barrier. Type B LEDs show a significantly smaller circular polarization at the e1h1 feature than type A devices. Other differences include the presence of the e1l1 exciton as well as excitonic phonon replicas in type B LEDs. Possible mechanisms for these differences are discussed. [J775]

"Probing radical kinetics in the afterglow of pulsed discharges by absorption spectroscopy with light emitting diodes: Application to BCl radical"

Measuring decay rates of radical densities in the afterglow of pulsed plasmas is a powerful approach to determine their gas phase and surface loss kinetics. We show that this measurement can be achieved by absorption spectroscopy with low cost and simple apparatus by using light emitting diodes as a light source. The feasibility is demonstrated by monitoring BCl radicals in pulsed low pressure high-density BCl₃ plasmas. It is shown that BCl is lost both in the gas phase by reacting with Cl₂ with a cross section of 9E-2 and in the chamber walls with a sticking coefficient of about 0.3. [J776]

"Light extraction from GaN-based light emitting diode structures with a noninvasive two-dimensional photonic crystal"

A noninvasive fabrication process involving soft nanoimprint lithography is used to pattern a photonic crystal (PhC) in titania film for enhanced light extraction from a GaN light emitting diode (LED). This technique avoids damaging the LED structure by the etching process, while photoluminescence measurements show extracted modes emitted from the quantum wells which agree well with modeling. A light extraction improvement of 1.8 times is measured using this noninvasive PhC. [J777]

"The right word, anywhere"

First Page of the Article [J778]

"Phosphor-Free Monolithic White-Light LED"

Phosphor-free monolithic InGaN-based white-light LED has the advantages of simpler device process and potentially higher efficiency. Several techniques have been developed for implementing such white-light LEDs. Among them, the key issue is the growth of a high-quality high-indium InGaN/GaN quantum well (QW). An underlying InGaN layer growth technique is introduced for enhancing the crystal quality of a high-indium QW. To demonstrate the superior properties of a QW grown with this technique, a green LED is fabricated based on the underlying growth technique to compare with another LED of the same emission wavelength based on the conventional growth method. Then, the underlying growth technique is used to grow three yellow-emitting QWs of high efficiency. The yellow photons mix with blue light from an overgrown blue-emitting QW to produce white light. The improved properties of the phosphor-free monolithic white-light LED are discussed in detail. [J779]

"Adaptive equalization system for visible light wireless communication utilizing multiple white LED lighting equipment"

White LEDs were invented the 1990's. Since then they have been extensively researched and applied in various ways. Compared with conventional lighting devices, the white LED has lower power consumption, lower voltage requirements, longer lifetime, smaller size, faster response, and cooler operation. The white LED will eventually replace incandescent or fluorescent lights in offices and homes. We have proposed an indoor visible light wireless communication system that utilizes multiple white LED lighting equipment. In this system, the equipment is used not only for illuminating rooms but also for an optical wireless communication system. The system has significantly higher power levels than infrared wireless communication systems, since it also functions as the main lighting equipment. One problem is we tend to install many lighting sources on a ceiling in order to illuminate the room as evenly as possible. While the number of sources permits site diversity transmission over

LOS links, the optical path difference between the multiple sources triggers intersymbol interference (ISI), which significantly degrades system performance. This paper overcomes the ISI problem by proposing an adaptive equalization system. We elucidate the most effective training sequence interval for channel estimation in a mobile environment. And we show that the adaptive equalization system with the effectual interval alleviates the influence of shadowing. [J780]

"Time is on your side"

There's no longer any excuse for having the wrong time. Computers, set-top boxes, and even some wristwatches can get their time from the U.S. Naval Observatory or some other authoritative source. But what about a device you build yourself? Many will come with a timing chip that you can use as a counter, but they won't tell you what time it is in the real world or self-adjust for daylight saving time. What you want is a microprocessor on a computer board that will query a network for the correct time and pass it on to the rest of your device. This month's project is just that, a clock on a singleboard computer that uses the Network Time Protocol (NTP) to give you millisecond accuracy for about US \$115. [J781]

"Substrate thermal conductivity effect on heat dissipation and lifetime improvement of organic light-emitting diodes"

We report substrate thermal conductivity effect on heat dissipation and lifetime improvement of organic light-emitting diodes (OLEDs). Heat dissipation behavior of top-emission OLEDs fabricated on silicon, glass, and planarized stainless steel substrates was measured by using an infrared camera. Peak temperature measured from the backside of each substrate was saturated to be 21.4, 64.5, and 40.5 °C, 180 s after the OLED was operated at luminance of 10 000cd/m² and 80% luminance lifetime was about 198, 31, and 96 h, respectively. Efficient heat dissipation through the highly thermally conductive substrates reduced temperature increase, resulting in much improved OLED lifetime. [J782]

"Spontaneous charge transfer from indium tin oxide to organic molecules for effective hole injection"

Naphthalene tetracarboxylic dianhydride (NTCDA) shows strong chemical interaction with metal atoms in an indium tin oxide (ITO) substrate to form charge transfer (CT) complexes. The CT complex at the ITO/NTCDA interface can lower the energy barrier height for hole injection from ITO into the hole transporting layer of N,N'-diphenyl-N, N'-bis(1-naphthyl)(1,1'-biphenyl)-4,4'-diamine (NPB). The operational voltage of an emissive device at a current density of 100mA/cm² was significantly reduced from 12.2 to 9.2 V by simply inserting a thin layer of NTCDA between the ITO and NPB. The results enable the achievement of organic light-emitting diodes that consume relatively less power. [J783]

"Design Analysis of Staggered InGaN Quantum Wells Light-Emitting Diodes at 500-540 nm"

Staggered InGaN quantum wells (QWs) are analyzed as improved active region for light-emitting diodes (LEDs) emitting at 500 nm and 540 nm, respectively. The calculation of band structure is based on a self-consistent 6-band k-middot-p formalism taking into account the valence band mixing, strain effect, and spontaneous and piezoelectric polarizations as well as the carrier screening effect. Both two-layer staggered In_xGa_{1-x}N/In_yGa_{1-y}N QW and three-layer staggered In_yGa_{1-y}N/In_xGa_{1-x}N/In_yGa_{1-y}N QW structures are investigated as active region to enhance the spontaneous emission radiative recombination rate (R_{sp}) for LEDs emitting at 500 nm and 540 nm. Analysis of the spontaneous emission radiative recombination rate (R_{sp}) shows significant enhancement for both two-layer staggered InGaN QW and three-layer staggered InGaN QW, in comparison to that of the conventional In_zGa_{1-z}N QW. The studies of the carrier lifetime indicate a significant reduction of the carrier lifetime for staggered InGaN QWs, which contribute to the enhancement of the radiative efficiency for both two-layer staggered InGaN QW and three-layer staggered InGaN QW LEDs emitting at 500 nm and 540 nm. [J784]

"Enhancing current spreading by simple electrode pattern design methodology in lateral GaN/InGaN LEDs"

An electrode pattern design methodology that improves the current uniformity in mesa-structured GaN/InGaN blue light-emitting diodes (LEDs) is investigated. Comparisons between an LED with a new electrode pattern adopting the proposed methodology and an LED with a commercially used electrode are made in view of both current and luminance distributions. Simulations as well as experimental results show that the proposed simple design methodology is very effective to spread current more uniformly in the active layer. [J785]

"A Simple, Low-Cost Double Beam Spectrophotometer for Colorimetric Detection of Nitrite in"

Seawater"

This paper reports on the optical detection system of a prototype nitrite sensor for seawater analysis. The sensor uses a colorimetric Griess reaction that produces an Azo dye with an absorption peak at 540 nm. A simple low-cost double beam spectrophotometer using a green light emitting diode (LED) light source, two integrated photo detectors and lock-in detection is described. A log-ratio amplifier is used to produce an output proportional to absorbance. The optical devices were mounted in a cast resin block to prevent shock and vibration. Experimental results show the detection system has a limit of detection of 0.1 μM . [J786]

"Reliable thin film encapsulation for organic light emitting diodes grown by low-temperature atomic layer deposition"

We report on highly efficient gas diffusion barriers for organic light emitting diodes (OLEDs). Nanolaminate (NL) structures composed of alternating Al_2O_3 and ZrO_2 sublayers grown by atomic layer deposition at 80 °C are used to realize long-term stable OLED devices. While the brightness of phosphorescent p-i-n OLEDs sealed by a single Al_2O_3 layer drops to 85% of the initial luminance of 1000 cd/m^2 after 1000 h of continuous operation, OLEDs encapsulated with the NL retain more than 95% of their brightness. An extrapolated device lifetime substantially in excess of 10 000 h can be achieved, clearly proving the suitability of the NLs as highly dense and reliable thin film encapsulation of sensitive organic electronic devices. [J787]

"Improved Transient Current Feedforward Output Buffer for Fast and Compact Active-Matrix OLED Column Drivers"

An improved transient current feedforward driver is designed for compact implementation and low-power consumption by adopting the demultiplexing operation of the proposed driver based on the fast driving speed of 6 μs for the panel load of 6 k Ω /40 pF, which is equivalent to that of extended-graphic-array active-matrix organic light-emitting diode displays. The driver has the structural advantages of simple frequency compensation and low-power consumption, which come from the elimination of an internal operational transconductance amplifier (OTA). The chip implementation confers that the area of the driver is 32.5 times 217 μm^2 , and the power consumption is 6.5 μA for each channel. [J788]

"Far-Field and Near-Field Distribution of GaN-Based Photonic Crystal LEDs With Guided Mode Extraction"

The near-field and far-field distribution of GaN LEDs with square photonic crystal (PhC) lattice are experimentally investigated. The optical images of the near-field pattern are obtained from the guided electroluminescent light generated at the center of a special annular structure. For increasing lattice constant, symmetric patterns with varying number of petals according to the symmetry of the PhC are observed. The far-field distribution is studied with GaN-based film-transferred PhC LEDs with the thickness about 1500 nm. Angular-resolved measurements under electrical injection revealed guided modes extraction behavior and polarization based on the Bragg's diffraction with the PhC lattice. Good agreement with the two-dimension free photon band structure is obtained. [J789]

"Composition Optimization and Phase Transformation of Si-Nanocrystal-Doped for Enhancing Luminescence From MOSLED"

Near-infrared (NIR) photo- and electroluminescence (PL and EL) of Si nanocrystals buried in Si-rich SiO_x film, and their correlation with the structural phase transformation and the varied oxygen composition of SiO_x , are investigated. By detuning the N_2O flowing ratio ($\text{YN}_2\text{O} = [\text{N}_2\text{O}/(\text{N}_2\text{O} + \text{SiH}_4)] \times 100\%$) from 93% to 80% during plasma-enhanced chemical vapor deposition growth, the oxygen composition ratio of the Si-rich SiO_x can be adjusted from 1.64 to 0.88. The grazing incident X-ray diffraction and X-ray photoelectron spectroscopy spectra indicate that the SiO_x transforms its structural phase from Si + SiO_2 isomer to Si + SiO + SiO_2 isomer. With O/Si ratio > 1.24, the SiO_x matrix becomes SiO_2 isomer, whereas the SiO_x structure approaches SiO phase at O/Si ratio that is nearly 1.0. The formation of SiO matrix in SiO_x , grown at YN_2O below 85% reduces the precipitated Si nanocrystal density from 2.8 times 10^{18} to 7 times 10^{16} cm^{-3} , and monotonically attenuates the NIR PL by one order of magnitude. Such a structural phase transformation from SiO_2 to SiO in SiO_x with lower O/Si ratio causes the degradation in EL power conversion efficiency and external quantum efficiency (EQE). Maximum EL power of 0.5 μW and EQE of 0.06% are obtained from MOSLED made on SiO_x , with optimized O/Si ratio of 1.24. [J790]

"Silicon Nanocrystals as an Enabling Material for Silicon Photonics"

Silicon nanocrystals (Si-nc) is an enabling material for silicon photonics, which is no longer an emerging field of

research but an available technology with the first commercial products available on the market. In this paper, properties and applications of Si-nc in silicon photonics are reviewed. After a brief history of silicon photonics, the limitations of silicon as a light emitter are discussed and the strategies to overcome them are briefly treated, with particular attention to the recent achievements. Emphasis is given to the visible optical gain properties of Si-nc and to its sensitization effect on Er ions to achieve infrared light amplification. The state of the art of Si-nc applied in a few photonic components is reviewed and discussed. The possibility to exploit Si-nc for solar cells is also presented. In addition, nonlinear optical effects, which enable fast all-optical switches, are described. [J791]

"A Comparative Study of Fast Photomultipliers for Timing Experiments and TOF PET"

The new 1 inch and 1.5 inch in diameter photomultipliers for timing applications from Photonis and Hamamatsu have been tested. Time resolution of XP1020, XP3060, R9800 and R9420 was measured with a 10 times 10 times 5 mm³LSO crystal in coincidence experiments with 511 keV annihilation quanta from ²²Na gamma source. Results were discussed in terms of measured photoelectron number and time jitter. Single photoelectron spectra were recorded and excess noise factor for each tube was also calculated. The final comparison of the tested tubes and their timing properties were presented in relation to large amount of experimental data of various types of PMTs collected during last few years. Especially, observed linear dependency between the time resolution normalized to the number of photoelectrons and time jitter was pointed out. Inconsistency of the data collected with the Hamamatsu R9420 PMT resulting from the overestimated photoelectron number was reported and further studied. Additional experiments with LED light source and different experimental set-ups were discussed and comparison of the two methods of the photoelectron number measurements was performed. [J792]

"Quantum Dots for Single- and Entangled-Photon Emitters"

The efficient generation of polarized single or entangled photons is a crucial requirement for the implementation of quantum key distribution (QKD) systems. Self-organized semiconductor quantum dots (QDs) are capable of emitting one polarized photon or an entangled photon pair at a time using appropriate electrical current injection. We realized a highly efficient single-photon source (SPS) based on well-established semiconductor technology: In a pin structure, a single electron and a single hole are funneled into a single InAs QD using a submicron AlOx current aperture. Efficient radiative recombination leads to emission of single polarized photons with an all-time record purity of the spectrum. Non-classicality of the emitted light without using additional spectral filtering is demonstrated. The out-coupling efficiency and the emission rate are increased by embedding the SPS into a micro-cavity. The design of the micro-cavity is based on detailed modeling to optimize its performance. The resulting resonant single-QD diode is driven at a repetition rate of 1 GHz, exhibiting a second-order correlation function of $g(2)(0) = 0$. Eventually, QDs grown on (111)-oriented substrates are proposed as a source of entangled photon pairs. Intrinsic symmetry-lowering effects leading to the splitting of the exciton bright states are shown to be absent for this substrate orientation. As a result, the XXrrrr Xrrrr 0 recombination cascade of a QD can be used for the generation of entangled photons without further tuning of the fine-structure splitting via QD size and/or shape. [J793]

"Silicon-Germanium Nanostructures for Light Emitters and On-Chip Optical Interconnects"

In this paper, we review the present status of light emitters based on SiGe nanostructures. In order to be commercially valuable, these light emitters should be efficient, fast, operational at room temperature, and, perhaps most important, compatible with the "mainstream" complementary metal-oxide-semiconductor (CMOS) technology. Another important requirement is in the emission wavelength, which should match the optical waveguide low-loss spectral region, i.e., 1.3-1.6 μm . Among other approaches, epitaxially grown Si/SiGe quantum wells and quantum dot/quantum well complexes produce efficient photoluminescence and electroluminescence in the required spectral range. Until recently, the major roadblocks for practical applications of these devices were strong thermal quenching of the luminescence quantum efficiency and a long carrier radiative lifetime. The latest progress in the understanding of physics of carrier recombination in Si/SiGe nanostructures is reviewed, and a new route toward CMOS compatible light emitters for on-chip optical interconnects is proposed. [J794]

"Dramatic efficiency improvement in phosphorescent organic light-emitting diodes with ultraviolet-ozone treated poly(3,4-ethylenedioxythiophene):poly(styrenesulfonate)"

The treatment of poly(3,4-ethylenedioxythiophene):poly(styrenesulfonate) (PEDOT:PSS) films by ultraviolet (UV) light-ozone to improve device efficiency was investigated utilizing two simple phosphorescent organic light-emitting diodes (PHOLEDs) architectures. The maximum external quantum efficiency in the first device increased from 3.5% for the untreated anode to 10.5%, while in the second device comprising an exciton blocking layer increased from 15.8% to 18.5%. The time dependence of the UV-ozone treatment on the performance was

studied. The dramatic improvement in the PHOLED performance is attributed to the change in the PEDOT:PSS work function and more balanced charge injection, suggesting promising easy-to-do method to improve PHOLED performance. [J795]

"The relationship of current transfer ratio and input light wavelengths in the organic photocoupler"

In this article we have fabricated an organic photocoupler with different wavelengths of organic light-emitting diodes as light source (input unit) and photodiode based on poly(3-hexylthiophene):1-(3-methoxycarbonyl)propyl-1-phenyl-(6,6)-C61as detector (output unit). The relationship between the current transfer ratio (CTR) and input light wavelengths was studied. The output current and CTR are increasing with the input light wavelengths decreasing from 624 to 470 nm, and the CTR value with 470 nm input wavelength is 3-12 times higher than that with other longer input wavelengths, indicating that the short wavelength input light generates photocurrent and CTR efficiently. [J796]

"Origin of the abnormal behavior of contact resistance in Ohmic contacts to laser-irradiated n-type GaN"

Abnormal behavior of contact resistance with annealing in Ohmic contacts to laser-irradiated n-GaN is investigated. Ti/Al contacts on as-grown n-GaN shows no change in contact resistivity with annealing at the temperature range of 100-400 °C. However, the annealing results in the significant increase in contact resistivity in the contacts on laser-irradiated n-GaN. Synchrotron radiation photoemission study reveals the reduction of the concentration of donor-like N vacancies near the surface by the annealing. These results suggest that preventing the annihilation of N vacancies in the laser-irradiated n-GaN is important in improving the performance of vertical-structure GaN-based light-emitting diodes fabricated by laser lift-off. [J797]

"Auger recombination rates in nitrides from first principles"

We report Auger recombination rates for wurtzite InGa_N calculated from first-principles density-functional and many-body-perturbation theory. Two different mechanisms are examined-inter- and intra-band recombination-that affect different parts of the emission spectrum. In the blue to green spectral region and at room temperature the Auger coefficient can be as large as 2410-30cm⁶ s⁻¹; in the infrared it is even larger. Since Auger recombination scales with the cubic power of the free-carrier concentration it becomes an important nonradiative loss mechanism at high current densities. Our results indicate that Auger recombination may be responsible for the loss of quantum efficiency that affects InGa_N-based light emitters. [J798]

"Effect of annealing on the performance of CrO₃/ZnO light emitting diodes"

Heterojunction CrO₃/ZnO light emitting diodes have been fabricated. Their performance was investigated for different annealing temperature for ZnO nanorods. Annealing in oxygen atmosphere had significant influence on carrier concentration in the nanorods, as well as on the emission spectra of the nanorods. Surprisingly, annealing conditions, which yield the lowest band edge-to-defect emission ratio in the photoluminescence spectra, result in the highest band edge-to-defect emission ratio in the electroluminescence spectra. The influence of the native defects on ZnO light emitting diode performance is discussed. [J799]

"Ga_N/In_{1-x}Ga_xN/GaN/ZnO nanoarchitecture light emitting diode microarrays"

We studied the fabrication and electroluminescent (EL) characteristics of Ga_N/In_{1-x}Ga_xN/GaN/ZnO nanoarchitecture light emitting diode (LED) microarrays consisting of position-controlled GaN/ZnO coaxial nanotube heterostructures. For the fabrication of nanoarchitecture LED arrays, n-GaN, GaN/In_{0.24}Ga_{0.76}N multi-quantum well (MQW) structures and p-GaN layers were deposited coaxially over the entire surface of position-controlled ZnO nanotube arrays grown vertically on c-plane sapphire substrates. The nanoarchitecture LEDs exhibited strong green and blue emission from the GaN/GaN/In_{0.24}Ga_{0.76}N MQWs at room temperature. Furthermore, the origins of dominant EL peaks are also discussed. [J800]

"Enhanced efficiency and reduced roll-off in blue and white phosphorescent organic light-emitting diodes with a mixed host structure"

We report a significant enhancement and a reduced efficiency roll-off in blue and white phosphorescent organic light-emitting diodes (PHOLEDs) based on a mixed host structure. The combination of a hole-transport-type host and an electron-transport-type host as a mixed host emissive layer resulted in an effective charge carrier injection and distribution of the recombination zone, and therefore highly efficient blue PHOLEDs with peak external quantum and power efficiencies of 21.6% and 44.9 lm/W were achieved. Moreover, white PHOLEDs with a mixed host structure showed a power efficiency of 37 lm/W, which is over four times higher than 8.7 lm/W

in a single host structure device at a luminance of 1000cd/m². [J801]

"Controlling the carrier recombination zone for improved color stability in a two-dopant fluorophore/phosphor white organic light-emitting diode"

A white organic light-emitting diode (WOLED) is produced upon systematic introduction of deep-blue fluorescence from 4,4'-bis(9-ethyl-3-carbazovinylen)-1,1'-biphenyl to broad-band yellow phosphorescence from bis[3,5-bis(2-pyridyl)-1,2,4-triazolato]platinum(II) in the common host 4,4'-bis(carbazol-9-yl)biphenyl. The carrier recombination zone is first identified upon investigating alternative device structures, then optimized by varying the thickness of the electron-transport layer. The WOLED exhibits striking stability of color and efficiency, as manifest by parameters at high brightness of 1000cd/m²sustaining 94%-122% their values at 50cd/m². [J802]

"Electroluminescent measurement of the internal quantum efficiency of light emitting diodes"

An experimental method is demonstrated for the determination of internal quantum efficiency (IQE) in III-nitride-based light-emitting diodes (LEDs). LED devices surrounded with an optically absorbing material have been fabricated to limit collected light to photons emitted directly from the quantum wells across a known fraction of the recombination area. The emission pattern for this device configuration was modeled to estimate the extraction efficiency. IQE can then be calculated from the measured input current and output power. This method was applied to c-plane In_xGa_{1-x}N-based LEDs emitting at 445 nm. Initial measurements estimate an IQE of 43%±1%at a current density of 7.9A/cm². [J803]

"Full-wave simulation of enhanced outcoupling of organic light-emitting devices with an embedded low-index grid"

Enhancement of light outcoupling into substrate modes by a grid of low-refractive-index material embedded into the organic layer of an organic light-emitting device (OLED) is analyzed using full-wave electromagnetic simulations. The low-index grid (LIG) redirects modes normally trapped within the high-index organic and indium tin oxide layers (waveguide modes) into the substrate where they can be further extracted into free space using methods such as microlens arrays or roughened surfaces. This increases the external quantum and power efficiencies without affecting the electroluminescent spectrum. The dependence on grid geometry, dimensions, and refractive index is explored to optimize the structure. Simulations show that up to 50% more light can be extracted from the high-index region using an ultralow-index (n=1.03)grid than a conventional device, and provided efficient substrate-to-air outcoupling, the external quantum efficiencies of LIG OLEDs can reach 50%. [J804]

"Intramolecular energy transfer between the triplet of ancillary ligand and the metal to ligand charge transfer state existed in heterocyclometalated iridium (III) complexes"

Higher efficiency red organic light emitting devices (OLEDs) were obtained by employing Ir (III) complexes with 1-phenylbutane-1, 3-dione (ba) as the second ligand than that with acetylacetone (acac) as the second ligand, which were attributed to the intramolecular energy transfer existed in these complexes. The reason were attributed to the intramolecular energy transfer existed in these complexes and were approved by their photoluminescence characteristics at 77 K, as well the phosphorescence decay lifetime. Because of the lower triplet energy level of ba (Tba,19 230cm⁻¹)whose energy was suitable to transfer to the triplet of the metal to ligand charge transfer (MLCT) (3MLCT,16 260cm⁻¹)state compared to Tacac(25 500cm⁻¹), more efficient OLEDs were obtained (7.0 cd/A) using Ir[2-(4'-methanoxystyryl)-benzothiazole]2ba(ba-2) than Ir[2-(4'-methanoxystyryl)-benzothiazole]2acacacac-2 (6.1 cd/A). [J805]

"White phosphorescent organic light-emitting devices with dual triple-doped emissive layers"

We demonstrate high efficiency white organic light-emitting devices with two adjacent emissive layers each doped with three phosphorescent emitters (blue, green, and red). Efficient charge and exciton confinement is realized by employing charge transport layers with high triplet energy, leading to a maximum external quantum efficiency of (19±1)%. Using the p-i-ndevice structure, we have achieved a peak power efficiency of (40±2)lm/Wand (36±2)lm/Wat 100cd/m², a color rendering index of 79, and Commission Internationale de L'Eclairage coordinates of (0.37, 0.40) for the white light emission. [J806]

"GaN-based light-emitting diode with textured indium tin oxide transparent layer coated with Al₂O₃ powder"

Surface-textured InGaN/GaN light-emitting diodes (LEDs) coated with transparent Al₂O₃powder were fabricated

by natural lithography combined with inductively coupled plasma etching. For surface texturing, 300 nm size Al₂O₃ powder is used as an etching mask by simply coating the surface using a spin-coating process. Also, the powders are left on the surface after surface texturing to further increase extraction efficiency. At 20 mA, the light output power of the textured indium tin oxide (ITO) InGaN/GaN LEDs coated with the Al₂O₃ powder is enhanced by 112% compared with the conventional nontextured ITO LED. The enhanced light output power is attributed to the improved extraction efficiency resulting from an overall decrease in the total internal reflection due to the textured surface and the Al₂O₃ powder coating. [J807]

"Erratum: "ZnO light-emitting diode grown by plasma-assisted metal organic chemical vapor deposition" [JAppl. Phys. Lett. 88, 173506 (2006)]"

First Page of the Article [J808]

"Surface plasmon-enhanced spontaneous emission rate in an organic light-emitting device structure: Cathode structure for plasmonic application"

The surface plasmon-enhanced spontaneous emission based on an organic light-emitting device is reported in this paper. For surface plasmon localization, silver nanoparticles were thermally deposited in a high vacuum on cathode that had a 1-nm-thick LiF spacer. Since plasmons provide a strong oscillator decay channel, time-resolved photoluminescence (PL) results displayed a 1.75-fold increased emission rate, and continuous wave PL results showed a twofold enhanced intensity. In addition, LiF film/Ag cluster/LiF film structure resolved the carrier injection problem between the cathode and the organic layer. Thus, the suggested design may follow plasmonic applications for a wider organic optoelectronics. [J809]

"Highly phosphorescent organic mixed films: The effect of aggregation on triplet-triplet annihilation"

The efficiency roll-off at high brightness levels is a key factor limiting the application of organic light emitting diodes. We investigate triplet-triplet annihilation in an archetype phosphorescent host-guest system. We show that the currently used host-guest systems are not at the physical limit set by intrinsic annihilation, but have an increased roll-off due to aggregate formation. The existence of these aggregates is directly proven by transmission electron microscopy. [J810]

"Comment on "Control of magnetic-field effect on electro-luminescence in Alq 3 -based organic light emitting diodes" [JAppl. Phys. Lett. 88, 123501 (2006)]"

In a recently published paper by [Odaka et al, Appl. Phys. Lett. 88, 123501 (2006)], the authors explain their experimental observations of a weak magnetic field effect on electroluminescence from Alq₃-based light emitting diodes by the magnetic field-induced evolution of singlet-to-triplet spin conversion of loosely bound electron-hole pairs, suggesting the originality of their explanation. [J811]

"The Structure of GaN-Based Transverse Junction Blue LED Array for Uniform Distribution of Injected Current/Carriers"

In this study, we demonstrate a GaN-based transverse junction blue LED array. This device was realized by the regrowth of n-type GaN layers on the sidewall of p-type GaN and undoped multiple quantum wells (MQWs). Due to the transverse flow of injection carriers, problems related to nonuniform current distribution, nonuniform carrier distribution among different MQWs, and bias-dependent shape of the electroluminescence spectra such as that occurring in traditional GaN-based blue LEDs with vertical p-n junctions and large active area (>1 mm²) are all greatly minimized in our structure. [J812]

"Improved Output Power of 380 nm InGaN-Based LEDs Using a Heavily Mg-Doped GaN Insertion Layer Technique"

High-performance InGaN-based 380 nm UV LEDs are fabricated by using a heavily Mg-doped GaN insertion layer (HD-IL) technique. Based on the transmission electron microscopy, etch pit density, and cathodoluminescence results, the HD-IL technique can substantially reduce the defect density of GaN layer. The double-crystal X-ray diffraction results are in good agreement with those observations. The internal quantum efficiency of LED sample with an HD-IL shows around 40% improvement compared with the LED sample without the use of HD-IL. When the vertical-type LED chips (size: 1 mm times 1 mm) are driven by a 350 mA current, the output powers of the LEDs with and without an HD-IL are measured to be 203.4 and 158.9 mW, respectively. As much as 28% increased light output power is achieved. [J813]

"Enhanced Light Extraction by Photonic Quasi-Crystals in GaN Blue LEDs"

The far-field profile of photonic quasi-crystal patterned and unpatterned LEDs, fabricated from commercial epitaxial substrates by electron beam lithography, has been measured prior to lapping and dicing. Emission enhancements reach a maximum of 62%, and are strongly dependent on the filling factor. Qualitative agreement is achieved between 2-D finite-difference time-domain calculations and the experimental data. [J814]

"Novel Epitaxial Nanostructures for the Improvement of InGaN LEDs Efficiency"

We demonstrated that the efficiency of an InGaN LED can be improved by using a novel epitaxial nanostructure, namely, the nanostructured semipolar (NSSP) gallium nitride (GaN). The NSSP GaN template was fabricated on a c-plane GaN surface using a standard GaN metal-organic chemical vapor deposition tool on c-plane sapphire substrates. We showed that the surface of NSSP GaN consisted of two semipolar orientations: (10-11) and (11-22). InGaN/GaN multiple quantum wells (MQWs) fabricated on NSSP GaN exhibited negligible quantum-confined Stark effect (QCSE) and a 30% improvement in internal quantum efficiency as compared to planar c-plane InGaN/GaN MQWs. Using time-resolved photoluminescence (PL), a considerable improvement in radiative recombination lifetime was also observed. We fabricated and characterized semipolar InGaN LEDs on NSSP GaN that emitted at 543 nm and showed negligible QCSE. The NSSP GaN structure can also be applied to improve the photon extraction efficiency of InGaN-based LEDs. The surface texturing was performed insitotogether with the LED epitaxy without additional exsituetching processes. The insitusurface texturing improved the PL intensity by a factor of two. An electrical injection LED structure employing insitusurface texturing was also demonstrated. [J815]

"Design Optimization of Photonic Crystal Structure for Improved Light Extraction of GaN LED"

We performed a theoretical analysis on improved light extraction efficiency of LEDs with photonic crystals (PCs). The light propagation and extraction of PC LEDs were simulated using the finite-difference time-domain method for various PC LED structures. LEDs with both top and bottom PCs and PC LEDs grown on patterned substrates were considered to maximize light extraction efficiency. The design parameters of the PC were varied, and optimized values were obtained. A disordered PC was simulated, and we showed that the light extraction efficiency of a disordered PC was nearly equivalent to that of an ordered PC with the same pattern periodicity. This result revealed that the increased light extraction of PC LEDs was mainly due to scattering. Moreover, by comparing the enhancement of PC LEDs with different shapes of air holes, we showed that only the density of holes and the area occupied by holes play important roles in light extraction. The shapes of the holes have no strong effect on the enhancement of light extraction. [J816]

"Control of Quantum-Confined Stark Effect in InGaN-Based Quantum Wells"

This paper reviews current technological developments in polarization engineering and the control of the quantum-confined Stark effect (QCSE) for $\text{In}_x\text{Ga}_{1-x}\text{N}$ -based quantum-well active regions, which are generally employed in visible LEDs for solid-state lighting applications. First, the origin of the QCSE in III-N wurtzite semiconductors is introduced, and polarization-induced internal fields are discussed in order to provide contextual background. Next, the optical and electrical properties of $\text{In}_x\text{Ga}_{1-x}\text{N}$ -based quantum wells that are affected by the QCSE are described. Finally, several methods for controlling the QCSE of $\text{In}_x\text{Ga}_{1-x}\text{N}$ -based quantum wells are discussed in the context of performance metrics of visible light emitters, considering both pros and cons. These strategies include doping control, strain/polarization field/electronic band structure control, growth direction control, and crystalline structure control. [J817]

"High Energy Gap OLED Host Materials for Green and Blue PHOLED Materials"

In this paper, we developed a series of novel arylamino-containing spiro triplet state host materials for green and blue phosphorescent emitters. With high enough energy gap and compatible HOMO, LUMO levels, we demonstrated the green PHOLED with a low driving voltage of 2.5 V and a high power efficiency of 38.5 lm/W. We also demonstrated blue PHOLED with a very low driving voltage of 3.0 V and a current efficiency of 9.2 cd/A. [J818]

"Innovative Voltage Driving Pixel Circuit Using Organic Thin-Film Transistor for AMOLEDs"

In this work, we propose a novel active-matrix organic light-emitting diode displays (AMOLED) pixel circuit based on organic thin-film transistor (OTFT) architecture, which consisted of four switches, one driving transistor, and a capacitor. The pentacene-based OTFT device possesses a field-effect mobility of 0.1 $\text{cm}^2/\text{V s}$, a threshold voltage of -1.5 V, subthreshold slope of 1.8 V/decade and an on/off current ratio 106. The resultant voltage-driving pixel circuit, named I^2C (complementary voltage-induced coupling driving) (CVICD), is different from

the current-driving scheme and can appropriately operate at low gray level for the low-mobility OTFT circuitry. The current non-uniformity less than 2.9% is achieved for data voltage ranging from 1 to 17 V by SPICE simulation work. In addition, the new external driving method can effectively reduce the complexity of OLED pixel circuitry. [J819]

"Human Gait Acquisition and Characterization"

This paper analyzes human motion, more specifically the human gait in the sagittal plane. A video camera is used to acquire images of a walking person, fitted with a set of white light-emitting diodes (LEDs). The acquired trajectories of the light points are then used to specify joint trajectories in a biped robot. To analyze the stability of the human gait, a system was also developed to acquire the center of pressure (CoP). This system uses eight force sensors, four under each foot. The influence of the human torso angle on the CoP position during walking was confirmed. Some experiments were carried out on a biped robot, and the results show that the acquired human gait can be used in a biped robot, after scale conversion. [J820]

"Mitigating energy wastage of light-emitting diodes using discretised multilevel pulsation"

There is a recent trend and growing popularity of using the technique of light pulsation for achieving the dimming control of light-emitting diodes. However, it is found that such a dimming control technique can result in a significant power loss in terms of luminous efficacy. This contradicts the original motive of energy saving through illumination dimming. Total energy consumed for lighting is an overwhelming 8% of depleting energy resources. A potential loss of 2% or more of these resources could go unnoticed owing to poor handling of dimming technology. It is demonstrated that, driving the LEDs with discretised multilevel pulsation, can achieve a quasi-optimally-efficient state of dimming control with a saving of up to 26.7% of the luminous efficacy. [J821]

"Surface Texturing of High-Power Flip-Chip LEDs by Femtosecond Laser Direct Structuring"

We report on the femtosecond laser direct structuring of the sapphire flipside surfaces of high-power flip-chip LEDs. It is found that diameter and depth of the created submicrometer-sized holes can be manipulated by varying the laser power at a constant number of laser pulses. This method enables the control of the structure sizes with high precision. Our study shows that the light extraction from such LEDs increases strongly with increasing hole sizes. [J822]

"Investigation of Ce:YAG Doping Effect on Thermal Aging for High-Power Phosphor-Converted White-Light-Emitting Diodes"

In this paper, high-power phosphor-converted white-light-emitting diodes (PC-LEDs) with selected concentration and thickness of cerium-doped yttrium aluminum garnet (Ce:YAG) phosphor-doped silicones are investigated to study the thermal-degradation effect of the Ce:YAG phosphor-silicone layer. The experimental results showed that the lumen loss, chromaticity (CIE shift), and spectrum intensity reduction increase as the concentration of Ce:YAG phosphor-doped silicone increases. Although silicone degradation attributed to the final thermal degradation, it is not a dominant factor until a much thicker silicone is employed in PC-LEDs. The major degradation mechanism of the PC-LEDs results from the higher doping concentration of Ce:YAG in silicone. We found that 94% lumen loss was attributed to 5.5 wt% Ce:YAG doping and only 6% of the lumen loss was due to a 1-mm thickness of silicone degradation. However, the negligible differences of measured fluorescent lifetimes among the test samples before and after thermal aging (at 150 degC for 500 h) eliminated any significant nonradioactive quenching processes that existed in the aged samples. The emission spectra indicate that a higher doping concentration in silicone causes a higher degree of loss at the emission wavelength of Ce:YAG. Therefore, minimizing any unwanted interactions, such as refractive index and thermal-expansion mismatches, between the phosphor and the silicone during thermal aging is a new direction of addressing thermal reliability for high-power PC-LEDs. From practical points of view, we found that a lower doping concentration of the Ce:YAG phosphor in thin silicone is a better choice in terms of having less thermal degradation for use in packaging of the high-power PC-LEDs modules and is essential to extend the operating lifetime of the phosphor-based white LED modules. [J823]

"Means of Eliminating Electrolytic Capacitor in AC/DC Power Supplies for LED Lightings"

This paper proposes two methods of reducing the storage capacitance in the ac/dc power supplies for light emitting diode (LED) lighting. In doing so, film capacitors can be adopted instead of electrolytic capacitors to achieve a long power supplies lifetime. The voltage ripple of the storage capacitor is intentionally increased to reduce the storage capacitance. The method of determining the storage capacitance for ensuring that the boost power factor correction converter operates normally in the whole input voltage range is also discussed. For the purpose of further reducing the storage capacitance, a method of injecting the third harmonic current into the

input current flow is proposed. While ensuring that the input power factor is always higher than 0.9 to comply with regulation standards such as ENERGY STAR, the storage capacitance can be reduced to 65.6% of that with an input power factor of 1. A 60-W experimental prototype is built to verify the proposed methods. [J824]

"Geometrical Shaping of InGaN Light-Emitting Diodes by Laser Micromachining"

Geometrical shaping of InGaN light-emitting diodes (LEDs) by laser micromachining is introduced. The sapphire substrate is shaped with inclined sidewalls at 50deg, serving as a prism favoring light redirection for out-coupling from the top window. Compared to conventional cuboid LEDs with a calculated light extraction efficiency η_{ext} of 18.3%, these shaped LEDs offers a pronounced increase in η_{ext} up to 85.2%, verified by experimental results. [J825]

"Application of Nanosphere Lithography to LED Surface Texturing and to the Fabrication of Nanorod LED Arrays"

In this study, the process of nanosphere lithography was developed and applied to LED surface texturing and nanorod device fabrication. We observed a texture-size-dependent improvement of total light output. While the increase of output optical power from the textured LEDs can be attributed to surface roughening in the GaN-air surface and to the increase of internal quantum efficiency as the strain is relaxed with the surface texturing, the size-dependent device performance is related to the interaction of generated photons with the textured surface. We further etched through the p-GaN and quantum well region to form p-i-n nanorods on the sample. By inserting a spacer to prevent p-type contact from shorting the n-GaN, we successfully demonstrated nanorod LED arrays. For such a device, a narrower radiation profile was demonstrated from the nanorod LED array as compared with that from the planar LED. The result is associated with the vertical guiding effect along the nanorod cylinder and the Bragg scattering of photons extracted from the sidewall by the rest of the rods. Furthermore, the electroluminescence spectra showed a nearly constant peak wavelength of the nanorod LED arrays, which is due to the suppression of the effect of quantum confined Stark effect. [J826]

"LED Permanent Emergency Lighting System Based on a Single Magnetic Component"

The use of high-efficiency LEDs in low-power lighting applications is growing continuously due to new advances in LED features. The lifetime of a low-power fluorescent lamp is around 5000 h. This implies short lamp-replacement times and high maintenance costs. The use of high-efficiency LEDs reduces drastically the maintenance costs due to the long lifetime (>50 000 h). One of the applications where using LED is very interesting is permanent emergency light systems. Generally, these circuits are based on a two-stage design, using two magnetic cores. This paper presents offline power LED driver and battery charger integrated in one magnetic core topology. Besides, the converter allows driving the LEDs in case of a line failure and it complies with the IEC 61000-3-2 Class C Standard. [J827]

"100-Mb/s NRZ Visible Light Communications Using a Postequalized White LED"

This letter describes a high-speed visible light communications link that uses a white-light light-emitting diode (LED). Such devices have bandwidths of few megahertz, severely limiting the data rates of any communication system. Here, we demonstrate that by detecting only the blue component of the LED, and using a simple first-order analogue equalizer, a data rate of 100 Mb/s can be achieved using on-off keying nonreturn-to-zero modulation. [J828]

"Optimization of Light Extraction Efficiency of III-Nitride LEDs With Self-Assembled Colloidal-Based Microlenses"

Improvement of light extraction efficiency of InGaN LEDs using colloidal-based SiO₂/polystyrene (PS) microlens arrays was demonstrated. The size effect of the SiO₂ microspheres and the thickness effect of the PS layer on the light extraction efficiency of III-nitride LEDs were studied. The monolayer rapid convective deposition conditions for SiO₂ microspheres were also investigated. Ray tracing simulations show that the use of microlens arrays can lead to increase in light extraction efficiency of InGaN LEDs by 2.64 times. This is consistent with experiments that demonstrated 2.49 times improvement in light extraction utilizing SiO₂/PS microlens arrays. The enhancement in light extraction efficiency is attributed to increase in effective photon escape cone due to SiO₂/PS microlens arrays, and reduced Fresnel reflection within the photon escape cone due to the grading of refractive index change between GaN/SiO₂/PS/air interface. [J829]

"Effect of Residual Stress and Sidewall Emission of InGaN-Based LED by Varying Sapphire Substrate Thickness"

The effect of residual stress and the sidewall emission in InGaN-GaN films with different thickness of sapphire substrate were investigated. The peak wavelength of electroluminescence was blue-shifted as thinning the sapphire substrate, because the wafer bowing-induced mechanical stress alters the piezoelectric field in the InGaN-GaN multiple quantum-well active region of the light-emitting diode (LED). A sideview LED with 170- μm -thick sapphire exhibited the highest output power of 14.04 mW at a forward current of 20 mA, improved by 7% compared to that with 80- μm -thick sapphire. The maximum output power can be obtained by considering both the photon escaping probability from the edges of the sapphire and the photon absorption probability in the sapphire as well as the residual mechanical stress induced by the wafer bowing. [J830]

"Tolerance Design of an Optomechanical Transmitter Assembly for Automotive Applications"

We report on different optical coupling concepts between resonant-cavity light-emitting diodes and plastic optical fiber for the automotive according to the multimedia oriented systems transport standard. We present five different candidate optical coupling schemes. Two coupling schemes were investigated in depth regarding manufacturing and assembly tolerances using a Monte Carlo simulation method: a system using a ball lens and another made by clear molding. We select the best suited system according to manufacturing and assembly capabilities as well as its suitability for automotive applications. [J831]

"Fabrication of the InGaN-Based Light-Emitting Diodes Through a Photoelectrochemical Process"

InGaN-based light-emitting diodes (LEDs) with a lateral-etched (LE) undercut structure were fabricated through a photoelectrochemical-etching process. The LE-LED was fabricated with an undercut structure, where the InGaN layer acted as a sacrificial layer without reducing the effective emission area. The electroluminescence (EL) spectrum of the LE-LED had a wavelength blueshift phenomenon of 4.6 nm when compared with a standard-LED (ST-LED) at a 30-A/cm² current density. The wavelength blueshift phenomenon of the EL emission peaks were measured as 5.5 and 4.3 nm by varying the injection current density from 1.5 to 30 A/cm² for the ST-LED and the LE-LED. In a bias-dependent micro-photoluminescence measurement, the blueshift phenomenon of a peak wavelength for the LE-LED was smaller than for the ST-LED. These results were attributed to a partially reduced piezoelectric field in the InGaN active layer and larger light extraction efficiency in the LE-LED structure. [J832]

"Code Division-Based Sensing of Illumination Contributions in Solid-State Lighting Systems"

Light-emitting diodes (LEDs) have emerged as a prime candidate for the light source of the future. To enable easy user interaction with a future lighting system consisting of many LEDs, this paper proposes a method to accurately measure and estimate the local light contributions of a large set of LEDs. This is enabled through tagging the light of each LED with a unique identifier. To this end, we propose a new family of modulation and multiple access schemes in this paper, named code-time division multiple access-pulse position modulation (CTDMA-PPM) and CTDMA-pulse width modulation (CTDMA-PWM). These schemes satisfy illumination constraints, are compatible with the commonly used PWM dimming of LEDs, and meet the multi-signal separation requirements for simultaneous measurement of illumination strengths. Based on these modulation methods, the paper develops algorithms to estimate illumination. Finally, performance analyses show that even for a very large number of LEDs, the sensing performance of the proposed system satisfies the requirements up to an adequate range. [J833]

"Illumination Sensing in LED Lighting Systems Based on Frequency-Division Multiplexing"

Recently, light emitting diode (LED) based illumination systems have attracted considerable research interest. Such systems normally consist of a large number of LEDs. In order to facilitate the control of such high-complexity system, a novel signal processing application, namely illumination sensing, is thus studied. In this paper, the system concept and research challenges of illumination sensing are presented. Thereafter, we investigate a frequency-division multiplexing (FDM) scheme to distinguish the signals from different LEDs, such that we are able to estimate the illuminances of all the LEDs simultaneously. Moreover, a filter bank sensor structure is proposed to study the key properties of the FDM scheme. Conditions on the design of the filter response are imposed for the ideal case without the existence of any frequency inaccuracy, as well as for the case with frequency inaccuracies. The maximum number of LEDs that can be supported for each case is also derived. In particular, it is shown that, among all the other considered functions, the use of the triangular function is able to give a better tradeoff between the number of LEDs that can be supported and the allowable clock inaccuracies within a practical range. Moreover, through numerical investigations, we show that many tens of LEDs can be supported for the considered system parameters. Remark on the low-cost implementations of the proposed sensor structure is also provided. [J834]

"Multiwavelength Optical Source for OCDM Using Sinusoidally Modulated Laser Diode"

This paper reports a novel cost-effective multiwavelength optical source for OCDM. This source has a simple configuration and emits well-flattened light with a precisely controlled wavelength spacing by using a directly sinusoidally modulated laser diode technique. The flattened multiwavelength light generation is analytically evaluated by using a small signal approximation. The application of the proposed optical source to OCDM was demonstrated experimentally. [J835]

"Wireless UV sensor based on photocapacitive effect in GaN"

The LC oscillator with the interdigitated aluminium-on-GaN/sapphire photo capacitor has been demonstrated. Upon illumination with a 375 nm UV LED, an oscillator frequency downshift owing to the photo capacitive effect attains 5.2 MHz (3.5 of the dark frequency value 149 MHz) with sensitivity up to 170 kHz/($\mu\text{W}/\text{cm}^2$). The oscillator can be employed as a visible-blind UV sensor with a remote wireless pickup of the RF output signal. [J836]

"Technique Makes Strong Encryption Easier to Use"

Organizations are beginning to adopt identity-based encryption (IBE), a communications-protection process that promises to make public-key cryptography easier to use. Public-key cryptography uses paired keys for encrypting and decrypting messages, to protect electronic communications over public networks such as the Internet. [J837]

"LEDs for Solid-State Lighting: Performance Challenges and Recent Advances"

Over the past decade, advances in LEDs have enabled the potential for wide-scale replacement of traditional lighting with solid-state light sources. If LED performance targets are realized, solid-state lighting will provide significant energy savings, important environmental benefits, and dramatically new ways to utilize and control light. In this paper, we review LED performance targets that are needed to achieve these benefits and highlight some of the remaining technical challenges. We describe recent advances in LED materials and novel device concepts that show promise for realizing the full potential of LED-based white lighting. [J838]

"The Effect of the Phosphor Particle Sizes on the Angular Homogeneity of Phosphor-Converted High-Power White LED Light Sources"

Based on optical ray tracing, we discuss the effect of the phosphor particle sizes on the angular homogeneity of the light emitted from phosphor-converted LEDs. Since the blue LED and the yellow-converted light have rather different emission characteristics, which have to be harmonized to one another by the scattering processes within the color conversion element, the phosphor particle size turns out to be an essential parameter in order to attain angular homogeneity. This can be attributed, on the one hand, to the number of scattering processes within a specific unit volume for a given phosphor concentration, and on the other hand, to the specific scattering functions, both of which depend on the phosphor particle diameter. [J839]

"Metalorganic Vapor Phase Epitaxy of III-Nitride Light-Emitting Diodes on Nanopatterned AGOG Sapphire Substrate by Abbreviated Growth Mode"

Metalorganic vapor phase epitaxial (MOVPE) growth of GaN on nanopatterned AGOG sapphire substrates was performed, and characteristics of the light-emitting diode (LED) devices grown on patterned sapphire and planar substrates were compared. The nanopatterned sapphire substrates were fabricated by a novel process (AGOG) whereby aluminum nanomesas were epitaxially converted into crystalline Al_2O_3 via a two-stage annealing process. The GaN template grown on the nanopatterned sapphire substrate was done via an abbreviated growth mode, where a 15-nm thick, low-temperature GaN buffer layer was used, without the use of an etch-back and recovery process during the epitaxy. InGaN quantum wells (QWs) LEDs were grown on the GaN template on the nanopatterned sapphire, employing the abbreviated growth mode. The optimized InGaN QW LEDs grown on the patterned AGOG sapphire substrate exhibited a 24% improvement in output power as compared to LEDs on GaN templates grown using the conventional method. The increase in output power of the LEDs is attributed to improved internal quantum efficiency of the LEDs. [J840]

"Electrically pumped, micro-cavity based single photon source driven at 1 GHz"

A resonant cavity light emitting diode combined with a submicron oxide current aperture, to pump individual InGaAs/GaAs quantum dots electrically, has been designed and fabricated. Pulsed correlation measurements demonstrated true single photon emission with $g_2(0)=0$ at a rate of 1 GHz. [J841]

"High-Power MWIR Cascaded InAs-GaSb Superlattice LEDs"

Midwave IR LEDs operating at 3.8 μm with output powers approaching 25 mW at 77 K are reported. Devices based on the InAs-GaSb superlattice material system grown by solid source molecular beam epitaxy are demonstrated in a cascaded active region configuration as high-power IR emitters. Optical and electronic characteristics of 16-stage devices with variable mesa size were examined to assess the performance dependence on device size and injection current. The results are suggestive that output power saturation was due to thermal management limitations and carrier leakage out of the active region. Reported output power measurements were taken without the use of an immersion lens or other collection optics, thus representing the upper hemisphere output. Devices were also demonstrated to generate an upper hemisphere power exceeding 1.4 mW at 220 K under quasi-DC excitation conditions. [J842]

"The reality: Academic research to commercial product, part 2-[Tried and true]"

The NRE for even a conceptually simple system (the car parking system) can easily be US \$1 million or more. Development can take a year or more to complete the design and prepare for manufacturing, distribution, and installation. The NRE for a medical device or safety-critical system can easily cost more than US \$12 million and take five or more years to complete. That cost represents only development up to the point at which one would be ready to manufacture, distribute, and install (or implant) products. Obviously, these numbers vary according to the project, but they do indicate that a lot of engineering and effort go into taking a proof-of-concept and realizing a commercial product that is ready for sale. If your proof-of-concept cost is US \$50,000 to develop, then you have only realized 5% or less of the cost and effort required to render it a commercial product. [J843]

"Decay Mechanisms of Radiation Pattern and Optical Spectrum of High-Power LED Modules in Aging Test"

Decay of radiation pattern and optical spectrum of high-power LED modules fabricated by different manufacturers after a thermal-aging test were investigated experimentally and numerically. Samples were aged at 65degC, 85degC, and 95degC under a constant current of 350 mA. The results showed that the radiation pattern of the LED modules at the two view angles of plusmn(45deg ~ 75deg) decreased more than the other angles as aging time increased. This was due to the reduction of optical power from corner shape of lens. Due to the degradation of lens material after thermal aging, the center wavelength of the LED spectrum shifted 5 nm. Furthermore, the radius curvature of plastic lens was observed to have 6-70 μm contraction as aging times increased. The key module package related to the decrease of power density, the change of radiation pattern, and the shift of optical spectrum in high-power LED modules under thermal aging were due to the degradation of lens material and lens structure. Both experimental and simulated results clearly indicated that improving the lens structure and lens material is essential to extend the operating life of the high-power LED modules. This study may provide practical LED package guidelines in low-cost consumer applications. [J844]

"Optical Feedback Self-Mixing Interferometry With a Large Feedback Factor : Behavior Studies"

This paper studies the behavior of optical feedback self-mixing interferometric (OFSMI) systems, where the semiconductor lasers operate at a single mode (perturbed external cavity mode) with a large optical feedback factor C . Based on analysis of the spectral linewidth associated with all the possible lasing modes at different C values, a set of mode jumping rules are proposed following the minimum linewidth mode competition principle proposed in . According to the rules, the C factor can be classified into different regions, on which an OFSMI system will exhibit distinct phenomena. In particular, for the same amount of displacement associated with the external cavity, the fringe number reduction on the OFSMI signal should be observed when C increases from one region to the next. An experimental setup with a laser diode HL7851G was implemented and employed to verify the proposed rules. The behavior of the OFSMI predicted by the paper has been confirmed by the experiments with C value up to 8.0. [J845]

"Probing of carrier behavior in organic electroluminescent diode using electric field induced optical second-harmonic generation measurement"

By using the electric field induced optical second-harmonic generation (EFISHG) measurements, we probed the transient electric field in a double-layer indium zinc oxide (IZO)/N, N'-di-[(1-naphthyl)-N,N'-diphenyl]-(1,1'-biphenyl)-4, 4'-diamine(alpha -NPD)/tris(8-hydroxy-quinolinato)aluminum(III)(Alq3)/Al electroluminescent (EL) diode. Results evidently showed that EL was initiated by the injected hole transport across alpha -NPD layer, and holes accumulated at the alpha -NPD/Alq3 interface while EL was enhanced. Analysis based on the Maxwell-Wagner effect model well accounted for the hole accumulation. EFISHG measurement is useful as a tool for probing carrier behavior in organic EL devices. [J846]

"Role of photovoltaic effects on characterizing emission properties of InGaN/GaN light emitting diodes"

Strong photovoltaic effects on photoluminescence (PL) spectra in InGaN/GaN blue light emitting diodes were investigated. Due to severe carrier escape from quantum wells, significant photovoltaic effects occur in PL measurement in open-circuit condition, which strongly affect the PL peak position and intensity. We reveal that proper correlation between electroluminescence and PL peak positions cannot be obtained without proper consideration of the photovoltaic effects. By changing sample temperature and the PL excitation power, the generated photovoltage varies in the range of 2.0 to 2.6 V. We show that in the open-circuit condition, which is the usual case, the determination of radiative efficiency by measuring the PL intensity ratio of low- and high-temperature cannot be accurate, and the excitation intensity dependent PL cannot be solely intrinsic either. Both the absorption of incident laser and the carrier escape from the quantum well are bias-sensitive. By a simple and straightforward method, we determined that 51% of photogenerated carriers escaped in short-circuit condition.

[J847]

"In situ measurement of the internal luminescence quantum efficiency in organic light-emitting diodes"

The internal luminescence quantum efficiency is one limiting factor for the performance of organic light-emitting diodes. Photoluminescence measurements are frequently used to estimate η_{int} but these neglect effects of the local environment of the emissive sites and the electrical excitation mechanism. We present a method for the in situ measurement of η_{int} under electrical operation. The current efficiency of several devices with different emitter-cathode distances is quantitatively compared. Precise optical simulation allows determining η_{int} without additional assumptions. [J848]

"Triplet annihilation exceeding spin statistical limit in highly efficient fluorescent organic light-emitting diodes"

We have demonstrated that the exemplary red fluorescent organic light-emitting diodes (OLEDs) gain as much as half of their electroluminescence from annihilation of triplet states generated by recombining charge carriers. The magnitude of triplet-triplet annihilation (TTA) contribution in combination with the remarkably high total efficiencies [11% external quantum efficiency (EQE)] indicates that the absolute amount of electroluminescence attributable to TTA substantially exceeds the limit imposed by spin statistics, which was independently confirmed by studying magnetic field effects on delayed luminescence. We determined the value of 1.3 for the ratio of the rate constants of singlet and triplet channels of annihilation, which is indeed substantially higher than the value of 0.33 expected for a purely statistical annihilation process. It is, however, in an excellent quantitative agreement with the extent of the experimental contribution of delayed luminescence to steady-state electroluminescence. The nonstatistical branching ratio of the two annihilation channels is attributed to the favorable relationship between the energies of the excited singlet and triplet states of rubrene-emissive layer host. We surmise that, with the appropriate emissive layer materials, the fluorescent OLED devices are capable of using a considerably larger fraction of triplet states than was previously believed. In principle, the upper limit for the singlet excited state yield in the TTA process is 0.5, which makes the maximum internal quantum efficiency of fluorescent OLEDs to be $25\% + 0.5 \times 47.5\% = 62.5\%$. The estimates of maximum EQE of the fluorescent OLEDs should be revised to at least $0.2 \times 62.5\% = 12.5\%$ and, likely, even higher to account for optical outcoupling exceeding 0.2. [J849]

"Data driver architecture and driving scheme of AMOLED microdisplay for mobile projectors"

For a mobile projector application that can be embedded in a cellular phone, a 6-bit data driver integrated in a 0.4-inch diagonal VGA AMOLED on silicon substrate is proposed. The proposed data driver has a couple of features tailored for a microdisplay application: To be integrated with a very fine pixel pitch of 4.2 μm , the data driver uses a 33-degree demultiplexing scheme, thereby taking circuit area within the peripheral height of 810 μm . In addition, the separate gamma correction is provided to resolve the color shift problem due to the transmittance mismatch of red, green, and blue color filters. In spite of the separate gamma correction involved, the height of the data driver is not increased, because it is realized by making use of a time sharing method synchronized with the 33-degree demultiplexing. [J850]

"A real time video data adjusting method for active matrix organic light emitting diode displays with high image quality"

A real time video data adjusting method for television applications of active matrix organic light emitting diode

(AMOLED) displays with high image quality is proposed. The proposed method senses electrical characteristics of polycrystalline silicon (poly-Si) thin film transistors (TFTs) and organic light emitting diode (OLED) of pixels and compensates nonuniform luminance due to the electrical characteristic variations of TFTs and the degradation of OLEDs by adjusting video data. The sensing and compensation operations are performed while the image is displayed on the screen. Experimental results show that the luminance error is improved from 92.1% to 0.8% when the proposed adjusting method is used. The proposed method is demonstrated on 14.1-inch AMOLED display panel. [J851]

"Linearly polarized light emission from InGaN light emitting diode with subwavelength metallic nanograting"

Surface emitting linearly polarized InGaN/GaN light emitting diode (LED) is demonstrated using a subwavelength metallic nanograting. The aluminum based grating with a period of 150 nm is fabricated on top of the p-contact layer in a conventional InGaN LED structure grown on (0001) oriented sapphire substrate. Polarization ratio can reach 7:1, the highest ever reported polarization ratio directly from a light emitting diode. The polarization characteristics are studied in details both experimentally and theoretically, suggesting an effective way to make polarized light emission devices. [J852]

"An optical feedback system for local dimming backlight with RGB LEDs"

One of the major issues plaguing RGB LED backlight is color shift. This phenomenon is due to the characteristic changes of each Red, Green, and Blue LEDs as the time and temperature variation. To compensate this variation, many researchers are proposed color control method for the stable color management. However, their method is not suitable for the local dimming backlight because of the light interference between blocks. Therefore, we proposed an optical feedback system for the stable color control regardless of its dimming method. The test results show that our proposed method is very suitable for RGB LED backlights. [J853]

"Improved performance of GaN-based blue light emitting diodes with InGaN/GaN multilayer barriers"

Multi-layer barrier structure is suggested as an alternative approach to single-layer polarization matching barrier structure for the reduction of efficiency droop. Time resolved photoluminescence measurement showed that polarization field was reduced by 19% in the multilayer barrier light emitting diodes structures. Optical power measurements on packaged devices showed overall increase of external quantum efficiency for all currents up to the current density of 150A/cm². Increase of optical power is attributed to reduced polarization and decreased current overflow to p-side cladding layers. These results provide additional evidences that polarization is important in addressing the droop problem. [J854]

"Enhanced photoluminescence of strained Ge with a delta -doping SiGe layer on silicon and silicon-on-insulator"

An enhancement of the direct bandgap photoluminescence from Ge layer on silicon with boron or phosphorous delta -doping SiGe layers at room temperature is reported. The n-type delta -doping SiGe layer is proposed to transfer extra electrons to L valley in Ge, which decreases the possibility of the excited electrons in the Gamma valley to be scattered to the L valley, and improve the photoluminescence of the direct band transition in the Ge layer. Additionally, 2.5 fold enhancement of luminescence from the strained Ge layer on a silicon-on-insulator substrate is demonstrated due to the resonant effect. This investigation is very promising for efficient Si-based Ge light emitting diodes compatible with silicon technology. [J855]

"Using copper substrate to enhance the thermal conductivity of top-emission organic light-emitting diodes for improving the luminance efficiency and lifetime"

The influence of heat dissipation on the performances of organic light-emitting diode (OLED) is investigated by measuring junction temperature and by calculating the rate of heat flow. The calculated rate of heat flow reveals that the key factors include the thermal conductivity, the substrate thickness, and the UV glue. Moreover, the use of copper substrate can effectively dissipate the joule heat, which then reduces the temperature gradient. Finally, it is shown that the use of a high thermal conductivity thinner substrate can enhance the thermal conductivity of OLED and the luminance efficiency as well. [J856]

"A combined electro-optical method for the determination of the recombination parameters in InGaN-based light-emitting diodes"

We present an electro-optical method for the extrapolation of the nonradiative and Auger recombination coefficients in InGaN/GaN Light-emitting diodes (LEDs). The method has the advantage of permitting the extrapolation of the recombination parameters of packaged devices, contrary to conventional techniques based on the analysis of quasibulk structures. For the analyzed devices, the average values of the nonradiative and Auger recombination coefficients have been determined to be equal to $2.34 \cdot 10^{-1} \text{ s}^{-1}$ and $1.04 \cdot 10^{-30} \text{ cm}^6 \text{ s}^{-1}$, respectively. These results are consistent with previous reports based on the analysis of quasibulk structures and on theoretical simulations. The method described in this paper constitutes an efficient tool for the analysis of the recombination dynamics in GaN-based LEDs. The results obtained within this work support the hypothesis on the importance of Auger recombination in determining the so-called efficiency droop in LED structures. [J857]

"Demonstration on GaN-based light-emitting diodes grown on 3C-SiC/Si(111)"

GaN-based light-emitting diodes (LEDs) grown on template of 3C-SiC/Si(111) were demonstrated. The structural properties have been investigated systematically by means of atomic force microscopy, x-ray diffraction, and transmission electron microscopy. It is found that the intermediate layer (IL) of 3C-SiC leads to not only a significant improvement in the crystalline quality of GaN, but also better interfaces between the buffer layer and the initial layers of strained-layer superlattice. The device properties were also evaluated using the measurements of current-voltage, electroluminescence, and light output power-current. Compared to conventional LEDs that do not contain 3C-SiC IL, the device with IL exhibits enhanced output power by more than 200% at an injection current of 20 mA, and the operating voltage is slightly increased from 3.7 to 3.9 V. These results indicate that using 3C-SiC as IL is one of the promising approaches to improve the performance of LEDs on silicon. [J858]

"Improved hole injection and transport of organic light-emitting devices with an efficient p-doped hole-injection layer"

A 4,4',4"-tris(3-methylphenylphenylamino)triphenylamine thin film doped with Fe₃O₄ has been demonstrated an efficient p-type hole-injection layer (HIL) in organic light-emitting devices (OLEDs). The tris-(8-hydroxyquinoline) aluminum-based OLEDs with the p-type HIL exhibit a very low turn-on voltage of 2.4 V and a high luminance of 29 360 cd/m² at 8 V, while it is 3 V and 6005 cd/m², respectively, for the nondoped devices. The improvement in the device performance is clarified as arising from the improved hole injection and transport by the results of ultraviolet/visible/near-infrared absorption, x-ray photoelectron spectra and current density-voltage characteristics of hole-only devices. [J859]

"Hybrid p-n junction light-emitting diodes based on sputtered ZnO and organic semiconductors"

We fabricated light-emitting hybrid p-n junction devices using low temperature deposited ZnO and organic films, in which the ZnO and the organic films served as the n- and p-type component, respectively. The devices have a rectification factor as high as 10³ and a current density greater than 2 A/cm². Electroluminescence of the hybrid device shows the mixture of the emission bands arising from radiative charge recombination in organic and ZnO. The substantial device properties could provide various opportunities for low cost and large area multicolor light-emitting sources. [J860]

"Improved performance of blue phosphorescent organic light-emitting diodes with a mixed host system"

We have investigated a relationship between device performances and host properties in the emissive layer (EML) of iridium(III) bis(4',6'-difluorophenylpyridinato)tetrakis(1-pyrazolyl)borate doped blue phosphorescent organic light-emitting diodes (PHOLEDs). We found that the recombination zone as well as charge carrier injection properties of the EML could be systematically engineered through a mixed host system. Therefore, light-emitting performances of blue PHOLEDs were greatly improved with external quantum and power efficiencies of 20.5% and 43.5 lm/W at a luminance of 56 cd/m², respectively. [J861]

"Low-Oxygen-Saturation Quantification in Human Arterial and Venous Circulation"

Conventional pulse oximetry has limited accuracy in measuring blood oxygen saturation in low-saturation and -perfusion scenarios. This limits the application of pulse oximetry in patients suffering from peripheral vascular afflictions. We present a novel pulse oximetry system that proposes solutions to these low-saturation and -perfusion scenarios by inducing an artificial pulse in the detected photoplethysmograph (PPG). A novel arteriovenous hypothesis was formulated to extract arterial and venous saturation data from the artificial PPG using arterial-to-venous compliance ratios. Sensor wavelengths were selected to provide high- and low-saturation accuracy, followed by an invivosensor calibration procedure. System performance was validated by

means of an invivoprocedure. Invivoresults indicate good accuracy for high saturation, with limited accuracy in low-saturation scenarios. The arteriovenous hypothesis was validated, indicating that venous saturation can be extracted from the artificial PPG. The results indicate that the proposed system might be able to accurately monitor arterial and venous saturation in low- or no-perfusion scenarios. It is recommended that further studies into the system's performance are conducted. [J862]

"Efficient Alternating Current Operated White Light-Emitting Diode Chip"

The structure of a single light-emitting diode (LED) chip for operation under high voltage alternating current (ac) conditions was proposed. The chip was designed and fabricated as an integrated circuit with several isolated LED structures grown on a single insulated sapphire substrate. The efficient blue LED chip for operation directly from 220-V ac power source has been designed, fabricated, and analyzed. The white ac operated LED (ACOLED) chip demonstrates a value of averaged luminous flux ~ 320 lm and luminous efficiency 80 lm/W under operation from 220-V ac source with 4 W of power consumption. The ladder type of circuit and the efficient ACOLED chip configuration results in proficient operation under ac conditions. [J863]

"Extraction Efficiency Enhancement of GaN-Based Light-Emitting Diodes by Microhole Array and Roughened Surface Oxide"

The light-output power of GaN-based light-emitting diodes (LEDs) was enhanced by microhole array pattern and roughened GaOxfilm grown on the exposed surface. The GaOxfilm was grown by photoelectrochemical (PEC) oxidation via H₂O and formed a naturally rough oxide surface and GaOx/GaN interface. Compared with that of conventional broad-area LEDs, the output power of the microhole array LED and the surface-oxidized microhole array LED increased by 1.38 and 1.82 times at 20-mA forward current, respectively. The results show that the microhole array pattern with the roughened surface oxide method could significantly enhance light extraction efficiency and be a candidate for manufacturing high-efficient low-cost GaN-based LEDs. [J864]

"Identification and Control of a Grating-Stabilized External-Cavity Diode Laser"

Diode lasers have many useful properties and have found a variety of uses including CD and DVD players, barcode scanners, laser surgery, water purification, quantum-key cryptography, spectroscopic sensing, etc. Nevertheless, their intrinsic linewidth or the precision of their emitted wavelengths, is not good enough for many cutting-edge applications such as atomic interferometry or high-performance atomic clocks. Using active feedback control, we can narrow the linewidth of a diode laser by not allowing the frequency of emitted light to drift away from a reference value. Nevertheless, such feedback designs are challenging because of a lack of first principles models and difficult sensor dynamics. This brief describes our diode laser system and reports our results identifying the system using black-box techniques, validating the empirical models, and designing controllers to achieve desired performance while preserving stability and satisfying implementation constraints. [J865]

"Self-Consistent Analysis of Strain-Compensated InGaN-AlGaIn Quantum Wells for Lasers and Light-Emitting Diodes"

Strain-compensated InGaIn-AlGaIn quantum wells (QW) are investigated as improved active regions for lasers and light emitting diodes. The strain-compensated QW structure consists of thin tensile-strained AlGaIn barriers surrounding the InGaIn QW. The band structure was calculated by using a self-consistent 6-band knddotpformalism, taking into account valence band mixing, strain effect, spontaneous and piezoelectric polarizations, as well as the carrier screening effect. The spontaneous emission and gain properties were analyzed for strain-compensated InGaIn-AlGaIn QW structures with indium contents of 28%, 22%, and 15% for lasers (light-emitting diodes) emitting at 480 (500), 440 (450), and 405 nm (415 nm) spectral regimes, respectively. The spontaneous emission spectra show significant improvement of the radiative emission for strain-compensated QW for all three structures compared to the corresponding conventional InGaIn QW, which indicates the enhanced radiative efficiency for light emitting diodes. Our studies show the improvement of the optical gain and reduction of the threshold current density from the use of strain-compensated InGaIn-AlGaIn QW as active regions for diode lasers. [J866]

"A Study of Semitransparent Cathodes on the Performance of Top-Emitting Polymer Light-Emitting Diodes"

This work reports the influence of semitransparent cathodes, which were made of Ca or Al covered with a thin layer of Ag, on the performance of poly(2-methoxy-5-(2'-ethylhexyloxy)-1,4-phenylene vinylene) (MEH-PPV)-based top-emitting polymer light-emitting diodes (T-PLEDs). The physical properties of the semitransparent

cathodes alter the optical microcavity of T-PLEDs and adjust the output characteristics of the electroluminescence (EL). The bright, red-emissive, MEH-PPV-based T-PLED, with Ca(10 nm)/Ag(20 nm) as the semitransparent cathode, exhibited 3.6 cd/A, 38.7 nm, and ($x=0.67$, $y=0.33$) for the luminous efficiency, full-width at half-maximum of the EL, and Commission International de l'Eclairage coordinate, respectively. The favorable performance can be attributed to the formation of an appropriate microcavity structure, which results in spatial redistribution and enhances the out-coupling of EL emission in the direction of the surface normal. [J867]

"Poly(Dimethylsiloxane) Waveguide Cantilevers for Optomechanical Sensing"

The optical and structural properties of poly(dimethylsiloxane) (PDMS) are considered to define disposable cantilever-based micropoptoelectromechanical systems (MOEMS) by ways of soft lithography and with a high degree of monolithic integration. The very low Young's modulus of this material relaxes the dimensions' requirements, being then possible to define thick PDMS structures with a sensitivity comparable to nanometer scale silicon counterparts. Experimental results using a light-emitting diode working at 670 nm have determined the resonant frequencies of the proposed MOEMS and are in agreement with the numerical simulations done. Finally, when a 2- μ L droplet of ethanol (1.58 mg) is dispensed on the cantilever, relative losses rise to 25 dB, returning to its initial value when the droplet evaporates. [J868]

"Uniform Illumination Rendering Using an Array of LEDs: A Signal Processing Perspective"

An array of a large number of LEDs will be widely used in future indoor illumination systems. In this paper, we investigate the problem of rendering uniform illumination by a regular LED array on the ceiling of a room. We first present two general results on the scaling property of the basic illumination pattern, i.e., the light pattern of a single LED, and the setting of LED illumination levels, respectively. Thereafter, we propose to use the relative mean squared error as the cost function to measure the uniformity of the realized illumination pattern, and provide an analysis for this cost function. Based on the analysis, the design of a basic illumination pattern is discussed. The performances of a few basic illumination patterns are compared, and an approach for optimizing the basic illumination pattern through a weighted combination of these basic patterns is also proposed. A weighted combination of Gaussian and raised-cosine functions is found to yield the best results. Finally, three basic regular grid shapes for an LED array are compared. The results show that 13% and 39% of LEDs can be saved for the same degree of uniformity, using the hexagonal instead of the rectangular and triangular grid, respectively. [J869]

"Improvement in the Light Output Power of GaN-Based Light-Emitting Diodes by Natural-Cluster Silicon Dioxide Nanoparticles as the Current-Blocking Layer"

In this study, the fabrication and characterization of InGaN-GaN multiple-quantum-well light-emitting diodes (LEDs) with silicon dioxide (SiO₂) nanoparticles as the current-blocking layer (CBL) are described. The performance was improved by introducing SiO₂nanoparticles, not deposited by commonly used plasma-enhanced chemical vapor deposition, as the CBL beneath the p-pad. The injected current was forced to spread outside instead of flowing directly downward. At 20 mA, the light output power of the LED with a CBL was increased 15.7% as compared to that of the conventional LED. The forward voltage of the LED with the SiO₂nanoparticle CBL was 3.34 V at 20 mA, which was slightly higher than that of the conventional LED (3.29 V). The increase in the light output power can be attributed to the injection of additional current into the light-emitting active layer of the LED by the SiO₂nanoparticles CBL and thus a reduction in optical absorption at the p-pad. [J870]

"Aluminum Nitride Ceramic Substrates-Bonded Vertical Light-Emitting Diodes"

We confirmed the potential of an aluminum nitride (AlN) substrate to be used as a bonding material for the high current operation of vertical light-emitting diodes (VLEDs). For the electrical connection to the top and bottom of the AlN substrate, via-holes were formed by laser drilling and then filled with Ag, which plays a role in improving the thermal dissipation from the VLEDs. The forward voltage of the fabricated AlN-bonded VLEDs was 3.54 V at 350 mA, which is similar to that of the Si-bonded VLEDs. It was also found that the light output power of the AlN-bonded VLEDs increased steadily with increasing injection current up to 1 A, while that of the Si-bonded VLEDs started to decrease at around 850 mA. In addition, the thermal resistance of the AlN-bonded VLEDs was significantly reduced, as compared with that of the Si-bonded VLEDs and conventional LEDs, under the same package conditions. [J871]

"Image integrity-based gray-level error control for low power liquid crystal displays"

In this paper, we present a new approach to dynamic gray-level error control for global dimming of liquid crystal display (LCD) devices. In the LCD devices, global dimming is used to reduce power consumption by limiting the

maximum luminance and lowering the brightness of backlight. The existing approaches, based on the fixed rate of clipped pixels, deteriorate the image quality seriously for some images even after gray level compensation. The proposed approach, on the other hand, dynamically chooses the maximum luminance for a given image, based on final image integrity. Thus, it has an advantage of preserving the worst image quality at any desired level, while reducing power consumption as much as possible. In the experiments, the proposed approach successfully maintained the minimum target peak signal to noise ratio (PSNR) for test sequences. [J872]

"The multi-touch system with high applicability using tri-axial coordinate infrared LEDs"

In these days, multi-touch technology becomes an important interface in various environments. However, most of multi-touch systems have a characteristic of low applicability so that it is difficult to apply to diverse applications. In this paper, we compare the main three methods of multi-touch systems, and analyze the pros and cons of these systems. By considering applicability and economical efficiency, we propose an infrared LED based system suitable to be used in multi users. To solve coordinate recognition problems in collinear in a 2-dimensional bi-axial coordinate system, we design a 2-dimensional tri-axial coordinate multi-touch system using infrared LEDs. The comparing result between two systems shows that the recognition rate in the biaxial coordinate system is 49 percent and the recognition rate in the tri-axial coordinate system is 99 percent. [J873]

"Individually Addressable AlInGaN Micro-LED Arrays With CMOS Control and Subnanosecond Output Pulses"

We report the fabrication and characterization of an ultraviolet (370 nm) emitting AlInGaN-based micro-light-emitting diode (micro-LED) array integrated with complementary metal-oxide-semiconductor control electronics. This configuration allows an 8 × 8 array of micro-LED pixels, each of 72-μm diameter, to be individually addressed. The micro-LED pixels can be driven in direct current (dc), square wave, or pulsed operation, with linear feedback shift registers (LFSRs) allowing the output of the micro-LED pixels to mimic that of an optical data transmitter. We present the optical output power versus drive current characteristics of an individual pixel, which show a micro-LED output power of up to 570 μW in dc operation. Representative optical pulse trains demonstrating the micro-LEDs driven in square wave and LFSR modes, and controlled optical pulsewidths from 300 ps to 40 ns are also presented. [J874]

"Pixel-to-Pixel Fiber-Coupled Emissive Micro-Light-Emitting Diode Arrays"

We report on an integrated fiber-coupled bi-linear micro-light-emitting diode array, serving as a portable microdisplay system. The fiber bundle transforms the bi-linearly arranged optical signals from the emissive array into a 6-by-8 pixel microdisplay, offering a crisp and clear optical output. The pixel-to-pixel coupling arrangement ensures optical coupling efficiency. Due to the narrow acceptance cones of optical fibers, individual pixels can be well resolved with minimal crosstalk. The performance and functionality of this optical system is fully evaluated. A model to determine the fiber-coupling efficiency was constructed; it was found that the simulated results compare well with the measured data. [J875]

"Study of the Excitation Power Dependent Internal Quantum Efficiency in InGaN/GaN LEDs Grown on Patterned Sapphire Substrate"

The mechanisms of the excitation power dependent internal quantum efficiency in InGaN/GaN multiple quantum wells (MQWs) LEDs grown on the planar and the patterned sapphire substrates (PSS) at temperature of 15 and 300 K were investigated. From observation the tendency of emission peak energy and carrier lifetime variation in MQWs with different excitation power for both LED samples, we conclude the internal quantum efficiency would increase as coulomb screening effect dominates at lower carrier injection stage and decrease due to the band-filling effect at higher density stage. At room temperature, the majority of the initial injected carriers would be first consumed by the thermal activated nonradiative centers that hinder the further achievement of high-efficiency LED devices. Experimentally, the internal quantum efficiency of the LED grown on the PSS is ~70% and that of the LED grown on the planar sapphire substrate is ~62%. For the LED grown on the PSS, the observed higher internal quantum efficiency is due to the larger activation energy. Therefore, the reduction of dislocation defects and the prevention of injected carriers escaping from extended states would be a promising prospective for InGaN/GaN MQWs LEDs to achieve high internal quantum efficiency. [J876]

"High-Brightness InGaN-GaN Power Flip-Chip LEDs"

We report the fabrication of InGaN-GaN power flip-chip (FC) light-emitting diodes (LEDs) with a roughened sapphire backside surface prepared by grinding. It was found that we can increase output power of the FC LED by about 35% by roughening the backside surface of the sapphire substrate. The reliability of the proposed

device was also better, as compared to power FC LEDs with a conventional flat sapphire backside surface.

[J877]

"Organic vapor phase deposition for the growth of large area organic electronic devices"

We demonstrate that material utilization efficiencies of 50% and deposition nonuniformities $\leq 2.5\%$ are achievable over substrate diameters of 200 mm using a simplified, organic vapor phase deposition (OVPD) system. The OVPD system is used to demonstrate doped electrophosphorescent organic light emitting diodes whose performance is comparable to those grown by vacuum thermal evaporation. Through continuum modeling, we demonstrate that analogous systems whose chamber dimensions are comparable to the substrate width are scalable to substrate sizes of at least 1500 \times 1800 mm² with deposition nonuniformities between 1.5% and 2.5%. These results indicate that OVPD is useful in the large area deposition of displays, lighting, and other organic electronic devices. [J878]

"On carrier spillover in c- and m-plane InGaN light emitting diodes"

The internal quantum efficiency (IQE) and relative external quantum efficiency (EQE) in InGaN light-emitting diodes (LEDs) emitting at 400 nm with and without electron blocking layers (EBLs) on c-plane GaN and m-plane GaN were investigated in order to shed some light on any effect of polarization charge induced field on efficiency killer carrier spillover. Without an EBL the EQE values suffered considerably (by 80%) for both orientations, which is clearly attributable to carrier spillover. Substantial carrier spillover in both polarities, therefore, suggests that the polarization charge is not the major factor in efficiency degradation observed, particularly at high injection levels. Furthermore, the m-plane variety with EBL did not show any discernable efficiency degradation up to a maximum current density of 2250 A cm⁻² employed while that on c-plane showed a reduction by 40%. In addition, IQE of m-plane LED structure determined from excitation power dependent photoluminescence was 80% compared to 50% in c-plane LEDs under resonant and moderate excitation condition. This too is indicative of the superiority of m-plane LED structures, most probably due to relatively larger optical matrix elements for m-plane orientation. [J879]

"Efficient inverted top-emitting organic light-emitting diodes using ultrathin MoO₃/C₆₀ bilayer structure to enhance hole injection"

Efficient inverted top-emitting organic light-emitting diodes with aluminum (Al) as both the cathode and semitransparent anode are investigated. It is found that introduction of the ultrathin molybdenum trioxide (MoO₃)/fullerene(C₆₀) bilayer structure between the low work function Al top anode and the hole-transporting layer dramatically enhances the device performance as compared to the devices with sole MoO₃ or C₆₀ buffer layer. The ultraviolet photoemission spectroscopy and x-ray photoelectron spectroscopy indicate that the hole injection barrier between Al anode and hole-transporting layer is effectively reduced via strong dipole effect at Al/MoO₃/C₆₀ interfaces with its direction pointing from Al to C₆₀. [J880]

"Fully bendable polymer light emitting devices with carbon nanotubes as cathode and anode"

Polymer light emitting devices were fabricated by roll lamination using single-walled carbon nanotubes as both anode and cathode. The devices exhibited a low turn-on voltage of 3.8 V, high brightness of 1400 cd/m² at 10 V and maximum efficiency of 2.2 cd/A at 480 cd/m². The devices are also highly transparent and exhibited very high flexibility. No failure was observed after bending the devices down to 2.5 mm radius. [J881]

"Optocouplers: Fundamentals and Hardness Assurance for Space Applications"

Operating principles and hardness assurance methods are discussed for various types of optocouplers. Radiation damage in light-emitting diodes is addressed, along with the impact of phototransistors and internal amplifiers on overall performance. Hardness assurance for optocouplers is contrasted with the approach used for conventional microelectronics. Methods of detecting abnormal devices are discussed, along with the implementation of special screening measurements. [J882]

"Highly efficient yellow organic light emitting diode based on a layer-cross faded emission layer allowing easy color tuning"

An easy way to adjust the color of yellow organic light emitting diodes (OLED) is realized by basing the emission layer on a cross-fading zone of two unipolar-conducting host materials doping parts of it either with a red or green phosphorescent emitter at varying thickness ratios. At color coordinates of 0.47/0.50, a current efficacy of 42.2 cd/A (16.2% external quantum efficiency) and a power efficacy of 32.9 lm/W (1000 cd/m²) are measured without light extraction enhancement. Mixed-host emission layer OLED without cross-fading are processed for

comparison. Exciton distributions are studied. The concept is suggested to be useful for white OLED. [J883]

"Enhancement of electrical property by oxygen doping to copper phthalocyanine in inverted top emitting organic light emitting diodes"

We reported the evidence of oxygen doping to copper-phthalocyanine (CuPc) by O₂-plasma treatment to inverted top-emitting organic light-emitting diodes (ITOLEDs). In situ synchrotron-radiation photoelectron spectroscopy results showed that a new Cu-O bond appeared and the energy difference between the highest-occupied molecular orbital and EF is lowered by 0.15 eV after plasma treatment. The oxygen ions chemically interacted with Cu atoms and transferred charges to the CuPc. Thus the hole injection barrier was lowered, enhancing the electroluminescent property of ITOLEDs. [J884]

"High data rate multiple input multiple output (MIMO) optical wireless communications using white led lighting"

Solid-state lighting is a rapidly growing area of research and applications, due to the reliability and predicted high efficiency of these devices. The white LED sources that are typically used for general illumination can also be used for data transmission, and Visible Light Communications (VLC) is a rapidly growing area of research. One of the key challenges is the limited modulation bandwidth of sources, typically several MHz. However, as a room or coverage space would typically be illuminated by an array of LEDs there is the potential for parallel data transmission, and using optical MIMO techniques is potentially attractive for achieving high data rates. In this paper we investigate non-imaging and imaging MIMO approaches: a non-imaging optical MIMO system does not perform properly at all receiver positions due to symmetry, but an imaging based system can operate under all foreseeable circumstances. Simulations show such systems can operate at several hundred Mbit/s, and up to Gbit/s in many circumstances. [J885]

"Magnetoelectroluminescence in tris (8-hydroxyquinolato) aluminum-based organic light-emitting diodes doped with fluorescent dyes"

The influences of fluorescent dye doping on the magnetoelectroluminescence in tris (8-hydroxyquinolato) aluminum (Alq₃)-based organic light-emitting diodes have been investigated systematically by varying the dopant concentrations and its energy band gap. Our results show that the decrease in electroluminescence intensity at high magnetic field, which survives only at low temperatures for pure Alq₃-based devices, persists in dye-doped devices even at room temperature. This is explained here as the result of magnetic field dependent triplet-triplet annihilation process, in which the triplet excitons trapped on the dye molecules play the most important role. [J886]

"Blue light-emitting diodes with a roughened backside fabricated by wet etching"

The InGaN-based light-emitting diodes (LEDs) with a roughened patterned backside on the N-face GaN surface were fabricated through a crystallographic etching process to increase light-extraction efficiency. After laser decomposition, laser scribing, and a lateral crystallographic wet etching process at the GaN/Al₂O₃ interface, stable crystallographic etching planes were formed as the GaN {1011} planes that included an angle with the top GaN (0001) plane measured at 58°. The GaN buffer layer acted as the sacrificial layer for the laser decomposition process and the lateral wet etching process with a 26mcm/min etching rate. The LED with the inverted pyramidal N-face GaN surface close to the GaN/Al₂O₃ interface has a larger light-scattering process than the conventional LED. The light-output power of the LED with the backside roughened surface had a 47% enhancement when measured in LED chip form. [J887]

"Barbot, the automated bartender"

At NYC Resistor, a communal hacker space in downtown Brooklyn, N.Y., we do two things really well, hack and party. An automated bartender seemed like a natural, but as we searched the U.S. patent database for ideas, it became clear we'd have to hack one up ourselves. And so we have. An ongoing series of them, in fact. [J888]

"Effect of indium content on performance and reliability of InGaN/GaN light-emitting diodes"

While longer wavelength emission from InGaN/GaN light-emitting diodes (LEDs) can be achieved by increasing the indium (In) content in the quantum wells, the increased In content gives rise to side effects to the material and device performance and reliability. It was found that the induced strain in the wafer and the density of threading dislocations increase with increasing In content. From current-voltage and 1/f noise measurements, it was observed that the leakage currents, static resistance, and noise magnitudes rise monotonically with

increasing emission wavelength (In composition), which can be attributed to higher defect concentrations. After undergoing a 1000 h reliability test, it was discovered that the optical degradation rates for the longer wavelength green LEDs were significantly higher than those of shorter wavelength. [J889]

"Measurement system of the refractive power of spherical and spherocylindrical lenses with the magnification ellipse fitting method"

This paper proposes a new measurement system for measuring the refractive power of spherical and spherocylindrical lenses with a six-point light source, which is composed of a light emitting diode and a six-hole pattern aperture, and magnification ellipse fitting method. The position of the six light sources is changed into a circular or elliptical form subjected to the lens refractive power and meridian rotation angle. The magnification ellipse fitting method calculates the lens refractive power based on the ellipse equation with magnifications that are the ratios between initial diagonal lengths and measured diagonal lengths of the conjugated light sources changed by the target lens. The refractive powers of the spherical and spherocylindrical lenses certified in the Korea Research Institute of Standard and Science were measured to verify the measurement performance. The proposed method is estimated to have a repeatability of $\pm 0.01\text{D}$ and an error value below 1%. [J890]

"Randomly packed n-SnO₂ nanorods/p-SiC heterojunction light-emitting diodes"

A layer of randomly packed n-SnO₂ nanorods is grown by vapor transport method on the p-SiC(4H) substrate to realize heterojunction light-emitting diodes. Diodelike rectifying current-voltage characteristics, with a turn-on voltage of 4.5 V and reverse leakage current density of 0.25 A/m², are obtained at room temperature. Furthermore, electroluminescent spectra with emission peaks at around 395, 434, and 497 nm are observed from the heterojunction under forward bias. This is due to the relaxation of electrons in the conduction band of SnO₂ to the surface defect states and subsequent radiative recombination with holes injected from the p-SiC substrate. [J891]

"Spin-polarization dynamics in InGaAs quantum dots during pulsed electrical spin-injection"

We investigate the fidelity of electron spin initialization in quantum dots utilizing nanosecond-pulsed electrical spin injection through a semimagnetic spin aligner in a spin light-emitting diode. At the onset of the electroluminescence signal, the circular polarization degree of the emitted light, corresponding to the spin polarization degree, is distinctively higher than under constant-current excitation. The observed spin-polarization dynamics are attributed to state filling effects. Additional contributions due to spin-flip mechanisms within the optically active region are identified. [J892]

"Go big or go home"

When Prithviraj Banerjee arrived at HP Laboratories, in Palo Alto, Calif., as the organization's new director in August 2007, he was intent on pushing the researchers to swing big. HP Labs, a sprawling enterprise with some 500 researchers spread over seven locations worldwide, is the company's advanced research arm, spending about US \$150 million annually. The first commercially available LED, the pocket scientific calculator, thermal inkjet printing, and reduced instruction-set computer architecture were all born in the labs. The labs got the company into digital printing, and HP is counting on those researchers for future wins. [J893]

"Direct measurement of Auger recombination in In_{0.1}Ga_{0.9}N/GaN quantum wells and its impact on the efficiency of In_{0.1}Ga_{0.9}N/GaN multiple quantum well light emitting diodes"

The Auger recombination coefficient in In_{0.1}Ga_{0.9}N/GaN quantum wells, emitting at 407 nm has been determined from large signal modulation measurements on lasers in which these quantum wells form the gain region. A value of $1.5 \times 10^{-30} \text{ cm}^6 \text{ s}^{-1}$ is determined for the Auger coefficient at room temperature, which is used to analyze the reported efficiency characteristics of 410 nm In_{0.1}Ga_{0.9}N/GaN quantum wells light emitting diodes. The calculated efficiencies agree remarkably well with the measured ones. It is apparent that Auger recombination is largely responsible for limiting device efficiencies at high injection currents. [J894]

"Amorphous silicon as electron transport layer for colloidal semiconductor nanocrystals light emitting diode"

We demonstrate the fabrication of light-emitting diodes (LEDs) made from all-inorganic colloidal semiconducting nanocrystals (NCs). The diode utilizes a sandwich structure formed by placing CdSe/CdS NCs between two layers of Si and Ag_xO, which act as electron- and hole-transporting materials, respectively. The photoluminescence properties of NCs are rendered less dependent upon surface chemistry and chemical

environment by growing a thick CdS shell. It also enhances stability of the NCs during the process of magnetron sputtering for silicon deposition. The resulting LED device exhibits a low turn-on voltage of 2.5 V and the maximum external quantum efficiency of nearly 0.08%. [J895]

"Enhanced performance of organic light-emitting diodes using two-dimensional zinc sulfide photonic crystals"

The light extraction efficiency of an organic light-emitting diode (OLED) was significantly enhanced upon incorporating a photonic-crystal (PC) pattern consisting of ZnS pillars residing on top of the transparent anode-glass substrate. The luminance efficiency of the PC-OLED is enhanced by a factor of 2.1 to 2.4 depending on the periodicity of the PC structure, when compared to that of a control OLED operating under the same conditions. [J896]

"Impact of two-floor air prism arrays as an embedded reflector for enhancing the output power of InGaN/GaN light emitting diodes"

This paper reports on the impact of two-floor air prism (TFAP) arrays InGaN/GaN light emitting diodes (LEDs) as an embedded reflector with low refractive indices. The reflectance spectra, measured over the entire visible spectral region, shows strong reflectance modulations due to the TFAP arrays in GaN. The light output powers of TFAP LEDs is seen to be 2.62 times higher than that of conventional LEDs, and 1.55 times higher than that of LEDs with one floor air prism arrays, respectively, at injection currents of 100 mA. This significant enhancement is attributable to a combined effect of effective shaping with 62° angled sidewalls and high refractive index difference between the embedded air prism and the GaN. [J897]

"Photothermal determination of thermal diffusivity and polymerization depth profiles of polymerized dental resins"

The degree and depth of curing due to photopolymerization in a commercial dental resin have been studied using photothermal radiometry. The sample consisted of a thick layer of resin on which a thin metallic gold layer was deposited, thus guaranteeing full opacity. Purely thermal-wave inverse problem techniques without the interference of optical profiles were used. Thermal depth profiles were obtained by heating the gold coating with a modulated laser beam and by performing a frequency scan. Prior to each frequency scan, photopolymerization was induced using a high power blue light emitted diode (LED). Due to the highly light dispersive nature of dental resins, the polymerization process depends strongly on optical absorption of the blue light, thereby inducing a depth dependent thermal diffusivity profile in the sample. A robust depth profilometric method for reconstructing the thermal diffusivity depth dependence on degree and depth of polymerization has been developed. The thermal diffusivity depth profile was linked to the polymerization kinetics. [J898]

"Planar silicon light emitting arrays for the 3-12 mcm spectral band"

Silicon light emitting diode arrays made by industrial planar technology and operating at T = 300K in the double injection mode have been shown to be an efficient emitters of the infrared (IR) radiation in the 3-12mcm spectral band. We show that due to free carrier injection in an optically thin base, which makes its emissivity to increase at the wavelengths of the free carrier absorption, the devices have thermal emission output power of 2-3 mW and local power density up to 1mW/mm² at T=473K. The 0.5-mm-thick 646mm² emitting pixel of an array demonstrates the power conversion efficiency of 13%, a time response of 300μs, and an apparent temperature of the IR radiation of 400 K, which make the device practical for use in IR dynamic scene simulation techniques. [J899]

"High-efficiency turquoise-blue electrophosphorescence from a Pt(II)-pyridyltriazolate complex in a phosphine oxide host"

We demonstrate high-efficiency turquoise-blue electrophosphorescence from bis[3,5-bis(2-pyridyl)-1,2,4-triazolato]platinum(II) [Pt(ftp)₂] doped in 4-(diphenylphosphoryl)-N,N-diphenylaniline (HM-A1). Organic light-emitting diodes (OLEDs) with 5% Pt(ftp)₂:HM-A1 attain peak power efficiency of 61.2 lm/W, versus 40.8 lm/W for analogous devices employing the standard turquoise-blue phosphor bis[(4,6-difluorophenyl)-pyridinato-N,C2'] (picolinato) iridium(III) (Flrpic). Devices with x% Pt(ftp)₂:HM-A1 exhibit blue emission maxima (λ_{max} 480nm) with monotonic increase in excimer/monomer intensity ratio at higher doping levels within 1%-10%, causing color shift toward green and less charge balance. This work represents a significant step toward optimizing future white OLEDs from the same phosphor via combination of low-doped and higher-doped or neat films. [J900]

"Molecular beam epitaxial (MBE) growth and spectroscopy of dilute nitride InAsN:Sb for mid-infrared applications"

The molecular beam epitaxial (MBE) growth and spectroscopy of dilute nitride InAsN:Sb epilayers are presented. Nitrogen incorporation in InAsN epilayers grown by radio-frequency plasma-assisted MBE was investigated as a function of growth conditions. High-quality InAsN epilayers containing up to 2.5% nitrogen were successfully grown using optimal growth conditions. The optical properties of InAsN were studied by photoluminescence (PL). Intense PL emission at 4% K was observed with double-peak features, which were attributed to free carrier recombination and localised carrier recombination. Strong room temperature PL emission extending up to a wavelength of 4.5 μm was obtained and a bandgap reduction of 63% meV for 1% N was deduced. The electronic properties of InAsN such as residual carrier concentration and mobility were also studied by Hall effect measurements. Further improvement of InAsN by addition of Sb during growth is also discussed. The authors observed that the introduction of Sb flux dramatically enhances nitrogen incorporation and significantly improves optical properties. In addition, Sb incorporation is enhanced with the presence of nitrogen. The authors also report the realisation of InAsN:Sb/InAs mid-infrared light emitting diodes operating at 4.0 μm at 4% K. [J901]

"Design and characteristics of staggered InGaN quantum-well light-emitting diodes in the green spectral regime"

Staggered InGaN quantum wells (QWs) are investigated both numerically and experimentally as improved active region for light-emitting diodes (LEDs) emitting at 520-525-nm. Based on a self-consistent six-band $k \cdot p$ method, band structures of both two-layer staggered $\text{In}_x\text{Ga}_{1-x}\text{N}/\text{In}_y\text{Ga}_{1-y}\text{N}$ QW and three-layer staggered $\text{In}_y\text{Ga}_{1-y}\text{N}/\text{In}_x\text{Ga}_{1-x}\text{N}/\text{In}_y\text{Ga}_{1-y}\text{N}$ QW structures are investigated as active region to enhance the spontaneous emission radiative recombination rate (R_{sp}) for LEDs emitting at 520-525-nm. Numerical analysis shows significant enhancement of R_{sp} for both two-layer and three-layer staggered InGaN QWs as compared to that of the conventional $\text{In}_z\text{Ga}_{1-z}\text{N}$ QW. Significant reduction of the radiative carrier lifetime contributes to the enhancement of the radiative efficiency for both two-layer and three-layer staggered InGaN QW LEDs emitting at 520-525-nm. Three-layer staggered InGaN QW LEDs emitting at 520-525-nm was grown by metal-organic chemical vapour deposition (MOCVD) by employing graded-temperature profile. Power density-dependent cathodoluminescence (CL) measurements show the enhancement of peak luminescence by up to 3 times and integrated luminescence by 1.8-2.8 times for the three-layer staggered InGaN QW LED. Electroluminescence (EL) output power of the staggered InGaN QW LED exhibits 2.0-3.5 times enhancement as compared to that of the conventional InGaN QW LED. The experimental results show the good agreement with theory. [J902]

"Solution-processed conjugated polymer organic p-i-n light-emitting diodes with high built-in potential by solution- and solid-state doping"

Polymer p-i-n homojunction light-emitting diodes (LEDs) comprising p-doped poly(dioctylfluorene-alt-benzothiadiazole) (F8BT) hole-injection, intrinsic F8BT emitter, and n-doped F8BT electron-injection layers have been demonstrated. A thin F8BT film was photocrosslinked and bulk p-doped by nitronium oxidation, then overcoated with an F8BT layer which was then surface n-doped by contact printing with naphthalenide on an elastomeric stamp. These LEDs exhibit high built-in potential ($V_{\text{bi}}=2.2\text{V}$), efficient bipolar injection, and greatly improved external electroluminescence efficiency compared to control devices without the p-i-n structure. A modulated photocurrent technique was used to measure this V_{bi} , which systematically improves with diode structure. [J903]

"Electroluminescence induced by Ge nanocrystals obtained by hot ion implantation into SiO₂"

Commonly, electroluminescence (EL) from Ge nanocrystals (Ge NCs) has been obtained by room temperature (RT) Ge implantation into a SiO₂ matrix followed by a high temperature anneal. In the present work, we have used a novel experimental approach: we have performed the Ge implantation at high temperature (T_i) and subsequently a high temperature anneal at 900 °C in order to grow the Ge NCs. By performing the implantation at $T_i=350$ °C, the electrical stability of the MOSLEDs were enhanced, as compared to the ones obtained from RT implantation. Moreover, by changing the implantation fluence from $\Phi=0.54 \times 10^{16}$ and $1.04 \times 10^{16} \text{ Ge/cm}^2$ we have observed a blueshift in the EL emission peak. The results show that the electrical stability of the hot implanted devices is higher than the ones obtained by RT implantation. [J904]

"Defect selective passivation in GaN epitaxial growth and its application to light emitting diodes"

A defect selective passivation method to block the propagation of threading dislocations in GaN epitaxial growth is demonstrated. The defect selective passivation is done by using defect selective chemical etching to locate defect sites, followed by silicon oxide passivation of the etched pits, and epitaxial over growth. The threading

dislocation density in the regrown epilayer is significantly improved from 1.4×10^9 to $4.4 \times 10^7 \text{ cm}^{-2}$. The defect passivated epiwafer is used to grow light emitting diode and the output power of the fabricated chip is enhanced by 45% at 20 mA compared to a reference one without using defect passivation. [J905]

"High spontaneous emission rate asymmetrically graded 480 nm InGaN/GaN quantum well light-emitting diodes"

Spontaneous emission property of an asymmetrically graded 480 nm InGaN/GaN quantum well (QW) is investigated via k-p theory. Comparing to rectangular QW, band profiles of the graded QW change into parabolalike due to the variation of internal piezoelectric field along the growth direction, and the spontaneous emission rates of the graded QW are three times larger than rectangular case under various carrier densities. This can be attributed to the fact that the graded QW has much larger matrix element $(M_e)_{n\sigma}$ than rectangular QW considering that the wave function overlap of the graded QW is less affected by the quantum confined Stark effect. [J906]

"Real-time external sensing and compensation method for organic light emitting diode displays"

A real-time external sensing and compensation method for active matrix organic light emitting diode displays is proposed. The proposed method senses and compensates for the variation of electrical characteristics of poly-Si thin-film transistors (TFTs) during display time. Experimental results show that the proposed method successfully senses the electrical characteristics of TFTs in real-time and compensates for the non-uniform emission current error. [J907]

"Electroluminescence from n-ZnO nanowires/p-GaN heterostructure light-emitting diodes"

The investigation explores the fabrication and characteristics of ZnO nanowire (NW)/p-GaN/ZnO NW heterojunction light-emitting diodes (LEDs). Vertically aligned ZnO NWs arrays were grown on the p-GaN substrate. The n-p-n heterojunction LED was fabricated by combining indium tin oxide/glass substrate with the prepared ZnO NWs/p-GaN substrate. The symmetrical rectifying behavior demonstrates that the heterostructure herein was formed with two p-n junction diodes and connected back to back. The room-temperature electroluminescent emission peak at 415 nm was attributed to the band offset at the interface between n-ZnO and p-GaN and defect-related emission from ZnO and GaN. Finally, the photograph indicated the LED clearly emitted blue light. [J908]

"Active Lighting for Video Conferencing"

In consumer video conferencing, lighting conditions are usually not ideal thus the image qualities are poor. Lighting affects image quality on two aspects: brightness and skin tone. While there has been much research on improving the brightness of the captured images including contrast enhancement and noise removal (which can be thought of as components for brightness improvement), little attention has been paid to the skin tone aspect. In contrast, it is a common knowledge for professional stage lighting designers that lighting affects not only the brightness but also the color tone which plays a critical role in the perceived look of the host and the mood of the stage scene. Inspired by stage lighting design, we propose an active lighting system which automatically adjusts the lighting so that the image looks visually appealing. The system consists of computer controllable light emitting diode light sources of different colors so that it improves not only the brightness but also the skin tone of the face. Given that there is no quantitative formula on what makes a good skin tone, we use a data driven approach to learn a good skin tone model from a collection of photographs taken by professional photographers. We have developed a working system and conducted user studies to validate our approach. [J909]

"Electron-hole pair mechanism for the magnetic field effect in organic light emitting diodes based on poly(paraphenylene vinylene)"

We investigated the magnetic field effect (MFE) on current and electroluminescence in organic light emitting diodes based on poly(paraphenylene vinylene). The MFE was strictly positive in the full range of device operation and showed nonmonotonic dependencies on applied voltage and temperature. Furthermore, the MFE on current obtained in bipolar devices was significantly larger than in hole-dominated devices. We discuss our results in the framework of an electron-hole pair model and show that the model can explain all functional dependencies observed in our devices. [J910]

"On the use of silicon photonics--Part II"

For Part I see *ibid.*, vol. 28, no. 1 (2009). With optical input and output devices integrated on chip, chips could be tested in a contactless manner using an easy optical test setup. The contactless optical testing approach can

address many challenges associated with increases in the number of physical test probes required to test increasingly complex integrated circuits (ICs). [J911]

"Fabrication of a Blue Pixel Organic Light-Emitting Diode Video Display Incorporating a Thermally Stable Emitter"

A 7 times 11 pixel blue OLED display was fabricated using a patterned indium-tin-oxide (ITO) substrate. The fabrication process for an M times N pixel organic light-emitting diode (OLED) video display including an electrical insulating layer and a physical pixel separator layer is presented. An efficient and thermally stable blue fluorescent organic material, 6,6'-bis((2-p -biphenyl)-4-phenylquinoline) (B2PPQ), was used in combination with an evaporated hole-transport small molecule with a high ionization potential. [J912]

"Prolog to The Transition to Solid-State Lighting"

This is an introduction to the above titled paper. [J913]

"On an AlGaInP Light-Emitting Diode With a Modulation-Doped Multiquantum-Well (MD-MQW) Structure"

An interesting AlGaInP multiquantum-well (MQW) light-emitting diode (LED) with an n-type modulation-doped (MD) structure, grown by low-pressure metal-organic vapor-phase epitaxy (LP-MOVPE), is fabricated and studied. This n-type MD-MQW LED exhibits lower dynamic resistance, higher luminescence, and higher luminous efficiency than those of a conventional undoped-MQW LED. Experimental results show a higher luminous efficiency of 16.05 lm/W and higher luminescence of 2.53 lm are obtained for the MD-MQW LED which are superior to the corresponding values of 14.49 lm/W and 2.04 lm for the undoped-MQW LED under dc operation. In addition, the n-type MD-MQW LED exhibits a higher quantum efficiency of 7.2% under dc operation as compared with the 6.7% of the undoped-MQW LED. The reduced junction temperature of 12degC at 200 mA is also acquired for the MD-MQW LED. Moreover, the brightness reliability of this new device is found to be comparable to the undoped-MQW LED. These positive results could be attributed to the presence of a higher electron concentration in the active region of the MD-MQW structure which causes the suppression of electron thermal velocity especially at a high level injection condition, and a reduced junction heating effect. [J914]

"GaN-Based Light-Emitting Diode With Three-Dimensional Silver Reflectors"

We present a simple and robust method to fabricate three-dimensional Ag reflectors on GaN light-emitting diodes (LEDs) using SiO₂ nanospheres as the template. First, the hexagonal arrays of SiO₂ nanosphere monolayer were spun-cast on a benzocyclobutene (BCB) layer, which was prepared on a sapphire surface. Then, the bottom half of the SiO₂ nanospheres were embedded into the BCB layer after heating, resulting in arrays of "nano-lenses" that were in the shape of convex hemispheres. The concave-shaped hemisphere arrays were produced by etching the SiO₂ nanospheres with an HF solution. Ag was deposited onto both patterns, concave and convex hemispheres, resulting in the formation of three-dimensional Ag reflectors. From the electroluminescence measurements, these Ag reflectors, which contained either concave or convex hemisphere patterns, were found to enhance the light output of GaN LEDs by as much as 29%-33%. [J915]

"A Synchronous Multioutput Step-Up/Down DC-DC Converter With Return Current Control"

This brief presents a new return-current control method for a multioutput step-up/down dc-dc converter. Compared with prior multioutput dc-dc converters, the presently described converter can generate outputs higher or lower than the input voltage with simple control-loop compensation while guaranteeing stability in a wide load range. Using a 0.5-μm bipolar CMOS (BiCMOS) process, a converter having five outputs has been implemented for an LG active-matrix organic light-emitting diode (AM-OLED) display panel. The implemented converter operates at 1-MHz switching frequency with 4.7- μH inductor and 10-μF capacitor. Experimental results show that the proposed control method can generate tightly regulated stepped-up or -down outputs stably under a wide load variation. The conversion efficiency is higher than 80% at a typical AM-OLED panel grey level. [J916]

"Enhancement of Light Extraction Efficiency Using Lozenge-Shaped GaN-Based Light-Emitting Diodes"

We have demonstrated both theoretically and experimentally that a lozenge-shaped light-emitting diode (LED) enhances light extraction efficiency compared with a conventional rectangular LED. The total light output power of the lozenge-shaped LED on a transmitter optical can (TO-can)-type package shows an increase of 12% at an

injection current of 20 mA when compared with that of a rectangular LED. Moreover, the series resistance and the forward voltage of the lozenge-shaped LED slightly decrease compared with those of the rectangular LED. The far-field emission pattern shows that the light escaping from the lozenge-shaped LED along the horizontal direction is larger than that from the rectangular LED. [J917]

"Light Output Improvement of Oxide-Textured InGaN-Based Light-Emitting Diodes by Bias-Assisted Photoelectrochemical Oxidation With Imprint Technique"

The improvement of light output power in InGaN-GaN multiple quantum-well (MQW) light-emitting diodes (LEDs) with oxide textural films are observed. The oxide textural films are grown by alternating current bias-assisted photoelectrochemical oxidation with an imprint technique. At an injection current of 20 mA, the light output power of the oxide-textured InGaN-GaN MQW LEDs is 22% higher than that of the conventional LEDs. Relatively low values in leakage current for the oxide-textured are also observed, as compared to the conventional LEDs. This enhancement in the oxide-textured LEDs performance is attributed to the increase in external quantum efficiency by the nanoscale roughness of the convex oxide films and to the passivation in possible leakage paths of the devices. [J918]

"ITO/AlN_dN/Al contact process for active matrix OLED displays"

Integrating circuits into organic light emitting diode displays requires fabrication of polycrystalline silicon (poly-Si) based thin-film transistors (TFTs) on glass substrates. A novel ITO/AlN_dN/Al contact process has been developed for the pixel step. In metallisation, ITO/Al interconnection is metallurgically undesirable. An AlN_dN layer is selected for a pixel material and ITO/AlN_dN/Al structure is applied to the pixel line. Reported is the feasibility for the multilevel ITO/AlN_dN/Al contact, which can make the poly-Si TFTs competitive in the market. [J919]

"Triple wavelength LED driver for optical brain-computer interfaces"

A dedicated triple wavelength LED driver is presented for optical brain-computer interfacing (BCI). The solution caters for the constraints of a common-anode grounded case and modulation up to several kilohertz that allows source separation of light that has back-scattered from the brain. With total harmonic distortion of 0.95- and a frequency range of ~40-kHz, the driver has application in a continuous wave optical BCI. Other modulation strategies such as time division multiplexing (TDM) are catered for, owing to input DC coupling. Linearity in the optical output is maintained by the -load sensing- differential op-amp on the LED-s current limiting resistor, which is the basis for the V-I conversion. [J920]

"Designing Uniform Illumination Systems by Surface-Tailored Lens and Configurations of LED Arrays"

Light-emitting diodes (LEDs) are gradually becoming the preferred choice for many lighting applications that require uniform illumination distribution. LED sources are usually composed of several individual LEDs which must be mounted on a panel as a lighting module. Therefore, the design is quite important for achieving a good uniform illumination distribution before a LED lighting module is produced. This paper presents a theory and design method by systemic concepts and focuses on the study of optical properties. We can design, efficiently, a LED lighting module and achieve a satisfactory uniformity by this theory and method, the design of a uniform LED illumination system. By this method, we not only obtain the maximally flat illumination distribution but also the emitting angle of the system can be designed at will. This method and theory will offer a preferable choice when LED lighting modules become the main stream for the lighting market in the future. Here, the light source is approximately defined as a point light source with cosine irradiance distribution. [J921]

"Investigation of Light Extraction of InGaN LEDs With Surface-Textured Indium Tin Oxide by Holographic and Natural Lithography"

Blue InGaN LEDs with periodically surface-textured indium tin oxide by holographic lithography were compared with those textured randomly by natural lithography where polystyrene spheres (PSs) with required diameter were employed as a mask for dry-etching process. It was found that the employed texturing processes not only exhibit unchanged I-V characteristics but also improve light output power. The turn-on threshold voltages of all the textured InGaN LEDs are similar to that of a conventional LED chip. An LED textured with a regular pattern with 600 nm pitch exhibits a maximum power enhancement of 65.2% at an injection current of 350 mA as compared with that of an original one. In addition, the LEDs with this 600 nm array pattern present much better light extraction than that textured with equal dimensioned PSs, which is indicative of the superior diffraction-dominated light extraction behavior. [J922]

"Application of Two Hopfield Neural Networks for Automatic Four-Element LED Inspection"

A system for the automatic inspection of LED wafer defects is proposed to detect defective dies in a four-element (aluminum gallium indium phosphide, AlGaInP) wafer. There are over 80000 dies on an LED wafer. Defective dies are typically visually identified with the aid of a scanning electron microscope. This process involves dozens of operators or engineers visually checking the wafers and hand marking the defective dies. However, wafers may not be fully and thoughtfully checked, and different observers usually find different results. These shortcomings lead to significant labor and production costs. Therefore, a solution that consists of two Hopfield neural networks, of which one is used to identify the LED die regions and the other is used to cluster the die into three groups, is proposed to facilitate the detection of defective dies in wafer images. The experimental results show that the proposed method successfully detects defective dies in a four-element wafer.

[J923]

"The Transition to Solid-State Lighting"

Lighting constitutes more than 20% of total U.S. electricity consumption, a similar fraction in the European Union, and an even higher fraction in many developing countries. Because many current lighting technologies are highly inefficient, improved technologies for lighting hold great potential for energy savings and for reducing associated greenhouse gas emissions. Solid-state lighting shows great promise as a source of efficient, affordable, color-balanced white light. Indeed, assuming market discount rates, engineering-economic analysis demonstrates that white solid-state lighting already has a lower levelized annual cost (LAC) than incandescent bulbs. The LAC for white solid-state lighting will be lower than that of the most efficient fluorescent bulbs by the end of this decade. However, a large literature indicates that households do not make their decisions in terms of simple expected economic value. After a review of the technology, we compare the electricity consumption, carbon emissions, and cost-effectiveness of current lighting technologies, accounting for expected performance evolution through 2015. We then simulate the lighting electricity consumption and implicit greenhouse gases emissions for the U.S. residential and commercial sectors through 2015 under different policy scenarios: voluntary solid-state lighting adoption, implementation of lighting standards in new construction, and rebate programs or equivalent subsidies. Finally, we provide a measure of cost-effectiveness for solid-state lighting in the context of other climate change abatement policies. [J924]

"Primary colors"

Presents the work of British artist Paul Cockshedge. [J925]

"Substrate Cleaning Methods for Fabricating OLEDs and Its Effect on Current Leakage Defect Formation"

Various methods for cleaning the large glass substrates (300 times 400 mm) used in organic light-emitting diode (OLED) fabrication processes were investigated. Horizontal roller-bed cleaning methods using a shower-rinse with megasonic (MS)-irradiation, or brush-scrubbing, were investigated for use with anode sputtering processes. Substrates were contaminated with particulate contaminants (0.3-0.5 particles/cm²) generated from anode sputtering targets. Large particles (≥ 5 μm) were easily removed with the MS irradiation (efficiency ≥ 95%). Small particles (< 3 μm) were harder to remove. The brush-scrubbing cleaning removed them with 80-90% efficiency, while the MS-irradiation cleaning had an efficiency of 60%-70%. spin-rinse-dry cleaning methods using ozonized or electrolyzed cathode water were investigated for use with pre-organic deposition processes. Glass substrates were intentionally contaminated by exposing them to a clean room atmosphere for either 24 or 100 hours. The number of particles was reduced from around 0.4 to 0.03/cm² and from around 1.7 to 0.08/cm² by the MS-irradiation cleaning using de-ionized water alone, respectively. The effect of the ozonized water treatment was evident for the longer exposure substrates: it reduced the number of particles to 0.03. The electrolyzed-cathode water cleaning was successful in removing submicrometer size particles. We also investigated the effect of particulate contaminants on the current leakage defect formation. [J926]

"Optical Detection of Partial Discharges on Insulator Strings of High-Voltage Transmission Lines"

Leakage current detection is a promising method for measuring pollution levels on insulators of overhead transmission lines. This paper describes the development of a leakage current sensor based on a fiber-coupled light-emitting diode, as well as the development of a processing module that detects, stores, and classifies leakage current peaks that are directly related to partial discharges on the surface of the high-voltage insulators. The relative humidity is also detected and stored for further analysis. The processing module uses a PIC 16F877A microcontroller and can register the rate of partial discharges for two months on three different levels.

[J927]

"On an AlGaInP-Based Light-Emitting Diode With an ITO Direct Ohmic Contact Structure"

An interesting AlGaInP multiple-quantum-well light-emitting diode (LED) with a direct ohmic contact structure, formed by an indium-tin-oxide (ITO) transparent film and AuBe diffused thin layer, is fabricated and studied. The direct ohmic contact structure is performed by the deposition of an AuBe diffused thin layer and the following activation process on the surface of a Mg-doped GaP window layer. Experimental results demonstrate that a dynamic resistance of 5.7 Ω and a forward voltage of 1.91 V, under an injection current of 20 mA, are obtained. In addition, the studied LED exhibits a higher external quantum efficiency of 9.7% and a larger maximum light-output power of 26.6 mW. The external quantum efficiency is increased by 26% under the injection current of 100 mA, as compared with the conventional LED without this structure. This is mainly attributed to the reduced series resistance resulted from the relatively uniform distribution of AuBe atoms near the GaP layer surface and the effective current spreading ability by the use of ITO film. Moreover, the life behavior of the studied LED, under a 20-mA operation condition, is comparable to the conventional LED without this structure. [J928]

"Novel Device Design for High-Power InGaN/Sapphire LEDs Using Copper Heat Spreader With Reflector"

Direct integration of InGaN/sapphire LED with a cup-shaped copper heat spreader was proposed for enhancing light extraction and heat dissipation by self-aligned photolithography and copper electroforming techniques. Based on optical simulation results, geometric design for a copper heat spreader is crucial to luminous property of an LED chip. An InGaN/sapphire LED embedded with the optimized cup-shaped copper heat spreader was demonstrated to exhibit superior light output power than a conventional LED by a factor of 2.68 times at an injection current of 1 A. Moreover, the power efficiency is remarkably increased from 4.2% to 15.7% at the same driven current. The improved device performance can be attributed to both of the enhanced light extraction of the laterally emitted light from an LED chip and efficient heat dissipation by the highly reflective and excellently thermal conductive copper heat spreader. These results suggest an efficient alternative simultaneously with two functions of thermal management and light extraction for high-power InGaN/sapphire LEDs application from chip to package design. [J929]

"Printed Nonvolatile Memory for a Sheet-Type Communication System"

By using state-of-the-art printing technologies and functional inks, we have demonstrated organic nonvolatile flexible random-access-memory matrices with a nondestructive read-out capability and a time-continuous current output; these functionalities have not been simultaneously achieved even by silicon-based conventional memory. A memory cell comprising three transistors becomes possible with inkjet printing and other solution-based processes, which can use ferroelectric copolymer ink comprising poly(vinylidene fluoride-co-trifluoroethylene) and insulating ink comprising polyimide precursors properly within the planer plastic substrate. A large "on/off" current ratio of 10⁵ is observed in air when it is annealed at 135°C, which is sufficiently low to be compatible with many plastic substrates. When stored in air, the "on/off" ratio was still 10⁴ after 15 days and 10³ after 5 months, which is sufficient for practical applications. Furthermore, human-scale communication sheets were manufactured as the first demonstration utilizing large-area organic memories. [J930]

"GaN-Based LEDs Output Power Improved by Textured GaN/Sapphire Interface Using In Situ Treatment Process During Epitaxial Growth"

In this study, we demonstrate an insitu roughening technique at the GaN/sapphire interface in GaN-based LEDs using a silane treatment (SiH₄ treatment) process that forms a thin SiNx layer with nanometer-sized holes on the sapphire surface that behave like a patterned sapphire substrate. A plurality of voids at the GaN/sapphire interface is observed according to the transmission electron microscopy analysis. With a 20 mA current injection, the results indicate that the typical output power of LEDs grown with and without the SiH₄ treatment process are approximately 18.0 and 15.6 mW, respectively. In other words, the output power can be enhanced by 15% with the use of the SiH₄ treatment process. The enhancement of output power is mainly due to light scattering at the naturally textured GaN/sapphire interface, which can lead to a higher escape probability for the photons emitted from the active layer in an LED. [J931]

"Angle-Dependent Spectral Width of Resonant-Cavity Light-Emitting Diode"

Characteristics of spectral width of a resonant-cavity light-emitting diode are theoretically and experimentally presented for an angular emission. To clarify the influence of the reflectivity of the distributed Bragg reflector on the spectral width, the optical matrix method was used for both the transverse-magnetic and transverse-electric

waves. The calculated results were in good agreement with the experimental ones that showed the spectral broadening at the greater angle. [J932]

"External Compensation of Nonuniform Electrical Characteristics of Thin-Film Transistors and Degradation of OLED Devices in AMOLED Displays"

The variation of electrical characteristics of polycrystalline-silicon thin-film transistor (TFT) and degradation of organic light-emitting-diode (OLED) device cause nonuniform intensity of luminance and image sticking in active-matrix OLED (AMOLED) displays. An external compensation method that senses and compensates variations of threshold voltage and mobility of TFTs and degradation of OLED device is proposed. The effect of the external compensation method on AMOLED pixel is experimentally verified by measuring the luminance of OLEDs and the electrical characteristics of TFTs in AMOLED pixels. [J933]

"Size-Dependent Strain Relaxation and Optical Characteristics of InGaN/GaN Nanorod LEDs"

In this paper, InGaN/GaN nanorod LEDs with various sizes are fabricated using self-assembled Ni nanomasks and inductively coupled plasma-reactive ion etching. Photoluminescence (PL) characteristics exhibit size-dependent, wavelength blue shifts of the emission spectra from the nanorod LEDs. Numerical analyses using a valence force field model and a self-consistent Poisson, Schrodinger, and drift-diffusion solver quantitatively describe the correlation between the wavelength blue shifts and the strain relaxation of multiple quantum wells embedded in nanorods with different averaged sizes. Time-resolved PL studies confirm that the array with a smaller size exhibits a shorter carrier lifetime at low temperature, giving rise to a stronger PL intensity. However, the PL intensity deteriorates at room temperature, compared to that of a larger size, possibly due to an increased number of surface states, which decreases the nonradiative lifetime, and hence reduces the internal quantum efficiency. [J934]

"Optical Analysis of Phosphor's Location for High-Power Light-Emitting Diodes"

High-power-light-emitting-diode (LED) packaging is crucial for the development of solid-state lighting. Phosphor's location could affect the LED packaging performance such as light extraction and correlated color temperature (CCT). This paper systematically analyzes first the effects of phosphor's location on LED packaging performance. A two-light-source step computation method based on the Monte Carlo theory is developed, and five different optical structures are discussed. Results show that the location of phosphor has small impact on light extraction but could greatly affect CCT. Remote phosphor location presents higher light extraction than proximate phosphor location. However, the increase is slight, and too remote location could reduce light extraction. A convex phosphor layer has higher light extraction but lower yellow-blue ratio than a plane phosphor layer. Considering the significant variation of CCT, it is suggested that an optical structure with plane and remote phosphor location should be a suitable choice for LED packaging. [J935]

"A Field Sequential Color LCD Based on Color Fields Arrangement for Color Breakup and Flicker Reduction"

The field sequential color (FSC) mechanism can effectively generate multi-primary color fields in temporal sequence to form a full-color image. Color breakup (CBU), however, has appeared intrinsically in conventional FSC displays to degrade visual qualities. A novel CBU suppression method, color fields arrangement (CFA), was proposed to eliminate the artifacts for FSC liquid crystal displays (LCDs). The modified order of consecutive color fields results in superimposed color images on a retina without CBU. Additionally, the 4-CFA method with a field rate of 240 Hz was found to avoid the flicker phenomenon on static images. The proposed method was successfully implemented on a 5.6-in optically compensated bend (OCB) LC panel. Our results confirm that the visibility of CBU artifacts can be reduced as the evaluation of dynamic and static models. [J936]

"Improving Light Output Power of the GaN-Based Vertical-Injection Light-Emitting Diodes by Mg Implanted Current Blocking Layer"

A method for forming a current blocking layer (CBL) by ion implantation in GaN-based vertical-injection light-emitting diodes (VI-LEDs) was proposed. It was found that the use of CBL in VI-LEDs can effectively reduce the current crowding effect and enhance the light output power. The uniform emission intensity distribution of VI-LEDs with CBL was demonstrated by electroluminescence measurements. Experimental results show that the wall-plug efficiency was enhanced by 12.3% at an injection current of 20 mA, compared to that of VI-LEDs without CBL, and by 56.2% compared to that of conventional LEDs. The device simulation results reveal that the current path can be blocked by CBL, resulting in high light extraction efficiencies and large current densities within the effective emission region of active layers. [J937]

"GaN-Based Power Flip-Chip LEDs With Cu Submount"

Nitride-based power flip-chip (FC) LEDs with Cu submount were proposed and prepared. With a much higher thermal conductivity, it was found that we can achieve a lower operation voltage under high-current injections and lower junction temperature from the FC LEDs with Cu submount. Compared with the power FC LEDs with Si submount, the reliability of the proposed device was also better. [J938]

"Fast-Response Single Cell Gap Transflective Liquid Crystal Displays"

A single cell gap transflective liquid crystal display (TR-LCD) using dual fringing field switching mode is proposed, in which a positive dielectric anisotropy liquid crystal is vertically aligned and driven by fringing fields from both substrates. By optimizing the electrode width and gap of the transmissive and reflective regions, this TR-LCD exhibits a fast response time, high optical efficiency, single gamma curve, and wide viewing angle. Fast response time enables color sequential operation using red, green, and blue light-emitting diodes without noticeable color breakup. Potential application of this TR-LCD for sunlight readable mobile displays is emphasized. [J939]

"Method for determining the junction temperature of alternating current light-emitting diodes"

A numerical simulation was used to simulate the temperature distribution during AC and DC operations of an alternating current light-emitting diode (AC LED). The relationship between the junction temperature and the temperature at the centre of the bottom surface of the submount of an AC LED was measured under DC operation. This relationship was confirmed by numerical simulation. The numerical results were consistent with the experimental observations in that the temperature at the centre of the bottom surface of the submount was insensitive to the current variations that occur in an AC LED, probably because of the large mass of the submount. However, it was difficult to measure the temperature oscillation at the junctions in an AC LED, although this oscillation can be clearly seen in the numerical results. Thus, the authors propose a formula for predicting the range of the oscillating junction temperature for an AC LED. [J940]

"A Novel Two-Dimensional Adaptive Dimming Technique of X-Y Channel Drivers for LED Backlight System in LCD TVs"

In this paper, a novel two-dimensional (2-D) adaptive dimming technique with X-Y channels for light-emitting diode (LED) backlight system in LCD TVs is proposed. The proposed LED backlight has matrix-structured LED modules with row and column switches to control the brightness of individual division block. It shows local dimming effects such as reduced power consumption and high dynamic contrast ratio even with much less number of LED drivers than that of the conventional 2-D local dimming method. Therefore, low cost and compact design of LED drivers can be achieved. This paper also contains a new adaptive dimming algorithm and image manipulation technique for the proposed LED backlight system. The proposed dimming technique is verified by simulation and experimental results based on a RGB-LED backlight of a 32-in LCD TV. [J941]

"Guiding Light From LED Array Via Tapered Light Pipe for Illumination Systems Design"

In illumination systems, it is often necessary to get a structure that can have good performance on uniformity. Although light-emitting diodes (LEDs) are replacing conventional light sources in illumination systems, they have nonuniformity and a large view angle. In this paper, an LED illumination system has been designed that can use color sequential to replace the color wheel for projector and also can mix color to get the color you want. An optical element tapered light pipe is also used in this structure, and we investigate the mechanism of irradiance distribution. It assists in the design of light pipe for different applications. The efficiency is above 80% and the uniformity is better than 60%. The formation of irradiance distribution in the tapered light pipe is discussed, both analytically and numerically. The result of the simulation verifies that efficiency of this structure is well enough for the illumination of both car headlights and interior lighting. This illumination system also provides a good color-mixing effect that can replace arc lamps or fluorescent lamps. [J942]

"Thermal Measurement and Modeling of Multi-Die Packages"

Thermal measurement and modeling of multi-die packages with vertical (stacked) and lateral arrangement became a hot topic recently in different fields like RAM chip packaging or LEDs and LED assemblies. In our present study, we present results for a more complex structure: an opto-coupler device with four chips in a combined lateral and vertical arrangement. The paper gives an overview of measurement and modeling techniques and results for stacked and multichip module (MCM) structures. It describes actual measurement results along with our structure function-based methodology which helps validating the detailed model of the

package being studied. For stack-die packages, we suggest an extension of the DELPHI model topology. Also, we show how one can derive junction-to-pin thermal resistances with a technique using structure functions.

[J943]

"A New Thin-Film Transistor Pixel Structure Suppressing the Leakage Current Effects on AMOLED"

We propose a new pixel structure employing solid-phase crystallized silicon thin-film transistors which suppresses the leakage current effects on active-matrix organic light-emitting diode (AMOLED) displays. The pixel structure has been fabricated on a glass substrate employing the field-enhanced rapid thermal annealing technology. In the proposed pixel, the charge holding capability is considerably enhanced due to the capacitor located between two series-connected switch transistors. Our experimental results shows that the average variation range of the OLED current is suppressed less than 0.5% while the conventional one exceeded 4%.

[J944]

"AlGaIn/GaN Schottky Barrier Photodetector With Multi- /GaN Buffer"

AlGaIn/GaN heterostructure Schottky barrier photodetector (PD) with multi-MgxNy/GaN buffer was proposed and fabricated. Compared with AlGaIn/GaN heterostructure PD prepared on conventional low-temperature GaN buffer, it was found that we can reduce dark leakage current by more than three orders of magnitude. It was also found that we can use the multi-MgxNy/GaN buffer to suppress photoconductance gain, enhance UV-to-visible rejection ratio, reduce noise level and enhance the detectivity. [J945]

"An Improved Optical Feedback Pixel Driver Circuit"

An improved optical feedback circuit is proposed with only a few components and a wide range of Vdatavoltages. Its operation is verified by simulation using the HSPICE simulator, PSIA2 thin-film transistor (TFT) model, and our previously published light-impact model of polycrystalline TFTs. In addition, the new optical feedback pixel driver (OFPD) is compared with previously published OFPDs, and its advantages are pointed out and discussed. [J946]

"Flip Chip Bonding of 68 68 MWIR LED Arrays"

The flip chip bonding process is optimized by varying the bonding pressure, temperature, and time. The 68times68 mid wave infrared (MWIR) LED array was hybridized onto Si-CMOS driver array with same number of pixels. Each pixel has two indium bumps, one for cathode and another for anode. Both LED array and CMOS drivers have 15-mum-square Indium bump contact pads. We used Karl Suss FC150 flip chip machine for bonding of CMOS driver array onto LED array. From the LED current-voltage characteristics, it is concluded that the optimized flip chip bonding process results in uniform contact and very low contact resistance. Both electrical and optical characteristics of LED array after flip chip bonding are presented. [J947]

"Single-Stage Soft-Switching Converter With Boost Type of Active Clamp for Wide Input Voltage Ranges"

A single-stage soft-switching converter is proposed for universal line voltage applications. A boost type of active-clamp circuit is used to achieve zero-voltage switching operation of the power switches. A simple DC-link voltage feedback scheme is applied to the proposed converter. A resonant voltage-doubler rectifier helps the output diodes to achieve zero-current switching operation. The reverse-recovery losses of the output diodes can be eliminated without any additional components. The DC-link capacitor voltage can be reduced, providing reduced voltage stresses of switching devices. Furthermore, power conversion efficiency can be improved by the soft-switching operation of switching devices. The performance of the proposed converter is evaluated on a 160-W (50 V/3.2 A) experimental prototype. The proposed converter complies with International Electrotechnical Commission (IEC) 1000-3-2 Class-D requirements for the light-emitting diode power supply of large-sized liquid crystal displays, maintaining the DC-link capacitor voltage within 400 V under the universal line voltage (90-265 Vrms). [J948]

"Polarization-Resolved Modulation Response of Single-Transverse-Mode Vertical-Cavity Surface-Emitting Lasers"

The small-signal modulation response of vertical-cavity surface-emitting lasers (VCSELs) is studied numerically, based on the spin-flip model. A detailed characterization of the influence of various parameters, such as the dichroism, the birefringence, the spin-flip rate and the noise level is done. The analysis is performed in regions of the parameter space where the operating conditions, in the absence of modulation, are such that there is

either stable single linear polarization, or bistability of two orthogonal linear polarizations or polarization instability. In the instability region the intensities of the orthogonal polarizations display anticorrelated self-sustained oscillations that result in a complex small-signal modulation response, exhibiting multiple resonance peaks with frequencies that vary with the injection current and the spin-flip rate. In contrast, in parameter regions where there is stable single polarization the modulation response of the total intensity is as that of a single-mode laser, exhibiting a conventional single-resonance peak, and is almost not influenced by the value of the spin-flip rate. Polarization mode-hopping results in a distortion of the polarization-resolved modulation response at low frequencies. [J949]

"Where Is Waldo? [JMicrowave Surfing]"

Professor Pendry's (Imperial College, London) observation [1] from 2006 is an example of the excitement in the electromagnetic research community on the potential of metamaterials to create the equivalent of Harry Potter's invisibility cloak. Back then, a research group at Duke University demonstrated [2] how a twodimensional (2-D) structure composed of ten fiberglass rings covered with subwavelength arrays of copper elements could help "channel" an incident electromagnetic (EM) wave in the microwave frequency range around a copper cylinder, minimizing a scattered signal. Earlier this year, a group at the University of California (UC) Berkeley [3] raised the stakes by fabricating the "cloak" using nanotechnology (for the subwavelength elements) so that the target could be made to "disappear" at wavelengths approaching the visible spectrum. Exciting as these metamaterial-based developments have been, they remain far from real-life applications. A recent report in The Economist [4] discusses what is achievable in practice using the current hide-and-seek military technology. Here are some highlights from the report [4]. [J950]

"Establishment of All Digital Closed-Loop Interferometric Fiber-Optic Gyroscope and Scale Factor Comparison for Open-Loop and All Digital Closed-Loop Configurations"

This paper covers the design details of an all digital closed-loop interferometric fiber-optic gyroscope (ADCL-IFOG) prototype, constructed in TUBITAK UME, and scale factor comparison between open-loop and ADCL-IFOG prototypes with sine wave biasing modulation. The output of demodulation circuit, proportional to the applied rotation rate, was sampled by AD7714YN analog-to-digital converter (ADC), operated in 16 bit resolution. Error voltage, generated by microcomputer-controlled LTC 1667CG, 14 bit digital to analog converter (DAC), was sent to the phase modulator through a linear summing circuit to make Sagnac phase shift zero, depending on the rotation direction. For this implementation, the ultimate rotation rate of 1.84 (deg/h) was nullified. The averaged sensitivity of the proposed closed-loop IFOG in unit of error voltage applied to the phase modulator was determined as 132.65 $\mu\text{V}/(\text{deg/h})$. The scale factors of both the open-loop and ADCL-IFOG prototypes were compared in a range of 1-15270 (deg/h) rotation rate, corresponding to Sagnac phase shifts varying from 0.00115 (deg) to 17.57448 (deg). The maximum peak to peak noise and the bias stability of ADCL-IFOG prototype were determined as 4.97 (deg/h) and 1.48 (deg/h) at 23.0degC, respectively. [J951]

"GaN nanowire light emitting diodes based on templated and scalable nanowire growth"

GaN optoelectronic devices based on nanowires offer potential advantages that merit further investigation for applications in solid-state lighting and displays. Reported is the operation GaN nanowire, light-emitting diodes that are based on a uniform and scalable nanowire process. For light-emitting diodes consisting of approximately 300 nanowire pn-homojunctions, operating in parallel, the electroluminescence intensity was found to grow superlinearly with current. For individual nanowire light-emitting diodes the forward and reverse leakage current was <1 pA. The low leakage current of individual light-emitting nanowire diodes indicates that surface effects do not dominate the electrical behaviour of these LEDs. [J952]

"Influence of Insulator Length on the Downstream Electron Temperature and Density in the Coaxial Plasma Focus Device"

We have generated the Ar plasma in the diode chamber based on the established coaxial electrode type and investigated the emitted visible light for emission spectroscopy. The optical emission spectrum data have been obtained for the focused plasma in the cylindrical diode chamber under the input voltage of 4.5 kV and pressure of 40 mtorr. We observed the nine emission lines of Ar II: 407.3, 410.6, 422.4, 426.8, 427.9, 435.0, 438.1, 444.5, and 488.0 nm. The downstream electron temperature and density have been measured by the Boltzmann plot and Stark broadening, respectively, from the assumption of local thermodynamic equilibrium. The length of the acrylic insulator has been changed to 30, 40, and 45 mm, respectively, which is covered on the inner cathode surface, to investigate the influence of insulator length on the downstream electron temperature and density in this experiment. Our results show that the downstream electron temperature and density of focused plasma are 2.5 eV and $1.6 \times 10^{16} \text{cm}^{-3}$, respectively, for the coaxial plasma focus with cylindrical electrodes at the

insulator length of 40 mm. [J953]

"Performance Improvement of Carbon-Nanotube-Incorporated Transparent Conducting Anode Film for Organic Device Application"

Carbon nanotubes (CNTs) were incorporated into indium tin oxide and polythiophene by mixing and then spin coating or screen printing to form the transparent conducting electrode (TCE). With only approximately 0.005%, by weight, of CNTs in the TCE, the sheet resistance was found to drop by about 25% to 40%, without any significant decrease in the transmittance. Organic light-emitting devices (OLEDs) were then fabricated using these composite TCEs as the anode. In comparison with a device without the CNTs, there was an increase in the current density for the same applied voltage, mainly due to the contribution of hole current. In addition, the mechanical strength was improved, as seen from bending test of the device. [J954]

"Effects of Hydrogenation on Optoelectronic Properties of a-C:H Thin-Film White-Light-Emitting Diodes With Composition-Graded Carrier-Injection Layers"

In this paper, thin-film white-light-emitting diodes (TFWLEDs) were fabricated with a hydrogenated intrinsic amorphous carbon (i-a-C:H) film as the luminescent layer and a composition-graded (CG) hydrogenated intrinsic amorphous silicon carbide (i-a-SiC:H) film as the carrier-injection layers. The demonstrated TFWLEDs could be operated under direct-current (dc) forward or reverse bias or sinusoidal alternating-current (ac) voltage. The hydrogenation process for the luminescent or CG carrier-injection layer has been investigated to greatly enhance the optoelectronic properties of the obtained TFWLEDs. For the hydrogenated TFWLEDs, the highest obtainable brightnesses were 813 and 507 cd/m² at an injection-current density of 0.6 A/cm², and the lowest electroluminescence (EL) threshold voltages were 9.1 and 8.9 V, under dc forward and reverse biases, respectively. These enhanced optoelectronic properties were attributed to the passivation of dangling bonds and the forming of more H₂-compensated amorphous film by the employed hydrogenation process. In addition, the electrical transport mechanisms of the TFWLEDs were studied. In the low-applied-bias range, the ohmic current was the dominated one. In the high-applied-bias range, a Poole-Frenkel emission current resulted from the field-assisted hopping along the traps in amorphous film was observed. Moreover, a significant red-shift in EL spectra has been observed while the applied ac frequencies were higher than 1 kHz, and its origin has been attributed to the lower mobilities of charge carriers. [J955]

"Optical Sensors for Real-Time Measurement of Motorcycle Tilt Angle"

This paper addresses the analysis and design of an optical sensor for the real-time measurement of the tilt angle in hypersport motorcycles. The aim of this paper is to design a compact, reliable, and low-cost optical triangulator that is capable of accurate in-field measurements in the harsh environment of sport motorcycles. An analytical computation of the required system sensitivity and achievable accuracy is carried out. The detrimental effects of solar interference are also described and discussed. The proposed instrumentation, which is realized with ad hoc laser emitters, is shown to have superior performance with respect to a previous solution based on light-emitting diode (LED) emitters. Such novel triangulators are shown to provide good and reliable performances for the proposed application to maintain low costs and small sizes, overcoming the problem of solar interference. The performance of the proposed sensor is assessed by experiments on an instrumented motorbike in a racetrack. [J956]

"UV-LEDs for Monitoring Dialysis Adequacy"

New Ultraviolet (C band: 280 nm - 100 nm) light emitting diodes (UV-C LEDs) have been characterized to evaluate their potential applicability in the development of a simple low-cost optical adequacy sensor for continuous online measurements on spent dialysate. This approach would allow us to avoid the use of bulky and expensive spectrometers in the monitor systems. The reported results could be useful for the system development even if different critical aspects such as LED reliability, mean lifetime, and emitted and transmitted power monitoring should be taken into consideration. Nevertheless, the experimental activity has shown that the system can be implemented with few optical components and that the assembly can be made simple. [J957]

"Efficiency Enhancement and Beam Shaping of GaN-InGaN Vertical-Injection Light-Emitting Diodes via High-Aspect-Ratio Nanorod Arrays"

The enhanced light extraction and collimated output beam profile from GaN-InGaN vertical-injection light-emitting diodes (VI-LEDs) are demonstrated utilizing high-aspect-ratio nanorod arrays. The nanorod arrays are patterned by self-assembled silica spheres, followed by inductively coupled-plasma reactive ion etching. The fabricated nanorod arrays not only provide an omnidirectional escaping zone for photons, but also serve as waveguiding

channels for the emitted light, resulting in a relatively collimated beam profile. The light output power of the VI-LED with nanorod arrays is enhanced by 40%, compared to a conventional VI-LED. The measured far-field profiles indicate that the enhancement is mainly along the surface normal direction, within a view angle of 20deg. [J958]

"Nitride-Based Thin-Film Light-Emitting Diodes With Photonic Quasi-Crystal Surface"

In this letter, the nitride-based thin-film light-emitting diodes (TFLEDs) with eight-fold photonic quasi-crystal (PQC) surfaces are proposed and demonstrated by a combination of wafer bonding, laser lift-off, and electron-beam lithography processes. By adopting a PQC surface, the light-output power (at 350 mA) of the PQC-TFLEDs exhibits 140% output power enhancement as compared with that of TFLEDs without a PQC surface. [J959]

"Performance enhancement of outdoor visible-light communication system using selective combining receiver"

New generation of high-intensity aluminium gallium arsenide (AlGaAs) and aluminium indium gallium phosphide (AlInGaP) light-emitting diodes (LEDs) which have permitted the replacement of incandescent-based traffic lights with LED-based traffic lights, unfolds the potential of implementing visible-light communication (VLC) system on outdoor environment. The feasibility of outdoor VLC system is undoubtedly questionable because of the significant ambient-light noise caused by daylight. Existing performance studies related to this system have not taken into account the effect of ambient-light noise which varies largely from day time to night time. The authors propose an analytical daylight noise model based on a modified Blackbody radiation model to capture the effect of ambient-light noise and conduct an in-depth study on the impact of daylight on the system performance. The proposed daylight noise model allows us to perform analytical analysis which produces relatively accurate results with less complexity, as compared to the existing time-consuming simulation. The authors also introduce a new receiver structure employing the selective combining technique to significantly reduce the effect of background noise. From numerical analysis, the authors show that the new receiver structure is able to achieve a signal-to-noise ratio (SNR) improvement of approximately 5 dB and establish a stable communication link at any time of the day. [J960]

"Development of street lighting system-based novel high-brightness LED modules"

The development of high-power light emitting diode (LED) for street lighting is growing continuously owing to its greater energy efficiency, long operating life and light control. Users of street lighting are compelled to adopt this technology over traditional light sources. An alternative solution based on a novel 9LEDM (9-LED module) and adaptive driver is shown. The design of the 9LEDM is derived from the thermal, photometric, power electronics techniques to meet the application of street lighting. The 9LEDM performances with a price less than 1\$/Watt (W) and luminous flux higher than 110 Lumens (Lm)/W compared with traditional ones. Furthermore, several restrictions of driving the solid-state lighting loads are overcome by an adaptive street lighting driver with an AC/DC converter of a quasi-resonant operation flyback topology and with Soft Startup, Full ON, Half ON functions by sensing the ambient light and working temperature. Finally, a high performance/cost 50 W pole head as a design example is conducted to illustrate the complete design process, and the results from the demonstration projection with two pole heads of 50 W for a 12 m pole show a luminous intensity range from 38 to 19 lux with a heat sink temperature of 58degC and an energy saving more by 72% compared with conventional street lighting after three months of running. [J961]

"Fast and Offset-Leakage Insensitive Current-Mode Line Driver for Active Matrix Displays and Sensors"

Current-programmed active matrix (AM) architectures that are independent of fabrication technology are attractive for display and sensor because of their ability to tolerate mismatches and nonuniformity caused by aging. However, the long settling time due to low current levels and large parasitic capacitance can be a significant limitation. In this paper, we present a fast current-mode line driver based on positive feedback which controls the effect of parasitic capacitance. The driver was fabricated in 0.8- μm 20-V CMOS technology. While the measured settling time of a conventional current source is around 2 ms for a 100-nA input current and 200-pF parasitic capacitance, it is less than 4 μs for the driver presented here. Moreover, an offset-leakage cancellation technique is implemented for the fabricated driver to reduce the effect of leakage and offset currents to few nA. [J962]

"Optical Replacement of pH Electrode"

The development of a noninvasive, self-contained optical pH sensor probe intended as a direct replacement for a pH electrode is presented. It uses a fluorescent excitation-ratiometric pH sensing dye in a patch. The patch is excited by light emitting diodes of differing wavelengths which are controlled by a microcontroller (MCU). The emission levels are measured by analog circuitry and their ratio is converted by the MCU into a linear output which mirrors that of a conventional pH electrode. The optical sensor readings were consistent with readings from a glass pH electrode with average difference .061 pH. This sensor allows noninvasive, low-cost optical pH sensing with the ability to interface with existing pH monitoring equipment. [J963]

"Model Parameterization of Nonlinear Devices Using Impedance Spectroscopy"

In this paper, a new approach is used to identify the parameters of a large-signal lumped-element model for nonlinear devices based on small-signal impedance measurements at several operating points. Starting from the large-signal impedance of an equivalent circuit with nonlinear devices, the relationship between current and voltage is derived by the determining nonlinear system equation. This differential equation for a first-order model is then linearized via nonlinear series expansion using the perturbation approach. The linearized ac part (which is the fundamental frequency part) is then transformed into the frequency domain to find a representation of the complex small-signal impedance for a given operating point. Large-signal modeling based on small-signal measurements is successfully demonstrated for organic light-emitting diodes. [J964]

"Dimming of High-Brightness LEDs by Means of Luminous Flux Thermal Estimation"

Usually, pulsewidth modulation (PWM) operation is selected as the best dimming strategy to drive high-brightness LEDs. Nevertheless, to obtain an enhanced full linear dimming control of the device, the luminous flux should be measured. This paper proposes a control method based on an estimator of the luminous flux emitted by the LED. Based on the characterization of the LEDs, this estimator is defined. The estimator provides the flux value from only two temperature values (the case temperature and the ambient temperature). Once the estimator is validated, the electronic driver to supply the LEDs, as well as the digital control scheme, are presented. Such a control scheme is suitable for both AM and PWM dimming strategies. A prototype of the electronic driver has been built and tested, and experimental measurements of AM and PWM dimming are presented. It can be concluded that with the proposed estimator, the flux emitted by the LEDs can be accurately estimated. Thus, the output light control of the LEDs can be accomplished by sensing temperature rather than luminous flux. The final output characteristic of the system shows linearity between the output flux and the reference value, with AM as well as with PWM dimming of the LEDs. [J965]

"Chromatic dispersion penalty by angular coupling between resonant cavity light-emitting diode and plastic optical fibre"

Chromatic dispersion penalty by angular coupling between a resonant cavity light-emitting diode (RCLED) and a plastic optical fibre is presented. To evaluate the influence of the angular-dependent spectral characteristics of the RCLED on the chromatic dispersion penalty, the effective spectral linewidth of the RCLED was defined and the bit error rate performances for 500 Mbit/s by 50 m transmission were calculated. The calculated results were in good agreement with the experimental ones that showed the chromatic dispersion penalty of 1.2 dB at BER 10⁻¹² in the angle of 26deg. [J966]

"Optical impulse modulation for indoor diffuse wireless communications"

Current lasers and LEDs have far higher pulse rates than can be supported by the lowpass indoor diffuse optical wireless channel. Although high-frequency emissions are attenuated by the channel and are not detected by the receiver, a key insight of this paper is that these bands can be used to satisfy the channel non-negativity constraint. We define optical impulse modulation (OIM) in which data are confined to the lowpass region while the highpass region, which is attenuated by the channel, is used to satisfy the channel amplitude constraints. A mathematical framework for OIM is presented, and a simple suboptimal receiver filter is designed which is channel independent. Using a well-known exponential model for indoor diffuse optical channels, at a normalized delay spread of 0.2, the gain in optical average power of OIM with a simple lowpass receiver is shown to be 4.9 dBo which exceeds the gain of rectangular on-off keying (Rect-OOK) with a complex decision feedback equalizer. From an information theory point of view, at the same normalized delay spread of 0.2, the information rate of OIM with a lowpass receiver is shown to be 11.5% higher than that of Rect-OOK with a more complex whitened matched filter receiver. [J967]

"Methods of Increasing Luminous Efficiency of Phosphor-Converted LED Realized by Conformal Phosphor Coating"

White light output was realized through combining a cerium-doped yttrium aluminum garnet (YAG:Ce³⁺) phosphor with a gallium nitride (GaN)-based blue light-emitting diode (LED). In order to coat a phosphor layer of high quality on a GaN chip, the slurry coating technique was applied and investigated because of the coating efficiency and uniformity. The phosphor layer of conformal structure was realized on the LED chip with the self-exposure method. The influences of ammonium dichromate (ADC) as photosensitizer of photoresist in the slurry are discussed. Two methods are brought forward to reduce the absorption of Cr ions introduced by ADC. And experimental results indicate that these two methods are feasible to increase the luminous efficiency of white LEDs. [J968]

"Design and Evaluation of Light Spread Function for Area-Adaptive LCD System"

A methodology, based on two-dimensional super-Gaussian light spread functions (LSFs), was studied for the light-emitting-diode (LED) backlighting system in the high dynamic range (HDR) liquid crystal displays (LCDs). We proposed a novel LED-based optomechanical configuration to implement the desirable luminous pattern. A dual-liquid-crystal-panel system was constructed as a pseudo-HDR LCD to evaluate the super-Gaussian illumination. The proposed HDR scheme was verified via the current platform: overall luminance uniformity, contrast ratio and processing speed could be improved by factors of 1.55, 1.95-4.15, and 4.82, respectively. The design flexibility made the methodology applicable to any panel dimension and backlight division of the HDR LCDs, and to the conventional full-on backlighting LCDs as well. [J969]

"A Single-Inductor Step-Up DC-DC Switching Converter With Bipolar Outputs for Active Matrix OLED Mobile Display Panels"

A single-inductor step-up DC-DC switching converter with bipolar outputs is implemented for active-matrix OLED mobile display panels. The positive output voltage is regulated by a boost operation with a modified comparator control (MCC), and the negative output voltage is regulated by a charge-pump operation with a proportional-integral (PI) control. The proposed adaptive current-sensing technique successfully supports the implementation of the proposed converter topology and enables the converter to work in both discontinuous-conduction mode (DCM) and continuous-conduction mode (CCM). In addition, with the MCC method, the converter can guarantee a positive output voltage that has both a fast transient response of the comparator control and a small output voltage ripple of the PWM control. A 4.1 mm² converter IC fabricated in a 0.5 μm power BiCMOS process operates at a switching frequency of 1 MHz with a maximum efficiency of 82.3% at an output power of 330 mW. [J970]

"Nitride-Based Asymmetric Two-Step Light-Emitting Diode With In Ga N Shallow Step"

A nitride-based asymmetric two-step light-emitting diode (LED) with In_{0.08}Ga_{0.92}N shallow step was proposed and fabricated. It was found that the low indium content In_{0.08}Ga_{0.92}N layer can significantly enhance phase separation and/or inhomogeneous indium distribution in the active In_{0.27}Ga_{0.73}N layer. It was also found that we can enhance LED output power by a factor of 2.27 by simply inserting an In_{0.08}Ga_{0.92}N shallow step. [J971]

"Nitride-Based LEDs With Phosphoric Acid Etched Undercut Sidewalls"

We propose a simple defect-selective wet etching method to form oblique sidewalls for GaN-based epitaxial layers with phosphoric acid. Using the same defect-selective wet etching, we also prepared GaN-based light-emitting diodes (LEDs) with undercut sidewalls. Compared with conventional LEDs with vertical sidewalls, it was found that output intensity of the LEDs prepared by defect-selective wet etching was 30% higher. [J972]

"Study of an AlGaInP-Based Light-Emitting Diode With a Modulation-Doped Multiquantum-Well (MD-MQW) Structure"

An AlGaInP-based multiquantum-well (MQW) light-emitting diode (LED) with an n-type modulation-doped (MD) structure, grown by metal-organic vapor-phase epitaxy, is fabricated and studied. Experimental results indicate that a lower turn-on voltage and dynamic resistance, higher output power, and smaller wavelength shift, as compared to a conventional undoped-MQW LED, are obtained. The studied n-type MD-MQW LED also exhibits a higher external quantum efficiency of 7.2% and a larger maximum light output power. The junction temperature of the studied MD-MQW LED also shows a 12 degC reduction, at 200 mA, as compared to a conventional one. These positive results are mainly attributed to the presence of a higher electron concentration in the MD-MQW active region. [J973]

"Improvement of the Efficiency of InGaN-GaN Quantum-Well Light-Emitting Diodes Grown With a

Pulsed-Trimethylindium Flow Process"

This study demonstrated the enhancement of the light output power of InGaN-GaN multiple quantum-well light-emitting diodes (LEDs) that are grown with a pulsed-trimethylindium (pulsed-TMIn) flow process by metal-organic vapor-phase epitaxy. At an injection current of 20 mA, the output power of the pulsed-TMIn treated LEDs was improved by 16% as compared to that of the conventional LEDs. In addition, a minor droop (versus injection current) in terms of external quantum efficiency was also observed in the pulsed-TMIn treated LEDs as compared to conventional LEDs. This improvement could be attributed to the fact that the significant carrier localization effect in the pulsed-TMIn treated LEDs can lead to higher recombination efficiency. This contention is perhaps tentatively evidenced by the temperature-dependent photoluminescence results in which the activation energy of the pulsed-TMIn treated LEDs was increased by 21.8% as compared to that of conventional LEDs.

[J974]

"Improvement on Optical Properties of GaN Light-Emitting Diode With Mesh-Textured Sapphire Back Delineated by Laser Scriber"

The optical properties of gallium nitride light-emitting diode with mesh-textured sapphire back delineated by laser scriber and subsequently coated with silver-copper layers were investigated. This new structure improves the optical characteristics. The electroluminescence and luminous intensities are 30% and 20% stronger than that without mesh-textured trench and silver-copper at 20 mA, respectively. The maximum luminous intensity has 1.6 times enhancement, which is mainly from higher light extraction by the mesh-textured trench. [J975]

"Growths of staggered InGaN quantum wells light-emitting diodes emitting at 520-525 nm employing graded growth-temperature profile"

Three-layer staggered InGaN quantum wells (QWs) light-emitting diodes (LEDs) emitting at 520-525 nm were grown by metal-organic chemical vapor deposition by employing graded growth-temperature profile. The use of staggered InGaN QW, with improved electron-hole wave functions overlap design, leads to an enhancement of its radiative recombination rate. Both cathodoluminescence and electroluminescence measurements of three-layer staggered InGaN QW LED exhibited enhancements by 1.8-2.8 and 2.0-3.5 times, respectively, over those of conventional InGaN QW LED. [J976]

"Transport of Photogenerated Charge Carriers in Polymer Semiconductors"

The electrical transport of photogenerated charge carriers in disordered polymer semiconductors is reviewed. We emphasize that the mobility parameter in these disordered semiconducting systems is not a well-defined quantity. We highlight the utility of scanning probe photocurrent technique on variety of polymers in an asymmetric-electrode patterned configuration. The multiple length and time scales present in carrier transport processes are indicated by the large observed decay length scales in these systems. [J977]

"High-Efficiency Current-Regulated Charge Pump for a White LED Driver"

This brief presents a high-efficiency current-regulated charge pump for a white light-emitting diode driver. The charge pump incorporates no series current regulator, unlike conventional voltage charge pump circuits. Output current regulation is accomplished by the proposed pumping current control. The experimental system, with two 1- μ F flying and load capacitors, delivers a regulated 20-mA current from an input supply voltage of 2.8-4.2 V. The measured variation is less than 0.6% at a pumping frequency of 200 kHz. The active area of the designed chip is 0.43 mm² in a 0.5- μ m CMOS process. [J978]

"Dip-shaped InGaN/GaN quantum-well light-emitting diodes with high efficiency"

Optical properties of dip-shaped InGaN/GaN quantum well (QW) light-emitting diodes are investigated using the multiband effective-mass theory. These results are compared with those of conventional and staggered InGaN/GaN QW light-emitting diodes. In the case of a dip-shaped QW structure, the carrier density dependence of the transition wavelength is reduced due to a relatively small internal field effect. Also, we observe that the heavy-hole effective mass around the topmost valence band is greatly reduced with the inclusion of the dip-shaped layer. The spontaneous emission peak of a dip-shaped QW structure is shown to be larger than that of a staggered QW structure or a conventional QW structure. This is mainly due to the fact that a dip-shaped QW structure has larger optical matrix elements produced by Kane's parameter. [J979]

"Low-voltage onset of electroluminescence in nanocrystalline-Si /SiO₂ multilayers"

Thin film metal-oxide-semiconductor light emitting devices (LEDs) based on nanocrystalline silicon multilayer

structure were grown by plasma-enhanced chemical vapor deposition. Room temperature electroluminescence was studied under direct current and time-resolved pulsed-current injection schemes. Multilayer LEDs operating at voltages below 5 V and electroluminescence turn-on voltage of 1.4-1.7 V are demonstrated. The turn-on voltage is less than 3.2 V which corresponds to the barrier height at the silicon oxide interface for electrons. Electrical injection in the multilayer LED is controlled by direct tunneling of electrons and holes among silicon nanocrystals. This injection regime is different than the Fowler-Nordheim tunneling that controls the electron injection in single thick layer LED operating at high voltages. A comparison of the power efficiency for the multilayer based LED and a similar single thick layer LED shows larger power efficiency for the former than for the second. Our results open new directions in the development of highly efficient room temperature silicon based LED. [J980]

"Quantitative Analysis of Dopant Distribution and Activation Across p-n Junctions in AlGaAs/GaAs Light-Emitting Diodes Using Off-Axis Electron Holography"

Off-axis electron holography has been used to measure the electrostatic potential profile across the p-n junction of an AlGaAs/GaAs light-emitting diode with linearly graded triangular AlGaAs barriers. Simulations of the junction profile showed small discrepancies with experiment when the nominal dopant concentrations of Si and Be impurities were used. Revised simulations reproduced the measurements reasonably using reduced dopant levels that reflected the efficiency of dopant activation. Band-edge diagrams simulated with the nominal and revised dopant concentrations were also compared in terms of the effect that activation efficiency had on the AlGaAs barrier shape and carrier transport. It is concluded that electron holography measurements combined with modeling offer device designers and growers a helpful tool for analyzing and confirming doping profiles in complex heterostructures. [J981]

"Organic Semiconductor Optical Amplifiers"

Organic semiconducting materials have been researched for novel optoelectronic devices due to their efficient light emission and high gain properties. Such devices range from organic light-emitting diodes and solar cells to lasers and amplifiers. This paper explores the research carried out on one of these devices: organic semiconductor amplifiers that have shown to give high gains of 20-40 dB in solution and solid state. [J982]

"Multiscale Modeling of Charge and Energy Transport in Organic Light-Emitting Diodes and Photovoltaics"

Modelling organic devices is an outstanding challenge because device performance is very sensitive to how the molecules are packed and the films are highly disordered. An understanding of charge and exciton (bound electron-hole pair) transport in these materials is important if organic light-emitting diodes are to be exploited in displays, lighting, photovoltaics, transistors, and sensors. This paper discusses methods we have pioneered for predicting charge and exciton transport, in which polymer chains are explicitly modeled and charge and exciton transfer rates are taken from electronic structure theory. Monte Carlo and drift diffusion device models that link device performance with morphology are also covered. The focus here is on polymers, but there is much in common with small molecule organic materials. [J983]

"Study on the formation of dodecagonal pyramid on nitrogen polar GaN surface etched by hot H₃PO₄"

Hot phosphoric acid (H₃PO₄) etching is presented to form a roughened surface with dodecagonal pyramids on laser lift-off N face GaN grown by metalorganic chemical vapor deposition. A detailed analysis of time evolution of surface morphology is described as a function of etching temperature. The activation energy of the H₃PO₄ etching process is 1.25 eV, indicating the process is reaction-limited scheme. And it is found that the oblique angle between the facets and the base plane increases as the temperature increases. Thermodynamics and kinetics related factors of the formation mechanism of the dodecagonal pyramid are also discussed. The light output power of a vertical injection light-emitting-diode (LED) with proper roughened surface shows about 2.5 fold increase compared with that of LED without roughened surface. [J984]

"Effect of efficiency 'droop' in violet and blue InGaN laser diodes"

We have studied two types of InGaN laser diodes emitting at 410 and 440 nm. Each device was characterized by measuring light-current characteristics in two geometries for which the light was collected: along the resonator and perpendicularly to the cavity. In the first configuration, the 410 nm device displays no reduction of differential efficiency while 440 nm laser shows evidence of droop. In the perpendicular configuration both devices show the pronounced droop. We associate the suppression of the droop for 410 nm laser in the "along cavity"

configuration with the appearance of the stimulated recombination. [J985]

"Space charge effects on the electroluminescence efficiency and stability of organic light-emitting devices with mixed emitting layers"

In organic light-emitting devices (OLEDs), the decay rate of triplet state population in the electron/hole recombination zone is found to be highly sensitive to space charge densities, providing an avenue for inferring variations in their formation. In OLEDs containing mixtures of N,N'-Bis(naphthalen-1-yl)-N'-bis(phenyl)benzidine (NPB) and tris(8-hydroxyquinoline) aluminum (AlQ3) in the emitting layer, optimizing the NPB/AlQ3 is found to reduce hole space charges, and leads to an increase in electroluminescence stability. Conversely, electroluminescence efficiency is found to be only weakly dependent on the mixture composition, suggesting that hole space charges are not effective quenchers of AlQ3 singlet excitons in mixed emitting layer OLEDs. [J986]

"Enhanced performance of silicon quantum dot light-emitting diodes grown on nanoroughened silicon substrate"

We report the effect of a nanoroughened Si substrate on silicon quantum dot (Si QD) light-emitting diodes (LEDs). The electroluminescence of Si QD LEDs grown on the nanoroughened Si substrate was remarkably improved by 493% at an injection current of 90 mA compared to those of Si QD LEDs grown on the flat Si substrate. The electrical and optical enhancements were attributed to the enhanced inhomogeneous local electric field on the nanoroughened Si surface and the angular randomization of photons emitted from Si QDs at the nanoroughened surface of silicon nitride layer containing Si QDs. [J987]

"Demonstration of nonpolar a-plane InGaN/GaN light emitting diode on r-plane sapphire substrate"

High crystalline a-plane (1120)GaN epitaxial layers with smooth surface morphology were grown on r-plane (1102)sapphire substrate by metalorganic chemical vapor deposition. The full width at half maximum of x-ray rocking curve was measured as 407 arc sec along c-axis direction, and the root mean square roughness was 1.23 nm. Nonpolar a-plane InGaN/GaN light emitting diodes were subsequently grown on a-plane GaN template, and the optical output power of 0.72 mW was obtained at drive current of 20 mA (3.36 V) and 2.84 mW at 100 mA (4.62 V) with the peak emission wavelength of 477 nm. [J988]

"Does the Estimation of Light Attenuation in Tissue Increase the Accuracy of Reflectance Pulse Oximetry at Low Oxygen Saturations In Vivo ?"

A new technique was validated in vivo in reflectance pulse oximetry for measuring low oxygen saturations. Two pairs of light emitter/detector diodes allow for estimation of light attenuation (LA) in tissue, which is assumed to be responsible for the inaccuracy of pulse oximetry at less than 70% arterial oxygen saturation. For validation, 17 newborn piglets were desaturated stepwise from 21% to 1.25% inspiratory oxygen concentration during general anesthesia, and arterial oxygen saturation was measured with the reflectance pulse oximeter adjusted for LA in tissue, with a standard transmission pulse oximeter and a hemoximeter. LA in tissue could be quantified and was different between snout and foreleg (probability level (p) < 0.05). At arterial oxygen saturations above 70%, the bias between the methods was at 0%-1% and the variability 4%-5%. From 2% to 100% arterial oxygen saturation, the reflectance pulse oximeter estimated oxyhemoglobin saturation more accurately than a conventional transmission pulse oximeter (p < 0.05). At low oxygen saturations below 70%, the bias and variability of the reflectance pulse oximeter calibration were closer to the hemoximeter measurements than the transmission pulse oximeter (p < 0.05). The variability of the reflectance pulse oximeter was slightly lower than the traditional oximeter by taking into account the LA in tissue (9% versus 11%-15%, ns), and thus, the quality of the individual calibration lines improved (correlation coefficient, p < 0.05). [J989]

"For your eye only"

A contact lens with one LED that is powered wirelessly with radiofrequency (RF) is built. The conventional contact lenses made up of polymers are integrated with control circuits, communication circuits, and miniature antennas using custom-built optoelectronic components that include hundreds of LEDs. The lenses are successfully tested with live rabbits and can be a multipurpose, whether used as biosensors, displays, etc. [J990]

"Publisher's Note: "Opening the light extraction cone of high index substrates with plasmonic gratings: Light emitting diode applications" [JAppl. Phys. Lett. 95, 021101 (2009)]"

"Blue-emitting LaSi₃N₅:Ce³⁺ fine powder phosphor for UV-converting white light-emitting diodes"

We have synthesized the pure ternary nitride phosphor, LaSi₃N₅:Ce³⁺ from the multicomponent oxide system La₂O₃-CeO₂-SiO₂, by using the gas-reduction-nitridation method. Highly pure, single-phase LaSi₃N₅:Ce³⁺ powders possessing particle sizes of 0.4-0.6 μm were obtained with the processing temperature ≤1500 °C. The synthesized LaSi₃N₅:Ce³⁺ exhibits tunable blue broadband emission with the dominant wavelength of 464-475 nm and the external quantum efficiency of 34%-67% under excitation of 355-380 nm. A high thermal stability of LaSi₃N₅:Ce³⁺ compared to the existing La-Si-O-N hosts was demonstrated, indicating the promising applicability as a blue-emitting phosphor for UV-converting white light-emitting diodes. [J992]

"Singlet Generation Yields in Organic Light-Emitting Diodes"

A major potential difference between polymer and small molecule organic light-emitting devices is the possibility of spin-dependent charge recombination in the latter. In this case, the singlet exciton formation yield, one of the key parameters that determines device efficiencies, deviates from the simple quantum mechanical spin statistics prediction of 25%. For polymers, the departure from this limit has been demonstrated by several indirect measurements yielding a wide spread values from 25% up to 95% and by ourselves using a direct measurement on working devices at 44%. These results clearly indicate that polymer-based devices hold a unique advantage over small molecule-based devices. Comment will be made to these various measurement techniques along with an insight into current theoretical ideas that can explain the departure from the quantum spin statistical limit. OLEDs. [J993]

"Bilevel Current Driving Technique for LEDs"

The significant improvements recently achieved in LED technology in terms of lifetime, luminous efficacy, power rating, and color property render LED one of the most promising candidates to replace conventional light sources in various residential and industrial applications. The rapid advancement in the device characteristics has simultaneously stimulated interests in developing efficient LED drivers with optimized control circuitries. The two conventional techniques currently employed in most LED drivers, namely the amplitude-mode and pulsewidth modulation (PWM) mode driving techniques, suffer from the disadvantage that high luminous efficacy in the amplitude mode has to be traded for control flexibility in the PWM mode and vice versa. In this paper, a method is proposed to improve the luminous efficacy of conventional PWM-mode driving technique while retaining their control flexibility by introducing a dc-offset component into the PWM current. Two LEDs were used in the experimental verifications. Improvements of 17.6% and 18.1% on average were measured by maintaining a dc offset of 100 and 200 mA, respectively, in the LED current. Further improvement can be achieved by increasing the dc-offset current. The main tradeoff is the reduction of the dynamic range over which the average LED current can be controlled. For a given set of performance criteria, the proposed method offers designers of LED drivers the flexibility of balancing between luminous efficacy and dynamic range for control. [J994]

"Electron injection via pentacene thin films for efficient inverted organic light-emitting diodes"

We report on the fabrication of efficient inverted organic light-emitting diodes (IOLEDs) using pentacene films as an electron injection/transport layer between Al and Alq₃ layers. These IOLED devices turn on at 4.7 V and exhibit a luminous efficiency of 9.5 cd/A without any dopants or reactive metals. Analysis using space-charge-limited characteristics of electron-only devices and ultraviolet photoelectron spectroscopy measurement of metal/organic interfaces indicates that the efficient IOLED characteristics can be attributed partly to the electron mobility of pentacene that is 10²-10⁴ times larger than that of Alq₃ and to the effective reduction in injection barrier at contacts. [J995]

"Modeling Highly Efficient RCLED-Type Quantum-Dot-Based Single Photon Emitters"

Highly efficient single photon sources are of particular importance for quantum cryptography and quantum computation. Cavity-induced enhancement of spontaneous emission can improve photon generation efficiency in quantum-dot-based single photon sources dramatically. Using the eigenmode-technique, the authors calculate the 3-D distribution of the optical electromagnetic field inside a RCLED-type single photon source and consequently the Purcell-factor as a function of the wavelength. Under systematic variation of device design parameters such as cavity length and aperture diameter, an optimized device design was determined, providing Purcell-factors up to 5.5. [J996]

"Morphological changes of InGaN epilayers during annealing assessed by spectral analysis of atomic force microscopy images"

During annealing, the morphologies of thin InGaN epilayers have been observed to change from a terraced structure to a network of interlinking InGaN strips separated by troughs. This change in morphology may contribute to high efficiencies in some GaN-based light emitting diodes (LEDs) if the InGaN is exposed to elevated temperatures without a protective GaN capping layer. Here, we investigate the changes in morphology which occur when InGaN epilayers are annealed at their growth temperature under NH₃, N₂, and a small H₂ flux. We observe that while the layers initially roughen, more extended anneals lead to the surface becoming smooth and terraced once again. Power spectral density analysis of atomic force microscopy data is used to show that the dominant mechanism for roughening is loss of material from pre-existing pits, while the dominant smoothing mechanism is surface diffusion. This mechanistic analysis may be relevant to the growth of InGaN quantum wells in LED structures. [J997]

"Organic Devices for Integrated Photonics"

This paper describes the application of organic photonic devices including organic light-emitting diodes (OLEDs) and organic photodetectors (OPDs) to integrated photonic devices for the realization of an all-polymeric local-area network. OLEDs and OPDs fabricated by vacuum and solution processes are also discussed. Signal transmission of moving picture signals is demonstrated, with clear signals transmitted and received by the organic devices. [J998]

"Driver circuits for temperature-invariant performance of junction diodes"

Different types of driver circuits for the temperature-invariant brightness of light emitting diodes and the RF performance of Schottky barrier diodes, p-i-n diodes and p-n junction diodes are presented. The sensitivities of the proposed driver circuits with ambient temperature, bias voltage and other component variations are presented. Novel techniques are proposed and demonstrated to compensate the performance variation of diode-based circuits due to the temperature sensitivity of the components of driver circuits. The proposed driver circuits eliminate the requirement of conventional temperature compensation techniques with temperature sensors. The driver circuits respond directly to the junction temperature of the diodes itself; thus, there will be no compensation error due to the temperature gradient or self-heating of the diodes. This technique is very simple, accurate and easy to implement. [J999]

"Application of Taguchi Method in Light-Emitting Diode Backlight Design for Wide Color Gamut Displays"

This paper utilizes the Taguchi design method to optimize the design parameters of a light-emitting diode (LED) backlight unit for wide color gamut liquid crystal displays (LCDs). In optimizing the design, the parametric analyses consider two particular regions of the backlight unit, namely, the color-mixing zone and the extractor zone. The Taguchi experiments are configured in L₉(3⁴) orthogonal arrays and are designed to evaluate the effects of the design parameters on the color-difference, optical efficiency and luminance of the unit. The analysis of variance (ANOVA) results reveal that the optical efficiency and color-difference properties are determined primarily by the reflector design and the length of the color mixing zone, respectively, while the luminance to the LCD panel is affected principally by the taper angle of the optical microstructures in the extractor zone. The optimal design parameters of the color-mixing zone and extractor zone are estimated from the Taguchi S/N ratio data and the ANOVA results, and are verified via ray-tracing simulations. For an input flux of 1501 lm, the optimal design shows 0.01 of the color differences in CIE 1976 color space, 85% of the optical efficiency, and 10675 nits of luminance. Thus, the optimized backlight unit provides an ideal solution for the illumination of large-scale LCD display devices. [J1000]

"A Very Simple Control Strategy for Power Factor Correctors Driving High-Brightness LEDs"

This paper presents a new control strategy for power factor correctors (PFCs) that are used to drive high-brightness LEDs. This control strategy is extremely simple and is based on the use of a conventional peak-current-mode controller with a suitable selection of the compensation ramp waveform. Neither an analog multiplier nor an input voltage sensor is needed to achieve quasi-sinusoidal line waveforms at nominal conditions and full load. If the converter belongs to the flyback family (flyback, buck-boost, SEPIC, Cuk and Zeta), the line waveform appears notably distorted if the compensation function is a linear ramp, but becomes almost sinusoidal if the linear ramp is substituted by a properly chosen exponential function. The line waveform is slightly distorted when the load varies or when the converter works under either overvoltage or undervoltage conditions. However, the waveform maintains a very high power factor (PF) even under these conditions. Moreover, the line current is cycle-by-cycle-controlled due to the peak-current-mode control, and hence, the input-current feedback loop is

extremely fast, thereby allowing this type of control to be used with high-frequency lines (above 400 Hz). [J1001]

"Electrooptical Analysis of Effects Induced by Floating Metallic Interlayers in Organic LEDs"

The aim of this paper is to investigate the electrical and optical property modifications that can be related to the presence of a nanometric metallic layer at the interface between two organic emissive materials in a stacked structure. For purposes of comparison, reference devices have also been analyzed to emphasize the increase of electrical switching and hysteresis behaviors in current-voltage plots and spectral variations in electroluminescence. In this paper, we have tried to summarize the electrical effects of the floating nanometric thin metallic layer by extracting a small number of parameters which can represent the current state of the device. [J1002]

"Organic light-emitting diode with liquid emitting layer"

We demonstrate an original organic light-emitting diode (OLED) having a neat liquid host of 9-(2-ethylhexyl)carbazole (EHCz) doped with a guest emitter of 5,6,11,12-tetraphenylnaphthacene (rubrene). The device structure is composed of indium tin-oxide (ITO)/poly(3,4-ethylenedioxythiophene):poly(styrenesulphonate)/EHCz:rubrene/Cs₂CO₃/ITO. We demonstrate that the liquid organic semiconducting layer surely transports charge carriers, leading to electroluminescence from rubrene with the highest external quantum efficiency of $\eta_{\text{ext}}=0.03\%$ at a current density of 0.26 mA/cm². Our demonstration of the liquid-OLEDs will open another possibility of organic semiconductors and light-emitting applications. [J1003]

"White Light Wireless Transmission at 200 Mb/s Net Data Rate by Use of Discrete-Multitone Modulation"

Spectrally efficient data transmission with white light-emitting diodes (LEDs) is a topic of increasing interest. In this letter, we report a visible light communication link operating at 200 Mb/s net transmission rate (230 Mb/s gross) with a bit-error ratio for uncoded data below 10^{-3} . The link is based on a thin-film high-power phosphorescent white LED and offline signal processing of discrete multitone signals. Transmission at the brightness levels of about 1100 and 550 lx was investigated. Our results indicate that the achievable data rates are limited by detector noise. [J1004]

"GaN-Based LEDs With GaN -Pillars Around Mesa, Patterned Substrate, and Reflector Under Pads"

Nitride-based light-emitting diodes (LEDs) with textured sidewall, GaN μ -pillars around mesa region, patterned sapphire substrate (PSS), and highly reflective Ag-Cr-Au electrode pads were fabricated using the conventional lithography method (labeled as experimental LEDs). When a 20-mA injection current was applied, forward voltages were 3.18 and 3.4 V for the conventional and experimental LEDs, respectively. The high 20-mA V_{of} LEDs with Ag-Cr-Au electrode pads could be attributed to the fact that the specific contact resistance of n⁺-GaN-Ag-Cr-Au is slightly higher than that of the n⁺-GaN-Cr-Au contact. It was found that we could achieve much stronger LED output power with textured sidewalls, GaN μ -pillars around mesa region, PSS, and highly reflective Ag-Cr-Au electrode pads. It was also found that we could enhance LED output power by more than 80% compared with the conventional LEDs. [J1005]

"A General Photo-Electro-Thermal Theory for Light Emitting Diode (LED) Systems"

The photometric, electrical, and thermal features of LED systems are highly dependent on one another. By considering all these factors together, it is possible to optimize the design of LED systems. This paper presents a general theory that links the photometric, electrical, and thermal behaviors of an LED system together. The theory shows that the thermal design is an indispensable part of the electrical circuit design and will strongly influence the peak luminous output of LED systems. It can be used to explain why the optimal operating power, at which maximum luminous flux is generated, may not occur at the rated power of the LEDs. This theory can be used to determine the optimal operating point for an LED system so that the maximum luminous flux can be achieved for a given thermal design. The general theory has been verified favorably by experiments using high-brightness LEDs. [J1006]

"A Charge-Recycling Buck-Store and Boost-Restore (BSBR) Technique With Dual Outputs for RGB LED Backlight and Flashlight Module"

A boost converter with buck-store and boost-restore (BSBR) technique fabricated by 0.25 μ m CMOS BCD process can provide different supply voltages to drive series red, green, and blue LEDs in sequence for reducing

the power consumption on the constant current generator. The proposed technique not only stores and restores extra energy during the transient time of the reference tracking response to improve the efficiency but also enhances the reference tracking response to greatly reduce load transition time. Experimental results show that the period of reference tracking response can be improved. When the load current is 100 mA, the periods of reference down-tracking and up-tracking are smaller than 10 and 20 μ s, respectively. Furthermore, this technique can also provide a regulated voltage to drive the subblock implemented in the liquid crystal display system. The maximum efficiency of charge recycling is up to 94%, and the maximum efficiency of this boost converter is 94.5%. Experimental results demonstrate fast and efficient reference tracking performance is achieved by the proposed BSBR technique. [J1007]

"Effects of Defects on the Thermal and Optical Performance of High-Brightness Light-Emitting Diodes"

Defects in terms of voids, cracks, and delaminations are often generated in light-emitting diodes (LEDs) devices and modules. During various manufacturing processes, accelerated testing, inappropriate handling, and field applications, defects are most frequently induced in the early stage of process development. One loading is due to the nonuniform loads caused by temperature, moisture, and their gradients. In this research, defects in various cases are modeled by a nonlinear finite-element method (FEM) to investigate the existence of interfaces, interfacial open and contacts in terms of thermal contact resistance, stress force nonlinearity, and optical discontinuity, in order to analyze their effects on the LED's thermal and optical performance. The simulation results show that voids and delaminations in the die attachment would enhance the thermal resistance greatly and decrease the LED's light extraction efficiency, depending on the defects' sizes and locations generated in packaging. [J1008]

"Verification of p-n junctions in polymer light-emitting electrochemical cells via electrical characterization"

We report micrometer thick sandwich light-emitting electrochemical cells (LECs) based on a blend of poly[5-(2'-ethylhexyloxy)-2-methoxy-1, 4-phenylene vinylene] and poly(ethylene oxide) complexed with lithium trifluoromethanesulfonate. These LECs exhibit very similar properties as those of thin LECs including bipolar current-voltage characteristics and light emission. Mixing of aluminum nanoparticles into polymer layers improves electroluminescence because of smaller series resistance and larger light-emitting area. Taking series resistance into account, we confirm the operating mechanism of an LEC is the formation of a p-n junction by in situ electrochemical doping via fitting the steady state current-voltage characteristics to the expression for the Shockley model of a p-n diode. [J1009]

"Efficient multiple triplet quantum well structures in organic light-emitting devices"

We demonstrate the multiple quantum well (MQW) structures with the charge control layers (CCLs) to produce highly efficient red phosphorescent organic light-emitting devices (OLEDs). Various triplet quantum well devices from a single to five quantum wells are realized using wide band-gap hole and electron transporting layers, narrow band-gap host and dopant materials, and CCLs. Triplet energies in such MQW devices are confined at the emitting layers. The maximum external quantum efficiency of 14.8% with a two quantum well device structure is obtained. The described MQW device concept has been proposed to be very useful to future OLED display and lighting applications. [J1010]

"Temperature estimation of high-power light emitting diode street lamp by a multi-chip analytical solution"

Light emitting diodes (LEDs) are now widely used in many fields including traffic lights, vehicle backlights and liquid crystal display (LCD) displays because of their long life, good illumination efficiency and low energy consumption. At present, LEDs are increasingly replacing the traditional lighting and are being used in general illumination such as the street lamp. For the high-power LED street lamps, good light extraction is the most important thing, but low junction temperature of the LED modules is also critical for achieving a long lifetime and a high optical efficiency. Actually, there have been many reports about early failures of street lamps, called dead lamps that have been regarded as a barrier in the public and administration acceptance of LED street lamps. Therefore temperature estimation is always a crucial issue for LED product development. A multi-chip spreading thermal resistance model was applied to estimate the temperature distribution of LED street lamp. The experiment was first done to obtain temperatures of several locations in a prototype LED street lamp. Then the multi-chip spreading resistance model was established to calculate the full temperature distribution. Comparison between the model calculation and experimental measurement showed a good agreement, which demonstrates that the present model can be used in engineering design to estimate the temperature distribution of high-power

LED street lamps. [J1011]

"Local electroluminescence and time-resolved photoluminescence study of InGaN light-emitting diodes"

Uniformity of luminescence properties in blue InGaN light-emitting diodes has been studied and analyzed by local time-resolved photoluminescence and microelectroluminescence measurements at different biasing. For studied structures, some nonuniform distribution of photoluminescence properties has been observed at reverse biasing conditions. This nonuniformity revealed inhomogeneous distribution of electric field over the active region. It is supposed that nonuniform distribution of acceptors concentration in p-GaN is a source of electric field fluctuations. Microelectroluminescence measurements showed that areas with locally lower acceptor concentration in p-GaN layer emit lower electroluminescence intensity. This was caused by limited hole injection efficiency into multiple quantum wells region at high current. [J1012]

"Self-pulsing 1050 nm quantum dot edge emitting laser diodes"

We examine self-pulsing, edge emitting, quantum dot laser diodes as continuous broad spectrum light sources emitting at 1050 nm. Devices are configured with split contacts. When operated without a saturable absorber, the laser emits a number of discrete narrow modes, which merge to form a broad continuous lasing spectrum on application of the saturable absorber. The broadened spectra are consistent with the modulated carrier density expected under Q-switched operation. This provides a simple technique for generating emission suitable for biomedical applications. The spectral width achieved is 10 nm, and the average output power is 7.5 mW.

[J1013]

"Degradation of High-Brightness Green LEDs Submitted to Reverse Electrical Stress"

This letter describes an extensive analysis of the reverse-bias degradation of green light-emitting diodes. The analysis consists in a wide set of stress tests carried out under different negative-bias levels. The results presented in this letter indicate the following: 1) Leakage current is strongly correlated to the presence of reverse-bias luminescence; 2) reverse current flows through preferential leakage paths and is due to a soft-breakdown mechanism that is possibly correlated to the presence of structural defects; 3) reverse-bias stress can induce an increase in the leakage current, with a corresponding decrease in the breakdown voltage of the samples; and 4) the degradation rate has a linear dependence on the (reverse) stress-current level, suggesting that degradation is induced by hot carriers. On the basis of the evidence collected in this letter, degradation can be ascribed to the generation/propagation of point defects due to the injection of highly accelerated carriers.

[J1014]

"Evaluation of Peripheral Visual Performance When Using Incandescent and LED Miner Cap Lamps"

Illumination plays a critical role in an underground miner's safety because miners depend most heavily on visual cues to recognize hazards. Mobile mining machinery, located in the miner's peripheral field of view (plusmn10deg to about plusmn60deg off-axis), may pose potential pinning and striking hazards. The main objective of this research was to determine if there were peripheral visual performance improvements for the detection of moving objects when using cool-white light-emitting diode (LED) cap lamps as compared to incandescent (INC) light bulbs commonly used in miner cap lamps. The cap lamp variable of interest is the spectral power distribution. The illuminances were normalized by a diffusion filter. The second objective was to determine if age is a factor for the peripheral visual performance. This is important because the workforce is aging-the average miner age is about 43 years old. Thirty subjects participated in the study, ten subjects each in the age groups of younger (18-25 years), middle (40-50 years), and older (51+ years). Visual performance was quantified by the subjects' speed and accuracy of response to detect the rotation of high-contrast (white) circular targets located 3.83 m away at -20deg, 40deg, and 50deg off-axis. The speed of detection and the number of missed target rotations (accuracy) were measured. The prototype LED cap lamp results were best with an 11%-15% improvement compared to the INC and LED cap lamps, respectively. Age does appear to be a significant factor. For the middle and older age groups, the target movement detection time increased 75% and 60%, and the number of missed targets increased 500% and 450%, respectively, in comparison to the youngest age group. The results also suggest that target location is a significant factor. The subjects' target movement detection time for the 40deg and 50deg target movements increased 16% and 69%, respectively, as compared to the -20deg target. [J1015]

"Band alignment at SrCu₂O₂/ZnO heterointerface"

SrCu₂O₂/ZnO interface is interesting for application in blue and UV light emission devices. Measurements of the valence band offset at SrCu₂O₂/ZnO interface using photoelectron spectroscopy result in an offset of 2.0 eV (cliff), meaning that the interface band gap is reduced to 1.4 eV. Blue and UV light emission observed previously can be attained in this material system presumably by injection of minority carriers involving tunneling through a narrow barrier at the interface. Additional intensive infrared light emission due to interface recombination can be predicted. [J1016]

"InGaN-Based Light-Emitting Diodes With Nanoporous Microhole Structures"

InGaN-based light-emitting diodes (LEDs) with nanoporous microhole array (NMA) structures were fabricated through photoelectrochemical wet oxidation and oxide-removing processes. The average size of the nanoporous structure at the microhole regions was measured at 60-80 nm. Forward voltages were measured at 3.47 and 3.68 V for a standard LED (ST-LED) and an NMA-LED, respectively, the latter caused by the higher contact resistance at the nanoporous GaN:Mg surface. The light output power of the NMA-LED had a 40.5% enhancement compared with the ST-LED on nonencapsulated LEDs in chip form. The higher light scattering process occurred at the NMA structure on the GaN:Mg surface and at the ringlike patterns on the GaN:Si structure. The results were a higher light extraction efficiency and a larger divergent angle in the NMA-LED. [J1017]

"On Driving Techniques for LEDs: Toward a Generalized Methodology"

LEDs must be externally driven by power sources to emit light. One problem associated with driving LEDs is its inherent nonlinear relation between the emission intensity and the forward current. Thus, the light output obtained from an LED is strongly dependent on the actual current waveforms employed to drive it. It is found that driving an LED with dc produces light output that surpasses all other techniques including the commonly used pulse-width modulation (PWM) technique. On the other hand, for dimming function, it is found that the PWM technique offers greater dimming flexibility in comparison to dc technique. In this paper, a generalized methodology for driving LEDs inheriting the features of both of these techniques is proposed. It employs a pulsating current switching between two discrete current levels, where the current levels and their durations can be concurrently varied for a more precise mapping of the driving conditions to the light output. The existing dc and PWM techniques can be viewed alternatively as being special cases of this more general approach. [J1018]

"Micro-pixel array of organic light-emitting diodes applying imprinting technique with a polymer replica"

Efficient micro-pixel array of small molecule organic light-emitting diodes (OLEDs) has been fabricated by an imprinting technique which uses a polymer replica. To confirm the effect of the oxygen plasma for removing the residual layer, the performance of two kinds of OLEDs with varying thicknesses of resin as the micro-pixel array, have been compared. The measured results of the OLEDs have shown comparable device performances that are significantly characterized depending on the residues on the substrate. The performance of enhanced device has achieved efficiencies of 3.6 cd/A and 1.9 lm/W at 20mA/cm². [J1019]

"GaN-Based Light-Emitting Diode Prepared on Nano-Inverted Pyramid GaN Template"

Using self-aligned SiO₂ nano-spheres as an etching mask, the authors demonstrated the formation of a GaN-based nano-inverted pyramid (NIP) structure. It was found that crystal quality of the GaN epilayer prepared on an NIP/GaN template was significantly better than that prepared with conventional low-temperature GaN nucleation layer. With the NIP structure, it was found that 20-mA light-emitting-diode (LED) output power can be enhanced by 32%, as compared with the conventional LED. [J1020]

"Study of trap states in polyspirobifluorene based devices: Influence of aging by electrical stress"

The influence of aging by electrical stress on the formation of defects has been studied in two types of polymers: blue emitting spiro copolymer and white emitting spiro blend polymer. The white emitting spiro polymer was obtained by adding green and red chromophores into the host blue copolymer. The defect states were investigated by using two complementary techniques: charge based deep level transient spectroscopy and thermally stimulated current (TSC). Six trap levels were retrieved in blue emitting diodes with a depth of 0.17-0.85 eV, and the onset of an additional trap with a depth of 0.49 eV was observed in white emitting ones. The density of these traps is of the order of 10¹⁶-10¹⁷cm⁻³. The fractional TSC experiments allowed us to determine the distribution of five trap types in white emitting diodes, which could be described by Gaussian functions. The aging of devices was performed by electrical stress and not by exposure of samples to air or oxygen, in contrast to previous investigations on other organic materials. Upon aging, no new traps have been created or suppressed in both doped and undoped polymers. Furthermore, an enhancement in trap density has been

observed. The analysis of the trap characteristics has highlighted that the aging would not uniformly affect the defect levels in the polymer. The density of deeper traps (above 0.3 eV) is increased, and their distribution is also modified, while the shallow traps (below 0.3 eV) remain stable. Furthermore, the investigation of the doping influence on the degradation process has shown that the chromophore addition seems to stabilize the polymer, whose degradation rate is slower than that of the undoped material. [J1021]

"ZnO-Based Fairly Pure Ultraviolet Light-Emitting Diodes With a Low Operation Voltage"

A ZnO-based metal-insulator (HfO₂)-semiconductor diode was synthesized on a commercially available n+-GaN/sapphire substrate using a radio-frequency magnetron sputtering system. Electroluminescence measurements revealed that the diode exhibited fairly pure ultraviolet (UV) emission peaking at ~ 370 nm with a line width of less than 8 nm. By choosing a proper thickness of the insulator HfO₂ layer, the threshold voltage of the emission could be reduced to 2 V, demonstrating that this ZnO-based fairly pure UV light-emitting diode can be driven by two ordinary dry batteries. The reason for low threshold voltage is proposed in terms of the n+-GaN/sapphire substrate and the high-insulator HfO₂ layer. [J1022]

"Polarization-Dependent Sidewall Light Diffraction of LEDs Surrounded by Nanorod Arrays"

The polarization behavior of the light-emitting diodes (LEDs) with nanorods surrounding the p-mesa is investigated. The nanorods were fabricated using a natural nanosphere lithography and are intended to diffract laterally propagated light. In the horizontal direction, s-polarized light is dominated since the injected carriers choose to fill up the lowest energy state in a direction parallel to the quantum-well layers. The p/s-polarized ratio starts to increase with the increase of radiated angles and eventually saturates. Since the Bragg diffraction of laterally propagated p-polarized mode by nanorods is more efficient than the s-polarized light, the p/s-ratio of the device with nanorods is higher than that without rods. The p/s-ratio of the LED with nanorods is 1.96 at 90deg, and is 1.52 when the integrating intensity between 0deg and 90deg is considered. [J1023]

"Transient measurement of light-emitting diode characteristic parameters for production lines"

A new instrument has been developed for transient measurement of light-emitting diodes (LEDs), including photometric parameters, colorimetric parameters, and electrical parameters in a matter of milliseconds, by combining spectrometer with a human photopic vision detector and data acquisition card (DAQ). The instrument can provide communication interface for sorter to realize automatic sorting of measured LEDs samples. The light emitted from the measured LEDs, which are illuminated under pulse current operation condition, is captured by the spectrometer and the human photopic vision detector. The spectral power distributions of LEDs are recorded by spectrometer, and processed to provide colorimetric parameters. We employ two novel algorithms including look-up table method and curve fitting method to determine the dominant wavelength of LED. In combination with linear interpolation, the look-up table method can locate dominant wavelength with a resolution of 0.1 nm. A programmable constant current source/voltage source is designed for power supply to drive LED. The luminous intensity of LED can be derived by detecting the photocurrent of human photopic vision detector. We also describe the calibration of the human photopic vision detector. This calibration provides detector-specific correction factor that enables accurate extraction of luminous intensity of LED. The instrument has been used to measure and inspect the quality of packaging LED. [J1024]

"Degradation of organic light emitting diodes by nucleated telephone cord blisters"

This letter presents the results of a study into adhesion-related degradation mechanisms in single layer polymer light emitting diodes with poly[2-methoxy-5-(2-ethylhexyloxy)-1,4-phenylenevinylene] as the active layer. These studies reveal spiral-shaped blister patterns that are associated with rapid degradation of the device. Scanning electron microscopy and atomic force microscopy images of these defects reveal that these patterns are spiral telephone cord failures that form as a result of compressive stresses in the device. [J1025]

"Carrier lifetime and spin relaxation time study for electrical spin injection into GaAs"

We fabricated spin light emitting diodes using oxide tunneling barriers between ferromagnetic materials (Ni_{0.8}Fe_{0.2}/Co_{0.9}Fe_{0.1}) and semiconductors (GaAs) and investigated the temperature-dependent carrier lifetime and spin relaxation time of the active GaAs layer. We observed the circular polarization of the free exciton from the electroluminescence spectra due to the spin injection from the ferromagnetic material, whereas the circular polarization of the conduction band to acceptor transition was negligible. From the temperature-dependent carrier lifetime and spin relaxation time of the active GaAs layer, we found that the spin injection efficiency was larger than 25% between 20 and 180 K, where the magnetic field dependence of the spin lifetime was ignored. [J1026]

"Enhanced Light Extraction in Wafer-Bonded AlGaInP-Based Light-Emitting Diodes via Micro- and Nanoscale Surface Textured"

AlGaInP-based metal-bonding light-emitting diodes (LEDs) with micro- and nanoscale textured surface were investigated. The device surface with microbowls and nanorods were formed by a chemical wet-etching and dry-etching technique for enhancing light-extraction purpose. The luminous intensity could be enhanced 65.8% under 20-mA current injection as compared with the plane surface LEDs. The maximum wall-plug efficiency was achieved 14.1% at 7.5-mA operation. [J1027]

"Optical Power Transmission Through Adhesive and Bonding Layers"

In this paper, we analyze the optical power transmission in structures that include a low-index intermediate layer and sources with a wide angular distribution. Special attention is paid to the angular average of the transmission coefficient, which can be cast in a universal form for two practically relevant classes of source layers. Due to the so-called frustrated total internal reflection, the structure transparency is highly sensitive to the intermediate layer thickness and index contrast. We show that the transmission coefficient for isotropic radiation may remain low even for optically thin low-index intermediate layers, so that the usual comparison between the optical thickness and the wavelength is no longer a reliable criterion. Calculations are presented for exemplary structures, such as a semiconductor scintillator bonded to a photodiode. The angular dependence of the transmission coefficient is shown to satisfy a simple and universal sum rule. [J1028]

"Energy band alignment of SiO₂/ZnO interface determined by x-ray photoelectron spectroscopy"

Thin SiO₂ interlayer is the key to improving the electroluminescence characteristics of light emitting diodes based on ZnO heterojunctions, but little is known of the band offsets of SiO₂/ZnO. In this letter, energy band alignment of SiO₂/ZnO interface was determined by x-ray photoelectron spectroscopy. The valence band offset ΔE_{V} of SiO₂/ZnO interface is determined to be 0.93 ± 0.15 eV. According to the relationship between the conduction band offset ΔE_{C} and the valence band offset ΔE_{V} : $\Delta E_{\text{C}} = E_{\text{gSiO}_2} - E_{\text{gZnO}} - \Delta E_{\text{V}}$, and taking the room-temperature band-gaps of 9.0 and 3.37 eV for SiO₂ and ZnO, respectively, a type-I band-energy alignment of SiO₂/ZnO interface with a conduction band offset of 4.70 ± 0.15 eV is found. The accurate determination of energy band alignment of SiO₂/ZnO is helpful for designing of SiO₂/ZnO hybrid devices and is also important for understanding their carrier transport properties. [J1029]

"Boost DC-DC Converter With Fast Reference Tracking (FRT) and Charge-Recycling (CR) Techniques for High-Efficiency and Low-Cost LED Driver"

An RGB LED driver with the fast reference tracking (FRT) and charge-recycling (CR) techniques is proposed to implement a high-efficiency and low-cost RGB backlight module in color sequential notebook computers' display. The proposed LED driver composed of an asynchronous 1.5 MHz DC/DC boost converter with the FRT and CR techniques was fabricated in TSMC 0.25 μm BCD 40 V technology to generate 16 V for 6-series red (R) LEDs or 21 V for 6-series green (G), or blue (B) LEDs. The FRT technique can speed up the reference tracking performance and effectively improve the up-tracking performance. However, the down-reference tracking depends on the load current and output capacitor. It is difficult to enhance the transient response without reducing the efficiency. Therefore, the CR technique is proposed to store extra energy on the recycling capacitor when the output voltage is switched from high- to low-supplying voltage level and releases the reserved energy back to the output node at next period. Furthermore, the output voltage can be rapidly switched between two different voltage levels by FRT technique without consuming much power owing to the restored energy by the CR technique. Experimental results show that the total power consumption of a notebook computer's 15.4" LCD panel can be reduced from 5 W in cold-cathode fluorescent lamp (CCFL) backlight module to about 2-3 W in RGB LED backlight module with the field color sequential (FCS) algorithm. Furthermore, after the implementation of the LED driver with the FRT and CR techniques, the power loss can be reduced to about 24% of that without the FRT and CR techniques. [J1030]

"A step forward toward smart white lighting: Combination of glass phosphor and light emitting diodes"

We present our recent achievements of a glass able to produce smart white light combining a glass phosphor with light emitting diodes (LEDs). The combined emissions of Ce³⁺-doped calcium aluminosilicate glass and the 405 nm LED using the Commission Internationale de l'Éclairage 1931 chromatic diagram showed that this system presents an emission close to the ideal white light and allows tunability. In addition, the glass blue emission overlaps with the spectral range of the retinal photoreceptors involved in circadian responses. This glass combined with UV LED emission is suitable for circadian lights and therefore may contribute to improve environmental lighting and human well being. [J1031]

"Broadband blue superluminescent light-emitting diodes based on GaN"

We report on the achievement of III-nitride blue superluminescent light-emitting diodes on GaN substrates. The epitaxial structure includes an active region made of $\text{In}_{0.12}\text{Ga}_{0.88}\text{N}$ quantum wells in a GaN/AlGaIn waveguide. Superluminescence under cw operation is observed at room temperature for a current of 130 mA and a current density of 8 kA/cm^2 . The central emission wavelength is 420 nm and the emission bandwidth is 5 nm in the superluminescence regime. A peak optical output power of 100 mW is obtained at 630 mA under pulsed operation and an average power of 10 mW is achieved at a duty cycle of 20%. [J1032]

"Erratum: "Charged particle-display" [JJ. Appl. Phys. 106, 033505 (2009)]"

First Page of the Article [J1033]

"Electroluminescence from Ge on Si substrate at room temperature"

A Ge/Si heterojunction light emitting diode with a $p^+-\text{Ge}/i\text{-Ge}/n^+\text{-Si}$ structure was fabricated using the ultrahigh vacuum chemical vapor deposition technology on $n^+\text{-Si}$ substrate. The device had a good I-V rectifying behavior. Under forward bias voltage ranging from 1.1 to 2.5 V, electroluminescence around 1565 nm was observed at room temperature. The mechanism of the light emission is discussed by the radiative lifetime and the scattering rate. The results indicate that germanium is a potential candidate for silicon-based light source material. [J1034]

"A Reliability Study on Green InGaIn-GaN Light-Emitting Diodes"

In this letter, the reliability of green InGaIn-GaN light-emitting diodes (LEDs) has been analyzed by correlating the defect density of wafers with various device parameters, including leakage current, $1/f$ noise, and degradation rate. It was found that as the wavelength of green LEDs increases from 520 to 550 nm by increasing the indium content in the quantum wells, the defect density also increases, thus leading to larger leakage current, enhanced noise magnitude, and shortened device lifetime. [J1035]

"Erbium-doped GaN optical amplifiers operating at 1.54 μm "

Strip optical waveguides based on erbium (Er)-doped AlGaIn/GaN:Er/AlGaIn heterostructures have been fabricated and characterized in the optical communication wavelength window near 1.54 μm . The propagation loss of these waveguide amplifiers have been measured at 1.54 μm and found to be 3.5 cm^{-1} . Moreover, the optical amplification properties of the waveguides were measured using a signal input at 1.54 μm and a broadband GaN light-emitting diode at 365 nm as pump source. A relative signal enhancement of 8 cm^{-1} was observed. The implications of such devices in photonic integrated circuits for optical communications are discussed. [J1036]

"Mid-Infrared Light-Emitting Diodes and Photodiodes for Hydrocarbon Sensing"

The properties of $\text{Al}_x\text{In}_{1-x}\text{Sb}$ light-emitting diodes (LEDs) and photodetectors have been investigated to establish their suitability for methane sensing. Using these components it is possible to achieve good signal-to-noise values at both the characteristic absorption wavelength and also at 4 μm , an attractive wavelength for use as a reference channel. A limit of sensitivity of approximately 400 ppm, with an integration time of 10 s and a path length of 5 cm, was estimated for methane detection. [J1037]

"Characterizations of GaN-Based LEDs Encompassed With Self-Aligned Nanorod Arrays of Various Distribution Densities"

We designed and fabricated GaN-based light emitting diodes encompassed with self-aligned nanorod arrays of three different distribution densities. The radiation profiles show that the device with less dense nanorod distribution has the highest optical power enhancement factor. By regarding the nanorod arrays as sidewall reflectors, the enhancement is due to the light diffraction of the laterally guided mode to radiative modes in the surface normal direction. As for the densest nanorods in our experiment, the radiation profile shows a better emission directionality as the guided modes are phase matched to the radiation modes. However, they show less optical output enhancement since some of the laterally propagated light is diffracted back to p-mesa by the first several columns of nanorods. [J1038]

"Evolution of surface morphology of dry-etched ZnO with Cl_2/Ar plasma"

This work elucidates the surface morphologies of dry-etched ZnO films formed by reactive ion etching using a

Cl₂/Ar mixture. The root-mean-square (rms) roughness and etching rate were obtained by varying the gas flow ratio, the radio-frequency (rf) plasma power, and the chamber pressure. Atomic force microscopy results and surface topographies are discussed. The rms roughness is highest, 24.20 nm, at a Cl₂/Ar flow rate of 150/10 SCCM (SCCM denotes cubic centimeter per minute at STP), a working pressure of 190 mTorr, and a rf power of 300 W. Such films are suitable for use as roughened transparent contact layers in light-emitting diodes. Bearing ratio analysis reveals that under the aforementioned condition, the nanorods covered 25.4% of the total surface area and their maximum height was approximately 150.83 nm. Moreover, high and low etching rates of 300 and 16 E/min were obtained at rf powers of 300 and 50 W, respectively, supporting the ZnO-based devices and the gate-recess process. [J1039]

"Rate equation analysis of efficiency droop in InGaN light-emitting diodes"

Efficiency droop in InGaN light-emitting diodes (LEDs) is analyzed based on the rate equation model. By using the peak point of the efficiency versus current-density relation as the parameters of the rate equation analysis, internal quantum efficiency and each recombination current at arbitrary current density can be unambiguously determined without any knowledge of A, B, and C coefficients. The theoretical analysis is compared with measured efficiency of a LED sample and good agreement between the model and experiment is found. The investigation of recombination coefficients shows that Auger recombination alone is not sufficient to explain the efficiency droop of InGaN LEDs. [J1040]

"Anisotropic optical constants of in-plane oriented polyfluorene thin films on rubbed substrate"

We present a photometric method to determine the anisotropic optical constants of several aligned polyfluorene films. These polymers exhibit liquid crystal characteristic under heat treatment and polymer chains are preferentially in-plane oriented on a rubbed alignment layer. A self-consistent dispersion formula of Forouhi-Bloomer model is introduced to fit the measured polarized reflectance and transmittance curves by a global optimization algorithm. The very good agreements between the experimental and theoretical spectra allow us to shed light on the parallel and perpendicular components of optical constant. On this basis, light-emitting devices are fabricated using the anisotropic active films. The measured polarized electroluminescence spectra confirm the optical birefringence. [J1041]

"Plastic solar cells roll into unlit villages"

By day, the electronic devices that Frederik Krebs rolls off his printing presses could be mistaken for old plastic overhead-projector transparencies. Nightfall reveals their ingenious purpose: Snap the metal fasteners at the corners together and the sheets glow with reading-quality light. Krebs's sheets may prove to be much more than a curiosity, for the senior scientist at Denmark's Riso National Laboratory for Sustainable Energy has found a cheap way to integrate LEDs, photovoltaic (PV) cells, and ultrathin lithium batteries into a potentially life-saving lamp. He hopes to see them on sale next year, providing an affordable alternative to kerosene lighting for the more than 1.5 billion people in developing countries who lack access to electricity. [J1042]

"Enhancement of p -type conductivity by modifying the internal electric field in Mg- and Si- delta -codoped Al_xGa_{1-x}N/Al_yGa_{1-y}N superlattices"

The internal electric field is modified by using Mg- and Si-delta -codoped Al_xGa_{1-x}N/Al_yGa_{1-y}N superlattices (SLs). The first-principles simulation results show that the internal electric field in SL has been significantly intensified due to the charge transferring from Si-doped interface to Mg-doped interface. Accordingly, the Mg- and Si-delta -codoped p-type Al_{0.2}Ga_{0.8}N/GaN SLs are grown by metalorganic vapor phase epitaxy and higher hole concentration as much as twice of that in modulation-doped SL has been achieved, as determined by Hall effect measurements. Furthermore, by applying Mg- and Si-delta -codoped Al_xGa_{1-x}N/Al_yGa_{1-y}N SLs with high Al content as the p-type layers, we have fabricated deep ultraviolet light emitting diodes with superior current-voltage characteristics by lowering Mg-acceptor activation energy. [J1043]

"Bright three-band white light generated from CdSe/ZnSe quantum dot-assisted Sr₃SiO₅:Ce³⁺,Li⁺-based white light-emitting diode with high color rendering index"

In this study, bright three-band white light was generated from the CdSe/ZnSe quantum dot (QD)-assisted Sr₃SiO₅:Ce³⁺,Li⁺-based white light-emitting diode (WLED). The CdSe/ZnSe core/shell structure was confirmed by energy dispersive x-ray spectroscopy and x-ray photoelectron spectroscopy. The CdSe/ZnSe QDs showed high quantum efficiency (79%) and contributed to the high luminous efficiency (eta_L) of the fabricated WLED. The WLED showed bright natural white with excellent color rendering property (eta_L=26.8lm/W, color temperature=6140K, and color rendering index=85) and high stability against the increase in forward bias

currents from 20 to 70 mA. [J1044]

"Removing plasma-induced sidewall damage in GaN-based light-emitting diodes by annealing and wet chemical treatments"

The effects of thermal annealing and wet chemical treatments on the electrical characteristics of GaN-based light emitting diodes (LEDs) integrated with a microhole array were studied. It was found that KOH can etch off the plasma-damaged materials, leading to a complete suppression of surface leakage currents. It, however, attacked metal contacts and compromised the forward turn-on characteristics. Thermal annealing removed damage in the near-surface bulk region, whereas (NH₄)₂S treatment only passivated surface states. Both methods produced a partial recovery of the electrical characteristics of the perforated LEDs. It has been found that a complete removal of plasma damage in the perforated LEDs can be realized by thermal annealing used in conjunction with sulfide passivation. [J1045]

"Leakage current and reverse-bias luminescence in InGaN-based light-emitting diodes"

This paper reports an electro-optical analysis of the correlation between reverse-bias leakage current and luminescence in light-emitting diodes based on InGaN. The results of the analysis suggest that (i) the main mechanism responsible for leakage current conduction is tunneling, (ii) leakage current is correlated with the presence of reverse-bias luminescence, (iii) leakage current flows through preferential paths, that can be identified by means of emission microscopy, and (iv) reverse-bias luminescence could be ascribed to the recombination of electron-hole pairs in the quantum well region. [J1046]

"The Thermal Resistance of Solder Joints in High Brightness Light Emitting Diode (HB LED) Packages"

We present a framework to calculate the thermal resistance of Au-Sn eutectic solder joint (R_{th} , Au-Sn joint) in high brightness light emitting diode (HB LED) packages whose heat extraction capability controls the optical efficiency and reliability of HB LEDs. Using the transient thermal measurement combined with the structure function based analytical method and the finite element method, we find that the thermal conductivity (k) of the thin solder joint becomes significantly smaller than the Au-Sn alloy after joining; hence, R_{th} , Au-Sn joint constitutes a large portion of the total R_{th} of the package (R_{thPKG}). [J1047]

"Efficiency droop behavior of direct current aged GaN-based blue light-emitting diodes"

By direct current (dc) stressing, GaN-based blue light-emitting diodes (LEDs) with different density of nonradiative recombination centers in the active region of InGaN/GaN multiple quantum wells were obtained and studied for injection-current-induced efficiency droop. It is found that with increasing stressing time, the overall quantum efficiency of the aged LEDs drops while the peak-efficiency-current shifts toward higher magnitude. At selected injection current levels, the electroluminescence spectra of the aged LEDs show little change in peak position and shape. The shift in peak-efficiency-current, which follows the same trend as the degree of luminescence decay, is explained by a rate-equation model in which the newly created defects by dc stressing enlarge the dominant low-current region of nonradiative recombinations. [J1048]

"Highly efficient tris(8-hydroxyquinoline) aluminum-based organic light-emitting diodes utilized by balanced energy transfer with cosensitizing fluorescent dyes"

We report on the development of highly efficient organic light-emitting diodes (OLEDs) utilized by balancing the energy transfer between multiple dopants, that is, multiple emissions from the multiple dopants were realized by balanced distributed energy transfer. From the cosensitizing fluorescent OLEDs, the peak external quantum efficiency (EQE) of 4.8% at 130 cd/m² is demonstrated, which realized theoretical limits of 5.0% and means that nearly 100% of the singlet excitons are radiative. Also, the optimized device accompanying thickness-modulated electron transport layer for the enhanced light outcoupling demonstrated the highly improved peak EQE and current efficiency of 6.7%, and 23.4 cd/A. [J1049]

"Carrier distribution in InGaN/GaN tricolor multiple quantum well light emitting diodes"

Carrier transport in InGaN light emitting diodes has been studied by comparing the electroluminescence (EL) from a set of triple quantum well structures with different indium content in each well, leading to multicolor emission. Both the sequence and width of the quantum wells have been varied. Comparison of the EL spectra reveals the current dependent carrier transport between the quantum wells, with a net carrier flow toward the deepest quantum well. [J1050]

"Time-resolved photoluminescence analysis of two-peak emission behavior in $\text{Sr}_2\text{Si}_5\text{N}_8:\text{Eu}^{2+}$ "

$\text{Sr}_2\text{Si}_5\text{N}_8:\text{Eu}^{2+}$, one of the most recently developed phosphors for use in white light emitting diodes, exhibits a two-peak emission. Namely, the emission band of $\text{Sr}_2\text{Si}_5\text{N}_8:\text{Eu}^{2+}$ is deconvoluted into two Gaussian peaks irrespective of the Eu^{2+} concentration. We examined the two-peak emission of $\text{Sr}_2\text{Si}_5\text{N}_8:\text{Eu}^{2+}$ by analyzing the time-resolved photoluminescence spectra. We revealed that the two-peak emission was closely associated with the energy transfer taking place between Eu^{2+} activators located at two different crystallographic sites in the $\text{Sr}_2\text{Si}_5\text{N}_8$ structure. The experimental results coincided well with the rate equation model involving the crystallographic information of the host. [J1051]

"Self-assembled microarray of organic light-emitting diodes using a self-assembled monolayer by microcontact printing"

A self-assembled microarray (SAMA) of organic light-emitting diodes (OLEDs) has been fabricated using self-assembled monolayers (SAMs) by microcontact printing (μCP). The hydrophobic methyl-terminated SAMs modify the surface properties of the substrates to become hydrophobic, i.e., with low surface energy. Thus, the hydrophobic SAMs pattern, by the μCP , can be applied to form SAMAs on the patterned SAMs since the difference of the local surface energy modifies the patterns on the substrates. In this study, octadecyltrichlorosilane based hydrophobic methyl-terminated SAMs have been used and the fabricated OLEDs, with the SAMAs show local light emissions on the micron scale with efficient performances. [J1052]

"Electroluminescence enhancement in polymer light-emitting diodes through hole injection layer insertion"

After a hole injection layer is inserted into a polymer light-emitting diode (PLED), the positive polaron is easily injected into the polymer layer. An applied electrical field drives the positive polaron to approach and collide with the nonemissive triplet exciton. The collision between the positive polaron and neutral triplet exciton induces the exciton to emit light. Based on this physical picture, the maximum quantum efficiency of the PLEDs, 61.6%, is consistent with the experimental result of 60%. With the help of an external magnetic field, a structure of PLEDs with high electroluminescent efficiency is designed. [J1053]

"Forster resonance energy transfer enhanced color-conversion using colloidal semiconductor quantum dots for solid state lighting"

In this paper, we present Forster resonance energy transfer (FRET)-enhanced color-conversion using colloidal semiconductor quantum dot nanocrystals (NCs) to make reddish-orange light-emitting diodes for use in ultraefficient solid state lighting. To achieve FRET enhancement at 614 nm, we use an energy gradient hybrid structure made of cyan- and orange-emitting CdSe/ZnS NCs ($\lambda_{\text{PL}}=492$ and 588 nm in solution, respectively). This enables recycling of trapped excitons using FRET and achieves a relative quantum efficiency enhancement of 15.1% in reddish-orange full color-conversion for the integrated hybrid cyan-orange NC layer with respect to the case of full color-conversion using only orange NCs without FRET. [J1054]

"Effect of injection current density on electroluminescence in silicon quantum dot light-emitting diodes"

We report the effect of injection current density on the electroluminescence (EL) from silicon quantum dot (QD) light-emitting diodes. The EL spectra as a function of injection current density were blueshifted and broad. These results are attributed to both the increase in the contribution of small Si QDs in the silicon nitride film due to the increase in the injection current density and the recombination of electron-hole pairs between excited states in the Si QDs due to band bending under high bias. [J1055]

"Spectral shape and broadening of emission from AlGaInP light-emitting diodes"

This work presents a model for describing the shape of the spontaneous emission spectrum from a quantum-well structure. A function is introduced to specify the probability distribution for the effective band gap. Based on this model, the coexisting carrier thermal broadening and effective band gap broadening in the spontaneous emission spectrum can be separated from each other. Applying this model to the spectra of AlGaInP light-emitting diodes reveals that the probability distribution functions are almost Gaussian. Therefore, the emission spectra can be described by an analytical expression with fitted parameters. Possible reasons for this band gap broadening are discussed. The determination of the junction temperatures from the emission spectra and possible deviations of the results thus determined are also elaborated. [J1056]

"Transparent Electronics for See-Through AMOLED Displays"

Transparent thin-film-transistors (TFTs) with a channel semiconductor based on the zinc-tin-oxide (ZTO) system are presented. Specifically, the technological and material aspects of the plasma-assisted pulsed laser deposition of these materials are discussed. The supply of additional radical oxygen species will be evidenced to significantly reduce defects in the material and as a consequence allows for well-behaved n-channel TFTs with mobilities higher than $10 \text{ cm}^2\text{V}^{-1}\text{s}^{-1}$ and a threshold voltage in the range of 0 V. In addition the devices are extremely stable versus bias/current stress, which is especially important for active matrix OLED applications. Based on a detailed understanding of the interaction of the TFT channels with oxygen a strategy for the thin-film encapsulation of the TFTs will be presented, which leaves their device characteristics unaffected. [J1057]

"Energy Efficient RGBW Pixel Configuration for Light-Emitting Displays"

A study on LED displays has been conducted exploring a more efficient method for color generation than the traditional method. The study is comprehensive and thoroughly performed employing various sets of experiments in order to examine the functionality of the new proposed scheme which includes a literature review, theoretical modeling based on a scientific study, experimental data measurements of a developed prototype, and statistical data based on a survey. This study resulted in very interesting outcomes that may lead to a tremendous change in the existing LED display technology. [J1058]

"Chemical changes on the green emitter tris(8-hydroxy-quinolino)aluminum during device aging of p-i-n -structured organic light emitting diodes"

Metal organic fluorescent and phosphorescent emitters are widely used in organic light emitting devices (OLEDs). Iridium-based triplet emitters are known to undergo chemical reactions with other materials during OLED aging. The material tris(8-hydroxy-quinolino)aluminum (Alq3), which is widely used as electron transporting material and green fluorescent emitter, degrades mainly during hole transport. We investigate the chemical changes in Alq3 during device aging: using laser desorption ionization time-of-flight mass spectrometry, we study the reaction products found in degraded OLEDs. Similar to the reactions known from the phosphorescent iridium-based emitters, Alq3 undergoes a dissociation and further reaction with the hole blocking material 4,7-diphenyl-1,10-phenanthroline. [J1059]

"Guest Editorial Special Issue on Transparent Electronics"

From material and design advancements to new innovative processing methods, there have been significant recent achievements in the area of transparent electronics. The papers in this issue focus on this emerging technology and recent work in the field spanning from fundamental research to technology development. The articles cover the general topics of materials & performance, fabrication techniques, and devices & applications. Application articles focused on the benefits of transparent electronics display and organic light emitting diode devices. [J1060]

"Electroluminescence induced by photoluminescence excitation in GaInN/GaN light-emitting diodes"

Optical emission resulting from 405 nm selective photoexcitation of carriers in the GaInN/GaN quantum well (QW) active region of a light-emitting diode reveals two recombination channels. The first recombination channel is the recombination of photoexcited carriers in the GaInN QWs. The second recombination channel is formed by carriers that leak out of the GaInN QW active region, self-bias the device in forward direction, induce a forward current, and subsequently recombine in the GaInN active region in a spatially distributed manner. The results indicate dynamic carrier transport involving active, confinement, and contact regions of the device. [J1061]

"Tb 3+ luminescence by energy transfer from Eu 2+ in (Sr ,Ba)2 SiO 4 phosphor"

(Sr,Ba)₂SiO₄ phosphors co-doped with Tb³⁺ and Eu²⁺ were prepared by a conventional solid-state reaction method. Prepared (Sr,Ba)₂SiO₄:Tb,Eu phosphors had characteristic luminescent spectra excited under near-UV excitation in which both the broadband spectrum assigned to Eu²⁺ and the narrowband spectrum assigned to Tb³⁺ are observed, although Tb³⁺ is inactive with this photon energy in general. The sudden emergence of the Tb³⁺ luminescence shows that Eu²⁺-Tb³⁺ energy transfer is possible in the phosphor. We also studied the energy transfer mechanism in terms of the resonant energy transfer theory and found that the crystal structure of the host material Sr₂SiO₄ plays an important role in the luminescence properties of the phosphor. The Eu²⁺-Tb³⁺ energy transfer is ascribed to the overlap between the shorter Eu²⁺ luminescence band from the Sr₂SiO₄ crystal structure with two Sr sites and 5D₄ energy level of Tb³⁺ ion. Therefore, this phosphor has a

potential for application to white light-emitting diodes excited by near-UV light. [J1062]

"Dual-Plate OLED Display (DOD) Embedded With White OLED"

White organic light-emitting diode (WOLED) with color filter adopting dual-plate OLED display (DOD) structure is proposed. In order to prevent outgassing from color filter and overcoat, the SiN_x passivation film was deposited on the overcoat film. This structure does not show any defects after it has been kept over 500 hours of storage tests at 90 degC. By fabricating 1 stacked WOLED consisting of fluorescent blue layer/ phosphorescent red:green layer, luminance efficiency of 20 cd/A with CIE_x = 0.29, CIE_y = 0.37 was achieved. [J1063]

"Optimization of 2-Stack WOLED Structure With Consideration on Color Gamut and Power Consumption"

We fabricated 2-stack white organic light-emitting diode (WOLED) structure with luminance efficiency of 27.4 cd/A and color point of (0.32, 0.29) where one unit device emitted blue color and the other emitted red and green colors. Comparing with other configurations possible for 2-stack WOLED, it was found that our structure had merits of higher color gamut and lower power consumption, in spite of low luminance efficiency. In our 2-stack structure, we found that the blue efficiency which determines the power consumption of panel was strongly dependent on the position of the blue emitting layer. Based on an optical simulation and a viewing-angle analysis, we proved that the change of the luminance of blue color came from the microcavity effect depending on the distances between anode and cathode and between blue emitting layer and cathode. [J1064]

"UV Plasmonic Structures: Direct Observations of UV Extraordinary Optical Transmission and Localized Field Enhancement Through Nanoslits"

The ultraviolet (UV) extraordinary optical transmission through nanoslit structures in the far field and the localized field enhancement in the near field are directly observed and compared with each other. Numerical modeling results are also presented, and the distribution properties of the UV Surface Plasmon polaritons (SPPs) are analyzed, showing agreement with the experiment results. These phenomena may enrich the studies on subwavelength optics on a chip and especially be useful for performance optimization of UV active devices, e.g., UV light-emitting diodes (LEDs) and UV detectors. [J1065]

"Singlet energy transfer and singlet-singlet annihilation in light-emitting blends of organic semiconductors"

Excitation energy transfer from host to guest is studied in spin-cast blends of 4,4'-bis(N-carbazolyl)biphenyl (CBP) and a phosphorescent fac-tris(2-phenylpyridyl)iridium(III)-cored dendrimer using time resolved fluorescence. The kinetics of energy transfer are consistent with homogeneous dispersion of the dendrimers in the CBP host. Diffusion-controlled singlet-singlet exciton annihilation is observed in the CBP host at moderate excitation densities, similar to those encountered in high brightness light-emitting devices and organic lasers. The results are important for organic lighting and the understanding of exciton diffusion in guest-host systems for electrophosphorescence. [J1066]

"Drain Current Centric Modality: Instrumentation and Evaluation of ISFET for Monitoring Myocardial Ischemia Like Variations in pH and Potassium Ion Concentration"

Variations in concentrations of ions in biological systems can be important events in the onset of a physiological disorder. In an episode of myocardial ischemia, acidosis and elevation of potassium ion concentration has been observed in the extra-cellular matrix of the myocardium. As a spectrum of markers, they can help detect onset of ischemia as well as infarctions. In this study, Flexible Organic Ion-Sensitive Field-Effect Transistors (ISFETs) have been characterized to detect Ischemia-like variations in pH and potassium ion concentration. Detection capabilities, of the sensors, have been shown as pure chemical concentration to current signal transduction of the ISFET. Independent of peripheral amplifier-converter circuits, they are standalone sensors. The sensors have been evaluated for their sensitivity and signal resolution. Calibration expression, following a thermo-electric model for device operation, represents an explicit relations between transistor drain current and ion concentrations. Signal conditioning, by normalization, has been attempted to make the calibration expression explicit in ion-concentration. Finally a reliable detection strategy, in differential mode, is proposed for a reference electrode free device. [J1067]

"Analysis and implementation of an integrated sepic-forward converter for photovoltaic based light emitting diode lighting"

This study presents an integrated sepic-forward converter for photovoltaic (PV)-based light emitting diode (LED) lighting system. In the proposed converter, the sepic converter is used to deliver the solar energy via PV cell modules to battery bank in charging mode during the daytime. During the nighttime, the soft switching forward converter is adopted to drive LED lighting system in discharging mode. Power switches of sepic and soft switching forward converters are integrated to reduce the component count and the synchronous switch technique is used in the circuit to reduce the conduction losses. Thus, the smaller size, lighter weight and higher efficiency can be achieved in the proposed converter. Finally, experimental results, taken from a laboratory prototype rated at 100 W, are presented to verify the effectiveness of the proposed converter. [J1068]

"Spectrally narrowed edge emission from leaky waveguide modes in organic light-emitting diodes"

A dramatic spectral line narrowing of the edge emission at room temperature from tris(quinolinolate) Al (Alq3), N,N'-diphenyl-N,N'-bis(1-naphthylphenyl)-1,1'-biphenyl-4,4'-diamine (NPD), 4,4'-bis(2,2'-diphenyl-vinyl)-1,1'-biphenyl (DPVBi), and some guest-host small molecular organic light-emitting diodes (OLEDs), fabricated on indium tin oxide (ITO)-coated glass, is described. In all but the DPVBi OLEDs, the narrowed emission band emerges above a threshold thickness of the emitting layer, and narrows down to a full width at half maximum of only 5-10 nm. The results demonstrate that this narrowed emission is due to irregular waveguide modes that leak from the ITO to the glass substrate at a grazing angle. While measurements of variable stripe length ldevices exhibit an apparent weak optical gain $0 \leq g \leq 1.86 \text{ cm}^{-1}$, there is no observable threshold current or bias associated with this spectral narrowing. In addition, in the phosphorescent guest-host OLEDs, there is no decrease in the emission decay time of the narrowed edge emission relative to the broad surface emission. It is suspected that the apparent weak optical gain is due to misalignment of the axis of the waveguided mode and the axis of the collection lens of the probe. However, it is not clear if such a misalignment can account for all the effects of the observed evolution of the edge-emission spectra with l. [J1069]

"Aging of AlGaIn quantum well light emitting diode studied by scanning near-field optical spectroscopy"

Emission from a 285 nm AlGaIn quantum well light emitting diode has been studied by scanning near-field optical spectroscopy. The scans revealed micrometer-size domainlike areas emitting with a higher intensity and at a longer wavelength; presumably, because of a lower AlIn molar fraction in these regions. Experiments performed on different days have shown that with time, intensity from these spots increases and emission wavelength shifts to the red, indicating a further change in the quantum well alloy composition. This has allowed distinguishing an aging mechanism that involves locally increased current, heating, and atom migration. [J1070]

"4-GHz Modulation Bandwidth of Integrated 2x2 LED Array"

We demonstrate a 4.3-GHz high-speed "tilted-charge" integrated 2x2 light-emitting diode (LED) array. With an array of four LEDs operating in parallel, the optical output power can be as much as tripled while the peak high-speed performance of its individual LED component is preserved. The gigahertz bandwidth is achieved by utilizing a "drain" layer, common to all the devices in the array, to enforce a "tilted-charge" condition where only fast recombination is employed for the modulation of optical output. The successful integration of four "tilted-charge" LEDs in a parallel array paves the way towards a simple viable solution for ultra-high-speed short range optical communication. [J1071]

"Strong High Order Diffraction of Guided Modes in Micro-Cavity Light-Emitting Diodes With Hexagonal Photonic Crystals"

Photonic crystals (PhCs) have now been firmly established as an efficient means for light extraction from light emitting diodes (LEDs). We analyze the diffraction properties from thin GaN micro-cavity LEDs with hexagonal lattices that feature three guided TE modes only. In contrast to common design rules, we find that high order diffraction contributes significantly to the light extraction and increases the directionality of the emitted light. The implementation of the PhC leads to an enhancement in light extraction by a factor of up to 1.8 and the directionality of the light is greatly improved with a radiant intensity enhancement factor of 4.3, which can only be explained by the higher order diffraction that has been hitherto neglected. Furthermore, we show that higher order diffraction contributes significantly to the high azimuthal extraction uniformity we observe, suggesting that the use of quasi-crystal lattices is not necessary. We use a model including mode absorption where each in-plane angle of the guided modes is treated separately in order to explain the experimental results. [J1072]

"Inversion of magnetic field effects on electrical current and electroluminescence in tri-(8-hydroxyquinoline)-aluminum based light-emitting diodes"

The magnetic field effects on electrical current and electroluminescence have been investigated for tri-(8-hydroxyquinoline)-aluminum based organic light emitting diodes through the transient electroluminescence method. By applying rectangular pulse to drive the devices, the influence of the degradation is dramatically decreased; and a full-range evolution for the magnetoconductance (MC) and magnetoelectroluminescence (MEL) with the driving voltage has been obtained. The transition voltages for MC (1.6 V) from the negative to positive value and MEL (7 V) from the positive to negative value are different, which suggests that the magnetic field effect on the MC and MEL may have different mechanisms. [J1073]

"High efficiency p-i-n top-emitting organic light-emitting diodes with a nearly Lambertian emission pattern"

We report high efficiency phosphorescent green p-i-ntop-emitting organic light-emitting diodes consisting of metal anodes (Ag and Al), a rhenium oxide p-dopant, a rubidium carbonate n-dopant, and a semitransparent Ag cathode. Significantly high peak current efficiencies of 88 and 73 cd/A are demonstrated for the devices using Ag and Al anodes, respectively, through the optimization of organic layer thickness. The electroluminescence intensities of the Ag-based device with viewing angles show a nearly Lambertian distribution, whereas those of the Al-based device exhibit a relatively strong angular dependence, which is mainly attributed to the change in the resonance wavelength of the microcavity of the devices. Efficiencies, emission spectra, and angular dependence of the emission of the devices are further successfully analyzed using an optical model. [J1074]

"Efficiency and Stability of p-i-n Type Organic Light Emitting Diodes for Display and Lighting Applications"

Recent advances in the field of p-i-n type organic light emitting diodes (OLEDs) are reviewed. OLEDs are energy efficient light sources, which will be used in the near future in commercial display and lighting applications. In particular, p-i-n type OLEDs consisting of doped charge transport layers and intrinsic emission layers have been very successful in reducing the operational voltages and increasing the power efficiency. After shortly introducing the p-i-n concept, the advantages of this concept in terms of low operating voltages, high power efficiency and long lifetime are described. In particular, the latest reports on monochrome, white, and top-emission p-i-n OLEDs are summarized. [J1075]

"Effect of dye concentrations in blended-layer white organic light-emitting devices based on phosphorescent dyes"

The electronic and optoelectronic behavior of white organic light-emitting devices (OLEDs) based on blue (Flrpic) and red [Ir(piq)₂(acac)] phosphorescent dyes doped into the same layer of a polyvinylcarbazole (PVK) host are reported. The conductivity of all the OLEDs studied appeared to be dominated by space-charge injection effects, exhibiting a current I versus voltage V dependence of the form $I \propto V^n$, with $n \approx 7$ at applied voltages at which electroluminescence was observed. Systematic studies of the current versus voltage and light-emitting behavior of the OLEDs have identified different excitation processes for the two dyes. It is suggested that electroluminescence from the Flrpic molecules originates by direct transfer of the exciton energy from the PVK to the dye molecules, while the process of light emission from the Ir(piq)₂(acac) molecules involves carrier trapping. The efficiency of the devices can be tuned, to some extent, by varying the thickness of the organic film. Luminous efficiencies and luminous power efficiencies of 8 cd A⁻¹ and 3 lm W⁻¹ were measured for these blended-layer OLEDs, with Commission Internationale de l'Eclairage coordinates of 0.35, 0.35. [J1076]

"Diode breakdown related to recombination active defects in block-cast multicrystalline silicon solar cells"

Solar cells in modules are reverse biased when they are shaded. This can lead to diode breakdown and eventually to the occurrence of hot spots, which may, in the extreme case, destroy the module by thermal degradation. We observed at least three different types of diode breakdown in multicrystalline silicon solar cells. One of them is found to be related to the recombination activity of defects. This type is indicated by a slow increase in the reverse current with reverse bias and a relatively low breakdown voltage around -10 V. The local breakdown voltage depends significantly on the level of contamination of the material. When the solar cell is reverse biased, the breakdown sites emit bright light which shows a broad spectral distribution in the visible range with a maximum at 700 nm. [J1077]

"The LED's dark secret"

The blue light-emitting diode, arguably the greatest optoelectronic advance of the past 25 years, harbors a dark secret: crank up the current and its efficiencies will plummet. The problem is known as droop, and it's not only

puzzling the brightest minds in the field, it's also threatening the future of the electric lighting industry. [J1078]

"Impedance spectroscopy investigation of conjugated polymer coated core-shell nanoparticles"

Poly(styrene) nanoparticles decorated at their surface with poly(styrene sulfonate) brushes and subsequently loaded with polypyrrole have been prepared as film-forming materials to serve as hole injection layers in organic light-emitting diodes. Thin compressed pellets of these nanoparticles have been studied by impedance spectroscopy. Measurements were carried out in the temperature range between 123.15 and 453.15 K and frequency range from 10-1 to 106 Hz. The polypyrrole volume fraction ϕ PPy was varied as well. The film-forming nanoparticles exhibit a core-shell-type morphology with a core of electrically insulating poly(styrene) and a shell consisting of a corona of poly(styrene sulfonate) chains, which form the matrix in which the electrically conducting complex of polypyrrole and poly(styrene sulfonate) is embedded. This conducting complex exists in forms of domains with nanoscale dimensions. It is demonstrated that the charge transport in samples with ϕ PPy [for the calculation of the polypyrrole volume fractions the poly(styrene) volume was excluded] lower than 0.52 is dominated by ionic conductivity. At higher volume fractions the charge transport is mainly electronic in nature. The fluctuation-induced tunneling model can be used to describe the temperature dependence of the dc conductivity. For a sample with ϕ PPy of 0.52, a transition from insulating to conducting behavior at 385 K has been found. An electrical percolating behavior has been observed with a percolation threshold at ϕ PPy of 0.65, suggesting that polypyrrole rich and poor domains are present in the poly(styrene sulfonate) matrix and indicating a "transition" from electronically insulating to conducting behavior. A detailed analysis of the impedance spectra suggests a lower limit of the conducting domains of 2.5 nm. [J1079]

"Organic Memory and Electrical Bistability in a Quinone-Based Charge-Transfer Complex"

We present an overview of the issues of organic memory devices and discuss the mechanisms involved in conductance switching. To make the memory elements addressable, we introduce nanostructures of a quinone-based charge-transfer complex. The devices based on charge-transfer complexes exhibit electrical bistability. Apart from characterizing complex formation, we study characteristics of memory devices based on the complexes. The mechanism of bistability has been discussed in terms of electroreduction of the quinone derivative with the formation of a percolating network of conducting molecules or channels across the device. Depending on the device architecture, a device may exhibit memory-switching or threshold-switching phenomenon. The former system has displayed read-only and random-access memory applications. [J1080]

"Improvement of Electrostatic Discharge Characteristics and Optical Properties of GaN-Based Light-Emitting Diodes"

To improve the positive- and negative-voltage electrostatic discharge (ESD) characteristics of GaN light-emitting diodes (LEDs), an air gap was introduced as an ESD protection structure in an Al film on the bottom side of a sapphire substrate. The negative-voltage ESD characteristic of GaN LEDs with an air gap was remarkably improved from -0.3 to -4 kV. The degradation of electroluminescent intensity of GaN LEDs, which was caused by ESD stress, was also suppressed by an air gap in GaN LEDs. An ESD-stress-induced current is believed to flow in an air gap to protect the multiquantum well of GaN LEDs. [J1081]

"Near-Field Scanning Nanophotonic Microscopy-Breaking the Diffraction Limit Using Integrated Nano Light-Emitting Probe Tip"

We introduce a novel scanning nanophotonic microscope through monolithic integration of a nanoscale LED (Nano-LED) on a silicon cantilever. We review two recent trends of incorporating miniature light sources on the scanning probes for near-field scanning optical microscopy: one is to attach fluorophores at the tip to define a small light source, while the other is to integrate an LED and a nanometer aperture into scanning probes, based on silicon microfabrication techniques. The creation of Nano-LED combines the advantages of previous two approaches: no external sources are required and the reduction of the light source size directly leads to resolution improvement. Two types of Nano-LEDs have been successfully demonstrated utilizing nanofabrication and microelectromechanical systems technologies: 1) formation of thin silicon dioxide light-emitting layer between heavily doped p+ and n+ silicon layers created by a focused ion beam and 2) electrostatic trapping and excitation of CdSe/ZnS core-shell nanoparticles in a nanogap. We employed these probes into a standard near-field scanning and excitation setup. The probe successfully measured optical as well as topographic images of chromium test patterns with imaging resolutions of 400 and 50 nm, respectively. In addition, the directional resolution dependence of the acquired images suggests the size and shape of the light source. To our knowledge, these results are probably the first successful near-field images directly measured by such tip-embedded light sources. With the potential emission capability from near UV to IR and additional mass producibility, the nanophotonic microscope presents exciting opportunities in near-field optics, integrated circuit

technology, nanomanufacturing and molecular imaging, and sensing in biomedicine. [J1082]

"Simulation of Light Emission From Planar Multilayer OLEDs, Using a Transmission-Line Model"

In this paper, we propose a fast, accurate, and easy to implement transmission-line model, which evaluates light emission from planar multilayer OLED devices. Total radiated power and radiation patterns of OLED devices are calculated adopting the classic consideration, which relates photon emission in the active layer with the power that is radiated by a randomly oriented dipole antenna. The simulation model considers the under study configurations as equivalent electric and magnetic transmission lines in Fourier space, which are excited by voltage or current sources properly calculated. The proposed model demonstrates also an inherent ability to calculate the waveguided modes and can be also easily transformed to tackle problems of material inhomogeneity and nonlinearity. The accuracy of the transmission-line model has been verified against alternative but also exact calculation methods. Finally, numerical results are provided and discussed for OLED devices, which are constructed by materials with a complex refractive index and emit light within a zone inside the active layer. [J1083]

"Theoretical Investigation of the Radiation Pattern From LEDs Incorporating Shallow Photonic Crystals"

A theoretical approach based on coupled-mode theory is presented in order to determine the radiation pattern of LEDs incorporating a shallow photonic crystal. From this, a fundamental limit for the directionality of the diffraction of a single guided mode is given. Additionally, the Fabry-Perot resonances are shown to have significant impact on the directionality of diffracted light. For a realistic green-emitting InGaN LED in thin-film configuration the optimum reciprocal lattice vector is derived in terms of absolute diffracted intensity and directionality within a limited acceptance angle. The latter can be as high as 1.8 times the directionality of a Lambertian emitter. Furthermore, the spontaneous emission distribution between guided modes heavily influences the diffracted intensity. [J1084]

"Impact of LED Nonlinearity on Discrete Multitone Modulation"

In the context of communications based on light-emitting diodes (LEDs), spectrally efficient modulation has been considered for overcoming their limited bandwidth, and one scheme under investigation is quadrature-amplitude modulation on discrete multitones. The dependence of the output optical power on the driving current of practical LEDs is nonlinear, which distorts the transmitted signal. We investigate the impact of the nonlinear LED transfer function, i.e., the dependence of the emitted optical power on the driving current, on discrete multitone modulation. The effect incurred by this distortion was analyzed by using detailed numerical simulations addressing the impact of clipping, individual subcarriers, signal-to-noise ratio, and bit-error ratio. The approach was generalized to describe the impact of the nonlinearity of arbitrary LEDs and laser diodes, resulting in a powerful tool for assessing the impact of the nonlinearity on the link performance. This approach was applied to three types of LED, showing anything from a minuscule effect to the case in which error-free data transmission is made impossible by the transfer-function nonlinearity. [J1085]

"On a GaN-Based Light-Emitting Diode With a p-GaN/i-InGaN Superlattice Structure"

An interesting GaN-based light-emitting diode (LED) with a ten-period i-InGaN/p-GaN (5-nm/5-nm) superlattice (SL) structure, inserted between a multiple-quantum-well structure and a p-GaN layer, is fabricated and studied. This inserted SL can be regarded as a confinement layer of holes to enhance the hole injection efficiency. As compared with a conventional LED device without the SL structure, the studied LED exhibits better current-spreading performance and an improved quality. The turn-on voltage, at 20 mA, is decreased from 3.32 to 3.14 V due to the reduced contact resistance as well as the more uniformity of carrier injection. A substantially reduced leakage current (10^{-7} - 10^{-9} A) and higher endurance of the reverse current pulse are found. As compared with the conventional LED without the SL structure, the significant enhancement of 25.4% in output power and the increment of 5% in external quantum efficiency are observed. [J1086]

"Improved Light Output Power of GaN-Based Light-Emitting Diodes Using Double Photonic Quasi-Crystal Patterns"

The enhancement of light extraction from GaN-based light-emitting diodes (LEDs) with a double 12-fold photonic quasi-crystal (PQC) structure using nanoimprint lithography is presented. At a driving current of 20 mA on a transistor-outline-can package, the light output power of an LED with a nanohole patterned sapphire substrate (NHPSS) and an LED with a double PQC structure are enhanced by 34% and 61%, compared with the conventional LED. In addition, the higher output power of the LED with the double PQC structure is due to better

reflectance on NHPSS and higher scattering effect on p-GaN surface using a 12-fold PQC structure pattern. These results provide promising potential to increase the output powers of commercial light-emitting devices.

[J1087]

"Indoor broadcasting via white LEDs and OFDM"

Recently, visible light communication (VLC) technology has been gaining attention in both academia and industry. This is driven by the progress of white light emitting diode (LED) technology for solid-state lighting (SSL) and the potential of simultaneously using such LEDs for illumination and indoor wireless data transmission. This paper provides an overview about the technology and describes the physical layer implementation of a VLC system based on a modified version of the classical orthogonal frequency division multiplexing (OFDM) modulation technique. Besides, the paper presents a hardware prototype for short-range broadcasting using a white LED lamp. The OFDM system runs on DSP development boards. Off-the-shelf 9 LEDs and a single photodiode (PD) are utilized to build the analog frontends. The prototype allows investigating the influence of the electrical signal-to-noise ratio (SNR), constellation order, and channel coding on the bit-error performance. Theoretical and experimental results on optical path loss show close match. In this context, the influence of the LED beam angle on the horizontal coverage is highlighted. [J1088]

"Wide color-gamut improvement of LCM using multi-phosphor white LED and modified rich color method"

This paper presents an improved wide color-gamut technique for liquid crystal modules (LCM) with multiphosphor white (MPW) light emitting diodes (LED) and an modified rich color image processing method. The MPW LED improves 13% of the display color gamut in comparison with standard white LED under the assumption of equal power consumption and brightness. Via many simulation results, the pixel-level rich color method is shown to obtain a superior image data by giving about 45% saturation enhancement without hue distortion. The performance and merit of the proposed technique are exemplified by conducting several experimental results on a 2.8-inch thin-film-transistor (TFT) LCM. [J1089]

"Highly efficient nondoped green organic light-emitting devices based on a substituted triphenylpyridine derivative"

Highly efficient nondoped green organic light-emitting devices based on a triphenylpyridine derivative, 4-[4-(dimethylamino)phenyl]-2,6-diphenylnicotinonitrile (NPDPN), were fabricated and characterized. The double-organic-layer device with a structure of ITO/ α -naphthylphenylbiphenyl diamine /NPDPN/LiF/Al, in which NPDPN was used as both the emitter and the electron transporter, exhibits a green emission with Commission Internationale de L'Eclairage (CIE) coordinates of (0.23,0.52) and a power efficiency of 5.5 lm/W. The result is much better than that of similarly structured device based on tris(8-hydroxyquinoline)aluminum. Furthermore, a high current efficiency of 8.4 cd/A was achieved with an optimized device configuration. [J1090]

"Enhancement in current efficiency in organic light-emitting diodes with incorporation of subphthalocyanine"

A highly efficient hole injection material, boron subphthalocyanine chloride (SubPc), was incorporated in organic light-emitting diodes. Device performance is greatly enhanced by inserting an ultrathin layer of SubPc between anodes and N,N'-di(naphthalene-1-yl)-N,N'-diphenyl-benzidine (NPB). Electronic structures and chemical reaction at the interface between NPB and SubPc are also investigated by photoemission spectroscopy with synchrotron radiation sources. Extra states are observed at the forbidden gap of SubPc with deposition of NPB, resulting from the broken bonds between boron and chlorine on SubPc with presence of NPB. These gap states are attributed to the improvement of device performance. [J1091]

"Enhancement of Light Power for Blue InGaN LEDs by Using Low-Indium-Content InGaN Barriers"

The optical properties of blue InGaN LEDs that emit in a spectral range from 410 to 445 nm are theoretically investigated by using the APSYS simulation program. It is found that the light performance can be enhanced effectively when the conventional GaN barrier layers are replaced by In_{0.02}Ga_{0.98}N and In_{0.05}Ga_{0.95}N barrier layers. The numerical results indicate that the output power of LEDs with In_{0.02}Ga_{0.98}N barrier layers is improved gradually above the emission wavelength of 410 nm. However, when the In_{0.05}Ga_{0.95}N barrier layers are used, the emitting power of LEDs varies significantly when the emission wavelength changes. When the emission wavelength is 410 nm, the use of GaN and In_{0.02}Ga_{0.98}N barrier layers can lead to higher output power. However, if the emission wavelength is 445 nm, the use of In_{0.05}Ga_{0.95}N barrier layers is beneficial for maintaining high output power. [J1092]

"Erratum: "High efficiency GaN-based light-emitting diodes fabricated on dielectric-mask-embedded structures" [JAppl. Phys. Lett. 95, 011108 (2009)]"

First Page of the Article [J1093]

"Influence of interlayer on the performance of stacked white organic light-emitting devices"

Stacked white organic light-emitting devices (WOLEDs) comprising of blue fluorescent and orange phosphorescent emissive units employing tri(8-hydroxyquinoline) aluminum (Alq3):Mg/MoO₃ as charge generation layer are fabricated. The working mechanism of Alq3:Mg/MoO₃ is also discussed using a simple method. We demonstrate charge-carrier separation takes place only in MoO₃ layer. Stacked WOLED with better performance was obtained by adjusting the thickness of MoO₃. The stacked WOLED with efficiency of 39.2 cd/A has excellent color stability with the Commission Internationale de l'Eclairage coordinates only changing from (0.407, 0.405) to (0.398, 0.397) when luminance increases from 22 to 10 000 cd/m². [J1094]

"Efficiency retention at high current injection levels in m -plane InGaN light emitting diodes"

We investigated the internal quantum efficiency (IQE) and the relative external quantum efficiency (EQE) of m-plane InGaN light emitting diodes (LEDs) grown on m-plane freestanding GaN emitting at 400 nm for current densities up to 2500 A/cm². IQE values extracted from intensity and temperature dependent photoluminescence measurements were consistently higher, by some 30%, for the m-plane LEDs than for reference c-plane LEDs having the same structure, e.g., 80% versus 60% at an injected steady-state carrier concentration of $1.24 \times 10^{18} \text{ cm}^{-3}$. With increasing current injection up to 2500 A/cm², the maximum EQE is nearly retained in m-plane LEDs, whereas c-plane LEDs exhibit approximately 25% droop. The negligible droop in m-plane LEDs is consistent with the reported enhanced hole carrier concentration and light holes in m-plane orientation, thereby enhanced hole transport throughout the active region, and lack of polarization induced field. A high quantum efficiency and in particular its retention at high injection levels bode well for m-plane LEDs as candidates for general lighting applications. [J1095]

"Output power enhancement of light-emitting diodes via two-dimensional hole arrays generated by a monolayer of microspheres"

The output power enhancement of the GaN-based light-emitting diodes (LEDs) featuring two-dimensional (2D) hole arrays is demonstrated. The 2D air hole arrays were first generated in the photoresist by utilizing the focusing nature of microspheres, and then transferred onto the GaN surface through dry etching. The maximum output power of the surface-textured LEDs was enhanced by 45% compared with the LEDs without surface texturing. The finite-difference time-domain calculation was performed and revealed that the light extraction efficiency of the textured LEDs increased with increasing etching depth. [J1096]

"Enhanced light extraction in nitride light-emitting diodes by epitaxially grown photonic-crystal nanopillar arrays"

A photonic crystal has been created on the p-layer of an InGaN light-emitting diode wafer by selective area growth, thus avoiding the etch processes that are detrimental to the active region. Nanopillar arrays with either hexagonal or Archimedian lattices were grown in apertures defined by nanoimprint lithography. Electroluminescence measurements show that the pillars improve the on-axis light output by up to 1.9-2.0 times. This technique could be extended to higher aspect ratio nanostructures that will have stronger coupling between the guided modes and the photonic crystal. [J1097]

"Improving efficiency roll-off in organic light emitting devices with a fluorescence-interlayer-phosphorescence emission architecture"

Organic light emitting devices (OLEDs) with a fluorescence-interlayer-phosphorescence emission layer structure (FIP EML) has been proposed to solve the efficiency roll-off issue effectively. Efficient green OLED based on FIP EML exhibiting only 26% roll-off in the luminance efficiency, which is lower than the typical roll-off of 51% for conventional phosphorescent OLEDs with single EML operated at 5-150 mA/cm² range, has been demonstrated. Such enhancement should be attributed to the improved carrier balance, the exciton redistribution in recombination zone, the suppression of nonradiative exciton quenching processes, and the elimination of energy transfer loss offered by the FIP EML structure. [J1098]

"The future's so bright"

Anyone who thinks that LED illumination is for wimps should look at-not into-one of Wayne Johnson's new flashlights. With 4 four-chip LED modules, it puts out roughly the same light as a 200-watt incandescent bulb. Parabolic reflectors point most of that light into a beam that can illuminate the landscape dozens of meters away. [J1099]

"Double side electroluminescence from p-NiO /n-ZnO nanowire heterojunctions"

Double side light emission devices based on p-NiO/n-ZnO nanowire heterojunctions have been fabricated on indium tin oxide substrate by radio frequency magnetron sputtering combined with hydrothermal process. According to the energy band alignment, the detected broad visible and narrow ultraviolet electroluminescence arise from defect and band edge transitions in ZnO nanowires, respectively. The unique property of the double side emission is due to the nature of the large band gap of NiO film. It provides a good opportunity for the emission of a light emitting device with different colors on the top and back sides, simultaneously. [J1100]

"Ultraviolet emission from a ZnO rod homojunction light-emitting diode"

Ultraviolet electroluminescence was demonstrated at room temperature from a ZnO rod homojunction light-emitting diode array. The p-type doping was realized by phosphorous (P) ion implantation into defect-free ZnO rods followed by annealing. High resolution transmission electron microscopy shows the lattice compression of annealed single crystalline P-doped ZnO rod compared to the as-grown ZnO rod, suggesting atomically incorporation of P into the ZnO wurtzite structure. p-type doping was confirmed by low temperature photoluminescence spectra and single rod current-voltage characterization. [J1101]

"High efficiency light emitting diode with anisotropically etched GaN-sapphire interface"

We report the fabrication and study of high efficiency ultraviolet light emitting diodes with inverted micropylam structures at GaN-sapphire interface. The micropylam structures were created by anisotropic chemical wet etching. The pyram structures have significantly enhanced the light output efficiency and at the same time also improved the crystal quality by partially relieving the strain and reducing the dislocation defects in GaN. The electroluminescent output power at normal direction was enhanced by 120% at 20 mA injection current and the output power integrated over all directions was enhanced by 85% compared to a reference sample. [J1102]

"Impact of Nonlinear LED Transfer Function on Discrete Multitone Modulation: Analytical Approach"

Light-emitting diodes constitute a low-cost choice for optical transmitters in medium-bit-rate optical links. An example for the latter is local-area networks. However, one of the disadvantageous properties of light-emitting diodes is their nonlinear characteristic, which may limit the data transmission performance of the system, especially in the case of multiple subcarrier modulation, which is starting to attract attention in various applications, such as visible-light communications and data transmission over polymer optical fibers. In this paper, the influence of the nonlinear transfer function of the light-emitting diodes on discrete multitone modulation is studied. The transfer function describes the dependence of the emitted optical power on the driving current. Analytical expressions for an idealized link were derived, and these equations allow the estimation of the power of the noise-like, nonlinear crosstalk between the orthogonal subcarriers. The crosstalk components of the quadrature and in-phase subcarrier components were found to be independent and approximately normally distributed. Using these results, the influence of light-emitting-diode nonlinearity on the performance of the system was investigated. The main finding was that systems using a small number of subcarriers and/or high QAM level exhibit a large signal-to-noise-ratio penalty due to the nonlinear crosstalk. The model was applied to systems with white and resonant-cavity light-emitting diodes. It is shown that the nonlinearity may severely limit the performance of the system, particularly in the case of resonant-cavity light-emitting diodes, which exhibit a strong nonlinear behavior. [J1103]

"Foundry giant sees the light"

What do you do when you dominate your market? You find other markets to dominate. That's the plan for Taiwan Semiconductor Manufacturing Co. (TSMC), the world's biggest semiconductor foundry, according to its founding chairman, who retook the reins of the company in mid-June. Morris Chang, the recently reappointed chairman and CEO, says that a better future lies ahead for the firm if it pushes into green energy- specifically solar power and LEDs. [J1104]

"The Spectrum Dimpling Gang"

Dean Kamen is a throwback to the era of Edison, Tesla, and Westinghouse, when a charismatic engineer-entrepreneur could be famous. And when Kamen, the multimillionaire inventor of the Segway, wants to escape

the limelight, he flies his helicopter to his private island off the coast of Connecticut. [J1105]

СПИСОК ЛИТЕРАТУРЫ

- J1. McGraw Gregory J. Organic vapor jet printing at micrometer resolution using microfluidic nozzle arrays. / McGraw Gregory J., Peters Diane L., Forrest Stephen R. // Applied Physics Letters. - 2011. - Vol. 98, No. 1. - P. 013302-013302-3. ↑
- J2. Brinkley Stuart E. Polarized spontaneous emission from blue-green m-plane GaN-based light emitting diodes. / Brinkley Stuart E., Lin You-Da, Chakraborty Arpan, Pfaff Nathan, Cohen Daniel, Speck James S., Nakamura Shuji, DenBaars Steven P. // Applied Physics Letters. - 2011. - Vol. 98, No. 1. - P. 011110-011110-3. ↑
- J3. Kim Sun-Kyung. Surface-plasmon-induced light absorption on a rough silver surface. / Kim Sun-Kyung, Ee Ho-Seok, Choi Woonkyung, Kwon Soon-Hong, Kang Ju-Hyung, Kim Yoon-Ho, Kwon Hoki, Park Hong-Gyu. // Applied Physics Letters. - 2011. - Vol. 98, No. 1. - P. 011109-011109-3. ↑
- J4. Ting-Wei Kuo. Improved Extraction Efficiency of Light-Emitting Diodes by Wet-Etching Modifying AZO Surface Roughness. / Ting-Wei Kuo, Shi-Xiong Lin, Yueh-Yu Hung, Jui-Hong Horng, Mau-Phon Hong. // IEEE Photonics Technology Letters. - 2011. - Vol. 23, No. 6. - P. 362-364. ↑
- J5. Marchetti A. P. Integer charge transfer states in organic light-emitting diodes: Optical detection of hole carriers at the anode |organic interface. / Marchetti A. P., Sassini K. E., Young R. H., Rothberg L. J., Kondakov D. Y. // Journal of Applied Physics. - 2011. - Vol. 109, No. 1. - P. 013709-013709-8. ↑
- J6. Zhu Dandan. Efficiency measurement of GaN-based quantum well and light-emitting diode structures grown on silicon substrates. / Zhu Dandan, McAleese Clifford, Haberlen Maik, Salcianu Carmen, Thrush Ted, Kappers Menno, Phillips Andrew, Lane Penelope, Kane Michael, Wallis David, Martin Trevor, Astles Mike, Hylton Nicolas, Dawson Phil, Humphreys Colin. // Journal of Applied Physics. - 2011. - Vol. 109, No. 1. - P. 014502-014502-6. ↑
- J7. Wen-Yu Lin. Enhanced Output Power of Near-Ultraviolet InGaN/AlGaN LEDs With Patterned Distributed Bragg Reflectors. / Wen-Yu Lin, Dong-Sing Wu, Shih-Cheng Huang, Ray-Hua Horng. // IEEE Transactions on Electron Devices. - 2011. - Vol. 58, No. 1. - P. 173-179. ↑
- J8. Preezant Yevgeni. Exciton formation as a rate limiting step for charge recombination in disordered organic molecules or polymers. / Preezant Yevgeni, Tessler Nir. // Journal of Applied Physics. - 2011. - Vol. 109, No. 1. - P. 013701-013701-8. ↑
- J9. Jenn-Bin Huang. Improvement of ESD Level of GaN-Based LEDs Using Antiparallel Ga- and N-Polar Domains in p-GaN Layer. / Jenn-Bin Huang, Lu-Sheng Hong, Chen-Chia Chou. // IEEE Electron Device Letters. - 2011. - Vol. 32, No. 3. - P. 342-344. ↑
- J10. Ching-Ting Lee. Ultraviolet Electroluminescence From ZnO-Based n-i-p Light-Emitting Diodes. / Ching-Ting Lee, Jheng-Tai Yan. // IEEE Photonics Technology Letters. - 2011. - Vol. 23, No. 6. - P. 353-355. ↑
- J11. Kwonhyung Lee. Indoor Channel Characteristics for Visible Light Communications. / Kwonhyung Lee, Hyuncheol Park, Barry J.R. // IEEE Communications Letters. - 2011. - Vol. 15, No. 2. - P. 217-219. ↑
- J12. Tonheim C.R. Enhancement in Light Emission From Hg-Cd-Te Due to Surface Patterning. / Tonheim C.R., Sudbush, A.S., Selvig E., Haakenaasen R. // IEEE Photonics Technology Letters. - 2011. - Vol. 23, No. 1. - P. 36-38. ↑
- J13. Hsin-Tao Huang. Planar Lighting System Using Array of Blue LEDs to Excite Yellow Remote Phosphor Film. / Hsin-Tao Huang, Yi-Pai Huang, Chuang-Chuang Tsai. // Journal of Display Technology. - 2011. - Vol. 7, No. 1. - P. 44-51. ↑
- J14. Daeyoun Cho. A Novel Adaptive Dimming LED Backlight System With Current Compensated X-Y

Channel Drivers for LCD TVs. / Daeyoun Cho, Won-Sik Oh, Gun Woo Moon. // Journal of Display Technology. - 2011. - Vol. 7, No. 1. - P. 29-35. ↑

J15. Mao An. Characteristics of dotlike green satellite emission in GaInN light emitting diodes. / Mao An, Cho Jaehee, Dai Qi, Schubert E. Fred, Son Joong Kon, Park Yongjo. // Applied Physics Letters. - 2011. - Vol. 98, No. 2. - P. 023503-023503-3. ↑

J16. Yang Xiaohui. Efficient organic light-emitting devices with platinum-complex emissive layer. / Yang Xiaohui, Wu Fang-ly, Haverinen Hanna, Li Jian, Cheng Chien-Hong, Jabbour Ghassan E. // Applied Physics Letters. - 2011. - Vol. 98, No. 3. - P. 033302-033302-3. ↑

J17. Balci Sinan. Localization of surface plasmon polaritons in hexagonal arrays of Moire cavities. / Balci Sinan, Kocabas Askin, Kocabas Coskun, Aydinli Atilla. // Applied Physics Letters. - 2011. - Vol. 98, No. 3. - P. 031101-031101-3. ↑

J18. Zhen-min Zhu. Uniform Illumination Design by Configuration of LED Array and Diffuse Reflection Surface for Color Vision Application. / Zhen-min Zhu, Xing-hua Qu, Guo-xin Jia, Jian-fei Ouyang. // Journal of Display Technology. - 2011. - Vol. 7, No. 2. - P. 84-89. ↑

J19. Jeong H. H. Improved Electrostatic Discharge Protection in GaN-Based Vertical Light-Emitting Diodes by an Internal Diode. / Jeong H. H., Lee S. Y., Bae J.-H., Choi K. K., Song J.-O., Son S. J., Lee Y.-H., Seong T.-Y. // IEEE Photonics Technology Letters. - 2011. - Vol. 23, No. 7. - P. 423-425. ↑

J20. Hochreiner A. Midinfrared electroluminescence from PbTe/CdTe quantum dot light-emitting diodes. / Hochreiner A., Schwarzl T., Eibelhuber M., Heiss W., Springholz G., Kolkovsky V., Karczewski G., Wojtowicz T. // Applied Physics Letters. - 2011. - Vol. 98, No. 2. - P. 021106-021106-3. ↑

J21. Mak Giuseppe Y. Interconnected alternating-current light-emitting diode arrays isolated by laser micromachining. / Mak Giuseppe Y., Lam Edmund Y., Choi H. W. // Journal of Vacuum Science & Technology B: Microelectronics and Nanometer Structures. - 2011. - Vol. 29, No. 1. - P. 011025-011025-4. ↑

J22. Starvaggi P. Design of selective emitting media within a cylindrical tube for conversion of wasted heat energy to electrical energy. / Starvaggi P., Hoffman M., Clemons C. B., Young G. W. // Journal of Applied Physics. - 2011. - Vol. 109, No. 1. - P. 013112-013112-10. ↑

J23. Lehnhardt T. Influence of GaSb and AlGaInAsSb as Barrier Material on 2.8- μ m GaSb-Based Diode Laser Properties. / Lehnhardt T., Herrmann A., Kamp M., Hojfling S., Worschech L., Forchel A. // IEEE Photonics Technology Letters. - 2011. - Vol. 23, No. 6. - P. 371-373. ↑

J24. Yi-Lun Chou. Improvement of Surface Emission for GaN-Based Light-Emitting Diodes With a Metal-Via-Hole Structure Embedded in a Reflector. / Yi-Lun Chou, Ray-Ming Lin, Min-Hung Tung, Chia-Lung Tsai, Jen-Chih Li, I-Chun Kuo, Meng-Chyi Wu. // IEEE Photonics Technology Letters. - 2011. - Vol. 23, No. 7. - P. 393-395. ↑

J25. Dambul K.D. Indoor Optical Wireless MIMO System With an Imaging Receiver. / Dambul K.D., O'Brien D.C., Faulkner G. // IEEE Photonics Technology Letters. - 2011. - Vol. 23, No. 2. - P. 97-99. ↑

J26. Jin-Wei Shi. Investigation of the Carrier Dynamic in GaN-Based Cascade Green Light-Emitting Diodes Using the Very Fast Electrical-Optical Pump-Probe Technique. / Jin-Wei Shi, Huang H.-W., Kuo F.-M., Lai W.-C., Ming-Lun Lee, Jinn-Kong Sheu. // IEEE Transactions on Electron Devices. - 2011. - Vol. 58, No. 2. - P. 495-500. ↑

J27. Koerperick E.J. Cascaded Superlattice InAs/GaSb Light-Emitting Diodes for Operation in the Long-Wave Infrared. / Koerperick E.J., Norton D.T., Olesberg J.T., Olson B.V., Prineas J.P., Boggess T.F. // IEEE Journal of Quantum Electronics. - 2011. - Vol. 47, No. 1. - P. 50-54. ↑

J28. Sumpf B. Nearly Diffraction-Limited Tapered Lasers at 675 nm With 1-W Output Power and Conversion Efficiencies Above 30%. / Sumpf B., Adamiec P., Zorn M., Wenzel H., Erbert G. // IEEE Photonics Technology Letters. - 2011. - Vol. 23, No. 4. - P. 266-268. ↑

J29. Yu-Hsuan Sun. Optical Properties of the Partially Strain Relaxed InGaN/GaN Light-Emitting Diodes Induced by p-Type GaN Surface Texturing. / Yu-Hsuan Sun, Yun-Wei Cheng, Szu-Chieh Wang, Ying-Yuan

Huang, Chun-Hsiang Chang, Sheng-Chieh Yang, Liang-Yi Chen, Min-Yung Ke, Chi-Kang Li, Yuh-Renn Wu, JianJang Huang. // IEEE Electron Device Letters. - 2011. - Vol. 32, No. 2. - P. 182-184. ↑

J30. Wern-Yarng Shieh. Design of Infrared Electronic-Toll-Collection Systems With Extended Communication Areas and Performance of Data Transmission. / Wern-Yarng Shieh, Chen-Chien Hsu, Shen-Lung Tung, Po-Wen Lu, Ti-Ho Wang, Shyang-Lih Chang. // IEEE Transactions on Intelligent Transportation Systems. - 2011. - Vol. 12, No. 1. - P. 25-35. ↑

J31. Wenzl F.P. On the Adjustment of the Color Temperature of White Light-Emitting Diodes by Femtosecond Laser Patterning. / Wenzl F.P., Kuna L., Sommer C., Reil F., Krenn J.R., Pachler P., Hartmann P. // IEEE Photonics Technology Letters. - 2011. - Vol. 23, No. 2. - P. 124-126. ↑

J32. Gacio D. A Universal-Input Single-Stage High-Power-Factor Power Supply for HB-LEDs Based on Integrated Buck-Flyback Converter. / Gacio D., Alonso J.M., Calleja A.J., Garcia J., Rico-Secades M. // IEEE Transactions on Industrial Electronics. - 2011. - Vol. 58, No. 2. - P. 589-599. ↑

J33. Il-Suk Kang. A Method for Fabricating Practically Channel-Corner-Free Polycrystalline Silicon Thin-Film Transistors. / Il-Suk Kang, Cheol-Ho Park, Young-Su Kim, Nam-Kyu Song, Seung-Ki Joo, Hyun-Sang Seo, Chi Won Ahn, Jun-Mo Yang, Wook-Jung Hwang. // IEEE Transactions on Electron Devices. - 2011. - Vol. 58, No. 1. - P. 271-275. ↑

J34. Dan-Dan Zhang. Efficiency Enhancement in Organic Light-Emitting Devices With a Magnetic Doped Hole-Transport Layer. / Dan-Dan Zhang, Jing Feng, Hai Wang, Yue-Feng Liu, Lu Chen, Yu Jin, Yu-Qing Zhong, Yu Bai, Qi-Dai Chen, Hong-Bo Sun. // IEEE Photonics Journal. - 2011. - Vol. 3, No. 1. - P. 26-30. ↑

J35. Zhu L. Vertically Mounted InGaN-on-Sapphire Light-Emitting Diodes. / Zhu L., Ma Z.T., Lai P.T., Choi H.W. // IEEE Transactions on Electron Devices. - 2011. - Vol. 58, No. 2. - P. 490-494. ↑

J36. Yun Shuai. Angular CCT Uniformity of Phosphor Converted White LEDs: Effects of Phosphor Materials and Packaging Structures. / Yun Shuai, Yongzhi He, Tran N.T., Shi F.G. // IEEE Photonics Technology Letters. - 2011. - Vol. 23, No. 3. - P. 137-139. ↑

J37. Kissinger J. Portable Fluorescence Lifetime Detection for Chlorophyll Analysis in Marine Environments. / Kissinger J., Wilson D. // IEEE Sensors Journal. - 2011. - Vol. 11, No. 2. - P. 288-295. ↑

J38. Ross P.E. Top 11 technologies of the decade. IEEE Spectrum. - 2011. - Vol. 48, No. 1. - P. 27-63. ↑

J39. Wallich P. The lightbulb that really is a better idea [Tools & Toys]. IEEE Spectrum. - 2011. - Vol. 48, No. 1. - P. 20-22. ↑

J40. Dong-Long Lin. Color Range Images Captured by a Four-Phase CMOS Image Sensor. / Dong-Long Lin, Ching-Chun Wang, Chia-Ling Wei. // IEEE Transactions on Electron Devices. - 2011. - Vol. 58, No. 3. - P. 732-739. ↑

J41. Ray-Hua Horng. Light Extraction Investigation for Thin-Film GaN Light-Emitting Diodes With Imbedded Electrodes. / Ray-Hua Horng, Yi-An Lu, Dong-Sing Wu. // IEEE Photonics Technology Letters. - 2011. - Vol. 23, No. 1. - P. 54-56. ↑

J42. Miao-Chan Tsai. Numerical Study of Blue InGaN Light-Emitting Diodes With Varied Barrier Thicknesses. / Miao-Chan Tsai, Sheng-Horng Yen, Ying-Chung Lu, Yen-Kuang Kuo. // IEEE Photonics Technology Letters. - 2011. - Vol. 23, No. 2. - P. 76-78. ↑

J43. Hwu K.I. Powering LED Using High-Efficiency SR Flyback Converter. / Hwu K.I., Yau Y.T., Li-Ling Lee. // IEEE Transactions on Industry Applications. - 2011. - Vol. 47, No. 1. - P. 376-386. ↑

J44. Yao-Ching Hsieh. An Interleaved Flyback Converter Featured With Zero-Voltage Transition. / Yao-Ching Hsieh, Ming-Ren Chen, Hung-Liang Cheng. // IEEE Transactions on Power Electronics. - 2011. - Vol. 26, No. 1. - P. 79-84. ↑

J45. Chiang T. H. Improved Optical and ESD Characteristics for GaN-Based LEDs With an Layer. / Chiang T. H., Chiou Y. Z., Chang S. J., Wang C. K., Ko T. K., Lin T. K., Chiu C. J., Chang S. P. // IEEE Transactions on Device and Materials Reliability. - 2011. - Vol. 11, No. 1. - P. 76-80. ↑

- J46.** Wern-Yarng Shieh. A Problem of Infrared Electronic-Toll-Collection Systems: The Irregularity of LED Radiation Pattern and Emitter Design. / Wern-Yarng Shieh, Hsu C.-C.J., Ti-Ho Wang. // IEEE Transactions on Intelligent Transportation Systems. - 2011. - Vol. 12, No. 1. - P. 152-163. ↑
- J47.** Hsiao-Chiu Hsu. Enhanced Performance of Nitride-Based Blue LED With Step-Stage MQW Structure. / Hsiao-Chiu Hsu, Yan-Kuin Su, Shyh-Jer Huang, Chi-Yao Tseng, Chiao-Yang Cheng, Kuan-Chun Chen. // IEEE Photonics Technology Letters. - 2011. - Vol. 23, No. 5. - P. 287-289. ↑
- J48.** Ntogari G. Combining Illumination Dimming Based on Pulse-Width Modulation With Visible-Light Communications Based on Discrete Multitone. / Ntogari G., Kamalakis T., Walewski J., Sphicopoulos T. // IEEE/OSA Journal of Optical Communications and Networking. - 2011. - Vol. 3, No. 1. - P. 56-65. ↑
- J49.** Kim Hyunsoo. Performance characteristics of GaN-based light-emitting diodes fabricated with AgNi, AgCu, and AgAl-alloy reflectors. / Kim Hyunsoo, Lee Sung-Nam. // Journal of Vacuum Science & Technology B: Microelectronics and Nanometer Structures. - 2011. - Vol. 29, No. 1. - P. 011032-011032-5. ↑
- J50.** Tanaka S. Droop improvement in high current range on PSS-LEDs. / Tanaka S., Zhao Y., Koslow I., Pan C.-C., Chen H.-T., Sonoda J., DenBaars S.P., Nakamura S. // Electronics Letters. - 2011. - Vol. 47, No. 5. - P. 335-336. ↑
- J51.** Sharbati M.T. Electroluminescence From Polar Nonlinear Optical Chromophore With Low Turn-On Voltage. / Sharbati M.T., Gharavi A., Emami F. // Journal of Display Technology. - 2011. - Vol. 7, No. 4. - P. 181-185. ↑
- J52.** Gago-Caldero. Multicolor Virtual Matrix LED Display Controlled by D-Type Flip-Flop Drivers. / Gago-Caldero, n A., Fernandez-Ramos J., Gago-Boho, rquez A. // Journal of Display Technology. - 2011. - Vol. 7, No. 4. - P. 174-180. ↑
- J53.** Chung Dae-Young. Flexible multilayer inverted polymer light-emitting diodes with a gravure contact printed Cs₂CO₃ electron injection layer. / Chung Dae-Young, Leem Dong-Seok, Bradley Donal D. C., Campbell Alasdair J. // Applied Physics Letters. - 2011. - Vol. 98, No. 10. - P. 103306-103306-3. ↑
- J54.** Zhang L. Theoretical study of polarization-doped GaN-based light-emitting diodes. / Zhang L., Ding K., Liu N. X., Wei T. B., Ji X. L., Ma P., Yan J. C., Wang J. X., Zeng Y. P., Li J. M. // Applied Physics Letters. - 2011. - Vol. 98, No. 10. - P. 101110-101110-3. ↑
- J55.** Lee Sang Wuk. Vertical ZnO nanorod/Si contact light-emitting diode. / Lee Sang Wuk, Cho Hak Dong, Panin Gennady, Won Kang Tae. // Applied Physics Letters. - 2011. - Vol. 98, No. 9. - P. 093110-093110-3. ↑
- J56.** Chen Yan. A host sensitized reddish-orange Gd²⁺MoO₆:Sm³⁺ phosphor for light emitting diodes. / Chen Yan, Wang Jing, Liu Chunmeng, Kuang Xiaojun, Su Qiang. // Applied Physics Letters. - 2011. - Vol. 98, No. 8. - P. 081917-081917-3. ↑
- J57.** Endo Ayataka. Efficient up-conversion of triplet excitons into a singlet state and its application for organic light emitting diodes. / Endo Ayataka, Sato Keigo, Yoshimura Kazuaki, Kai Takahiro, Kawada Atsushi, Miyazaki Hiroshi, Adachi Chihaya. // Applied Physics Letters. - 2011. - Vol. 98, No. 8. - P. 083302-083302-3. ↑
- J58.** Liao Yitao. AlGaIn based deep ultraviolet light emitting diodes with high internal quantum efficiency grown by molecular beam epitaxy. / Liao Yitao, Thomidis Christos, Kao Chen-kai, Moustakas Theodore. D. // Applied Physics Letters. - 2011. - Vol. 98, No. 8. - P. 081110-081110-3. ↑
- J59.** Chen E.-C. Polymer Infrared Proximity Sensor Array. / Chen E.-C., Shih C.-Y., Dai M.-Z., Yeh H.-C., Chao Y.-C., Meng H.-F., Zan H.-W., Liu W.-R., Chiu Y.-C., Yeh Y.-T., Sun C.-J., Horng S.-F., Hsu C.-S. // IEEE Transactions on Electron Devices. - 2011. - Vol. 58, No. 4. - P. 1215-1220. ↑
- J60.** Kuik Martijn. Determination of the trap-assisted recombination strength in polymer light emitting diodes. / Kuik Martijn, Nicolai Herman T., Lenes Martijn, Wetzelaer Gert-Jan A. H., Lu Mingtao, Blom Paul W. M. // Applied Physics Letters. - 2011. - Vol. 98, No. 9. - P. 093301-093301-3. ↑
- J61.** Thomschke Michael. Improvement of voltage and charge balance in inverted top-emitting organic electroluminescent diodes comprising doped transport layers by thermal annealing. / Thomschke Michael, Hofmann Simone, Olthof Selina, Anderson Merve, Kleemann Hans, Schober Matthias, Lussem Bjorn, Leo Karl. //

Applied Physics Letters. - 2011. - Vol. 98, No. 8. - P. 083304-083304-3. ↑

J62. Vasilopoulou Maria. Reduced molybdenum oxide as an efficient electron injection layer in polymer light-emitting diodes. / Vasilopoulou Maria, Palilis Leonidas C., Georgiadou Dimitra G., Argitis Panagiotis, Kennou Stella, Sygellou Labrini, Kostis Ioannis, Papadimitropoulos Giorgos, Konofaos Nikos, Iliadis Agis A., Davazoglou Dimitris. // Applied Physics Letters. - 2011. - Vol. 98, No. 12. - P. 123301-123301-3. ↑

J63. Huang Yong. InP/InAlGaAs light-emitting transistors and transistor lasers with a carbon-doped base layer. / Huang Yong, Ryou Jae-Hyun, Dupuis Russell D., Dixon Forest, Feng Milton, Holonyak Nick. // Journal of Applied Physics. - 2011. - Vol. 109, No. 6. - P. 063106-063106-6. ↑

J64. Tsai Miao-Chan. Deep-ultraviolet light-emitting diodes with gradually increased barrier thicknesses from n-layers to p-layers. / Tsai Miao-Chan, Yen Sheng-Horng, Kuo Yen-Kuang. // Applied Physics Letters. - 2011. - Vol. 98, No. 11. - P. 111114-111114-3. ↑

J65. Fu Yi-Keng. The effect of trimethylgallium flows in the AlInGa_N barrier on optoelectronic characteristics of near ultraviolet light-emitting diodes grown by atmospheric pressure metalorganic vapor phase epitaxy. / Fu Yi-Keng, Jiang Ren-Hao, Lu Yu-Hsuan, Chen Bo-Chun, Xuan Rong, Fang Yen-Hsiang, Lin Chia-Feng, Su Yan-Kuin, Chen Jenn-Fang. // Applied Physics Letters. - 2011. - Vol. 98, No. 12. - P. 121115-121115-3. ↑

J66. Chiaria S. Numerical Study of ZnO-Based LEDs. / Chiaria S., Goano M., Bellotti E. // IEEE Journal of Quantum Electronics. - 2011. - Vol. 47, No. 5. - P. 661-671. ↑

J67. Lee Y.-J. Effect of Surface Texture and Backside Patterned Reflector on the AlGaInP Light-Emitting Diode: High Extraction of Waveguided Light. / Lee Y.-J., Lee C.-J., Chen C.-H. // IEEE Journal of Quantum Electronics. - 2011. - Vol. 47, No. 5. - P. 636-641. ↑

J68. Yang Y. GaAs-based near-infrared up-conversion device fabricated by wafer fusion. / Yang Y., Liu H.C., Shen W.Z., Gupta J.A., Luo H., Buchanan M., Wasilewski Z.R. // Electronics Letters. - 2011. - Vol. 47, No. 6. - P. 393-395. ↑

J69. Yang Shinhyuk. Water-related abnormal instability of transparent oxide/organic hybrid thin film transistors. / Yang Shinhyuk, Hwang Chi-Sun, Lee Jeong-Ik, Yoon Sung-Min, Ryu Min-Ki, Cho Kyoung-Ik, Park Sang-Hee Ko, Kim Se-Hyun, Park Chan-Eon, Jang Jin. // Applied Physics Letters. - 2011. - Vol. 98, No. 10. - P. 103515-103515-3. ↑

J70. Wang Z. B. Optical design of organic light emitting diodes. / Wang Z. B., Helander M. G., Xu X. F., Puzzo D. P., Qiu J., Greiner M. T., Lu Z. H. // Journal of Applied Physics. - 2011. - Vol. 109, No. 5. - P. 053107-053107-7. ↑

J71. Hsieh J.-C. Optimization of Thermal Management by Integration of an SCGM, a Finite-Element Method, and an Experiment on a High-Power LED Array. / Hsieh J.-C., Lin D. T. W., Cheng C.-H. // IEEE Transactions on Electron Devices. - 2011. - Vol. 58, No. 4. - P. 1141-1148. ↑

J72. Asshoff Pablo. A spintronic source of circularly polarized single photons. / Asshoff Pablo, Merz Andreas, Kalt Heinz, Hetterich Michael. // Applied Physics Letters. - 2011. - Vol. 98, No. 11. - P. 112106-112106-3. ↑

J73. van Mensfoort S. L. M. Predictive modeling of the current density and radiative recombination in blue polymer-based light-emitting diodes. / van Mensfoort S. L. M., Billen J., Carvelli M., Vulto S. I. E., Janssen R. A. J., Coehoorn R. // Journal of Applied Physics. - 2011. - Vol. 109, No. 6. - P. 064502-064502-8. ↑

J74. Rangel Elizabeth. Directionality control through selective excitation of low-order guided modes in thin-film InGa_N photonic crystal light-emitting diodes. / Rangel Elizabeth, Matioli Alison, Choi Yong-Seok, Weisbuch Claude, Speck James S., Hu Evelyn L. // Applied Physics Letters. - 2011. - Vol. 98, No. 8. - P. 081104-081104-3. ↑

J75. Cho Chu-Young. Enhanced optical output power of green light-emitting diodes by surface plasmon of gold nanoparticles. / Cho Chu-Young, Lee Sang-Jun, Song Jung-Hoon, Hong Sang-Hyun, Lee Song-Mae, Cho Yong-Hoon, Park Seong-Ju. // Applied Physics Letters. - 2011. - Vol. 98, No. 5. - P. 051106-051106-3. ↑

J76. Wu F. Misfit dislocation formation at heterointerfaces in (Al,In)Ga_N heteroepitaxial layers grown on semipolar free-standing Ga_N substrates. / Wu F., Tyagi A., Young E. C., Romanov A. E., Fujito K., DenBaars S.

- P., Nakamura S., Speck J. S. // Journal of Applied Physics. - 2011. - Vol. 109, No. 3. - P. 033505-033505-7. ↑
- J77. Han J. 6-DOF tracker using LED directivity. / Han J., Heo S., Lee G., Bang W.-C., Kim D.K., Kim C.Y. // Electronics Letters. - 2011. - Vol. 47, No. 3. - P. 177-178. ↑
- J78. Han N. Self-Assembled Periodic Silica Nanosphere Arrays on Wet-Etched Patterned Sapphire Substrate for a High-Light-Extraction-Efficiency Light-Emitting Diode. / Han N., Kim H.-G., Kim H.-Y., Kang J.-H., Ryu B.-D., Park Y.-J., Han M., Jeong H., Chandramohan S., Suh E.-K., Hong C.-H. // IEEE Electron Device Letters. - 2011. - Vol. 32, No. 4. - P. 527-529. ↑
- J79. Dai Qi. On the symmetry of efficiency-versus-carrier-concentration curves in GaInN/GaN light-emitting diodes and relation to droop-causing mechanisms. / Dai Qi, Shan Qifeng, Cho Jaehee, Schubert E. Fred, Crawford Mary H., Koleske Daniel D., Kim Min-Ho, Park Yongjo. // Applied Physics Letters. - 2011. - Vol. 98, No. 3. - P. 033506-033506-3. ↑
- J80. Lew Yan Voon L. C. Electromechanical phenomena in semiconductor nanostructures. / Lew Yan Voon L. C., Willatzen M. // Journal of Applied Physics. - 2011. - Vol. 109, No. 3. - P. 031101-031101-24. ↑
- J81. Zeolla D. DFE Versus MLSE Electronic Equalization for Gigabit/s SI-POF Transmission Systems. / Zeolla D., Antonino A., Bosco G., Gaudino R. // IEEE Photonics Technology Letters. - 2011. - Vol. 23, No. 8. - P. 510-512. ↑
- J82. Huang Y.-H. Top-Emitting Organic Light-Emitting Diodes With Step-Doped Emission Layers. / Huang Y.-H., Liou B.-T., Chen J.-D., Kuo Y.-K. // IEEE Photonics Technology Letters. - 2011. - Vol. 23, No. 8. - P. 480-482. ↑
- J83. Kim K.-S. Leakage Current Characteristics of Nitride-Based InGaN Light-Emitting Diode. / Kim K.-S., Kim J.-H., Cho S. N. // IEEE Photonics Technology Letters. - 2011. - Vol. 23, No. 8. - P. 483-485. ↑
- J84. Linping Mu. Towards Color Stable Blue Primary for Displays: Suppress Field-Dependent Color Change in a Multilayered Electroluminescent Device. / Linping Mu, Zhiqun He, Xiangfei Kong, Chunjun Liang, Yongsheng Wang, Danel A., Kulig E., Milburn G.H.W. // Journal of Display Technology. - 2011. - Vol. 7, No. 2. - P. 96-104. ↑
- J85. Sun T. Erratum: "Multilayered graphene used as anode of organic light emitting devices" [Appl. Phys. Lett. 96, 133301 (2010)]. / Sun T., Wang Z. L., Shi Z. J., Ran G. Z., Xu W. J., Wang Z. Y., Li Y. Z., Dai L., Qin G. G. // Applied Physics Letters. - 2011. - Vol. 98, No. 5. - P. 059901-059901-1. ↑
- J86. Onural L. Digital Holographic Three-Dimensional Video Displays. / Onural L., Yaras F., Kang H. // Proceedings of the IEEE. - 2011. - Vol. 99, No. 4. - P. 576-589. ↑
- J87. Kim Byung-Jae. Emission enhancement from nonpolar a-plane III-nitride nanopillar. / Kim Byung-Jae, Jung Younghun, Mastro Michael A., Hite Jennifer, Nepal Neeraj, Eddy Charles R., Kim Jihyun. // Journal of Vacuum Science & Technology B: Microelectronics and Nanometer Structures. - 2011. - Vol. 29, No. 2. - P. 021004-021004-4. ↑
- J88. Lin N.-M. Nitride-Based LEDs With High-Reflectance and Wide-Angle Ag Mirror SiO₂/TiO₂ DBR Backside Reflector. / Lin N.-M., Shei S.-C., Chang S.-J. // Journal of Lightwave Technology. - 2011. - Vol. 29, No. 7. - P. 1033-1038. ↑
- J89. Jin Wook Jeong. The Emission Properties of Integrated Organic Light Emitting Diodes With Organic Photo Sensor for Emotional Lighting Applications. / Jin Wook Jeong, Young Wook Park, Tae Hyun Park, Jin Hwan Choi, Hyun Ju Choi, Eun Ho Song, Jeong Ik Lee, Hye Yong Chu, Byeong Kwon Ju. // IEEE Electron Device Letters. - 2011. - Vol. 32, No. 3. - P. 348-350. ↑
- J90. Zamani Siboni Hossein. Luminescence degradation in phosphorescent organic light-emitting devices by hole space charges. / Zamani Siboni Hossein, Luo Yichun, Aziz Hany. // Journal of Applied Physics. - 2011. - Vol. 109, No. 4. - P. 044501-044501-6. ↑
- J91. Wang Z. B. Highly simplified phosphorescent organic light emitting diode with >20% external quantum efficiency at >10,000 cd/m². / Wang Z. B., Helander M. G., Qiu J., Puzzo D. P., Greiner M. T., Liu Z. W., Lu Z. H. // Applied Physics Letters. - 2011. - Vol. 98, No. 7. - P. 073310-073310-3. ↑

- J92.** Chi-Che Tseng. Influence of as on the Morphologies and Optical Characteristics of GaSb/GaAs Quantum Dots. / Chi-Che Tseng, Shu-Cheng Mai, Wei-Hsun Lin, Shung-Yi Wu, Bang-Ying Yu, Shu-Han Chen, Shih-Yen Lin, Jing-Jong Shyue, Meng-Chyi Wu. // IEEE Journal of Quantum Electronics. - 2011. - Vol. 47, No. 3. - P. 335-339. ↑
- J93.** Dong Yanqun. Raman and emission characteristics of a-plane InGaN/GaN blue-green light emitting diodes on r-sapphire substrates. / Dong Yanqun, Song Jae-Ho, Kim Ho-Jong, Kim Tae-Soo, Ahn Byung-Jun, Song Jung-Hoon, Cho In-Sung, Im Won-Taek, Moon Youngboo, Hwang Sung-Min, Hong Soon-Ku, Lee Seog-Woo. // Journal of Applied Physics. - 2011. - Vol. 109, No. 4. - P. 043103-043103-4. ↑
- J94.** Saccomandi Paola. A novel target-type low pressure drop bidirectional optoelectronic air flow sensor for infant artificial ventilation: Measurement principle and static calibration. / Saccomandi Paola, Schena Emiliano, Silvestri Sergio. // Review of Scientific Instruments. - 2011. - Vol. 82, No. 2. - P. 024301-024301-9. ↑
- J95.** Chhajed Sameer. Strong light extraction enhancement in GaInN light-emitting diodes by using self-organized nanoscale patterning of p-type GaN. / Chhajed Sameer, Lee Wonseok, Cho Jaehee, Schubert E. Fred, Kim Jong Kyu. // Applied Physics Letters. - 2011. - Vol. 98, No. 7. - P. 071102-071102-3. ↑
- J96.** Jeon Soon Ok. Mechanism for the direct electron injection from Al cathode to the phosphine oxide type electron transport layer. / Jeon Soon Ok, Yook Kyoung Soo, Lee Jun Yeob, Park Soon Mi, Won Kim Jeong, Kim Ji-Hoon, Hong Jong-Am, Park Yongsup. // Applied Physics Letters. - 2011. - Vol. 98, No. 7. - P. 073306-073306-3. ↑
- J97.** Mamada Masashi. Charge transport, carrier balance, and blue electrophosphorescence in diphenyl[4-(triphenylsilyl)phenyl]phosphine oxide devices. / Mamada Masashi, Ergun Selin, Perez-Bolivar Cesar, Anzenbacher Pavel. // Applied Physics Letters. - 2011. - Vol. 98, No. 7. - P. 073305-073305-3. ↑
- J98.** Ahn Jaehui. Violet electroluminescence from p-GaN thin film/n-GaN nanowire homojunction. / Ahn Jaehui, Mastro Michael A., Hite Jennifer, Eddy Charles R., Kim Jihyun. // Applied Physics Letters. - 2010. - Vol. 96, No. 13. - P. 132105-132105-3. ↑
- J99.** Chang-yu Shen. White LED Based on YAG : Ce,Gd Phosphor and CdSe-ZnS Core/Shell Quantum Dots. / Chang-yu Shen, Ke Li, Qiang-long Hou, Hua-jun Feng, Xin-yong Dong. // IEEE Photonics Technology Letters. - 2010. - Vol. 22, No. 12. - P. 884-886. ↑
- J100.** Bochkareva N. I. Defect-related tunneling mechanism of efficiency droop in III-nitride light-emitting diodes. / Bochkareva N. I., Voronenkov V. V., Gorbunov R. I., Zubrilov A. S., Lelikov Y. S., Latyshev P. E., Rebane Y. T., Tsyuk A. I., Shreter Y. G. // Applied Physics Letters. - 2010. - Vol. 96, No. 13. - P. 133502-133502-3. ↑
- J101.** Gopal Ashwini. Photolithographic patterning of subwavelength top emitting colloidal quantum dot based inorganic light emitting diodes on silicon. / Gopal Ashwini, Hoshino Kazunori, Zhang Xiaojing. // Applied Physics Letters. - 2010. - Vol. 96, No. 13. - P. 131109-131109-3. ↑
- J102.** Thurgood Clementine. Development of a light-emitting diode tachistoscope. / Thurgood Clementine, Patterson John, Simpson David, Whitfield T. W. Allan. // Review of Scientific Instruments. - 2010. - Vol. 81, No. 3. - P. 035117-035117-3. ↑
- J103.** Im Jisun. Photometer for monitoring the thickness of inkjet printed films for organic electronic and sensor applications. / Im Jisun, Sengupta Sandip K., Whitten James E. // Review of Scientific Instruments. - 2010. - Vol. 81, No. 3. - P. 034103-034103-6. ↑
- J104.** Hsieh Ming-Ta. Study of electric characteristics and diffusion effects of 2-methyl-9,10-di(2-naphthyl)anthracene doped with cesium fluoride by admittance spectroscopy. / Hsieh Ming-Ta, Ho Meng-Huan, Lin Kuan-Heng, Chen Jenn-Fang, Chen Teng-Ming, Chen Chin H. // Applied Physics Letters. - 2010. - Vol. 96, No. 13. - P. 133310-133310-3. ↑
- J105.** Tu S. H. InGaN gallium nitride light-emitting diodes with reflective electrode pads and textured gallium-doped ZnO contact layer. / Tu S. H., Lan C. J., Wang S. H., Lee M. L., Chang K. H., Lin R. M., Chang J. Y., Sheu J. K. // Applied Physics Letters. - 2010. - Vol. 96, No. 13. - P. 133504-133504-3. ↑
- J106.** Jun-Rong Chen. Study of InGaN-GaN Light-Emitting Diodes With Different Last Barrier Thicknesses. /

- Jun-Rong Chen, Tien-Chang Lu, Hao-Chung Kuo, Fang K.L., Huang K.F., Kuo C.W., Chang C.J., Kuo C.T., Shing-Chung Wang. // IEEE Photonics Technology Letters. - 2010. - Vol. 22, No. 12. - P. 860-862. ↑
- J107. Bagheri M. Fast Voltage-Programmed Pixel Architecture for AMOLED Displays. / Bagheri M., Ashtiani S.J., Nathan A.N. // Journal of Display Technology. - 2010. - Vol. 6, No. 5. - P. 191-195. ↑
- J108. Cao X. A. Electroluminescence observation of nanoscale phase separation in quaternary AlInGaN light-emitting diodes. / Cao X. A., Yang Y. // Applied Physics Letters. - 2010. - Vol. 96, No. 15. - P. 151109-151109-3. ↑
- J109. Meneghini M. Soft and Hard Failures of InGaN-Based LEDs Submitted to Electrostatic Discharge Testing. / Meneghini M., Tazzoli A., Butendeich R., Hahn B., Meneghesso G., Zanoni E. // IEEE Electron Device Letters. - 2010. - Vol. 31, No. 6. - P. 579-581. ↑
- J110. Kato Y. Large-Area Flexible Ultrasonic Imaging System With an Organic Transistor Active Matrix. / Kato Y., Sekitani T., Noguchi Y., Yokota T., Takamiya M., Sakurai T., Someya T. // IEEE Transactions on Electron Devices. - 2010. - Vol. 57, No. 5. - P. 995-1002. ↑
- J111. Seungjun Yi. Microplasma Current Switch and Its Characteristics. / Seungjun Yi, Jie Yu Cai, Cheol-Hee Moon. // IEEE Transactions on Plasma Science. - 2010. - Vol. 38, No. 5. - P. 1106-1110. ↑
- J112. Huang H.W. Efficiency Improvement of GaN-Based LEDs With a Nanorod Array and a Patterned Sapphire Substrate. / Huang H.W., Huang J.K., Lin C.H., Lee K.Y., Hsu H.W., Yu C.C., Kuo H.C. // IEEE Electron Device Letters. - 2010. - Vol. 31, No. 6. - P. 582-584. ↑
- J113. Huang H.W. Light-Output-Power Enhancement of GaN-Based Light-Emitting Diodes on an n-GaN Layer Using a Photonic Quasi-Crystal Overgrowth. / Huang H.W., Huang J.K., Lee K.Y., Lin C.F., Kuo H.C. // IEEE Electron Device Letters. - 2010. - Vol. 31, No. 6. - P. 573-575. ↑
- J114. Young June Hong. Measurement of Electron Temperature and Density Using Stark Broadening of the Coaxial Focused Plasma for Extreme Ultraviolet Lithography. / Young June Hong, Gi Chung Kwon, Guangsup Cho, Hee Myoung Shin, Eun Ha Choi. // IEEE Transactions on Plasma Science. - 2010. - Vol. 38, No. 5. - P. 1111-1117. ↑
- J115. Xue Zheng-Qun. Laser-induced Zn doping in GaN based light-emitting diode. / Xue Zheng-Qun, Huang Sheng-Rong, Zhang Bao-Ping, Chen Chao. // Applied Physics Letters. - 2010. - Vol. 96, No. 14. - P. 141101-141101-3. ↑
- J116. Cheng-Hung Lin. Light Extraction Enhancement of a GaN-Based Light-Emitting Diode Through Grating-Patterned Photoelectrochemical Surface Etching With Phase Mask Interferometry. / Cheng-Hung Lin, Cheng-Yen Chen, Dong-Ming Yeh, Chih-Chung Yang. // IEEE Photonics Technology Letters. - 2010. - Vol. 22, No. 9. - P. 640-642. ↑
- J117. Elgala H. An LED Model for Intensity-Modulated Optical Communication Systems. / Elgala H., Mesleh R., Haas H. // IEEE Photonics Technology Letters. - 2010. - Vol. 22, No. 11. - P. 835-837. ↑
- J118. Jou Jwo-Huei. Highly efficient orange-red phosphorescent organic light-emitting diode using 2,7-bis(carbazol-9-yl)-9,9-difluorene as the host. / Jou Jwo-Huei, Shen Shih-Ming, Chen Szu-Hao, Wu Ming-Hsuan, Wang Wei-Ben, Wang Hsi-Ching, Lin Chuen-Ren, Chou Yi-Chieh, Wu Po-Hsien, Shyue Jing-Jong. // Applied Physics Letters. - 2010. - Vol. 96, No. 14. - P. 143306-143306-3. ↑
- J119. Noguchi Yutaka. Light- and ion-gauge-induced space charges in tris-(8-hydroxyquinolate) aluminum-based organic light-emitting diodes. / Noguchi Yutaka, Sato Naoki, Miyazaki Yukimasa, Ishii Hisao. // Applied Physics Letters. - 2010. - Vol. 96, No. 14. - P. 143305-143305-3. ↑
- J120. Leung K. K. Physical mechanisms for hot-electron degradation in GaN light-emitting diodes. / Leung K. K., Fong W. K., Chan P. K. L., Surya C. // Journal of Applied Physics. - 2010. - Vol. 107, No. 7. - P. 073103-073103-6. ↑
- J121. Zhang Meng. Mg doping of GaN grown by plasma-assisted molecular beam epitaxy under nitrogen-rich conditions. / Zhang Meng, Bhattacharya Pallab, Guo Wei, Banerjee Animesh. // Applied Physics Letters. - 2010. - Vol. 96, No. 13. - P. 132103-132103-3. ↑

- J122.** Young Wook Park. Enhanced Electroluminescence Efficiency of Phosphorescent Organic Light-Emitting Diodes by Controlling the Triplet Energy of the Hole-Blocking Layer. / Young Wook Park, Young Min Kim, Jin Hwan Choi, Tae Hyun Park, Jin-Wook Jeong, Hyun Ju Choi, Byeong Kwon Ju. // IEEE Electron Device Letters. - 2010. - Vol. 31, No. 5. - P. 452-454. ↑
- J123.** Malkin R. A Novel Phototherapy Device. / Malkin R., Anand V. // IEEE Engineering in Medicine and Biology Magazine. - 2010. - Vol. 29, No. 2. - P. 37-43. ↑
- J124.** Flemming B. New Technologies in Electric-Powered Vehicles [Automotive Electronics]. IEEE Vehicular Technology Magazine. - 2010. - Vol. 5, No. 1. - P. 4-103. ↑
- J125.** Bakin A. ZnO-GaN Hybrid Heterostructures as Potential Cost-Efficient LED Technology. / Bakin A., Behrends A., Waag A., Lugauer H., Laubsch A., Streubel K. // Proceedings of the IEEE. - 2010. - Vol. 98, No. 7. - P. 1281-1287. ↑
- J126.** Zhigang Zang. High-Power (110" > mW) Superluminescent Diodes by Using Active Multimode Interferometer. / Zhigang Zang, Minato T., Navaretti P., Hinokuma Y., Duelk M., Velez C., Hamamoto K. // IEEE Photonics Technology Letters. - 2010. - Vol. 22, No. 10. - P. 721-723. ↑
- J127.** Sciuto A. On the Aging Effects of 4H-SiC Schottky Photodiodes Under High Intensity Mercury Lamp Irradiation. / Sciuto A., Mazzillo M., Raineri V., Catania G., D'Arrigo G., Roccaforte F. // IEEE Photonics Technology Letters. - 2010. - Vol. 22, No. 11. - P. 775-777. ↑
- J128.** Matioli Elison. Measurement of extraction and absorption parameters in GaN-based photonic-crystal light-emitting diodes. / Matioli Elison, Fleury Blaise, Rangel Elizabeth, Hu Evelyn, Speck James, Weisbuch Claude. // Journal of Applied Physics. - 2010. - Vol. 107, No. 5. - P. 053114-053114-6. ↑
- J129.** Lin Wei. Near-ultraviolet light emitting diodes using strained ultrathin InN/GaN quantum well grown by metal organic vapor phase epitaxy. / Lin Wei, Li Shuping, Kang Junyong. // Applied Physics Letters. - 2010. - Vol. 96, No. 10. - P. 101115-101115-3. ↑
- J130.** Snyman L.W. Photonic Transitions (1.4 eV-2.8 eV) in Silicon p np Injection-Avalanche CMOS LEDs as Function of Depletion Layer Profiling and Defect Engineering. / Snyman L.W., du Plessis M., Bellotti E. // IEEE Journal of Quantum Electronics. - 2010. - Vol. 46, No. 6. - P. 906-919. ↑
- J131.** Kim Hee Jin. Improvement of quantum efficiency by employing active-layer-friendly lattice-matched InAlN electron blocking layer in green light-emitting diodes. / Kim Hee Jin, Choi Suk, Kim Seong-Soo, Ryou Jae-Hyun, Yoder P. Douglas, Dupuis Russell D., Fischer Alec M., Sun Kewei, Ponce Fernando A. // Applied Physics Letters. - 2010. - Vol. 96, No. 10. - P. 101102-101102-3. ↑
- J132.** Nowy Stefan. Impedance spectroscopy as a probe for the degradation of organic light-emitting diodes. / Nowy Stefan, Ren Wei, Elschner Andreas, Lovenich Wilfried, Brutting Wolfgang. // Journal of Applied Physics. - 2010. - Vol. 107, No. 5. - P. 054501-054501-9. ↑
- J133.** Seidler Nico. Influence of the hole blocking layer on blue phosphorescent organic light-emitting devices using 3,6-di(9-carbazolyl)-9-(2-ethylhexyl)carbazole as host material. / Seidler Nico, Reineke Sebastian, Walzer Karsten, Lussem Bjorn, Tomkeviciene Ausra, Grazulevicius Juozas V., Leo Karl. // Applied Physics Letters. - 2010. - Vol. 96, No. 9. - P. 093304-093304-3. ↑
- J134.** Kasai J. Properties of TiO₂-based transparent conducting oxide thin films on GaN(0001) surfaces. / Kasai J., Hitosugi T., Moriyama M., Goshonoo K., Hoang N. L. H., Nakao S., Yamada N., Hasegawa T. // Journal of Applied Physics. - 2010. - Vol. 107, No. 5. - P. 053110-053110-4. ↑
- J135.** Ye Tengling. Detailed studies on energy loss mechanism in phosphor-sensitized fluorescent polymer light-emitting devices. / Ye Tengling, Shao Shiyang, Chen Jiangshan, Chen Zhenyu, Wang Lixiang, Ma Dongge. // Journal of Applied Physics. - 2010. - Vol. 107, No. 5. - P. 054515-054515-6. ↑
- J136.** Huang Shanjin. A chip-level electrothermal-coupled design model for high-power light-emitting diodes. / Huang Shanjin, Wu Hao, Fan Bingfeng, Zhang Baijun, Wang Gang. // Journal of Applied Physics. - 2010. - Vol. 107, No. 5. - P. 054509-054509-8. ↑
- J137.** David Aurelien. Droop in InGaN light-emitting diodes: A differential carrier lifetime analysis. / David

Aurelien, Grundmann Michael J. // Applied Physics Letters. - 2010. - Vol. 96, No. 10. - P. 103504-103504-3. ↑

J138. Lee Wonseok. Growth and characteristics of GaInN/GaN multiple quantum well light-emitting diodes. / Lee Wonseok, Kim Min-Ho, Zhu Di, Noemaun Ahmed N., Kim Jong Kyu, Schubert E. F. // Journal of Applied Physics. - 2010. - Vol. 107, No. 6. - P. 063102-063102-6. ↑

J139. Feng L.F. Negative Terminal Capacitance of Light Emitting Diodes at Alternating Current (AC) Biases. / Feng L.F., Li Y., Zhu C.Y., Cong H.X., Wang C.D. // IEEE Journal of Quantum Electronics. - 2010. - Vol. 46, No. 7. - P. 1072-1075. ↑

J140. Chen P.H. GaN-Based Light-Emitting Diodes With Pillar Structures Around the Mesa Region. / Chen P.H., Li Chuan Chang, Tsai C.H., Lee Y.C., Wei-Chih Lai, Wu M.-L., Cheng-Huang Kuo, Jinn-Kong Sheu. // IEEE Journal of Quantum Electronics. - 2010. - Vol. 46, No. 7. - P. 1066-1071. ↑

J141. Zhu Di. Enhanced electron capture and symmetrized carrier distribution in GaInN light-emitting diodes having tailored barrier doping. / Zhu Di, Noemaun Ahmed N., Schubert Martin F., Cho Jaehee, Schubert E. Fred, Crawford Mary H., Koleske Daniel D. // Applied Physics Letters. - 2010. - Vol. 96, No. 12. - P. 121110-121110-3. ↑

J142. Chia-Feng Lin. InGaN Light-Emitting Diodes With the Inverted Cone-Shaped Pillar Structures. / Chia-Feng Lin, Chun-Min Lin, Kuei-Ting Chen, Jing-Jie Dai, Ming-Shiou Lin. // IEEE Electron Device Letters. - 2010. - Vol. 31, No. 5. - P. 458-460. ↑

J143. Varghese P Benjamin. Fiber optic sensor for the measurement of concentration of silica in water with dual wavelength probing. / Varghese P Benjamin, John Satish, Madhusoodanan K. N. // Review of Scientific Instruments. - 2010. - Vol. 81, No. 3. - P. 035111-035111-5. ↑

J144. Sun T. Multilayered graphene used as anode of organic light emitting devices. / Sun T., Wang Z. L., Shi Z. J., Ran G. Z., Xu W. J., Wang Z. Y., Li Y. Z., Dai L., Qin G. G. // Applied Physics Letters. - 2010. - Vol. 96, No. 13. - P. 133301-133301-3. ↑

J145. Orava J. Large Gamut Backlight for an LCD With Four Primaries. / Orava J., Jaaskelainen T., Parkkinen J. // Journal of Display Technology. - 2010. - Vol. 6, No. 5. - P. 170-177. ↑

J146. Fiorentin P. Detector-Based Calibration for Illuminance and Luminance Meters-Experimental Results. / Fiorentin P., Scroccaro A. // IEEE Transactions on Instrumentation and Measurement. - 2010. - Vol. 59, No. 5. - P. 1375-1381. ↑

J147. Jae-Hoon Lee. Enhanced Output Power of InGaN-Based Light-Emitting Diodes With AlGaIn/GaN Two-Dimensional Electron Gas Structure. / Jae-Hoon Lee, Jung-Hee Lee. // IEEE Electron Device Letters. - 2010. - Vol. 31, No. 5. - P. 455-457. ↑

J148. Kuo-Kai Shyu. Development of a Low-Cost FPGA-Based SSVEP BCI Multimedia Control System. / Kuo-Kai Shyu, Po-Lei Lee, Ming-Huan Lee, Ming-Hong Lin, Ren-Jie Lai, Yun-Jen Chiu. // IEEE Transactions on Biomedical Circuits and Systems. - 2010. - Vol. 4, No. 2. - P. 125-132. ↑

J149. Han D.P. Relationship between thermal and luminance distributions in high-power lateral GaN/InGaN light-emitting diodes. / Han D.P., Shim J.I., Shin D.S. // Electronics Letters. - 2010. - Vol. 46, No. 6. - P. 437-439. ↑

J150. Turner J. Board certified. IEEE Spectrum. - 2010. - Vol. 47, No. 4. - P. 24-25. ↑

J151. Lin Shih-Yen. Room-temperature operation type-II GaSb/GaAs quantum-dot infrared light-emitting diode. / Lin Shih-Yen, Tseng Chi-Che, Lin Wei-Hsun, Mai Shu-Cheng, Wu Shung-Yi, Chen Shu-Han, Chyi Jen-Inn. // Applied Physics Letters. - 2010. - Vol. 96, No. 12. - P. 123503-123503-3. ↑

J152. Yoonsik Uhm. Design and implementation of power-aware LED light enabler with location-aware adaptive middleware and context-aware user pattern. / Yoonsik Uhm, Insung Hong, Gwanyeon Kim, Byoungjoo Lee, Sehyun Park. // IEEE Transactions on Consumer Electronics. - 2010. - Vol. 56, No. 1. - P. 231-239. ↑

J153. Torricelli Fabrizio. Space-charge-limited current in organic light emitting diodes. / Torricelli Fabrizio, Zappa Dario, Colalongo Luigi. // Applied Physics Letters. - 2010. - Vol. 96, No. 11. - P. 113304-113304-3. ↑

- J154.** Papadopoulos N.P. Current-Based Testing of Optical Feedback Pixel Driver. / Papadopoulos N.P., Papakostas D.K., Hatzopoulos A.A. // Journal of Display Technology. - 2010. - Vol. 6, No. 4. - P. 150-157. ↑
- J155.** Swanson J. Light-Rail Transit Systems. / Swanson J., Thornes C. // IEEE Vehicular Technology Magazine. - 2010. - Vol. 5, No. 2. - P. 22-27. ↑
- J156.** Cherenack K.H. Woven Thin-Film Metal Interconnects. / Cherenack K.H., Kinkeldei T., Zysset C., Trojster G. // IEEE Electron Device Letters. - 2010. - Vol. 31, No. 7. - P. 740-742. ↑
- J157.** Bo Ling. Electroluminescence From Ferromagnetic Fe-Doped ZnO Nanorod Arrays on p-Si. / Bo Ling, Jun Liang Zhao, Xiao Wei Sun, Swee Tiam Tan, Yi Yang, Zhi Li Dong. // IEEE Transactions on Electron Devices. - 2010. - Vol. 57, No. 8. - P. 1948-1952. ↑
- J158.** Choi Suk. Improvement of peak quantum efficiency and efficiency droop in III-nitride visible light-emitting diodes with an InAlN electron-blocking layer. / Choi Suk, Kim Hee Jin, Kim Seong-Soo, Liu Jianping, Kim Jeomoh, Ryou Jae-Hyun, Dupuis Russell D., Fischer Alec M., Ponce Fernando A. // Applied Physics Letters. - 2010. - Vol. 96, No. 22. - P. 221105-221105-3. ↑
- J159.** Hsi-Hsuan Yen. Particular Failure Mechanism of GaN-Based Alternating Current Light-Emitting Diode Induced by GaO Oxidation. / Hsi-Hsuan Yen, Hao-Chung Kuo, Wen-Yung Yeh. // IEEE Photonics Technology Letters. - 2010. - Vol. 22, No. 15. - P. 1168-1170. ↑
- J160.** Rakshit A. A Microcontroller-Based IR Range Finder System With Dynamic Range Enhancement. / Rakshit A., Chatterjee A. // IEEE Sensors Journal. - 2010. - Vol. 10, No. 10. - P. 1635-1636. ↑
- J161.** Meining C. J. Spin injection and circular polarized electroluminescence from InAs-based spin-light emitting diode structures. / Meining C. J., Stier A. V., McCombe B. D., Chado I., Grabs P., Schmidt G., Molenkamp L. W. // Journal of Applied Physics. - 2010. - Vol. 107, No. 11. - P. 114510-114510-10. ↑
- J162.** Tao Y. B. Polarization modification in InGaN/GaN multiple quantum wells by symmetrical thin low temperature-GaN layers. / Tao Y. B., Chen Z. Z., Zhang F. F., Jia C. Y., Qi S. L., Yu T. J., Kang X. N., Yang Z. J., You L. P., Yu D. P., Zhang G. Y. // Journal of Applied Physics. - 2010. - Vol. 107, No. 10. - P. 103529-103529-5. ↑
- J163.** Qiao Xianfeng. Observation of hole hopping via dopant in MoO_x-doped organic semiconductors: Mechanism analysis and application for high performance organic light-emitting devices. / Qiao Xianfeng, Chen Jiangshan, Li Xinglin, Ma Dongge. // Journal of Applied Physics. - 2010. - Vol. 107, No. 10. - P. 104505-104505-6. ↑
- J164.** Li Songzhan. Enhancement of ultraviolet electroluminescence based on n-ZnO /n-GaN isotype heterojunction with low threshold voltage. / Li Songzhan, Fang Guojia, Long Hao, Mo Xiaoming, Huang Huihui, Dong Binzhong, Zhao Xingzhong. // Applied Physics Letters. - 2010. - Vol. 96, No. 20. - P. 201111-201111-3. ↑
- J165.** Chih-Chien Lin. Enhanced Light Extraction Mechanism of GaN-Based Light-Emitting Diodes Using Top Surface and Side-Wall Nanorod Arrays. / Chih-Chien Lin, Ching-Ting Lee. // IEEE Photonics Technology Letters. - 2010. - Vol. 22, No. 15. - P. 1132-1134. ↑
- J166.** Brovelli Sergio. White luminescence from single-layer devices of nonresonant polymer blends. / Brovelli Sergio, Guan Hao, Winroth Gustaf, Fenwick Oliver, Di Stasio Francesco, Daik Rusli, Feast W. James, Meinardi Francesco, Cacialli Franco. // Applied Physics Letters. - 2010. - Vol. 96, No. 21. - P. 213301-213301-3. ↑
- J167.** Jae Hyuk Jang. A PDM-Based Digital Driving Technique Using Delta-Sigma ($\Delta\Sigma$) Modulation for QVGA Full-Color AMOLED Display Applications. / Jae Hyuk Jang, Minho Kwon, Tjandranegara E., Kwiro Lee, Byunghoo Jung. // Journal of Display Technology. - 2010. - Vol. 6, No. 7. - P. 269-278. ↑
- J168.** Jae-Hoon Lee. InGaN-Based High-Power Flip-Chip LEDs With Deep-Hole-Patterned Sapphire Substrate by Laser Direct Beam Drilling. / Jae-Hoon Lee, Seok-Min Hwang, Nam-Seung Kim, Jung-Hee Lee. // IEEE Electron Device Letters. - 2010. - Vol. 31, No. 7. - P. 698-700. ↑
- J169.** Kakue T. Parallel Phase-Shifting Digital Holography Capable of Simultaneously Capturing Visible and Invisible Three-Dimensional Information. / Kakue T., Ito K., Tahara T., Awatsuji Y., Nishio K., Ura S., Kubota T., Matoba O. // Journal of Display Technology. - 2010. - Vol. 6, No. 10. - P. 472-478. ↑

- J170.** Xianping Fu. Telescope Aiming Point Tracking Method for Bioptic Driving Surveillance. / Xianping Fu, Gang Luo, Eli Peli. // IEEE Transactions on Neural Systems and Rehabilitation Engineering. - 2010. - Vol. 18, No. 6. - P. 628-636. ↑
- J171.** Morkoc H. Challenges and Opportunities in GaN and ZnO Devices and Materials. / Morkoc H., Chyi J.-I., Krost A., Nanishi Y., Silversmith D. J. // Proceedings of the IEEE. - 2010. - Vol. 98, No. 7. - P. 1113-1117. ↑
- J172.** Wu Feng. Stacking fault formation in the long wavelength InGaN/GaN multiple quantum wells grown on m-plane GaN. / Wu Feng, Lin You-Da, Chakraborty Arpan, Ohta Hiroaki, DenBaars Steven P., Nakamura Shuji, Speck James S. // Applied Physics Letters. - 2010. - Vol. 96, No. 23. - P. 231912-231912-3. ↑
- J173.** Kang E.-C. Sequential low-voltage detecting method for multistring LED BLU circuit. / Kang E.-C., Yeon J.-E., Kim D.-S., Kwon D. // Electronics Letters. - 2010. - Vol. 46, No. 12. - P. 839-840. ↑
- J174.** Fujita K. High-Performance Quantum Cascade Lasers With Single Phonon-Continuum Depopulation Structures. / Fujita K., Furuta S., Sugiyama A., Ochiai T., Edamura T., Akikusa N., Yamanishi M., Kan H. // IEEE Journal of Quantum Electronics. - 2010. - Vol. 46, No. 5. - P. 683-688. ↑
- J175.** Riedel Boris. Enhancing outcoupling efficiency of indium-tin-oxide-free organic light-emitting diodes via nanostructured high index layers. / Riedel Boris, Hauss Julian, Geyer Ulf, Guetlein Johanna, Lemmer Uli, Gerken Martina. // Applied Physics Letters. - 2010. - Vol. 96, No. 24. - P. 243302-243302-3. ↑
- J176.** Haase M. A. II-VI semiconductor color converters for efficient green, yellow, and red light emitting diodes. / Haase M. A., Xie J., Ballen T. A., Zhang J., Hao B., Yang Z. H., Miller T. J., Sun X., Smith T. L., Leatherdale C. A. // Applied Physics Letters. - 2010. - Vol. 96, No. 23. - P. 231116-231116-3. ↑
- J177.** Yu-Sheng Tsai. Easy Process and Performance Improvement for Top-Emission Organic Light-Emitting Diodes by Using UV Glue as the Insulation Layer on Copper Substrate. / Yu-Sheng Tsai, Shun-Hsi Wang, Fuh-Shyang Juang, Shu-Wei Chang, Chuan-hung Chen, Ming-Hua Chung, Tsung-Eong Hsieh, Liu M.-O., Teh-Chao Liao. // Journal of Display Technology. - 2010. - Vol. 6, No. 7. - P. 279-283. ↑
- J178.** van Mensfoort S. L. M. Hole transport in the organic small molecule material alpha -NPD : evidence for the presence of correlated disorder. / van Mensfoort S. L. M., Shabro V., de Vries R. J., Janssen R. A. J., Coehoorn R. // Journal of Applied Physics. - 2010. - Vol. 107, No. 11. - P. 113710-113710-8. ↑
- J179.** Lei Yao. CMOS Imaging of Pin-Printed Xerogel-Based Luminescent Sensor Microarrays. / Lei Yao, Ka Yi Yung, Khan R., Chodavarapu V.P., Bright F.V. // IEEE Sensors Journal. - 2010. - Vol. 10, No. 12. - P. 1824-1832. ↑
- J180.** Taniyasu Yoshitaka. Surface 210 nm light emission from an AlN p-n junction light-emitting diode enhanced by A-plane growth orientation. / Taniyasu Yoshitaka, Kasu Makoto. // Applied Physics Letters. - 2010. - Vol. 96, No. 22. - P. 221110-221110-3. ↑
- J181.** Tesfamichael T. Electron Beam Evaporation of Tungsten Oxide Films for Gas Sensors. IEEE Sensors Journal. - 2010. - Vol. 10, No. 11. - P. 1796-1802. ↑
- J182.** Marimuthu P.N. Corrosion Estimation of Stainless Steel in Nitric Acid by an Optoelectronic Instrument Based on Diffuse Light Scattering Pattern Measurement. / Marimuthu P.N., Kabilan A.P. // IEEE Sensors Journal. - 2010. - Vol. 10, No. 10. - P. 1658-1665. ↑
- J183.** Sakamoto Kenji. Highly polarized polymer-based light-emitting diodes fabricated by using very thin photoaligned polyimide layers. / Sakamoto Kenji, Miki Kazushi, Misaki Masahiro, Sakaguchi Koichi, Hijikata Yuzuru, Chikamatsu Masayuki, Azumi Reiko. // Journal of Applied Physics. - 2010. - Vol. 107, No. 11. - P. 113108-113108-9. ↑
- J184.** Sekiguchi Hiroto. Emission color control from blue to red with nanocolumn diameter of InGaN/GaN nanocolumn arrays grown on same substrate. / Sekiguchi Hiroto, Kishino Katsumi, Kikuchi Akihiko. // Applied Physics Letters. - 2010. - Vol. 96, No. 23. - P. 231104-231104-3. ↑
- J185.** Ling Shih-Chun. Low efficiency droop in blue-green m-plane InGaN/GaN light emitting diodes. / Ling Shih-Chun, Lu Tien-Chang, Chang Shih-Pang, Chen Jun-Rong, Kuo Hao-Chung, Wang Shing-Chung. // Applied Physics Letters. - 2010. - Vol. 96, No. 23. - P. 231101-231101-3. ↑

- J186.** Avrutin V. Growth of Bulk GaN and AlN: Progress and Challenges. / Avrutin V., Silversmith D.J., Mori Y., Kawamura F., Kitaoka Y., Morkoc H. // Proceedings of the IEEE. - 2010. - Vol. 98, No. 7. - P. 1302-1315. ↑
- J187.** Hofstetter D. Intersubband Transition-Based Processes and Devices in AlN/GaN-Based Heterostructures. / Hofstetter D., Baumann E., Giorgetta F.R., The,ron R., Hong Wu, Schaff W.J., Dawlaty J., George P.A., Eastman L.F., Rana F., Kandaswamy P.K., Guillot F., Monroy E. // Proceedings of the IEEE. - 2010. - Vol. 98, No. 7. - P. 1234-1248. ↑
- J188.** Nicolai H. T. Space-charge-limited hole current in poly(9,9-dioctylfluorene) diodes. / Nicolai H. T., Wetzelaer G. A. H., Kuik M., Kronemeijer A. J., de Boer B., Blom P. W. M. // Applied Physics Letters. - 2010. - Vol. 96, No. 17. - P. 172107-172107-3. ↑
- J189.** Wang Qi. Evidence of intermolecular species formation with electrical aging in anthracene-based blue organic light-emitting devices. / Wang Qi, Luo Yichun, Aziz Hany. // Journal of Applied Physics. - 2010. - Vol. 107, No. 8. - P. 084506-084506-6. ↑
- J190.** Chen-Fu Chu. High Brightness GaN Vertical Light-Emitting Diodes on Metal Alloy for General Lighting Application. / Chen-Fu Chu, Chao-Chen Cheng, Wen-Huan Liu, Jiunn-Yi Chu, Feng-Hsu Fan, Hao-Chun Cheng, Trung Doan, Chuong Anh Tran. // Proceedings of the IEEE. - 2010. - Vol. 98, No. 7. - P. 1197-1207. ↑
- J191.** Jin-Wei Shi. Very-High Temperature (200 C) and High-Speed Operation of Cascade GaN-Based Green Light- Emitting Diodes With an InGaN Insertion Layer. / Jin-Wei Shi, Huang H.-W., Kuo F.-M., Sheu J.-K., Lai W.-C., Lee M.L. // IEEE Photonics Technology Letters. - 2010. - Vol. 22, No. 14. - P. 1033-1035. ↑
- J192.** Harigai Takakiyo. Vibration energy harvesting using highly (001)-oriented Pb (Zr ,Ti)O 3 thin film. / Harigai Takakiyo, Adachi Hideaki, Fujii Eiji. // Journal of Applied Physics. - 2010. - Vol. 107, No. 9. - P. 096101-096101-3. ↑
- J193.** Kao C.C. Localized Surface Plasmon-Enhanced Nitride-Based Light-Emitting Diode With Ag Nanotriangle Array by Nanosphere Lithography. / Kao C.C., Su Y.K., Lin C.L., Chen J.J. // IEEE Photonics Technology Letters. - 2010. - Vol. 22, No. 13. - P. 984-986. ↑
- J194.** Tsao J.Y. Solid-State Lighting: An Integrated Human Factors, Technology, and Economic Perspective. / Tsao J.Y., Coltrin M.E., Crawford M.H., Simmons J.A. // Proceedings of the IEEE. - 2010. - Vol. 98, No. 7. - P. 1162-1179. ↑
- J195.** Yen-Kuang Kuo. Effect of P-Type Last Barrier on Efficiency Droop of Blue InGaN Light-Emitting Diodes. / Yen-Kuang Kuo, Miao-Chan Tsai, Sheng-Horng Yen, Ta-Cheng Hsu, Yu-Jiun Shen. // IEEE Journal of Quantum Electronics. - 2010. - Vol. 46, No. 8. - P. 1214-1220. ↑
- J196.** Hui S.Y. A Novel Passive Offline LED Driver With Long Lifetime. / Hui S.Y., Si Nan Li, Xue Hui Tao, Wu Chen, Ng W.M. // IEEE Transactions on Power Electronics. - 2010. - Vol. 25, No. 10. - P. 2665-2672. ↑
- J197.** Potfajova J. Microcavity enhanced silicon light emitting pn-diode. / Potfajova J., Schmidt B., Helm M., Gemming T., Benyoucef M., Rastelli A., Schmidt O. G. // Applied Physics Letters. - 2010. - Vol. 96, No. 15. - P. 151113-151113-3. ↑
- J198.** Lee Hyunkoo. Improvement of electron injection in inverted bottom-emission blue phosphorescent organic light emitting diodes using zinc oxide nanoparticles. / Lee Hyunkoo, Park Insun, Kwak Jeonghun, Yoon Do Y., Lee Changhee. // Applied Physics Letters. - 2010. - Vol. 96, No. 15. - P. 153306-153306-3. ↑
- J199.** Chivukula Venkata. AlGaIn based highly sensitive radio-frequency UV sensor. / Chivukula Venkata, Ciplys Daumantas, Sereika Albertas, Shur Michael, Yang Jinwei, Gaska Remis. // Applied Physics Letters. - 2010. - Vol. 96, No. 16. - P. 163504-163504-3. ↑
- J200.** Lincoln J. The latest video projectors can fit inside tiny cameras or cellphones yet still produce big pictures [Little Gizmo, Big Picture]. IEEE Spectrum. - 2010. - Vol. 47, No. 5. - P. 41-45. ↑
- J201.** You J. B. Electroluminescence behavior of ZnO/Si heterojunctions: Energy band alignment and interfacial microstructure. / You J. B., Zhang X. W., Zhang S. G., Tan H. R., Ying J., Yin Z. G., Zhu Q. S., Chu Paul K. // Journal of Applied Physics. - 2010. - Vol. 107, No. 8. - P. 083701-083701-5. ↑

- J202.** Oksanen Jani. Thermophotonic heat pump-a theoretical model and numerical simulations. / Oksanen Jani, Tulkki Jukka. // Journal of Applied Physics. - 2010. - Vol. 107, No. 9. - P. 093106-093106-8. ↑
- J203.** Ming-Hsin Huang. Energy-Recycling (ER) Technique for a Direct-Lit Intelligent Power Management Backlight Unit (BLU). / Ming-Hsin Huang, Yueh-Chang Tsai, Ke-Horng Chen. // IEEE Transactions on Power Electronics. - 2010. - Vol. 25, No. 10. - P. 2588-2598. ↑
- J204.** You J. B. Improved electroluminescence from n-ZnO/AlN/p-GaN heterojunction light-emitting diodes. / You J. B., Zhang X. W., Zhang S. G., Wang J. X., Yin Z. G., Tan H. R., Zhang W. J., Chu P. K., Cui B., Wowchak A. M., Dabiran A. M., Chow P. P. // Applied Physics Letters. - 2010. - Vol. 96, No. 20. - P. 201102-201102-3. ↑
- J205.** Jongwoon Park. Power Recycling of Large-Area OLEDs Using Solar Cells. / Jongwoon Park, Jongho Lee, Dongchan Shin. // Journal of Display Technology. - 2010. - Vol. 6, No. 7. - P. 247-251. ↑
- J206.** Mont F. W. Erratum: "High-refractive-index TiO₂ -nanoparticle-loaded encapsulants for light-emitting diodes" [J. Appl. Phys. 103, 083120 (2008)]. / Mont F. W., Schubert E. F. // Journal of Applied Physics. - 2010. - Vol. 107, No. 10. - P. 109901-109901-1. ↑
- J207.** Kisin Mikhail V. Modeling of injection characteristics of polar and nonpolar III-nitride multiple quantum well structures. / Kisin Mikhail V., El-Ghoroury Hussein S. // Journal of Applied Physics. - 2010. - Vol. 107, No. 10. - P. 103106-103106-9. ↑
- J208.** Chen P. Control of magnetoconductance through modifying the amount of dissociated excited states in tris-(8-hydroxyquinoline) aluminum-based organic light-emitting diodes. / Chen P., Lei Y. L., Song Q. L., Zhang Q. M., Zhang Y., Liu R., Xiong Z. H. // Applied Physics Letters. - 2010. - Vol. 96, No. 20. - P. 203303-203303-3. ↑
- J209.** Deng Dongmei. InGaN-based light-emitting diodes grown and fabricated on nanopatterned Si substrates. / Deng Dongmei, Yu Naisen, Wang Yong, Zou Xinbo, Kuo Hao-Chung, Chen Peng, Lau Kei May. // Applied Physics Letters. - 2010. - Vol. 96, No. 20. - P. 201106-201106-3. ↑
- J210.** Yunchan Yim. Solution-Processed Flexible ITO-Free Organic Light-Emitting Diodes Using Patterned Polymeric Anodes. / Yunchan Yim, Jongwoon Park, Byoungchoo Park. // Journal of Display Technology. - 2010. - Vol. 6, No. 7. - P. 252-256. ↑
- J211.** Ojzgujr U. ZnO Devices and Applications: A Review of Current Status and Future Prospects. / Ojzgujr U., Hofstetter D., Morkoz, H. // Proceedings of the IEEE. - 2010. - Vol. 98, No. 7. - P. 1255-1268. ↑
- J212.** Ozgur U. GaN-Based Light-Emitting Diodes: Efficiency at High Injection Levels. / Ozgur U., Huiyong Liu, Xing Li, Xianfeng Ni, Morkoz, H. // Proceedings of the IEEE. - 2010. - Vol. 98, No. 7. - P. 1180-1196. ↑
- J213.** Avrutin V. Doping Asymmetry Problem in ZnO: Current Status and Outlook. / Avrutin V., Silversmith D.J., Morkoz, H. // Proceedings of the IEEE. - 2010. - Vol. 98, No. 7. - P. 1269-1280. ↑
- J214.** Cho Chu-Young. Enhanced light extraction in light-emitting diodes with photonic crystal structure selectively grown on p -GaIn. / Cho Chu-Young, Kang Se-Eun, Kim Ki Seok, Lee Sang-Jun, Choi Yong-Seok, Han Sang-Heon, Jung Gun-Young, Park Seong-Ju. // Applied Physics Letters. - 2010. - Vol. 96, No. 18. - P. 181110-181110-3. ↑
- J215.** Torres-Peiro. Sensor Applications Based on the Cutoff Properties of Liquid-Filled Ge-Doped Microstructured Fibers. / Torres-Peiro, S., Díez A., Cruz J.L., Andre,s M.V. // IEEE Sensors Journal. - 2010. - Vol. 10, No. 7. - P. 1174-1179. ↑
- J216.** Van Dormael A. Heinrich Welker. IEEE Annals of the History of Computing. - 2010. - Vol. 32, No. 2. - P. 72-79. ↑
- J217.** Jung Seungyong. Dual wavelength GaSb based type I quantum well mid-infrared light emitting diodes. / Jung Seungyong, Suchalkin Sergey, Kipshidze Gela, Westerfeld David, Golden Eric, Snyder Donald, Belenky Gregory. // Applied Physics Letters. - 2010. - Vol. 96, No. 19. - P. 191102-191102-3. ↑
- J218.** Lin Chang-Ting. Influences of evaporation temperature on electronic structures and electrical properties of molybdenum oxide in organic light emitting devices. / Lin Chang-Ting, Yeh Cheng-Hung, Chen Mei-Hsin, Hsu

Shu-Han, Wu Chih-I, Pi Tun-Wen. // Journal of Applied Physics. - 2010. - Vol. 107, No. 5. - P. 053703-053703-3. ↑

J219. Ka Ming Wong. Transfer of GaN-Based Light-Emitting Diodes From Silicon Growth Substrate to Copper. / Ka Ming Wong, Xinbo Zou, Peng Chen, Kei May Lau. // IEEE Electron Device Letters. - 2010. - Vol. 31, No. 2. - P. 132-134. ↑

J220. Chao-Hsuan Liu. SAR-Controlled Adaptive Off-Time Technique Without Sensing Resistor for Achieving High Efficiency and Accuracy LED Lighting System. / Chao-Hsuan Liu, Chun-Yu Hsieh, Yu-Chiao Hsieh, Ting-Jung Tai, Ke-Horng Chen. // IEEE Transactions on Circuits and Systems I: Regular Papers. - 2010. - Vol. 57, No. 6. - P. 1384-1394. ↑

J221. Schols S. Pulsed Excitation of OLEDs With a Remote Metallic Cathode. / Schols S., Van Willigenburg L., Steudel S., Genoe J., Heremans P. // IEEE Journal of Quantum Electronics. - 2010. - Vol. 46, No. 1. - P. 62-67. ↑

J222. Deshayes Y. Stark Effects Model Used to Highlight Selective Activation of Failure Mechanisms in MQW InGaN/GaN Light-Emitting Diodes. / Deshayes Y., Bechou L., Ousten Y. // IEEE Transactions on Device and Materials Reliability. - 2010. - Vol. 10, No. 1. - P. 164-170. ↑

J223. Duun S.B. A Ring-Shaped Photodiode Designed for Use in a Reflectance Pulse Oximetry Sensor in Wireless Health Monitoring Applications. / Duun S.B., Haahr R.G., Birkelund K., Thomsen E.V. // IEEE Sensors Journal. - 2010. - Vol. 10, No. 2. - P. 261-268. ↑

J224. Khoshnagar M. Design of a GaN White Light-Emitting Diode Through Envelope Function Analysis. / Khoshnagar M., Sodagar M., Eftekharian A., Khorasani S. // IEEE Journal of Quantum Electronics. - 2010. - Vol. 46, No. 2. - P. 228-237. ↑

J225. Xiaobing Luo. Effects of Moist Environments on LED Module Reliability. / Xiaobing Luo, Bulong Wu, Sheng Liu. // IEEE Transactions on Device and Materials Reliability. - 2010. - Vol. 10, No. 2. - P. 182-186. ↑

J226. Yu-Chung Lien. Si Nano-Dots and Nano-Pyramids Dependent Light Emission and Charge Accumulation in ITO/SiO₂/p-Si MOS Diode. / Yu-Chung Lien, Yi-Hao Pai, Gong-Ru Lin. // IEEE Journal of Quantum Electronics. - 2010. - Vol. 46, No. 1. - P. 121-127. ↑

J227. Tavakoli M. An Ultra-Low-Power Pulse Oximeter Implemented With an Energy-Efficient Transimpedance Amplifier. / Tavakoli M., Turicchia L., Sarpeshkar R. // IEEE Transactions on Biomedical Circuits and Systems. - 2010. - Vol. 4, No. 1. - P. 27-38. ↑

J228. Chiaria S. Design Criteria for Near-Ultraviolet GaN-Based Light-Emitting Diodes. / Chiaria S., Furno E., Goano M., Bellotti E. // IEEE Transactions on Electron Devices. - 2010. - Vol. 57, No. 1. - P. 60-70. ↑

J229. Swee Tiam Tan. Heterostructured White Light-Emitting Diode: Nanoscale Interface Analysis and Electroluminescence Studies. / Swee Tiam Tan, Junliang Zhao, Iwan S., Xiao Wei Sun, Xiaohong Tang, Jiandong Ye, Bosman M., Leijun Tang, Guo-Qiang Lo, Teo K.L. // IEEE Transactions on Electron Devices. - 2010. - Vol. 57, No. 1. - P. 129-133. ↑

J230. Kumar M. J. Guest Editorial Special Issue on Light-Emitting Diodes. / Kumar M. J., Lunardi L., Meneghesso G., Pearton S. J., Schubert E. F. // IEEE Transactions on Electron Devices. - 2010. - Vol. 57, No. 1. - P. 7-11. ↑

J231. Young Chul Shin. High Efficiency GaN Light-Emitting Diodes With Two Dimensional Photonic Crystal Structures of Deep-Hole Square Lattices. / Young Chul Shin, Dong Ho Kim, Eun Hong Kim, Joong-Mok Park, Kai-Ming Ho, Constant K., Jong Ho Choe, Park Q.H., Han-Youl Ryu, Jong Hyeob Baek, Tak Jung, Tae Geun Kim. // IEEE Journal of Quantum Electronics. - 2010. - Vol. 46, No. 1. - P. 116-120. ↑

J232. Tsung-Yi Tang. Nitride Nanocolumns for the Development of Light-Emitting Diode. / Tsung-Yi Tang, Cheng-Hung Lin, Yung-Sheng Chen, Wen-Yu Shiao, Wen-Ming Chang, Che-Hao Liao, Kun-Ching Shen, Chih-Chung Yang, Ming-Chi Hsu, Jui-Hung Yeh, Ta-Cheng Hsu. // IEEE Transactions on Electron Devices. - 2010. - Vol. 57, No. 1. - P. 71-78. ↑

J233. Hui-Chuan Cheng. Five-Primary-Color LCDs. / Hui-Chuan Cheng, Ben-David I., Shin-Tson Wu. // ↑

Journal of Display Technology. - 2010. - Vol. 6, No. 1. - P. 3-7.

J234. Lee Hsin-Ying. Mechanisms of lighting enhancement of Al nanoclusters-embedded Al-doped ZnO film in GaN-based light-emitting diodes. / Lee Hsin-Ying, Chou Ying-Hung, Lee Ching-Ting, Yeh Wen-Yung, Chu Mu-Tao. // Journal of Applied Physics. - 2010. - Vol. 107, No. 1. - P. 014503-014503-5. ↑

J235. Zhou Zhang-Lin. Multilayer structured polymer light emitting diodes with cross-linked polymer matrices. / Zhou Zhang-Lin, Sheng Xia, Nauka K., Zhao Lihua, Gibson Gary, Lam Sity, Yang Chung Ching, Brug James, Elder Rich. // Applied Physics Letters. - 2010. - Vol. 96, No. 1. - P. 013504-013504-3. ↑

J236. Zhang J. C. Low-temperature electroluminescence quenching of AlGaIn deep ultraviolet light-emitting diodes. / Zhang J. C., Sakai Y., Egawa T. // Applied Physics Letters. - 2010. - Vol. 96, No. 1. - P. 013503-013503-3. ↑

J237. Gong Zheng. Size-dependent light output, spectral shift, and self-heating of 400 nm InGaIn light-emitting diodes. / Gong Zheng, Jin Shirong, Chen Yujie, McKendry Jonathan, Massoubre David, Watson Ian. M., Gu Erdan, Dawson Martin D. // Journal of Applied Physics. - 2010. - Vol. 107, No. 1. - P. 013103-013103-6. ↑

J238. Qi Xiangfei. Analysis of metal-oxide-based charge generation layers used in stacked organic light-emitting diodes. / Qi Xiangfei, Li Ning, Forrest Stephen R. // Journal of Applied Physics. - 2010. - Vol. 107, No. 1. - P. 014514-014514-8. ↑

J239. Habibi M. Geometric centre tracking of tagged objects using a low power demodulation smart vision sensor. / Habibi M., Sayedi M. // IET Circuits, Devices & Systems. - 2010. - Vol. 4, No. 1. - P. 67-77. ↑

J240. Kim Hong-Yeol. Effect of neutron irradiation on electrical and optical properties of InGaIn/GaN light-emitting diodes. / Kim Hong-Yeol, Kim Jihyun, Ren F., Jang Soohwan. // Journal of Vacuum Science & Technology B: Microelectronics and Nanometer Structures. - 2010. - Vol. 28, No. 1. - P. 27-29. ↑

J241. Wu I-Wen. Correlation of energy band alignment and turn-on voltage in organic light emitting diodes. / Wu I-Wen, Chen Yu-Hung, Wang Po-Sheng, Wang Chao-Gong, Hsu Shu-Han, Wu Chih-I. // Applied Physics Letters. - 2010. - Vol. 96, No. 1. - P. 013301-013301-3. ↑

J242. Mphepo W. Enhancing the Brightness of Parallax Barrier Based 3D Flat Panel Mobile Displays Without Compromising Power Consumption. / Mphepo W., Yi-Pai Huang, Shieh H.-P.D. // Journal of Display Technology. - 2010. - Vol. 6, No. 2. - P. 60-64. ↑

J243. Yi-Jung Liu. Characteristics of an AlGaInP-Based Light Emitting Diode With an Indium-Tin-Oxide (ITO) Direct Ohmic Contact Structure. / Yi-Jung Liu, Chih-Hung Yen, Kuo-Hui Yu, Pei-Ling Lin, Li-Yang Chen, Tsung-Han Tsai, Tsung-Yuan Tsai, Wen-Chau Liu. // IEEE Journal of Quantum Electronics. - 2010. - Vol. 46, No. 2. - P. 246-252. ↑

J244. Hsing-Chao Chen. UV Electroluminescence and Structure of n-ZnO/p-GaN Heterojunction LEDs Grown by Atomic Layer Deposition. / Hsing-Chao Chen, Miin-Jang Chen, Mong-Kai Wu, Wei-Chih Li, Hung-Ling Tsai, Jer-Ren Yang, Hon Kuan, Shiojiri M. // IEEE Journal of Quantum Electronics. - 2010. - Vol. 46, No. 2. - P. 265-271. ↑

J245. Ross P.E. Target Practice. IEEE Spectrum. - 2010. - Vol. 47, No. 1. - P. 8. ↑

J246. Saito H. Efficient spin injection into semiconductor from an Fe /GaO x tunnel injector. / Saito H., Le Breton J. C., Zayets V., Mineno Y., Yuasa S., Ando K. // Applied Physics Letters. - 2010. - Vol. 96, No. 1. - P. 012501-012501-3. ↑

J247. {no data available}. You've got that glow. IEEE Spectrum. - 2010. - Vol. 47, No. 1. - P. 22-23. ↑

J248. Cherry S. 4G in the U.S.A.. IEEE Spectrum. - 2010. - Vol. 47, No. 1. - P. 15. ↑

J249. Li-Chi Peng. III-Nitride-Based Light-Emitting Diodes With GaN Micropillars Around Mesa and Patterned Substrate. / Li-Chi Peng, Wei-Chih Lai, Ming-Nan Chang, Tao-Hung Hsueh, Shih-Chang Shei, Jinn-Kong Sheu. // IEEE Transactions on Electron Devices. - 2010. - Vol. 57, No. 1. - P. 140-144. ↑

J250. Yan B. Influence of Die Attach Layer on Thermal Performance of High Power Light Emitting Diodes. / Yan B., Jiun Pyng You, Tran N.T., Yongzhi He, Shi F.G. // IEEE Transactions on Components and Packaging

Technologies. - 2010. - Vol. 33, No. 4. - P. 722-727. ↑

J251. Min-An Tsai. Self-Assembled Two-Dimensional Surface Structures for Beam Shaping of GaN-Based Vertical-Injection Light-Emitting Diodes. / Min-An Tsai, Peichen Yu, Chiu C.H., Kuo H.C., Lu T.C., Lin S.H. // IEEE Photonics Technology Letters. - 2010. - Vol. 22, No. 1. - P. 12-14. ↑

J252. Xiaochen Sun. Toward a Germanium Laser for Integrated Silicon Photonics. / Xiaochen Sun, Jifeng Liu, Kimerling L.C., Michel J. // IEEE Journal of Selected Topics in Quantum Electronics. - 2010. - Vol. 16, No. 1. - P. 124-131. ↑

J253. Ching-Ting Lee. Mechanism Investigation of p-i-n ZnO-Based Light-Emitting Diodes. / Ching-Ting Lee, Yung-Hao Lin, Li-Wen Lai, Li-Ren Lou. // IEEE Photonics Technology Letters. - 2010. - Vol. 22, No. 1. - P. 30-32. ↑

J254. Cox M.P. LED-Based Optical Device for Chronic In Vivo Cerebral Blood Volume Measurement. / Cox M.P., Hongtao Ma, Bahlke M.E., Beck J.H., Schwartz T.H., Kymissis I. // IEEE Transactions on Electron Devices. - 2010. - Vol. 57, No. 1. - P. 174-177. ↑

J255. Yong-Seok Choi. Recent Advances in ZnO-Based Light-Emitting Diodes. / Yong-Seok Choi, Jang-Won Kang, Dae-Kue Hwang, Seong-Ju Park. // IEEE Transactions on Electron Devices. - 2010. - Vol. 57, No. 1. - P. 26-41. ↑

J256. Chen P.H. GaN-Based LEDs With AZO:Y Upper Contact. / Chen P.H., Lai W.C., Li-Chi Peng, Kuo C.H., Chi-Li Yeh, Sheu J.K., Tun C.J. // IEEE Transactions on Electron Devices. - 2010. - Vol. 57, No. 1. - P. 134-139. ↑

J257. Xiaohui Qu. Temperature Measurement Technique for Stabilizing the Light Output of RGB LED Lamps. / Xiaohui Qu, Siu-Chung Wong, Tse C.K. // IEEE Transactions on Instrumentation and Measurement. - 2010. - Vol. 59, No. 3. - P. 661-670. ↑

J258. Kok-Kiong Tan. Bridging Physics to Electronics-An Outreach Effort. / Kok-Kiong Tan, Kok-Zuea Tang, Ng V., Tay A., Shih-Cheng Yen, Tong-Heng Lee. // IEEE Transactions on Education. - 2010. - Vol. 53, No. 1. - P. 3-11. ↑

J259. Huang-Jen Chiu. A High-Efficiency Dimmable LED Driver for Low-Power Lighting Applications. / Huang-Jen Chiu, Yu-Kang Lo, Jun-Ting Chen, Shih-Jen Cheng, Chung-Yi Lin, Shann-Chyi Mou. // IEEE Transactions on Industrial Electronics. - 2010. - Vol. 57, No. 2. - P. 735-743. ↑

J260. Young-Suk Son. Transient Charge Feedforward Driver for High-Speed Current-Mode Data Driving in Active-Matrix OLED Displays. / Young-Suk Son, Yong-Joon Jeon, Jin-Yong Jeon, Gyu-Hyeong Cho. // IEEE Transactions on Circuits and Systems I: Regular Papers. - 2010. - Vol. 57, No. 3. - P. 539-547. ↑

J261. Qin Y.X. Comparative Study on the Structural Designs of LED Devices and Systems Based on the General Photo-Electro-Thermal Theory. / Qin Y.X., Hui S.Y.R. // IEEE Transactions on Power Electronics. - 2010. - Vol. 25, No. 2. - P. 507-513. ↑

J262. Zanchi M.G. An Optically Coupled System for Quantitative Monitoring of MRI-Induced RF Currents Into Long Conductors. / Zanchi M.G., Venook R., Pauly J.M., Scott G.C. // IEEE Transactions on Medical Imaging. - 2010. - Vol. 29, No. 1. - P. 169-178. ↑

J263. Beibei Wang. A Method of Reducing the Peak-to-Average Ratio of LED Current for Electrolytic Capacitor-Less AC-DC Drivers. / Beibei Wang, Xinbo Ruan, Kai Yao, Ming Xu. // IEEE Transactions on Power Electronics. - 2010. - Vol. 25, No. 3. - P. 592-601. ↑

J264. Qingcong Hu. LED Driver Circuit with Series-Input-Connected Converter Cells Operating in Continuous Conduction Mode. / Qingcong Hu, Zane R. // IEEE Transactions on Power Electronics. - 2010. - Vol. 25, No. 3. - P. 574-582. ↑

J265. Paskova T. GaN Substrates for III-Nitride Devices. / Paskova T., Hanser D.A., Evans K.R. // Proceedings of the IEEE. - 2010. - Vol. 98, No. 7. - P. 1324-1338. ↑

J266. Pinato A. Impact of Trapped Charge and Interface Defects on the Degradation of the Optical and

Electrical Characteristics in OLEDs. / Pinato A., Cester A., Meneghini M., Wrachien N., Tazzoli A., Xia S., Adamovich V., Weaver M.S., Brown J.J., Zanoni E., Meneghesso G. // IEEE Transactions on Electron Devices. - 2010. - Vol. 57, No. 1. - P. 178-187. ↑

J267. Chopra N. High-Efficiency Blue Emitting Phosphorescent OLEDs. / Chopra N., Jaewon Lee, Jiangeng Xue, So F. // IEEE Transactions on Electron Devices. - 2010. - Vol. 57, No. 1. - P. 101-107. ↑

J268. Jheng-Tai Yan. Ultraviolet ZnO Nanorod/P-GaN-Heterostructured Light-Emitting Diodes. / Jheng-Tai Yan, Chia-Hsun Chen, Shiu-Fang Yen, Ching-Ting Lee. // IEEE Photonics Technology Letters. - 2010. - Vol. 22, No. 3. - P. 146-148. ↑

J269. Laubsch A. High-Power and High-Efficiency InGaN-Based Light Emitters. / Laubsch A., Sabathil M., Baur J., Peter M., Hahn B. // IEEE Transactions on Electron Devices. - 2010. - Vol. 57, No. 1. - P. 79-87. ↑

J270. Gokdel Y.D. Polymer-MEMS-Based Optoelectronic Display. / Gokdel Y.D., Sevim A.O., Mutlu S., Yalcinkaya A.D. // IEEE Transactions on Electron Devices. - 2010. - Vol. 57, No. 1. - P. 145-152. ↑

J271. Song J.O. Ohmic-Contact Technology for GaN-Based Light-Emitting Diodes: Role of P-Type Contact. / Song J.O., Jun-Seok Ha, Tae-Yeon Seong. // IEEE Transactions on Electron Devices. - 2010. - Vol. 57, No. 1. - P. 42-59. ↑

J272. Liann-Be Chang. Electrostatic Reliability Characteristics of GaN Flip-Chip Power Light-Emitting Diodes With Metal-Oxide-Silicon Submount. / Liann-Be Chang, Kuo-Ling Chiang, Hsin-Yi Chang, Ming-Jer Jeng, Chia-Yi Yen, Cheng-Chen Lin, Yuan-Hsiao Chang, Mu-Jen Lai, Yu-Lin Lee, Tai-Wei Soong. // IEEE Transactions on Electron Devices. - 2010. - Vol. 57, No. 1. - P. 119-124. ↑

J273. Jae-Hoon Lee. Comparison of InGaN-Based LEDs Grown on Conventional Sapphire and Cone-Shape-Patterned Sapphire Substrate. / Jae-Hoon Lee, Dong-Yul Lee, Bang-Won Oh, Jung-Hee Lee. // IEEE Transactions on Electron Devices. - 2010. - Vol. 57, No. 1. - P. 157-163. ↑

J274. Masui H. Nonpolar and Semipolar III-Nitride Light-Emitting Diodes: Achievements and Challenges. / Masui H., Nakamura S., DenBaars S.P., Mishra U.K. // IEEE Transactions on Electron Devices. - 2010. - Vol. 57, No. 1. - P. 88-100. ↑

J275. Meneghini M. A Review on the Physical Mechanisms That Limit the Reliability of GaN-Based LEDs. / Meneghini M., Tazzoli A., Mura G., Meneghesso G., Zanoni E. // IEEE Transactions on Electron Devices. - 2010. - Vol. 57, No. 1. - P. 108-118. ↑

J276. Chien-Chih Kao. Efficiency Improvement of GaN-Based LEDs With Microrod Array and Textured Sidewalls. / Chien-Chih Kao, Yan-Kuin Su, Chuang-Liang Lin, Jian-Jhong Chen. // IEEE Electron Device Letters. - 2010. - Vol. 31, No. 1. - P. 35-37. ↑

J277. Subbarao S.P. Laboratory Thin-Film Encapsulation of Air-Sensitive Organic Semiconductor Devices. / Subbarao S.P., Bahlke M.E., Kymissis I. // IEEE Transactions on Electron Devices. - 2010. - Vol. 57, No. 1. - P. 153-156. ↑

J278. Shur M.S. Deep-Ultraviolet Light-Emitting Diodes. / Shur M.S., Gaska R. // IEEE Transactions on Electron Devices. - 2010. - Vol. 57, No. 1. - P. 12-25. ↑

J279. Zhang H.M. Blue Organic LEDs With Improved Power Efficiency. / Zhang H.M., Choy W., Li K. // IEEE Transactions on Electron Devices. - 2010. - Vol. 57, No. 1. - P. 125-128. ↑

J280. Kondakova Marina E. Highly efficient fluorescent-phosphorescent triplet-harvesting hybrid organic light-emitting diodes. / Kondakova Marina E., Deaton Joseph C., Pawlik Thomas D., Giesen David J., Kondakov Denis Y., Young Ralph H., Royster Tommie L., Comfort Dustin L., Shore Joel D. // Journal of Applied Physics. - 2010. - Vol. 107, No. 1. - P. 014515-014515-13. ↑

J281. Fu-Cheng Wang. Multivariable Robust Control for a Red-Green-Blue LED Lighting System. / Fu-Cheng Wang, Chun-Wen Tang, Bin-Juine Huang. // IEEE Transactions on Power Electronics. - 2010. - Vol. 25, No. 2. - P. 417-428. ↑

J282. Perlin P. Degradation Mechanisms of InGaN Laser Diodes. / Perlin P., Marona L., Leszczynski M., Suski

T., Wisniewski P., Czernecki R., Grzegory I. // Proceedings of the IEEE. - 2010. - Vol. 98, No. 7. - P. 1214-1219. ↑

J283. Kim Tae-Gon. Effects of additional Ce 3+ doping on the luminescence of Li 2 SrSiO 4 :Eu 2+ yellow phosphor. / Kim Tae-Gon, Lee Hyo-Sug, Lin Chun Che, Kim Taehyung, Liu Ru-Shi, Chan Ting-Shan, Im Seoung-Jae. // Applied Physics Letters. - 2010. - Vol. 96, No. 6. - P. 061904-061904-3. ↑

J284. Frischeisen Jorg. Determination of molecular dipole orientation in doped fluorescent organic thin films by photoluminescence measurements. / Frischeisen Jorg, Yokoyama Daisuke, Adachi Chihaya, Brutting Wolfgang. // Applied Physics Letters. - 2010. - Vol. 96, No. 7. - P. 073302-073302-3. ↑

J285. Chu Ryang Wie. Nonsaturating Drain Current Characteristic in Short-Channel Amorphous-Silicon Thin-Film Transistors. IEEE Transactions on Electron Devices. - 2010. - Vol. 57, No. 4. - P. 846-854. ↑

J286. {no data available}. Intermix and match. Electronics Letters. - 2010. - Vol. 46, No. 4. - P. 262. ↑

J287. Niu Xiaodi. Balanced charge transport and enhanced white electroluminescence from a single white emissive polymer via thermal annealing. / Niu Xiaodi, Zhang Baohua, Xie Zhiyuan, Cheng Yanxiang, Wang Lixiang. // Applied Physics Letters. - 2010. - Vol. 96, No. 7. - P. 073303-073303-3. ↑

J288. Sun W. Efficiency droop in 245-247 nm AlGaIn light-emitting diodes with continuous wave 2 mW output power. / Sun W., Shatalov M., Deng J., Hu X., Yang J., Lunev A., Bilenko Y., Shur M., Gaska R. // Applied Physics Letters. - 2010. - Vol. 96, No. 6. - P. 061102-061102-3. ↑

J289. Jong In Park. Direct Prediction Methods on Lifetime Distribution of Organic Light-Emitting Diodes From Accelerated Degradation Tests. / Jong In Park, Suk Joo Bae. // IEEE Transactions on Reliability. - 2010. - Vol. 59, No. 1. - P. 74-90. ↑

J290. Park Tae-Young. Enhanced optical power and low forward voltage of GaN-based light-emitting diodes with Ga-doped ZnO transparent conducting layer. / Park Tae-Young, Choi Yong-Seok, Kang Jang-Won, Jeong Jae-Ho, Park Seong-Ju, Jeon Dong Min, Kim Je Won, Kim Yong Chun. // Applied Physics Letters. - 2010. - Vol. 96, No. 5. - P. 051124-051124-3. ↑

J291. Haverinen H.M. Inkjet Printed RGB Quantum Dot-Hybrid LED. / Haverinen H.M., Myllyla R.A., Jabbour G.E. // Journal of Display Technology. - 2010. - Vol. 6, No. 3. - P. 87-89. ↑

J292. Yi-Jung Liu. Characteristics of a GaN-Based Light-Emitting Diode With an Inserted p-GaN/i-InGaN Superlattice Structure. / Yi-Jung Liu, Tsung-Yuan Tsai, Chih-Hung Yen, Li-Yang Chen, Tsung-Han Tsai, Wen-Chau Liu. // IEEE Journal of Quantum Electronics. - 2010. - Vol. 46, No. 4. - P. 492-498. ↑

J293. Heikkila Oskari. The challenge of unity wall plug efficiency: The effects of internal heating on the efficiency of light emitting diodes. / Heikkila Oskari, Oksanen Jani, Tulkki Jukka. // Journal of Applied Physics. - 2010. - Vol. 107, No. 3. - P. 033105-033105-6. ↑

J294. Li Z.Q. Comprehensive Modeling of Superluminescent Light-Emitting Diodes. / Li Z.Q., Li Z. // IEEE Journal of Quantum Electronics. - 2010. - Vol. 46, No. 4. - P. 454-461. ↑

J295. Chung-Hsun Jang. Improved Performance of GaN-Based Blue LEDs With the InGaN Insertion Layer Between the MQW Active Layer and the n-GaN Cladding Layer. / Chung-Hsun Jang, Jinn-Kong Sheu, Tsai C.M., Shouu-Jinn Chang, Wei-Chih Lai, Ming-Lun Lee, Ko T.K., Shen C.F., Shei S.C. // IEEE Journal of Quantum Electronics. - 2010. - Vol. 46, No. 4. - P. 513-517. ↑

J296. Turner J. The smart power strip. IEEE Spectrum. - 2010. - Vol. 47, No. 3. - P. 22-23. ↑

J297. Liu Huihui. Remarkable increase in the efficiency of N,N'-dimethylquinacridone dye heavily doped organic light emitting diodes under high current density. / Liu Huihui, Yan Fei, Li Wenlian, Chu Bei, Su Wenming, Su Zisheng, Wang Junbo, Hu Zhizhi, Zhang Zhiqiang. // Applied Physics Letters. - 2010. - Vol. 96, No. 8. - P. 083301-083301-3. ↑

J298. Han-Youl Ryu. Structural Parameter Dependence of Light Extraction Efficiency in Photonic Crystal InGaN Vertical Light-Emitting Diode Structures. / Han-Youl Ryu, Jong-In Shim. // IEEE Journal of Quantum Electronics. - 2010. - Vol. 46, No. 5. - P. 714-720. ↑

- J299.** Lobo N. Enhancement of light extraction in ultraviolet light-emitting diodes using nanopixel contact design with Al reflector. / Lobo N., Rodriguez H., Knauer A., Hoppe M., Einfeldt S., Vogt P., Weyers M., Kneissl M. // Applied Physics Letters. - 2010. - Vol. 96, No. 8. - P. 081109-081109-3. ↑
- J300.** Kim Kyu Sang. Stable temperature characteristics of InGaN blue light emitting diodes using AlGaIn/GaN/InGaN superlattices as electron blocking layer. / Kim Kyu Sang, Kim Jin Ha, Jung Su Jin, Park Yong Jo, Cho S. N. // Applied Physics Letters. - 2010. - Vol. 96, No. 9. - P. 091104-091104-3. ↑
- J301.** Cheng-Yu Chang. Study of Light Emission Enhancement in Nanostructured InGaN/GaN Quantum Wells. / Cheng-Yu Chang, Yuh-Renn Wu. // IEEE Journal of Quantum Electronics. - 2010. - Vol. 46, No. 6. - P. 884-889. ↑
- J302.** Yan Dawei. Forward tunneling current in GaN-based blue light-emitting diodes. / Yan Dawei, Lu Hai, Chen Dunjun, Zhang Rong, Zheng Youdou. // Applied Physics Letters. - 2010. - Vol. 96, No. 8. - P. 083504-083504-3. ↑
- J303.** Litvinov V.I. Resonant Tunneling in III-Nitrides. Proceedings of the IEEE. - 2010. - Vol. 98, No. 7. - P. 1249-1254. ↑
- J304.** Kwang Hyeon Baik. Effects of Basal Stacking Faults on Electrical Anisotropy of Nonpolar a-Plane () GaN Light-Emitting Diodes on Sapphire Substrate. / Kwang Hyeon Baik, Yong Gon Seo, Soon-Ku Hong, Seogwoo Lee, Jaebum Kim, Ji-Su Son, Sung-Min Hwang. // IEEE Photonics Technology Letters. - 2010. - Vol. 22, No. 9. - P. 595-597. ↑
- J305.** Ming-Te Lin. Ring Remote Phosphor Structure for Phosphor-Converted White LEDs. / Ming-Te Lin, Shang-Ping Ying, Ming-Yao Lin, Kuang-Yu Tai, Sheng-Chieh Tai, Chih-Hsuan Liu, Jyh-Chen Chen, Ching-Cherng Sun. // IEEE Photonics Technology Letters. - 2010. - Vol. 22, No. 8. - P. 574-576. ↑
- J306.** Horng R.-H. Performance of Flip-Chip Thin-Film GaN Light-Emitting Diodes With and Without Patterned Sapphires. / Horng R.-H., Hung-Lieh Hu, Mu-Tao Chu, Yu-Li Tsai, Yao-Jun Tsai, Chen-Peng Hsu, Dong-Sing Wu. // IEEE Photonics Technology Letters. - 2010. - Vol. 22, No. 8. - P. 550-552. ↑
- J307.** Dae-Whan Kim. Direct Submount Cooling of High-Power LEDs. / Dae-Whan Kim, Rahim E., Bar-Cohen A., Bongtae Han. // IEEE Transactions on Components and Packaging Technologies. - 2010. - Vol. 33, No. 4. - P. 698-712. ↑
- J308.** Wang Liang. Highly efficient blue organic light emitting device using indium-free transparent anode Ga:ZnO with scalability for large area coating. / Wang Liang, Matson Dean W., Polikarpov Evgueni, Swensen James S., Bonham Charles C., Cosimbescu Lelia, Berry Joseph J., Ginley David S., Gaspar Daniel J., Padmaperuma Asanga B. // Journal of Applied Physics. - 2010. - Vol. 107, No. 4. - P. 043103-043103-8. ↑
- J309.** Masui Hisashi. Technique to evaluate the diode ideality factor of light-emitting diodes. / Masui Hisashi, Nakamura Shuji, DenBaars Steven P. // Applied Physics Letters. - 2010. - Vol. 96, No. 7. - P. 073509-073509-3. ↑
- J310.** Fang-Cheng Lin. Color Filter-Less LCDs in Achieving High Contrast and Low Power Consumption by Stencil Field-Sequential-Color Method. / Fang-Cheng Lin, Yi-Pai Huang, Ching-Ming Wei, Shieh H.-P.D. // Journal of Display Technology. - 2010. - Vol. 6, No. 3. - P. 98-106. ↑
- J311.** Netzel C. Temperature and excitation power dependent photoluminescence intensity of GaInN quantum wells with varying charge carrier wave function overlap. / Netzel C., Hoffmann V., Wernicke T., Knauer A., Weyers M., Kneissl M., Szabo N. // Journal of Applied Physics. - 2010. - Vol. 107, No. 3. - P. 033510-033510-9. ↑
- J312.** Namdas Ebinazar B. Organic light emitting complementary inverters. / Namdas Ebinazar B., Samuel Ifor D. W., Shukla Deepak, Meyer Dianne M., Sun Yanming, Hsu Ben B. Y., Moses Daniel, Heeger Alan J. // Applied Physics Letters. - 2010. - Vol. 96, No. 4. - P. 043304-043304-3. ↑
- J313.** Wang Z. B. Controlling carrier accumulation and exciton formation in organic light emitting diodes. / Wang Z. B., Helander M. G., Liu Z. W., Greiner M. T., Qiu J., Lu Z. H. // Applied Physics Letters. - 2010. - Vol. 96, No. 4. - P. 043303-043303-3. ↑
- J314.** Kondakov Denis Y. Chemical reactivity of aromatic hydrocarbons and operational degradation of organic

light-emitting diodes. / Kondakov Denis Y., Brown Christopher T., Pawlik Thomas D., Jarikov Viktor V. // Journal of Applied Physics. - 2010. - Vol. 107, No. 2. - P. 024507-024507-8. ↑

J315. Wang Xuhua. Device physics of highly sensitive thin film polyfluorene copolymer organic phototransistors. / Wang Xuhua, Wasapinyokul Kamol, De Tan Wei, Rawcliffe Ruth, Campbell Alasdair J., Bradley Donal D. C. // Journal of Applied Physics. - 2010. - Vol. 107, No. 2. - P. 024509-024509-10. ↑

J316. Gosnell J.D. White Light Emission Characteristics of Polymer-Encapsulated CdSe Nanocrystal Films. / Gosnell J.D., Rosenthal S.J., Weiss S.M. // IEEE Photonics Technology Letters. - 2010. - Vol. 22, No. 8. - P. 541-543. ↑

J317. Bruckner Jan. ac excitation of organic light emitting devices utilizing conductive charge generation layers. / Bruckner Jan, Christ Nico, Bauder Olga, Gartner Christian, Seyfried Moritz, Glockler Felix, Lemmer Uli, Gerken Martina. // Applied Physics Letters. - 2010. - Vol. 96, No. 4. - P. 041107-041107-3. ↑

J318. Fujiki A. Enhanced fluorescence by surface plasmon coupling of Au nanoparticles in an organic electroluminescence diode. / Fujiki A., Uemura T., Zettsu N., Akai-Kasaya M., Saito A., Kuwahara Y. // Applied Physics Letters. - 2010. - Vol. 96, No. 4. - P. 043307-043307-3. ↑

J319. Kobayashi Takeyuki. Near-infrared electroluminescence and stimulated emission from semiconducting nonconjugated polymer thin films. / Kobayashi Takeyuki, Django Martin, Blau Werner J. // Journal of Applied Physics. - 2010. - Vol. 107, No. 2. - P. 023103-023103-5. ↑

J320. Krautz D. Interchain and intrachain emission branching in polymer light-emitting diode doped by organic molecules. / Krautz D., Lunedei E., Puigdollers J., Badenes G., Alcubilla R., Cheylan S. // Applied Physics Letters. - 2010. - Vol. 96, No. 3. - P. 033301-033301-3. ↑

J321. Karlin S. Engineer on a mission. IEEE Spectrum. - 2010. - Vol. 47, No. 2. - P. 24. ↑

J322. Schubert Martin F. Polarization-charge tunnel junctions for ultraviolet light-emitters without p-type contact. Applied Physics Letters. - 2010. - Vol. 96, No. 3. - P. 031102-031102-3. ↑

J323. Cho J. Analysis of reverse tunnelling current in GaInN light-emitting diodes. / Cho J., Mao A., Kim J.K., Son J.K., Park Y., Schubert E.F. // Electronics Letters. - 2010. - Vol. 46, No. 2. - P. 156-158. ↑

J324. Liao L. S. Recoverable electroluminescence from a contaminated organic/organic interface in an organic light-emitting diode. / Liao L. S., Klubek K. P., Madathil J. K., Tang C. W., Giesen D. J. // Applied Physics Letters. - 2010. - Vol. 96, No. 4. - P. 043302-043302-3. ↑

J325. Matioli Elison. High extraction efficiency light-emitting diodes based on embedded air-gap photonic-crystals. / Matioli Elison, Rangel Elizabeth, Iza Micheal, Fleury Blaise, Pfaff Nathan, Speck James, Hu Evelyn, Weisbuch Claude. // Applied Physics Letters. - 2010. - Vol. 96, No. 3. - P. 031108-031108-3. ↑

J326. Rusak David A. Note: Investigation of a null measurement of optical absorbance using a pulse width modulated light-emitting diode. / Rusak David A., Kawka Ernest A., Trexler E. Brady. // Review of Scientific Instruments. - 2010. - Vol. 81, No. 1. - P. 016107-016107-2. ↑

J327. Han Sang-Heon. Effect of Mg doping in the barrier of InGaN/GaN multiple quantum well on optical power of light-emitting diodes. / Han Sang-Heon, Cho Chu-Young, Lee Sang-Jun, Park Tae-Young, Kim Tae-Hun, Park Seung Hyun, Won Kang Sang, Won Kim Je, Kim Yong Chun, Park Seong-Ju. // Applied Physics Letters. - 2010. - Vol. 96, No. 5. - P. 051113-051113-3. ↑

J328. Fadhil H.A. Design considerations of high performance optical code division multiple access: a new spectral amplitude code based on laser and light emitting diode light source. / Fadhil H.A., Aljunid S.A., Ahmad R.B. // IET Optoelectronics. - 2010. - Vol. 4, No. 1. - P. 29-34. ↑

J329. Nakanotani Hajime. Organic light-emitting diodes containing multilayers of organic single crystals. / Nakanotani Hajime, Adachi Chihaya. // Applied Physics Letters. - 2010. - Vol. 96, No. 5. - P. 053301-053301-3. ↑

J330. Poikonen Tuomas. Multifunctional integrating sphere setup for luminous flux measurements of light emitting diodes. / Poikonen Tuomas, Manninen Pasi, Karha Petri, Ikonen Erkki. // Review of Scientific Instruments. - 2010. - Vol. 81, No. 2. - P. 023102-023102-7. ↑

- J331.** Polikarpov Evgueni. Emission zone control in blue organic electrophosphorescent devices through chemical modification of host materials. / Polikarpov Evgueni, Swensen James S., Cosimbescu Lelia, Koech Phillip K., Rainbolt James E., Padmaperuma Asanga B. // Applied Physics Letters. - 2010. - Vol. 96, No. 5. - P. 053306-053306-3. ↑
- J332.** Löffler W. Doping and optimal electron spin polarization in n-ZnMnSe for quantum-dot spin-injection light-emitting diodes. / Löffler W., Hopcke N., Kalt H., Li S. F., Grun M., Hetterich M. // Applied Physics Letters. - 2010. - Vol. 96, No. 5. - P. 052113-052113-3. ↑
- J333.** Cheng Ji-Hao. Improved crystal quality and performance of GaN-based light-emitting diodes by decreasing the slanted angle of patterned sapphire. / Cheng Ji-Hao, Wu YewChung Sermon, Liao Wei-Chih, Lin Bo-Wen. // Applied Physics Letters. - 2010. - Vol. 96, No. 5. - P. 051109-051109-3. ↑
- J334.** Detchprohm Theeradetch. Wavelength-stable cyan and green light emitting diodes on nonpolar m-plane GaN bulk substrates. / Detchprohm Theeradetch, Zhu Mingwei, Li Yufeng, Zhao Liang, You Shi, Wetzel Christian, Preble Edward A., Paskova Tanya, Hanser Drew. // Applied Physics Letters. - 2010. - Vol. 96, No. 5. - P. 051101-051101-3. ↑
- J335.** Shih-Yung Huang. Study on Hydrogen Ion-Implanted Characteristic of Thin-Film Green Resonant-Cavity Light-Emitting Diodes. / Shih-Yung Huang, Ray-Hua Horng, Po-Han Tseng, Jen-Hung Tu, Li-Wei Tu, Dong-Sing Wu. // IEEE Photonics Technology Letters. - 2010. - Vol. 22, No. 6. - P. 404-406. ↑
- J336.** Buss I.J. Finite-Difference Time-Domain Modeling of Periodic and Disordered Surface Gratings in AlInSb Light Emitting Diodes With Metallic Back-Reflectors. / Buss I.J., Nash G.R., Rarity J.G., Cryan M.J. // Journal of Lightwave Technology. - 2010. - Vol. 28, No. 8. - P. 1190-1200. ↑
- J337.** Zhu L. Angularly Uniform White Light-Emitting Diodes Using an Integrated Reflector Cup. / Zhu L., Wang X.H., Lai P.T., Choi H.W. // IEEE Photonics Technology Letters. - 2010. - Vol. 22, No. 7. - P. 513-515. ↑
- J338.** Sun Y.X. GaN-Based Power Flip-Chip LEDs With an Internal ESD Protection Diode on Cu Sub-Mount. / Sun Y.X., Chen W.S., Hung S.C., Lam K.T., Liu C.H., Shouu-Jinn Chang. // IEEE Transactions on Advanced Packaging. - 2010. - Vol. 33, No. 2. - P. 433-437. ↑
- J339.** Cheng-Huang Kuo. Efficiency Dependence on Degree of Localization States in GaN-Based Asymmetric Two-Step Light-Emitting Diode With a Low Indium Content InGaN Shallow Step. / Cheng-Huang Kuo, Fu Y.K., Chi G.C., Shouu-Jinn Chang. // IEEE Journal of Quantum Electronics. - 2010. - Vol. 46, No. 3. - P. 391-395. ↑
- J340.** Terry B.S. An Integrated Port Camera and Display System for Laparoscopy. / Terry B.S., Ruppert A.D., Steinhilber K.R., Schoen J.A., Rentschler M.E. // IEEE Transactions on Biomedical Engineering. - 2010. - Vol. 57, No. 5. - P. 1191-1197. ↑
- J341.** Zhu H. A route to improved extraction efficiency of light-emitting diodes. / Zhu H., Shan C. X., Wang L. K., Yang Y., Zhang J. Y., Yao B., Shen D. Z., Fan X. W. // Applied Physics Letters. - 2010. - Vol. 96, No. 4. - P. 041110-041110-3. ↑
- J342.** Yin X. R. Internal potential distribution in organic light emitting diodes measured by dc bridge. / Yin X. R., Le Y. K., Gao X. D., Sun Z. Y., Hou X. Y. // Applied Physics Letters. - 2010. - Vol. 97, No. 15. - P. 153305-153305-3. ↑
- J343.** Kondakov Denis Y. Variable sensitivity of organic light-emitting diodes to operation-induced chemical degradation: Nature of the antagonistic relationship between lifetime and efficiency. / Kondakov Denis Y., Young Ralph H. // Journal of Applied Physics. - 2010. - Vol. 108, No. 7. - P. 074513-074513-11. ↑
- J344.** Damilano B. Blue-green and white color tuning of monolithic light emitting diodes. / Damilano B., Demoloni P., Brault J., Huault T., Natali F., Massies J. // Journal of Applied Physics. - 2010. - Vol. 108, No. 7. - P. 073115-073115-6. ↑
- J345.** Kavehrad M. Sustainable energy-efficient wireless applications using light. IEEE Communications Magazine. - 2010. - Vol. 48, No. 12. - P. 66-73. ↑
- J346.** Youn Hongseok. Solution processed polymer light-emitting diodes utilizing a ZnO/organic ionic interlayer

with Al cathode. / Youn Hongseok, Yang Minyang. // Applied Physics Letters. - 2010. - Vol. 97, No. 24. - P. 243302-243302-3. ↑

J347. Liang Zhiwen. GaN nanostructure design for optimal dislocation filtering. / Liang Zhiwen, Colby Robert, Wildeson Isaac H., Ewoldt David A., Sands Timothy D., Stach Eric A., Garcia R. Edwin. // Journal of Applied Physics. - 2010. - Vol. 108, No. 7. - P. 074313-074313-8. ↑

J348. Lee Hsin-Ying. Mechanisms of high quality i-ZnO thin films deposition at low temperature by vapor cooling condensation technique. / Lee Hsin-Ying, Xia Shang-Da, Zhang Wei-Ping, Lou Li-Ren, Yan Jheng-Tai, Lee Ching-Ting. // Journal of Applied Physics. - 2010. - Vol. 108, No. 7. - P. 073119-073119-6. ↑

J349. Dahal R. 1.54 mcm emitters based on erbium doped InGaN p-i-n junctions. / Dahal R., Ugolini C., Lin J. Y., Jiang H. X., Zavada J. M. // Applied Physics Letters. - 2010. - Vol. 97, No. 14. - P. 141109-141109-3. ↑

J350. Zhu Jihong. The fabrication of GaN-based nanopillar light-emitting diodes. / Zhu Jihong, Wang Liangji, Zhang Shuming, Wang Hui, Zhao Degang, Zhu Jianjun, Liu Zongshun, Jiang Desheng, Yang Hui. // Journal of Applied Physics. - 2010. - Vol. 108, No. 7. - P. 074302-074302-4. ↑

J351. Meneghini Matteo. Analysis of the physical processes responsible for the degradation of deep-ultraviolet light emitting diodes. / Meneghini Matteo, Barbisan Diego, Rodighiero Luca, Meneghesso Gaudenzio, Zanoni Enrico. // Applied Physics Letters. - 2010. - Vol. 97, No. 14. - P. 143506-143506-3. ↑

J352. Konezny S. J. The effects of energetic disorder and polydispersity in conjugation length on the efficiency of polymer-based light-emitting diodes. / Konezny S. J., Rothberg L. J., Galvin M. E., Smith D. L. // Applied Physics Letters. - 2010. - Vol. 97, No. 14. - P. 143305-143305-3. ↑

J353. Renyong Yu. Effect of the Phosphor Geometry on the Luminous Flux of Phosphor-Converted Light-Emitting Diodes. / Renyong Yu, Shangzhong Jin, Songyuan Cen, Pei Liang. // IEEE Photonics Technology Letters. - 2010. - Vol. 22, No. 23. - P. 1765-1767. ↑

J354. Wildeson Isaac H. Publisher's Note: "III-nitride nanopillar light emitting diodes grown by organometallic vapor phase epitaxy" [J. Appl. Phys. 108, 044303 (2010)]. / Wildeson Isaac H., Colby Robert, Ewoldt David A., Liang Zhiwen, Zakharov Dmitri N., Zaluzec Nestor J., Garcia R. Edwin, Stach Eric A., Sands Timothy D. // Journal of Applied Physics. - 2010. - Vol. 108, No. 7. - P. 079907-079907-1. ↑

J355. Zhu Y. Effects of strain on defect structure in II-VI green color converters. / Zhu Y., McKernan S., Xie J., Miller T. J., Haase M. A., Sun X., Smith T. L., Leatherdale C. A. // Journal of Applied Physics. - 2010. - Vol. 108, No. 12. - P. 123104-123104-4. ↑

J356. Sheng-Horng Yen. Investigation of Optical Performance of InGaN MQW LED With Thin Last Barrier. / Sheng-Horng Yen, Meng-Lun Tsai, Miao-Chan Tsai, Shu-Jeng Chang, Yen-Kuang Kuo. // IEEE Photonics Technology Letters. - 2010. - Vol. 22, No. 24. - P. 1787-1789. ↑

J357. Bertoli B. Equilibrium strain and dislocation density in exponentially graded Si 1-x Ge x /Si (001). / Bertoli B., Sidoti D., Khurshi S., Kujofsa T., Cheruku S., Correa J. P., Rago P. B., Suarez E. N., Jain F. C., Ayers J. E. // Journal of Applied Physics. - 2010. - Vol. 108, No. 11. - P. 113525-113525-5. ↑

J358. Bhattacharya Pallab. Tunnel injection In 0.25 Ga 0.75 N /GaN quantum dot light-emitting diodes. / Bhattacharya Pallab, Zhang Meng, Hinckley John. // Applied Physics Letters. - 2010. - Vol. 97, No. 25. - P. 251107-251107-3. ↑

J359. Shan Qifeng. Analysis of thermal properties of GaInN light-emitting diodes and laser diodes. / Shan Qifeng, Dai Qi, Chhajed Sameer, Cho Jaehee, Schubert E. Fred. // Journal of Applied Physics. - 2010. - Vol. 108, No. 8. - P. 084504-084504-8. ↑

J360. Cha-Hsin Chao. Influence of Architecture-Controlled GaN Rod Arrays on the Output Power of GaN LEDs. / Cha-Hsin Chao, Shih-Che Hung, Shu-Chia Shiu, Ming-Tung Kuo, Chang-Ho Chen, Ching-Hua Changjean, Ching-Fuh Lin. // IEEE Photonics Technology Letters. - 2010. - Vol. 22, No. 24. - P. 1847-1849. ↑

J361. Yang Zhaohui H. Enhanced efficiency of CdMgZnSe down-converted light emitting diodes using light extraction features fabricated by laser-speckle lithography. / Yang Zhaohui H., Haase Michael A., Leatherdale Catherine A., Smith Terry L. // Journal of Applied Physics. - 2010. - Vol. 108, No. 12. - P. 123106-123106-4. ↑

- J362.** Malyutenko V. K. Current crowding effect on the ideality factor and efficiency droop in blue lateral InGaN/GaN light emitting diodes. / Malyutenko V. K., Bolgov S. S., Podoltsev A. D. // Applied Physics Letters. - 2010. - Vol. 97, No. 25. - P. 251110-251110-3. ↑
- J363.** Rosenow Thomas C. Highly efficient white organic light-emitting diodes based on fluorescent blue emitters. / Rosenow Thomas C., Furno Mauro, Reineke Sebastian, Olthof Selina, Lussem Bjorn, Leo Karl. // Journal of Applied Physics. - 2010. - Vol. 108, No. 11. - P. 113113-113113-5. ↑
- J364.** Rufo J. Experimental evaluation of video transmission through LED illumination devices. / Rufo J., Rabadan J., Delgado F., Quintana C., Perez-Jimenez R. // IEEE Transactions on Consumer Electronics. - 2010. - Vol. 56, No. 3. - P. 1411-1416. ↑
- J365.** Li Z. L. Mechanism of optical degradation in microstructured InGaN light-emitting diodes. / Li Z. L., Li K. H., Choi H. W. // Journal of Applied Physics. - 2010. - Vol. 108, No. 11. - P. 114511-114511-4. ↑
- J366.** Bertazzi Francesco. A numerical study of Auger recombination in bulk InGaN. / Bertazzi Francesco, Goano Michele, Bellotti Enrico. // Applied Physics Letters. - 2010. - Vol. 97, No. 23. - P. 231118-231118-3. ↑
- J367.** Bleicher A. Bright Lights, Big City. / Bleicher A., Klett R.S. // IEEE Spectrum. - 2010. - Vol. 47, No. 11. - P. 50-55. ↑
- J368.** Toyama Toshihiko. Solution-processed ZnO nanocrystals in thin-film light-emitting diodes for printed electronics. / Toyama Toshihiko, Takeuchi Hisazumi, Yamaguchi Daisaku, Kawasaki Hayato, Itatani Kazuki, Okamoto Hiroaki. // Journal of Applied Physics. - 2010. - Vol. 108, No. 8. - P. 084302-084302-6. ↑
- J369.** Zion Hwang. Development of LED smart switch with light-weight middleware for location-aware services in smart home. / Zion Hwang, Yoonsik Uhm, Yong Kim, Gwanyeon Kim, Sehyun Park. // IEEE Transactions on Consumer Electronics. - 2010. - Vol. 56, No. 3. - P. 1395-1402. ↑
- J370.** Hai-Jung In. A luminance adjusting algorithm for high resolution and high image quality AMOLED displays of mobile phone applications. / Hai-Jung In, Kyong-Hwan Oh, Oh-Kyong Kwon, Chang Ho Hyun, Sung-Chul Kim. // IEEE Transactions on Consumer Electronics. - 2010. - Vol. 56, No. 3. - P. 1191-1195. ↑
- J371.** Drapiko E. Improved calibration technique of the infrared imaging bolometer using ultraviolet light-emitting diodes. / Drapiko E., Peterson B., Alekseev A., Seo D. C. // Review of Scientific Instruments. - 2010. - Vol. 81, No. 10. - P. 10E116-10E116-3. ↑
- J372.** Lo M. F. Operation stability enhancement in organic photovoltaic device by a metal doped organic exciton blocking layer. / Lo M. F., Ng T. W., Lai S. L., Wong F. L., Fung M. K., Lee S. T., Lee C. S. // Applied Physics Letters. - 2010. - Vol. 97, No. 14. - P. 143304-143304-3. ↑
- J373.** Schuster E. Epitaxial growth and interfacial magnetism of spin aligner for remanent spin injection: [Fe /Tb]n /Fe /MgO /GaAs -light emitting diode as a prototype system. / Schuster E., Brand R. A., Stromberg F., Lo F.-Y., Ludwig A., Reuter D., Wieck A. D., Hovel S., Gerhardt N. C., Hofmann M. R., Wende H., Keune W. // Journal of Applied Physics. - 2010. - Vol. 108, No. 6. - P. 063902-063902-4. ↑
- J374.** Hai-Jung In. An Advanced External Compensation System for Active Matrix Organic Light-Emitting Diode Displays With Poly-Si Thin-Film Transistor Backplane. / Hai-Jung In, Kyong-Hwan Oh, Inhwan Lee, Do-Hyung Ryu, Sang-Moo Choi, Keum-Nam Kim, Hye-Dong Kim, Oh-Kyong Kwon. // IEEE Transactions on Electron Devices. - 2010. - Vol. 57, No. 11. - P. 3012-3019. ↑
- J375.** Hung-Pin Shiao. Enhancing the Brightness of GaN Light-Emitting Diodes by Manipulating the Illumination Direction in the Photoelectrochemical Process. / Hung-Pin Shiao, Chi-Yu Wang, Wu M.-L., Chia-Hao Chiu. // IEEE Photonics Technology Letters. - 2010. - Vol. 22, No. 22. - P. 1653-1655. ↑
- J376.** Jang Ji-Hyang. Polymer grating imbedded organic light emitting diodes with improved out-coupling efficiency. / Jang Ji-Hyang, Oh Min-Cheol, Yoon Tae-Hoon, Kim Jae Chang. // Applied Physics Letters. - 2010. - Vol. 97, No. 12. - P. 123302-123302-3. ↑
- J377.** Ishizawa A. Octave-spanning frequency comb generated by 250 fs pulse train emitted from 25 GHz externally phase-modulated laser diode for carrier-envelope-offset-locking. / Ishizawa A., Nishikawa T., Mizutori A., Takara H., Aozasa S., Mori A., Nakano H., Takada A., Koga M. // Electronics Letters. - 2010. - Vol. 46, No.

19. - P. 1343-1344. ↑

J378. Liao J. Integration of LED chip within patch antenna geometry for hybrid FSO/RF communication. / Liao J., Mirvakili A., Boryssenko A., Joyner V., Huang Z.R. // Electronics Letters. - 2010. - Vol. 46, No. 19. - P. 1332-1333. ↑

J379. Forget S. Red-emitting fluorescent organic light emitting diodes with low sensitivity to self-quenching. / Forget S., Chenais S., Tondelier D., Geffroy B., Gozhyk I., Lebental M., Ishow E. // Journal of Applied Physics. - 2010. - Vol. 108, No. 6. - P. 064509-064509-6. ↑

J380. Zhou Mi. Determination of the interface delta -hole density in a blue-emitting organic semiconductor diode by electromodulated absorption spectroscopy. / Zhou Mi, Png Rui-Qi, Sivaramakrishnan Sankaran, Chia Perq-Jon, Yong Chaw-Keong, Chua Lay-Lay, Ho Peter K. H. // Applied Physics Letters. - 2010. - Vol. 97, No. 11. - P. 113505-113505-3. ↑

J381. Gan Zhengqing. Transient electroluminescence dynamics in small molecular organic light-emitting diodes. / Gan Zhengqing, Liu Rui, Shinar Ruth, Shinar Joseph. // Applied Physics Letters. - 2010. - Vol. 97, No. 11. - P. 113301-113301-3. ↑

J382. Wu Honglei. C and Si codoping method for p -type AlN. / Wu Honglei, Zheng Ruisheng, Liu Wen, Meng Shu, Huang Junyi. // Journal of Applied Physics. - 2010. - Vol. 108, No. 5. - P. 053715-053715-4. ↑

J383. Tatebayashi J. Visible light emission from self-catalyzed GaInP/GaP core-shell double heterostructure nanowires on silicon. / Tatebayashi J., Lin A., Wong P. S., Hick R. F., Huffaker D. L. // Journal of Applied Physics. - 2010. - Vol. 108, No. 3. - P. 034315-034315-5. ↑

J384. Rath Arup K. Mn-doped nanocrystals in light-emitting diodes: Energy-transfer to obtain electroluminescence from quantum dots. / Rath Arup K., Bhaumik Saikat, Pal Amlan J. // Applied Physics Letters. - 2010. - Vol. 97, No. 11. - P. 113502-113502-3. ↑

J385. Lorenz K. Lattice site location of optical centers in GaN:Eu light emitting diode material grown by organometallic vapor phase epitaxy. / Lorenz K., Alves E., Roqan I. S., O'Donnell K. P., Nishikawa A., Fujiwara Y., Bockowski M. // Applied Physics Letters. - 2010. - Vol. 97, No. 11. - P. 111911-111911-3. ↑

J386. Lee Hsin-Ying. Emission mechanisms of passivated single n-ZnO:In/i-ZnO/p-GaN-heterostructured nanorod light-emitting diodes. / Lee Hsin-Ying, Lee Ching-Ting, Yan Jheng-Tai. // Applied Physics Letters. - 2010. - Vol. 97, No. 11. - P. 111111-111111-3. ↑

J387. Patterson M. D. Note: Scanned multi-light-emitting-diode illumination for volumetric particle image velocimetry. / Patterson M. D., Wettlaufer J. S. // Review of Scientific Instruments. - 2010. - Vol. 81, No. 9. - P. 096101-096101-3. ↑

J388. Everdell N. L. Multispectral imaging of the ocular fundus using light emitting diode illumination. / Everdell N. L., Styles I. B., Calcagni A., Gibson J., Hebden J., Claridge E. // Review of Scientific Instruments. - 2010. - Vol. 81, No. 9. - P. 093706-093706-9. ↑

J389. Yilmaz Y.O. Multiwavelength Blue Light Source Based on MgO : PPLN SHG Using Vertically Stacked Grating-Coupled Surface-Emitting Lasers. / Yilmaz Y.O., Smolski V.O., Smolski O.V., Johnson E.G. // IEEE Photonics Technology Letters. - 2010. - Vol. 22, No. 23. - P. 1711-1713. ↑

J390. Luka G. The properties of tris (8-hydroxyquinoline) aluminum organic light emitting diode with undoped zinc oxide anode layer. / Luka G., Stakhira P., Cherpak V., Volynuk D., Hotra Z., Godlewski M., Guzewicz E., Witkowski B., Paszkowicz W., Kostruba A. // Journal of Applied Physics. - 2010. - Vol. 108, No. 6. - P. 064518-064518-4. ↑
















J391. Prabhakar Sanjay. Influence of electromechanical effects and wetting layers on band structures of AlN/GaN quantum dots and spin control. / Prabhakar Sanjay, Melnik Roderick. // Journal of Applied Physics. - 2010. - Vol. 108, No. 6. - P. 064330-064330-7. ↑

J392. Mehta M. An intentionally positioned (In,Ga)As quantum dot in a micron sized light emitting diode. / Mehta M., Reuter D., Wieck A. D., Michaelis de Vasconcellos S., Zrenner A., Meier C. // Applied Physics Letters. - 2010. - Vol. 97, No. 14. - P. 143101-143101-3. ↑

- J393.** Zhao Hongping. Analysis of InGaN-delta-InN quantum wells for light-emitting diodes. / Zhao Hongping, Liu Guangyu, Tansu Nelson. // Applied Physics Letters. - 2010. - Vol. 97, No. 13. - P. 131114-131114-3. ↑
- J394.** Dai Qi. Carrier recombination mechanisms and efficiency droop in GaInN/GaN light-emitting diodes. / Dai Qi, Shan Qifeng, Wang Jing, Chhaged Sameer, Cho Jaehee, Schubert E. Fred, Crawford Mary H., Koleske Daniel D., Kim Min-Ho, Park Yongjo. // Applied Physics Letters. - 2010. - Vol. 97, No. 13. - P. 133507-133507-3. ↑
- J395.** Oksanen Jani. Drooping as a simple characterization tool for extraction efficiency and optical losses in light emitting diodes. / Oksanen Jani, Tulkki Jukka. // Applied Physics Letters. - 2010. - Vol. 97, No. 13. - P. 131105-131105-3. ↑
- J396.** Chow W. W. Internal efficiency of InGaN light-emitting diodes: Beyond a quasiequilibrium model. / Chow W. W., Crawford M. H., Tsao J. Y., Kneissl M. // Applied Physics Letters. - 2010. - Vol. 97, No. 12. - P. 121105-121105-3. ↑
- J397.** Sharbati M.T. Near-Infrared Organic Light-Emitting Diodes Based on Donor-pi-Acceptor Oligomers. / Sharbati M.T., Panahi F., Gharavi A. // IEEE Photonics Technology Letters. - 2010. - Vol. 22, No. 22. - P. 1695-1697. ↑
- J398.** Sommer C. The Impact of Inhomogeneities in the Phosphor Distribution on the Device Performance of Phosphor-Converted High-Power White LED Light Sources. / Sommer C., Reil F., Krenn J.R., Hartmann P., Pachler P., Tasch S., Wenzl F.P. // Journal of Lightwave Technology. - 2010. - Vol. 28, No. 22. - P. 3226-3232. ↑
- J399.** Park Seoung-Hwan. Enhancement of light power for strain-compensated hybrid InGaN/InGaIn/MgZnO light-emitting diodes. / Park Seoung-Hwan, Moon Yong-Tae, Lee Jeong Sik, Kwon Ho Ki, Park Joong Seo, Ahn Doyeol. // Applied Physics Letters. - 2010. - Vol. 97, No. 12. - P. 121107-121107-3. ↑
- J400.** Setoguchi Yousuke. Suppression of roll-off characteristics of electroluminescence at high current densities in organic light emitting diodes by introducing reduced carrier injection barriers. / Setoguchi Yousuke, Adachi Chihaya. // Journal of Applied Physics. - 2010. - Vol. 108, No. 6. - P. 064516-064516-7. ↑
- J401.** Liao Chih-Teng. Improvement in output power of a 460 nm InGaN light-emitting diode using staggered quantum well. / Liao Chih-Teng, Tsai Miao-Chan, Liou Bo-Ting, Yen Sheng-Horng, Kuo Yen-Kuang. // Journal of Applied Physics. - 2010. - Vol. 108, No. 6. - P. 063107-063107-6. ↑
- J402.** Baik K. H. Light output enhancement of GaN-based flip-chip light-emitting diodes fabricated with SiO₂/TiO₂ distributed Bragg reflector coated on mesa sidewall. / Baik K. H., Min B. K., Kim J. Y., Kim H. K., Sone C., Park Y., Kim H. // Journal of Applied Physics. - 2010. - Vol. 108, No. 6. - P. 063105-063105-4. ↑
- J403.** Shih-Chang Hsia. Cost effective design and implementation of scanning-based LED backlight for LCD module. / Shih-Chang Hsia, Jung-Ming Kuo. // IEEE Transactions on Consumer Electronics. - 2010. - Vol. 56, No. 4. - P. 2037-2042. ↑
- J404.** Chia-Feng Lin. Blue Light-Emitting Diodes With an Embedded Native Gallium Oxide Pattern Structure. / Chia-Feng Lin, Kuei-Ting Chen, Kun-Pin Huang. // IEEE Electron Device Letters. - 2010. - Vol. 31, No. 12. - P. 1431-1433. ↑
- J405.** Kolbe Tim. Optical polarization characteristics of ultraviolet (In)(Al)GaN multiple quantum well light emitting diodes. / Kolbe Tim, Knauer Arne, Chua Chris, Yang Zhihong, Einfeldt Sven, Vogt Patrick, Johnson Noble M., Weyers Markus, Kneissl Michael. // Applied Physics Letters. - 2010. - Vol. 97, No. 17. - P. 171105-171105-3. ↑
- J406.** Yomogida Yohei. Green light emission from the edges of organic single-crystal transistors. / Yomogida Yohei, Takenobu Taishi, Shimotani Hidekazu, Sawabe Kosuke, Bisri Satria Zulkarnaen, Yamao Takeshi, Hotta Shu, Iwasa Yoshihiro. // Applied Physics Letters. - 2010. - Vol. 97, No. 17. - P. 173301-173301-3. ↑
- J407.** Pandey J. A Fully Integrated RF-Powered Contact Lens With a Single Element Display. / Pandey J., Yu-Te Liao, Lingley A., Mirjalili R., Parviz B., Otis B. // IEEE Transactions on Biomedical Circuits and Systems. - 2010. - Vol. 4, No. 6. - P. 454-461. ↑

- J408.** Soh C. B. Generation of amber III-nitride based light emitting diodes by indium rich InGaN quantum dots with InGaN wetting layer and AlN encapsulation layer. / Soh C. B., Liu W., Chua S. J., Ang S. S., Tan Rayson J. N., Chow S. Y. // Journal of Applied Physics. - 2010. - Vol. 108, No. 9. - P. 093501-093501-5. ↑
- J409.** Wang C. H. Efficiency droop alleviation in InGaN/GaN light-emitting diodes by graded-thickness multiple quantum wells. / Wang C. H., Chang S. P., Chang W. T., Li J. C., Lu Y. S., Li Z. Y., Yang H. C., Kuo H. C., Lu T. C., Wang S. C. // Applied Physics Letters. - 2010. - Vol. 97, No. 18. - P. 181101-181101-3. ↑
- J410.** Guo Zhen. The ultralow driven current ultraviolet-blue light-emitting diode based on n-ZnO nanowires/i-polymer/p-GaN heterojunction. / Guo Zhen, Zhang Hong, Zhao Dongxu, Liu Yichun, Yao Bin, Li Binghui, Zhang Zhenzhong, Shen Dezhen. // Applied Physics Letters. - 2010. - Vol. 97, No. 17. - P. 173508-173508-3. ↑
- J411.** Park Byoungchoo. Electrical annealing for flexible organic light-emitting diodes having poly(3,4-ethylenedioxythiophene):poly(styrene sulfonate) anodes. / Park Byoungchoo, Park Chan Hyuk, Yim Yunchan, Park Jongwoon. // Journal of Applied Physics. - 2010. - Vol. 108, No. 8. - P. 084508-084508-6. ↑
- J412.** Wang Zhaokui. Competitive emission process in mixed single layer top-emission organic light emitting device with reduced efficiency roll-off. / Wang Zhaokui, Lou Yanhui, Naka Shigeki, Okada Hiroyuki. // Applied Physics Letters. - 2010. - Vol. 97, No. 20. - P. 203302-203302-3. ↑
- J413.** Jiang Z. Y. Stress-induced current and luminescence modulations in an organic light-emitting device. / Jiang Z. Y., Cao X. A. // Applied Physics Letters. - 2010. - Vol. 97, No. 20. - P. 203304-203304-3. ↑
- J414.** Kim Jeongho. Organic light emitting diodes using NaCl:N,N'-bis(naphthalene-1-yl)-N,N'-bis(phenyl)benzidine composite as a hole injection buffer layer. / Kim Jeongho, Kim Myungseop, Won Kim Jeong, Yi Yeonjin, Kang Heon. // Journal of Applied Physics. - 2010. - Vol. 108, No. 10. - P. 103703-103703-5. ↑
- J415.** Lo H.M. AlGaInP LEDs Prepared by Contact-Transferred and Mask-Embedded Lithography. / Lo H.M., Hsieh Y.T., Shei S.C., Lee Y.C., Zeng X.F., Weng W.Y., Lin N.M., Chang S.J. // IEEE Journal of Quantum Electronics. - 2010. - Vol. 46, No. 12. - P. 1834-1839. ↑
- J416.** Steenbergen E. H. Optically-addressed two-terminal multicolor photodetector. / Steenbergen E. H., DiNezza M. J., Dettlaff W. H. G., Lim S. H., Zhang Y.-H. // Applied Physics Letters. - 2010. - Vol. 97, No. 16. - P. 161111-161111-3. ↑
- J417.** Dang Po-Yuan. Optical polarization anisotropy of tensile strained InGaN/AlInN quantum wells for TM mode lasers. / Dang Po-Yuan, Wu Yuh-Renn. // Journal of Applied Physics. - 2010. - Vol. 108, No. 8. - P. 083108-083108-4. ↑
- J418.** Zhang Y. Q. Concentration quenching of electroluminescence in neat Ir (ppy)₃ organic light-emitting diodes. / Zhang Y. Q., Zhong G. Y., Cao X. A. // Journal of Applied Physics. - 2010. - Vol. 108, No. 8. - P. 083107-083107-5. ↑
- J419.** Pinos A. Optical studies of degradation of AlGaIn quantum well based deep ultraviolet light emitting diodes. / Pinos A., Marcinkevicius S., Yang J., Gaska R., Shatalov M., Shur M. S. // Journal of Applied Physics. - 2010. - Vol. 108, No. 9. - P. 093113-093113-6. ↑
- J420.** Bera D. Optimization of the Yellow Phosphor Concentration and Layer Thickness for Down-Conversion of Blue to White Light. / Bera D., Maslov S., Lei Qian, Jae Soo Yoo, Holloway P.H. // Journal of Display Technology. - 2010. - Vol. 6, No. 12. - P. 645-651. ↑
- J421.** Hofmann Simone. Top-emitting organic light-emitting diodes: Influence of cavity design. / Hofmann Simone, Thomschke Michael, Freitag Patricia, Furno Mauro, Lussem Bjorn, Leo Karl. // Applied Physics Letters. - 2010. - Vol. 97, No. 25. - P. 253308-253308-3. ↑
- J422.** Nazeran Motlagh A.A. Minimal Viewing Distance Calculation in LED Display Panels. / Nazeran Motlagh A.A., Hashemi B.M.R. // Journal of Display Technology. - 2010. - Vol. 6, No. 12. - P. 620-624. ↑
- J423.** David Aurelien. Droop in III-nitrides: Comparison of bulk and injection contributions. / David Aurelien, Gardner Nathan F. // Applied Physics Letters. - 2010. - Vol. 97, No. 19. - P. 193508-193508-3. ↑
- J424.** Soon-Kwang Hong. New Pixel Design on Emitting Area for High Resolution Active-Matrix Organic Light-

- Emitting Diode Displays. / Soon-Kwang Hong, Jea-Ho Sim, In-Gyo Seo, Keun-Choul Kim, Sung-II Bae, Hee-Young Lee, Nam-Yang Lee, Jin Jang. // Journal of Display Technology. - 2010. - Vol. 6, No. 12. - P. 601-606. ↑
- J425. Pappas I. Polycrystalline Silicon TFTs Threshold Voltage Compensated Bias Current Generator for Analog Circuit Design. / Pappas I., Siskos S., Dimitriadis C.A. // Journal of Display Technology. - 2010. - Vol. 6, No. 12. - P. 633-638. ↑
- J426. Jicai Zhang. Study on the Electron Overflow in 264 nm AlGaIn Light-Emitting Diodes. / Jicai Zhang, Sakai Y., Egawa T. // IEEE Journal of Quantum Electronics. - 2010. - Vol. 46, No. 12. - P. 1854-1859. ↑
- J427. Park Byoungchoo. Solution processable single layer organic light-emitting devices with a single small molecular ionic iridium compound. / Park Byoungchoo, Huh Yoon Ho, Jeon Hong Goo, Park Chan Huk, Kang Tae Kyung, Kim Byeong Hyo, Park Jongwoon. // Journal of Applied Physics. - 2010. - Vol. 108, No. 9. - P. 094506-094506-6. ↑
- J428. Rakhshani A. E. Optoelectronic properties of p-n and p-i-n heterojunction devices prepared by electrodeposition of n-ZnO on p-Si. Journal of Applied Physics. - 2010. - Vol. 108, No. 9. - P. 094502-094502-5. ↑
- J429. Lin Ray-Ming. Effect of an asymmetry AlGaIn barrier on efficiency droop in wide-well InGaIn double-heterostructure light-emitting diodes. / Lin Ray-Ming, Lai Mu-Jen, Chang Liann-Be, Huang Chou-Hsiung. // Applied Physics Letters. - 2010. - Vol. 97, No. 18. - P. 181108-181108-3. ↑
- J430. McGovern B. A New Individually Addressable Micro-LED Array for Photogenetic Neural Stimulation. / McGovern B., Palmini R.B., Grossman N., Drakakis E., Poher V., Neil M.A.A., Degenaar P. // IEEE Transactions on Biomedical Circuits and Systems. - 2010. - Vol. 4, No. 6. - P. 469-476. ↑
- J431. El Basaty A. B. Optical second harmonic generation at heterojunction interfaces of a molybdenum trioxide layer and an organic layer. / El Basaty A. B., Miyauchi Y., Mizutani G., Matsushima T., Murata H. // Applied Physics Letters. - 2010. - Vol. 97, No. 19. - P. 193302-193302-3. ↑
- J432. Nakamura Kazuki. Color-tunable multilayer organic light emitting diode composed of DNA complex and tris(8-hydroxyquinolino)aluminum. / Nakamura Kazuki, Ishikawa Takayuki, Nishioka Daisuke, Ushikubo Takahiro, Kobayashi Norihisa. // Applied Physics Letters. - 2010. - Vol. 97, No. 19. - P. 193301-193301-3. ↑
- J433. Yang H. Y. Electroluminescence from AlN nanowires grown on p-SiC substrate. / Yang H. Y., Yu S. F., Hui Y. Y., Lau S. P. // Applied Physics Letters. - 2010. - Vol. 97, No. 19. - P. 191105-191105-3. ↑
- J434. Arik M. Development of a High-Lumen Solid State Down Light Application. / Arik M., Sharma R., Jackson J., Prabhakaran S., Seeley C., Utturkar Y., Weaver S., Kuenzler G., Bongtae Han. // IEEE Transactions on Components and Packaging Technologies. - 2010. - Vol. 33, No. 4. - P. 668-679. ↑
- J435. Meerheim Rico. Quantification of energy loss mechanisms in organic light-emitting diodes. / Meerheim Rico, Furno Mauro, Hofmann Simone, Lussem Bjorn, Leo Karl. // Applied Physics Letters. - 2010. - Vol. 97, No. 25. - P. 253305-253305-3. ↑
- J436. Shen Kun-Ching. Effects of the intermediate SiO₂ layer on polarized output of a light-emitting diode with surface plasmon coupling. / Shen Kun-Ching, Liao Che-Hao, Yu Zan-Yao, Wang Jyh-Yang, Lin Cheng-Hung, Kiang Yean-Woei, Yang C. C. // Journal of Applied Physics. - 2010. - Vol. 108, No. 11. - P. 113101-113101-8. ↑
- J437. Yan L. J. Polarized edge emission from GaN-based light-emitting diodes sandwiched by dielectric/metal hybrid reflectors. / Yan L. J., Sheu J. K., Huang F. W., Lee M. L. // Journal of Applied Physics. - 2010. - Vol. 108, No. 11. - P. 113102-113102-5. ↑
- J438. Yang J. P. Light out-coupling enhancement of organic light-emitting devices with microlens array. / Yang J. P., Bao Q. Y., Xu Z. Q., Li Y. Q., Tang J. X., Shen S. // Applied Physics Letters. - 2010. - Vol. 97, No. 22. - P. 223303-223303-3. ↑
- J439. Lee Sung-Nam. Thermal stability of Si-doped InGaIn multiple-quantum wells for high efficiency light emitting diodes. / Lee Sung-Nam, Kim Jihoon, Kim Kyoung-Kook, Kim Hyunsoo, Kim Han-Ki. // Journal of Applied Physics. - 2010. - Vol. 108, No. 10. - P. 102813-102813-4. ↑

- J440.** Chang S. P. Characteristics of efficiency droop in GaN-based light emitting diodes with an insertion layer between the multiple quantum wells and n -GaN layer. / Chang S. P., Wang C. H., Chiu C. H., Li J. C., Lu Y. S., Li Z. Y., Yang H. C., Kuo H. C., Lu T. C., Wang S. C. // Applied Physics Letters. - 2010. - Vol. 97, No. 25. - P. 251114-251114-3. 
- J441.** Zhou D. Y. Efficiency dependence on alkali metal compound/Al bilayer cathode in organic light-emitting diodes. / Zhou D. Y., Cai S. D., Gu W., Liao L. S., Lee S. T. // Applied Physics Letters. - 2010. - Vol. 97, No. 22. - P. 223302-223302-3. 
- J442.** Alarcon-Llado Esther. Temperature rise in InGaN/GaN vertical light emitting diode on copper transferred from silicon probed by Raman scattering. / Alarcon-Llado Esther, Bin-Dolmanan Surani, Lin Vivian Kai Xin, Teo Siew Lang, Dadgar Armin, Krost Alois, Tripathy Sudhiranjan. // Journal of Applied Physics. - 2010. - Vol. 108, No. 11. - P. 114501-114501-5. 
- J443.** Ding B. F. Magnetic field effects on the electroluminescence of organic light emitting devices: A tool to indicate the carrier mobility. / Ding B. F., Yao Y., Sun Z. Y., Wu C. Q., Gao X. D., Wang Z. J., Ding X. M., Choy W. C. H., Hou X. Y. // Applied Physics Letters. - 2010. - Vol. 97, No. 16. - P. 163302-163302-3. 
- J444.** Vuc. 513 Mbit/s Visible Light Communications Link Based on DMT-Modulation of a White LED. / Vuc,ic, J., Kottke C., Nerreter S., Langer K., Walewski J.W. // Journal of Lightwave Technology. - 2010. - Vol. 28, No. 24. - P. 3512-3518. 
- J445.** Lu I-Lin. A study of the role of dislocation density, indium composition on the radiative efficiency in InGaN/GaN polar and nonpolar light-emitting diodes using drift-diffusion coupled with a Monte Carlo method. / Lu I-Lin, Wu Yuh-Renn, Singh Jasprit. // Journal of Applied Physics. - 2010. - Vol. 108, No. 12. - P. 124508-124508-6. 
- J446.** Hyunsuk Cho. A local dimming algorithm for low power LCD TVs using edge-type LED backlight. / Hyunsuk Cho, Oh-Kyong Kwon. // IEEE Transactions on Consumer Electronics. - 2010. - Vol. 56, No. 4. - P. 2054-2060. 
- J447.** Meneghini M. Degradation of InGaN-based laser diodes analyzed by means of electrical and optical measurements. / Meneghini M., Trivellini N., Orita K., Takigawa S., Tanaka T., Ueda D., Meneghesso G., Zanoni E. // Applied Physics Letters. - 2010. - Vol. 97, No. 26. - P. 263501-263501-3. 
- J448.** Yang L. Correlations for predicting the surface wettability for organic light-emitting-diode patterns by x-ray photoelectron spectroscopy analysis. / Yang L., Svarnas P., Shard A. G., Bradley J. W., Seah M. P. // Journal of Applied Physics. - 2010. - Vol. 108, No. 11. - P. 114901-114901-8. 
- J449.** Ran G. Z. Experimental observation of polarized electroluminescence from edge-emission organic light emitting devices. / Ran G. Z., Jiang D. F., Kan Q., Chen H. D. // Applied Physics Letters. - 2010. - Vol. 97, No. 23. - P. 233304-233304-3. 
- J450.** Ming-Yi Tsai. Thermal Resistance and Reliability of High-Power LED Packages Under WHTOL and Thermal Shock Tests. / Ming-Yi Tsai, Chun-Hung Chen, Wan-Lin Tsai. // IEEE Transactions on Components and Packaging Technologies. - 2010. - Vol. 33, No. 4. - P. 738-746. 
- J451.** Yi-Hua Liu. A novel sequential-color RGB-LED backlight driving system with local dimming control and dynamic bus voltage regulation. / Yi-Hua Liu, Zong-Zhen Yang, Shun-Chung Wang. // IEEE Transactions on Consumer Electronics. - 2010. - Vol. 56, No. 4. - P. 2445-2452. 
- J452.** Rae B.R. A Vertically Integrated CMOS Microsystem for Time-Resolved Fluorescence Analysis. / Rae B.R., Jingbin Yang, McKendry J., Zheng Gong, Renshaw D., Girkin J.M., Erdan Gu, Dawson M.D., Henderson R.K. // IEEE Transactions on Biomedical Circuits and Systems. - 2010. - Vol. 4, No. 6. - P. 437-444. 
- J453.** Kuramoto M. Die Bonding for a Nitride Light-Emitting Diode by Low-Temperature Sintering of Micrometer Size Silver Particles. / Kuramoto M., Ogawa S., Niwa M., Keun-Soo Kim, Suganuma K. // IEEE Transactions on Components and Packaging Technologies. - 2010. - Vol. 33, No. 4. - P. 801-808. 
- J454.** Wang C. H. Hole injection and efficiency droop improvement in InGaN/GaN light-emitting diodes by band-engineered electron blocking layer. / Wang C. H., Ke C. C., Lee C. Y., Chang S. P., Chang W. T., Li J. C., Li Z. Y., Yang H. C., Kuo H. C., Lu T. C., Wang S. C. // Applied Physics Letters. - 2010. - Vol. 97, No. 26. - P. 

261103-261103-3. ↑

J455. Wei-Hao Chi. Analysis of Thermal and Luminous Performance of MR-16 LED Lighting Module. / Wei-Hao Chi, Tsung-Lin Chou, Cheng-Nan Han, Shin-Yueh Yang, Kuo-Ning Chiang. // IEEE Transactions on Components and Packaging Technologies. - 2010. - Vol. 33, No. 4. - P. 713-721. ↑

J456. Bongtae Han. Coupled Thermal and Thermo-Mechanical Design Assessment of High Power Light Emitting Diode. / Bongtae Han, Changsoo Jang, Bar-Cohen A., Bongmin Song. // IEEE Transactions on Components and Packaging Technologies. - 2010. - Vol. 33, No. 4. - P. 688-697. ↑

J457. Wang Jiaying. Understanding efficiency droop effect in InGaN/GaN multiple-quantum-well blue light-emitting diodes with different degree of carrier localization. / Wang Jiaying, Wang Lai, Zhao Wei, Hao Zhibiao, Luo Yi. // Applied Physics Letters. - 2010. - Vol. 97, No. 20. - P. 201112-201112-3. ↑

J458. Wang Po-Sheng. Enhancement of current injection in inverted organic light emitting diodes with thermal annealing. / Wang Po-Sheng, Wu I.-Wen, Wu Chih-I. // Journal of Applied Physics. - 2010. - Vol. 108, No. 10. - P. 103714-103714-4. ↑

J459. Lorke M. Influence of carrier dynamics on the modulation bandwidth of quantum-dot based nanocavity devices. / Lorke M., Nielsen T. R., Mørk J. // Applied Physics Letters. - 2010. - Vol. 97, No. 21. - P. 211106-211106-3. ↑

J460. Kim Nam-Soo. Future direction of direct writing. / Kim Nam-Soo, Han Kenneth N. // Journal of Applied Physics. - 2010. - Vol. 108, No. 10. - P. 102801-102801-6. ↑

J461. Malyutenko V. K. Silicon emitter for shortwave infrared (1.6-3 μm) band by light down-conversion. / Malyutenko V. K., Bogatyrenko V. V., Tykhonov A. M. // Applied Physics Letters. - 2010. - Vol. 97, No. 21. - P. 211104-211104-3. ↑

J462. Harris M. 3-D without four eyes. IEEE Spectrum. - 2010. - Vol. 47, No. 12. - P. 50-56. ↑

J463. Li Xiao. Reduced efficiency roll-off in electrophosphorescent devices by a short-living rhenium emitter with well-matched energy levels. / Li Xiao, Zhang Dongyu, Chi Haijun, Xiao Guoyong, Dong Yan, Wu Shuanghong, Su Zisheng, Zhang Zhiqiang, Lei Peng, Hu Zhizhi, Li Wenlian. // Applied Physics Letters. - 2010. - Vol. 97, No. 26. - P. 263303-263303-3. ↑

J464. Zhang Y. Q. Electroluminescence of green CdSe/ZnS quantum dots enhanced by harvesting excitons from phosphorescent molecules. / Zhang Y. Q., Cao X. A. // Applied Physics Letters. - 2010. - Vol. 97, No. 25. - P. 253115-253115-3. ↑

J465. Qiao Xianfeng. Controlling charge balance and exciton recombination by bipolar host in single-layer organic light-emitting diodes. / Qiao Xianfeng, Tao Youtian, Wang Qiang, Ma Dongge, Yang Chuluo, Wang Lixiang, Qin Jingui, Wang Fosong. // Journal of Applied Physics. - 2010. - Vol. 108, No. 3. - P. 034508-034508-8. ↑

J466. Young Chul Shin. Effects of Nanometer-Scale Photonic Crystal Structures on the Light Extraction From GaN Light-Emitting Diodes. / Young Chul Shin, Dong Ho Kim, Dong Ju Chae, Ji Won Yang, Jae In Shim, Joong Mok Park, Kai-Ming Ho, Constant K., Han Youl Ryu, Tae Geun Kim. // IEEE Journal of Quantum Electronics. - 2010. - Vol. 46, No. 9. - P. 1375-1380. ↑

J467. Epstein A. The Impact of Spectral and Spatial Exciton Distributions on Optical Emission From Thin-Film Weak-Microcavity Organic Light-Emitting Diodes. / Epstein A., Tessler N., Einziger P.D. // IEEE Journal of Quantum Electronics. - 2010. - Vol. 46, No. 9. - P. 1388-1395. ↑

J468. Dalui S. Light Output Enhancement of GaN-Based Light-Emitting Diodes Using ZnO Nanorod Arrays Produced by Aqueous Solution Growth Technique. / Dalui S., Lin C.-C., Lee H.-Y., Chao C.-H., Lee C.-T. // IEEE Photonics Technology Letters. - 2010. - Vol. 22, No. 16. - P. 1220-1222. ↑

J469. Eun Hong Kim. InGaN/GaN White Light-Emitting Diodes Embedded With Europium Silicate Thin Film Phosphor. / Eun Hong Kim, Kyoung Chan Kim, Dong Ho Kim, Jong Hyeob Baek, Tae Geun Kim. // IEEE Journal of Quantum Electronics. - 2010. - Vol. 46, No. 9. - P. 1381-1387. ↑

↑

- J470.** Lai Chun-Feng. Highly-directional emission patterns based on near single guided mode extraction from GaN-based ultrathin microcavity light-emitting diodes with photonic crystals. / Lai Chun-Feng, Kuo Hao-Chung, Yu Peichen, Lu Tien-Chang, Chao Chia-Hsin, Yen Hsi-Hsuan, Yeh Wen-Yung. // Applied Physics Letters. - 2010. - Vol. 97, No. 1. - P. 013108-013108-3. ↑
- J471.** Seifert Ruben. Comparison of ultraviolet- and charge-induced degradation phenomena in blue fluorescent organic light emitting diodes. / Seifert Ruben, Scholz Sebastian, Lussem Bjorn, Leo Karl. // Applied Physics Letters. - 2010. - Vol. 97, No. 1. - P. 013308-013308-3. ↑
- J472.** Ni X. InGaN staircase electron injector for reduction of electron overflow in InGaN light emitting diodes. / Ni X., Li X., Lee J., Liu S., Avrutin V., Ozgur U., Morkoc H., Matulionis A., Paskova T., Mulholland G., Evans K. R. // Applied Physics Letters. - 2010. - Vol. 97, No. 3. - P. 031110-031110-3. ↑
- J473.** Chopra Neetu. High efficiency and low roll-off blue phosphorescent organic light-emitting devices using mixed host architecture. / Chopra Neetu, Swensen James S., Polikarpov Evgueni, Cosimbescu Lelia, So Franky, Padmaperuma Asanga B. // Applied Physics Letters. - 2010. - Vol. 97, No. 3. - P. 033304-033304-3. ↑
- J474.** Uno M. High-power and high-speed organic three-dimensional transistors with submicrometer channels. / Uno M., Hirose Y., Uemura T., Takimiya K., Nakazawa Y., Takeya J. // Applied Physics Letters. - 2010. - Vol. 97, No. 1. - P. 013301-013301-3. ↑
- J475.** Nakahara K. Nitrogen doped Mg x Zn 1-x O /ZnO single heterostructure ultraviolet light-emitting diodes on ZnO substrates. / Nakahara K., Akasaka S., Yuji H., Tamura K., Fujii T., Nishimoto Y., Takamizu D., Sasaki A., Tanabe T., Takasu H., Amaike H., Onuma T., Chichibu S. F., Tsukazaki A., Ohtomo A., Kawasaki M. // Applied Physics Letters. - 2010. - Vol. 97, No. 1. - P. 013501-013501-3. ↑
- J476.** Lin Gong-Ru. Comparison on the electroluminescence of Si-rich SiN x and SiO x based light-emitting diodes. / Lin Gong-Ru, Pai Yi-Hao, Lin Cheng-Tao, Chen Chun-Chieh. // Applied Physics Letters. - 2010. - Vol. 96, No. 26. - P. 263514-263514-3. ↑
- J477.** Ling Bo. Color tunable light-emitting diodes based on p+ -Si /p-CuAlO 2 /n-ZnO nanorod array heterojunctions. / Ling Bo, Zhao Jun Liang, Sun Xiao Wei, Tan Swee Tiam, Kyaw Aung Ko Ko, Divayana Yoga, Dong Zhi Li. // Applied Physics Letters. - 2010. - Vol. 97, No. 1. - P. 013101-013101-3. ↑
- J478.** Qiang Wang. Manipulating the Microcavity Structure for Highly Efficient Inverted Top-Emitting Organic Light-Emitting Diodes: Simulation and Experiment. / Qiang Wang, Zhaoqi Deng, Jiangshan Chen, Dongge Ma. // IEEE Transactions on Electron Devices. - 2010. - Vol. 57, No. 9. - P. 2221-2226. ↑
- J479.** Kimura M. Degradation Evaluation of -IGZO TFTs for Application to AM-OLEDs. / Kimura M., Imai S. // IEEE Electron Device Letters. - 2010. - Vol. 31, No. 9. - P. 963-965. ↑
- J480.** Wong A. K. Y. A 0.5-Hz High-Pass Cutoff Dual-Loop Transimpedance Amplifier for Wearable NIR Sensing Device. / Wong A. K. Y., Leung K. N., Pun K.-P., Zhang Y.-T. // IEEE Transactions on Circuits and Systems II: Express Briefs. - 2010. - Vol. 57, No. 7. - P. 531-535. ↑
- J481.** Ray-Hua Horng. Optimized Thermal Management From a Chip to a Heat Sink for High-Power GaN-Based Light-Emitting Diodes. / Ray-Hua Horng, Jhih-Sin Hong, Yu-Li Tsai, Dong-Sing Wu, Chih-Ming Chen, Chia-Ju Chen. // IEEE Transactions on Electron Devices. - 2010. - Vol. 57, No. 9. - P. 2203-2207. ↑
- J482.** Chun-Li Chu. Pseudo Zero-Dimension Dimming for Power Reduction in Field Sequential Color Liquid Crystal Display Systems. / Chun-Li Chu, Ta-Liang Chiu, Ke-Horng Chen. // Journal of Display Technology. - 2010. - Vol. 6, No. 8. - P. 323-331. ↑
- J483.** Long Christopher M. Lateral current injection photonic crystal membrane light emitting diodes. / Long Christopher M., Giannopoulos Antonios V., Choquette Kent D. // Journal of Vacuum Science & Technology B: Microelectronics and Nanometer Structures. - 2010. - Vol. 28, No. 2. - P. 359-364. ↑
- J484.** Yi-Jung Liu. Investigation of the Electrostatic Discharge Performance of GaN-Based Light-Emitting Diodes With Naturally Textured p-GaN Contact Layers Grown on Miscut Sapphire Substrates. / Yi-Jung Liu, Der-Feng Guo, Li-Yang Chen, Tsung-Han Tsai, Chien-Chang Huang, Tai-You Chen, Chi-Hsiang Hsu, Wen-Chau Liu. // IEEE Transactions on Electron Devices. - 2010. - Vol. 57, No. 9. - P. 2155-2162. ↑

- J485.** Hongming Yang. Enhanced Illumination Sensing Using Multiple Harmonics for LED Lighting Systems. / Hongming Yang, Schenk T.C.W., Bergmans J.W.M., Pandharipande A. // IEEE Transactions on Signal Processing. - 2010. - Vol. 58, No. 11. - P. 5508-5522. ↑
- J486.** de Kersauson M. Direct and indirect band gap room temperature electroluminescence of Ge diodes. / de Kersauson M., Jakomin R., El Kurdi M., Beaudoin G., Zerounian N., Aniel F., Sauvage S., Sagnes I., Boucaud P. // Journal of Applied Physics. - 2010. - Vol. 108, No. 2. - P. 023105-023105-4. ↑
- J487.** Akande Wali O. Thermally induced surface instabilities in polymer light emitting diodes. / Akande Wali O., Akogwu Onobu, Tong Tiffany, Soboyejo Wole. // Journal of Applied Physics. - 2010. - Vol. 108, No. 2. - P. 023510-023510-6. ↑
- J488.** Mak G. Y. Precision laser micromachining of trenches in GaN on sapphire. / Mak G. Y., Lam E. Y., Choi H. W. // Journal of Vacuum Science & Technology B: Microelectronics and Nanometer Structures. - 2010. - Vol. 28, No. 2. - P. 380-385. ↑
- J489.** Fraser E. D. Efficient electron spin injection in MnAs-based spin-light-emitting-diodes up to room temperature. / Fraser E. D., Hegde S., Schweidenback L., Russ A. H., Petrou A., Luo H., Kioseoglou G. // Applied Physics Letters. - 2010. - Vol. 97, No. 4. - P. 041103-041103-3. ↑
- J490.** Kao Chien-Chih. The aspect ratio effects on the performances of GaN-based light-emitting diodes with nanopatterned sapphire substrates. / Kao Chien-Chih, Su Yan-Kuin, Lin Chuang-Liang, Chen Jian-Jhong. // Applied Physics Letters. - 2010. - Vol. 97, No. 2. - P. 023111-023111-3. ↑
- J491.** Wu Jiun-Shian. Polyethyleneoxide/sodium dodecyl sulfate as hole-blocking/electron-transporting layer for high-performance blue polymer light-emitting diode with oxygen- and moisture-stable aluminum cathode. / Wu Jiun-Shian, Lu Hsin-Hung, Hung Wei-Chun, Lin Guan-Hong, Chen Show-An. // Applied Physics Letters. - 2010. - Vol. 97, No. 2. - P. 023304-023304-3. ↑
- J492.** Holc Katarzyna. Temperature dependence of superluminescence in InGaN-based superluminescent light emitting diode structures. / Holc Katarzyna, Marona Ł., ucja, Czernecki Robert, Bockowski Michał., Suski Tadeusz, Najda Stephen, Perlin Piotr. // Journal of Applied Physics. - 2010. - Vol. 108, No. 1. - P. 013110-013110-4. ↑
- J493.** David Aurelien. Influence of polarization fields on carrier lifetime and recombination rates in InGaN-based light-emitting diodes. / David Aurelien, Grundmann Michael J. // Applied Physics Letters. - 2010. - Vol. 97, No. 3. - P. 033501-033501-3. ↑
- J494.** Son Jun Ho. Numerical analysis of efficiency droop induced by piezoelectric polarization in InGaN/GaN light-emitting diodes. / Son Jun Ho, Lee Jong-Lam. // Applied Physics Letters. - 2010. - Vol. 97, No. 3. - P. 032109-032109-3. ↑
- J495.** Miin-Jang Chen. Structure and Ultraviolet Electroluminescence of Nanocomposite/ -GaN Heterostructure Light-Emitting Diodes. / Miin-Jang Chen, Ying-Tsang Shih, Mong-Kai Wu, Hsing-Chao Chen, Hung-Ling Tsai, Wei-Chih Li, Jer-Ren Yang, Hon Kuan, Shiojiri M. // IEEE Transactions on Electron Devices. - 2010. - Vol. 57, No. 9. - P. 2195-2202. ↑
- J496.** An Min-Jun. Air stable, ambipolar organic transistors and inverters based upon a heterojunction structure of pentacene on N,N' -ditridecylperylene-3,4,9,10-tetracarboxylic di-imide. / An Min-Jun, Seo Hoon-Seok, Zhang Ying, Oh Jeong-Do, Choi Jong-Ho. // Applied Physics Letters. - 2010. - Vol. 97, No. 2. - P. 023506-023506-3. ↑
- J497.** Kim Kyu Sang. Investigation of dominant effect on efficiency droop in InGaN light emitting device. / Kim Kyu Sang, Kim Jin Ha, Park Young Min, Jung Su Jin, Park Yong Jo, Cho S. N. // Applied Physics Letters. - 2010. - Vol. 97, No. 3. - P. 031113-031113-3. ↑
- J498.** Lee M.H. High-Performance Poly-Si TFTs Using Ultrathin Gate Dielectric for Monolithic Three-Dimensional Integrated Circuits and System on Glass Applications. / Lee M.H., Wu S.L., Yang M.-J., Chen K.-J., Luo G.-L., Lee L.-S., Kao M.-J. // IEEE Electron Device Letters. - 2010. - Vol. 31, No. 8. - P. 824-826. ↑
- J499.** Wei-Chi Lee. Enhanced Light Output of GaN-Based Vertical-Structured Light-Emitting Diodes With Two-Step Surface Roughening Using KrF Laser and Chemical Wet Etching. / Wei-Chi Lee, Shui-Jinn Wang, Kai-Ming Uang, Tron-Min Chen, Der-Ming Kuo, Pei-Ren Wang, Po-Hong Wang. // IEEE Photonics Technology Letters. -

2010. - Vol. 22, No. 17. - P. 1318-1320. ↑

J500. Kim Ja-Yeon. Enhancement of light extraction from GaN-based green light-emitting diodes using selective area photonic crystal. / Kim Ja-Yeon, Kwon Min-Ki, Park Seong-Ju, Kim Sang Hoon, Lee Ki-Dong. // Applied Physics Letters. - 2010. - Vol. 96, No. 25. - P. 251103-251103-3. ↑

J501. Wenbin Xu. Modeling of Tunable Luminescence in Multiple Rare Earth Co-Doped Glasses. / Wenbin Xu, Chun Jiang. // Journal of Display Technology. - 2010. - Vol. 6, No. 8. - P. 298-305. ↑

J502. Deepak. Evidence of electron conductivity in polysilanes and its implications in design of ultraviolet emitting devices. / Deepak, Banerjee Niladri, Seki Shu. // Journal of Applied Physics. - 2010. - Vol. 107, No. 12. - P. 124513-124513-9. ↑

J503. Sang-Mook Kim. Effects of Patterned Sapphire Substrates on Piezoelectric Field in Blue-Emitting InGaN Multiple Quantum Wells. / Sang-Mook Kim, Hwa Sub Oh, Jong Hyeob Baek, Kwang-Ho Lee, Gun Young Jung, Jae-Ho Song, Ho-Jong Kim, Byung-Jun Ahn, Dong Yanqun, Jung-Hoon Song. // IEEE Electron Device Letters. - 2010. - Vol. 31, No. 8. - P. 842-844. ↑

J504. Nasibov H. Performance Analysis of the CCD Pixel Binning Option in Particle-Image Velocimetry Measurements. / Nasibov H., Kholmatov A., Akselli B., Nasibov A., Baytaroglu S. // IEEE/ASME Transactions on Mechatronics. - 2010. - Vol. 15, No. 4. - P. 527-540. ↑

J505. Elliott Stella N. Time resolved studies of catastrophic optical mirror damage in red-emitting laser diodes. / Elliott Stella N., Snowton Peter M., Ziegler Mathias, Tomm Jens W., Zeimer Ute. // Journal of Applied Physics. - 2010. - Vol. 107, No. 12. - P. 123116-123116-7. ↑

J506. Juhn-Suk Yoo. Highly Flexible AM-OLED Display With Integrated Gate Driver Using Amorphous Silicon TFT on Ultrathin Metal Foil. / Juhn-Suk Yoo, Sang-Hoon Jung, Yong-Chul Kim, Seung-Chan Byun, Jong-Moo Kim, Nack-Bong Choi, Soo-Young Yoon, Chang-Dong Kim, Yong-Kee Hwang, In-Jae Chung. // Journal of Display Technology. - 2010. - Vol. 6, No. 11. - P. 565-570. ↑

J507. Chih-Chien Lin. GaN-Based Resonant-Cavity Light-Emitting Diodes With Top and Bottom Dielectric Distributed Bragg Reflectors. / Chih-Chien Lin, Ching-Ting Lee. // IEEE Photonics Technology Letters. - 2010. - Vol. 22, No. 17. - P. 1291-1293. ↑

J508. Park Ji Sun. Efficient hybrid organic-inorganic light emitting diodes with self-assembled dipole molecule deposited metal oxides. / Park Ji Sun, Lee Bo Ram, Lee Ju Min, Kim Ji-Seon, Kim Sang Ouk, Song Myoung Hoon. // Applied Physics Letters. - 2010. - Vol. 96, No. 24. - P. 243306-243306-3. ↑

J509. Ya-Ju Lee. Stable Temperature Characteristics and Suppression of Efficiency Droop in InGaN Green Light-Emitting Diodes Using Pre-TMIn Flow Treatment. / Ya-Ju Lee, Yi-Ching Chen, Chia-Jung Lee, Chun-Mao Cheng, Shih-Wei Chen, Tien-Chang Lu. // IEEE Photonics Technology Letters. - 2010. - Vol. 22, No. 17. - P. 1279-1281. ↑

J510. Benor Amare. Energy barrier, charge carrier balance, and performance improvement in organic light-emitting diodes. / Benor Amare, Takizawa Shin-ya, Perez-Bolivar C., Anzenbacher Pavel. // Applied Physics Letters. - 2010. - Vol. 96, No. 24. - P. 243310-243310-3. ↑

J511. Latini Gianluca. Enhanced luminescence properties of highly threaded conjugated polyelectrolytes with potassium counter-ions upon blending with poly(ethylene oxide). / Latini Gianluca, Winroth Gustaf, Brovelli Sergio, McDonnell Shane O., Anderson Harry L., Mativetsky Jeffrey M., Samori Paolo, Cacialli Franco. // Journal of Applied Physics. - 2010. - Vol. 107, No. 12. - P. 124509-124509-9. ↑

J512. In-Kui Cho. Optical Chip-to-Chip Link System by Using Optical Wiring Method for Reducing EMI. / In-Kui Cho, Jae-Hoon Yun, Myung-Yung Jeong, Hyo-Hoon Park. // IEEE Transactions on Advanced Packaging. - 2010. - Vol. 33, No. 3. - P. 722-728. ↑

J513. Renaud Cedric. Identification of the nature of trapping centers in polyspirobifluorene based diodes by using electrical characterization. / Renaud Cedric, Nguyen Thien-Phap. // Journal of Applied Physics. - 2010. - Vol. 107, No. 12. - P. 124505-124505-8. ↑

J514. Jung J. Measurement of initial motion of a flying golf ball with multi-exposure images for screen-golf. /

Jung J., Park H., Kang S., Lee S., Hahn M. // IEEE Transactions on Consumer Electronics. - 2010. - Vol. 56, No. 2. - P. 516-523. ↑

J515. Woo-Chan Kim. Efficient resource allocation for rapid link recovery and visibility in visible-light local area networks. / Woo-Chan Kim, Chi-Sung Bae, Soo-Yong Jeon, Sung-Yeop Pyun, Dong-Ho Cho. // IEEE Transactions on Consumer Electronics. - 2010. - Vol. 56, No. 2. - P. 524-531. ↑

J516. McKendry J.J.D. High-Speed Visible Light Communications Using Individual Pixels in a Micro Light-Emitting Diode Array. / McKendry J.J.D., Green R.P., Kelly A.E., Zheng Gong, Guilhabert B., Massoubre D., Gu E., Dawson M.D. // IEEE Photonics Technology Letters. - 2010. - Vol. 22, No. 18. - P. 1346-1348. ↑

J517. Yong-Joon Jeon. Design method for area-efficient and uniform channel DACs. / Yong-Joon Jeon, Jin-Yong Jeon, Sung-Woo Lee, Gyu-Hyeong Cho. // IEEE Transactions on Consumer Electronics. - 2010. - Vol. 56, No. 2. - P. 271-279. ↑

J518. Sung Jun-Ho. Enhancement of electroluminescence in GaN-based light-emitting diodes by metallic nanoparticles. / Sung Jun-Ho, Yang Jeong Su, Kim Bo-Soon, Choi Chul-Hyun, Lee Min-Woo, Lee Seung-Gol, Park Se-Geun, Lee El-Hang, O Beom-Hoan. // Applied Physics Letters. - 2010. - Vol. 96, No. 26. - P. 261105-261105-3. ↑

J519. Huang Hung-Wen. High extraction efficiency GaN-based light-emitting diodes on embedded SiO₂ nanorod array and nanoscale patterned sapphire substrate. / Huang Hung-Wen, Huang Jhi-Kai, Kuo Shou-Yi, Lee Kang-Yuan, Kuo Hao-Chung. // Applied Physics Letters. - 2010. - Vol. 96, No. 26. - P. 263115-263115-3. ↑

J520. Byong-Deok Choi. Data driving methods and circuits for compact and high-image-quality AMOLED mobile displays. / Byong-Deok Choi, Chun-Won Byun. // IEEE Transactions on Consumer Electronics. - 2010. - Vol. 56, No. 2. - P. 1102-1107. ↑

J521. Bernardo G. Synergistic effect on the efficiency of polymer light-emitting diodes upon blending of two green-emitting polymers. / Bernardo G., Ferreira Q., Brotas G., Di Paolo R. E., Charas A., Morgado J. // Journal of Applied Physics. - 2010. - Vol. 108, No. 1. - P. 014503-014503-8. ↑

J522. Chen Shr-Jia. Fabrication of ZnO photonic crystals by nanosphere lithography using inductively coupled-plasma reactive ion etching with CH₄/H₂/Ar plasma on the ZnO/GaN heterojunction light emitting diodes. / Chen Shr-Jia, Chang Chun-Ming, Kao Jiann-Shiun, Chen Fu-Rong, Tsai Chuen-Horng. // and Films Journal of Vacuum Science & Technology A: Vacuum, Surfaces. - 2010. - Vol. 28, No. 4. - P. 745-749. ↑

J523. Oka Nobuto. Study on MoO_{3-x} films deposited by reactive sputtering for organic light-emitting diodes. / Oka Nobuto, Watanabe Hiroki, Sato Yasushi, Yamaguchi Hiroshi, Ito Norihiro, Tsuji Hiroya, Shigesato Yuzo. // and Films Journal of Vacuum Science & Technology A: Vacuum, Surfaces. - 2010. - Vol. 28, No. 4. - P. 886-889. ↑

J524. Yeong-Her Lin. Development of High-Performance Optical Silicone for the Packaging of High-Power LEDs. / Yeong-Her Lin, Jiun Pyng You, Yuan-Chang Lin, Tran N.T., Shi F.G. // IEEE Transactions on Components and Packaging Technologies. - 2010. - Vol. 33, No. 4. - P. 761-766. ↑

J525. Paraskevopoulos A. Optical Wireless Communication Systems in the Mb/s to Gb/s Range, Suitable for Industrial Applications. / Paraskevopoulos A., Vucic, J., Voss S.-H., Swoboda R., Langer K.-D. // IEEE/ASME Transactions on Mechatronics. - 2010. - Vol. 15, No. 4. - P. 541-547. ↑

J526. An Hu. CMOS Optoelectronic Lock-In Amplifier With Integrated Phototransistor Array. / An Hu, Chodavarapu V.P. // IEEE Transactions on Biomedical Circuits and Systems. - 2010. - Vol. 4, No. 5. - P. 274-280. ↑

J527. Yung Hsun Lin. Light Output Enhancement of Near UV-LED by Using Ti-Doped ITO Transparent Conducting Layer. / Yung Hsun Lin, Liu Y.S., Liu C.Y. // IEEE Photonics Technology Letters. - 2010. - Vol. 22, No. 19. - P. 1443-1445. ↑

J528. Vickers S. V. Light-emitting dendrimer film morphology: A neutron reflectivity study. / Vickers S. V., Barcena H., Knights K. A., Thomas R. K., Ribierre J.-C., Gambino S., Samuel I. D. W., Burn P. L., Fragneto Giovanna. // Applied Physics Letters. - 2010. - Vol. 96, No. 26. - P. 263302-263302-3. ↑

- J529.** Lu Chih-Feng. Reduction in the efficiency droop effect of a light-emitting diode through surface plasmon coupling. / Lu Chih-Feng, Liao Che-Hao, Chen Chih-Yen, Hsieh Chieh, Kiang Yean-Woei, Yang C. C. // Applied Physics Letters. - 2010. - Vol. 96, No. 26. - P. 261104-261104-3. ↑
- J530.** Knapp E. Numerical simulation of charge transport in disordered organic semiconductor devices. / Knapp E., Hausermann R., Schwarzenbach H. U., Ruhstaller B. // Journal of Applied Physics. - 2010. - Vol. 108, No. 5. - P. 054504-054504-8. ↑
- J531.** Kim Hyun Sung. Revised hole injection mechanism of a thin LiF layer introduced between pentacene and an indium tin oxide anode. / Kim Hyun Sung, Lee Hyunbok, Jeon Pyung Eun, Jeong Kwangho, Lee Jung Han, Yi Yeonjin. // Journal of Applied Physics. - 2010. - Vol. 108, No. 5. - P. 053701-053701-4. ↑
- J532.** Naidu D. The measured dependence of the lateral ambipolar diffusion length on carrier injection-level in Stranski-Krastanov quantum dot devices. / Naidu D., Smowton P. M., Summers H. D. // Journal of Applied Physics. - 2010. - Vol. 108, No. 4. - P. 043108-043108-10. ↑
- J533.** Wang C. Si-based packaging platform for LED module using electroplating method. / Wang C., Lee W.S., Zhang F., Kim N.Y. // Electronics Letters. - 2010. - Vol. 46, No. 17. - P. 1220-1221. ↑
- J534.** Ya-Ju Lee. Determination of Junction Temperature in InGaN and AlGaInP Light-Emitting Diodes. / Ya-Ju Lee, Chia-Jung Lee, Chih-Hao Chen. // IEEE Journal of Quantum Electronics. - 2010. - Vol. 46, No. 10. - P. 1450-1455. ↑
- J535.** Spreemann M. Modal Behavior, Spatial Coherence, and Beam Quality of a High-Power Gain-Guided Laser Array. / Spreemann M., Eppich B., Schnieder F., Wenzel H., Erbert G. // IEEE Journal of Quantum Electronics. - 2010. - Vol. 46, No. 11. - P. 1619-1625. ↑
- J536.** Yong-Joon Jeon. A High-Speed Current-Mode Data Driver With Push-Pull Transient Current Feedforward for Full-HD AMOLED Displays. / Yong-Joon Jeon, Jin-Yong Jeon, Young-Suk Son, Jin Huh, Gyu-Hyeong Cho. // IEEE Journal of Solid-State Circuits. - 2010. - Vol. 45, No. 9. - P. 1881-1895. ↑
- J537.** Conley J.F. Instabilities in Amorphous Oxide Semiconductor Thin-Film Transistors. IEEE Transactions on Device and Materials Reliability. - 2010. - Vol. 10, No. 4. - P. 460-475. ↑
- J538.** Bong-Min Song. Hierarchical Life Prediction Model for Actively Cooled LED-Based Luminaire. / Bong-Min Song, Bongtae Han, Bar-Cohen A., Sharma R., Arik M. // IEEE Transactions on Components and Packaging Technologies. - 2010. - Vol. 33, No. 4. - P. 728-737. ↑
- J539.** Yong Xia. Boosting Green GaInN/GaN Light-Emitting Diode Performance by a GaInN Underlying Layer. / Yong Xia, Wenting Hou, Liang Zhao, Mingwei Zhu, Detchprohm T., Wetzel C. // IEEE Transactions on Electron Devices. - 2010. - Vol. 57, No. 10. - P. 2639-2643. ↑
- J540.** Bano N. ZnO-organic hybrid white light emitting diodes grown on flexible plastic using low temperature aqueous chemical method. / Bano N., Zaman S., Zainelabdin A., Hussain S., Hussain I., Nur O., Willander M. // Journal of Applied Physics. - 2010. - Vol. 108, No. 4. - P. 043103-043103-5. ↑
- J541.** Zong-Yuan Liu. Studies on Optical Consistency of White LEDs Affected by Phosphor Thickness and Concentration Using Optical Simulation. / Zong-Yuan Liu, Sheng Liu, Kai Wang, Xiao-Bing Luo. // IEEE Transactions on Components and Packaging Technologies. - 2010. - Vol. 33, No. 4. - P. 680-687. ↑
- J542.** Keppens A. Modeling high power light-emitting diode spectra and their variation with junction temperature. / Keppens A., Ryckaert W. R., Deconinck G., Hanselaer P. // Journal of Applied Physics. - 2010. - Vol. 108, No. 4. - P. 043104-043104-7. ↑
- J543.** Jongwoon Park. Speedup of Dynamic Response of Organic Light-Emitting Diodes. Journal of Lightwave Technology. - 2010. - Vol. 28, No. 19. - P. 2873-2880. ↑
- J544.** Arnaboldi C. Crosstalk Study of the Single-Photon Response of a Flat-Panel PMT for the RICH Upgrade at LHCb. / Arnaboldi C., Artuso M., Calvi M., Fanchini E., Gotti C., Maino M., Matteuzzi C., Perego D.L., Pessina G., Jianchun Wang. // IEEE Transactions on Nuclear Science. - 2010. - Vol. 57, No. 4. - P. 2267-2272. ↑
- J545.** Martinez-Torres P. Optical and thermal depth profile reconstructions of inhomogeneous

photopolymerization in dental resins using photothermal waves. / Martinez-Torres P., Mandelis A., Alvarado-Gil J. J. // Journal of Applied Physics. - 2010. - Vol. 108, No. 5. - P. 054902-054902-10. ↑

J546. Rangel Elizabeth. Interplay of cavity thickness and metal absorption in thin-film InGaN photonic crystal light-emitting diodes. / Rangel Elizabeth, Matioli Elison, Chen Hung-Tse, Choi Yong-Seok, Weisbuch Claude, Speck James S., Hu Evelyn L. // Applied Physics Letters. - 2010. - Vol. 97, No. 6. - P. 061118-061118-3. ↑

J547. Park Soon Mi. Insertion of an organic interlayer for hole current enhancement in inverted organic light emitting devices. / Park Soon Mi, Kim Yoon Hak, Yi Yeonjin, Oh Hyoung-Yun, Won Kim Jeong. // Applied Physics Letters. - 2010. - Vol. 97, No. 6. - P. 063308-063308-3. ↑

J548. Wang Qi. Photodegradation of the organic/metal cathode interface in organic light-emitting devices. / Wang Qi, Luo Yichun, Aziz Hany. // Applied Physics Letters. - 2010. - Vol. 97, No. 6. - P. 063309-063309-3. ↑

J549. Lai Wei-Chih. GaN-based light emitting diodes with embedded SiO₂ pillars and air gap array structures. / Lai Wei-Chih, Yang Ya-Yu, Peng Li-Chi, Yang Shih-Wei, Lin Yu-Ru, Sheu Jinn-Kong. // Applied Physics Letters. - 2010. - Vol. 97, No. 8. - P. 081103-081103-3. ↑

J550. Yamada-Takamura Yukiko. Surface electronic structure of ZrB₂ buffer layers for GaN growth on Si wafers. / Yamada-Takamura Yukiko, Bussolotti Fabio, Fleurence Antoine, Bera Sambhunath, Friedlein Rainer. // Applied Physics Letters. - 2010. - Vol. 97, No. 7. - P. 073109-073109-3. ↑

J551. Li Feng. Direct measurement of the magnetic field effects on carrier mobilities and recombination in tri-(8-hydroxyquinoline)-aluminum based light-emitting diodes. / Li Feng, Xin Linyuan, Liu Shiyong, Hu Bin. // Applied Physics Letters. - 2010. - Vol. 97, No. 7. - P. 073301-073301-3. ↑

J552. Liu Shumei. Enhanced efficiency and reduced roll-off in nondoped phosphorescent organic light-emitting devices with triplet multiple quantum well structures. / Liu Shumei, Li Bin, Zhang Liming, Song Hang, Jiang Hong. // Applied Physics Letters. - 2010. - Vol. 97, No. 8. - P. 083304-083304-3. ↑

J553. Nishikawa A. Improved luminescence properties of Eu-doped GaN light-emitting diodes grown by atmospheric-pressure organometallic vapor phase epitaxy. / Nishikawa A., Furukawa N., Kawasaki T., Terai Y., Fujiwara Y. // Applied Physics Letters. - 2010. - Vol. 97, No. 5. - P. 051113-051113-3. ↑

J554. Trieu S.S. Study of Top and Bottom Photonic Gratings on GaN LED With Error Grating Models. / Trieu S.S., Xiaomin Jin. // IEEE Journal of Quantum Electronics. - 2010. - Vol. 46, No. 10. - P. 1456-1463. ↑

J555. Halzen Francis. Invited Review Article: IceCube: An instrument for neutrino astronomy. / Halzen Francis, Klein Spencer R. // Review of Scientific Instruments. - 2010. - Vol. 81, No. 8. - P. 081101-081101-24. ↑

J556. Ozdol V. B. A non-damaging electron microscopy approach to map In distribution in InGaN light-emitting diodes. / Ozdol V. B., Koch C. T., van Aken P. A. // Journal of Applied Physics. - 2010. - Vol. 108, No. 5. - P. 056103-056103-3. ↑

J557. Bao Q. Y. Electronic structures of MoO₃-based charge generation layer for tandem organic light-emitting diodes. / Bao Q. Y., Yang J. P., Li Y. Q., Tang J. X. // Applied Physics Letters. - 2010. - Vol. 97, No. 6. - P. 063303-063303-3. ↑

J558. Flemish J.R. Optimization of a Photonic Controlled Microwave Switch and Attenuator. / Flemish J.R., Haupt R.L. // IEEE Transactions on Microwave Theory and Techniques. - 2010. - Vol. 58, No. 10. - P. 2582-2588. ↑

J559. Fiene J. The RoboCup. IEEE Robotics & Automation Magazine. - 2010. - Vol. 17, No. 3. - P. 78-82. ↑

J560. Lin Hon-Way. InGaN/GaN nanorod array white light-emitting diode. / Lin Hon-Way, Lu Yu-Jung, Chen Hung-Ying, Lee Hong-Mao, Gwo Shangjr. // Applied Physics Letters. - 2010. - Vol. 97, No. 7. - P. 073101-073101-3. ↑

J561. Montes M. External efficiency and carrier loss mechanisms in InAs/GaInNAs quantum dot light-emitting diodes. / Montes M., Hierro A., Ulloa J. M., Guzman A., Al Khalfoui M., Hugues M., Damilano B., Massies J. // Journal of Applied Physics. - 2010. - Vol. 108, No. 3. - P. 033104-033104-8. ↑

- J562.** Ahn Jaehui. Electroluminescence from ZnO nanoflowers/GaN thin film p-n heterojunction. / Ahn Jaehui, Mastro Michael A., Hite Jennifer, Eddy Charles R., Kim Jihyun. // Applied Physics Letters. - 2010. - Vol. 97, No. 8. - P. 082111-082111-3. ↑
- J563.** Wang Z. B. Direct hole injection in to 4,4' -N ,N ' -dicarbazole-biphenyl: A simple pathway to achieve efficient organic light emitting diodes. / Wang Z. B., Helander M. G., Qiu J., Liu Z. W., Greiner M. T., Lu Z. H. // Journal of Applied Physics. - 2010. - Vol. 108, No. 2. - P. 024510-024510-4. ↑
- J564.** Wang X. H. The contribution of sidewall light extraction to efficiencies of polygonal light-emitting diodes shaped with laser micromachining. / Wang X. H., Lai P. T., Choi H. W. // Journal of Applied Physics. - 2010. - Vol. 108, No. 2. - P. 023110-023110-5. ↑
- J565.** Zhang Baohua. On the origin of efficient electron injection at phosphonate-functionalized polyfluorene/aluminum interface in efficient polymer light-emitting diodes. / Zhang Baohua, Qin Chuanjiang, Niu Xiaodi, Xie Zhiyuan, Cheng Yanxiang, Wang Lixiang, Li Xinglin. // Applied Physics Letters. - 2010. - Vol. 97, No. 4. - P. 043506-043506-3. ↑
- J566.** Yen-Sheng Lin. High-Luminance White-Light Point Source Using Ce,Sm : YAG Double-Clad Crystal Fiber. / Yen-Sheng Lin, Tzu-Chieh Cheng, Chien-Chung Tsai, Kuang-Yu Hsu, Dong-Yo Jheng, Chia-Yao Lo, Yeh P.-H.S., Sheng-Lung Huang. // IEEE Photonics Technology Letters. - 2010. - Vol. 22, No. 20. - P. 1494-1496. ↑
- J567.** Yamamoto H. Viewing-Zone Control of Light-Emitting Diode Panel for Stereoscopic Display and Multiple Viewing Distances. / Yamamoto H., Kimura T., Matsumoto S., Suyama S. // Journal of Display Technology. - 2010. - Vol. 6, No. 9. - P. 359-366. ↑
- J568.** Jae Kyun Kwon. Inverse Source Coding for Dimming in Visible Light Communications Using NRZ-OOK on Reliable Links. IEEE Photonics Technology Letters. - 2010. - Vol. 22, No. 19. - P. 1455-1457. ↑
- J569.** Capaccioni F. VIS-NIR Imaging Spectroscopy of Mercury's Surface: SIMBIO-SYS/VIHI Experiment Onboard the BepiColombo Mission. / Capaccioni F., De Sanctis M.C., Filacchione G., Piccioni G., Ammannito E., Tommasi L., Fikai Veltroni I., Cosi M., Debei S., Calamai L., Flamini E. // IEEE Transactions on Geoscience and Remote Sensing. - 2010. - Vol. 48, No. 11. - P. 3932-3940. ↑
- J570.** Kimura M. Pulsewidth Modulation With Current Uniformization for AM-OLEDs. / Kimura M., Suzuki D., Koike M., Sawamura S., Kato M. // IEEE Transactions on Electron Devices. - 2010. - Vol. 57, No. 10. - P. 2624-2630. ↑
- J571.** Chun-Feng Lai. Structural Effects on Highly Directional Far-Field Emission Patterns of GaN-Based Micro-Cavity Light-Emitting Diodes With Photonic Crystals. / Chun-Feng Lai, Hao-Chung Kuo, Chia-Hsin Chao, Peichen Yu, Wen-Yung Yeh. // Journal of Lightwave Technology. - 2010. - Vol. 28, No. 19. - P. 2881-2889. ↑
- J572.** Ni X. Hot electron effects on efficiency degradation in InGaN light emitting diodes and designs to mitigate them. / Ni X., Li X., Lee J., Liu S., Avrutin V., Ozgur U., Morkoc H., Matulionis A. // Journal of Applied Physics. - 2010. - Vol. 108, No. 3. - P. 033112-033112-13. ↑
- J573.** Erickson Nicholas C. Highly efficient, single-layer organic light-emitting devices based on a graded-composition emissive layer. / Erickson Nicholas C., Holmes Russell J. // Applied Physics Letters. - 2010. - Vol. 97, No. 8. - P. 083308-083308-3. ↑
- J574.** Wildeson Isaac H. III-nitride nanopyramid light emitting diodes grown by organometallic vapor phase epitaxy. / Wildeson Isaac H., Colby Robert, Ewoldt David A., Liang Zhiwen, Zakharov Dmitri N., Zaluzec Nestor J., Garcia R. Edwin, Stach Eric A., Sands Timothy D. // Journal of Applied Physics. - 2010. - Vol. 108, No. 4. - P. 044303-044303-8. ↑
- J575.** Yerci S. Electroluminescence from Er-doped Si-rich silicon nitride light emitting diodes. / Yerci S., Li R., Dal Negro L. // Applied Physics Letters. - 2010. - Vol. 97, No. 8. - P. 081109-081109-3. ↑
- J576.** Svarnas P. Highly-selective wettability on organic light-emitting-diodes patterns by sequential low-power plasmas. / Svarnas P., Yang L., Munz M., Edwards A. J., Shard A. G., Bradley J. W. // Journal of Applied Physics. - 2010. - Vol. 107, No. 10. - P. 103313-103313-10. ↑

- J577.** Sulaeman Uyi. Solvothermal synthesis of designed nonstoichiometric strontium titanate for efficient visible-light photocatalysis. / Sulaeman Uyi, Yin Shu, Sato Tsugio. // *Applied Physics Letters*. - 2010. - Vol. 97, No. 10. - P. 103102-103102-3. ↑
- J578.** Ray-Hua Horng. Light Extraction Study on Thin-Film GaN Light-Emitting Diodes With Electrodes Covering by Wafer Bonding and Textured Surfaces. / Ray-Hua Horng, Yi-Anne Lu, Dong-Sing Wu. // *IEEE Transactions on Electron Devices*. - 2010. - Vol. 57, No. 10. - P. 2651-2654. ↑
- J579.** Chun-Feng Lai. Optimized Microcavity and Photonic Crystal Parameters of GaN-Based Ultrathin-Film Light-Emitting Diodes for Highly Directional Beam Profiles. / Chun-Feng Lai, Chia-Hsin Chao, Wen-Yung Yeh. // *IEEE Photonics Technology Letters*. - 2010. - Vol. 22, No. 21. - P. 1547-1549. ↑
- J580.** Ya-Ju Lee. Reduction in the Efficiency-Droop Effect of InGaN Green Light-Emitting Diodes Using Gradual Quantum Wells. / Ya-Ju Lee, Chih-Hao Chen, Chia-Jung Lee. // *IEEE Photonics Technology Letters*. - 2010. - Vol. 22, No. 20. - P. 1506-1508. ↑
- J581.** Ahn Chang-Geun. Photosensitive biosensor array system using optical addressing without an addressing circuit on array biochips. / Ahn Chang-Geun, Ah Chil Seong, Kim Tae-Youb, Park Chan Woo, Yang Jong-Heon, Kim Ansoon, Sung Gun Yong. // *Applied Physics Letters*. - 2010. - Vol. 97, No. 10. - P. 103703-103703-3. ↑
- J582.** Mansell R. Spin-injection device prospects for half-metallic Fe₃O₄/Al_{0.1}Ga_{0.9}As interfaces. / Mansell R., Laloe J.-B., Holmes S. N., Wong P. K. J., Xu Y. B., Farrer I., Jones G. A. C., Ritchie D. A., Barnes C. H. W. // *Journal of Applied Physics*. - 2010. - Vol. 108, No. 3. - P. 034507-034507-4. ↑
- J583.** Song Young Min. Disordered antireflective nanostructures on GaN-based light-emitting diodes using Ag nanoparticles for improved light extraction efficiency. / Song Young Min, Choi Eun Sil, Park Gyeong Cheol, Park Chang Young, Jang Sung Jun, Lee Yong Tak. // *Applied Physics Letters*. - 2010. - Vol. 97, No. 9. - P. 093110-093110-3. ↑
- J584.** Cheng Gang. Full spin-coated multilayer structure hybrid light-emitting devices. / Cheng Gang, Mazzeo Marco, Carallo Sonia, Wang Huiping, Ma Yuguang, Gigli Giuseppe. // *Applied Physics Letters*. - 2010. - Vol. 97, No. 10. - P. 103107-103107-3. ↑
- J585.** Jeong I.-H. Fast current programming method using current amplifier for active matrix organic light emitting diode displays. / Jeong I.-H., Kwon O.-K. // *Electronics Letters*. - 2010. - Vol. 46, No. 16. - P. 1118-1120. ↑
- J586.** Li C. C. Removing GaAs substrate by nitric acid solution. / Li C. C., Guan B. L., Chuai D. X., Guo X., Shen G. D. // *Journal of Vacuum Science & Technology B: Microelectronics and Nanometer Structures*. - 2010. - Vol. 28, No. 3. - P. 635-637. ↑
- J587.** Jeon Joon-Woo. Formation of low-resistance Ohmic contacts to N-face n-GaN for high-power GaN-based vertical light-emitting diodes. / Jeon Joon-Woo, Park Seong-Han, Jung Se-Yeon, Lee Sang Youl, Moon Jihyung, Song June-O, Seong Tae-Yeon. // *Applied Physics Letters*. - 2010. - Vol. 97, No. 9. - P. 092103-092103-3. ↑
- J588.** Bagnich S. A. Origin of magnetic field effect enhancement by electrical stress in organic light emitting diodes. / Bagnich S. A., Niedermeier U., Melzer C., Sarfert W., von Seggern H. // *Journal of Applied Physics*. - 2009. - Vol. 105, No. 12. - P. 123706-123706-6. ↑
- J589.** Sakanoue Tomo. Charge separation and transport behavior of a two-dimensional charge sheet at organic donor-acceptor heterointerfaces. / Sakanoue Tomo, Irie Toru, Adachi Chihaya. // *Journal of Applied Physics*. - 2009. - Vol. 105, No. 11. - P. 114502-114502-6. ↑
- J590.** Wu Yuh-Renn. Electronic and optical properties of InGaN quantum dot based light emitters for solid state lighting. / Wu Yuh-Renn, Lin Yih-Yin, Huang Hung-Hsun, Singh Jasprit. // *Journal of Applied Physics*. - 2009. - Vol. 105, No. 1. - P. 013117-013117-7. ↑
- J591.** Nenna G. Insights into thermal degradation of organic light emitting diodes induced by glass transition through impedance spectroscopy. / Nenna G., Barra M., Cassinese A., Miscioscia R., Fasolino T., Tassini P., Minarini C., della Sala D. // *Journal of Applied Physics*. - 2009. - Vol. 105, No. 12. - P. 123511-123511-6. ↑

- J592.** Suzuno Mitsushi. p-Si /beta -FeSi 2 /n-Si double-heterostructure light-emitting diodes achieving 1.6 mcm electroluminescence of 0.4 mW at room temperature. / Suzuno Mitsushi, Koizumi Tomoaki, Suemasu Takashi. // Applied Physics Letters. - 2009. - Vol. 94, No. 21. - P. 213509-213509-3. ↑
- J593.** Yang Su-Hua. Luminescence enhancement and emission color adjustment of white organic light-emitting diodes with quantum-well-like structures. / Yang Su-Hua, Hong Bo-Cheng, Huang Shih-Fong. // Journal of Applied Physics. - 2009. - Vol. 105, No. 11. - P. 113105-113105-7. ↑
- J594.** Hata Kazuki. Hadamard transform microchip electrophoresis combined with laser-induced fluorescence detection using a compact neodymium-doped yttrium aluminum garnet laser emitting at 532 nm. / Hata Kazuki, Kaneta Takashi, Imasaka Totaro. // Journal of Applied Physics. - 2009. - Vol. 105, No. 10. - P. 102018-102018-6. ↑
- J595.** Fujii Katsushi. Leakage current improvement of nitride-based light emitting diodes using CrN buffer layer and its vertical type application by chemical lift-off process. / Fujii Katsushi, Lee Seogwoo, Ha Jun-Seok, Lee Hyun-Jae, Lee Hyo-Jong, Lee Sang-Hyun, Kato Takashi, Cho Meoung-Whan, Yao Takafumi. // Applied Physics Letters. - 2009. - Vol. 94, No. 24. - P. 242108-242108-3. ↑
- J596.** Nizamoglu Sedat. Quantum efficiency enhancement in nanocrystals using nonradiative energy transfer with optimized donor-acceptor ratio for hybrid LEDs. / Nizamoglu Sedat, Akin Onur, Demir Hilmi Volkan. // Applied Physics Letters. - 2009. - Vol. 94, No. 24. - P. 243107-243107-3. ↑
- J597.** Zimmler Mariano A. Exciton-related electroluminescence from ZnO nanowire light-emitting diodes. / Zimmler Mariano A., Voss Tobias, Ronning Carsten, Capasso Federico. // Applied Physics Letters. - 2009. - Vol. 94, No. 24. - P. 241120-241120-3. ↑
- J598.** Liao Milton M. H. An investigation on the light-emission mechanism of metal-insulator-semiconductor light-emitting diodes with different SiGe quantum well structures. Applied Physics Letters. - 2009. - Vol. 94, No. 24. - P. 241908-241908-3. ↑
- J599.** Chang Shu-Tong. Light emission and photoluminescence from high-k dielectrics containing Ge nanocrystals. / Chang Shu-Tong, Liao Shu-Hui. // Journal of Vacuum Science & Technology B: Microelectronics and Nanometer Structures. - 2009. - Vol. 27, No. 1. - P. 535-537. ↑
- J600.** Sun Minghua. Enhanced ultraviolet electroluminescence from p-Si /n-Zn O nanorod array heterojunction. / Sun Minghua, Zhang Qi-Feng, Sun Hui, Zhang Junyan, Wu Jin-Lei. // Journal of Vacuum Science & Technology B: Microelectronics and Nanometer Structures. - 2009. - Vol. 27, No. 2. - P. 618-621. ↑
- J601.** Barlow Iain A. High-speed electroluminescence modulation of a conjugated-polymer light emitting diode. / Barlow Iain A., Kreouzis Theo, Lidzey David G. // Applied Physics Letters. - 2009. - Vol. 94, No. 24. - P. 243301-243301-3. ↑
- J602.** Vak Doojin. Efficient single-component light-emitting electrochemical cells with an ion-conducting water-soluble polyfluorene. / Vak Doojin, Oh Seung-Hwan, Kim Dong-Yu. // Applied Physics Letters. - 2009. - Vol. 94, No. 24. - P. 243305-243305-3. ↑
- J603.** Polikarpov Evgueni. An ambipolar phosphine oxide-based host for high power efficiency blue phosphorescent organic light emitting devices. / Polikarpov Evgueni, Swensen James S., Chopra Neetu, So Franky, Padmaperuma Asanga B. // Applied Physics Letters. - 2009. - Vol. 94, No. 22. - P. 223304-223304-3. ↑
- J604.** Walter G. Tilted-charge high speed (7 GHz) light emitting diode. / Walter G., Wu C. H., Then H. W., Feng M., Holonyak N. // Applied Physics Letters. - 2009. - Vol. 94, No. 23. - P. 231125-231125-3. ↑
- J605.** Zhang Dan-Dan. Enhanced hole injection in organic light-emitting devices by using Fe₃O₄ as an anodic buffer layer. / Zhang Dan-Dan, Feng Jing, Liu Yue-Feng, Zhong Yu-Qing, Bai Yu, Jin Yu, Xie Guo-Hua, Xue Qin, Zhao Yi, Liu Shi-Yong, Sun Hong-Bo. // Applied Physics Letters. - 2009. - Vol. 94, No. 22. - P. 223306-223306-3. ↑
- J606.** Han Sang-Heon. Effect of electron blocking layer on efficiency droop in InGaN/GaN multiple quantum well light-emitting diodes. / Han Sang-Heon, Lee Dong-Yul, Lee Sang-Jun, Cho Chu-Young, Kwon Min-Ki, Lee S. P., Noh D. Y., Kim Dong-Joon, Kim Yong Chun, Park Seong-Ju. // Applied Physics Letters. - 2009. - Vol. 94, No. 23. - P. 231123-231123-3. ↑

- J607.** Wang Qiang. Realization of high efficiency microcavity top-emitting organic light-emitting diodes with highly saturated colors and negligible angular dependence. / Wang Qiang, Deng Zhaoqi, Ma Dongge. // Applied Physics Letters. - 2009. - Vol. 94, No. 23. - P. 233306-233306-3. ↑
- J608.** Walter G. 4.3 GHz optical bandwidth light emitting transistor. / Walter G., Wu C. H., Then H. W., Feng M., Holonyak N. // Applied Physics Letters. - 2009. - Vol. 94, No. 24. - P. 241101-241101-3. ↑
- J609.** Fenwick William E. Metal organic chemical vapor deposition of crack-free GaN-based light emitting diodes on Si (111) using a thin Al₂O₃ interlayer. / Fenwick William E., Melton Andrew, Xu Tianming, Li Nola, Summers Christopher, Jamil Muhammad, Ferguson Ian T. // Applied Physics Letters. - 2009. - Vol. 94, No. 22. - P. 222105-222105-3. ↑
- J610.** Lu Yen-Cheng. Improving emission enhancement in surface plasmon coupling with an InGaN/GaN quantum well by inserting a dielectric layer of low refractive index between metal and semiconductor. / Lu Yen-Cheng, Chen Yung-Sheng, Tsai Fu-Ji, Wang Jyh-Yang, Lin Cheng-Hung, Chen Cheng-Yen, Kiang Yean-Woei, Yang C. C. // Applied Physics Letters. - 2009. - Vol. 94, No. 23. - P. 233113-233113-3. ↑
- J611.** Wang X. H. Laser micromachining of optical microstructures with inclined sidewall profile. / Wang X. H., Lai P. T., Choi H. W. // Journal of Vacuum Science & Technology B: Microelectronics and Nanometer Structures. - 2009. - Vol. 27, No. 3. - P. 1048-1052. ↑
- J612.** Na Jong H. Dual luminescence from organic/inorganic hybrid p-n junction light-emitting diodes. / Na Jong H., Kitamura M., Arita M., Arakawa Y. // Applied Physics Letters. - 2009. - Vol. 94, No. 21. - P. 213302-213302-3. ↑
- J613.** Li Zhen-Yu. Carrier localization degree of In_{0.2}Ga_{0.8}N/GaN multiple quantum wells grown on vicinal sapphire substrates. / Li Zhen-Yu, Lo Ming-Hua, Chiu Ching-Hua, Lin Po-Chun, Lu Tien-Chang, Kuo Hao-Chung, Wang Shing-Chung. // Journal of Applied Physics. - 2009. - Vol. 105, No. 1. - P. 013103-013103-7. ↑
- J614.** Kim Moojin. Effects of gate insulator using high pressure annealing on the characteristics of solid phase crystallized polycrystalline silicon thin-film transistors. / Kim Moojin, Jin GuangHai. // Journal of Applied Physics. - 2009. - Vol. 105, No. 7. - P. 074507-074507-4. ↑
- J615.** Wang Qi. A high-performance tandem white organic light-emitting diode combining highly effective white-units and their interconnection layer. / Wang Qi, Ding Junqiao, Zhang Zhiqiang, Ma Dongge, Cheng Yanxiang, Wang Lixiang, Wang Fosong. // Journal of Applied Physics. - 2009. - Vol. 105, No. 7. - P. 076101-076101-3. ↑
- J616.** Lee Ya-Ju. Erratum: "High output power density from GaN-based two-dimensional nanorod light-emitting diode arrays" [Appl. Phys. Lett. 94, 141111 (2009)]. / Lee Ya-Ju, Lin Shawn-Yu, Chiu Ching-Hua, Lu Tien-Chang, Kuo Hao-Chung, Wang Shing-Chung, Chhajed Sameer, Kim Jong Kyu, Schubert E. Fred. // Applied Physics Letters. - 2009. - Vol. 94, No. 21. - P. 219901-219901-1. ↑
- J617.** Nash G. R. Reduction in Shockley-Read-Hall generation-recombination in AlInSb light-emitting-diodes using spatial patterning of the depletion region. / Nash G. R., Ashley T. // Applied Physics Letters. - 2009. - Vol. 94, No. 21. - P. 213510-213510-3. ↑
- J618.** Yu Li-Zhen. Investigation of Forster-type energy transfer in organic light-emitting devices with 4-(dicyanomethylene)-2-t-butyl-6-(1,1,7,7-tetramethyljulolidin-4-yl-vinyl)-4H-pyran doped cohost emitting layer. / Yu Li-Zhen, Jiang Xue-Yin, Zhang Zhi-Lin, Lou Li-Ren, Lee Ching-Ting. // Journal of Applied Physics. - 2009. - Vol. 105, No. 1. - P. 013105-013105-4. ↑
- J619.** Mori M. J. Microstructure and luminescent properties of novel InGaP alloys on relaxed GaAsP substrates. / Mori M. J., Fitzgerald E. A. // Journal of Applied Physics. - 2009. - Vol. 105, No. 1. - P. 013107-013107-10. ↑
- J620.** Herman Tobias K. High power light emitting diode based setup for photobleaching fluorescent impurities. / Herman Tobias K., Mackowiak Stephan A., Kaufman Laura J. // Review of Scientific Instruments. - 2009. - Vol. 80, No. 1. - P. 016107-016107-3. ↑
- J621.** Neelamegam P. Measurement of urinary calcium using AT89C51RD2 microcontroller. / Neelamegam P., Jamaludeen A., Rajendran A., Raghunathan R. // Review of Scientific Instruments. - 2009. - Vol. 80, No. 4. - P. 044704-044704-5. ↑

- J622.** Tsai Chia-Lung. Fabrication and characterization of the substrate-free InGaN-based resonant-cavity light-emitting diodes for plastic optical fiber communications. / Tsai Chia-Lung, Lin Jia-Qing, Huang Ju-Ping. // Journal of Vacuum Science & Technology B: Microelectronics and Nanometer Structures. - 2009. - Vol. 27, No. 3. - P. 1080-1085. ↑
- J623.** Bayram C. Fabrication and characterization of novel hybrid green light emitting diodes based on substituting n-type ZnO for n-type GaN in an inverted p-n junction. / Bayram C., Razeghi M., Rogers D. J., Teherani F. Hosseini. // Journal of Vacuum Science & Technology B: Microelectronics and Nanometer Structures. - 2009. - Vol. 27, No. 3. - P. 1784-1788. ↑
- J624.** Li Ping. Light emitting diode fault detection using p-n junction photovoltaic effect. / Li Ping, Wen Yumei, Cai Youhai, Li Lian. // Review of Scientific Instruments. - 2009. - Vol. 80, No. 5. - P. 055108-055108-7. ↑
- J625.** Shatalov Max. Efficiency of light emission in high aluminum content AlGaIn quantum wells. / Shatalov Max, Yang Jinwei, Sun Wenhong, Kennedy Robert, Gaska Remis, Liu Kai, Shur Michael, Tamulaitis Gintautas. // Journal of Applied Physics. - 2009. - Vol. 105, No. 7. - P. 073103-073103-6. ↑
- J626.** Li L. T. Design and implementation of a system with a multielement thermopile for monitoring temperature of a plane. / Li L. T., Tsai C. F., Young M. S. // Review of Scientific Instruments. - 2009. - Vol. 80, No. 4. - P. 045111-045111-8. ↑
- J627.** Cornagliotti E. High sensitivity photoconductivity based measurement setup for the determination of effective recombination lifetime in silicon wafers. / Cornagliotti E., Kang X., Beaucarne G., John J., Poortmans J., Mertens R. // Review of Scientific Instruments. - 2009. - Vol. 80, No. 5. - P. 053906-053906-7. ↑
- J628.** Seungyong Jung. GaSb-Based Type I Quantum-Well Light-Emitting Diode Addressable Array Operated at Wavelengths Up to 3.66 μ m. / Seungyong Jung, Suchalkin S., Kipshidze G., Westerfeld D., Snyder D., Johnson M., Belenky G. // IEEE Photonics Technology Letters. - 2009. - Vol. 21, No. 15. - P. 1087-1089. ↑
- J629.** Nepal N. Optical enhancement of room temperature ferromagnetism in Er-doped GaN epilayers. / Nepal N., Zavada J. M., Dahal R., Ugolini C., Sedhain A., Lin J. Y., Jiang H. X. // Applied Physics Letters. - 2009. - Vol. 95, No. 2. - P. 022510-022510-3. ↑
- J630.** Arcelus A. Determination of Sit-to-Stand Transfer Duration Using Bed and Floor Pressure Sequences. / Arcelus A., Herry C.L., Goubran R.A., Knoefel F., Sveistrup H., Bilodeau M. // IEEE Transactions on Biomedical Engineering. - 2009. - Vol. 56, No. 10. - P. 2485-2492. ↑
- J631.** Sammarco J.J. Technological Aspects of Solid-State and Incandescent Sources for Miner Cap Lamps. / Sammarco J.J., Freyssinier J.P., Bullough J.D., Xin Zhang, Reyes M.A. // IEEE Transactions on Industry Applications. - 2009. - Vol. 45, No. 5. - P. 1583-1588. ↑
- J632.** Chia-Ta Chang. 460-nm InGaN-Based LEDs Grown on Fully Inclined Hemisphere-Shape-Patterned Sapphire Substrate With Submicrometer Spacing. / Chia-Ta Chang, Shih-Kuang Hsiao, Chang E.Y., Yu-Lin Hsiao, Jui-Chien Huang, Chung-Yu Lu, Huang-Choung Chang, Kai-Wen Cheng, Ching-Ting Lee. // IEEE Photonics Technology Letters. - 2009. - Vol. 21, No. 19. - P. 1366-1368. ↑
- J633.** Min-Ho Kim. Partial Polarization Matching in GaInN-Based Multiple Quantum Well Blue LEDs Using Ternary GaInN Barriers for a Reduced Efficiency Droop. / Min-Ho Kim, Wonseok Lee, Di Zhu, Schubert M.F., Jong Kyu Kim, Schubert E.F., Yongjo Park. // IEEE Journal of Selected Topics in Quantum Electronics. - 2009. - Vol. 15, No. 4. - P. 1122-1127. ↑
- J634.** Nguyen The Tran. Effect of Phosphor Particle Size on Luminous Efficacy of Phosphor-Converted White LED. / Nguyen The Tran, Jiun Pyng You, Shi F.G. // Journal of Lightwave Technology. - 2009. - Vol. 27, No. 22. - P. 5145-5150. ↑
- J635.** Cook N. B. Midinfrared electroluminescence from pentanary-quaternary heterojunction light-emitting diodes. / Cook N. B., Krier A. // Applied Physics Letters. - 2009. - Vol. 95, No. 2. - P. 021110-021110-3. ↑
- J636.** Hertkorn J. Highly conductive modulation doped composition graded p-AlGaIn/(AlIn)/GaIn multiheterostructures grown by metalorganic vapor phase epitaxy. / Hertkorn J., Thapa S. B., Wunderer T., Scholz F., Wu Z. H., Wei Q. Y., Ponce F. A., Moram M. A., Humphreys C. J., Vierheilg C., Schwarz U. T. // ↑

Journal of Applied Physics. - 2009. - Vol. 106, No. 1. - P. 013720-013720-6.

J637. Sheth A. Citizen Sensing, Social Signals, and Enriching Human Experience. IEEE Internet Computing. - 2009. - Vol. 13, No. 4. - P. 87-92. ↑

J638. Jou Jwo-Huei. Sunlight-style color-temperature tunable organic light-emitting diode. / Jou Jwo-Huei, Wu Ming-Hsuan, Shen Shih-Ming, Wang Hsi-Ching, Chen Sun-Zen, Chen Szu-Hao, Lin Chuen-Ren, Hsieh Yueh-Lin. // Applied Physics Letters. - 2009. - Vol. 95, No. 1. - P. 013307-013307-3. ↑

J639. Long Hao. Ultraviolet electroluminescence from ZnO/NiO-based heterojunction light-emitting diodes. / Long Hao, Fang Guojia, Huang Huihui, Mo Xiaoming, Xia Wei, Dong Binzhong, Meng Xianquan, Zhao Xingzhong. // Applied Physics Letters. - 2009. - Vol. 95, No. 1. - P. 013509-013509-3. ↑

J640. Kuo Yen-Kuang. Advantages of blue InGaN multiple-quantum well light-emitting diodes with InGaN barriers. / Kuo Yen-Kuang, Chang Jih-Yuan, Tsai Miao-Chan, Yen Sheng-Horng. // Applied Physics Letters. - 2009. - Vol. 95, No. 1. - P. 011116-011116-3. ↑

J641. Chan Chia-Hua. Improved output power of GaN-based light-emitting diodes grown on a nanopatterned sapphire substrate. / Chan Chia-Hua, Hou Chia-Hung, Tseng Shao-Ze, Chen Tsing-Jen, Chien Hung-Ta, Hsiao Fu-Li, Lee Chien-Chieh, Tsai Yen-Ling, Chen Chii-Chang. // Applied Physics Letters. - 2009. - Vol. 95, No. 1. - P. 011110-011110-3. ↑

J642. Jayasimhadri M. White light generation from Dy 3+ -doped ZnO -B₂O₃ -P₂O₅ glasses. / Jayasimhadri M., Jang Kiwan, Lee Ho Sueb, Chen Baojiu, Yi Soung-Soo, Jeong Jung-Hyun. // Journal of Applied Physics. - 2009. - Vol. 106, No. 1. - P. 013105-013105-4. ↑

J643. Christensen A.L. From Fireflies to Fault-Tolerant Swarms of Robots. / Christensen A.L., O'Grady R., Dorigo M. // IEEE Transactions on Evolutionary Computation. - 2009. - Vol. 13, No. 4. - P. 754-766. ↑

J644. Yu-Kang Lo. Design and Implementation of RGB LED Drivers for LCD Backlight Modules. / Yu-Kang Lo, Kuan-Hung Wu, Kai-Jun Pai, Huang-Jen Chiu. // IEEE Transactions on Industrial Electronics. - 2009. - Vol. 56, No. 12. - P. 4862-4871. ↑

J645. Kuo C.W. Optical Simulation and Fabrication of Nitride-Based LEDs With the Inverted Pyramid Sidewalls. / Kuo C.W., Lee Y.C., Fu Y.K., Tsai C.H., Wu M.L., Chi G.C., Kuo C.H., Tun C.J. // IEEE Journal of Selected Topics in Quantum Electronics. - 2009. - Vol. 15, No. 4. - P. 1264-1268. ↑

J646. Wang Bowen. Effects of disorder in a photonic crystal on the extraction efficiency of a light-emitting diode. / Wang Bowen, Jin Yi, He Sailing. // Journal of Applied Physics. - 2009. - Vol. 106, No. 1. - P. 014508-014508-5. ↑

J647. Drezet A. Opening the light extraction cone of high index substrates with plasmonic gratings: Light emitting diode applications. / Drezet A., Przybilla F., Laux E., Mahboub O., Genet C., Ebbesen T. W., Bouillard J. S., Zayats A., Spevak I. S., Zayats A. V., Nikitin A. Yu, Martin-Moreno L. // Applied Physics Letters. - 2009. - Vol. 95, No. 2. - P. 021101-021101-3. ↑

J648. Zhao Jun Liu. Monolithic LED Microdisplay on Active Matrix Substrate Using Flip-Chip Technology. / Zhao Jun Liu, Ka Ming Wong, Chi Wing Keung, Chak Wah Tang, Kei May Lau. // IEEE Journal of Selected Topics in Quantum Electronics. - 2009. - Vol. 15, No. 4. - P. 1298-1302. ↑

J649. Jun Chen. Near-IR Optical Upconverter With Integrated Heterojunction Phototransistor and Organic Light-Emitting Diode. / Jun Chen, Ban D., Helander M.G., Zhenghong Lu, Graf M., Poole P., Liu H.C. // IEEE Photonics Technology Letters. - 2009. - Vol. 21, No. 19. - P. 1447-1449. ↑

J650. Shih-Chun Ling. Characteristics of a-Plane Green Light-Emitting Diode Grown on r-Plane Sapphire. / Shih-Chun Ling, Te-Chung Wang, Jun-Rong Chen, Po-Chun Liu, Tsung-Shine Ko, Bao-Yao Chang, Tien-Chang Lu, Hao-Chung Kuo, Shing-Chung Wang, Jenq-Dar Tsay. // IEEE Photonics Technology Letters. - 2009. - Vol. 21, No. 16. - P. 1130-1132. ↑

J651. Ping-Wei Huang. Improved Performance of AlGaInP LEDs by a Periodic GaP-Dish Mirror Array. / Ping-Wei Huang, Wu Y.C.S. // IEEE Photonics Technology Letters. - 2009. - Vol. 21, No. 19. - P. 1441-1443. ↑

J652. Gather Malte C. Improving the lifetime of white polymeric organic light-emitting diodes. / Gather Malte C.,

Kober Sebastian, Heun Susanne, Meerholz Klaus. // Journal of Applied Physics. - 2009. - Vol. 106, No. 2. - P. 024506-024506-10. ↑

J653. Okamoto K. High-Efficiency InGaN/GaN Light Emitters Based on Nanophotonics and Plasmonics. / Okamoto K., Kawakami Y. // IEEE Journal of Selected Topics in Quantum Electronics. - 2009. - Vol. 15, No. 4. - P. 1199-1209. ↑

J654. Matioli Elison. Growth of embedded photonic crystals for GaN-based optoelectronic devices. / Matioli Elison, Keller Stacia, Wu Feng, Choi Yong-Seok, Hu Evelyn, Speck James, Weisbuch Claude. // Journal of Applied Physics. - 2009. - Vol. 106, No. 2. - P. 024309-024309-8. ↑

J655. Kye-Si Kwon. Waveform Design Methods for Piezo Inkjet Dispensers Based on Measured Meniscus Motion. Journal of Microelectromechanical Systems. - 2009. - Vol. 18, No. 5. - P. 1118-1125. ↑

J656. Chien-Chung Chen. Optical Design of LCOS Optical Engine and Optimization With Genetic Algorithm. / Chien-Chung Chen, Cheng-Mu Tsai, Yi Chin Fang. // Journal of Display Technology. - 2009. - Vol. 5, No. 8. - P. 293-305. ↑

J657. Jongwoon Park. Luminance Uniformity of Large-Area OLEDs With an Auxiliary Metal Electrode. / Jongwoon Park, Jongho Lee, Dongchan Shin, Seounghwan Park. // Journal of Display Technology. - 2009. - Vol. 5, No. 8. - P. 306-311. ↑

J658. Yaxiao Qin. A Simple Method for Comparative Study on the Thermal Performance of LEDs and Fluorescent Lamps. / Yaxiao Qin, Deyan Lin, Hui S.Y. // IEEE Transactions on Power Electronics. - 2009. - Vol. 24, No. 7. - P. 1811-1818. ↑

J659. Smolski O.V. Blue Light Source Based on a ppKTP SHG Using a Grating-Coupled Laser Diode. / Smolski O.V., Yilmaz Y.O., Smolski V.O., Johnson E.G. // IEEE Photonics Technology Letters. - 2009. - Vol. 21, No. 19. - P. 1420-1422. ↑

J660. Yun-Li Li. Investigation of Efficiency Droop Behaviors of InGaN/GaN Multiple-Quantum-Well LEDs With Various Well Thicknesses. / Yun-Li Li, Yi-Ru Huang, Yu-Hung Lai. // IEEE Journal of Selected Topics in Quantum Electronics. - 2009. - Vol. 15, No. 4. - P. 1128-1131. ↑

J661. Hsieh Ming-Ta. Study of electrical characterization of 2-methyl-9, 10-di (2-naphthyl)anthracene doped with tungsten oxide as hole-transport layer. / Hsieh Ming-Ta, Ho Meng-Huan, Lin Kuan-Heng, Chen Jenn-Fang, Chen Teng-Ming, Chen Chin H. // Applied Physics Letters. - 2009. - Vol. 95, No. 3. - P. 033501-033501-3. ↑

J662. Nizamoglu S. Green/Yellow Solid-State Lighting via Radiative and Nonradiative Energy Transfer Involving Colloidal Semiconductor Nanocrystals. / Nizamoglu S., Sari E., Jong-Hyeob Baek, In-Hwan Lee, Volkan Demir H. // IEEE Journal of Selected Topics in Quantum Electronics. - 2009. - Vol. 15, No. 4. - P. 1163-1170. ↑

J663. Yih-Peng Chiou. Wide-Angle Beam Propagation Method Using Local Reference Indices. / Yih-Peng Chiou, Cheng-Han Du. // Journal of Lightwave Technology. - 2009. - Vol. 27, No. 16. - P. 3381-3388. ↑

J664. Nakanotani Hajime. Highly balanced ambipolar mobilities with intense electroluminescence in field-effect transistors based on organic single crystal oligo(p-phenylenevinylene) derivatives. / Nakanotani Hajime, Saito Masatoshi, Nakamura Hiroaki, Adachi Chihaya. // Applied Physics Letters. - 2009. - Vol. 95, No. 3. - P. 033308-033308-3. ↑

J665. Huang Hung-Hsun. Study of polarization properties of light emitted from a -plane InGaN/GaN quantum well-based light emitting diodes. / Huang Hung-Hsun, Wu Yuh-Renn. // Journal of Applied Physics. - 2009. - Vol. 106, No. 2. - P. 023106-023106-6. ↑

J666. Li Y. Z. Top-emission Si-based phosphor organic light emitting diode with Au doped ultrathin n-Si film anode and bottom Al mirror. / Li Y. Z., Xu W. J., Ran G. Z., Qin G. G. // Applied Physics Letters. - 2009. - Vol. 95, No. 3. - P. 033307-033307-3. ↑

J667. Nakanishi T. Novel -Activated Glass Ceramics Precipitated With Green and Red Phosphors for High-Power White LED. / Nakanishi T., Tanabe S. // IEEE Journal of Selected Topics in Quantum Electronics. - 2009. - Vol. 15, No. 4. - P. 1171-1176. ↑

- J668.** Seok-Man Kim. A hybrid control scheme for driving current sources of pm-oled panel. / Seok-Man Kim, Je-Hoon Lee, Kyoung-Rok Cho. // IEEE Transactions on Consumer Electronics. - 2009. - Vol. 55, No. 2. - P. 644-649. ↑
- J669.** Tsai K. Y. F. Interfacial electronic structure of a hybrid organic-inorganic optical upconverter device: The role of interface states. / Tsai K. Y. F., Helander M. G., Lu Z. H. // Journal of Applied Physics. - 2009. - Vol. 105, No. 8. - P. 083706-083706-8. ↑
- J670.** Sharma Asha. Tailoring the work function of indium tin oxide electrodes in electrophosphorescent organic light-emitting diodes. / Sharma Asha, Hotchkiss Peter J., Marder Seth R., Kippelen Bernard. // Journal of Applied Physics. - 2009. - Vol. 105, No. 8. - P. 084507-084507-6. ↑
- J671.** Lim Jong Tae. Electronic structures of Ba-on-Alq 3 interfaces and device characteristics of organic light-emitting diodes based on these interfaces. / Lim Jong Tae, Yeom Geun Young, Lhm Kyuwook, Kang Tai-Hee. // Journal of Applied Physics. - 2009. - Vol. 105, No. 8. - P. 083705-083705-4. ↑
- J672.** Bai Shih Jung. Optical absorption and emission of fully conjugated heterocyclic aromatic rigid-rod polyelectrolytes containing sulfonated pendants. / Bai Shih Jung, Han Shen-Rong. // Journal of Applied Physics. - 2009. - Vol. 105, No. 8. - P. 083104-083104-5. ↑
- J673.** Nizamoglu Sedat. Excitation resolved color conversion of CdSe/ZnS core/shell quantum dot solids for hybrid white light emitting diodes. / Nizamoglu Sedat, Demir Hilmi Volkan. // Journal of Applied Physics. - 2009. - Vol. 105, No. 8. - P. 083112-083112-5. ↑
- J674.** Wang Fengxia. Tungsten oxide doped N,N'-di(naphthalen-1-yl)-N,N'-diphenyl-benzidine as hole injection layer for high performance organic light-emitting diodes. / Wang Fengxia, Qiao Xianfeng, Xiong Tao, Ma Dongge. // Journal of Applied Physics. - 2009. - Vol. 105, No. 8. - P. 084518-084518-6. ↑
- J675.** Heikkila Oskari. Ultimate limit and temperature dependency of light-emitting diode efficiency. / Heikkila Oskari, Oksanen Jani, Tulkki Jukka. // Journal of Applied Physics. - 2009. - Vol. 105, No. 9. - P. 093119-093119-9. ↑
- J676.** Gassmann Andrea. The Li 3 PO 4 /Al bilayer: An efficient cathode for organic light emitting devices. / Gassmann Andrea, Melzer Christian, von Seggern Heinz. // Journal of Applied Physics. - 2009. - Vol. 105, No. 8. - P. 084513-084513-6. ↑
- J677.** Ramuz Marc. Coupling light from an organic light emitting diode (OLED) into a single-mode waveguide: Toward monolithically integrated optical sensors. / Ramuz Marc, Burgi Lukas, Stanley Ross, Winnewisser Carsten. // Journal of Applied Physics. - 2009. - Vol. 105, No. 8. - P. 084508-084508-7. ↑
- J678.** Toyama Toshihiko. Ultraviolet-light-emitting AlN:Gd thin-film electroluminescence device using an energy transfer from Gd 3+ ions to N 2 molecules. / Toyama Toshihiko, Ota Jun, Adachi Daisuke, Niioka Yasumasa, Lee Dong-Hun, Okamoto Hiroaki. // Journal of Applied Physics. - 2009. - Vol. 105, No. 8. - P. 084512-084512-5. ↑
- J679.** Jarikov Viktor V. Studies of the degradation mechanism of organic light-emitting diodes based on tris(8-quinolinolate)aluminum Alq and 2-tert-butyl-9,10-di(2-naphthyl)anthracene TBADN. / Jarikov Viktor V., Kondakov Denis Y. // Journal of Applied Physics. - 2009. - Vol. 105, No. 3. - P. 034905-034905-8. ↑
- J680.** Jing Pengtao. Shell-dependent electroluminescence from colloidal CdSe quantum dots in multilayer light-emitting diodes. / Jing Pengtao, Zheng Jinju, Zeng Qinghui, Zhang Youlin, Liu Xiaomin, Liu Xueyan, Kong Xianggui, Zhao Jialong. // Journal of Applied Physics. - 2009. - Vol. 105, No. 4. - P. 044313-044313-5. ↑
- J681.** Tan Zhanao. Colloidal nanocrystal-based light-emitting diodes fabricated on plastic toward flexible quantum dot optoelectronics. / Tan Zhanao, Xu Jian, Zhang Chunfeng, Zhu Ting, Zhang Fan, Hedrick Brittany, Pickering Shawn, Wu Jian, Su Huaipeng, Gao Shuai, Wang Andrew Y., Kimball Brian, Ruzylo Jerzy, Dellas Nicholas S., Mohny Suzanne E. // Journal of Applied Physics. - 2009. - Vol. 105, No. 3. - P. 034312-034312-5. ↑
- J682.** Tang Tsung-Yi. Coalescence overgrowth of GaN nanocolumns on sapphire with patterned metal organic vapor phase epitaxy. / Tang Tsung-Yi, Shiao Wen-Yu, Lin Cheng-Hung, Shen Kun-Ching, Huang Jeng-Jie, Ting Shao-Ying, Liu Tzu-Chi, Yang C. C., Yao Chiu-Lin, Yeh Jui-Hung, Hsu Ta-Cheng, Chen Wei-Chao, Hsu Hsu-Cheng, Chen Li-Chyong. // Journal of Applied Physics. - 2009. - Vol. 105, No. 2. - P. 023501-023501-8. ↑

- J683.** Wu Chih-I. Electronic and chemical properties of molybdenum oxide doped hole injection layers in organic light emitting diodes. / Wu Chih-I, Lin Chang-Ting, Lee Guan-Ru, Cho Ting-Yi, Wu Chung-Chih, Pi Tun-Wen. // Journal of Applied Physics. - 2009. - Vol. 105, No. 3. - P. 033717-033717-4. ↑
- J684.** Lin Ke. Correlation analysis of electrical and optical low frequency fluctuation in organic device degradation. / Lin Ke, Cheng Lai Szu, Ramam Adelia, Jin Chua Soo. // Journal of Applied Physics. - 2009. - Vol. 105, No. 6. - P. 064504-064504-7. ↑
- J685.** Lee Jae-Hoon. Enhanced performance of GaN-based light emitting diode with isoelectronic Al doping layer. / Lee Jae-Hoon, Lee Jung-Hee. // Journal of Applied Physics. - 2009. - Vol. 105, No. 6. - P. 064508-064508-6. ↑
- J686.** Chang Mei-Ying. High-brightness, high-color-purity, white organic light-emitting diodes featuring multiple emission layers. / Chang Mei-Ying, Wang Chien-Hsiung, Lin Shih-Chin, Chen Yi-Fan. // Journal of Applied Physics. - 2009. - Vol. 105, No. 6. - P. 064318-064318-6. ↑
- J687.** Coya C. Full-solution-processed blue organic light emitting device based on a fluorescent 1,3,5-trisubstituted benzene stilbenoid small molecule. / Coya C., de Andres A., Zaldo C., Alvarez A. L., Arredondo B., Gomez R., Segura J. L., Seoane C. // Journal of Applied Physics. - 2009. - Vol. 105, No. 4. - P. 044510-044510-6. ↑
- J688.** Shklyayev A. A. Defect-related light emission in the 1.4-1.7 μm range from Si layers at room temperature. / Shklyayev A. A., Nakamura Y., Dultsev F. N., Ichikawa M. // Journal of Applied Physics. - 2009. - Vol. 105, No. 6. - P. 063513-063513-4. ↑
- J689.** Dinh Nguyen Nang. Enhancement of current-voltage characteristics of multilayer organic light emitting diodes by using nanostructured composite films. / Dinh Nguyen Nang, Chi Le Ha, Chung Thuy Tran Thi, Trung Tran Quang, Truong Vo-Van. // Journal of Applied Physics. - 2009. - Vol. 105, No. 9. - P. 093518-093518-5. ↑
- J690.** Sun Yongjian. Microanalyses of the reverse-bias leakage current increase in the laser lift off GaN-based light emitting diodes. / Sun Yongjian, Yu Tongjun, Zhao Huabo, Shan Xudong, Zhang Xinzheng, Chen Zhizhong, Kang Xiangning, Yu Dapeng, Zhang Guoyi. // Journal of Applied Physics. - 2009. - Vol. 106, No. 1. - P. 013101-013101-4. ↑
- J691.** Lee Ching-Ting. Light enhancement of Al nanoclusters embedded in Al-doped ZnO films of GaN-based light-emitting diodes. / Lee Ching-Ting, Chou Ying-Hung, Yan Jheng-Tai, Lee Hsin-Ying. // Journal of Vacuum Science & Technology B: Microelectronics and Nanometer Structures. - 2009. - Vol. 27, No. 4. - P. 1901-1903. ↑
- J692.** Lin You-Da. Characterization of blue-green m -plane InGaN light emitting diodes. / Lin You-Da, Chakraborty Arpan, Brinkley Stuart, Kuo Hsun Chih, Melo Thiago, Fujito Kenji, Speck James S., DenBaars Steven P., Nakamura Shuji. // Applied Physics Letters. - 2009. - Vol. 94, No. 26. - P. 261108-261108-3. ↑
- J693.** Gather Malte C. Measuring the profile of the emission zone in polymeric organic light-emitting diodes. / Gather Malte C., Flammich Michael, Danz Norbert, Michaelis Dirk, Meerholz Klaus. // Applied Physics Letters. - 2009. - Vol. 94, No. 26. - P. 263301-263301-3. ↑
- J694.** Loeser M. The Ultra Weak Variational Formulation Applied to Radiation Problems With Macroscopic Sources in Inhomogeneous Domains. / Loeser M., Witzigmann B. // IEEE Journal of Selected Topics in Quantum Electronics. - 2009. - Vol. 15, No. 4. - P. 1144-1155. ↑
- J695.** Lee J. W. High efficiency GaN-based light-emitting diodes fabricated on dielectric mask-embedded structures. / Lee J. W., Sone C., Park Y., Lee S.-N., Ryou J.-H., Dupuis R. D., Hong C.-H., Kim H. // Applied Physics Letters. - 2009. - Vol. 95, No. 1. - P. 011108-011108-3. ↑
- J696.** Yang Y. Complete suppression of surface leakage currents in microperforated blue light-emitting diodes. / Yang Y., Cao X. A. // Applied Physics Letters. - 2009. - Vol. 95, No. 1. - P. 011109-011109-3. ↑
- J697.** Park Jin-Seong. Flexible full color organic light-emitting diode display on polyimide plastic substrate driven by amorphous indium gallium zinc oxide thin-film transistors. / Park Jin-Seong, Kim Tae-Woong, Stryakhilev Denis, Lee Jae-Sup, An Sung-Guk, Pyo Yong-Shin, Lee Dong-Bum, Mo Yeon Gon, Jin Dong-Un, Chung Ho Kyoon. // Applied Physics Letters. - 2009. - Vol. 95, No. 1. - P. 013503-013503-3. ↑

- J698.** Chen J. Near-infrared optical upconverter based on i-In_{0.53}Ga_{0.47}As/C₆₀ photovoltaic heterojunction. / Chen J., Ban D., Helander M.G., Lu Z., Graf M., SpringThorpe A.J., Liu H.C. // Electronics Letters. - 2009. - Vol. 45, No. 14. - P. 753-755. ↑
- J699.** Cho J. Effect of chip geometry on breakdown voltage of GaInN light-emitting diodes. / Cho J., Zhu D., Schubert E.F., Kim J.K. // Electronics Letters. - 2009. - Vol. 45, No. 14. - P. 755-756. ↑
- J700.** Harris S. Sight and insight-[engineering vision]. Engineering & Technology. - 2009. - Vol. 4, No. 8. - P. 22-25. ↑
- J701.** Giebink N. C. Direct evidence for degradation of polaron excited states in organic light emitting diodes. / Giebink N. C., D'Andrade B. W., Weaver M. S., Brown J. J., Forrest S. R. // Journal of Applied Physics. - 2009. - Vol. 105, No. 12. - P. 124514-124514-7. ↑
- J702.** Ashtiani S.J. A Driving Scheme for Active-Matrix Organic Light-Emitting Diode Displays Based on Current Feedback. / Ashtiani S.J., Nathan A. // Journal of Display Technology. - 2009. - Vol. 5, No. 7. - P. 257-264. ↑
- J703.** Liu R. Magnetic field dependent triplet-triplet annihilation in Alq₃-based organic light emitting diodes at different temperatures. / Liu R., Zhang Y., Lei Y. L., Chen P., Xiong Z. H. // Journal of Applied Physics. - 2009. - Vol. 105, No. 9. - P. 093719-093719-5. ↑
- J704.** Sheng-Horng Yen. Effect of N-Type AlGaIn Layer on Carrier Transportation and Efficiency Droop of Blue InGaIn Light-Emitting Diodes. / Sheng-Horng Yen, Miao-Chan Tsai, Meng-Lun Tsai, Yu-Jiun Shen, Ta-Cheng Hsu, Yen-Kuang Kuo. // IEEE Photonics Technology Letters. - 2009. - Vol. 21, No. 14. - P. 975-977. ↑
- J705.** Li Lian. Temperature dependences of photoluminescence and electroluminescence spectra in light-emitting diodes. / Li Lian, Li Ping, Wen Yumei, Wen Jing, Zhu Yong. // Applied Physics Letters. - 2009. - Vol. 94, No. 26. - P. 261103-261103-3. ↑
- J706.** Wang Tong-Wen. Violet light-emitting diodes grown on crack-free AlGaIn templates. / Wang Tong-Wen, Chen Nie-Chuan, Lien Wei-Chieh, Wu Meng-Chyi, Shih Chuan-Feng. // Journal of Vacuum Science & Technology B: Microelectronics and Nanometer Structures. - 2009. - Vol. 27, No. 4. - P. 1881-1885. ↑
- J707.** Jimin Cheon. A Single-Chip CMOS Smoke and Temperature Sensor for an Intelligent Fire Detector. / Jimin Cheon, Jeonghwan Lee, Inhee Lee, Youngcheol Chae, Youngsin Yoo, Gunhee Han. // IEEE Sensors Journal. - 2009. - Vol. 9, No. 8. - P. 914-921. ↑
- J708.** Gassmann Andrea. Interface properties of a Li₃PO₄/Al cathode in organic light emitting diodes. / Gassmann Andrea, Melzer Christian, Mankel Eric, Jaegermann Wolfram, von Seggern Heinz. // Journal of Applied Physics. - 2009. - Vol. 105, No. 12. - P. 124517-124517-7. ↑
- J709.** Wei-Chih Lai. GaN-Based LEDs With Mesh ITO p-Contact and Nanopillars. / Wei-Chih Lai, Chen P.H., Chang L.C., Cheng-Huang Kuo, Jinn-Kong Sheu, Tun C.J., Shei S.C. // IEEE Photonics Technology Letters. - 2009. - Vol. 21, No. 18. - P. 1293-1295. ↑
- J710.** Simbrunner C. Para-sexiphenyl-CdSe/ZnS nanocrystal hybrid light emitting diodes. / Simbrunner C., Hernandez-Sosa G., Baumgartner E., Hesser G., Roither J., Heiss W., Sitter H. // Applied Physics Letters. - 2009. - Vol. 94, No. 7. - P. 073505-073505-3. ↑
- J711.** Mi Bao Xiu. Organic light-emitting diodes using 3,6-difluoro-2,5,7,8-tetracyanoquinodimethane as p-type dopant. / Mi Bao Xiu, Gao Zhi Qiang, Cheah Kok Wai, Chen Chin H. // Applied Physics Letters. - 2009. - Vol. 94, No. 7. - P. 073507-073507-3. ↑
- J712.** Hussain A. Mohammed. Improved performance of polymer light-emitting diodes with nanocomposites. / Hussain A. Mohammed, Neppolian B., Kim Sun Hee, Kim Jin Young, Choi Hee-Chul, Lee Kwanghee, Park Seong-Ju, Heeger Alan J. // Applied Physics Letters. - 2009. - Vol. 94, No. 7. - P. 073306-073306-3. ↑
- J713.** Cocchi Massimo. Color-variable highly efficient organic electrophosphorescent diodes manipulating molecular exciton and excimer emissions. / Cocchi Massimo, Kalinowski Jan, Fattori Valeria, Williams J. A. Gareth, Murphy Lisa. // Applied Physics Letters. - 2009. - Vol. 94, No. 7. - P. 073309-073309-3. ↑

- J714.** Thomschke Michael. Optimized efficiency and angular emission characteristics of white top-emitting organic electroluminescent diodes. / Thomschke Michael, Nitsche Robert, Furno Mauro, Leo Karl. // Applied Physics Letters. - 2009. - Vol. 94, No. 8. - P. 083303-083303-3. ↑
- J715.** Cocchi Massimo. High efficiency electroluminescence devices using a series of Ir(III)-tetrazolate phosphors: Mechanisms for the drive current evolution of quantum yield. / Cocchi Massimo, Kalinowski Jan, Stagni Stefano, Muzzioli Sara. // Applied Physics Letters. - 2009. - Vol. 94, No. 8. - P. 083306-083306-3. ↑
- J716.** Zhu Di. The origin of the high diode-ideality factors in GaInN/GaN multiple quantum well light-emitting diodes. / Zhu Di, Xu Jiuru, Noemaun Ahmed N., Kim Jong Kyu, Schubert E. Fred, Crawford Mary H., Koleske Daniel D. // Applied Physics Letters. - 2009. - Vol. 94, No. 8. - P. 081113-081113-3. ↑
- J717.** Schubert Martin F. On resonant optical excitation and carrier escape in GaInN/GaN quantum wells. / Schubert Martin F., Xu Jiuru, Dai Qi, Mont Frank W., Kim Jong Kyu, Schubert E. Fred. // Applied Physics Letters. - 2009. - Vol. 94, No. 8. - P. 081114-081114-3. ↑
- J718.** Haverinen Hanna M. Inkjet printing of light emitting quantum dots. / Haverinen Hanna M., Myllyla Risto A., Jabbour Ghassan E. // Applied Physics Letters. - 2009. - Vol. 94, No. 7. - P. 073108-073108-3. ↑
- J719.** Saito Makoto. Evaluation of GaN substrates grown in supercritical basic ammonia. / Saito Makoto, Yamada Hisashi, Iso Kenji, Sato Hitoshi, Hirasawa Hirohiko, Kamber Derrick S., Hashimoto Tadao, DenBaars Steven P., Speck James S., Nakamura Shuji. // Applied Physics Letters. - 2009. - Vol. 94, No. 5. - P. 052109-052109-3. ↑
- J720.** Vampola Kenneth J. Measurement of electron overflow in 450 nm InGaN light-emitting diode structures. / Vampola Kenneth J., Iza Michael, Keller Stacia, DenBaars Steven P., Nakamura Shuji. // Applied Physics Letters. - 2009. - Vol. 94, No. 6. - P. 061116-061116-3. ↑
- J721.** Scholz Sebastian. Laser desorption/ionization time-of-flight mass spectrometry: A predictive tool for the lifetime of organic light emitting devices. / Scholz Sebastian, Meerheim Rico, Lussem Bjorn, Leo Karl. // Applied Physics Letters. - 2009. - Vol. 94, No. 4. - P. 043314-043314-3. ↑
- J722.** Chang C. H. Broadband and omnidirectional antireflection from conductive indium-tin-oxide nanocolumns prepared by glancing-angle deposition with nitrogen. / Chang C. H., Yu Peichen, Yang C. S. // Applied Physics Letters. - 2009. - Vol. 94, No. 5. - P. 051114-051114-3. ↑
- J723.** Tsintzos S. I. Room temperature GaAs exciton-polariton light emitting diode. / Tsintzos S. I., Savvidis P. G., Deligeorgis G., Hatzopoulos Z., Pelekanos N. T. // Applied Physics Letters. - 2009. - Vol. 94, No. 7. - P. 071109-071109-3. ↑
- J724.** Kim Kyoung-Kook. Enhanced light extraction efficiency of GaN-based light-emitting diodes with ZnO nanorod arrays grown using aqueous solution. / Kim Kyoung-Kook, Lee Sam-dong, Kim Hyunsoo, Park Jae-Chul, Lee Sung-Nam, Park Youngsoo, Park Seong-Ju, Kim Sang-Woo. // Applied Physics Letters. - 2009. - Vol. 94, No. 7. - P. 071118-071118-3. ↑
- J725.** Takeuchi Misaichi. AlN/AlGaIn short-period superlattice sacrificial layers in laser lift-off for vertical-type AlGaIn-based deep ultraviolet light emitting diodes. / Takeuchi Misaichi, Maegawa Tomohiro, Shimizu Hiroshi, Ooishi Shin, Ohtsuka Takumi, Aoyagi Yoshinobu. // Applied Physics Letters. - 2009. - Vol. 94, No. 6. - P. 061117-061117-3. ↑
- J726.** Mariano F. Very low voltage and stable p-i-n organic light-emitting diodes using a linear S,S-dioxide oligothiophene as emitting layer. / Mariano F., Mazzeo M., Duan Y., Barbarella G., Favaretto L., Carallo S., Cingolani R., Gigli G. // Applied Physics Letters. - 2009. - Vol. 94, No. 6. - P. 063510-063510-3. ↑
- J727.** Sang-Mook Kim. Wafer-Level Packaged Light-Emitting Diodes Using Photodielectric Resin. / Sang-Mook Kim, Kwang-Cheol Lee, Young Moon Yu, Jong Hyeob Baek, Gun Young Jung. // IEEE Electron Device Letters. - 2009. - Vol. 30, No. 6. - P. 638-640. ↑
- J728.** Moore S.K. Some bright spots in the gloom. IEEE Spectrum. - 2009. - Vol. 46, No. 5. - P. 14. ↑
- J729.** Faxin Zang. Modulated Infrared Electroluminescence From Organic Light-Emitting Diodes. / Faxin Zang, Tze-Chien Sum, Furong Zhu, Zi-Ruo Hong, Xiaoyan Sun, Wen Lian Li, Huan C.H.A. // Journal of Lightwave

Technology. - 2009. - Vol. 27, No. 11. - P. 1522-1526. ↑

J730. Kok Beng Gan. Transabdominal Fetal Heart Rate Detection Using NIR Photoplethysmography: Instrumentation and Clinical Results. / Kok Beng Gan, Zahedi E., Ali M.A.M. // IEEE Transactions on Biomedical Engineering. - 2009. - Vol. 56, No. 8. - P. 2075-2082. ↑

J731. Uchida T. Blue Flexible Transparent Organic Light-Emitting Devices. / Uchida T., Wakana M., Yahata M., Dangtip S., Osotchan T., Satoh T., Sawada Y. // Journal of Display Technology. - 2009. - Vol. 5, No. 6. - P. 188-191. ↑

J732. Shih-Yung Huang. High-Performance InGaN-Based Green Resonant-Cavity Light-Emitting Diodes for Plastic Optical Fiber Applications. / Shih-Yung Huang, Ray-Hua Horng, Jin-Wei Shi, Hao-Chung Kuo, Dong-Sing Wu. // Journal of Lightwave Technology. - 2009. - Vol. 27, No. 18. - P. 4084-4094. ↑

J733. {no data available}. Robotic baby seal could diminish dementia. IEEE Spectrum. - 2009. - Vol. 46, No. 5. - P. 14. ↑

J734. Chen H.-L. Guest Editorial. / Chen H.-L., Hou J., McCulloch I., Raupp G. B., Subramanian V. // Journal of Display Technology. - 2009. - Vol. 5, No. 6. - P. 169-171. ↑

J735. Jongwoon Park. Electrical Properties of Trilayer Organic Light-Emitting Diodes With a Mixed Emitting Layer. / Jongwoon Park, Seoungwan Park, Dongchan Shin. // Journal of Lightwave Technology. - 2009. - Vol. 27, No. 13. - P. 2525-2529. ↑

J736. Jeon Soon Ok. Color control of multilayer stacked white polymer light-emitting diodes using a quantum dot as an interlayer. / Jeon Soon Ok, Joo Chul Woong, Yook Kyungsoo, Lee Jun Yeob. // Applied Physics Letters. - 2009. - Vol. 94, No. 9. - P. 093303-093303-3. ↑

J737. Yook Kyoung Soo. Correlation of lifetime and recombination zone in green phosphorescent organic light-emitting diodes. / Yook Kyoung Soo, Jeon Soon Ok, Joo Chul Woong, Lee Jun Yeob. // Applied Physics Letters. - 2009. - Vol. 94, No. 9. - P. 093501-093501-3. ↑

J738. Zhang Y. Low temperature magnetic field effects in Alq 3 -based organic light emitting diodes. / Zhang Y., Liu R., Lei Y. L., Xiong Z. H. // Applied Physics Letters. - 2009. - Vol. 94, No. 8. - P. 083307-083307-3. ↑

J739. Song Yanhua. Sr 3 Al 2 O 5 Cl 2 :Ce 3+ ,Eu 2+ : A potential tunable yellow-to-white-emitting phosphor for ultraviolet light emitting diodes. / Song Yanhua, Jia Guang, Yang Mei, Huang Yeju, You Hongpeng, Zhang Hongjie. // Applied Physics Letters. - 2009. - Vol. 94, No. 9. - P. 091902-091902-3. ↑

J740. Jing Rao. Enhancement of Light Extraction From Resonant Cavity Light-Emitting Diodes Using a 2-D Grating Embossed in TiO Sol-Gel. / Jing Rao, Winfield R., O'Brien S. // IEEE Photonics Technology Letters. - 2009. - Vol. 21, No. 13. - P. 941-943. ↑

J741. Huang-Jen Chiu. Design of an RGB LED Backlight Circuit for Liquid Crystal Display Panels. / Huang-Jen Chiu, Yu-Kang Lo, Ting-Peng Lee, Shann-Chyi Mou, Hsiu-Ming Huang. // IEEE Transactions on Industrial Electronics. - 2009. - Vol. 56, No. 7. - P. 2793-2795. ↑

J742. Yang Y. Near-infrared photon upconversion devices based on GaNAsSb active layer lattice matched to GaAs. / Yang Y., Shen W. Z., Liu H. C., Laframboise S. R., Wicaksono S., Yoon S. F., Tan K. H. // Applied Physics Letters. - 2009. - Vol. 94, No. 9. - P. 093504-093504-3. ↑

J743. Zhao J. L. Blue to deep UV light emission from a p-Si /AlN /Au heterostructure. / Zhao J. L., Tan S. T., Iwan S., Sun X. W., Liu W., Chua S. J. // Applied Physics Letters. - 2009. - Vol. 94, No. 9. - P. 093506-093506-3. ↑

J744. Wang X. H. Control performance of a single-chip white light emitting diode by adjusting strain in InGaN underlying layer. / Wang X. H., Guo L. W., Jia H. Q., Xing Z. G., Wang Y., Pei X. J., Zhou J. M., Chen H. // Applied Physics Letters. - 2009. - Vol. 94, No. 11. - P. 111913-111913-3. ↑

J745. Liu Z. W. Efficient bilayer phosphorescent organic light-emitting diodes: Direct hole injection into triplet dopants. / Liu Z. W., Helander M. G., Wang Z. B., Lu Z. H. // Applied Physics Letters. - 2009. - Vol. 94, No. 11. - P. 113305-113305-3. ↑

- J746.** Wang Qi. Highly efficient single-emitting-layer white organic light-emitting diodes with reduced efficiency roll-off. / Wang Qi, Ding Junqiao, Ma Dongge, Cheng Yanxiang, Wang Lixiang. // Applied Physics Letters. - 2009. - Vol. 94, No. 10. - P. 103503-103503-3. ↑
- J747.** Kim B. J. Output power enhancement of GaN light emitting diodes with p -type ZnO hole injection layer. / Kim B. J., Ryu Y. R., Lee T. S., White H. W. // Applied Physics Letters. - 2009. - Vol. 94, No. 10. - P. 103506-103506-3. ↑
- J748.** Zheng Tianhang. Nanoparticle-induced resonant tunneling behaviors in small molecule organic light-emitting devices. / Zheng Tianhang, Choy Wallace C. H., Sun Yuxiu. // Applied Physics Letters. - 2009. - Vol. 94, No. 12. - P. 123303-123303-3. ↑
- J749.** Jeon Soo-Kun. The effect of the internal capacitance of InGaN-light emitting diode on the electrostatic discharge properties. / Jeon Soo-Kun, Lee Jae-Gab, Park Eun-Hyun, Jang Jin, Lim Jae-Gu, Kim Seo-Kun, Park Joong-Seo. // Applied Physics Letters. - 2009. - Vol. 94, No. 13. - P. 131106-131106-2. ↑
- J750.** De Simoni Giorgio. Acoustoelectric luminescence from a field-effect n-i-p lateral junction. / De Simoni Giorgio, Piazza Vincenzo, Sorba Lucia, Biasiol Giorgio, Beltram Fabio. // Applied Physics Letters. - 2009. - Vol. 94, No. 12. - P. 121103-121103-3. ↑
- J751.** Lai Chun-Feng. Directional light extraction enhancement from GaN-based film-transferred photonic crystal light-emitting diodes. / Lai Chun-Feng, Chao Chia-Hsin, Kuo Hao-Chung, Yen His-Hsuan, Lee Chia-En, Yeh Wen-Yung. // Applied Physics Letters. - 2009. - Vol. 94, No. 12. - P. 123106-123106-3. ↑
- J752.** Uno Mayumi. Three-dimensional organic field-effect transistors with high output current and high on-off ratio. / Uno Mayumi, Doi I., Takimiya K., Takeya J. // Applied Physics Letters. - 2009. - Vol. 94, No. 10. - P. 103307-103307-3. ↑
- J753.** Jeon Soon Ok. High efficiency blue phosphorescent organic light emitting diodes using a simple device structure. / Jeon Soon Ok, Yook Kyoung Soo, Joo Chul Woong, Lee Jun Yeob. // Applied Physics Letters. - 2009. - Vol. 94, No. 1. - P. 013301-013301-3. ↑
- J754.** Chiu Tien-Lung. Optical and electrical characteristics of Ag-doped perylene diimide derivative. / Chiu Tien-Lung, Xu Wei-Feng, Lin Chi-Feng, Lee Jiun-Haw, Chao Chun-Chieh, Leung Man-Kit. // Applied Physics Letters. - 2009. - Vol. 94, No. 1. - P. 013307-013307-3. ↑
- J755.** Xu Jiuru. Reduction in efficiency droop, forward voltage, ideality factor, and wavelength shift in polarization-matched GaInN/GaN multi-quantum-well light-emitting diodes. / Xu Jiuru, Schubert Martin F., Noemaun Ahmed N., Zhu Di, Kim Jong Kyu, Schubert E. Fred, Kim Min Ho, Chung Hun Jae, Yoon Sukho, Sone Cheolsoo, Park Yongjo. // Applied Physics Letters. - 2009. - Vol. 94, No. 1. - P. 011113-011113-3. ↑
- J756.** Liu Deang. Organic light-emitting diodes with carbon nanotube cathode-organic interface layer. / Liu Deang, Fina Michael, Guo Jinghua, Chen Xiaobo, Liu Gao, Johnson Stephen G., Mao Samuel S. // Applied Physics Letters. - 2009. - Vol. 94, No. 1. - P. 013110-013110-3. ↑
- J757.** Kanjilal A. Correlation between the microstructure and electroluminescence properties of Er-doped metal-oxide semiconductor structures. / Kanjilal A., Rebohle L., Skorupa W., Helm M. // Applied Physics Letters. - 2009. - Vol. 94, No. 10. - P. 101916-101916-3. ↑
- J758.** Liu Chih-Che. Microcavity top-emitting organic light-emitting devices integrated with diffusers for simultaneous enhancement of efficiencies and viewing characteristics. / Liu Chih-Che, Liu Su-Hao, Tien Kun-Cheng, Hsu Min-Hung, Chang Hong-Wei, Chang Chih-Kai, Yang Chih-Jen, Wu Chung-Chih. // Applied Physics Letters. - 2009. - Vol. 94, No. 10. - P. 103302-103302-3. ↑
- J759.** Kim Sun-Kyung. Metal mirror assisting light extraction from patterned AlGaInP light-emitting diodes. / Kim Sun-Kyung, Song Hyun Don, Ee Ho-Seok, Choi Hyun Min, Cho Hyun Kyong, Lee Yong-Hee, Park Hong-Gyu. // Applied Physics Letters. - 2009. - Vol. 94, No. 10. - P. 101102-101102-3. ↑
- J760.** Lee Joonhee. GaN light-emitting diode with monolithically integrated photonic crystals and angled sidewall deflectors for efficient surface emission. / Lee Joonhee, Ahn Sungmo, Kim Sihan, Kim Dong-Uk, Jeon Heonsu, Lee Seung-Jae, Baek Jong Hyeob. // Applied Physics Letters. - 2009. - Vol. 94, No. 10. - P. 101105-101105-3. ↑

- J761.** Maier Markus. Reduced nonthermal rollover of wide-well GaInN light-emitting diodes. / Maier Markus, Kohler Klaus, Kunzer Michael, Pletschen Wilfried, Wagner Joachim. // Applied Physics Letters. - 2009. - Vol. 94, No. 4. - P. 041103-041103-3. ↑
- J762.** Park Seoung-Hwan. High-efficiency staggered 530 nm InGaN/InGaN/GaN quantum-well light-emitting diodes. / Park Seoung-Hwan, Ahn Doyeol, Kim Jong-Wook. // Applied Physics Letters. - 2009. - Vol. 94, No. 4. - P. 041109-041109-3. ↑
- J763.** Hoven Corey V. Direct measurement of electric field screening in light emitting diodes with conjugated polyelectrolyte electron injecting/transport layers. / Hoven Corey V., Peet Jeffrey, Mikhailovsky Alexander, Nguyen Thuc-Quyen. // Applied Physics Letters. - 2009. - Vol. 94, No. 3. - P. 033301-033301-3. ↑
- J764.** Tsuzuki Toshimitsu. Highly efficient and stable organic light-emitting diode using 4,4'-bis(N -carbazolyl)-9,9'-spirobifluorene as a thermally stable host material. / Tsuzuki Toshimitsu, Tokito Shizuo. // Applied Physics Letters. - 2009. - Vol. 94, No. 3. - P. 033302-033302-3. ↑
- J765.** Okachi Takayuki. Determination of localized-state distributions in organic light-emitting diodes by impedance spectroscopy. / Okachi Takayuki, Nagase Takashi, Kobayashi Takashi, Naito Hiroyoshi. // Applied Physics Letters. - 2009. - Vol. 94, No. 4. - P. 043301-043301-3. ↑
- J766.** Chen Fang-Chung. Single-layer triplet white polymer light-emitting diodes incorporating polymer oxides: Effect of charge trapping at phosphorescent dopants. / Chen Fang-Chung, Chien Shang-Chieh, Chen Yung-Shiuan. // Applied Physics Letters. - 2009. - Vol. 94, No. 4. - P. 043306-043306-3. ↑
- J767.** Yang Y. Rapid efficiency roll-off in high-quality green light-emitting diodes on freestanding GaN substrates. / Yang Y., Cao X. A., Yan C. H. // Applied Physics Letters. - 2009. - Vol. 94, No. 4. - P. 041117-041117-3. ↑
- J768.** Jeon Joon-Woo. TiN/Al Ohmic contacts to N-face n -type GaN for high-performance vertical light-emitting diodes. / Jeon Joon-Woo, Seong Tae-Yeon, Kim Hyunsoo, Kim Kyung-Kook. // Applied Physics Letters. - 2009. - Vol. 94, No. 4. - P. 042102-042102-3. ↑
- J769.** Grenet L. Spin injection in silicon at zero magnetic field. / Grenet L., Jamet M., Noe P., Calvo V., Hartmann J.-M., Nistor L. E., Rodmacq B., Auffret S., Warin P., Samson Y. // Applied Physics Letters. - 2009. - Vol. 94, No. 3. - P. 032502-032502-3. ↑
- J770.** Lee Ya-Ju. High output power density from GaN-based two-dimensional nanorod light-emitting diode arrays. / Lee Ya-Ju, Lin Shawn-Yu, Chiu Ching-Hua, Lu Tien-Chang, Kuo Hao-Chung, Wang Shing-Chung, Chhajed Sameer, Kim Jong Kyu, Schubert E. Fred. // Applied Physics Letters. - 2009. - Vol. 94, No. 14. - P. 141111-141111-3. ↑
- J771.** Liu Day-Shan. Light-extraction enhancement in GaN-based light-emitting diodes using grade-refractive-index amorphous titanium oxide films with porous structures. / Liu Day-Shan, Lin Tan-Wei, Huang Bing-Wen, Juang Fuh-Shyang, Lei Po-Hsun, Hu Chen-Ze. // Applied Physics Letters. - 2009. - Vol. 94, No. 14. - P. 143502-143502-3. ↑
- J772.** Kim Sun Young. Low voltage efficient simple p-i-n type electrophosphorescent green organic light-emitting devices. / Kim Sun Young, Jeon Woo Sik, Park Tae Jin, Pote Ramchandra, Jang Jin, Kwon Jang Hyuk. // Applied Physics Letters. - 2009. - Vol. 94, No. 13. - P. 133303-133303-3. ↑
- J773.** Truong V. G. High speed pulsed electrical spin injection in spin-light emitting diode. / Truong V. G., Binh P.-H., Renucci P., Tran M., Lu Y., Jaffres H., George J.-M., Deranlot C., Lemaitre A., Amand T., Marie X. // Applied Physics Letters. - 2009. - Vol. 94, No. 14. - P. 141109-141109-3. ↑
- J774.** Ho Meng-Huan. Study of efficient and stable organic light-emitting diodes with 2-methyl-9,10-di(2-naphthyl)anthracene as hole-transport material by admittance spectroscopy. / Ho Meng-Huan, Hsieh Ming-Ta, Lin Kuan-Heng, Chen Teng-Ming, Chen Jenn-Fang, Chen Chin H. // Applied Physics Letters. - 2009. - Vol. 94, No. 2. - P. 023306-023306-3. ↑
- J775.** Yasar M. Spin injection studies into GaAs quantum wells in the presence of confined electrons. / Yasar M., Mallory R., Petrou A., Hanbicki A. T., Kioseoglou G., Li C. H., vant Erve O. M. J., Jonker B. T. // Applied Physics Letters. - 2009. - Vol. 94, No. 3. - P. 032102-032102-3. ↑

- J776.** Vempaire D. Probing radical kinetics in the afterglow of pulsed discharges by absorption spectroscopy with light emitting diodes: Application to BCl radical. / Vempaire D., Cunge G. // Applied Physics Letters. - 2009. - Vol. 94, No. 2. - P. 021504-021504-3. ↑
- J777.** Truong T. A. Light extraction from GaN-based light emitting diode structures with a noninvasive two-dimensional photonic crystal. / Truong T. A., Campos L. M., Matoli E., Meinel I., Hawker C. J., Weisbuch C., Petroff P. M. // Applied Physics Letters. - 2009. - Vol. 94, No. 2. - P. 023101-023101-3. ↑
- J778.** Cherry S. The right word, anywhere. IEEE Spectrum. - 2009. - Vol. 46, No. 7. - P. 24. ↑
- J779.** Chih-Feng Lu. Phosphor-Free Monolithic White-Light LED. / Chih-Feng Lu, Chi-Feng Huang, Yung-Sheng Chen, Wen-Yu Shiao, Cheng-Yen Chen, Yen-Cheng Lu, Chih-Chung Yang. // IEEE Journal of Selected Topics in Quantum Electronics. - 2009. - Vol. 15, No. 4. - P. 1210-1217. ↑
- J780.** Komine T. Adaptive equalization system for visible light wireless communication utilizing multiple white LED lighting equipment. / Komine T., Jun Hwan Lee, Haruyama S., Nakagawa M. // IEEE Transactions on Wireless Communications. - 2009. - Vol. 8, No. 6. - P. 2892-2900. ↑
- J781.** Turner J. Time is on your side. IEEE Spectrum. - 2009. - Vol. 46, No. 7. - P. 24-25. ↑
- J782.** Chung Seungjun. Substrate thermal conductivity effect on heat dissipation and lifetime improvement of organic light-emitting diodes. / Chung Seungjun, Lee Jae-Hyun, Jeong Jaewook, Kim Jang-Joo, Hong Yongtaek. // Applied Physics Letters. - 2009. - Vol. 94, No. 25. - P. 253302-253302-3. ↑
- J783.** Koo Young-Mo. Spontaneous charge transfer from indium tin oxide to organic molecules for effective hole injection. / Koo Young-Mo, Song Ok-Keun. // Applied Physics Letters. - 2009. - Vol. 94, No. 15. - P. 153302-153302-3. ↑
- J784.** Hongping Zhao. Design Analysis of Staggered InGaN Quantum Wells Light-Emitting Diodes at 500-540 nm. / Hongping Zhao, Arif R.A., Tansu N. // IEEE Journal of Selected Topics in Quantum Electronics. - 2009. - Vol. 15, No. 4. - P. 1104-1114. ↑
- J785.** Yun J.S. Enhancing current spreading by simple electrode pattern design methodology in lateral GaN/InGaN LEDs. / Yun J.S., Shim J.I., Shin D.S. // Electronics Letters. - 2009. - Vol. 45, No. 13. - P. 703-705. ↑
- J786.** Weidong Gong. A Simple, Low-Cost Double Beam Spectrophotometer for Colorimetric Detection of Nitrite in Seawater. / Weidong Gong, Mowlem M., Kraft M., Morgan H. // IEEE Sensors Journal. - 2009. - Vol. 9, No. 7. - P. 862-869. ↑
- J787.** Meyer J. Reliable thin film encapsulation for organic light emitting diodes grown by low-temperature atomic layer deposition. / Meyer J., Schneidenbach D., Winkler T., Hamwi S., Weimann T., Hinze P., Ammermann S., Johannes H.-H., Riedl T., Kowalsky W. // Applied Physics Letters. - 2009. - Vol. 94, No. 23. - P. 233305-233305-3. ↑
- J788.** Yong-Joon Jeon. Improved Transient Current Feedforward Output Buffer for Fast and Compact Active-Matrix OLED Column Drivers. / Yong-Joon Jeon, Young-Suk Son, Jin-Yong Jeon, Gyu-Hyeong Cho. // IEEE Transactions on Circuits and Systems II: Express Briefs. - 2009. - Vol. 56, No. 7. - P. 560-564. ↑
- J789.** Chun-Feng Lai. Far-Field and Near-Field Distribution of GaN-Based Photonic Crystal LEDs With Guided Mode Extraction. / Chun-Feng Lai, Jim-Yong Chi, Hao-Chung Kuo, Hsi-Hsuan Yen, Chia-En Lee, Chia-Hsin Chao, Wen-Yung Yeh, Tien-Chang Lu. // IEEE Journal of Selected Topics in Quantum Electronics. - 2009. - Vol. 15, No. 4. - P. 1234-1241. ↑
- J790.** Yi-Hao Pai. Composition Optimization and Phase Transformation of Si-Nanocrystal-Doped for Enhancing Luminescence From MOSLED. / Yi-Hao Pai, Chung-Hsiang Chang, Gong-Ru Lin. // IEEE Journal of Selected Topics in Quantum Electronics. - 2009. - Vol. 15, No. 5. - P. 1387-1392. ↑
- J791.** Zhizhong Yuan. Silicon Nanocrystals as an Enabling Material for Silicon Photonics. / Zhizhong Yuan, Anopchenko A., Daldosso N., Guider R., Navarro-Urrios D., Pitanti A., Spano R., Pavesi L. // Proceedings of the IEEE. - 2009. - Vol. 97, No. 7. - P. 1250-1268. ↑

- J792.** Szczesniak T. A Comparative Study of Fast Photomultipliers for Timing Experiments and TOF PET. / Szczesniak T., Moszynski M., Swiderski L., Nassalski A., Syntfeld-Kazuch A., Dehaine A.-G., Kapusta M. // IEEE Transactions on Nuclear Science. - 2009. - Vol. 56, No. 3. - P. 1017-1023. ↑
- J793.** Bimberg D. Quantum Dots for Single- and Entangled-Photon Emitters. / Bimberg D., Stock E., Lochmann A., Schliwa A., Tofflinger J.A., Unrau W., Munnix M., Rodt S., Haisler V.A., Toropov A.I., Bakarov A., Kalagin A.K. // IEEE Photonics Journal. - 2009. - Vol. 1, No. 1. - P. 58-68. ↑
- J794.** Tsybeskov L. Silicon-Germanium Nanostructures for Light Emitters and On-Chip Optical Interconnects. / Tsybeskov L., Lockwood D.J. // Proceedings of the IEEE. - 2009. - Vol. 97, No. 7. - P. 1284-1303. ↑
- J795.** Benor Amare. Dramatic efficiency improvement in phosphorescent organic light-emitting diodes with ultraviolet-ozone treated poly(3,4-ethylenedioxythiophene):poly(styrenesulfonate). / Benor Amare, Takizawa Shinya, Chen Ping, Perez-Bolivar Cesar, Anzenbacher Pavel. // Applied Physics Letters. - 2009. - Vol. 94, No. 19. - P. 193301-193301-3. ↑
- J796.** Wang Zhongqiang. The relationship of current transfer ratio and input light wavelengths in the organic photocoupler. / Wang Zhongqiang, Deng Jiachun, Wu Xiaoming, Jing Na, Hu Ziyang, Cheng Xiaoman, Hua Yulin, Wei Jun, Yin Shougen. // Applied Physics Letters. - 2009. - Vol. 94, No. 19. - P. 193303-193303-3. ↑
- J797.** Jang Ho Won. Origin of the abnormal behavior of contact resistance in Ohmic contacts to laser-irradiated n -type GaN. / Jang Ho Won, Lee Jong-Lam. // Applied Physics Letters. - 2009. - Vol. 94, No. 18. - P. 182108-182108-3. ↑
- J798.** Delaney Kris T. Auger recombination rates in nitrides from first principles. / Delaney Kris T., Rinke Patrick, Van de Walle Chris G. // Applied Physics Letters. - 2009. - Vol. 94, No. 19. - P. 191109-191109-3. ↑
- J799.** Xi Y. Y. Effect of annealing on the performance of CrO₃/ZnO light emitting diodes. / Xi Y. Y., Ng A. M. C., Hsu Y. F., Djuricic A. B., Huang B. Q., Ge L., Chen X. Y., Chan W. K., Tam H. L., Cheah K. W. // Applied Physics Letters. - 2009. - Vol. 94, No. 20. - P. 203502-203502-3. ↑
- J800.** Lee Chul-Ho. GaN/In_{1-x}Ga_xN/GaN/ZnO nanoarchitecture light emitting diode microarrays. / Lee Chul-Ho, Yoo Jinkyung, Hong Young Joon, Cho Jeonghui, Kim Yong-Jin, Jeon Seong-Ran, Baek Jong Hyeob, Yi Gyu-Chul. // Applied Physics Letters. - 2009. - Vol. 94, No. 21. - P. 213101-213101-3. ↑
- J801.** Lee Jonghee. Enhanced efficiency and reduced roll-off in blue and white phosphorescent organic light-emitting diodes with a mixed host structure. / Lee Jonghee, Lee Jeong-Ik, Lee Jun Yeob, Chu Hye Yong. // Applied Physics Letters. - 2009. - Vol. 94, No. 19. - P. 193305-193305-3. ↑
- J802.** Bhansali Unnat S. Controlling the carrier recombination zone for improved color stability in a two-dopant fluorophore/phosphor white organic light-emitting diode. / Bhansali Unnat S., Jia Huiping, Lopez M. A. Quevedo, Gnade Bruce E., Chen Wei-Hsuan, Omary Mohammad A. // Applied Physics Letters. - 2009. - Vol. 94, No. 20. - P. 203501-203501-3. ↑
- J803.** Getty Amorette. Electroluminescent measurement of the internal quantum efficiency of light emitting diodes. / Getty Amorette, Matioli Elison, Iza Michael, Weisbuch Claude, Speck James S. // Applied Physics Letters. - 2009. - Vol. 94, No. 18. - P. 181102-181102-3. ↑
- J804.** Slightsky Michael. Full-wave simulation of enhanced outcoupling of organic light-emitting devices with an embedded low-index grid. / Slightsky Michael, Forrest Stephen R. // Applied Physics Letters. - 2009. - Vol. 94, No. 16. - P. 163302-163302-3. ↑
- J805.** Han Liangliang. Intramolecular energy transfer between the triplet of ancillary ligand and the metal to ligand charge transfer state existed in heterocyclometalated iridium (III) complexes. / Han Liangliang, Yang Dongfang, Li Wenlian, Chu Bei, Chen Yiren, Su Zisheng, Zhang Dongyu, Yan Fei, Wu Shuanghong, Wang Junbo, Hu Zhizhi, Zhang Zhiqiang. // Applied Physics Letters. - 2009. - Vol. 94, No. 16. - P. 163303-163303-3. ↑
- J806.** Eom Sang-Hyun. White phosphorescent organic light-emitting devices with dual triple-doped emissive layers. / Eom Sang-Hyun, Zheng Ying, Wrzesniewski Edward, Lee Jaewon, Chopra Neetu, So Franky, Xue Jiangeng. // Applied Physics Letters. - 2009. - Vol. 94, No. 15. - P. 153303-153303-3. ↑
- J807.** Kim T. K. GaN-based light-emitting diode with textured indium tin oxide transparent layer coated with Al

- 2 O 3 powder. / Kim T. K., Kim S. H., Yang S. S., Son J. K., Lee K. H., Hong Y. G., Shim K. H., Yang J. W., Lim K. Y., Bae S. J., Yang G. M. // Applied Physics Letters. - 2009. - Vol. 94, No. 16. - P. 161107-161107-3. ↑
- J808. Xu W. Z. Erratum: "ZnO light-emitting diode grown by plasma-assisted metal organic chemical vapor deposition" [Appl. Phys. Lett. 88, 173506 (2006)]. / Xu W. Z., Ye Z. Z., Zeng Y. J., Zhu L. P., Zhao B. H., Jiang L., Lu J. G., He H. P., Zhang S. B. // Applied Physics Letters. - 2009. - Vol. 94, No. 16. - P. 169901-169901-1. ↑
- J809. Yang Ki Youl. Surface plasmon-enhanced spontaneous emission rate in an organic light-emitting device structure: Cathode structure for plasmonic application. / Yang Ki Youl, Choi Kyung Cheol, Ahn Chi Won. // Applied Physics Letters. - 2009. - Vol. 94, No. 17. - P. 173301-173301-3. ↑
- J810. Reineke Sebastian. Highly phosphorescent organic mixed films: The effect of aggregation on triplet-triplet annihilation. / Reineke Sebastian, Schwartz Gregor, Walzer Karsten, Falke Meiken, Leo Karl. // Applied Physics Letters. - 2009. - Vol. 94, No. 16. - P. 163305-163305-3. ↑
- J811. Kalinowski J. Comment on "Control of magnetic-field effect on electro-luminescence in Alq 3 -based organic light emitting diodes" [Appl. Phys. Lett. 88, 123501 (2006)]. / Kalinowski J., Cocchi M., Di Marco P., Fattori V. // Applied Physics Letters. - 2009. - Vol. 94, No. 16. - P. 166104-166104-1. ↑
- J812. Jin-Wei Shi. The Structure of GaN-Based Transverse Junction Blue LED Array for Uniform Distribution of Injected Current/Carriers. / Jin-Wei Shi, Shi-Hao Guol, Lin C.-S., Jinn-Kong Sheu, Kuo-Hua Chang, Lai W.-C., Kuo C.-H., Tun C.-J., Jen-Inn Chyi. // IEEE Journal of Selected Topics in Quantum Electronics. - 2009. - Vol. 15, No. 4. - P. 1292-1297. ↑
- J813. Shih-Cheng Huang. Improved Output Power of 380 nm InGaN-Based LEDs Using a Heavily Mg-Doped GaN Insertion Layer Technique. / Shih-Cheng Huang, Dong-Sing Wu, Peng-Yi Wu, Shih-Hsiung Chan. // IEEE Journal of Selected Topics in Quantum Electronics. - 2009. - Vol. 15, No. 4. - P. 1132-1136. ↑
- J814. Shields P.A. Enhanced Light Extraction by Photonic Quasi-Crystals in GaN Blue LEDs. / Shields P.A., Charlton M., Lee T., Zoorob M.E., Allsopp D.W.E., Wang W.N. // IEEE Journal of Selected Topics in Quantum Electronics. - 2009. - Vol. 15, No. 4. - P. 1269-1274. ↑
- J815. Taeil Jung. Novel Epitaxial Nanostructures for the Improvement of InGaN LEDs Efficiency. / Taeil Jung, Lee L.K., Ku P.-C. // IEEE Journal of Selected Topics in Quantum Electronics. - 2009. - Vol. 15, No. 4. - P. 1073-1079. ↑
- J816. Dang Hoang Long. Design Optimization of Photonic Crystal Structure for Improved Light Extraction of GaN LED. / Dang Hoang Long, In-Kag Hwang, Sang-Wan Ryu. // IEEE Journal of Selected Topics in Quantum Electronics. - 2009. - Vol. 15, No. 4. - P. 1257-1263. ↑
- J817. Jae-Hyun Ryou. Control of Quantum-Confined Stark Effect in InGaN-Based Quantum Wells. / Jae-Hyun Ryou, Yoder P.D., Jianping Liu, Lochner Z., Hyunsoo Kim, Suk Choi, Hee Jin Kim, Dupuis R.D. // IEEE Journal of Selected Topics in Quantum Electronics. - 2009. - Vol. 15, No. 4. - P. 1080-1091. ↑
- J818. Chi-Jen Lin. High Energy Gap OLED Host Materials for Green and Blue PHOLED Materials. / Chi-Jen Lin, Heh-Lung Huang, Mei-Rung Tseng, Chien-Hong Cheng. // Journal of Display Technology. - 2009. - Vol. 5, No. 6. - P. 236-240. ↑
- J819. Po-Tsun Liu. Innovative Voltage Driving Pixel Circuit Using Organic Thin-Film Transistor for AMOLEDs. / Po-Tsun Liu, Li-Wei Chu. // Journal of Display Technology. - 2009. - Vol. 5, No. 6. - P. 224-227. ↑
- J820. Ferreira J.P. Human Gait Acquisition and Characterization. / Ferreira J.P., Crisostomo M.M., Coimbra A.P. // IEEE Transactions on Instrumentation and Measurement. - 2009. - Vol. 58, No. 9. - P. 2979-2988. ↑
- J821. Tan S.-C. Mitigating energy wastage of light-emitting diodes using discretised multilevel pulsation. Electronics Letters. - 2009. - Vol. 45, No. 10. - P. 522-524. ↑
- J822. Kuna L. Surface Texturing of High-Power Flip-Chip LEDs by Femtosecond Laser Direct Structuring. / Kuna L., Haase A., Reil F., Sommer C., Krenn J.R., Hartmann P., Pachler P., Tasch S., Wenzl F.P. // IEEE Journal of Selected Topics in Quantum Electronics. - 2009. - Vol. 15, No. 4. - P. 1250-1256. ↑
- J823. Chun-Chin Tsai. Investigation of Ce:YAG Doping Effect on Thermal Aging for High-Power Phosphor-

Converted White-Light-Emitting Diodes. / Chun-Chin Tsai, Yi-Cheng Hsu, Sheng-Bang Huang, Ying-Jyun Lin, Wang J., Ming-Hung Chen, Chao-Wei Lee, Hung-Lieh Hu, Wood-Hi Cheng. // IEEE Transactions on Device and Materials Reliability. - 2009. - Vol. 9, No. 3. - P. 367-371. ↑

J824. Linlin Gu. Means of Eliminating Electrolytic Capacitor in AC/DC Power Supplies for LED Lightings. / Linlin Gu, Xinbo Ruan, Ming Xu, Kai Yao. // IEEE Transactions on Power Electronics. - 2009. - Vol. 24, No. 5. - P. 1399-1408. ↑

J825. Fu W.Y. Geometrical Shaping of InGaN Light-Emitting Diodes by Laser Micromachining. / Fu W.Y., Hui K.N., Wang X.H., Wong K., Lai P.T., Choi H.W. // IEEE Photonics Technology Letters. - 2009. - Vol. 21, No. 15. - P. 1078-1080. ↑

J826. Min-Yung Ke. Application of Nanosphere Lithography to LED Surface Texturing and to the Fabrication of Nanorod LED Arrays. / Min-Yung Ke, Cheng-Yin Wang, Liang-Yi Chen, Hung-Hsien Chen, Hung-Li Chiang, Yun-Wei Cheng, Min-Yann Hsieh, Cheng-Pin Chen, JianJang Huang. // IEEE Journal of Selected Topics in Quantum Electronics. - 2009. - Vol. 15, No. 4. - P. 1242-1249. ↑

J827. Cardesin J. LED Permanent Emergency Lighting System Based on a Single Magnetic Component. / Cardesin J., Ribas J., Garcia-Garcia J., Rico-Secades M., Calleja A.J., Corominas E.L., Dalla Costa M.A. // IEEE Transactions on Power Electronics. - 2009. - Vol. 24, No. 5. - P. 1409-1416. ↑

J828. Hoa Le Minh. 100-Mb/s NRZ Visible Light Communications Using a Postequalized White LED. / Hoa Le Minh, O'Brien D., Faulkner G., Lubin Zeng, Kyungwoo Lee, Daekwang Jung, YunJe Oh, Eun Tae Won. // IEEE Photonics Technology Letters. - 2009. - Vol. 21, No. 15. - P. 1063-1065. ↑

J829. Yik-Khoon Ee. Optimization of Light Extraction Efficiency of III-Nitride LEDs With Self-Assembled Colloidal-Based Microlenses. / Yik-Khoon Ee, Kumnorkaew P., Arif R.A., Hua Tong, Hongping Zhao, Gilchrist J.F., Tansu N. // IEEE Journal of Selected Topics in Quantum Electronics. - 2009. - Vol. 15, No. 4. - P. 1218-1225. ↑

J830. Jae-Hoon Lee. Effect of Residual Stress and Sidewall Emission of InGaN-Based LED by Varying Sapphire Substrate Thickness. / Jae-Hoon Lee, Nam Seung Kim, Dong Yul Lee, Jung-Hee Lee. // IEEE Photonics Technology Letters. - 2009. - Vol. 21, No. 16. - P. 1151-1153. ↑

J831. Vervaeke M. Tolerance Design of an Optomechanical Transmitter Assembly for Automotive Applications. / Vervaeke M., Moens E., Meuret Y., Ottevaere H., Van Buggenhout C., De Pauw P., Thienpont H. // IEEE Photonics Technology Letters. - 2009. - Vol. 21, No. 17. - P. 1178-1180. ↑

J832. Chia-Feng Lin. Fabrication of the InGaN-Based Light-Emitting Diodes Through a Photoelectrochemical Process. / Chia-Feng Lin, Chung-Chieh Yang, Jui-Fen Chien, Chun-Min Lin, Kuei-Ting Chen, Yen S.K. // IEEE Photonics Technology Letters. - 2009. - Vol. 21, No. 16. - P. 1142-1144. ↑

J833. Linnartz J.-P. Code Division-Based Sensing of Illumination Contributions in Solid-State Lighting Systems. / Linnartz J.-P., Feri L., Hongming Yang, Colak S.B., Schenk T. // IEEE Transactions on Signal Processing. - 2009. - Vol. 57, No. 10. - P. 3984-3998. ↑

J834. Hongming Yang. Illumination Sensing in LED Lighting Systems Based on Frequency-Division Multiplexing. / Hongming Yang, Bergmans J.W.M., Schenk T. // IEEE Transactions on Signal Processing. - 2009. - Vol. 57, No. 11. - P. 4269-4281. ↑

J835. Yoshino M. Multiwavelength Optical Source for OCDM Using Sinusoidally Modulated Laser Diode. / Yoshino M., Miki N., Yoshimoto N., Kumozaki K. // Journal of Lightwave Technology. - 2009. - Vol. 27, No. 20. - P. 4524-4529. ↑

J836. Ciplys D. Wireless UV sensor based on photocapacitive effect in GaN. / Ciplys D., Chivukula V.S., Sereika A., Rimeika R., Shur M.S., Hu X., Gaska R. // Electronics Letters. - 2009. - Vol. 45, No. 12. - P. 653-654. ↑

J837. Paulson L.D. Technique Makes Strong Encryption Easier to Use. Computer. - 2009. - Vol. 42, No. 4. - P. 24-27. ↑

J838. Crawford M.H. LEDs for Solid-State Lighting: Performance Challenges and Recent Advances. IEEE

Journal of Selected Topics in Quantum Electronics. - 2009. - Vol. 15, No. 4. - P. 1028-1040. ↑

J839. Sommer C. The Effect of the Phosphor Particle Sizes on the Angular Homogeneity of Phosphor-Converted High-Power White LED Light Sources. / Sommer C., Krenn J.R., Hartmann P., Pachler P., Schweighart M., Tasch S., Wenzl F.P. // IEEE Journal of Selected Topics in Quantum Electronics. - 2009. - Vol. 15, No. 4. - P. 1181-1188. ↑

J840. Yik-Khoon Ee. Metalorganic Vapor Phase Epitaxy of III-Nitride Light-Emitting Diodes on Nanopatterned AGOG Sapphire Substrate by Abbreviated Growth Mode. / Yik-Khoon Ee, Biser J.M., Cao W., Chan H.M., Vinci R.P., Tansu N. // IEEE Journal of Selected Topics in Quantum Electronics. - 2009. - Vol. 15, No. 4. - P. 1066-1072. ↑

J841. Lochmann A. Electrically pumped, micro-cavity based single photon source driven at 1 GHz. / Lochmann A., Stock E., Tofflinger J.A., Unrau W., Toropov A., Bakarov A., Haisler V., Bimberg D. // Electronics Letters. - 2009. - Vol. 45, No. 11. - P. 566-567. ↑

J842. Koerperick E.J. High-Power MWIR Cascaded InAs-GaSb Superlattice LEDs. / Koerperick E.J., Olesberg J.T., Hicks J.L., Prineas J.P., Boggess T.F. // IEEE Journal of Quantum Electronics. - 2009. - Vol. 45, No. 7. - P. 849-853. ↑

J843. Fowler K. The reality: Academic research to commercial product, part 2-[tried and true]. IEEE Instrumentation & Measurement Magazine. - 2009. - Vol. 12, No. 3. - P. 34-37. ↑

J844. Chun-Chin Tsai. Decay Mechanisms of Radiation Pattern and Optical Spectrum of High-Power LED Modules in Aging Test. / Chun-Chin Tsai, Ming-Hung Chen, Yi-Chung Huang, Yi-Cheng Hsu, Yuan-Tsun Lo, Ying-Jyun Lin, Jao-Hwa Kuang, Sheng-Bang Huang, Hung-Lieh Hu, Yeh-I Su, Wood-Hi Cheng. // IEEE Journal of Selected Topics in Quantum Electronics. - 2009. - Vol. 15, No. 4. - P. 1156-1162. ↑

J845. Yanguang Yu. Optical Feedback Self-Mixing Interferometry With a Large Feedback Factor : Behavior Studies. / Yanguang Yu, Jiangtao Xi, Chicharo J.F., Bosch T.M. // IEEE Journal of Quantum Electronics. - 2009. - Vol. 45, No. 7. - P. 840-848. ↑

J846. Taguchi Dai. Probing of carrier behavior in organic electroluminescent diode using electric field induced optical second-harmonic generation measurement. / Taguchi Dai, Weis Martin, Manaka Takaaki, Iwamoto Mitsumasa. // Applied Physics Letters. - 2009. - Vol. 95, No. 26. - P. 263310-263310-3. ↑

J847. Song Jae-Ho. Role of photovoltaic effects on characterizing emission properties of InGaN/GaN light emitting diodes. / Song Jae-Ho, Kim Ho-Jong, Ahn Byung-Jun, Dong Yanqun, Hong Sayong, Song Jung-Hoon, Moon Youngboo, Yuh Hwan-Kuk, Choi Sung-Chul, Shee Sangkee. // Applied Physics Letters. - 2009. - Vol. 95, No. 26. - P. 263503-263503-3. ↑

J848. Flammich Michael. In situ measurement of the internal luminescence quantum efficiency in organic light-emitting diodes. / Flammich Michael, Gather Malte C., Danz Norbert, Michaelis Dirk, Meerholz Klaus. // Applied Physics Letters. - 2009. - Vol. 95, No. 26. - P. 263306-263306-3. ↑

J849. Kondakov D. Y. Triplet annihilation exceeding spin statistical limit in highly efficient fluorescent organic light-emitting diodes. / Kondakov D. Y., Pawlik T. D., Hatwar T. K., Spindler J. P. // Journal of Applied Physics. - 2009. - Vol. 106, No. 12. - P. 124510-124510-7. ↑

J850. In-Su Park. Data driver architecture and driving scheme of AMOLED microdisplay for mobile projectors. / In-Su Park, Tae-Wook Kim, Jae-Yoon Lee, Byong-Deok Choi. // IEEE Transactions on Consumer Electronics. - 2009. - Vol. 55, No. 4. - P. 2365-2371. ↑

J851. Ung-Gyu Min. A real time video data adjusting method for active matrix organic light emitting diode displays with high image quality. / Ung-Gyu Min, Hai-Jung In, Oh-Kyong Kwon. // IEEE Transactions on Consumer Electronics. - 2009. - Vol. 55, No. 4. - P. 2372-2376. ↑

J852. Zhang Liang. Linearly polarized light emission from InGaN light emitting diode with subwavelength metallic nanograting. / Zhang Liang, Teng Jing Hua, Chua Soo Jin, Fitzgerald Eugene A. // Applied Physics Letters. - 2009. - Vol. 95, No. 26. - P. 261110-261110-3. ↑

J853. Tae-Wook Lee. An optical feedback system for local dimming backlight with RGB LEDs. / Tae-Wook

Lee, Jae-Ho Lee, Chang-Gone Kim, Sin-Ho Kang. // IEEE Transactions on Consumer Electronics. - 2009. - Vol. 55, No. 4. - P. 2178-2183. ↑

J854. Chung Hun Jae. Improved performance of GaN-based blue light emitting diodes with InGaN/GaN multilayer barriers. / Chung Hun Jae, Choi Rak Jun, Kim Min Ho, Han Jae Woong, Park Young Min, Kim Yu Seung, Paek Ho Sun, Sone Cheol Soo, Park Yong Jo, Kim Jong Kyu, Schubert E. Fred. // Applied Physics Letters. - 2009. - Vol. 95, No. 24. - P. 241109-241109-3. ↑

J855. Li Cheng. Enhanced photoluminescence of strained Ge with a delta -doping SiGe layer on silicon and silicon-on-insulator. / Li Cheng, Chen Yanghua, Zhou Zhiwen, Lai Hongkai, Chen Songyan. // Applied Physics Letters. - 2009. - Vol. 95, No. 25. - P. 251102-251102-3. ↑

J856. Tsai Yu-Sheng. Using copper substrate to enhance the thermal conductivity of top-emission organic light-emitting diodes for improving the luminance efficiency and lifetime. / Tsai Yu-Sheng, Wang Shun-Hsi, Chen Chuan-Hung, Cheng Chien-Lung, Liao Teh-Chao. // Applied Physics Letters. - 2009. - Vol. 95, No. 23. - P. 233306-233306-3. ↑

J857. Meneghini Matteo. A combined electro-optical method for the determination of the recombination parameters in InGaN-based light-emitting diodes. / Meneghini Matteo, Trivellin Nicola, Meneghesso Gaudenzio, Zanoni Enrico, Zehnder Ulrich, Hahn Berthold. // Journal of Applied Physics. - 2009. - Vol. 106, No. 11. - P. 114508-114508-4. ↑

J858. Zhu Y. H. Demonstration on GaN-based light-emitting diodes grown on 3C-SiC/Si(111). / Zhu Y. H., Zhang J. C., Chen Z. T., Egawa T. // Journal of Applied Physics. - 2009. - Vol. 106, No. 12. - P. 124506-124506-4. ↑

J859. Zhang Dan-Dan. Improved hole injection and transport of organic light-emitting devices with an efficient p-doped hole-injection layer. / Zhang Dan-Dan, Feng Jing, Wang Hai, Bai Yu, Chen Qi-Dai, Liu Shi-Yong, Sun Hong-Bo. // Applied Physics Letters. - 2009. - Vol. 95, No. 26. - P. 263303-263303-3. ↑

J860. Na Jong H. Hybrid p-n junction light-emitting diodes based on sputtered ZnO and organic semiconductors. / Na Jong H., Kitamura M., Arita M., Arakawa Y. // Applied Physics Letters. - 2009. - Vol. 95, No. 25. - P. 253303-253303-3. ↑

J861. Lee Jonghee. Improved performance of blue phosphorescent organic light-emitting diodes with a mixed host system. / Lee Jonghee, Lee Jeong-Ik, Lee Jun Yeob, Chu Hye Yong. // Applied Physics Letters. - 2009. - Vol. 95, No. 25. - P. 253304-253304-3. ↑

J862. Schoevers J. Low-Oxygen-Saturation Quantification in Human Arterial and Venous Circulation. / Schoevers J., Scheffer C., Dippenaar R. // IEEE Transactions on Biomedical Engineering. - 2009. - Vol. 56, No. 3. - P. 846-854. ↑

J863. Onushkin G.A. Efficient Alternating Current Operated White Light-Emitting Diode Chip. / Onushkin G.A., Young-Jin Lee, Jung-Ja Yang, Hyung-Kun Kim, Joong-Kon Son, Gil-Han Park, YongJo Park. // IEEE Photonics Technology Letters. - 2009. - Vol. 21, No. 1. - P. 33-35. ↑

J864. Lai F.-I. Extraction Efficiency Enhancement of GaN-Based Light-Emitting Diodes by Microhole Array and Roughened Surface Oxide. / Lai F.-I., Ling S.C., Hsieh C.E., Hsueh T.H., Hao-Chung Kuo, Tien-Chang Lu. // IEEE Electron Device Letters. - 2009. - Vol. 30, No. 5. - P. 496-498. ↑

J865. Weyerman W. Identification and Control of a Grating-Stabilized External-Cavity Diode Laser. / Weyerman W., Neyenhuis B., Archibald J., Washburn M., Durfee D., Warnick S. // IEEE Transactions on Control Systems Technology. - 2009. - Vol. 17, No. 1. - P. 161-166. ↑

J866. Hongping Zhao. Self-Consistent Analysis of Strain-Compensated InGaN-AlGaN Quantum Wells for Lasers and Light-Emitting Diodes. / Hongping Zhao, Arif R.A., Yik-Khoon Ee, Tansu N. // IEEE Journal of Quantum Electronics. - 2009. - Vol. 45, No. 1. - P. 66-78. ↑

J867. Sung-Nien Hsieh. A Study of Semitransparent Cathodes on the Performance of Top-Emitting Polymer Light-Emitting Diodes. / Sung-Nien Hsieh, Tzu-Yin Kuo, Lai-Wan Chong, Ten-Chin Wen, Fun-Shun Yang, Tzung-Fang Guo, Chia-Tin Chung. // IEEE Photonics Technology Letters. - 2009. - Vol. 21, No. 2. - P. 109-111. ↑

- J868.** Llobera A. Poly(Dimethylsiloxane) Waveguide Cantilevers for Optomechanical Sensing. / Llobera A., Cadarso V.J., Zinoviev K., Dominguez C., Buttgenbach S., Vila J., Plaza J.A., Biittgenbach S. // IEEE Photonics Technology Letters. - 2009. - Vol. 21, No. 2. - P. 79-81. ↑
- J869.** Hongming Yang. Uniform Illumination Rendering Using an Array of LEDs: A Signal Processing Perspective. / Hongming Yang, Bergmans J.W.M., Schenk T.C.W., Linnartz J.-P.M.G., Rietman R. // IEEE Transactions on Signal Processing. - 2009. - Vol. 57, No. 3. - P. 1044-1057. ↑
- J870.** Chun-Fu Tsai. Improvement in the Light Output Power of GaN-Based Light-Emitting Diodes by Natural-Cluster Silicon Dioxide Nanoparticles as the Current-Blocking Layer. / Chun-Fu Tsai, Yan-Kuin Su, Chun-Liang Lin. // IEEE Photonics Technology Letters. - 2009. - Vol. 21, No. 14. - P. 996-998. ↑
- J871.** Tak Jeong. Aluminum Nitride Ceramic Substrates-Bonded Vertical Light-Emitting Diodes. / Tak Jeong, Kang Ho Kim, Seung Jae Lee, Sang Hern Lee, Seong Ran Jeon, Sue Hyun Lim, Jong Hyeob Baek, Lee J.K. // IEEE Photonics Technology Letters. - 2009. - Vol. 21, No. 13. - P. 890-892. ↑
- J872.** Suk-Ju Kang. Image integrity-based gray-level error control for low power liquid crystal displays. / Suk-Ju Kang, Young Hwan Kim. // IEEE Transactions on Consumer Electronics. - 2009. - Vol. 55, No. 4. - P. 2401-2406. ↑
- J873.** Lee B. The multi-touch system with high applicability using tri-axial coordinate infrared LEDs. / Lee B., Hong I., Uhm Y., Park S. // IEEE Transactions on Consumer Electronics. - 2009. - Vol. 55, No. 4. - P. 2416-2424. ↑
- J874.** McKendry J. Individually Addressable AlInGaN Micro-LED Arrays With CMOS Control and Subnanosecond Output Pulses. / McKendry J., Rae B.R., Zheng Gong, Muir K.R., Guilhabert B., Massoubre D., Gu E., Renshaw D., Dawson M.D., Henderson R.K. // IEEE Photonics Technology Letters. - 2009. - Vol. 21, No. 12. - P. 811-813. ↑
- J875.** Zhu L. Pixel-to-Pixel Fiber-Coupled Emissive Micro-Light-Emitting Diode Arrays. / Zhu L., Ng C.W., Wong N., Wong K.K.Y., Lai P.T., Choi H.W. // IEEE Photonics Journal. - 2009. - Vol. 1, No. 1. - P. 1-8. ↑
- J876.** Ya-Ju Lee. Study of the Excitation Power Dependent Internal Quantum Efficiency in InGaN/GaN LEDs Grown on Patterned Sapphire Substrate. / Ya-Ju Lee, Ching-Hua Chiu, Chih Chun Ke, Po Chun Lin, Tien-Chang Lu, Hao-Chung Kuo, Shing-Chung Wang. // IEEE Journal of Selected Topics in Quantum Electronics. - 2009. - Vol. 15, No. 4. - P. 1137-1143. ↑
- J877.** Shouu-Jinn Chang. High-Brightness InGaN-GaN Power Flip-Chip LEDs. / Shouu-Jinn Chang, Chen W.S., Shei S.C., Kuo C.T., Ko T.K., Shen C.F., Tsai J.M., Wei-Chi Lai, Jinn-Kong Sheu, Lin A.J. // Journal of Lightwave Technology. - 2009. - Vol. 27, No. 12. - P. 1985-1989. ↑
- J878.** Lunt Richard R. Organic vapor phase deposition for the growth of large area organic electronic devices. / Lunt Richard R., Lassiter Brian E., Benziger Jay B., Forrest Stephen R. // Applied Physics Letters. - 2009. - Vol. 95, No. 23. - P. 233305-233305-3. ↑
- J879.** Lee J. On carrier spillover in c- and m-plane InGaN light emitting diodes. / Lee J., Li X., Ni X., Ozgur U., Morkoc H., Paskova T., Mulholland G., Evans K. R. // Applied Physics Letters. - 2009. - Vol. 95, No. 20. - P. 201113-201113-3. ↑
- J880.** Hou Jianhua. Efficient inverted top-emitting organic light-emitting diodes using ultrathin MoO₃/C 60 bilayer structure to enhance hole injection. / Hou Jianhua, Wu Jiang, Xie Zhiyuan, Wang Lixiang. // Applied Physics Letters. - 2009. - Vol. 95, No. 20. - P. 203508-203508-3. ↑
- J881.** Yu Zhibin. Fully bendable polymer light emitting devices with carbon nanotubes as cathode and anode. / Yu Zhibin, Hu Liangbing, Liu Zhitian, Sun Mingliang, Wang Meiliang, Gruner George, Pei Qibing. // Applied Physics Letters. - 2009. - Vol. 95, No. 20. - P. 203304-203304-3. ↑
- J882.** Johnston A.H. Optocouplers: Fundamentals and Hardness Assurance for Space Applications. / Johnston A.H., Harris R.D., Miyahira T.F. // IEEE Transactions on Nuclear Science. - 2009. - Vol. 56, No. 6. - P. 3310-3317. ↑
- J883.** Lindla Florian. Highly efficient yellow organic light emitting diode based on a layer-cross faded emission

layer allowing easy color tuning. / Lindla Florian, Boesing Manuel, Zimmermann Christoph, Jessen Frank, van Gemmern Philipp, Bertram Dietrich, Keiper Dietmar, Meyer Nico, Heuken Michael, Kalisch Holger, Jansen Rolf H. // Applied Physics Letters. - 2009. - Vol. 95, No. 21. - P. 213305-213305-3. ↑

J884. Hong Kihyon. Enhancement of electrical property by oxygen doping to copper phthalocyanine in inverted top emitting organic light emitting diodes. / Hong Kihyon, Kim Kisoo, Lee Jong-Lam. // Applied Physics Letters. - 2009. - Vol. 95, No. 21. - P. 213307-213307-3. ↑

J885. Lubin Zeng. High data rate multiple input multiple output (MIMO) optical wireless communications using white led lighting. / Lubin Zeng, O'Brien D., Hoa Minh, Faulkner G., Kyungwoo Lee, Daekwang Jung, YunJe Oh, Eun Tae Won. // IEEE Journal on Selected Areas in Communications. - 2009. - Vol. 27, No. 9. - P. 1654-1662. ↑

J886. Chen P. Magnetoelectroluminescence in tris (8-hydroxyquinolato) aluminum-based organic light-emitting diodes doped with fluorescent dyes. / Chen P., Lei Y. L., Song Q. L., Zhang Y., Liu R., Zhang Q. M., Xiong Z. H. // Applied Physics Letters. - 2009. - Vol. 95, No. 21. - P. 213304-213304-3. ↑

J887. Lin Chia-Feng. Blue light-emitting diodes with a roughened backside fabricated by wet etching. / Lin Chia-Feng, Lin Chun-Min, Chen Kuei-Ting, Huang Wan-Chun, Lin Ming-Shiou, Dai Jing-Jie, Jiang Ren-Hao, Huang Yu-Chieh, Chang Chung-Ying. // Applied Physics Letters. - 2009. - Vol. 95, No. 20. - P. 201102-201102-3. ↑

J888. Pettis B. Barbot, the automated bartender. IEEE Spectrum. - 2009. - Vol. 46, No. 12. - P. 20-21. ↑

J889. Li Z. L. Effect of indium content on performance and reliability of InGaN/GaN light-emitting diodes. / Li Z. L., Tripathy S., Lai P. T., Choi H. W. // Journal of Applied Physics. - 2009. - Vol. 106, No. 9. - P. 094507-094507-5. ↑

J890. Ko Wooseok. Measurement system of the refractive power of spherical and spherocylindrical lenses with the magnification ellipse fitting method. / Ko Wooseok, Kim Soohyun. // Review of Scientific Instruments. - 2009. - Vol. 80, No. 11. - P. 115109-115109-5. ↑

J891. Yang H. Y. Randomly packed n-SnO₂ nanorods/p-SiC heterojunction light-emitting diodes. / Yang H. Y., Yu S. F., Cheng C. W., Tsang S. H., Liang H. K., Fan H. J. // Applied Physics Letters. - 2009. - Vol. 95, No. 20. - P. 201104-201104-3. ↑

J892. Asshoff Pablo. Spin-polarization dynamics in InGaAs quantum dots during pulsed electrical spin-injection. / Asshoff Pablo, Löffler Wolfgang, Zimmer Jochen, Fuser Heiko, Flugge Harald, Kalt Heinz, Hetterich Michael. // Applied Physics Letters. - 2009. - Vol. 95, No. 20. - P. 202105-202105-3. ↑

J893. Perry T.S. Go big or go home. IEEE Spectrum. - 2009. - Vol. 46, No. 12. - P. 42-46. ↑


J894. Zhang M. Direct measurement of auger recombination in In_{0.1}Ga_{0.9}N/GaN quantum wells and its impact on the efficiency of In_{0.1}Ga_{0.9}N/GaN multiple quantum well light emitting diodes. / Zhang M., Bhattacharya P., Singh J., Hinckley J. // Applied Physics Letters. - 2009. - Vol. 95, No. 20. - P. 201108-201108-3. ↑


J895. Song Tao. Amorphous silicon as electron transport layer for colloidal semiconductor nanocrystals light emitting diode. / Song Tao, Zhang Fute, Shen Xiaojuan, Zhang Xiaohong, Zhu Xiulin, Sun Baoquan. // Applied Physics Letters. - 2009. - Vol. 95, No. 23. - P. 233502-233502-3. ↑


J896. Kim C. S. Enhanced performance of organic light-emitting diodes using two-dimensional zinc sulfide photonic crystals. / Kim C. S., Kim M., Larrabee D. C., Vurgaftman I., Meyer J. R., Lee S. H., Kafafi Z. H. // Journal of Applied Physics. - 2009. - Vol. 106, No. 11. - P. 113105-113105-4. ↑


J897. Kim Hyung Gu. Impact of two-floor air prism arrays as an embedded reflector for enhancing the output power of InGaN/GaN light emitting diodes. / Kim Hyung Gu, Kim Hyun Kyu, Kim Hee Yun, Ryu Jae Hyoung, Kang Ji Hye, Han Nam, Uthirakumar Periyayya, Hong Chang-Hee. // Applied Physics Letters. - 2009. - Vol. 95, No. 22. - P. 221110-221110-3. ↑


J898. Martinez-Torres P. Photothermal determination of thermal diffusivity and polymerization depth profiles of polymerized dental resins. / Martinez-Torres P., Mandelis A., Alvarado-Gil J. J. // Journal of Applied Physics. - ↑


2009. - Vol. 106, No. 11. - P. 114906-114906-7. 


J899. Malyutenko V. K. Planar silicon light emitting arrays for the 3-12 mcm spectral band. / Malyutenko V. K., Malyutenko O. Yu., Bogatyrenko V. V., Tykhonov A. M., Piotrowski Tadeusz, Grodecki Remigiusz, Pultorak Jerzy, Wegrzecki Maciej. // Journal of Applied Physics. - 2009. - Vol. 106, No. 11. - P. 113106-113106-5. 


J900. Bhansali Unnat S. High-efficiency turquoise-blue electrophosphorescence from a Pt(II)-pyridyltriazolate complex in a phosphine oxide host. / Bhansali Unnat S., Polikarpov Evgueni, Swensen James S., Chen Wei-Hsuan, Jia Huiping, Gaspar Daniel J., Gnade Bruce E., Padmaperuma Asanga B., Omary Mohammad A. // Applied Physics Letters. - 2009. - Vol. 95, No. 23. - P. 233304-233304-3. 


J901. Zhuang Q. Molecular beam epitaxial (MBE) growth and spectroscopy of dilute nitride InAsN:Sb for mid-infrared applications. / Zhuang Q., Krier A. // IET Optoelectronics. - 2009. - Vol. 3, No. 6. - P. 248-258. 


J902. Zhao H.P. Design and characteristics of staggered InGaN quantum-well light-emitting diodes in the green spectral regime. / Zhao H.P., Liu G.Y., Li X.H., Arif R.A., Huang G.S., Poplawsky J.D., Tafon Penn S., Dierolf V., Tansu N. // IET Optoelectronics. - 2009. - Vol. 3, No. 6. - P. 283-295. 


J903. Sivaramakrishnan Sankaran. Solution-processed conjugated polymer organic p-i-n light-emitting diodes with high built-in potential by solution- and solid-state doping. / Sivaramakrishnan Sankaran, Zhou Mi, Kumar Aravind C., Chen Zhi-Li, Png Rui-Qi, Chua Lay-Lay, Ho Peter K. H. // Applied Physics Letters. - 2009. - Vol. 95, No. 21. - P. 213303-213303-3. 


J904. Bregolin F. L. Electroluminescence induced by Ge nanocrystals obtained by hot ion implantation into SiO₂. / Bregolin F. L., Behar M., Sias U. S., Reboh S., Lehmann J., Rebohle L., Skorupa W. // Journal of Applied Physics. - 2009. - Vol. 106, No. 10. - P. 106103-106103-3. 


J905. Lo M.-H. Defect selective passivation in GaN epitaxial growth and its application to light emitting diodes. / Lo M.-H., Tu P.-M., Wang C.-H., Cheng Y.-J., Hung C.-W., Hsu S.-C., Kuo H.-C., Zan H.-W., Wang S.-C., Chang C.-Y., Liu C.-M. // Applied Physics Letters. - 2009. - Vol. 95, No. 21. - P. 211103-211103-3. 

J906. Wang Lei. High spontaneous emission rate asymmetrically graded 480 nm InGaN/GaN quantum well light-emitting diodes. / Wang Lei, Li Rui, Yang Ziwen, Li Ding, Yu Tao, Liu Ningyang, Liu Lei, Chen Weihua, Hu Xiaodong. // Applied Physics Letters. - 2009. - Vol. 95, No. 21. - P. 211104-211104-3. 


J907. Min U.-G. Real-time external sensing and compensation method for organic light emitting diode displays. / Min U.-G., Kwon O.-K. // Electronics Letters. - 2009. - Vol. 45, No. 24. - P. 1232-1234. 


J908. Chen Chih-Han. Electroluminescence from n-ZnO nanowires/p-GaN heterostructure light-emitting diodes. / Chen Chih-Han, Chang Shouu-Jinn, Chang Sheng-Po, Li Meng-Ju, Chen I-Cherng, Hsueh Ting-Jen, Hsu Cheng-Liang. // Applied Physics Letters. - 2009. - Vol. 95, No. 22. - P. 223101-223101-3. 


J909. Mingxuan Sun. Active Lighting for Video Conferencing. / Mingxuan Sun, Zicheng Liu, Jingyu Qiu, Zhengyou Zhang, Sinclair M. // IEEE Transactions on Circuits and Systems for Video Technology. - 2009. - Vol. 19, No. 12. - P. 1819-1829. 

J910. Bagnich S. A. Electron-hole pair mechanism for the magnetic field effect in organic light emitting diodes based on poly(paraphenylene vinylene). / Bagnich S. A., Niedermeier U., Melzer C., Sarfert W., von Seggern H. // Journal of Applied Physics. - 2009. - Vol. 106, No. 11. - P. 113702-113702-7. 

J911. Sayil S. On the use of silicon photonics--Part II. IEEE Potentials. - 2009. - Vol. 28, No. 2. - P. 37-40. 

J912. Haldi A. Fabrication of a Blue Pixel Organic Light-Emitting Diode Video Display Incorporating a Thermally Stable Emitter. / Haldi A., Kim J.B., Domercq B., Kulkarni A.P., Barlow S., Gifford A.P., Jenekhe S.A., Marder S.R., Kippelen B. // Journal of Display Technology. - 2009. - Vol. 5, No. 4. - P. 120-125. 

J913. Esch J. Prolog to The Transition to Solid-State Lighting. Proceedings of the IEEE. - 2009. - Vol. 97, No. 3. - P. 478-480. 

J914. Chih-Hung Yen. On an AlGaInP Light-Emitting Diode With a Modulation-Doped Multiquantum-Well (MD-MQW) Structure. / Chih-Hung Yen, Yi-Jung Liu, Tzu-Pin Chen, Li-Yang Chen, Tsung-Han Tsai, Wen-Chau Liu. // IEEE Journal of Quantum Electronics. - 2009. - Vol. 45, No. 4. - P. 367-372. 

- J915.** Kim B.J. GaN-Based Light-Emitting Diode With Three-Dimensional Silver Reflectors. / Kim B.J., Jung H., Kim S.H., Bang J., Jihyun Kim. // IEEE Photonics Technology Letters. - 2009. - Vol. 21, No. 11. - P. 700-702. ↑
- J916.** Kyoung-Sik Seol. A Synchronous Multioutput Step-Up/Down DC-DC Converter With Return Current Control. / Kyoung-Sik Seol, Young-Jin Woo, Gyu-Hyeong Cho, Gyu-Ha Gho, Jae-Woo Lee. // IEEE Transactions on Circuits and Systems II: Express Briefs. - 2009. - Vol. 56, No. 3. - P. 210-214. ↑
- J917.** Dong-Hyun Jang. Enhancement of Light Extraction Efficiency Using Lozenge-Shaped GaN-Based Light-Emitting Diodes. / Dong-Hyun Jang, Jong-In Shim, Dong-Soo Shin. // IEEE Photonics Technology Letters. - 2009. - Vol. 21, No. 12. - P. 760-762. ↑
- J918.** Yeh C.Y. Light Output Improvement of Oxide-Textured InGaN-Based Light-Emitting Diodes by Bias-Assisted Photoelectrochemical Oxidation With Imprint Technique. / Yeh C.Y., Lai W.C., Hsueh T.H., Yang Y.Y., Sheu J.K., Ringer S.P., Gault B. // IEEE Photonics Technology Letters. - 2009. - Vol. 21, No. 11. - P. 718-720. ↑
- J919.** Kim M. ITO/AlN_dN/Al contact process for active matrix OLED displays. / Kim M., Jin G.H. // Electronics Letters. - 2009. - Vol. 45, No. 8. - P. 421-423. ↑
- J920.** Soraghan C.J. Triple wavelength LED driver for optical brain-computer interfaces. / Soraghan C.J., Markham C., Matthews F., Ward T.E. // Electronics Letters. - 2009. - Vol. 45, No. 8. - P. 392-394. ↑
- J921.** Whang A.J.-W. Designing Uniform Illumination Systems by Surface-Tailored Lens and Configurations of LED Arrays. / Whang A.J.-W., Yi-Yung Chen, Yuan-Ting Teng. // Journal of Display Technology. - 2009. - Vol. 5, No. 3. - P. 94-103. ↑
- J922.** Ray-Hua Horng. Investigation of Light Extraction of InGaN LEDs With Surface-Textured Indium Tin Oxide by Holographic and Natural Lithography. / Ray-Hua Horng, Yu-Li Tsai, Tzong-Ming Wu, Dong-Sing Wu, Chia-Hsin Chao. // IEEE Journal of Selected Topics in Quantum Electronics. - 2009. - Vol. 15, No. 5. - P. 1327-1331. ↑
- J923.** Chuan-Yu Chang. Application of Two Hopfield Neural Networks for Automatic Four-Element LED Inspection. / Chuan-Yu Chang, Chun-Hsi Li, Si-Yan Lin, MuDer Jeng. // IEEE Transactions on Systems, Man, and Cybernetics, Part C: Applications and Reviews. - 2009. - Vol. 39, No. 3. - P. 352-365. ↑
- J924.** Azevedo I.L. The Transition to Solid-State Lighting. / Azevedo I.L., Morgan M.G., Morgan F. // Proceedings of the IEEE. - 2009. - Vol. 97, No. 3. - P. 481-510. ↑
- J925.** {no data available}. Primary colors. IEEE Spectrum. - 2009. - Vol. 46, No. 4. - P. 18-19. ↑
- J926.** Nagai M. Substrate Cleaning Methods for Fabricating OLEDs and Its Effect on Current Leakage Defect Formation. Journal of Display Technology. - 2009. - Vol. 5, No. 4. - P. 126-132. ↑
- J927.** Oliveira S.C. Optical Detection of Partial Discharges on Insulator Strings of High-Voltage Transmission Lines. / Oliveira S.C., Fontana E. // IEEE Transactions on Instrumentation and Measurement. - 2009. - Vol. 58, No. 7. - P. 2328-2334. ↑
- J928.** Chih-Hung Yen. On an AlGaInP-Based Light-Emitting Diode With an ITO Direct Ohmic Contact Structure. / Chih-Hung Yen, Yi-Jung Liu, Kuo-Hui Yu, Pei-Ling Lin, Tzu-Pin Chen, Li-Yang Chen, Tsung-Han Tsai, Nan-Yi Huang, Chong-Yi Lee, Wen-Chau Liu. // IEEE Electron Device Letters. - 2009. - Vol. 30, No. 4. - P. 359-361. ↑
- J929.** Ray-Hua Horng. Novel Device Design for High-Power InGaN/Sapphire LEDs Using Copper Heat Spreader With Reflector. / Ray-Hua Horng, Hsiang-Yun Hsiao, Cheng-Chung Chiang, Dong-Sing Wu, Yu-Li Tsai, Heng-I Lin. // IEEE Journal of Selected Topics in Quantum Electronics. - 2009. - Vol. 15, No. 4. - P. 1281-1286. ↑
- J930.** Sekitani T. Printed Nonvolatile Memory for a Sheet-Type Communication System. / Sekitani T., Zaitzu K., Noguchi Y., Ishibe K., Takamiya M., Sakurai T., Someya T. // IEEE Transactions on Electron Devices. - 2009. - Vol. 56, No. 5. - P. 1027-1035. ↑
- J931.** Tsai C.M. GaN-Based LEDs Output Power Improved by Textured GaN/Sapphire Interface Using In Situ Treatment Process During Epitaxial Growth. / Tsai C.M., Jinn-Kong Sheu, Wei-Chih Lai, Ming-Lun Lee, Shouu-

Jinn Chang, Chang C.S., Ko T.K., Shen C.F. // IEEE Journal of Selected Topics in Quantum Electronics. - 2009. - Vol. 15, No. 4. - P. 1275-1280. ↑

J932. Morikura S. Angle-Dependent Spectral Width of Resonant-Cavity Light-Emitting Diode. / Morikura S., Okamura Y. // IEEE Photonics Technology Letters. - 2009. - Vol. 21, No. 10. - P. 660-662. ↑

J933. Hai-Jung In. External Compensation of Nonuniform Electrical Characteristics of Thin-Film Transistors and Degradation of OLED Devices in AMOLED Displays. / Hai-Jung In, Oh-Kyong Kwon. // IEEE Electron Device Letters. - 2009. - Vol. 30, No. 4. - P. 377-379. ↑

J934. Yuh-Renn Wu. Size-Dependent Strain Relaxation and Optical Characteristics of InGaN/GaN Nanorod LEDs. / Yuh-Renn Wu, Chinghua Chiu, Cheng-Yu Chang, Peichen Yu, Hao-Chung Kuo. // IEEE Journal of Selected Topics in Quantum Electronics. - 2009. - Vol. 15, No. 4. - P. 1226-1233. ↑

J935. Zongyuan Liu. Optical Analysis of Phosphor's Location for High-Power Light-Emitting Diodes. / Zongyuan Liu, Sheng Liu, Kai Wang, Xiaobing Luo. // IEEE Transactions on Device and Materials Reliability. - 2009. - Vol. 9, No. 1. - P. 65-73. ↑

J936. Chun-Ho Chen. A Field Sequential Color LCD Based on Color Fields Arrangement for Color Breakup and Flicker Reduction. / Chun-Ho Chen, Fang-Cheng Lin, Ya-Ting Hsu, Yi-Pai Huang, Shieh H.-P.D. // Journal of Display Technology. - 2009. - Vol. 5, No. 1. - P. 34-39. ↑

J937. Min-An Tsai. Improving Light Output Power of the GaN-Based Vertical-Injection Light-Emitting Diodes by Mg Implanted Current Blocking Layer. / Min-An Tsai, Peichen Yu, Chen J.R., Huang J.K., Chiu C.H., Kuo H.C., Lu T.C., Lin S.H., Wang S.C. // IEEE Photonics Technology Letters. - 2009. - Vol. 21, No. 11. - P. 688-690. ↑

J938. Chang S.J. GaN-Based Power Flip-Chip LEDs With Cu Submount. / Chang S.J., Chen W.S., Shei S.C., Shen C.F., Ko T.K., Tsai J.M., Lai W.C., Sheu J.K., Lin A.J., Hung S.C. // IEEE Journal of Selected Topics in Quantum Electronics. - 2009. - Vol. 15, No. 4. - P. 1287-1291. ↑

J939. Meizi Jiao. Fast-Response Single Cell Gap Transflective Liquid Crystal Displays. / Meizi Jiao, Shin-Tson Wu, Wing-Kit Choi. // Journal of Display Technology. - 2009. - Vol. 5, No. 3. - P. 83-85. ↑

J940. Hwu F.-S. Method for determining the junction temperature of alternating current light-emitting diodes. / Hwu F.-S., Sheu G.-J., Lin M.-T., Chen J.-C. // IET Science, Measurement & Technology. - 2009. - Vol. 3, No. 2. - P. 159-164. ↑

J941. Won-Sik Oh. A Novel Two-Dimensional Adaptive Dimming Technique of X-Y Channel Drivers for LED Backlight System in LCD TVs. / Won-Sik Oh, Daeyoun Cho, Kyu-Min Cho, Gun-Woo Moon, Byungchoon Yang, Taeseok Jang. // Journal of Display Technology. - 2009. - Vol. 5, No. 1. - P. 20-26. ↑

J942. Whang A.J.-W. Guiding Light From LED Array Via Tapered Light Pipe for Illumination Systems Design. / Whang A.J.-W., Pei-Chun Li, Yi-Yung Chen, Sheng-Liang Hsieh. // Journal of Display Technology. - 2009. - Vol. 5, No. 3. - P. 104-108. ↑

J943. Poppe A. Thermal Measurement and Modeling of Multi-Die Packages. / Poppe A., Yan Zhang, Wilson J., Farkas G., Szabo P., Parry J., Rencz M., Szekely V. // IEEE Transactions on Components and Packaging Technologies. - 2009. - Vol. 32, No. 2. - P. 484-492. ↑

J944. Hyun-Sang Park. A New Thin-Film Transistor Pixel Structure Suppressing the Leakage Current Effects on AMOLED. / Hyun-Sang Park, Hee-Sun Shin, Woocheul Lee, Seung-Hee Kuk, Yongtaek Hong, Min-Koo Han. // IEEE Electron Device Letters. - 2009. - Vol. 30, No. 3. - P. 240-242. ↑

J945. Chang S.J. AlGaIn/GaN Schottky Barrier Photodetector With Multi- /GaIn Buffer. / Chang S.J., Lee K.H., Chang P.C., Wang Y.C., Kuo C.H., Wu S.L. // IEEE Sensors Journal. - 2009. - Vol. 9, No. 2. - P. 87-92. ↑

J946. Papadopoulos N.P. An Improved Optical Feedback Pixel Driver Circuit. / Papadopoulos N.P., Hatzopoulos A.A., Papakostas D.K. // IEEE Transactions on Electron Devices. - 2009. - Vol. 56, No. 2. - P. 229-235. ↑

J947. Das N.C. Flip Chip Bonding of 68 68 MWIR LED Arrays. / Das N.C., Taysing-Lara M., Olver K.A., Kiamilev F., Prineas J.P., Olesberg J.T., Koerperick E.J., Murray L.M., Boggess T.F. // IEEE Transactions on

Electronics Packaging Manufacturing. - 2009. - Vol. 32, No. 1. - P. 9-13. ↑

J948. Woo-Young Choi. Single-Stage Soft-Switching Converter With Boost Type of Active Clamp for Wide Input Voltage Ranges. / Woo-Young Choi, Jung-Min Kwon, Jong-Jae Lee, Hyeon-Yong Jang, Bong-Hwan Kwon. // IEEE Transactions on Power Electronics. - 2009. - Vol. 24, No. 3. - P. 730-741. ↑

J949. Torre M.S. Polarization-Resolved Modulation Response of Single-Transverse-Mode Vertical-Cavity Surface-Emitting Lasers. / Torre M.S., Masoller C. // IEEE Journal of Quantum Electronics. - 2009. - Vol. 45, No. 2. - P. 206-212. ↑

J950. Bansal R. Where Is Waldo? [Microwave Surfing]. IEEE Microwave Magazine. - 2009. - Vol. 10, No. 1. - P. 22-174. ↑

J951. Celikel O. Establishment of All Digital Closed-Loop Interferometric Fiber-Optic Gyroscope and Scale Factor Comparison for Open-Loop and All Digital Closed-Loop Configurations. / Celikel O., San S.E. // IEEE Sensors Journal. - 2009. - Vol. 9, No. 2. - P. 176-186. ↑

J952. Hersee S.D. GaN nanowire light emitting diodes based on templated and scalable nanowire growth. / Hersee S.D., Fairchild M., Rishinaramangalam A.K., Ferdous M.S., Zhang L., Varangis P.M., Swartzentruber B.S., Talin A.A. // Electronics Letters. - 2009. - Vol. 45, No. 1. - P. 75-76. ↑

J953. Young June Hong. Influence of Insulator Length on the Downstream Electron Temperature and Density in the Coaxial Plasma Focus Device. / Young June Hong, Phil Yong Oh, Min Wug Moon, Hee Myung Shin, Yoonho Seo, Guangsup Cho, Eun Ha Choi. // IEEE Transactions on Plasma Science. - 2009. - Vol. 37, No. 1. - P. 184-189. ↑

J954. Ke Lin. Performance Improvement of Carbon-Nanotube-Incorporated Transparent Conducting Anode Film for Organic Device Application. / Ke Lin, Kumar R.S., Lai Szu Cheng, Chua Soo Jin. // IEEE Transactions on Electron Devices. - 2009. - Vol. 56, No. 1. - P. 31-37. ↑

J955. Shih-Yung Lo. Effects of Hydrogenation on Optoelectronic Properties of a-C:H Thin-Film White-Light-Emitting Diodes With Composition-Graded Carrier-Injection Layers. / Shih-Yung Lo, Rong-Hwei Yeh, Tai-Rong Yu, Jyh-Wong Hong. // IEEE Transactions on Electron Devices. - 2009. - Vol. 56, No. 1. - P. 57-64. ↑

J956. Norgia M. Optical Sensors for Real-Time Measurement of Motorcycle Tilt Angle. / Norgia M., Boniolo I., Tanelli M., Savaresi S.M., Svelto C. // IEEE Transactions on Instrumentation and Measurement. - 2009. - Vol. 58, No. 5. - P. 1640-1649. ↑

J957. Rovati L. UV-LEDs for Monitoring Dialysis Adequacy. / Rovati L., Cattini S. // IEEE Transactions on Instrumentation and Measurement. - 2009. - Vol. 58, No. 5. - P. 1720-1726. ↑

J958. Min-An Tsai. Efficiency Enhancement and Beam Shaping of GaN-InGaN Vertical-Injection Light-Emitting Diodes via High-Aspect-Ratio Nanorod Arrays. / Min-An Tsai, Peichen Yu, Chao C.L., Chiu C.H., Kuo H.C., Lin S.H., Huang J.J., Lu T.C., Wang S.C. // IEEE Photonics Technology Letters. - 2009. - Vol. 21, No. 4. - P. 257-259. ↑

J959. Chia-En Lee. Nitride-Based Thin-Film Light-Emitting Diodes With Photonic Quasi-Crystal Surface. / Chia-En Lee, Chun-Feng Lai, Yea-Chen Lee, Hao-Chung Kuo, Tien-Chang Lu, Shing-Chung Wang. // IEEE Photonics Technology Letters. - 2009. - Vol. 21, No. 5. - P. 331-333. ↑

J960. Lee I.E. Performance enhancement of outdoor visible-light communication system using selective combining receiver. / Lee I.E., Sim M.L., Kung F.W.L. // IET Optoelectronics. - 2009. - Vol. 3, No. 1. - P. 30-39. ↑

J961. Long X. Development of street lighting system-based novel high-brightness LED modules. / Long X., Liao R., Zhou J. // IET Optoelectronics. - 2009. - Vol. 3, No. 1. - P. 40-46. ↑

J962. Chaji G.R. Fast and Offset-Leakage Insensitive Current-Mode Line Driver for Active Matrix Displays and Sensors. / Chaji G.R., Nathan A. // Journal of Display Technology. - 2009. - Vol. 5, No. 2. - P. 72-79. ↑

J963. Sohanguhpurwala A. Optical Replacement of pH Electrode. / Sohanguhpurwala A., Rao G., Kostov Y. // IEEE Sensors Journal. - 2009. - Vol. 9, No. 3. - P. 219-220. ↑

- J964.** Kowal J. Model Parameterization of Nonlinear Devices Using Impedance Spectroscopy. / Kowal J., Hente D., Sauer D.U. // IEEE Transactions on Instrumentation and Measurement. - 2009. - Vol. 58, No. 7. - P. 2343-2350. ↑
- J965.** Garcia J. Dimming of High-Brightness LEDs by Means of Luminous Flux Thermal Estimation. / Garcia J., Dalla-Costa M.A., Cardesin J., Alonso J.M., Rico-Secades M. // IEEE Transactions on Power Electronics. - 2009. - Vol. 24, No. 4. - P. 1107-1114. ↑
- J966.** Morikura S. Chromatic dispersion penalty by angular coupling between resonant cavity light-emitting diode and plastic optical fibre. / Morikura S., Okamura Y. // Electronics Letters. - 2009. - Vol. 45, No. 4. - P. 202-203. ↑
- J967.** Mohamed M.D.A. Optical impulse modulation for indoor diffuse wireless communications. / Mohamed M.D.A., Hranilovic S. // IEEE Transactions on Communications. - 2009. - Vol. 57, No. 2. - P. 499-508. ↑
- J968.** Bin Hou. Methods of Increasing Luminous Efficiency of Phosphor-Converted LED Realized by Conformal Phosphor Coating. / Bin Hou, Haibo Rao, Junfei Li. // Journal of Display Technology. - 2009. - Vol. 5, No. 2. - P. 57-60. ↑
- J969.** Yu-Kuo Cheng. Design and Evaluation of Light Spread Function for Area-Adaptive LCD System. / Yu-Kuo Cheng, Yen-Hsing Lu, Chung-Hao Tien, Han-Ping Shieh. // Journal of Display Technology. - 2009. - Vol. 5, No. 2. - P. 66-71. ↑
- J970.** Chang-Seok Chae. A Single-Inductor Step-Up DC-DC Switching Converter With Bipolar Outputs for Active Matrix OLED Mobile Display Panels. / Chang-Seok Chae, Hanh-Phuc Le, Kwang-Chan Lee, Gyu-Ha Cho, Gyu-Hyeong Cho. // IEEE Journal of Solid-State Circuits. - 2009. - Vol. 44, No. 2. - P. 509-524. ↑
- J971.** Cheng-Huang Kuo. Nitride-Based Asymmetric Two-Step Light-Emitting Diode With In Ga N Shallow Step. / Cheng-Huang Kuo, Fu Y.K., Yeh C.L., Tun C.J., Chen P.H., Wei-Chih Lai, Shouu-Jinn Chang. // IEEE Photonics Technology Letters. - 2009. - Vol. 21, No. 6. - P. 371-373. ↑
- J972.** Kuo D.S. Nitride-Based LEDs With Phosphoric Acid Etched Undercut Sidewalls. / Kuo D.S., Shouu-Jinn Chang, Ko T.K., Shen C.F., Hon S.J., Hung S.C. // IEEE Photonics Technology Letters. - 2009. - Vol. 21, No. 8. - P. 510-512. ↑
- J973.** Chih-Hung Yen. Study of an AlGaInP-Based Light-Emitting Diode With a Modulation-Doped Multiquantum-Well (MD-MQW) Structure. / Chih-Hung Yen, Yi-Jung Liu, Tzu-Pin Chen, Li-Yang Chen, Tsung-Han Tsai, Wen-Chau Liu. // IEEE Photonics Technology Letters. - 2009. - Vol. 21, No. 10. - P. 609-611. ↑
- J974.** Tao-Hung Hsueh. Improvement of the Efficiency of InGaN-GaN Quantum-Well Light-Emitting Diodes Grown With a Pulsed-Trimethylindium Flow Process. / Tao-Hung Hsueh, Jinn-Kong Sheu, Wei-Chi Lai, Yi-Ting Wang, Hao-Chung Kuo, Shing-Chung Wang. // IEEE Photonics Technology Letters. - 2009. - Vol. 21, No. 7. - P. 414-416. ↑
- J975.** Ko-Tao Lee. Improvement on Optical Properties of GaN Light-Emitting Diode With Mesh-Textured Sapphire Back Delineated by Laser Scriber. / Ko-Tao Lee, Yeeu-Chang Lee, Jenq-Yang Chang, Jeng Gong. // IEEE Photonics Technology Letters. - 2009. - Vol. 21, No. 7. - P. 477-479. ↑
- J976.** Zhao Hongping. Growths of staggered InGaN quantum wells light-emitting diodes emitting at 520-525 nm employing graded growth-temperature profile. / Zhao Hongping, Liu Guangyu, Li Xiao-Hang, Huang G. S., Poplawsky Jonathan D., Penn S. Tafon, Dierolf Volkmar, Tansu Nelson. // Applied Physics Letters. - 2009. - Vol. 95, No. 6. - P. 061104-061104-3. ↑
- J977.** Gupta D. Transport of Photogenerated Charge Carriers in Polymer Semiconductors. / Gupta D., Vidhyadhiraja N.S., Narayan K.S. // Proceedings of the IEEE. - 2009. - Vol. 97, No. 9. - P. 1558-1569. ↑
- J978.** Chi-Hao Wu. High-Efficiency Current-Regulated Charge Pump for a White LED Driver. / Chi-Hao Wu, Chern-Lin Chen. // IEEE Transactions on Circuits and Systems II: Express Briefs. - 2009. - Vol. 56, No. 10. - P. 763-767. ↑
- J979.** Park Seoung-Hwan. Dip-shaped InGaN/GaN quantum-well light-emitting diodes with high efficiency. / Park Seoung-Hwan, Ahn Doyeol, Koo Bun-Hei, Kim Jong-Wook. // Applied Physics Letters. - 2009. - Vol. 95,

No. 6. - P. 063507-063507-3. ↑

J980. Anopchenko A. Low-voltage onset of electroluminescence in nanocrystalline-Si /SiO₂ multilayers. / Anopchenko A., Marconi A., Moser E., Prezioso S., Wang M., Pavesi L., Pucker G., Bellutti P. // Journal of Applied Physics. - 2009. - Vol. 106, No. 3. - P. 033104-033104-8. ↑

J981. Suk Chung. Quantitative Analysis of Dopant Distribution and Activation Across p-n Junctions in AlGaAs/GaAs Light-Emitting Diodes Using Off-Axis Electron Holography. / Suk Chung, Johnson S.R., Ding Ding, Yong-Hang Zhang, Smith D.J., McCartney M.R. // IEEE Transactions on Electron Devices. - 2009. - Vol. 56, No. 9. - P. 1919-1923. ↑

J982. Amarasinghe D. Organic Semiconductor Optical Amplifiers. / Amarasinghe D., Ruseckas A., Turnbull G.A., Samuel I.D.W. // Proceedings of the IEEE. - 2009. - Vol. 97, No. 9. - P. 1637-1650. ↑

J983. Walker A.B. Multiscale Modeling of Charge and Energy Transport in Organic Light-Emitting Diodes and Photovoltaics. Proceedings of the IEEE. - 2009. - Vol. 97, No. 9. - P. 1587-1596. ↑

J984. Qi S. L. Study on the formation of dodecagonal pyramid on nitrogen polar GaN surface etched by hot H₃PO₄. / Qi S. L., Chen Z. Z., Fang H., Sun Y. J., Sang L. W., Yang X. L., Zhao L. B., Tian P. F., Deng J. J., Tao Y. B., Yu T. J., Qin Z. X., Zhang G. Y. // Applied Physics Letters. - 2009. - Vol. 95, No. 7. - P. 071114-071114-3. ↑

J985. Grzanka S. Effect of efficiency "droop" in violet and blue InGaN laser diodes. / Grzanka S., Perlin P., Czernecki R., Marona L., Bockowski M., Łuczniak B., Leszczynski M., Suski T. // Applied Physics Letters. - 2009. - Vol. 95, No. 7. - P. 071108-071108-3. ↑

J986. Luo Yichun. Space charge effects on the electroluminescence efficiency and stability of organic light-emitting devices with mixed emitting layers. / Luo Yichun, Aziz Hany. // Applied Physics Letters. - 2009. - Vol. 95, No. 7. - P. 073304-073304-3. ↑

J987. Kim Baek Hyun. Enhanced performance of silicon quantum dot light-emitting diodes grown on nanoroughened silicon substrate. / Kim Baek Hyun, Davis Robert F., Cho Chang-Hee, Park Seong-Ju. // Applied Physics Letters. - 2009. - Vol. 95, No. 7. - P. 073113-073113-3. ↑

J988. Hwang Sung-Min. Demonstration of nonpolar a-plane InGaN/GaN light emitting diode on r-plane sapphire substrate. / Hwang Sung-Min, Seo Yong Gon, Baik Kwang Hyeon, Cho In-Sung, Baek Jong Hyeob, Jung Sukkoo, Kim Tae Geun, Cho Meoungwhan. // Applied Physics Letters. - 2009. - Vol. 95, No. 7. - P. 071101-071101-3. ↑

J989. Kisch-Wedel H. Does the Estimation of Light Attenuation in Tissue Increase the Accuracy of Reflectance Pulse Oximetry at Low Oxygen Saturations In Vivo ? / Kisch-Wedel H., Bernreuter P., Kemming G., Albert M., Zwissler B. // IEEE Transactions on Biomedical Engineering. - 2009. - Vol. 56, No. 9. - P. 2271-2279. ↑

J990. Parviz B.A. For your eye only. IEEE Spectrum. - 2009. - Vol. 46, No. 9. - P. 36-41. ↑

J991. Drezet A. Publisher's Note: "Opening the light extraction cone of high index substrates with plasmonic gratings: Light emitting diode applications" [Appl. Phys. Lett. 95, 021101 (2009)]. / Drezet A., Przybilla F., Laux E., Mahboub O., Genet C., Ebbesen T. W., Bouillard J. S., Zayats A. V., Spevak I. S., Kats A. V., Nikitin A. Yu, Martin-Moreno L. // Applied Physics Letters. - 2009. - Vol. 95, No. 6. - P. 069903-069903-1. ↑

J992. Suehiro Takayuki. Blue-emitting LaSi₃N₅:Ce³⁺ fine powder phosphor for UV-converting white light-emitting diodes. / Suehiro Takayuki, Hirosaki Naoto, Xie Rong-Jun, Sato Tsugio. // Applied Physics Letters. - 2009. - Vol. 95, No. 5. - P. 051903-051903-3. ↑

J993. Monkman A.P. Singlet Generation Yields in Organic Light-Emitting Diodes. / Monkman A.P., Rothe C., King S.M. // Proceedings of the IEEE. - 2009. - Vol. 97, No. 9. - P. 1597-1605. ↑

J994. Wai-Keung Lun. Bilevel Current Driving Technique for LEDs. / Wai-Keung Lun, Loo K.H., Siew-Chong Tan, Lai Y.M., Tse C.K. // IEEE Transactions on Power Electronics. - 2009. - Vol. 24, No. 12. - P. 2920-2932. ↑

J995. Yun Changhun. Electron injection via pentacene thin films for efficient inverted organic light-emitting diodes. / Yun Changhun, Cho Hyunsu, Kang Hyeseung, Lee Young Mi, Park Yongsup, Yoo Seunghyup. //

Applied Physics Letters. - 2009. - Vol. 95, No. 5. - P. 053301-053301-3. ↑

J996. Munnix M.C. Modeling Highly Efficient RCLED-Type Quantum-Dot-Based Single Photon Emitters. / Munnix M.C., Lochmann A., Bimberg D., Haisler V.A. // IEEE Journal of Quantum Electronics. - 2009. - Vol. 45, No. 9. - P. 1084-1088. ↑

J997. Oliver Rachel A. Morphological changes of InGaN epilayers during annealing assessed by spectral analysis of atomic force microscopy images. / Oliver Rachel A., Sumner Joy, Kappers Menno J., Humphreys Colin J. // Journal of Applied Physics. - 2009. - Vol. 106, No. 5. - P. 054319-054319-6. ↑

J998. Ohmori Y. Organic Devices for Integrated Photonics. / Ohmori Y., Kajii H. // Proceedings of the IEEE. - 2009. - Vol. 97, No. 9. - P. 1627-1636. ↑

J999. Bera S.C. Driver circuits for temperature-invariant performance of junction diodes. / Bera S.C., Singh R.V., Garg V.K. // IET Circuits, Devices & Systems. - 2009. - Vol. 3, No. 4. - P. 143-152. ↑

J1000. Chi-Feng Lin. Application of Taguchi Method in Light-Emitting Diode Backlight Design for Wide Color Gamut Displays. / Chi-Feng Lin, Chih-Cheng Wu, Po-Hua Yang, Tsung-Yuan Kuo. // Journal of Display Technology. - 2009. - Vol. 5, No. 8. - P. 323-330. ↑

J1001. Lamar D.G. A Very Simple Control Strategy for Power Factor Correctors Driving High-Brightness LEDs. / Lamar D.G., Zuniga J.S., Alonso A.R., Gonzalez M.R., Alvarez M.M.H. // IEEE Transactions on Power Electronics. - 2009. - Vol. 24, No. 8. - P. 2032-2042. ↑

J1002. Miscioscia R. Electrooptical Analysis of Effects Induced by Floating Metallic Interlayers in Organic LEDs. / Miscioscia R., Vacca P., Nenna G., Fasolino T., La Ferrara V., Tassini P., Minarini C., della Sala D. // IEEE Transactions on Electron Devices. - 2009. - Vol. 56, No. 9. - P. 1912-1918. ↑

J1003. Xu Denghui. Organic light-emitting diode with liquid emitting layer. / Xu Denghui, Adachi Chihaya. // Applied Physics Letters. - 2009. - Vol. 95, No. 5. - P. 053304-053304-3. ↑

J1004. Vucic J. White Light Wireless Transmission at 200 Mb/s Net Data Rate by Use of Discrete-Multitone Modulation. / Vucic J., Kottke C., Nerreter S., Buttner A., Langer K.-D., Walewski J. W. // IEEE Photonics Technology Letters. - 2009. - Vol. 21, No. 20. - P. 1511-1513. ↑

J1005. Li-Chi Peng. GaN-Based LEDs With GaN -Pillars Around Mesa, Patterned Substrate, and Reflector Under Pads. / Li-Chi Peng, Wei-Chih Lai, Ming-Nan Chang, Shih-Chang Shei, Jinn-Kong Sheu. // IEEE Photonics Technology Letters. - 2009. - Vol. 21, No. 22. - P. 1659-1661. ↑

J1006. Hui S.Y. A General Photo-Electro-Thermal Theory for Light Emitting Diode (LED) Systems. / Hui S.Y., Qin Y.X. // IEEE Transactions on Power Electronics. - 2009. - Vol. 24, No. 8. - P. 1967-1976. ↑

J1007. Chun-Yu Hsieh. A Charge-Recycling Buck-Store and Boost-Restore (BSBR) Technique With Dual Outputs for RGB LED Backlight and Flashlight Module. / Chun-Yu Hsieh, Chih-Yu Yang, Ke-Horng Chen. // IEEE Transactions on Power Electronics. - 2009. - Vol. 24, No. 8. - P. 1914-1925. ↑

J1008. Liuxi Tan. Effects of Defects on the Thermal and Optical Performance of High-Brightness Light-Emitting Diodes. / Liuxi Tan, Jia Li, Kai Wang, Sheng Liu. // IEEE Transactions on Electronics Packaging Manufacturing. - 2009. - Vol. 32, No. 4. - P. 233-240. ↑

J1009. Lei Yueqing. Verification of p-n junctions in polymer light-emitting electrochemical cells via electrical characterization. / Lei Yueqing, Teng Feng, Hou Yanbing, Lou Zhidong, Wang Yongsheng. // Applied Physics Letters. - 2009. - Vol. 95, No. 10. - P. 101105-101105-3. ↑

J1010. Park Tae Jin. Efficient multiple triplet quantum well structures in organic light-emitting devices. / Park Tae Jin, Jeon Woo Sik, Choi Jin Woo, Poda Ramchandra, Jang Jin, Kwon Jang Hyuk. // Applied Physics Letters. - 2009. - Vol. 95, No. 10. - P. 103303-103303-3. ↑

J1011. Luo X. Temperature estimation of high-power light emitting diode street lamp by a multi-chip analytical solution. / Luo X., Xiong W., Cheng T., Liu S. // IET Optoelectronics. - 2009. - Vol. 3, No. 5. - P. 225-232. ↑

J1012. Onushkin Grigory A. Local electroluminescence and time-resolved photoluminescence study of InGaN

light-emitting diodes. / Onushkin Grigory A., Hong Sang-Su, Lee Jin-Hyun, Park June-Sik, Son Joong-Kon, Kim Min-Ho, Park YongJo. // Applied Physics Letters. - 2009. - Vol. 95, No. 10. - P. 101904-101904-3. ↑

J1013. Liu Haoling. Self-pulsing 1050 nm quantum dot edge emitting laser diodes. / Liu Haoling, Smowton Peter, Summers Huw, Edwards Gareth, Drexler Wolfgang. // Applied Physics Letters. - 2009. - Vol. 95, No. 10. - P. 101111-101111-3. ↑

J1014. Meneghini M. Degradation of High-Brightness Green LEDs Submitted to Reverse Electrical Stress. / Meneghini M., Zehnder U., Hahn B., Meneghesso G., Zanoni E. // IEEE Electron Device Letters. - 2009. - Vol. 30, No. 10. - P. 1051-1053. ↑

J1015. Sammarco J.J. Evaluation of Peripheral Visual Performance When Using Incandescent and LED Miner Cap Lamps. / Sammarco J.J., Reyes M.A., Bartels J.R., Gallagher S. // IEEE Transactions on Industry Applications. - 2009. - Vol. 45, No. 6. - P. 1923-1929. ↑

J1016. Konovalov I. Band alignment at SrCu 2 O 2 /ZnO heterointerface. / Konovalov I., Hesse R. // Journal of Applied Physics. - 2009. - Vol. 106, No. 5. - P. 056102-056102-3. ↑

J1017. Chia-Feng Lin. InGaN-Based Light-Emitting Diodes With Nanoporous Microhole Structures. / Chia-Feng Lin, Kuei-Ting Chen, Chun-Min Lin, Chung-Chieh Yang. // IEEE Electron Device Letters. - 2009. - Vol. 30, No. 10. - P. 1057-1059. ↑

J1018. Loo K.H. On Driving Techniques for LEDs: Toward a Generalized Methodology. / Loo K.H., Wai-Keung Lun, Siew-Chong Tan, Lai Y.M., Tse C.K. // IEEE Transactions on Power Electronics. - 2009. - Vol. 24, No. 12. - P. 2967-2976. ↑

J1019. Park Tae Hyun. Micro-pixel array of organic light-emitting diodes applying imprinting technique with a polymer replica. / Park Tae Hyun, Kim Young Min, Park Young Wook, Choi Jin Hwan, Jeong Jin-Wook, Dong Ki Young, Choi Kyung Cheol, Ju Byeong-Kwon. // Applied Physics Letters. - 2009. - Vol. 95, No. 9. - P. 093301-093301-3. ↑

J1020. Kuo C.W. GaN-Based Light-Emitting Diode Prepared on Nano-Inverted Pyramid GaN Template. / Kuo C.W., Chang L.C., Cheng-Huang Kuo. // IEEE Photonics Technology Letters. - 2009. - Vol. 21, No. 21. - P. 1645-1647. ↑

J1021. Renaud Cedric. Study of trap states in polyspirobifluorene based devices: Influence of aging by electrical stress. / Renaud Cedric, Nguyen Thien-Phap. // Journal of Applied Physics. - 2009. - Vol. 106, No. 5. - P. 053707-053707-11. ↑

J1022. Huihui Huang. ZnO-Based Fairly Pure Ultraviolet Light-Emitting Diodes With a Low Operation Voltage. / Huihui Huang, Guojia Fang, Xiaoming Mo, Hao Long, Longyan Yuan, Binzhong Dong, Xianquan Meng, Xingzhong Zhao. // IEEE Electron Device Letters. - 2009. - Vol. 30, No. 10. - P. 1063-1065. ↑

J1023. Kun-Mao Pan. Polarization-Dependent Sidewall Light Diffraction of LEDs Surrounded by Nanorod Arrays. / Kun-Mao Pan, Yun-Wei Cheng, Liang-Yi Chen, Ying-Yuan Huang, Min-Yung Ke, Cheng-Pin Chen, Yuh-Renn Wu, JianJang Huang. // IEEE Photonics Technology Letters. - 2009. - Vol. 21, No. 22. - P. 1683-1685. ↑

J1024. Zhou Shengjun. Transient measurement of light-emitting diode characteristic parameters for production lines. / Zhou Shengjun, Liu Sheng. // Review of Scientific Instruments. - 2009. - Vol. 80, No. 9. - P. 095102-095102-7. ↑

J1025. Akande Wali O. Degradation of organic light emitting diodes by nucleated telephone cord blisters. / Akande Wali O., Soboyejo Wole. // Applied Physics Letters. - 2009. - Vol. 95, No. 11. - P. 113304-113304-3. ↑

J1026. Oh Eunsoon. Carrier lifetime and spin relaxation time study for electrical spin injection into GaAs. / Oh Eunsoon, Lee T. K., Park J. H., Choi J. H., Park Y. J., Shin K. H., Kim K. Y. // Journal of Applied Physics. - 2009. - Vol. 106, No. 4. - P. 043515-043515-4. ↑

J1027. Yea-Chen Lee. Enhanced Light Extraction in Wafer-Bonded AlGaInP-Based Light-Emitting Diodes via Micro- and Nanoscale Surface Textured. / Yea-Chen Lee, Hao-Chung Kuo, Bo-Siao Cheng, Chia-En Lee, Ching-Hua Chiu, Tien-Chang Lu, Shing-Chung Wang, Tien-Fu Liao, Chih-Sung Chang. // IEEE Electron Device

Letters. - 2009. - Vol. 30, No. 10. - P. 1054-1056. ↑

J1028. Subashiev A.V. Optical Power Transmission Through Adhesive and Bonding Layers. / Subashiev A.V., Luryi S. // Journal of Lightwave Technology. - 2009. - Vol. 27, No. 22. - P. 5192-5201. ↑

J1029. You J. B. Energy band alignment of SiO₂/ZnO interface determined by x-ray photoelectron spectroscopy. / You J. B., Zhang X. W., Song H. P., Ying J., Guo Y., Yang A. L., Yin Z. G., Chen N. F., Zhu Q. S. // Journal of Applied Physics. - 2009. - Vol. 106, No. 4. - P. 043709-043709-5. ↑

J1030. Chun-Yu Hsieh. Boost DC-DC Converter With Fast Reference Tracking (FRT) and Charge-Recycling (CR) Techniques for High-Efficiency and Low-Cost LED Driver. / Chun-Yu Hsieh, Ke-Horng Chen. // IEEE Journal of Solid-State Circuits. - 2009. - Vol. 44, No. 9. - P. 2568-2580. ↑

J1031. Andrade L. H. C. A step forward toward smart white lighting: Combination of glass phosphor and light emitting diodes. / Andrade L. H. C., Lima S. M., Novatski A., Steimacher A., Rohling J. H., Medina A. N., Bento A. C., Baesso M. L., Guyot Y., Boulon G. // Applied Physics Letters. - 2009. - Vol. 95, No. 8. - P. 081104-081104-3. ↑

J1032. Feltin E. Broadband blue superluminescent light-emitting diodes based on GaN. / Feltin E., Castiglia A., Cosendey G., Sulmoni L., Carlin J.-F., Grandjean N., Rossetti M., Dorsaz J., Laino V., Duell M., Velez C. // Applied Physics Letters. - 2009. - Vol. 95, No. 8. - P. 081107-081107-3. ↑

J1033. Cho Sung Nae. Erratum: "Charged particle-display" [J. Appl. Phys. 106, 033505 (2009)]. Journal of Applied Physics. - 2009. - Vol. 106, No. 4. - P. 049902-049902-1. ↑

J1034. Hu Weixuan. Electroluminescence from Ge on Si substrate at room temperature. / Hu Weixuan, Cheng Buwen, Xue Chunlai, Xue Haiyun, Su Shaojian, Bai Anqi, Luo Liping, Yu Yude, Wang Qiming. // Applied Physics Letters. - 2009. - Vol. 95, No. 9. - P. 092102-092102-3. ↑

J1035. Li Z.L. A Reliability Study on Green InGaN-GaN Light-Emitting Diodes. / Li Z.L., Lai P.T., Choi H.W. // IEEE Photonics Technology Letters. - 2009. - Vol. 21, No. 19. - P. 1429-1431. ↑

J1036. Dahal R. Erbium-doped GaN optical amplifiers operating at 1.54 μm . / Dahal R., Ugolini C., Lin J. Y., Jiang H. X., Zavada J. M. // Applied Physics Letters. - 2009. - Vol. 95, No. 11. - P. 111109-111109-3. ↑

J1037. Nash G.R. Mid-Infrared Light-Emitting Diodes and Photodiodes for Hydrocarbon Sensing. / Nash G.R., Forman H.L., Smith S.J., Robinson P.B., Buckle L., Coomber S.D., Emeny M.T., Gordon N.T., Ashley T. // IEEE Sensors Journal. - 2009. - Vol. 9, No. 10. - P. 1240-1243. ↑

J1038. Yun-Wei Cheng. Characterizations of GaN-Based LEDs Encompassed With Self-Aligned Nanorod Arrays of Various Distribution Densities. / Yun-Wei Cheng, Kun-Mao Pan, Liang-Yi Chen, Min-Yung Ke, Cheng-Pin Chen, Cheng-Yen Chen, Yang C.C., Jian Jang Huang. // IEEE Electron Device Letters. - 2009. - Vol. 30, No. 10. - P. 1060-1062. ↑

J1039. Hsueh Kuang-Po. Evolution of surface morphology of dry-etched ZnO with Cl₂/Ar plasma. / Hsueh Kuang-Po, Hou Ren-Jie, Tun Chun-Ju. // Journal of Vacuum Science & Technology B: Microelectronics and Nanometer Structures. - 2009. - Vol. 27, No. 5. - P. 2187-2191. ↑

J1040. Ryu Han-Youl. Rate equation analysis of efficiency droop in InGaN light-emitting diodes. / Ryu Han-Youl, Kim Hyun-Sung, Shim Jong-In. // Applied Physics Letters. - 2009. - Vol. 95, No. 8. - P. 081114-081114-3. ↑

J1041. Zhu De-Xi. Anisotropic optical constants of in-plane oriented polyfluorene thin films on rubbed substrate. / Zhu De-Xi, Shen Wei-Dong, Zhen Hong-Yu. // Journal of Applied Physics. - 2009. - Vol. 106, No. 8. - P. 084504-084504-5. ↑

J1042. Fairley P. Plastic solar cells roll into unlit villages. IEEE Spectrum. - 2009. - Vol. 46, No. 11. - P. 13-14. ↑

J1043. Li Jinchai. Enhancement of p-type conductivity by modifying the internal electric field in Mg- and Si-delta-codoped Al_xGa_{1-x}N/Al_yGa_{1-y}N superlattices. / Li Jinchai, Yang Weihuang, Li Shuping, Chen Hangyang, Liu Dayi, Kang Junyong. // Applied Physics Letters. - 2009. - Vol. 95, No. 15. - P. 151113-151113-3. ↑

- J1044.** Jang Ho Seong. Bright three-band white light generated from CdSe/ZnSe quantum dot-assisted Sr 3 SiO 5 :Ce 3+ ,Li + -based white light-emitting diode with high color rendering index. / Jang Ho Seong, Kwon Byoung-Hwa, Yang Heesun, Jeon Duk Young. // Applied Physics Letters. - 2009. - Vol. 95, No. 16. - P. 161901-161901-3. ↑
- J1045.** Yang Y. Removing plasma-induced sidewall damage in GaN-based light-emitting diodes by annealing and wet chemical treatments. / Yang Y., Cao X. A. // Journal of Vacuum Science & Technology B: Microelectronics and Nanometer Structures. - 2009. - Vol. 27, No. 6. - P. 2337-2341. ↑
- J1046.** Meneghini M. Leakage current and reverse-bias luminescence in InGaN-based light-emitting diodes. / Meneghini M., Trivellin N., Pavesi M., Manfredi M., Zehnder U., Hahn B., Meneghesso G., Zanoni E. // Applied Physics Letters. - 2009. - Vol. 95, No. 17. - P. 173507-173507-3. ↑
- J1047.** Young-Bok Yoon. The Thermal Resistance of Solder Joints in High Brightness Light Emitting Diode (HB LED) Packages. / Young-Bok Yoon, Jin-Woo Park. // IEEE Transactions on Components and Packaging Technologies. - 2009. - Vol. 32, No. 4. - P. 825-831. ↑
- J1048.** Shao Xianjie. Efficiency droop behavior of direct current aged GaN-based blue light-emitting diodes. / Shao Xianjie, Lu Hai, Chen Dunjun, Xie Zili, Zhang Rong, Zheng Youdou. // Applied Physics Letters. - 2009. - Vol. 95, No. 16. - P. 163504-163504-3. ↑
- J1049.** Park Young Wook. Highly efficient tris(8-hydroxyquinoline) aluminum-based organic light-emitting diodes utilized by balanced energy transfer with cosensitizing fluorescent dyes. / Park Young Wook, Kim Young Min, Choi Jin Hwan, Park Tae Hyun, Huh Jin Woo, Kim Hong Suk, Cho Min Ju, Choi Dong Hoon, Ju Byeong-Kwon. // Applied Physics Letters. - 2009. - Vol. 95, No. 14. - P. 143305-143305-3. ↑
- J1050.** Charash R. Carrier distribution in InGaN/GaN tricolor multiple quantum well light emitting diodes. / Charash R., Maaskant P. P., Lewis L., McAleese C., Kappers M. J., Humphreys C. J., Corbett B. // Applied Physics Letters. - 2009. - Vol. 95, No. 15. - P. 151103-151103-3. ↑
- J1051.** Sohn Kee-Sun. Time-resolved photoluminescence analysis of two-peak emission behavior in Sr 2 Si 5 N 8 :Eu 2+. / Sohn Kee-Sun, Lee Sangjun, Xie Rong-Jun, Hirotsuki Naoto. // Applied Physics Letters. - 2009. - Vol. 95, No. 12. - P. 121903-121903-3. ↑
- J1052.** Park Tae Hyun. Self-assembled microarray of organic light-emitting diodes using a self-assembled monolayer by microcontact printing. / Park Tae Hyun, Kim Young Min, Park Young Wook, Choi Jin Hwan, Jeong Jin-Wook, Choi Kyung Cheol, Ju Byeong-Kwon. // Applied Physics Letters. - 2009. - Vol. 95, No. 11. - P. 113310-113310-3. ↑
- J1053.** Li Sheng. Electroluminescence enhancement in polymer light-emitting diodes through hole injection layer insertion. / Li Sheng, Tong Guo-Ping, George Thomas F. // Journal of Applied Physics. - 2009. - Vol. 106, No. 7. - P. 074513-074513-4. ↑
- J1054.** Nizamoglu Sedat. Forster resonance energy transfer enhanced color-conversion using colloidal semiconductor quantum dots for solid state lighting. / Nizamoglu Sedat, Demir Hilmi Volkan. // Applied Physics Letters. - 2009. - Vol. 95, No. 15. - P. 151111-151111-3. ↑
- J1055.** Kim Baek Hyun. Effect of injection current density on electroluminescence in silicon quantum dot light-emitting diodes. / Kim Baek Hyun, Davis Robert F., Cho Chang-Hee, Park Seong-Ju. // Applied Physics Letters. - 2009. - Vol. 95, No. 15. - P. 153103-153103-3. ↑
- J1056.** Chen N. C. Spectral shape and broadening of emission from AlGaInP light-emitting diodes. / Chen N. C., Lien W. C., Yang Y. K., Shen C., Wang Y. S., Chen J. F. // Journal of Applied Physics. - 2009. - Vol. 106, No. 7. - P. 074514-074514-9. ↑
- J1057.** Riedl T. Transparent Electronics for See-Through AMOLED Displays. / Riedl T., Gorn P., Kowalsky W. // Journal of Display Technology. - 2009. - Vol. 5, No. 12. - P. 501-508. ↑
- J1058.** Shlayan N. Energy Efficient RGBW Pixel Configuration for Light-Emitting Displays. / Shlayan N., Venkat R., Ginobbi P., Singh A.K. // Journal of Display Technology. - 2009. - Vol. 5, No. 11. - P. 418-424. ↑
- J1059.** Scholz Sebastian. Chemical changes on the green emitter tris(8-hydroxy-quinolinato)aluminum during

device aging of p-i-n -structured organic light emitting diodes. / Scholz Sebastian, Lussem Bjorn, Leo Karl. // Applied Physics Letters. - 2009. - Vol. 95, No. 18. - P. 183309-183309-3. ↑

J1060. Garner S.M. Guest Editorial Special Issue on Transparent Electronics. / Garner S.M., Chung-Chih Wu, Yongtaek Hong, So F., Xin Jiang. // Journal of Display Technology. - 2009. - Vol. 5, No. 12. - P. 429-430. ↑

J1061. Schubert Martin F. Electroluminescence induced by photoluminescence excitation in GaInN/GaN light-emitting diodes. / Schubert Martin F., Dai Qi, Xu Jiuru, Kim Jong Kyu, Schubert E. Fred. // Applied Physics Letters. - 2009. - Vol. 95, No. 19. - P. 191105-191105-3. ↑

J1062. Hiramatsu Ryosuke. Tb 3+ luminescence by energy transfer from Eu 2+ in (Sr ,Ba)2 SiO 4 phosphor. / Hiramatsu Ryosuke, Ishida Kunio, Aiga Fumihiko, Fukuda Yumi, Matsuda Naotoshi, Asai Hironori. // Journal of Applied Physics. - 2009. - Vol. 106, No. 9. - P. 093513-093513-7. ↑

J1063. Chang-Wook Han. Dual-Plate OLED Display (DOD) Embedded With White OLED. / Chang-Wook Han, Hwa Kyung Kim, Hee Suk Pang, Sung-Hoon Pieh, Chang Je Sung, Hong Seok Choi, Woo-Chan Kim, Myung-Seop Kim, Yoon-Heung Tak. // Journal of Display Technology. - 2009. - Vol. 5, No. 12. - P. 541-545. ↑

J1064. Hong Seok Choi. Optimization of 2-Stack WOLED Structure With Consideration on Color Gamut and Power Consumption. / Hong Seok Choi, Sunghoon Pieh, Chang Je Sung, Hwa Kung Kim, Myung Seop Kim, Chang-Wook Han, Yoon Heung Tak. // Journal of Display Technology. - 2009. - Vol. 5, No. 12. - P. 546-551. ↑

J1065. Qiaoqiang Gan. UV Plasmonic Structures: Direct Observations of UV Extraordinary Optical Transmission and Localized Field Enhancement Through Nanoslits. / Qiaoqiang Gan, Liangcheng Zhou, Dierolf V., Bartoli F.J. // IEEE Photonics Journal. - 2009. - Vol. 1, No. 4. - P. 245-253. ↑

J1066. Ruseckas A. Singlet energy transfer and singlet-singlet annihilation in light-emitting blends of organic semiconductors. / Ruseckas A., Ribierre J. C., Shaw P. E., Staton S. V., Burn P. L., Samuel I. D. W. // Applied Physics Letters. - 2009. - Vol. 95, No. 18. - P. 183305-183305-3. ↑

J1067. Rai P. Drain Current Centric Modality: Instrumentation and Evaluation of ISFET for Monitoring Myocardial Ischemia Like Variations in pH and Potassium Ion Concentration. / Rai P., Soyoun Jung, Taeksoo Ji, Varadan V.K. // IEEE Sensors Journal. - 2009. - Vol. 9, No. 12. - P. 1987-1995. ↑

J1068. Lin B.-R. Analysis and implementation of an integrated sepic-forward converter for photovoltaicbased light emitting diode lighting. / Lin B.-R., Huang C.-L. // IET Power Electronics. - 2009. - Vol. 2, No. 6. - P. 635-645. ↑

J1069. Gan Zhengqing. Spectrally narrowed edge emission from leaky waveguide modes in organic light-emitting diodes. / Gan Zhengqing, Tian Yun, Lynch David W., Kang Ji-hun, Park Q-Han, Shinar Joseph. // Journal of Applied Physics. - 2009. - Vol. 106, No. 9. - P. 094502-094502-11. ↑

J1070. Pinos A. Aging of AlGaIn quantum well light emitting diode studied by scanning near-field optical spectroscopy. / Pinos A., Marcinkevicius S., Yang J., Bilenko Y., Shatalov M., Gaska R., Shur M. S. // Applied Physics Letters. - 2009. - Vol. 95, No. 18. - P. 181914-181914-3. ↑

J1071. Chao-Hsin Wu. 4-GHz Modulation Bandwidth of Integrated 2 2 LED Array. / Chao-Hsin Wu, Walter G., Han Wui Then, Feng M., Holonyak N. // IEEE Photonics Technology Letters. - 2009. - Vol. 21, No. 24. - P. 1834-1836. ↑

J1072. Bergenek K. Strong High Order Diffraction of Guided Modes in Micro-Cavity Light-Emitting Diodes With Hexagonal Photonic Crystals. / Bergenek K., Wiesmann C., Zull H., Rumbolz C., Wirth R., Linder N., Streubel K., Krauss T.F. // IEEE Journal of Quantum Electronics. - 2009. - Vol. 45, No. 12. - P. 1517-1523. ↑

J1073. Xin Linyuan. Inversion of magnetic field effects on electrical current and electroluminescence in tri-(8-hydroxyquinoline)-aluminum based light-emitting diodes. / Xin Linyuan, Li Chuannan, Li Feng, Liu Shiyong, Hu Bin. // Applied Physics Letters. - 2009. - Vol. 95, No. 12. - P. 123306-123306-3. ↑

J1074. Leem Dong-Seok. High efficiency p-i-n top-emitting organic light-emitting diodes with a nearly Lambertian emission pattern. / Leem Dong-Seok, Kim Sei-Yong, Lee Jae-Hyun, Kim Jang-Joo. // Journal of Applied Physics. - 2009. - Vol. 106, No. 6. - P. 063114-063114-5. ↑

↑

- J1075.** Meerheim R. Efficiency and Stability of p-i-n Type Organic Light Emitting Diodes for Display and Lighting Applications. / Meerheim R., Lussem B., Leo K. // Proceedings of the IEEE. - 2009. - Vol. 97, No. 9. - P. 1606-1626. ↑
- J1076.** Pearson C. Effect of dye concentrations in blended-layer white organic light-emitting devices based on phosphorescent dyes. / Pearson C., Cadd D. H., Petty M. C., Hua Y. L. // Journal of Applied Physics. - 2009. - Vol. 106, No. 6. - P. 064516-064516-10. ↑
- J1077.** Kwapil Wolfram. Diode breakdown related to recombination active defects in block-cast multicrystalline silicon solar cells. / Kwapil Wolfram, Kasemann Martin, Gundel Paul, Schubert Martin C., Warta Wilhelm, Bronsveld Paula, Coletti Gianluca. // Journal of Applied Physics. - 2009. - Vol. 106, No. 6. - P. 063530-063530-7. ↑
- J1078.** Stevenson R. The LED's dark secret. IEEE Spectrum. - 2009. - Vol. 46, No. 8. - P. 26-31. ↑
- J1079.** Mpoukouvalas Konstantinos. Impedance spectroscopy investigation of conjugated polymer coated core-shell nanoparticles. / Mpoukouvalas Konstantinos, Wang Jianjun, Tilch Robert, Butt Hans-Juergen, Wegner Gerhard. // Journal of Applied Physics. - 2009. - Vol. 106, No. 6. - P. 063706-063706-11. ↑
- J1080.** Rath A.K. Organic Memory and Electrical Bistability in a Quinone-Based Charge-Transfer Complex. / Rath A.K., Pal A.J. // Proceedings of the IEEE. - 2009. - Vol. 97, No. 9. - P. 1580-1586. ↑
- J1081.** Tae-Young Park. Improvement of Electrostatic Discharge Characteristics and Optical Properties of GaN-Based Light-Emitting Diodes. / Tae-Young Park, Min-Suk Oh, Seong-Ju Park. // IEEE Electron Device Letters. - 2009. - Vol. 30, No. 9. - P. 937-939. ↑
- J1082.** Hoshino K. Near-Field Scanning Nanophotonic Microscopy-Breaking the Diffraction Limit Using Integrated Nano Light-Emitting Probe Tip. / Hoshino K., Gopal A., Xiaojing Zhang. // IEEE Journal of Selected Topics in Quantum Electronics. - 2009. - Vol. 15, No. 5. - P. 1393-1399. ↑
- J1083.** Savaidis S.P. Simulation of Light Emission From Planar Multilayer OLEDs, Using a Transmission-Line Model. / Savaidis S.P., Stathopoulos N.A. // IEEE Journal of Quantum Electronics. - 2009. - Vol. 45, No. 9. - P. 1089-1099. ↑
- J1084.** Wiesmann C. Theoretical Investigation of the Radiation Pattern From LEDs Incorporating Shallow Photonic Crystals. / Wiesmann C., Bergenek K., Houdre R., Stanley R.P., Linder N., Schwarz U.T. // IEEE Journal of Quantum Electronics. - 2009. - Vol. 45, No. 10. - P. 1273-1283. ↑
- J1085.** Inan B. Impact of LED Nonlinearity on Discrete Multitone Modulation. / Inan B., Lee S.C.J., Randel S., Neokosmidis I., Koonen A.M.J., Walewski J.W. // IEEE/OSA Journal of Optical Communications and Networking. - 2009. - Vol. 1, No. 5. - P. 439-451. ↑
- J1086.** Yi-Jung Liu. On a GaN-Based Light-Emitting Diode With a p-GaN/i-InGaN Superlattice Structure. / Yi-Jung Liu, Chih-Hung Yen, Li-Yang Chen, Tsung-Han Tsai, Tsung-Yuan Tsai, Wen-Chau Liu. // IEEE Electron Device Letters. - 2009. - Vol. 30, No. 11. - P. 1149-1151. ↑
- J1087.** Hung-Wen Huang. Improved Light Output Power of GaN-Based Light-Emitting Diodes Using Double Photonic Quasi-Crystal Patterns. / Hung-Wen Huang, Chung-Hsiang Lin, Zhi-Kai Huang, Kang-Yuan Lee, Chang-Chin Yu, Hao-Chung Kuo. // IEEE Electron Device Letters. - 2009. - Vol. 30, No. 11. - P. 1152-1154. ↑
- J1088.** Elgala H. Indoor broadcasting via white LEDs and OFDM. / Elgala H., Mesleh R., Haas H. // IEEE Transactions on Consumer Electronics. - 2009. - Vol. 55, No. 3. - P. 1127-1134. ↑
- J1089.** Ching-Chih Tsai. Wide color-gamut improvement of LCM using multi-phosphor white LED and modified rich color method. / Ching-Chih Tsai, Chih-Chang Lai, Shih-Min Hsieh. // IEEE Transactions on Consumer Electronics. - 2009. - Vol. 55, No. 3. - P. 1566-1571. ↑
- J1090.** Li Na. Highly efficient nondoped green organic light-emitting devices based on a substituted triphenylpyridine derivative. / Li Na, Lai Shiu-Lun, Wang Pengfei, Teng Feng, Liu Zengtao, Lee Chun-Sing, Lee Shuit-Tong. // Applied Physics Letters. - 2009. - Vol. 95, No. 13. - P. 133301-133301-3. ↑
- J1091.** Chen Yu-Hung. Enhancement in current efficiency in organic light-emitting diodes with incorporation of

- subphthalocyanine. / Chen Yu-Hung, Chang Jung-Hung, Lee Guan-Ru, Wu I-Wen, Fang Jheng-Hao, Wu Chih-I, Pi Tun-Wen. // Applied Physics Letters. - 2009. - Vol. 95, No. 13. - P. 133302-133302-3. ↑
- J1092. Yen-Kuang Kuo. Enhancement of Light Power for Blue InGaN LEDs by Using Low-Indium-Content InGaN Barriers. / Yen-Kuang Kuo, Miao-Chan Tsai, Sheng-Horng Yen, Ta-Cheng Hsu, Yu-Jiun Shen. // IEEE Journal of Selected Topics in Quantum Electronics. - 2009. - Vol. 15, No. 4. - P. 1115-1121. ↑
- J1093. Lee J. W. Erratum: "High efficiency GaN-based light-emitting diodes fabricated on dielectric-mask-embedded structures" [Appl. Phys. Lett. 95, 011108 (2009)]. / Lee J. W., Sone C., Park Y., Lee S.-N., Ryou J.-H., Dupuis R. D., Hong C.-H., Kim H. // Applied Physics Letters. - 2009. - Vol. 95, No. 13. - P. 139902-139902-1. ↑
- J1094. Chen Ping. Influence of interlayer on the performance of stacked white organic light-emitting devices. / Chen Ping, Xue Qin, Xie Wenfa, Xie Guohua, Duan Yu, Zhao Yi, Liu Shiyong, Zhang Liying, Li Bin. // Applied Physics Letters. - 2009. - Vol. 95, No. 12. - P. 123307-123307-3. ↑
- J1095. Li X. Efficiency retention at high current injection levels in m-plane InGaN light emitting diodes. / Li X., Ni X., Lee J., Wu M., Ozgur U., Morkoc H., Paskova T., Mulholland G., Evans K. R. // Applied Physics Letters. - 2009. - Vol. 95, No. 12. - P. 121107-121107-3. ↑
- J1096. Hou Chia-Hung. Output power enhancement of light-emitting diodes via two-dimensional hole arrays generated by a monolayer of microspheres. / Hou Chia-Hung, Tseng Shao-Ze, Chan Chia-Hua, Chen Tsing-Jen, Chien Hung-Ta, Hsiao Fu-Li, Chiu Hua-Kung, Lee Chien-Chieh, Tsai Yen-Ling, Chen Chii-Chang. // Applied Physics Letters. - 2009. - Vol. 95, No. 13. - P. 133105-133105-3. ↑
- J1097. Shields P. A. Enhanced light extraction in nitride light-emitting diodes by epitaxially grown photonic-crystal nanopillar arrays. / Shields P. A., Liu C., Nasir M., Allsopp D. W. E., Wang W. N. // Applied Physics Letters. - 2009. - Vol. 95, No. 12. - P. 123120-123120-3. ↑
- J1098. Zheng Tianhang. Improving efficiency roll-off in organic light emitting devices with a fluorescence-interlayer-phosphorescence emission architecture. / Zheng Tianhang, Choy Wallace C. H., Ho Cheuk-Lam, Wong Wai-Yeung. // Applied Physics Letters. - 2009. - Vol. 95, No. 13. - P. 133304-133304-3. ↑
- J1099. Wallich P. The future's so bright. IEEE Spectrum. - 2009. - Vol. 46, No. 8. - P. 22. ↑
- J1100. Wang Jen-Yi. Double side electroluminescence from p-NiO /n-ZnO nanowire heterojunctions. / Wang Jen-Yi, Lee Chun-Yu, Chen Yung-Ting, Chen Chung-Tse, Chen Yung-Ling, Lin Ching-Fuh, Chen Yang-Fang. // Applied Physics Letters. - 2009. - Vol. 95, No. 13. - P. 131117-131117-3. ↑
- J1101. Sun X. W. Ultraviolet emission from a ZnO rod homojunction light-emitting diode. / Sun X. W., Ling B., Zhao J. L., Tan S. T., Yang Y., Shen Y. Q., Dong Z. L., Li X. C. // Applied Physics Letters. - 2009. - Vol. 95, No. 13. - P. 133124-133124-3. ↑
- J1102. Lo M. H. High efficiency light emitting diode with anisotropically etched GaN-sapphire interface. / Lo M. H., Tu P. M., Wang C. H., Hung C. W., Hsu S. C., Cheng Y. J., Kuo H. C., Zan H. W., Wang S. C., Chang C. Y., Huang S. C. // Applied Physics Letters. - 2009. - Vol. 95, No. 4. - P. 041109-041109-3. ↑
- J1103. Neokosmidis I. Impact of Nonlinear LED Transfer Function on Discrete Multitone Modulation: Analytical Approach. / Neokosmidis I., Kamalakis T., Walewski J.W., Inan B., Spicopoulos T. // Journal of Lightwave Technology. - 2009. - Vol. 27, No. 22. - P. 4970-4978. ↑
- J1104. Yu-Tzu Chiu. Foundry giant sees the light. IEEE Spectrum. - 2009. - Vol. 46, No. 8. - P. 19. ↑
- J1105. {no data available}. The Spectrum Dumping Gang. IEEE Spectrum. - 2009. - Vol. 46, No. 8. - P. 4. ↑